Gláucia Maria Dalfré

Flexural and shear
strengthening of RC elements

Flexural and shear
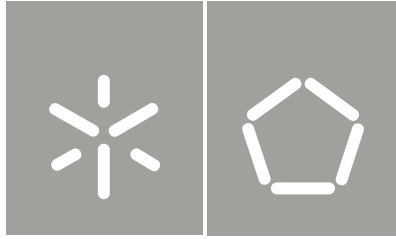strengthening of RC elements

Gláucia Maria Dalfré

UMinho | 2013

Fevereiro de 2013

Universidade do Minho
Escola de Engenharia

Gláucia Maria Dalfré

Flexural and shear
strengthening of RC elements

Tese de Mestrado / Doutoramento
Engenharia Civil

Trabalho efectuado sob a orientação do
Professor Doutor Joaquim António Oliveira de Barros

Fevereiro de 2013

Acknowledgements

Abstract

In a recent experimental program dealing with the Near Surface Mounted (NSM) technique for the flexural strengthening of continuous reinforced concrete (RC) slabs strips, the increase of load carrying and the moment redistribution was lower than the expected values. This experimental program was analysed in depth in this thesis and it was concluded that more efficient flexural strengthening arrangements can be applied if carbon fibre reinforced polymer (CFRP) laminates (of rectangular cross section) are applied not only in the intermediate support (hogging region), but also in the positive bending moment zones (sagging regions).

Thus, an experimental and a numerical research program were carried out, and it was verified the possibility of increasing the load carrying capacity in 25% and 50%, maintaining a relatively high level of moment redistribution, when correct NSM flexural strengthening arrangements are used.

For assessing the predictive performance of a FEM-based computer program, the experimental tests were simulated by considering the nonlinear relevant aspects of the intervening materials. After has been concluded about the capability of this model to simulate the behaviour of this type of structures, a parametric study was carried out to investigate the influence of the strengthening arrangement and CFRP percentage in terms of load carrying capacity and moment redistribution capacity of continuous RC slab strips flexurally strengthened by the NSM technique. Additionally, to predict the load-deflection response of this type of structures up to its collapse, an analytical model was developed and its performance was appraised by using the data obtained from the experimental program. This model is based on the flexibility method and requires the knowledge of the flexural stiffness of the representative cross sections of the structure, which can be determined from the moment-curvature relationship of these sections.

The increase of the load carrying capacity of the strengthened slabs can, however, can be limited by the formation of a shear failure crack in the hogging region. To avoid the occurrence of this brittle failure mode, a new technique, designated Embedded Trough Section (ETS) was developed, and its effectiveness was appraised by testing two series of RC beams of different cross section.

Finally, the most relevant conclusions extracted from the present study are presented, and further research developments are suggested.

Resumo

Num programa experimental recentemente realizado sobre o reforço à flexão de faixas de laje contínuas de betão armado (BA) reforçadas segundo a técnica NSM (Near Surface Mounted, nomenclatura inglesa), o aumento da capacidade de carga e de redistribuição de momento foi inferior ao esperado. Este programa experimental foi analisado em profundidade nesta tese e foi concluído que existem configurações de reforço à flexão mais eficientes que podem ser utilizadas se laminados de fibra de carbono (CFRP) forem aplicados não só na região de apoio central (momento negativo), mas também na região de momentos positivos.

Nesse sentido, um programa experimental e numérico foi levado a cabo, e verificou-se a possibilidade de aumentar a capacidade resistente em 25% e 50%, mantendo um nível de redistribuição de momentos relativamente elevada, quando se usam sistemas de reforço NSM adequados.

Para avaliar a capacidade de previsão um software baseado no Método dos Elementos Finitos (MEF), os resultados experimentais foram simulados considerando os aspectos mais relevantes do comportamento não-linear dos materiais intervenientes. Após a conclusão deste estudo sobre a capacidade de simulação do comportamento deste tipo de estruturas com este modelo, foi realizado um estudo paramétrico para investigar a influência da disposição do reforço e da percentagem de CFRP na capacidade de carga e capacidade de redistribuição de momento em faixas de laje contínuas reforçadas segundo a técnica NSM. Além disso, um modelo analítico foi desenvolvido para prever a relação força-flecha deste tipo de estruturas até o seu colapso e o seu desempenho foi avaliado usando os dados obtidos no programa experimental. Este modelo é baseado no método de flexibilidade e pressupõe o conhecimento da rigidez à flexão das secções transversais representativas da estrutura, a qual pode ser determinada a partir da relação momento-curvatura destas secções.

O aumento da capacidade de carga pode, no entanto, ser comprometido pela formação de fendas de corte junto aos apoios centrais dos elementos estruturais reforçados. Para evitar a ocorrência deste tipo de rotura frágil, uma nova técnica de reforço, designada por Embedded Trough Section (ETS, na nomenclatura inglesa) foi desenvolvida, e a sua eficácia foi avaliada por meio de ensaios de duas séries de vigas com diferentes seções transversais.

Finalmente, as principais conclusões extraídas da investigação desenvolvida ao longo deste trabalho são apresentadas, e desenvolvimentos futuros são sugeridos.

VI

Palavras chave

Faixas de laje de betão armado

Vigas de betão armado

Reforço a flexão

Reforço ao corte

Polímeros reforçados com fibras de carbono (CFRP)

NSM

ETS

Betão de recobrimento

Comportamento experimental

Simulação numérica

Modelo analítico

Ensaios de flexão

Ensaios de corte

Keywords

Reinforced concrete slab strips

Reinforced concrete beams

Flexural strengthening

Shear strengthening

Carbon fiber reinforced polymers (CFRP)

NSM

ETS

Concrete cover

Experimental behaviour

Numerical simulation

Analytical model

Bending tests

Shear tests

Chapter 2 - State-of-the-art

Chapter 3 – NSM technique to increase the load carrying capacity of continuous RC slab strips

regions.

Chapter 4 – Simulation of RC slab strips strengthened with NSM CFRP laminates

Chapter 5 – Description of the analytical strategy

Chapter 6 - Steel bar – concrete bond behaviour in the context of the ETS shear strengthening technique for RC beams

mm and bar diameter of 12 mm.

Chapter 7 - Assessment of the effectiveness of the embedded through-section technique for the shear strengthening of RC beams

Index of Tables

experimental program.

Chapter 3 – NSM technique to increase the load carrying capacity of continuous RC slab strips

Chapter 5 – Description of the analytical strategy

Chapter 6 - Steel bar – concrete bond behaviour in the context of the ETS shear strengthening technique for RC beams

Chapter 7 - Assessment of the effectiveness of the embedded through-section technique for the shear strengthening of RC beams

Contents

Technique

"Everything should be as simple as it is, but not simpler"

Albert Einstein

Chapter 1

INTRODUCTION

1.1 CONTEXT AND MOTIVATION

A large number of existing reinforced concrete (RC) and prestressed concrete (PC) structures are in a state of serious deterioration that can be attributed to the carbonation, chloride attack, aging, environmentally induced degradation, and corrosion of the embedded reinforcement. Some of them are not prepared to support loading demands of natural events such is the case of earthquakes. Moreover, many structures are no longer considered safe due to the increase of the load specifications in the design codes, poor initial design and/or construction, overloading, change of use, lack of quality control and maintenance. So, in order to maintain efficient serviceability, the structures must be repaired or strengthened in order to attain the demanded requirements. It is becoming both environmentally and economically preferable to repair or strengthen the structures rather than replacement, particularly if rapid, effective and simple strengthening methods are available.

In the last two decades, the use of FRP materials for the structural strengthening has become one of the most promising technologies in materials and structural engineering, and has gained increasing popularity in the civil engineering community. The intrinsic properties of these materials (e.g., lower weight, high strength, good corrosion and electromagnetic neutrality) can be used for the strengthening and/or rehabilitation of concrete, timber, steel and masonry structures. Furthermore, the decrease of FRC costs due to the market expansion is making FRP-based construction or strengthening/rehabilitation techniques more competitive.

In this context, the Externally Bonded Reinforcement (EBR) and the Near Surface Mounted (NSM) are the most used FRP-based techniques for the strengthening of RC elements. The efficiency of the NSM technique for the flexural and shear strengthening of RC members has already been assessed. However, most of the tests were carried out with NSM strengthened simply supported elements.

Although many in situ RC strengthened elements are of continuous construction nature, there is a lack of experimental and theoretical studies in the behaviour of statically indeterminate RC members strengthened with FRP materials. The majority of research

studies are dedicated to the analysis of the behaviour of continuous elements reports the use of the EBR technique. Limited information is available in literature dealing with the behaviour of continuous structures strengthened according to the NSM technique. Thus, in the present doctoral thesis the potentialities of the NSM technique are explored for the increase of the load carrying capacity of two spans continuous RC slabs. The NSM strengthening configurations applied in seventeen slab strips were designed to increase, in 25% and 50%, the load carrying capacity of its corresponding unstrengthened reference RC slab. Besides the load carrying capacity of the tested slabs, the moment redistribution issues are also discussed in this work.

The effectiveness of the NSM technique can be, however, compromised by the formation of shear cracks in the hogging region of the flexural strengthened elements. Moreover, in some cases, the failure mode shifts from ductile flexural failure to brittle shear failure after a flexural strengthening intervention. In fact, the shear failure of the retrofitted system should be avoided, once this failure is often brittle and occur with little or no visible warnings.

Concerning to the shear strengthening, there have been a number of studies on RC beams and slabs using different techniques. Existing approaches often involve the use of concrete jacketing, external prestressing and steel plate bonding. Recently, experimental studies on shear strengthening of reinforced concrete beams with Carbon Fibre Reinforced Polymer (CFRP) composites, according to the EBR (Externally Bonded Reinforcement) or NSM, show that these techniques are good alternatives to traditional shear strengthening solutions. However, in the EBR technique the external reinforcement frequently fails by premature debonding. Furthermore, EBR and NSM techniques have no applicability in the shear strengthening of slabs, and in the beams with very deficient concrete cover. Concerning to the slabs, in general, the shear strengthening involves installing external shear reinforcement and/or collars in the slab-column connections to increase the critical shear perimeter, the use of steel bars grouted into 45-degree inclined drilled holes, bolts to act as shear reinforcement, and carbon fiber reinforced polymers stirrups. A new shear strengthening technique is investigated in the present work, designated by Embedded Through-Section (ETS). According to this strengthening technique, holes are opened through the beam/slab's section, with the desired inclinations, and bars are introduced into these holes and bonded to the concrete substrate with adhesive material.

Limited research has been conducted on the use of embedded bars for shear strengthening. In this way, to explore the potentialities of the ETS shear strengthening technique, experimental programs were carried out. To assess the contribution of the bond mechanisms of ETS bars for the shear strengthening effectiveness of this technique, and to select the most convenient strengthening bars and adhesive materials for this strengthening technique, experimental programs of pull-out tests were executed.

1.2 SCOPE AND AIMS OF THE THESIS

The aim of the research conducted in this thesis is to increase the knowledge of the structural behaviour of continuous RC slab strips strengthened with NSM CFRP laminates. The aspects related to the strengthening effectiveness and moment redistribution capacity in such type of structures are analysed and discussed.

Another goal of the present work is to investigate the performance of the ETS technique for the shear strengthening of RC beams. The experimental research carried out is described, and the obtained results are presented and discussed. Additionally, the applicability of the ACI analytical formulations for the predicting of the shear resistance of RC beams strengthened according to the ETS technique was investigated.

Also, the characterization of the most relevant properties of the intervenient materials in the experimental programs is an additional aspect pursued in the present thesis.

It is expected that this thesis is of interest to structural engineers, composite material suppliers and testing institutions, as well as standardisation organizations and technical committees with the charge of developing design codes.

1.3 THESIS STRUCTURE

This thesis consists of nine chapters, eight forming the main body of the thesis, and one chapter with complementary sections, organized as follows.

The principal aims of this research work and an overview of the thesis is presented in the introductory part, chapter 1 (the present chapter).

The second chapter presents a state-of-art of the shear and flexural strengthening techniques investigated in the present study.

In chapter 3, the results of an experimental research program on the use of the NSM technique with CFRP laminates for the flexural strengthening of continuous RC slabs are presented. The performance of this technique in this type of structures is experimentally evaluated in terms of moment redistribution, ductility performance, and increase of the load carrying capacity.

The capability of a computer program, based on the finite element method (FEM), to simulate the behaviour of continuous RC slabs flexurally reinforced according to the NSM CFRP technique is investigated in Chapter 4. For this purpose, the results obtained in the experimental program detailed in chapter 3 are compared to those derived from the application of the numerical model. After the good predictive performance of the numerical model has been assessed, a parametric study composed of 144 numerical material nonlinear simulations was carried out to investigate the influence of the strengthening arrangement and CFRP percentage in terms of load carrying capacity and moment redistribution capacity of continuous RC slab strips flexurally strengthened by the NSM technique.

Chapter 5 is dedicated to the prediction of the load-deflection response of continuous RC slabs up to its collapse. For this purpose, an analytical model was developed and its performance was appraised by using the data obtained from the experimental program. The proposed model is based on the constitutive laws for the intervening materials, strain compatibility and equilibrium of the cross section representative of the structure. The predictive performance of the model was appraised by simulating two series of tests composed of seventeen RC slab strips strengthened with NSM CFRP laminates.

Chapter 6 deals with a comprehensive pullout program to assess the bond contribution mechanism for the shear strengthening effectiveness of the ETS technique. The

experimental program is described and the obtained results are presented and analysed in this chapter.

The assessment of the effectiveness of the Embedded Through-Section technique (ETS) for the shear strengthening of RC beams is presented in chapter 7. Some analyses using FEM based computer program were also executed and the results are presented and discussed.

Chapter 8 provides the major concluding remarks and findings from this research program, together with suggestions for future research.

Finally, a complementary section with annexes is also presented.

"The roots of education are bitter, but the fruit is sweet".
Aristotle

Chapter 2
STATE-OF-THE-ART

Prior the development of new strengthening schemes, it is important that the findings from research previously conducted on other strengthening techniques be known. This chapter presents a background and literature review on the strengthening of statically determinate or indeterminate RC structures. Thus, the overview about the development and applications of the strengthening materials is described, firstly for statically determinate elements, followed by a brief review for statically indeterminate elements. The review is presented in a chronological order to allow a better understanding on the evolution of the findings of the research effort, as well as the issues involved as the research progressed. For each paper, the review provides information on the objectives, the methodology, the experimental program, the test method, as well as the strengthening configuration used.

2.1 STATE-OF-THE-ART ON THE FLEXURAL STRENGTHENING OF RC ELEMENTS

2.1.1 Introduction

Structural rehabilitation represents an important area of the construction industry and its significance is increasing. Several methods are available, each one with different advantages, but also including certain weaknesses. The choice of the repair and/or strengthening method depends on the objectives of the structural intervention. The most popular techniques for strengthening of RC beams have involved the use of external epoxy-bonded steel plates. It has been found experimentally that the flexural strength of a structural member can be increased by using this technique. Although steel bonding technique is simple, cost-effective and efficient, it suffers from a serious problem of deterioration of bond at the steel and concrete interface due to corrosion of steel. Other common strengthening technique involves the construction of steel jackets, which is quite effective from strength, stiffness and ductility considerations. However, it increases overall cross-sectional dimensions, resulting strengthened structures with higher self-weight, which can be a concern in terms of dynamic response when submitted to natural events like an earthquake.

To eliminate these problems, instead of steel plates, it has been used corrosion resistant and light-weight fiber-reinforced polymer composite (FRP) plates. FRPs help to increase strength and the stiffness performance of a structure, but due to the linear-elastic brittle character of FRPs, the ductility of a FRP-based structure is a design concern. FRPs could be designed to meet specific requirements by optimizing the arrangement of fibers, which can be a great benefit of these materials. Thus, concrete members can be easily and effectively strengthened using FRP composites. During the past decade, the application of FRPs in structural rehabilitation has rising significantly due to the well-known advantages of FRP composites over conventional materials. Consequently, a great quantity of research, both experimental and theoretical, has been conducted on the behaviour of FRP strengthened reinforced concrete (RC) structures, including beams, slabs, and columns, mainly applied according to the Externally Bonded Reinforcement (EBR) and the Near-Surface Mounted (NSM) strengthening techniques.

In this way, a brief literature review of previous works on the strengthening materials was described, firstly for statically determinate elements and secondly for the statically indeterminate elements.

2.1.2   Statically determinate elements

2.1.2.1   Flexural strengthening of beams and slabs

For flexural strengthening, there are many methods such as: section enlargement, steel plate bonding, external post tensioning method, and EBR and NSM FRP-based techniques. While many methods of strengthening structures are available, strengthening structures via external bonding of FRP has become very popular worldwide. In the last decade, the use of conventional materials, like steel and concrete is being replaced by the use of FRP materials for the strengthening of concrete structures. These materials are available in the form of strips made by pultrusion, in the form of sheets or fabrics made by fibres in one or two different directions, respectively, and in the form of bars. Carbon (CFRP) and glass (GFRP) are the main fibres composing the fibrous phase of these materials, while epoxy is generally used on the matrix phase. Wet lay-up (sheets and fabrics) and prefabricated elements (laminates and bars) are the main types of FRP strengthening systems available in the market. The increasing demand of FRP for structural repair and strengthening is due to the following main advantages of these composites when compared to conventional materials: low weight, easy installation, high durability and tensile strength, large deformation capacity, electromagnetic permeability and practically unlimited availability in FRP sizes, geometry and dimensions.

In this context, a brief review of the literature dealing with the flexural strengthening of statically determinate elements is presented. This section is divided in four parts, as follows:

i) Beam jacketing;

ii) Externally Bonded Reinforcement (EBR) technique;

iii) Near-Surface Mounted (NSM) technique; and

iv) Mechanically Fastened FRP (MF-FRP) technique.

i) Beam Jacketing

Jacketing of beams is recommended for several purposes such as to give continuity to the columns and to increase the strength and stiffness of the structure. According to the proposed technique, additional stirrups are hanged to the beam by transverse threaded steel rods embedded in the RC beam. To evaluate the behaviour of the U-shape beam jacketing, eight RC beams were tested (Mahdy et al., 2004). The reference beam (BC0) had the

dimensions of 100x200x1300 mm^3 and was reinforced with two steel bars of 12 mm diameter (2ϕ12 mm) and two steel bars of 10 mm diameter (2ϕ10 mm) as tensile and compression reinforcement, respectively (Figure 2.1a). Steel stirrups of 8 mm diameter, at spacing of 100 mm, were used throughout the length of the beams.

To appraise the strengthening effectiveness of RC jacketed system, two beams (BS5R and BS9R) of dimensions 170x250x1300 mm^3 were tested (Figure 2.1b). These beams were cast in one phase (i.e., with no interface) and comprises the longitudinal reinforcement composed of 2ϕ12 mm and the stirrups of 5ϕ8 mm or 9ϕ10 mm, respectively. Three beams (BS0U, BS5U and BS9U) were strengthened in a second phase by casting a concrete jacket reinforced with longitudinal reinforcement formed by 2ϕ12 mm and stirrups (zero, 5ϕ8 mm or 9ϕ10 mm). Finally, two beams (BS5U, BS9U) were strengthened with a steel fibre reinforced concrete (SFRC) jacket reinforced with stirrups (5ϕ8 mm or 9ϕ10 mm) (Figure 2.1c). The mechanical properties of the materials used in this work were experimentally obtained. For the concrete, an average compressive strength (f_{cm}) of 30 MPa was determined at the age of 28 days. The tensile strength for the plain and concrete reinforced with 1% volume fraction of steel fibers was 4 MPa and 8 MPa, respectively.

From the obtained results, included in Table 2.1, it can be pointed out that the use of the concrete jacket provided significant increase of the load carrying capacity of RC beams. Based on the results of the unstrengthened beams (Reference, BC0), it was found that the beams cast in one phase, with longitudinal reinforcement composed of 2ϕ12 mm and additional stirrups presented an increase in the load carrying capacity of 108% and 106% when adding steel stirrups of 5ϕ8 (BS5R) and 9ϕ10 (BS9R), respectively. Concerning to the beams where the concrete jacket was applied in the first (BS5R and BS9R) or second (BS5U and BS9U) phase of the cast, a similar load carrying capacity was obtained when applying steel stirrups of 9ϕ10. However, a decrease of 17% was obtained for the beams with steel stirrups of 5ϕ8. The presence of the SFRC jacket enhanced the ultimate load in about 10% and 16% in comparison to the beams with plain concrete jacket (BS5U and BS9U), respectively.
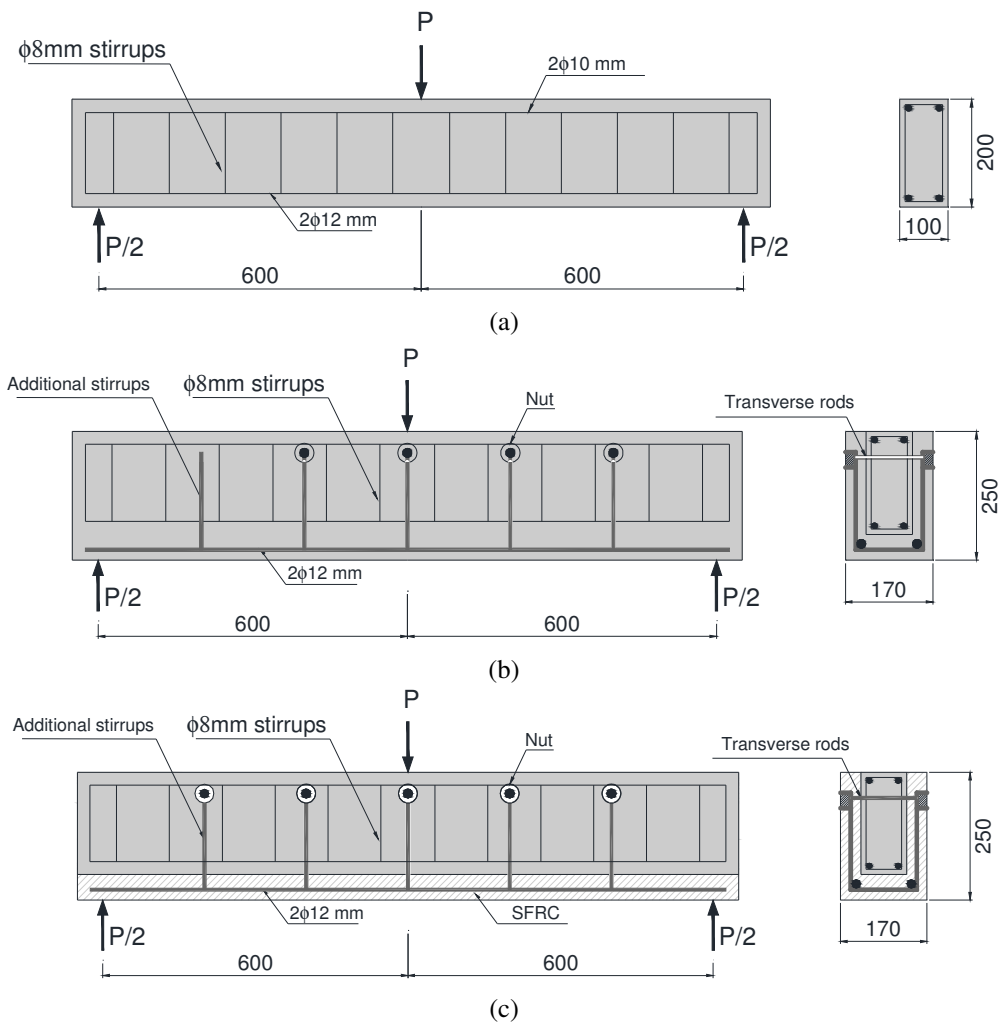
Figure 2.1: Details of the (a) reference beam (BC0) and (b-c) details of the reinforcement after the application of the strengthening technique (Mahdy et al., 2004, Dimensions in mm).

Table 2.1: Details of the experimental program.

Beam ID	Original Dimensions (mm)	Final Dimensions (mm)	Additional stirrups	V_f (%)	Depth of SFRC (mm)	Ultimate load (kN)
BC0	100x200	100x200	-----	-----	0	72
BS5R	170x250	170x250	5ϕ8	-----	0	150
BS9R	170x250	170x250	9ϕ10	-----	0	148
BS0U	100x200	170x250	Without	-----	0	95
BS5U	100x200	170x250	5ϕ8	-----	0	128
BS9U	100x200	170x250	9ϕ10	-----	0	145
BS5FU	100x200	170x250	5ϕ8	1	50*	140
BS9FU	100x200	170x250	9ϕ10	1	50*	168
*This value is the thickness of the bottom layer of U-shape jacket						

ii) Externally Bonded Reinforcement (EBR) technique

The first projects on the flexural strengthening of RC elements with FRP materials have been carried out by using EBR FRP strengthening (Meier, 1987; Kaiser, 1989; Triantafillou et al., 1992). The EBR strengthening technique is composed of the following steps: 1) on the zones of the beam's surfaces where the strips of CFRP sheet are planned to be glued, an emery is applied to remove the superficial cement paste; 2) the residues are removed by compressed air; 3) a layer of primer is applied to regularize the concrete surface and to enhance the adherence capacity of the CFRP to the concrete substrate; 4) the CFRP sheets are measured and cut in the desired shape and dimensions; and 5) U-shaped CFRP strips are glued to the bottom of the beam/slab by epoxy resin. The primer and the epoxy resin should be produced according to the supplier recommendations.

Grace et al. (2003)

The effectiveness of a triaxially braided ductile fabric for the strengthening of concrete beams was experimentally investigated by Grace et al. (2003). Twelve RC beams, divided into three different groups, were strengthened in flexure and shear by using fabrics applied according to the EBR technique. Groups A and B were used to investigate the contribution of fabrics for the flexural strengthening, while group C was used to investigate the effectiveness of fabrics for the shear strengthening. Groups A and B were composed of beams with dimensions of 152x254x2744 mm^3. Only the results of the flexurally strengthened beams are herein presented. The beams of the group A were reinforced with two steel bars of 16 mm diameter ($2\phi16$ mm) and two steel bars of 9.5 mm diameter ($2\phi9.5$ mm) as tensile and compression reinforcement, respectively. Steel stirrups of 9.5 mm diameter, at spacing of 102 mm, were used throughout the length of the beams. The beams of the group B were reinforced with two steel bars of 9.5 mm diameter ($2\phi9.5$ mm) and two steel bars of 9.5 mm diameter ($2\phi9.5$ mm) as tensile and compression reinforcement, respectively. Steel stirrups of 9.5 mm diameter, at spacing of 102 mm, were used throughout the length of the beams. Figure 2.2 shows the beam dimensions, reinforcement details, and loading setup for the beams of Groups A and B. Similar beams were strengthened with CFRP sheets. Additionally, one beam was strengthened with a steel plate to compare its behaviour with those strengthened with the fabrics and CFRP sheets.
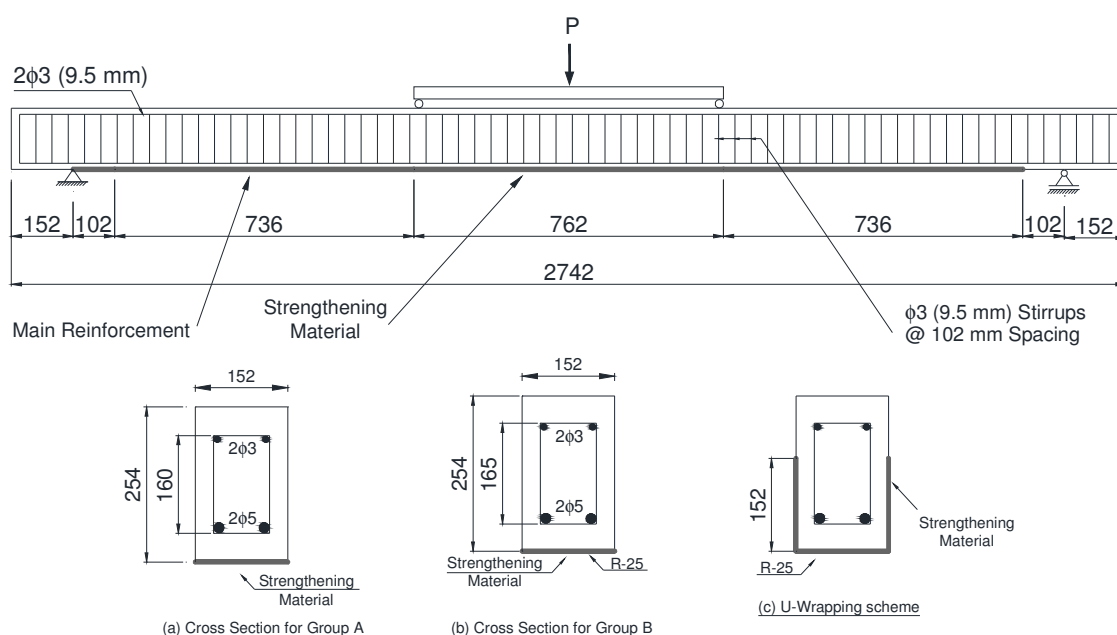
Figure 2.2: Details of test beams in Groups A and B (Grace et al., 2003; dimensions in mm).

The compressive strength of the concrete when beams were tested was 41.5 MPa and 55.2 MPa for Groups A and B, respectively. The steel reinforcement that was used had a yield stress of 490 MPa. Concerning to the strengthening materials, a 1.0 mm thickness triaxially braided ductile fabric was experimentally tested and presented an ultimate load of 0.33 kN/mm and 0.20 kN/mm for the 0-degree and 45-degree directions, respectively. A 0.13 mm thickness carbon fiber sheet was also used to strengthen beams. According to the results, an ultimate load of 0.34 kN/mm was obtained. Finally, a Grade 40 steel plate of 1.52 mm thickness was also used. This material presented an ultimate load of 0.58 kN/mm. Table 2.2 includes the details and the main results of the experimental program.

According to the results, for the beams of the group A, the use of the triaxial fabric applied in one layer in the U-wrap strengthening arrangement presented the higher increase of the load carrying capacity (taking into account the number of layers used for the strengthening), attaining a value of about 50%. Considering the strengthening configuration in which the materials are applied in the bottom face, an increase of about 62% and 39% was obtained when using four layers of carbon fiber sheet and steel plates, respectively. The beams of the group B have also presented better results with the U-shape strengthening configuration, attaining an increase of the lad carrying capacity of 119% when using the triaxial fabric (one layer) or the carbon fiber sheet (two layers). Based on the results, the beams strengthened in flexure with the triaxial fabric behaved in a more ductile manner than those strengthened with the CFRP sheet, and were generally less likely to exhibit debonding failures. The triaxial fabric produced a yield plateau similar to that of

the unstrengthened beam and also similar to that produced by a beam strengthened with a ductile material such as steel. Although the beam strengthened with the steel plate exhibited considerable ductility, the steel plate yielded at a lower load than the inner reinforcing steel because the plate has both a lower yield strain than the steel bars.

Table 2.2: Details of the experimental program.

Group	Beam ID	Strengthening squeme	Strengthening material	Failure Load (kN)	Deflection at failure (mm)	Type of failure
A	Control 1	-----	-----	87	44	Steel yield followed by concrete failure
	F-B-1*	Bottom face only	Triaxial fabric (two layers)			Steel and fabric yield followed by concrete failure
	F-B-2*			123	37	
	F-CB-1		Carbon fiber sheet (four layers)	141	29	Steel yield followed by sheet debonding
	F-ST-1		Steel plate	121	34	Steel yield followed by concrete failure
	F-BL3-1		Triaxial fabric (three layers)	141	36	Steel and fabric yield followed by concrete failure
	F-U-1**	U-wrap	Triaxial fabric (one layer)			Steel and fabric yield followed by concrete failure
	F-U-2**			130	37	
	F-CU-1		Carbon fiber sheet (two layers)	133	29	Steel yield followed by concrete failure
B	Control 2	-----	-----	42	57	Steel yield followed by concrete failure
	F3-B-1	Bottom face only	Triaxial fabric (two layers)	70	38	Steel and fabric yield followed by fabric debonding
	F3-CB-1		Carbon fiber sheet (four layers)	67	18	Steel yield followed by sheet debonding
	F3-U-1	U-wrap	Triaxial fabric (one layer)	91	45	Steel and fabric yield followed by fabric rupture
	F3-CU-1		Carbon fiber sheet (two layers)	92	25	Steel yield followed by sheet debonding

* The test results of beams F-B-1 and F-B-2 were very similar. Hence, the results herein presented will be focused on Beam F-B-2 to avoid repetition; ** The results of Beams F-U-1 and F-U-2 were very similar and, hence, the results herein presented is focused on Beam F-U-2 to avoid repetition.

iii) Near-Surface Mounted (NSM) Technique

The strengthening technique used for the rehabilitation of RC structures, based on the use carbon fibre reinforced polymer (CFRP) laminates installed into pre-cut slits opened on the concrete cover, designated as Near Surface Mounted (NSM), has been widely investigated and used mainly to increase the loading carrying capacity of statically determinate RC beams. The strengthening steps of the NSM technique is composed of the following steps: 1) using a diamond cutter, slits are opened on the concrete cover of the beam; 2) the slits

are cleaned by compressed air; 3) the laminates are cut with the desirable length and cleaned with acetone; 4) the epoxy adhesive should be produced according to the supplier recommendations; 5) the slits are filled with the adhesive; 6) a layer of adhesive is applied on the faces of the laminates; and 7) the laminates are inserted into the slits and adhesive in excess is removed.

Blaschko and Zilch (1999)

The first known experiments with near-surface mounted CFRP laminate strips as a strengthening technique were published by Blaschko and Zilch (1999). The mechanical behaviour of strengthened beams was tested in beam tests with CFRP strips glued into slits, according to the NSM technique, as well as with strips glued onto the concrete surface according to the EBR technique.

The beams were divided into two groups, with the dimensions of 350x150x3000 mm^3. The details of the beams are presented in Figure 2.3. It should be noted that the test specimens of series A reflect the behaviour of slabs, while series B the behaviour of beams. The longitudinal steel reinforcement is composed of bars with 6 mm diameter in the tension zone. All the beams were tested in 3 point loading at a span of 2.5 m. One test specimen of each series (A1, B1) was strengthened with one EBR CFRP strip 50 mm by 1.2 mm glued on the concrete surface. The other two (A2, B2) were strengthened with two NSM CFRP strips 25 mm by 1.2 mm glued in slits. The slits were 26 mm deep and 3 mm wide. Table 2.3 presents the main obtained results in the experimental program.
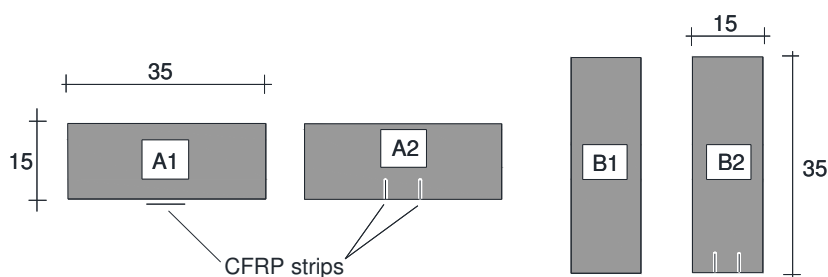
Figure 2.3: Cross sections of tested beams (Blaschko and Zilch, 1999)
Dimensions in cm.

Table 2.3: Main obtained results in the experimental program.

Group	Beam ID	Strengthening squeme	Maximum bending moment (kNm)	Type of failure
A	A1	EBR	12	Peeling-off of the glued strips
	A2	NSM	26	Tension failure of the CFRP strips
	B1	EBR	26	Peeling-off of the glued strips
	B2	NSM	52	Shear failure

Based on the obtained results, it was found that the NSM technique has provided a higher ductility and load carrying capacity than the EBR technique. In fact the NSM technique was capable of doubling the load carrying capacity of the corresponding beams strengthened with the EBR technique.

Carolin (2003)

The behaviour of concrete structures strengthened with NSM CFRP reinforcements was analysed by Carolin (2003). The first part of the experimental program (Series I) was composed by RC beams flexurally strengthened and submitted to a four point bending loading configuration (Figure 2.4a). In the static four point bending test, Series I, four rectangular concrete beams with dimensions of 200x300x4000 mm^3 were manufactured, three of them were strengthened with NSMR 10 mm square rods and the other one served as a reference beam. The beams were reinforced for shear with steel stirrups of ϕ10 mm at a spacing of 75 mm. The longitudinal steel reinforcement was composed of 2ϕ16 mm at the top and two at the bottom. Concerning to the properties of the materials used in this experimental program, NSMR laminates with a Young´s modulus of 230 GPa were applied. The adhesive used, BPE® Lim 465, had the following material properties: Young´s modulus (E_a) of 7.0 GPa, compressive strength (f_{ca}) of 103 MPa and tensile strength (f_{ta}) of 31 MPa. The mortar used, Bemix High Tech 305, had a compressive strength (f_{cc}) of 60 MPa after 28 days. Finally, the concrete average compressive strength of 60.7 MPa was obtained.

In the second part of the program (Series II), similar RC beams were flexurally strengthened with prestressed NSM rods of rectangular cross section (Figure 2.4b). Four beams were tested, one reference beam, one beam strengthened without prestress and two strengthened with prestress. The beams had the same dimensions and steel reinforcement presented for Series I. The rods were subjected to a prestressing force until a strain of approximately 2000 micro strain was achieved. However, about 5% of the prestress was lost due to problems with the equipment. The epoxy adhesive cured for 5 days before releasing the prestressing force, here an additional strain loss of 2% was recorded in the centre of both beams, BP1 and BP2. Concerning to the properties of the materials used in this experimental program, NSMR laminates with a Young´s modulus of 160 GPa were applied. The adhesive used is the same as for test Series I. Concerning to the concrete, an average compressive strength of 65.25 MPa was obtained. Table 2.4 presents the main results obtained in the experimental program.

(a)

(b)
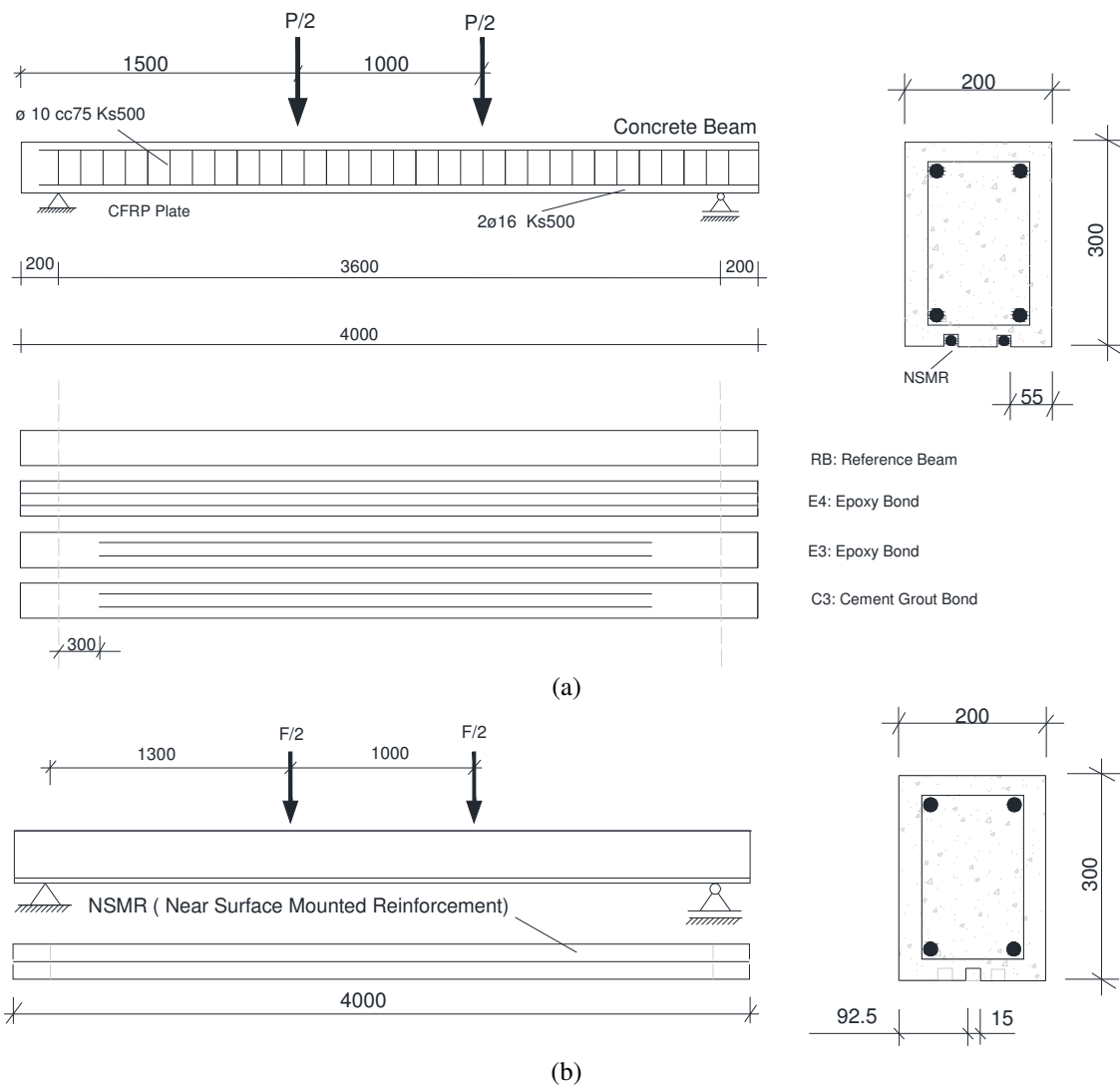
Figure 2.4: Test set-up and dimensions of the (a) Series I and (II) Series II (Carolin, 2003) - dimensions in m.

Table 2.4: Main results obtained in the experimental program.

Series I			Series II				
Beam ID	Ultimate load (kN)	Ultimate deflection (mm)	Beam ID	First crack (kN)	Steel Yielding (kN)	Ultimate load (kN)	Ultimate deflection (mm)
Reference	79.0	24.0	Reference	10	71	75	60
C3	123.5	43.0	BNP	16	84	118	55
E3	140.0	51.5	BP1	19	96	121	46
E4	152.0	58.5	BP2	21	99	121	44

For the Series I, according to the results, the use of steel NSMR rods provided significant increase of the load carrying capacity of RC beams. The effectiveness is also significant in terms of the deflection performance. An increase in the load carrying capacity of 56%, 77% and 92% were obtained when using cement grout (C3) and epoxy adhesives (E3 and

E4 configurations), respectively. In terms of deflection capacity, an increase of 79%, 115% and 144 %, respectively, was obtained.

For the Series II, similar increase in the load carrying capacity, of about 60%, was obtained for beams without prestress, as well as for the two strengthened with prestress. Beams BP1 and BP2 had a 37 % increase in load before the steel yielded compared with the unstressed beam BN, and an increase in the cracking load of about 100% compared with the reference beam; but the same ultimate load as BNP.

El-Hacha and Rizkalla (2004)

Eight simply supported concrete T–cross section beams were constructed and tested under a monotonically increasing concentrated load applied at midspan of the beam. The beams were 2700 mm long, with bottom tension reinforcement composed of 2ϕ12.7 mm and 2ϕ16 mm. The top compression reinforcement consisted of 2ϕ12.7 mm. The shear reinforcement consisted of double-legged steel stirrups of ϕ 12.7 mm at a spacing of 100 mm. One beam was tested as a control specimen, whereas the other seven beams were strengthened using different FRP reinforcements including CFRP reinforcing bars and strips, as well as GFRP thermoplastic strips. The test setup, beams details, instrumentation and the strengthening arrangements are presented in Figure 2.5. The mechanical properties of the materials are presented in Table 2.5 and main results obtained in the experimental program are presented in Table 2.6.

According to the results, the strengthening technique based on the use of NSM FRP reinforcing bars or strips has increased the flexural stiffness and the ultimate load-carrying capacity of the beams. The increase in the load carrying capacity ranged between 79.7% and 98.9% when using CFRP NSM technique. When using the CFRP EBR technique, an increase in the load carrying capacity of 16.1% was obtained. When using the GFRP NSM and the GFRP EBR techniques, an increase in the load carrying capacity of 85.4% and 28.3% was obtained.

Table 2.5: Mechanical properties.

FRP Materials						Adhesives	
Strengthening system	Type	Dimensions (mm)	Ultimate tensile strength (MPa)	Modulus of elasticity (GPa)	Ultimate tensile Strain (%)	Tensile strength (MPa)	Modulus of elasticity (MPa)
1	CFRP bars	9.5	1408	122.5	1.14	48	1200
2	CFRP strips	2x16	1525	140	1.08	70	3500
3	CFRP strips	1.2x25	2000	150	1.33	70	3500
4	GFRP strip	2x20	1000	45	2.22	70	3500

Table 2.6: Main results obtained in the experimental program.

Beam ID	FRP strengthening system	Ultimate load (kN)	Ultimate deflection (mm)
BO	No strengthening	55.4	64.4
B1	One NSM CFRP reinforcing bar	96.8	29.2
B2	Two Type 1 NSM CFRP strips	99.3	30.5
B2a	Two Type 1 externally bonded CFRP strips	64.6	43.7
B2b	Two Type 1 externally bonded CFRP strips	64.3	21.7
B3	Two Type 2 NSM CFRP strips	110.2	50.8
B4	Five NSM GFRP thermoplastic strips	102.7	44.3
B4a	Five externally bonded GFRP thermoplastic strips	71.1	22.2
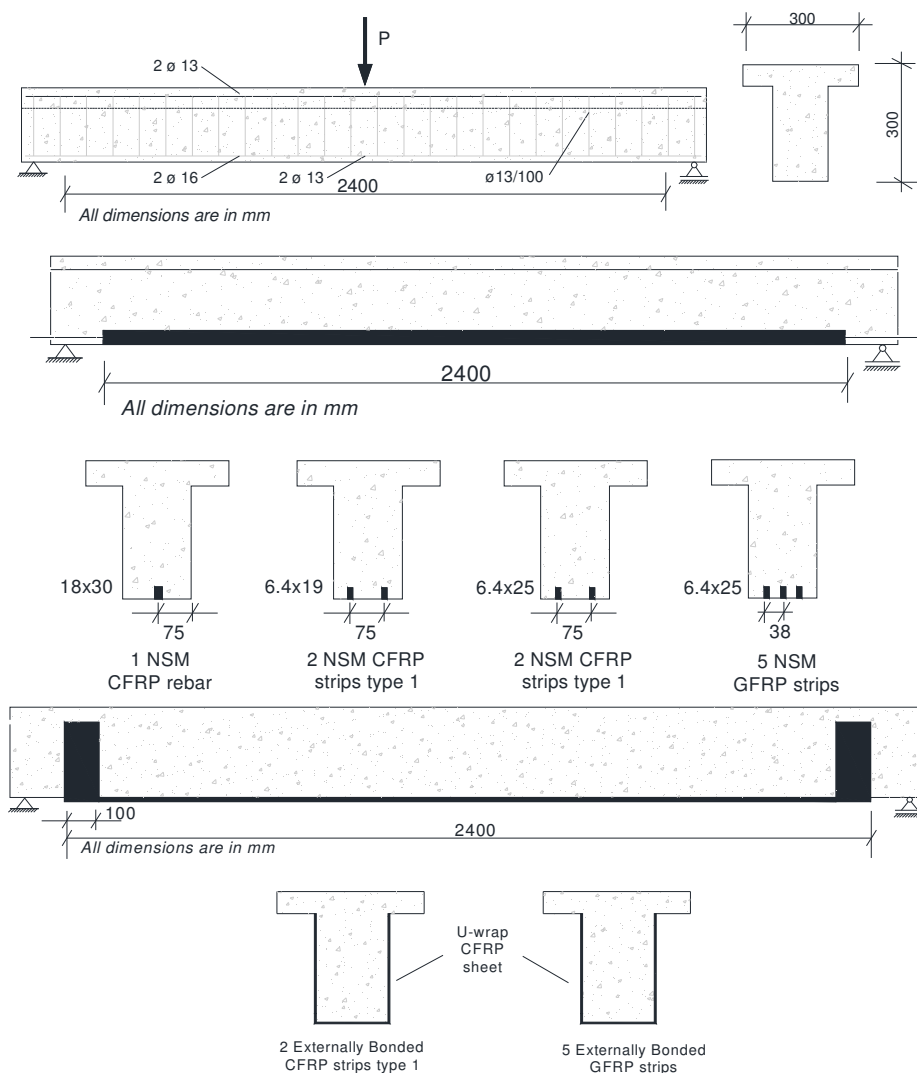
Figure 2.5:   Test setup and beam details (El-Hacha and Rizkalla, 2004).

Barros and Fortes (2005)

NSM strengthening technique using CFRP strips was applied for doubling the load carrying capacity of concrete beams failing in bending. To assess the efficacy of this strengthening technique, eight beams, divided in four series, were tested under four point

loads. The beams had a cross section of 100 mm width, and an height that varied between 170 mm to 180 mm (small differences were obtained due to the process of casting), while the distance between supports was 1600 mm. The compressive steel reinforcement in all series was composed of 2ϕ8 mm. The steel reinforcement in tension has varies for each series: 2ϕ6 mm for S1, 3ϕ6 mm for S2, 2ϕ6 mm and 1ϕ8 mm for S3 and 3ϕ8 mm for S4. The percentage of stirrups was determined to ensure bending failure modes for all beams, and the number of the CFRP laminates applied in the beam of each series (each series is composed of two beams) was evaluated for doubling the ultimate load of the corresponding reference beam. The test setup and beams details are presented in Figure 2.6, while the main results obtained in the experimental program are presented in Table 2.7. Concerning to the materials used in the experimental program, a concrete with an average compressive strength of 46.1 MPa was used. CFRP laminate strips were provided in rolls and had a cross section of 9.59 ± 0.09 mm width x 1.45 ± 0.005 mm thickness. From the tests, a Young´s modulus of 158.8 ± 2.6 GPa, a tensile strength of 2739.5 ±85.7 MPa and an ultimate strain of 17.0 ± 0.4 were obtained. An epoxy adhesive was used to bond the CFRP laminates to the concrete. From the uniaxial tensile tests, a Young´s modulus of 5.0 GPa and a tensile strength of 16-22 MPa, respectively, were obtained.
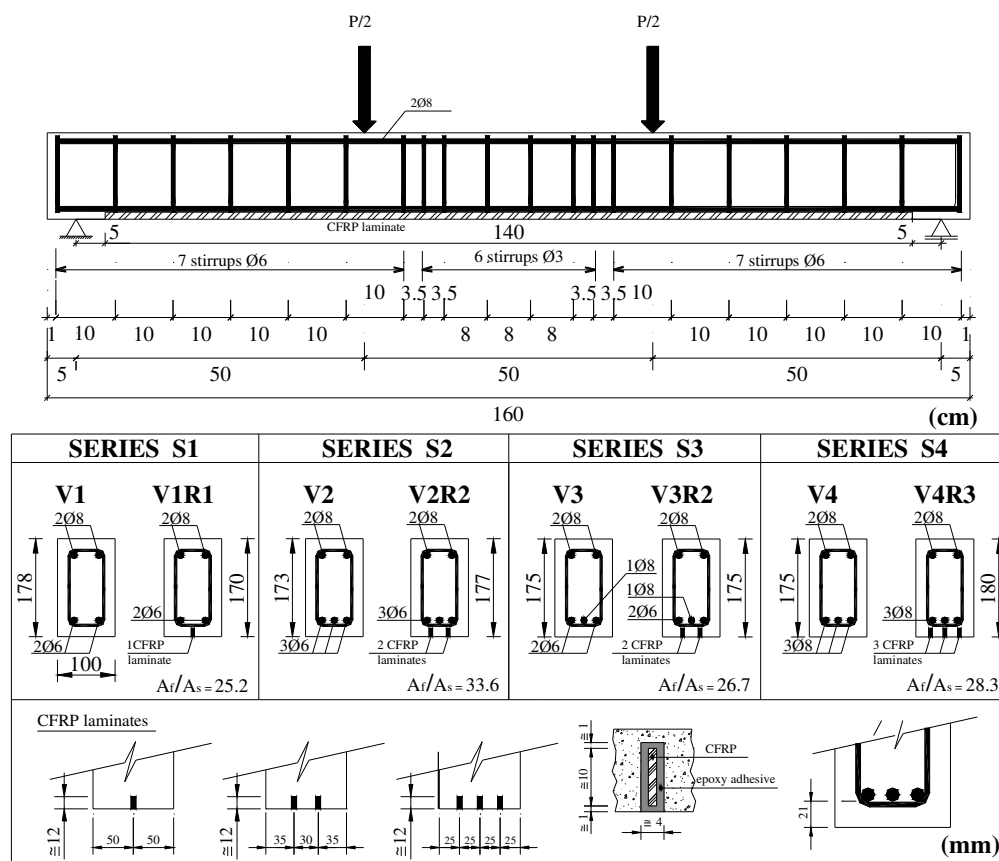
Figure 2.6:   Test setup and beam details (Barros and Fortes, 2005).

Table 2.7: Main results obtained in the experimental program.

Series	Beam ID	Cracking Load (kN)	Ultimate load (kN)	Maximum strains in CFRP laminates (‰)
S1	V1	8.5	28.2	-----
	V1R1	10.7	50.3	15.5
S2	V2	8.1	41.0	-----
	V2R2	12.3	78.5	12.8
S3	V3	7.9	41.3	-----
	V3R2	11.9	81.9	12.8
S4	V4	8.1	48.5	-----
	V4R3	14.1	94.9	10.6

According to the results, an average increase of 91% on the ultimate load of the tested RC beams was obtained when using the CFRP NSM technique. The deflection of the strengthened beams was similar to their corresponding reference beams. It was also observed that the proposed strengthening technique provided an average increase of 32% on the load corresponding to the deflection for the serviceability limit state (service load), 39% on the load corresponding to the yielding initiation of the longitudinal tensile steel bars, 28% on the stiffness for a load level corresponding to the service load of the strengthened beams, and 32% on the stiffness for a load level of 90% of the maximum load of the reference beams. The load corresponding to concrete cracking has also increased, but of minor significance. Finally, the maximum strains in the CFRP laminates ranged from 62% to 91% of its ultimate strain, indicating that this strengthening technique can mobilize stress levels in the CFRP reinforcing elements close to the tensile strength of this composite material.

Barros et al. (2007)

The efficacy of the NSM and EBR techniques for the flexural and shear strengthening of reinforced concrete beams were compared carrying out two experimental groups of tests. For the flexural strengthening, the influence of the longitudinal equivalent reinforcement ratio on the strengthening effectiveness of both techniques is assessed. The equivalent reinforcement ration is the addition of the steel and CFRP reinforcement ratio, by converting CFRP for an equivalent steel reinforcement. For the NSM technique the influence of the distance between two adjacent slits is also analysed. The experimental program was composed by twenty four beams with two beams for each reinforcement configuration. The dimensions of the beams were 120x170x1000 mm^3, with longitudinal steel reinforcement composed of 2ϕ 6.5 mm at the top face of all series and 2ϕ 5mm, 2ϕ6.5

mm and 3ϕ6.5 mm at bottom face of series S1, S2 and S3, respectively, with steel stirrups of ϕ6 mm at a spacing of 80 mm (Figure 2.7). Concerning to the materials used in the experimental program, a concrete with an average compressive strength of 44.2 MPa was used in the flexural strengthening program. Additionally, two distinct concretes an average compressive strength of 37.6 MPa and 49.5 MPa were used in shear strengthening program for the A and B series, respectively. CFRP sheets with Young´s modulus of 240 GPa and 390 GPa and tensile strengths of 3700 MPa and 3000 MPa were used in the flexural and shear strengthening programs, respectively. CFRP laminates with Young´s modulus of 158.8 GPa and 166.0 GPa and tensile strengths of 2740 MPa and 2286 MPa were used in the flexural and shear strengthening programs, respectively.

For the flexural strengthening, the NSM technique was the most effective, but the difference between the efficacy of NSM and EBR techniques decreased with the increase of the longitudinal equivalent reinforcement ratio.
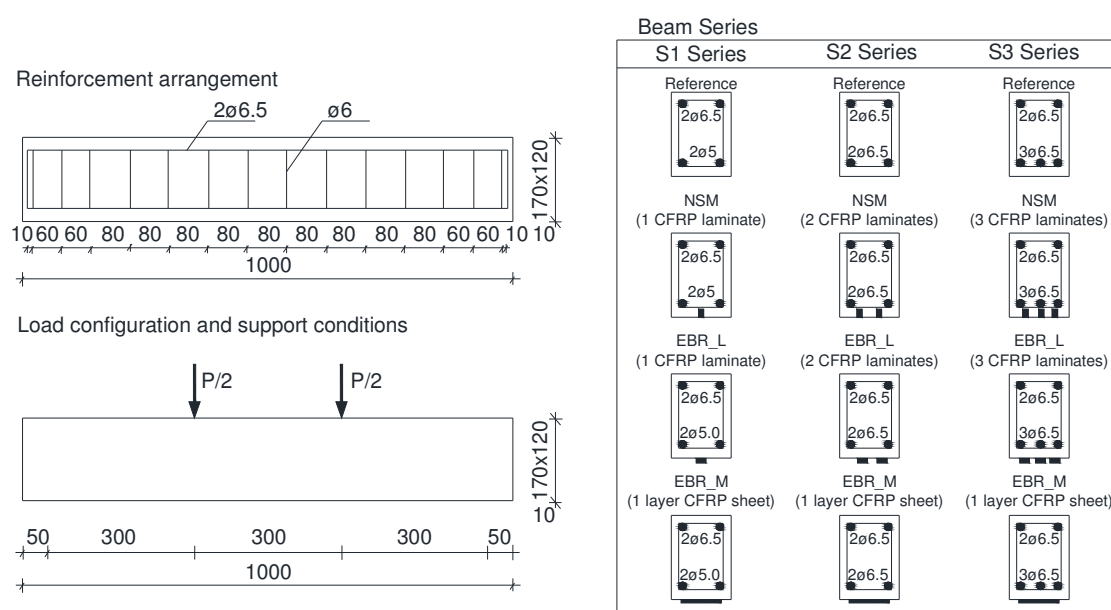
Figure 2.7: Beam series for the flexural strengthening (Barros et al., 2007) - dimension in mm.

Barros (2009)

An exploratory experimental program was carried out by Barros (2009) in order to evaluate the effectiveness of a new strengthening technique, based on applying NSM CFRP strips with a certain prestress level, to increase the flexural resistance of RC members (Figure 2.8). The preliminary experimental program was composed by three RC beams with dimensions of 120x200x2000 mm³. The longitudinal steel reinforcement is composed of 2ϕ12 mm, both in bottom and top surfaces. The shear reinforcement is composed of ϕ8 mm at a spacing of 100 mm. Concerning to the properties of the materials

used in this experimental program, an average compressive strength of 37.5 MPa, at 28 days, was obtained for the concrete of the beams. Steel bars of corrugated surface and with a characteristic yield stress of 500 MPa were used. An adhesive of fast curing was select and presented a tensile strength and Young´s modulus of 22.4 MPa and 2.78 GPa, respectively, at 24 hours.
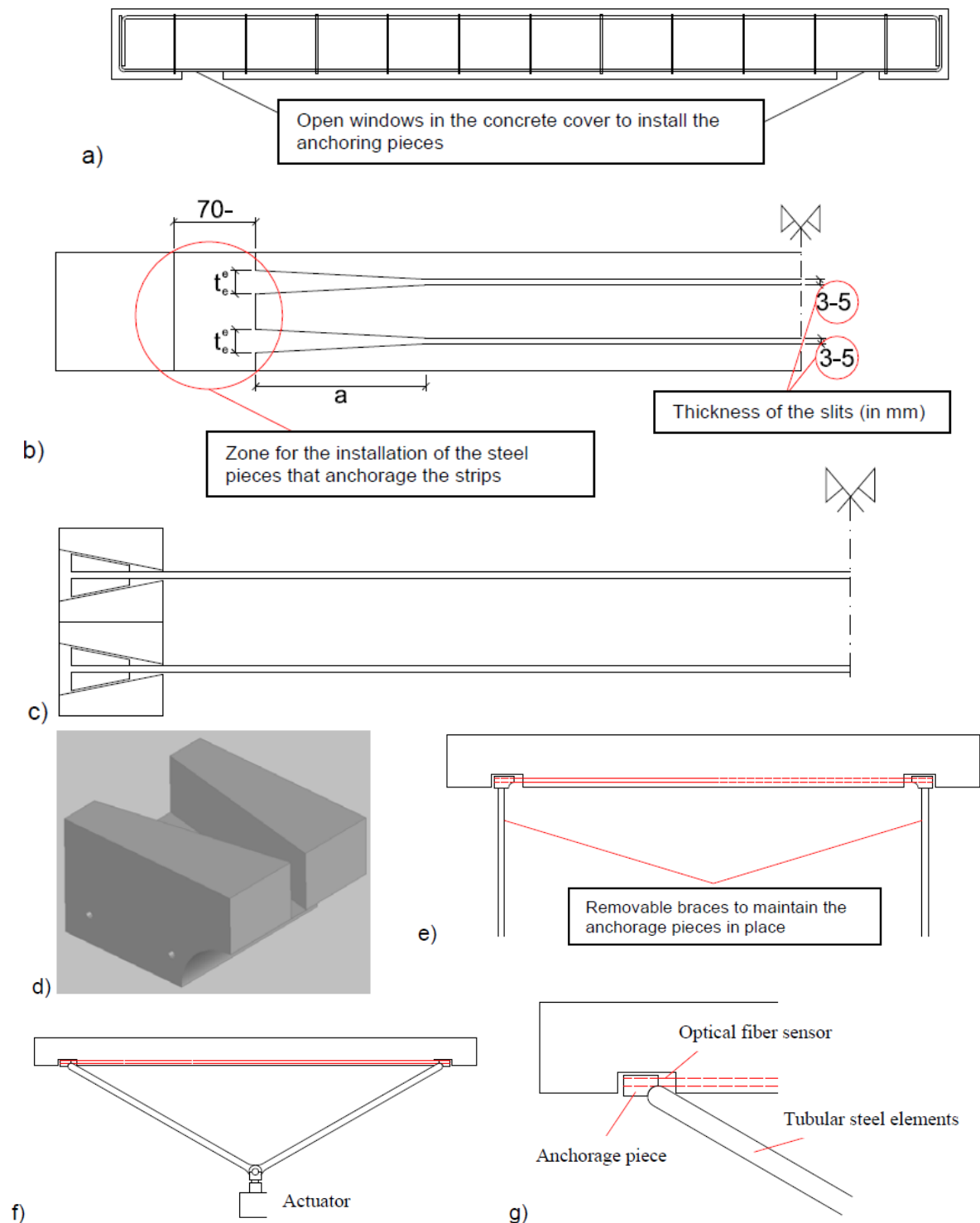
Figure 2.8: (a-g) Pre-stress technique for NSM CFRP strips (Barros, 2009).

The VLP and VRC20 beams, besides these steel reinforcements, were also strengthened with a CFRP strip of 10×1.2 mm^2 cross section, placed at the middle of the tensile bottom surface of the beams. In VLP beam the strip was applied without any pre-stress level (passive strip), while in VRC20 beam a pre-stress level of 20% of the tensile strength of the strip was applied. Main results of the experimental program are presented in Table 2.8.

Table 2.8: Main results obtained in the experimental program.

Beam ID	Cracking Load (kN)	Maximum load (kN)	Deflection at the maximum load (mm)
V00	10.07	54.72	30.475
VLP	11.50	76.72	19.859
VRC20	13.72	81.80	28.804

From the obtained results it can be concluded that a pre-stress level of 20% of the CFRP strip tensile strength provided an increment in terms of cracking load and maximum load of about 36% and 50%, respectively (taking the corresponding values of the V00 reference beam). If comparison is restricted to the maximum load of the VLP beam (strengthened with a passive strip), the pre-stress level only provided an increase of about 7%. However, the increment of load carrying capacity up to a midspan deflection corresponding to the verification of the serviceability limit states (SLS, L/400=4.5 mm) provided by the pre-stress level of 20%, exceeded 100% (VRC20 beam), while in VLP beam (with passive laminate) this increment was limited to 25%. It is also notable that for a deflection almost the double the corresponding deflection for SLS, the load increment provided by the pre-stress technique was about 60%, while in the VLP beam this increase was 25%. In conclusion, the proposed technique seems to be very effective.

El-Hacha and Gaafar (2011)

An experimental investigation for the assessment of the effectiveness of the NSM pre-stress technique for the flexural strengthening of RC beams was carried out by El-Hacha and Gaafar (2011). The effect of varying the prestressing level from 0% to 60% of the ultimate strength of the used CFRP bars on the overall flexural behaviour of the beams was examined. Five reinforced concrete beams, with dimensions of 200x400x5000 mm^3, were constructed and tested up to failure under quasi static monotonic four-point loading. The reinforcement consisted of steel bars, 3 of 16 mm diameter at the bottom and 2 of 10 mm diameter at the top. The clear cover over the top and bottom reinforcement was 19 mm and

38 mm, respectively. Steel stirrups of ϕ10 mm were used, at a spacing of 200 mm along the shear span and at 300 mm in the constant-moment region (Figure 2.9).

The yield strength and modulus of elasticity were 500 MPa and 200 GPa, respectively, for the ϕ10mm reinforcing bars and 475 MPa and 200 GPa for the ϕ16mm reinforcing bars. The concrete had a specified 28 days compressive strength of 40 MPa. The CFRP bars had a nominal diameter of 9 mm and, from the tests, a tensile strength and modulus of elasticity of 2167 MPa and 130 GPa, respectively, were obtained. Concerning to the adhesive, according to the manufacturer's product guide specification, the tensile strength of the epoxy is 24.8 MPa and the modulus of elasticity is 4482 MPa, respectively.
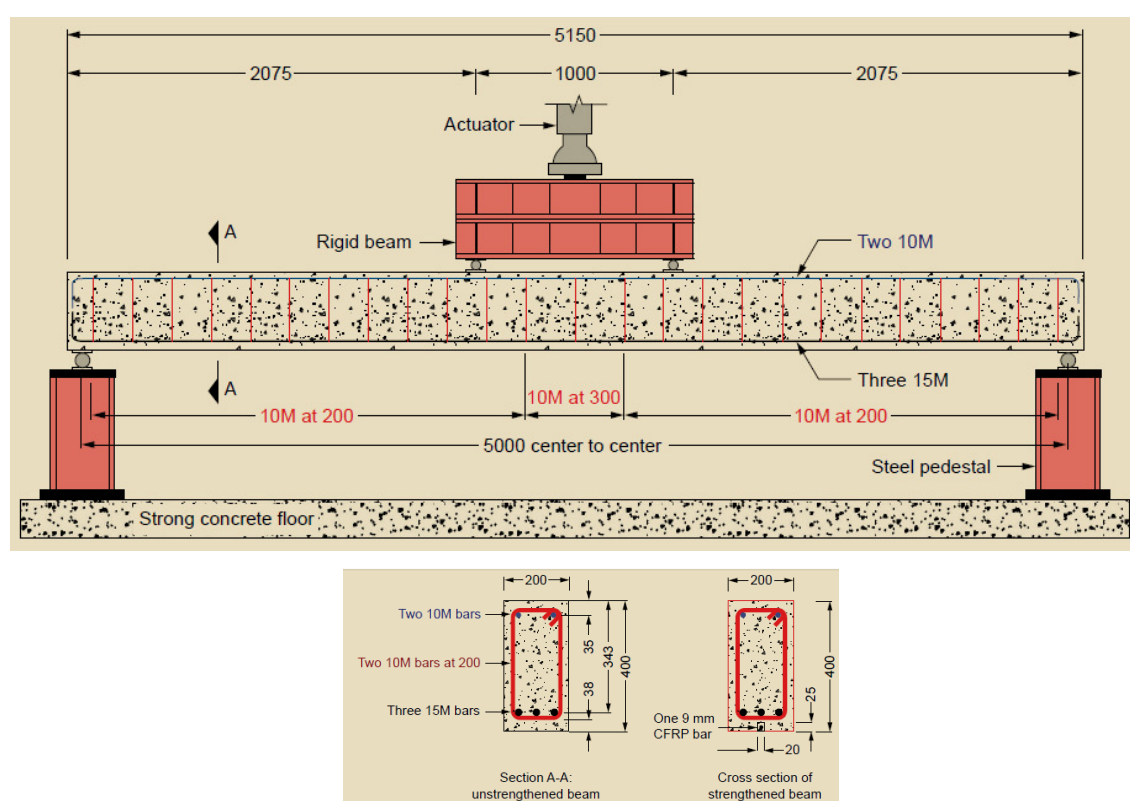
Figure 2.9: Test setup, elevation, cross-section, and reinforcement details (El-Hacha and Gaafar, 2011).
Note: All dimensions are in millimeters. CFRP = carbon-fiber-reinforced polymer.

According to the results obtained in the experimental program, the flexural strengthening of reinforced concrete beams using NSM CFRP bars has proved to be efficient. By inducing prestressing in the NSM CFRP bars the performance of the beams was significantly improved. When compared with the control unstrengthened beam, the prestressed beams presented for any load level smaller deflection and crack width. The prestress applied to the CFRP bars has delayed the formation of new cracks, and has increased the load at the crack initiation, at yielding initiation of the longitudinal steel bars,

and the ultimate load. All strengthened beams failed by rupture of the CFRP bar after yielding of the tension steel reinforcement, and no debonding or peeling of the CFRP bars was observed.

iv) Mechanically Fastened FRP (MF-FRP)

A new technique, called Mechanically Fastened FRP (MF-FRP), based on the use of steel fasteners applied along the laminate's length, has been proposed in alternative to EBR and NSM. One of the goals of this technique is the increase of the flexural capacity with little or no loss in ductility when used for the flexural strengthening of RC elements (Martin and Lamanna, 2008). This technique presents some benefits like quick installation with simple hand tools, no special labour skills are needed, no surface preparation is required, and the strengthened structure can be used immediately after installation of the FRP material. Nevertheless, some notable disadvantages of this system have been observed, including scale effects, cracking induced by the impact of fasteners in high-strength concrete, and less-effective stress transfer between the FRP and concrete due to the discrete attachment points (Ray et al., 2000).

Sena-Cruz et al. (2012)

Based on the MF-FRP technique, the Mechanically Fastened and Externally Bonded Reinforcement (MF-EBR) technique was proposed by Sena-Cruz et al. (2012). The strengthening steps of the MF-EBR technique is composed of the following steps: 1) a roughness concrete surface is made using a rotary hammer with a needle adapter; 2) the final surface is cleaned by compressed air; 3) holes are drilled in all the specimens with anchors. Later, compressed-air and a steel brush is used to clean the holes; 4) the holes in the laminates with anchors are performed with a current drill bit; 5) all the laminates are cleaned with a solvent (e.g. acetone); 6) the anchors are bonded to the concrete. This step is done according to the technical sheet of the supplier. To glue the laminate to the concrete, the epoxy adhesive is prepared according to the instructions of the technical sheet. A special care should be taken to assure a layer of adhesive of a thickness of about 1 to 2 mm; and 7) all remaining adhesive is removed (Sena-Cruz et al., 2010).

The experimental program was composed of two series of four beams each, being the distinction between the series associated to the loading configuration: one subjected to monotonic loading and the other to fatigue loading. Each series was composed of a reference beam (REF), and a beam for each investigated strengthening technique. The RC

beams had the dimensions of 200x300x2000 mm^3. All the beams had 3ϕ10 mm steel bars at the bottom and 2ϕ10 mm steel bars at the top as longitudinal reinforcement. The shear reinforcement was composed of steel stirrups of ϕ6 mm at a spacing of 100 mm (Figures 2.10 and 2.11). Concerning to the properties of the materials, the mechanical characterization of concrete was assessed by means of compression tests. From the compression tests, an average compressive strength and the modulus of elasticity of 53.08 MPa and 31.17 GPa were obtained, respectively.
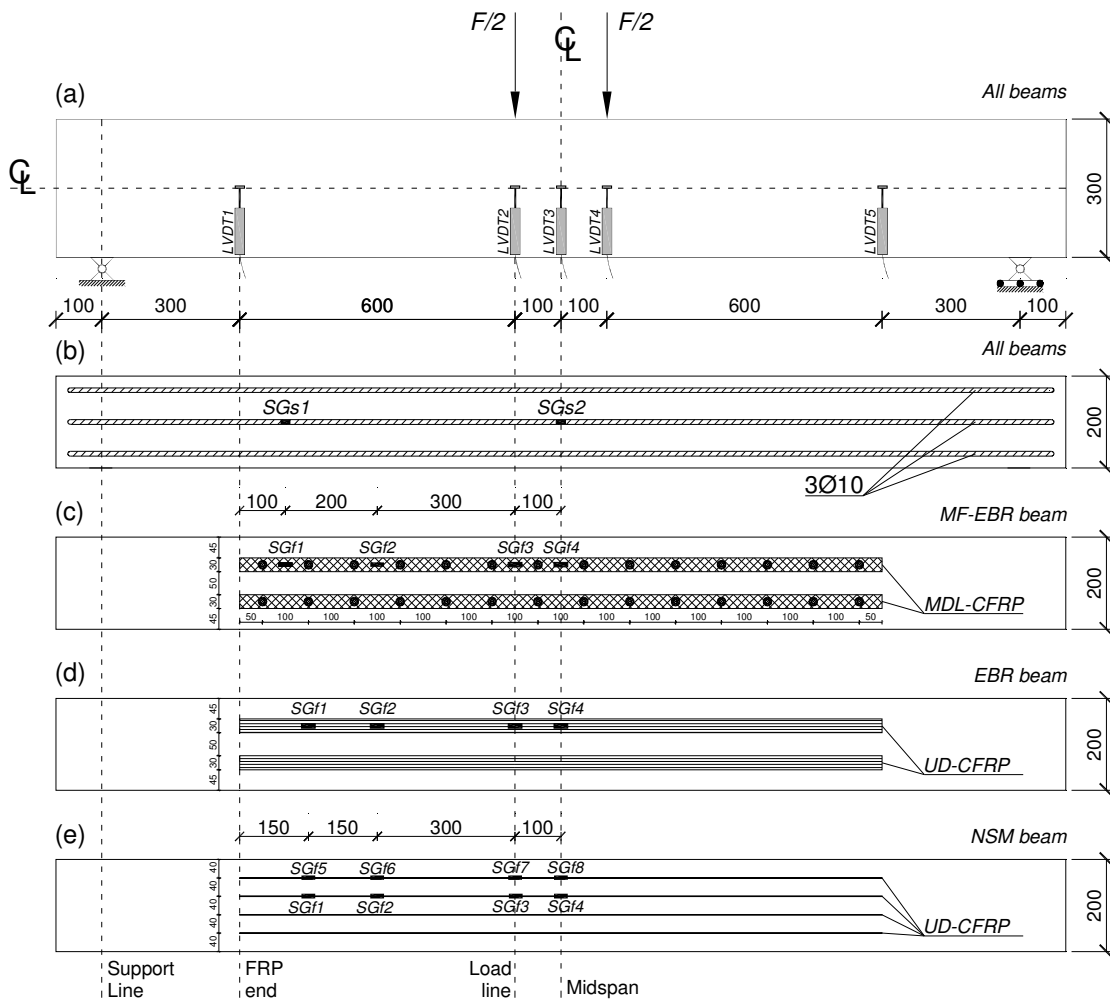
Figure 2.10: Dimensions, strengthening arrangements and instrumentation adopted: (a) vertical deflection; (b) strains on the steel bars; (c) strains on the laminate of the EBR beam; (d) strains on the laminate of the MF-EBR beam; (e) strains on the laminates of the NSM beam (Sena-Cruz et al., 2012).
All dimensions are in mm.
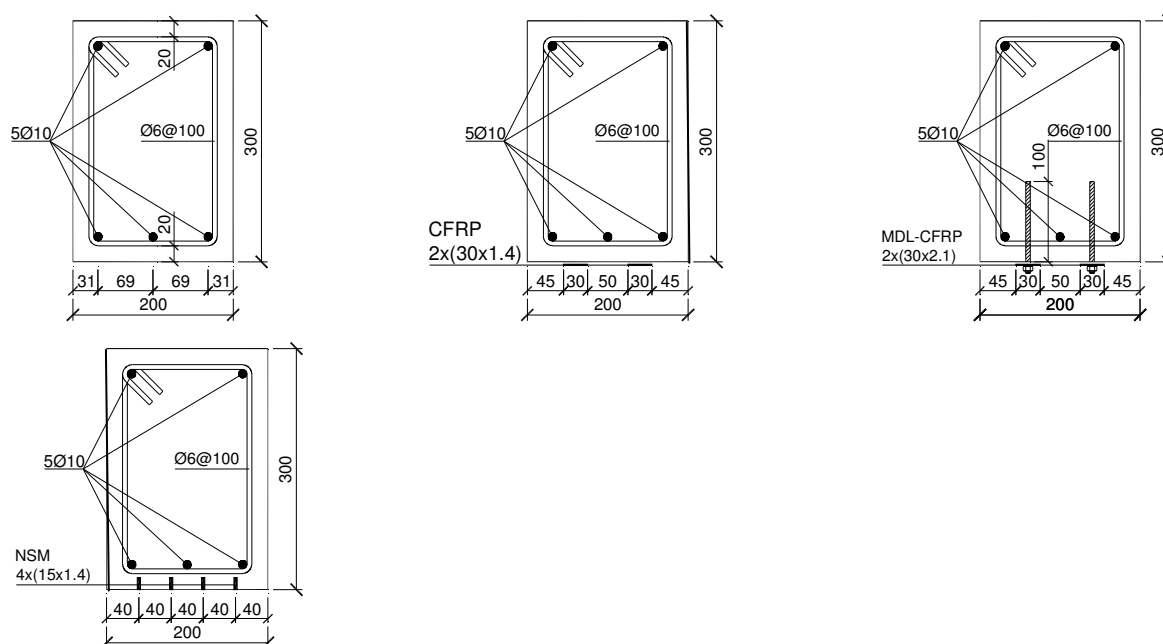
Figure 2.11: Cross section of the all beams: (a) REF; (b) EBR; (c) MF-EBR; (d) NSM (Sena-Cruz et al., 2012). All dimensions are in mm.

Two different types of CFRP laminates were used: unidirectional (UDCFRP) for the case of EBR and NSM techniques, and multidirectional (MDL-CFRP) for the case of the MF-EBR technique. From the experimental tests it was obtained a tensile strength, a modulus of elasticity and an ultimate strain of 1866 MPa, 118 GPa and 1.58 % for MDL-CFRP, and 2435 MPa, 158 GPa and 1.50 % for UD-CFRP, respectively. From the experimental tests, a bearing strength of 316.4 MPa and 604.4 MPa was obtained for the case of unclamped and clamped with a torque of 20 N×m, respectively. To bond the laminates to concrete the S&P Resin 220 epoxy adhesive was used. According to the supplier, this adhesive has a flexural tensile strength, a compressive strength and a bond concrete/laminate strength of 30 MPa, 90 MPa e 3 MPa, respectively. A Hilti chemical anchors system was adopted to fix mechanically the laminate to concrete for the case of the MF-EBR beam. The main results obtained in the experimental program are presented in Table 2.9.

From the results in the monotonic testes it was concluded that the most effective strengthening technique was the MF-EBR, since it provided the largest load, deflection at failure and strain level in the FRP at failure. When compared to the reference beam, an increase on the loading carrying capacity of 37%, 87% and 86% was obtained for the EBR, MF-EBR and NSM strengthened beams, respectively. When compared to the EBR beam, an increase of about 37% on the load carrying capacity was obtained for MF-EBR technique.

Table 2.9: Main results obtained in the tests.

Beam ID	Cracking initiation		Yielding		Ultimate		Failure mode
	Load (kN)	Deflection (mm)	Load (kN)	Deflection (mm)	Load (kN)	Deflection (mm)	
MONOTONIC							
REF	29	0.36	70	3.8	79.3	22.6	-----
EBR	25	0.27	90	4.1	108.4	7.4	Peeling
MF-EBR	32	0.38	96	4.2	148.2	18.3	Bearing
NSM	29	0.40	104	4.9	147.3	14.6	Rip-off
FATIGUE							
REF	20	0.26	66	2.5	79.9	23.3	-----
EBR	27	0.32	94	3.0	114.2	7.1	Peeling
MF-EBR	31	0.35	101	3.7	147.2	12.9	Bearing
NSM	N/A	N/A	105	3.3	160.7	22.2	Rip-off

The most favourable aspect of the MF-EBR technique is the more ductile failure mode. The prestressed anchors have contributed for this higher strengthening effectiveness of MF-EBR technique. The EBR FRP systems failed by FRP peeling, the NSM FRP systems failed by concrete cover rip-off (detachment of the concrete cover that includes the CFRP strips), and the MF-EBR FRP laminates failed by bearing.

In the fatigue tests, after having been subjected to 1 million cycles, the NSM beam has supported the highest ultimate load, corresponding to an increase of 101%, while the MF-EBR beams presented an increase of 84% and 43% in the load capacity, respectively, when compared with the maximum load of the reference beam. It should be noted that the presence of the anchors avoided the premature debonding (peeling) of the laminates, as well as the detachment of the concrete cover (rip-off).

2.1.2.2 Strengthening of columns

One of the earliest and the most common solutions for rehabilitation of concrete structures is to encase the existing column with additional layer of a material capable of increasing the axial and shear strength of columns. The following materials are the most used in the jacketing of columns: i) reinforced concrete, ii) steel and iii) composites of polymer matrix.

i) Reinforced concrete jacketing

A reinforced concrete jacket consists of a relatively thick layer of concrete cast around a column (Figure 2.12a). This new concrete layer is reinforced with longitudinal and transverse steel bars to increase the load carrying capacity and the ductility performance of

the column. Firstly, the cover concrete is removed to expose the main reinforcing bars. In addition, chipping away the concrete cover of the original member and roughening its surface can improve the bond between the old and new concrete. U-shaped steel links are then welded to the exposed bars to avoid the occurrence of separation of the additional RC layer from existing RC column. Additional bars are then welded to the U-shaped links to form the longitudinal reinforcement. Stirrups are added as required, and concrete is poured after the erection of the formwork (Monti, 2003).
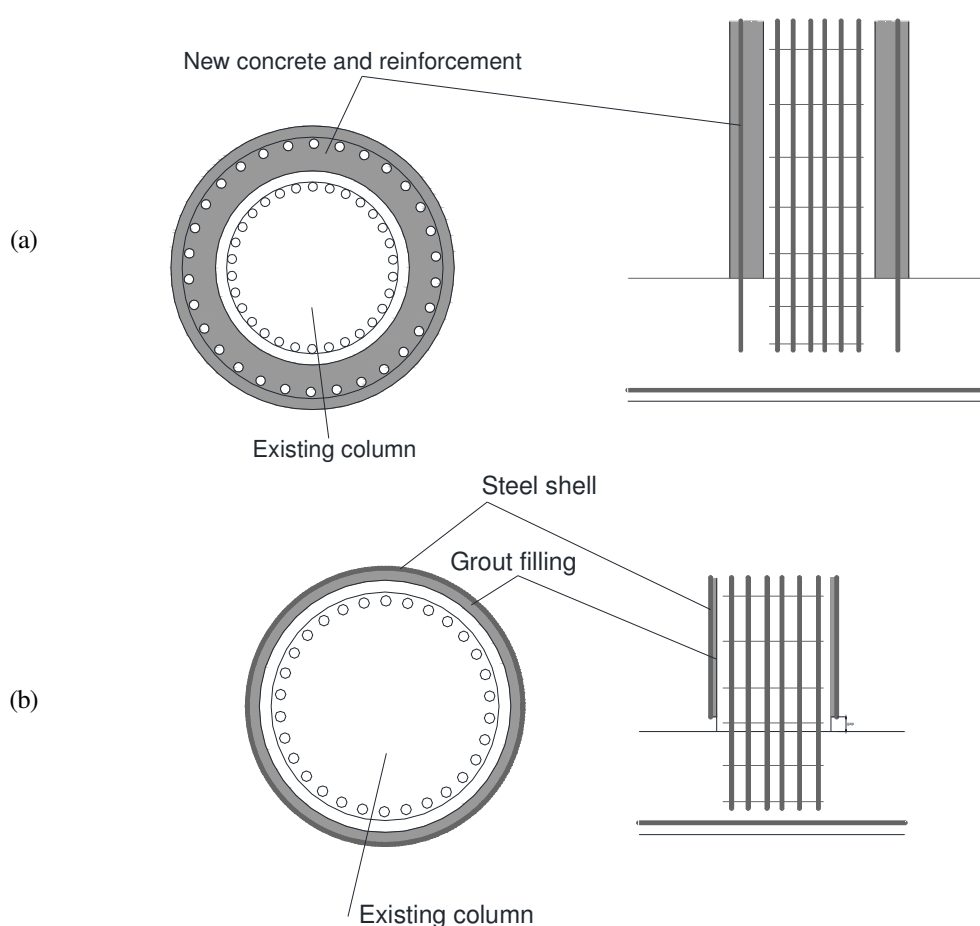
Figure 2.12: (a) Concrete jacketing and (b) Steel jacketing (encasing)
of a circular section column (Monti, 2003).

ii) Steel jacketing (caging and encasing)

In general, the techniques where either steel plate adhesion or steel welding in reinforced concrete is involved are relatively fast to execute and effective in terms of increasing the load carrying capacity and ductility performance of the RC column to strengthen. These favourable requisites turn this method appropriate for critical strengthening interventions such is the ones after the occurrence of a strong earthquake, particularly in special buildings such as hospitals and schools, and in bridges. An external steel cage is

constructed with longitudinal steel profiles connected with transversal steel strips, and the space between the steel cage and the existing concrete is usually filled with non-shrinkable mortars (Figure 2.12b). When required to provide corrosion or fire protection to the cage, a covering concrete layer can be added (Monti, 2003).

Wang et al. (2005)

Wang et al. (2005) carried out an experimental program by retrofitting rectangular RC columns with circular steel jackets. A total of ten specimens with and without circular steel-plate jacket were constructed and tested under lateral reversed cyclic loading with three different constant axial-stresses: 5.6 MPa (low axial-stress level), 13.2 MPa (medium axial-stress level), and 19.4 MPa (high axial-stress level).

The test specimens are approximately one third scale models of the actual existing R/C columns and their cross-sectional dimensions are 210 mm by 245 mm and presented eight bars of 10 mm diameter for the longitudinal reinforcement. Transverse (or hoop) reinforcement with 6 mm diameter bars applied at spacing of 130 mm was used. These specimens are divided into three major groups according to the applied axial-stresses (σ_o).

Three specimens (O-5.6, O-13.2, O-19.4) are the reference RC rectangular columns without any strengthening, and other seven specimens are retrofitted by the circular steel-plate with different thickness. The dimensions and the strengthening arrangement can be found in Figure 2.13. Details including size, shape, bar arrangement and the main resumes obtained in the experimental program of all the test specimens are presented in Table 2.10. According to the results, the seismic performances of three retrofit specimens with different steel-plate thickness are similar under the medium axial-stress of 13.2 MPa. In case of the high axial-stress of 19.4 MPa, the seismic performances were improved with the increase in the steel-plate thickness. Additionally, the difference in the ultimate lateral strengths between original specimens and retrofit specimens increased with the increase in the axial-stress.
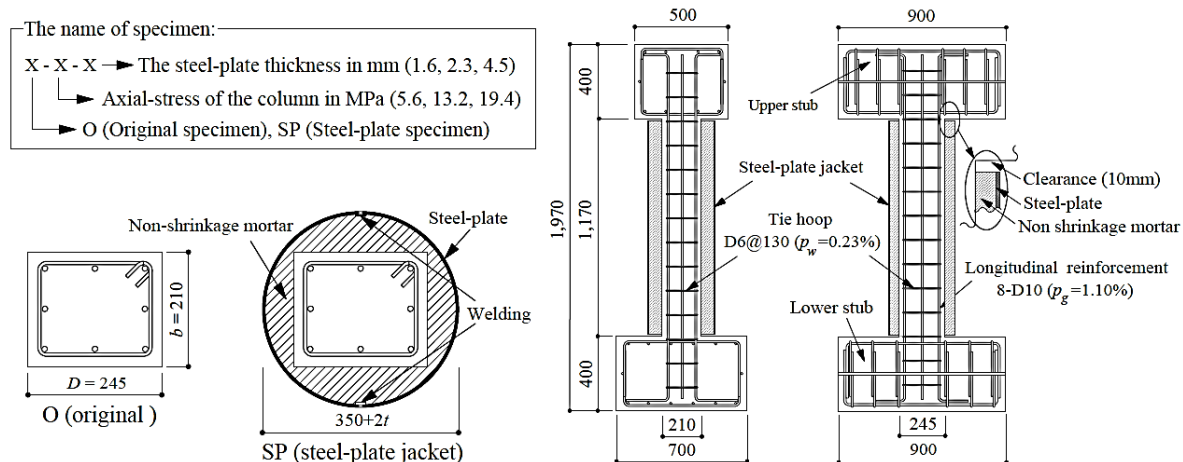
Figure 2.13: Details of test specimens (Wang et al., 2005).

Table 2.10: Main results obtained in the tests.

Specimens	Cross-section of column b×D (or d) (mm)	Steel-plate jacket thickness (mm)	Average concrete strength (MPa)	σ_o (MPa)	Experimental Value M (Kn.m)
O-5.6	210×245	-----	21.0	5.6	47.2
SP-5.6-1.6	φ350	1.6	21.5		54.3
O-13.2	210×245	-----	22.3	13.2	64.6
SP-13.2-1.6	φ350	1.6	19.5		83.9
SP-13.2-2.3		2.3	19.5		82.6
SP-13.2-4.5		4.5	20.1		84.1
O-19.4	210×245	-----	25.6	19.4	54.2
SP-19.4-1.6	φ350	1.6	20.8		94.8
SP-19.4-2.3		2.3	20.8		104.9
SP-19.4-4.5		4.5	22.9		103.8
b: breadth of R/C rectangular columns; D: depth of RC rectangular columns; d : column diameter in circular jacket part; t : thickness of steel-plate.					

iii) Composite materials jackets

Recently, the strengthening techniques based on the use of fibre reinforced polymer (FRP) materials have been recognised as very effective to increase the load and deformational capacity of reinforced concrete members. The remarkable properties of FRP, such as high specific strength and stiffness, low thickness and weight, and immunity to corrosion, allow them to be applied in a construction site without serious difficulties (Monti, 2003).

An FRP jacket can consist of active or passive layers, or a combination of different FRP materials. Normally carbon fibres and/or glass fibres are used, but aramid-fibers like Kevlar or Twaron are also used, in combination with a resin matrix, usually epoxy. Wrapping RC columns with wet lay-up fibre reinforced polymer sheets, using discrete (strips in between the existent steel hoops) or continuous (full wrapping) confinement arrangements, has proven to be an effective strategy to increase the load carrying capacity, ultimate deformability and energy absorption capacity of RC columns. The increase in

terms of the energy that a RC column can dissipate before its collapse, due to the concrete confinement provided by FRP arrangements, is one of the main reasons justifying the appropriateness of these composite materials to retrofit RC columns of the built heritage located in zones of high seismic risk.

Barros et al. (2000)

With the purpose of analysing the performance of the NSM technique for the flexural strengthening of RC columns, Barros et al. (2000) carried out some tests, where each specimen is composed of a RC column connected in one extremity to a RC foundation. Six CFRP laminate strips were used to strengthen each column, three in each face submitted to tension. The laminates were installed into slits and bonded to the concrete substrata by using an epoxy adhesive, according to the NSM technique, whereas epoxy mortar was used to bond the CFRP laminates to the foundation. According to the results, the flexural strengthening efficiency provided by this technique was high, due to the fact that the strengthening capacity of the laminates was almost fully mobilized without have occurred their detachment and rip-off failure mode. As expected this flexural strengthening technique was not effective to enhance the energy dissipation capacity of RC columns.

Ferreira and Barros (2006)

To assess the efficacy of the CFRP-based partial wrapping technique, Ferreira and Barros (2006) performed and experimental program where RC columns were confined by distinct CFRP arrangements and tested under direct compression (Figure 2.14).

The concrete specimens were confined by discrete and continuous CFRP systems, where the discrete confinement system is composed by strips of CFRP wet lay-up sheets, while the continuous confinement system corresponds to full wrapping the concrete specimen. The experimental program was composed of series of tests of two concrete strength classes (f_{cm} of 15 and 32 MPa), two longitudinal steel reinforcement ratios (ρ_{sl} of 0.64% and 1%), two transversal steel reinforcement ratios (ρ_{st} of 0.24% and 0.29%) and two thicknesses for the CFRP sheets (t_f of 0.113 mm and 0.176 mm), in order to evaluate influence of these parameters on the confinement performance provided by the confinement arrangements analysed. In the partial wrapping systems, the distance and width of the CFRP strips were also parameters considered in the experimental program. The CFRP sheets used have the trade name of CF 120 S&P 240 and CF 130 S&P 240.

W [mm]	ID	s' [mm]	W [mm]	ID	W [mm]	ID	s' [mm]	W [mm]	ID
45	W45S5L3	75	600	W600S1L3	45	W45S6L3	55	600	W600S1L3
45	W45S5L5	75	600	W600S1L3	45	W45S6L5	55	600	W600S1L3
60	W60S5L3	60	600	W600S1L5	60	W60S6L3	40	600	W600S1L5
60	W60S5L5	60	600	W600S1L5	60	W60S6L5	40	600	W600S1L5
Concrete average compressive strength: 15 MPa					Concrete average compressive strength: 32 MPa				
Longitudinal bars: $\phi10$					Longitudinal bars: $\phi8$				

Type of CFRP sheet	CF120 S&P 240 (200 gm/m²)	Group of test series	C15S200ϕ10	Type of CFRP sheet	CF120 S&P 240 (200 gm/m²)	Group of test series	C32S200ϕ8
	CF130 S&P 240 (300 gm/m²)		C15S300ϕ10		CF130 S&P 240 (300 gm/m²)		C32S300ϕ8

According to the supplier, CF 120 and CF 130 sheets have a thickness of 0.117 mm and 0.176 mm, respectively, and have a tensile strength higher than 3700 MPa, and an elasticity modulus and an ultimate strain in the fibre direction of about 240 GPa and 15‰, respectively. According to the obtained results for the group with a compressive strength of 15 MPa, confined by CFRP sheets of 0.113 mm and 0.176 mm thickness, an increase in terms of ultimate load carrying capacity between 1.7 for ρ_f =0.13% to 4.8 for ρ_f =0.88% was obtained. The maximum strains in the CFRP fibre direction varied from 44% to 84% of the CFRP ultimate strain. For the group with average compressive strength of 32 MPa and confined by CFRP sheets of 0.113 mm and 0.176 mm thickness, an increase in terms of ultimate load carrying capacity between 1.37 for ρ_f =0.15% to 3.55 for ρ_f =0.88% was obtained. The maximum strains in the CFRP fibre direction varied from 27% to 58% of the CFRP ultimate strain. Thus, the load carrying capacity of the tested specimens has increased with the CFRP confinement ratio, ρ_f. The confinement effectiveness was more

pronounced in the specimens manufactured with the lower concrete strength class. In comparison to the full wrapping confinement system, the partial confinement arrangements are easier and faster to apply, and consume few CFRP and epoxy adhesive materials. Based on the experimental results obtained in these programs, Barros and Ferreira (2008) developed an analytical model for the prediction of the compressive stress-strain response of CFRP-confined RC columns.

2.1.3   Statically indeterminate beams and slabs

Most of the tests were carried out with NSM strengthened simply supported elements. Although many in situ RC strengthened elements are of continuous construction nature, there is a lack of experimental and theoretical studies in the behaviour of statically indeterminate RC members strengthened with FRP materials. In addition, most design guidelines have been developed for simply supported beams with external FRP laminates. A literature review was done for addressing the strengthening of continuous beams and slabs using FRP materials.

i) Externally Bonded Reinforcement (EBR) technique

The majority of research studies dedicated to the analysis of the behaviour of continuous elements reports the use of the EBR technique. A brief review of the available literature is presented in the following paragraphs.

Park and Oehlers (2000)

Park and Oehlers (2000) performed tests on continuous beams with externally bonded steel or FRP reinforcement over the sagging and hogging regions. The beams had the dimensions of 240x200x5000 mm^3, with longitudinal reinforcement of 4ϕ16 mm and steel stirrups of ϕ10 mm at a spacing of 80 mm. The dimensions of the specimens and strengthening configuration are presented in Figure 2.15. The material properties for the concrete, reinforcing steel bars, adhesive plates and FRP plates are listed in Table 2.11. A concrete with an average compressive strength and the modulus of elasticity of 42.30 MPa and 34.84 GPa were obtained, respectively. The main results obtained in the experimental program are presented in Table 2.12.

(a) elevation steel tension face plated beam

994   850   850   994

240

adhesively bonded 3 mm
thick plate throughout

100 120   1700   580   580   1700   120 100

(a)

200

Y16 bars

Y10 at
80 mm centres

20 mm cover
throughout

3 mm plate

240

50   100   50

(b) sagging region

50   100   50   3 mm plate

Y16 bars

Y10 at
80 mm centres

20 mm cover
throughout

240

200

(c) hogging region

(a) elevation steel side plated beam

adhesively bonded 3 mm
thick plate throughout

994   850   850   994

100 120   1700   580   580   1700   120 100

(b)

200

Y16 bars

Y10 at
80 mm centres

20 mm cover
throughout

3 mm plate

126

80

34

(b) sagging region

3 mm plate

Y16 bars

Y10 at
80 mm centres

20 mm cover
throughout

34

80

126

200

(c) hogging region

(a) elevation FRP tension face plated beam

994   850   850   994

240

adhesively bonded 1.2 mm
thick plate throughout

100 120   1700   580   580   1700   120 100

(c)

200

Y16 bars

Y10 at
80 mm centres

20 mm cover
throughout

1.2 mm plate

240

75   50   75

(b) sagging region

75   50   75   1.2 mm plate

Y16 bars

Y10 at
80 mm centres

20 mm cover
throughout

240

200

(c) hogging region

Figure 2.15 (Continued)

37

Figure 2.15: (a) steel tension face plated beam, (b) steel side plated beam, (c) FRP tension face plated beam, (d) FRP side plated beam and (e) adhesively bonded and bolted steel tension face plated beam (Park and Oehlers, 2000). Dimensions in mm.

Table 2.11: Mechanical properties.

Steel bars			Steel bars				FRP Plates	
Diameter (mm)	Average yield strength (MPa)	Average ultimate strength (MPa)	ID	Average yield strength (MPa)	Average ultimate strength (MPa)	Young´s modulus (GPa)	Young´s modulus (GPa)	Average ultimate strength (MPa)
10 (Stirrup)	495	554	SP1	272	396	197.32	168.39	3050
16 (Main bar)	459	572	SP2	320	467	196.68		

Table 2.12: Main obtained results in the tests.

Specimens	Plate material	Bonding technique	Yield strength and deflection			Maximum strength and deflection			Failure strength and deflection		
			My (kN.m)	Vy (kN)	δy (mm)	Mmax (kN.m)	Vmax (kN)	δmax (mm)	Mf (kN.m)	Vf (kN)	δf (mm)
CB1	-----	-----	36.155	51.801	10.71	43.161	56.543	50.36	41.018	54.200	98.75
PBS1	Steel	Adhesion	48.895	69.817	7.51	49.421	70.359	7.74	46.020	66.100	8.31
PBS2	Steel	Adhesion	50.870	75.783	10.33	60.679	84.428	23.65	49.989	66.220	45.85
PBS3	Steel	Adhesion and bolting	60.129	87.800	13.09	70.650	92.900	49.13	62.544	70.500	111.91
PBF1	FRP	Adhesion	44.847	59.700	10.39	45.567	66.284	11.57	45.480	59.000	13.60
PBF2	FRP	Adhesion	53.536	75.900	11.95	59.466	80.400	16.19	59.056	67.100	18.15
My, Vy and δy: Moment, shear and deflection at which ductile plateau or brittle failure commences.											

From the results in the monotonic testes it was concluded that the most effective strengthening technique was obtained in the specimens with steel adhesively bonded and bolted steel tension face plated beam since it provided the largest load and deflection at failure. When compared to the reference beam, an increase on the loading carrying capacity of 22%, 22%, 30%, 9% and 24% was obtained for the PBS1, PBS2, PBS3, PBF1 and PBF2 strengthened specimens, respectively, at failure.

El-Refaie et al. (2003)

An experimental program with continuous RC two-span beams strengthened in flexure with externally bonded CFRP sheets was carried by El-Refaie et al. (2003). Eleven beams of 150x250x8500 mm^3 dimensions were tested. Both the compressive and the tensile steel reinforcement are composed of longitudinal reinforcement of 2ϕ16 mm steel bars and stirrups of 6 mm diameter at a spacing of 100 mm (Figure 2.16). The beams were made with a 28 days compressive strength of 30 N/mm^2. Concerning to the adhesives, from the experimental tests it was obtained a tensile strength, a modulus of elasticity of 17 MPa and 5.0 GPa for the bonding adhesive, and 19 MPa and 9.8 GPa for the structural adhesive, respectively. Concerning to the CFRP materials, a tensile strength and a modulus of elasticity of 3900 MPa and 240 GPa for the CFRP sheets, and 2500 MPa and 150 GPa for the CFRP plates were obtained, respectively. Details of CFRP laminates used in the test specimens and main results obtained in the tests are presented in Table 2.13.

According to the results, an increase of the load carrying and moment capacities of 55% and 57%, respectively, were obtained. However, the ductility of the strengthened beams was smaller than the corresponding reference beams. The peeling of the concrete cover adjacent to the CFRP composites was the dominant mode of failure for all the tested strengthened beams.

Table 2.13: Details of CFRP laminates used in the test specimens and main results obtained in the tests.

Specimens	Type	Size of the CFRP laminates		Bonding adhesive used	Ultimate load (kN)	Failure mode
		Central support (Hogging)	Mid-spans (Sagging)			
E1	None	None	None	None	149.67	Flexural mode
E2	Plate	2500mm long x 100mm wide x 1.2mm thick	None	Epoxy structural adhesive	178.64	Peeling failure
E3	Plate	None	3500mm long x 100mm wide x 1.2mm thick	Epoxy structural adhesive	207.06	Peeling failure
E4	Plate	2500mm long x 100mm wide x 1.2mm thick	3500mm long x 100mm wide x 1.2mm thick	Epoxy structural adhesive	231.42	Peeling failure
E5	Sheet	6 layers of 0.702mm total thickness x 110mm wide x 2500 mm long	None	Epoxy bonding adhesive	174.58	Peeling failure
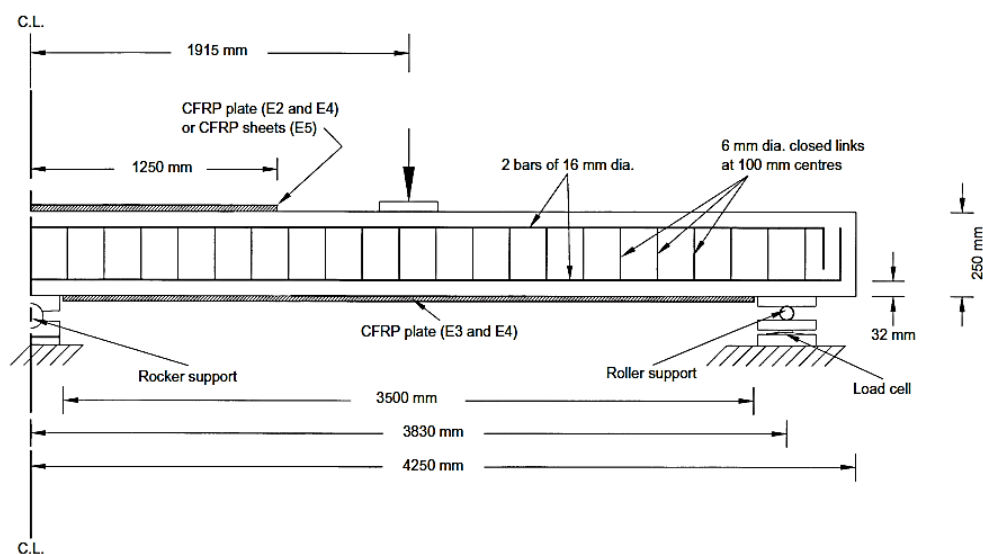
Figure 2.16: Details of CFRP laminates used in the test specimens (El-Refaie et al., 2003).

Ashour et al. (2004)

Sixteen RC continuous beams, classified into three groups (H, S and E) according to the arrangement of the internal steel reinforcement, were tested. Beams in group H were reinforced with 2ϕ8 mm steel bars on the top side of the beam and 2ϕ20 mm steel bars on the bottom side, whereas beams in group S were reinforced with an opposite arrangement of the internal longitudinal steel reinforcement. In the beams of group E the top and bottom steel reinforcement was equal and consisted of 2ϕ16 mm steel bars. Steel stirrups of 6 mm bar diameter at a spacing

of 100 mm were provided to prevent shear failure. The beams had the dimensions of 150x250x8500 mm^3 (Figure 2.17). Concerning to the strengthening materials, from the experimental tests it was obtained a tensile strength and a modulus of elasticity of 17 MPa and 5.0 GPa for the bonding adhesive, and 19 MPa and 9.8 GPa for the structural adhesive, respectively. Concerning to the CFRP materials, a tensile strength and a modulus of elasticity of 3900 MPa and 240 GPa for the CFRP sheets, and 2500 MPa and 150 GPa for the CFRP plates were obtained, respectively. Details of the strengthening arrangements and main results of the experimental program are presented in Table 2.14.
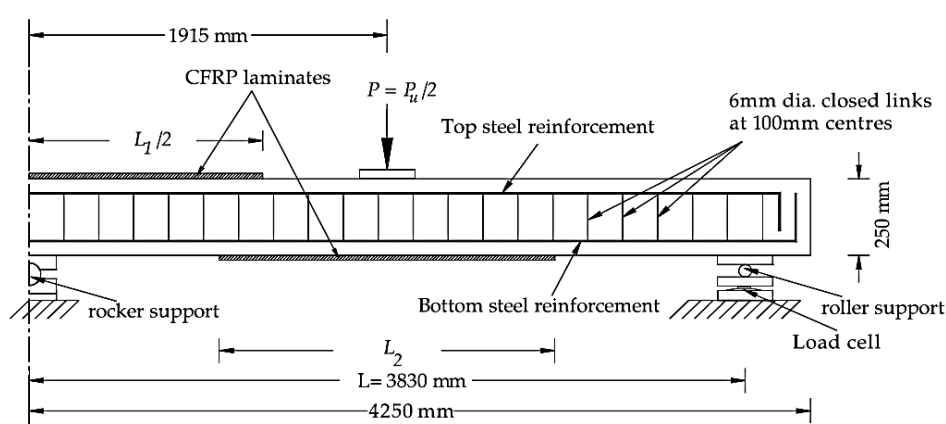
Figure 2.17: Details of CFRP laminates used in the test specimens (Ashour et al., 2004).

According to the results, all strengthened beams exhibited a higher beam load capacity but lower ductility compared with their respective unstrengthened control beams. The maximum increase in the load carrying capacity for the H, S and E series are 25%, 104% and 55%, respectively. For a specified length of CFRP sheets, there was an optimum number of CFRP layers above which the beam load capacity was not improved (beams H3 and H4 in group H and beams S2 and S3 in group S). Increasing the length of the CFRP sheets was found to increase the load capacity of the strengthened beams as in the case of beams H3 and H5 in group H and beams S3 and S4 in group S. Three distinct failure modes were observed, namely laminate FRP rupture, FRP separation and peeling failure of the concrete cover attached to the composite FRP. The increase of the CFRP sheet length to cover the entire negative (Hogging, H) or positive (sagging, S) moment zones did not prevent peeling failure of the CFRP laminate and was found to be ineffective when tensile rupture of the CFRP sheets was the failure mode.

Table 2.14: Details of CFRP laminates used in the test specimens and main results.

Group	Specimens	Main longitudinal steel		Type	Size of the CFRP laminates		Concrete average compressive strength (MPa)	Ultimate load (kN)	Failure mode
		Top	Bottom		Central support (Hogging)	Mid-spans (Sagging)			
H	H1	2T8	2T20	-----	-----	------	24.0	138.0	1
	H2	2T8	2T20	CFRP sheets	2 x 2.00m	-----	43.5	152.3	2 followed by 1
	H3	2T8	2T20	CFRP sheets	6 x 2.00m	-----	33.0	172.9	3
	H4	2T8	2T20	CFRP sheets	10 x 2.00m	-----	33.2	162.6	3
	H5	2T8	2T20	CFRP sheets	6 x 1.00m	-----	46.0	162.6	3
	H6	2T8	2T20	CFRP sheets	2 x 3.00m	2 x 1.00m	44.0	172.9	2 followed by 3
S	S1	2T20	2T8	-----	-----	-----	26.0	83.6	1
	S2	2T20	2T8	CFRP sheets	-----	2 x 2.00m	42.9	121.8	4
	S3	2T20	2T8	CFRP sheets	-----	6 x 2.00m	33.3	121.8	3
	S4	2T20	2T8	CFRP sheets	-----	6 x 3.50m	42.8	170.5	3
	S5	2T20	2T8	CFRP sheets	-----	10 x 3.50m	24.4	111.7	4
E	E1	2T16	2T16	-----	-----	-----	24.0	149.7	1
	E2	2T16	2T16	CFRP plate	1 x 2.50m	-----	43.6	178.6	3
	E3	2T16	2T16	CFRP plate	-----	1 x 3.50m	47.8	207.0	3
	E4	2T16	2T16	CFRP plate	1 x 2.50m	1 x 3.50m	46.1	231.4	3
	E5	2T16	2T16	CFRP sheets	6 x 2.50m	-----	44.7	174.6	3

Failure modes: 1 - Ductile flexural failure due to yielding of the internal tensile steel reinforcement followed by concrete crushing at both the central support and midspan sections; 2 - Tensile rupture of the CFRP sheets; 3 - Peeling failure of the concrete cover along the steel reinforcement level adjacent to the external CFRP laminates; 4 - CFRP sheet separation without concrete attached; Deflection ductility index at failure ($\mu_\Delta = \Delta_u / \Delta_y$), where Δ_u is the mid-span deflection at beam ultimate load and Δ_y is the mid-span deflection at the lower yielding load of the tensile reinforcement over the central support or the beam mid-span.

Oehlers et al. (2004)

An experimental program composed of seven continuous beams of two spans strengthened by adhesively bonding FRP or metal plates only in the hogging region was carried out by Oehlers et al. (2004). The specific aim of these tests was to both demonstrate and measure moment redistribution in externally bonded plated flexural members and not to demonstrate the effectiveness of the strengthening method. The beams had the dimensions of 120x375x5000 mm^3 (Figure 2.18). The steel reinforcement applied in the hogging region was designed to ensure that the cross section flexural capacity firstly occurs at the

hogging region. Concerning to the properties of the materials, the, specimens SS1, SF1, SF2 and SF3 had a concrete cylinder compressive strength of 39 MPa and a concrete Young's modulus of 35 GPa. The remaining specimens had a cylinder compressive strength of 48 MPa and Young's modulus of 41 GPa. The yield strength of the Y12 reinforcing bars was 601 MPa and that of the Y16 bars was 540 MPa. The main results of the experimental program are presented in Table 2.15.
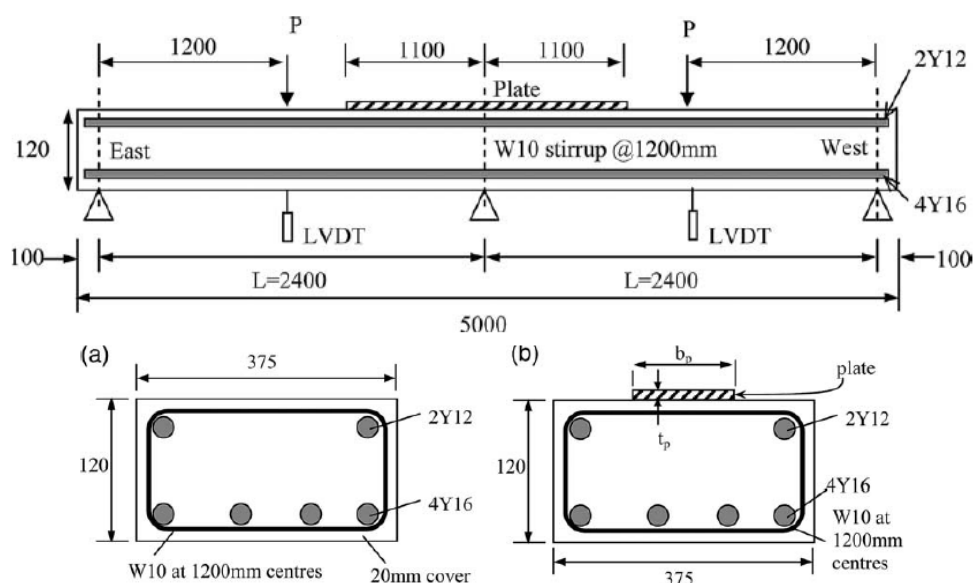
Figure 2.18: Two span continuous beam specimens and specimen cross-sectional details: (a) Sagging region; (b) hogging region (Oehlers et al., 2004) - dimensions in mm.

Table 2.15: Main results obtained in the experimental program.

Specimens ID	Plate material	Bonding technique	Plate Thickness (mm)	Plate Widths (mm)	Yield capacity of the plates (MPA)	Ultimate capacity of the plates (MPA)	Young's Modulus of the plates (GPa)	Moment redistribution percentage	
								At the maximum plate strain	At debonding
SS1	Steel	Adhesive	3	75	337	466	200	22	22
SS2	Steel	Adhesive	2	112	223	318	200	33	33
SS3	Steel	Adhesive	1	224	211	303	200	48	48
SF1	CFRP	Adhesive	2.4	25	-----	2800	144	30	35
SF2	CFRP	Adhesive	1.2	50	-----	2800	144	29	36
SF3	CFRP	Adhesive	1.2	80	-----	2800	144	28	28
SF4	CFRP	Wet lay-up (3 layers)	2.44	100	-----	350	43	35	44

Tests on seven plated beams have shown that substantial amounts of moment redistribution can occur. All the beams presented, at least, a moment redistribution capacity of 20% before plate debonding, and five beams had a moment redistribution level greater than the

upper limit of 30% recommended by international standards. For carbon FRP plated beams, this ranged from 28% to 35% and for steel plated beams from 22% to 48%. Hence plated beams have a scope for moment redistribution.

Grace et al. (2005)

Grace et al. (2005) performed an experimental program to analyse the effectiveness of a triaxially braided ductile FRP fabric for the flexural strengthening of continuous reinforced concrete beams. The experimental program was formed by three continuous beams with the dimensions of 152x254x4267 mm^3, where one of them is the reference beam and the other two beams were strengthened along their negative and positive moment regions around the top/bottom face on both sides as a U-wrap. The F-CT beam was strengthened with one layer of the triaxial ductile fabric, and the F-CTC beam was strengthened using two layers of carbon fibre sheet in order to compare their behavior with those strengthened with the new fabric (Figure 2.19). The longitudinal tensile reinforcement was formed by 2ϕ16 mm bars at top and bottom surfaces of the beam. To avoid shear failure, the beams were over reinforced for shear with steel stirrups of ϕ9.5 mm at a spacing of 102 mm. Concerning to the properties of the materials, the triaxial ductile fabric has a yield-equivalent load of 0.19 KN/mm and an initial modulus of 50 GPa, while the carbon fiber sheet has an ultimate load of 0.34 KN/mm. An epoxy resin was used to impregnate the fibers and to act as an adhesive between the strengthening material and the concrete surface. This epoxy has an ultimate tensile strength of 66.2 MPa with an ultimate strain of 4.4% and a compressive strength of 109.2 MPa. The compressive strength of the concrete at the time the beams were tested was 41.5 MPa. The steel reinforcement used had a yield stress of 490 MPa. Table 2.16 presents the main results obtained in the experimental program.

Table 2.16: Main results obtained in the experimental program.

Specimens ID	Strengthening squeme	Strengthening material	Positive moment strengthening		Negative moment strengthening		Failure load (kN)	Deflection at failure (mm)	Moment redistribution (%)
			Layers	Length (m)	Layers	Length (m)			
Control B	-----	-----	-----	-----	-----	-----	127	29.1	14.2
F-CT	U-wrap around tension face and sides	Triaxial ductile fabric	1	1.63	1	1.42	175	23.4	13.4
F-CTC		Carbon fiber sheet	2		2		185	16.1	6.5
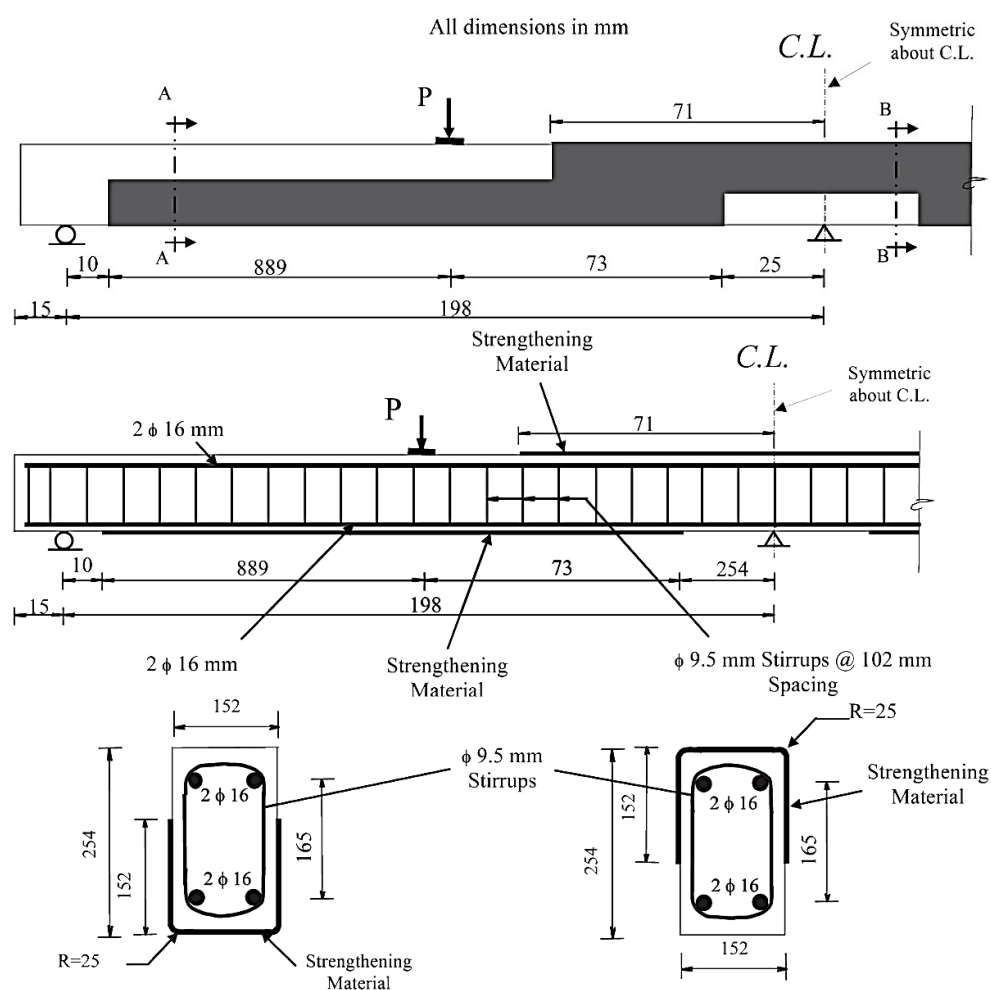
Figure 2.19: Beam specimens and specimen cross-sectional details (Grace et al., 2005).

According to the results, an increase of 37% and 46% were obtained when using the triaxial ductile fabric and carbon fibre sheets, respectively. However, the F-CTC beam had a moment redistribution ratio of 6.5%, which was significantly less than the one of F-CT beam (13.4%). Thus, the beam strengthened with the new fabric showed greater ductility than the one strengthened with carbon fibre sheet. The F-CT beam was characterized by the tensile rupture of the fabric over the central support followed by the rupture of the fabric at midspan. In case of F-CTC beam it failed suddenly by shear-tension failure at one end of the negative moment region, followed by debonding of the CFRP at the positive moment region.

Aiello et al. (2007)

Tests on six continuous RC beams, with and without strengthening, were carried out by Aiello et al. (2007). The internal flexural reinforcement consisted of 2ϕ12 mm steel bars at

both positive and negative moment regions. The shear reinforcement consisted of steel stirrups of 8 mm diameter at a spacing of 90 mm. The beams had different configurations of CFRP reinforcement: two beams were used as reference (unstrengthened) specimens; two beams were strengthened with one or two layers of EBR CFRP laminates applied in the sagging region; one layer of EBR CFRP laminates was applied in the hogging region of one specimen. Finally, one specimen was strengthened in both sagging and hogging regions by using EBR CFRP laminates (Figure 2.20).

The internal flexural steel reinforcement was designed to allow yield initiation of steel bars before the collapse of the beams. To prevent the premature failure due to delamination of the CFRP strengthening, a wrapping configuration was also applied. Table 2.17 presents the strengthening details and the main results obtained in the experimental program.
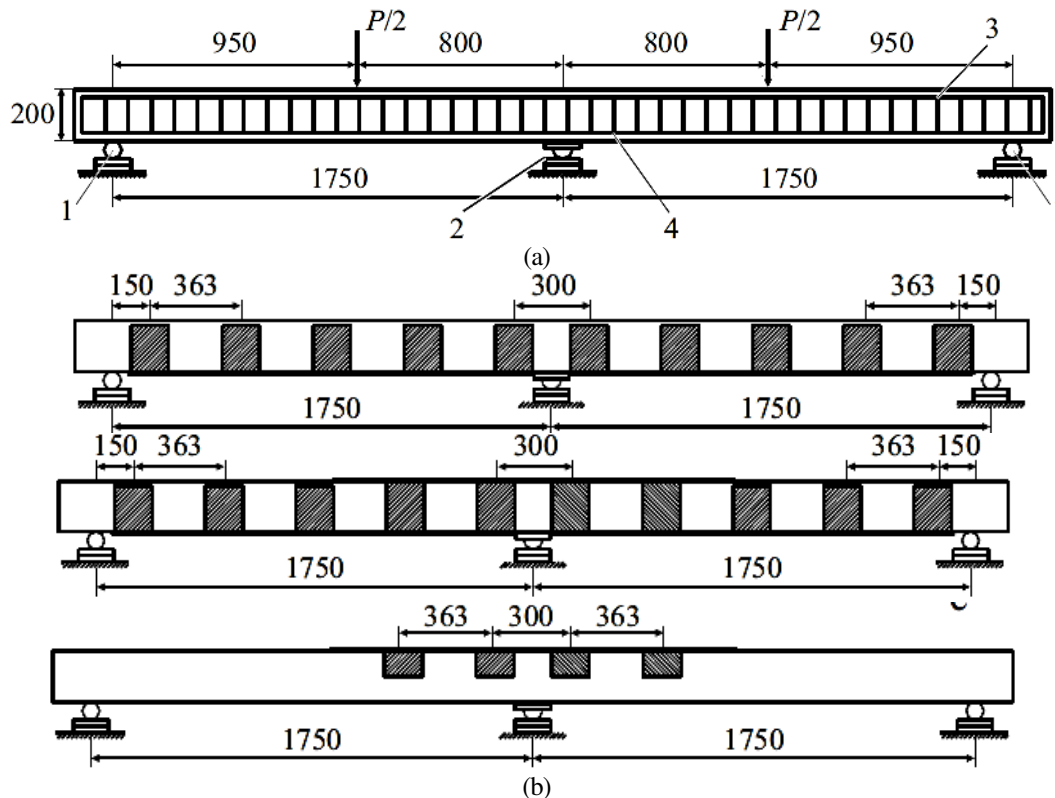
Figure 2.20: (a) Test setup (dimensions in mm). 1 - roller support; 2 - load cell; 3, 4 - top and bottom steel reinforcement, respectively, and (b) Details of strengthened beams S1-0 and S2-0 (a), S1-1 (b), and S0-1 (c). (Aiello et al., 2007) - Dimensions in mm.

Analysing the results, it can be noticed that an increase in the load carrying capacity and moment redistribution can be obtained if a proper strengthening configuration is applied. In fact, an about 32% and 20% of increase of the load carrying capacity and moment redistribution, respectively, were obtained when using EBR CFRP laminates in the sagging region. When CFRP sheets are only applied in the hogging region, a negative redistribution

of bending moments was obtained, with a maximum increase in the load carrying capacity of 4%. When the strengthening was applied in both hogging and sagging regions, the ultimate capacity of the beams was highest (36%) even if the percentage of moment redistribution was negligible. So, the experimental results obtained show that it is possible to achieve a sufficient degree of moment redistribution if the strengthening configuration is chosen properly. It should be noted that the failure of the strengthened beams occurred by detaching of the FRP sheets, together with concrete crushing.

Table 2.17: Strengthening details and main results obtained in the experimental program.

Specimens ID	Strengthening squeme	Number of CFRP sheets		Ultimate load (kN)	Moment redistribution (%)
		Sagging region	Hogging region		
C1	-----	-----	-----	149.09	0.07
C2				160.18	1.32
S1-0	Externally bonded CFRP laminate	1	0	203.96	10.50
S1-1		1	1	211.05	3.35
S2-0		2	0	197.95	22.14
S0-1		0	1	160.88	-13.87

Vasseur (2009)

Four RC beams with a cross section of a depth of 400 mm and a width of 200 mm and two-spans of 5000 mm were tested to verify the degree of moment redistribution when strengthened with FRP materials. The beams were loaded with one point load in each span. The beams had the same cross-section but different configurations of the internal and external reinforcement. The beam CB1 was reinforced with a small amount of internal reinforcement in the sagging region, where FRP EBR was applied, and a large amount at the hogging region. The beam CB2 had a large amount of internal reinforcement in the sagging region and a small amount at the hogging region, where FRP EBR was applied. The beam CB3 had almost the same amount of steel reinforcement in both sagging and hogging regions, and the FRPs were also applied in both sagging and hogging regions. Due to technical problems during the test of CB2, a new beam (CB4) of equal characteristics to CB2 beam was tested. The internal steel configuration of the beams and strengthening arrangements are presented in Figure 2.21. The properties of the materials are presented in Table 2.18, while the strengthening details and the results of the experimental program are presented in Table 2.19.
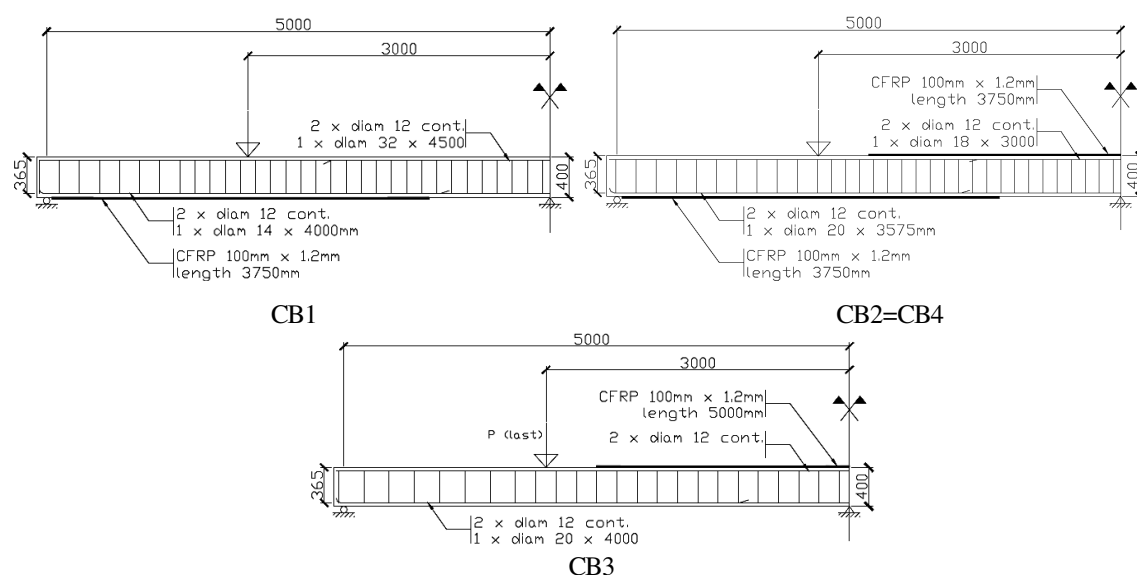
Figure 2.21: Internal steel configuration of the beams and strengthening arrangements (Vasseur, 2009).

Table 2.18: Mechanical properties of the materials.

	Steel						Concrete				CFRP	
	CB1		CB2		CB3		Properties	CB1	CB2	CB3	Properties	CB1/CB2/CB3
Properties	S	H	S	H	S	H						
Yielding strength (MPa)	601	530	570	570	589	589	Compressive strength (MPa)	38.0	36.0	35.5	Tensile strain (%)	2768
Tensile strength (MPa)	677	701	670	670	674	674	Tensile strain (%)	3.40	3.30	3.2	Failure strain (%)	1.46
Young´s modulus (GPa)	218	216	210	210	223	223	Young´s modulus (GPa)	35.50	32.0	32.0	Young´s modulus (GPa)	189.90
S: Sagging region, H: Hogging region												

Table 2.19: Strengthening details and main results obtained in the experimental program.

Specimens ID	Strengthening squeme	Ultimate load (kN)
CB1	EBR applied only in the spans	153
CB2	EBR applied in the spans and in the top of the beam above the mid-support	172
CB3	EBR applied only at the top of the beam above the mid-support	115

According to the results, the maximum increase was obtained when applying FRP materials in both sagging and hogging regions. In terms of moment redistribution, values of 32%, 28%, 13% and 23% were obtained. So, the experimental results show that it is possible to achieve a sufficient degree of moment redistribution if the strengthening configuration is chosen properly. Concerning to the failure modes, CB1 fails by debonding

of one the CFRP laminates in the span, CB2 and CB3 fails by the debonding of the top laminate above the mid support.

Akbarzadeh and Maghsoudi (2010)

Five RHSC continuous beams strengthened with CFRP and GFRP sheets, with the dimensions of 150X250x6000 mm^3, were tested by Akbarzadeh and Maghsoudi (2010) in order to assess the effectiveness of FRP type on the ductility and flexural strength of this type of beams. The beams were reinforced with 2ϕ16 mm steel bars at the top and bottom. Steel stirrups of ϕ10 mm diameter at a spacing of 100 mm were provided to avoid shear failure. The stirrups and reinforcement ratios are in accordance with the provision of American Concrete Institute. Thickness of CFRP sheets, strengthening configurations at both the hogging and sagging regions, and end anchorage technique were the main parameters investigated. Thickness and width of each layer of CFRP sheet were 0.11 mm and 145 mm. Thickness and width of each layer of GFRP sheet were 0.2 mm and 150 mm. The program is composed of an unstrengthened reference beam and four beams strengthened at both their negative and positive moment regions with different number of CFRP sheets. Additionally, an end anchorage system, which consisted of two or three layers of CFRP sheets of 150 mm width, was wrapped and bonded around the sides and the soffit of some strengthened beams near the end of longitudinal CFRP sheets (Figure 2.22). The average concrete strength was 77.6 MPa. Two bars of diameter 16 mm were tested in tensile and the measured yield strength was 412.5 MPa, and maximum tensile strength was 626.4 MPa. The modulus of elasticity of steel bars was 200 GPa. The Young's modulus and ultimate tensile stress of the CFRP and GFRP sheet and the properties of epoxies used for bonding the FRP sheets are presented in Table 2.20.

Table 2.20: Mechanical properties of the FRP sheets and the bonding adhesive.

FRP sheets				Bonding adhesive		
Material	Thickness (mm)	Ultimate tensile stress (MPa)	Young's Modulus (GPa)	Material	Tensile Strength (MPa)	Young's Modulus (MPa)
CFRP	0.11	3800	242	Epoxy resin adhesive	76.1	3600
GFRP	0.2	2250	73	Epoxy resin primer	>25	12800
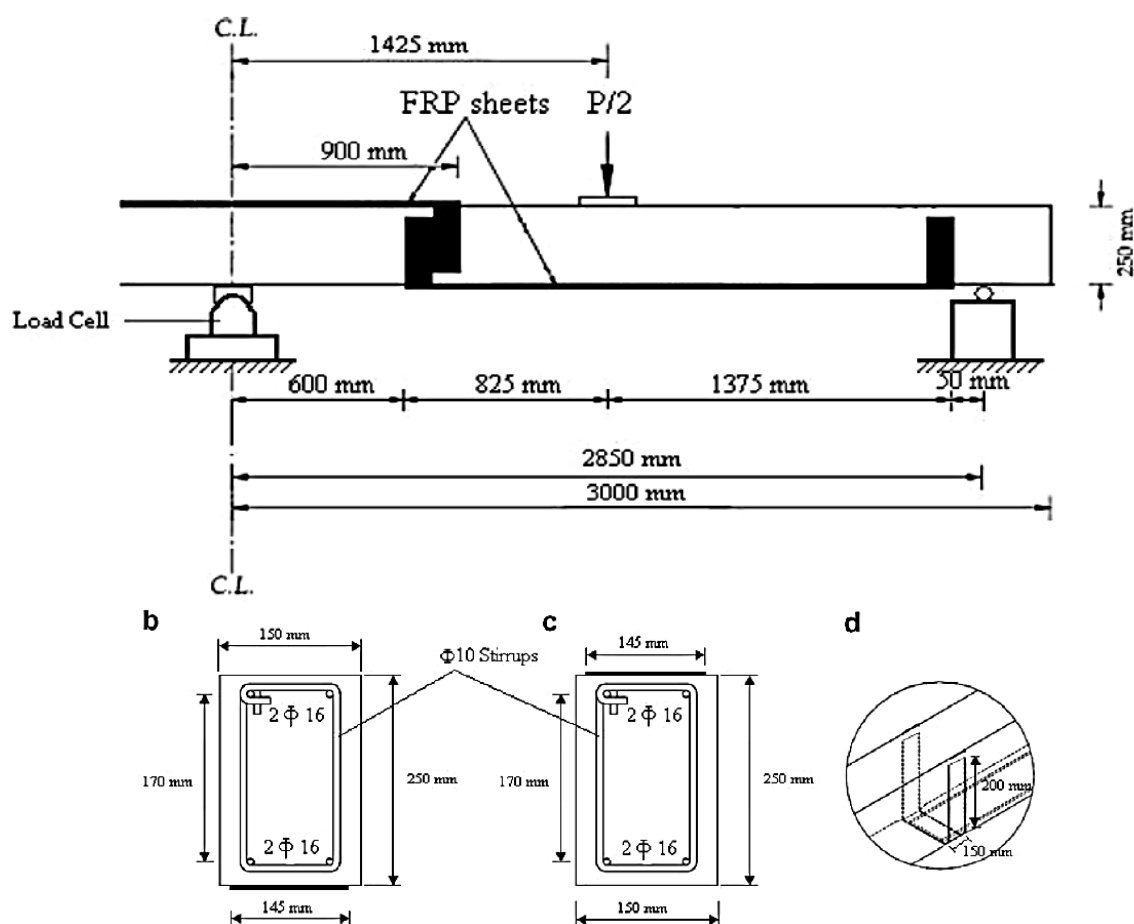
Figure 2.22: Test setup and strengthened RC continuous beam details: (a) longitudinal profile of beam, (b) typical cross section of beam in sagging region, (c) typical cross section of beam in hogging region and (d) end anchorage system (Akbarzadeh and Maghsoudi, 2010).

Table 2.21: Strengthening details and main results obtained in the experimental program.

Specimens ID	Concrete average compressive strength (MPa)	Type of FRP	Number of CFRP sheets		End anchorage	Ultimate load (kN)	Failure mode
			Sagging region	Hogging region			
Reference	74.2	-----	0	0	None	162.0	Flexural failure
SC1	74.6	CFRP	1	1	None	190.6	Rupture of top CFRP
SC2	74.1	CFRP	2	2	Yes	219.3	Debonding of the FRP sheet and rupture of end strap at hogging region
SC3	74.4	CFRP	3	3	Yes	259.3	Debonding at hogging region
SC4	79.7	GFRP	3	3	Yes	222.6	Debonding at hogging region

According to the results presented in Table 2.21, an increasing of the load carrying capacity was obtained when increasing the number of CFRP sheets, while ductility, moment redistribution, and maximum strain in the CFRP sheets have decreased. The

increase in the load carrying capacity obtained when using CFRP sheets has varied between 18% and 60%. However, when using GFRP sheets in strengthening the continuous beams an increase of 37% in the ultimate strength was achieved.

ii) Near-Surface Mounted (NSM) technique

Limited information is available in literature dealing with the behaviour of continuous structures (with redundant supports) strengthened according to the NSM technique. In this context, a brief review of the literature dealing with the flexural strengthening of statically indeterminate elements is presented in the following paragraphs.

Liu (2005); Liu et al. (2006)

An experimental program of nine RC continuous beams strengthened with NSM CFRP laminates and steel plates of various dimensions was carried out to determine the influence of these strengthening interventions on the ductility performance of statically indeterminate beams (Liu 2005; Liu et al 2006). The beams had the dimensions of 120x375x4800 mm^3 or 240x220x4800 mm^3 and were strengthened in the hogging region according to the NSM technique. The test program was divided into two series, NS and NB, where NS test series consists of six specimens with the slab shaped cross-section (Figure 2.23b) and NB test series consists of three specimens with the beam shaped cross-section (Figure 2.23c). All specimens were plated with CFRP or steel strips in the hogging region over interior support only. All beams in NS test series had stirrups with 10 mm diameter placed at a spacing of 1200 mm, while the specimens in the NB test series had stirrups with a diameter of 10 mm at a spacing of 70 mm. The strengthening arrangements are presented in Figure 2.23.

A concrete with an average compressive strength of 37.06 MPa and 34.99 MPa were used in the NS and NB series, respectively. Internal steel bars with an average tensile strength and young´s modulus of 575 MPa and 200 GPa, respectively, were used. Table 2.22 presents the properties of the NSM strips and Table 2.23 presents the strengthening details and main results obtained in the experimental program.
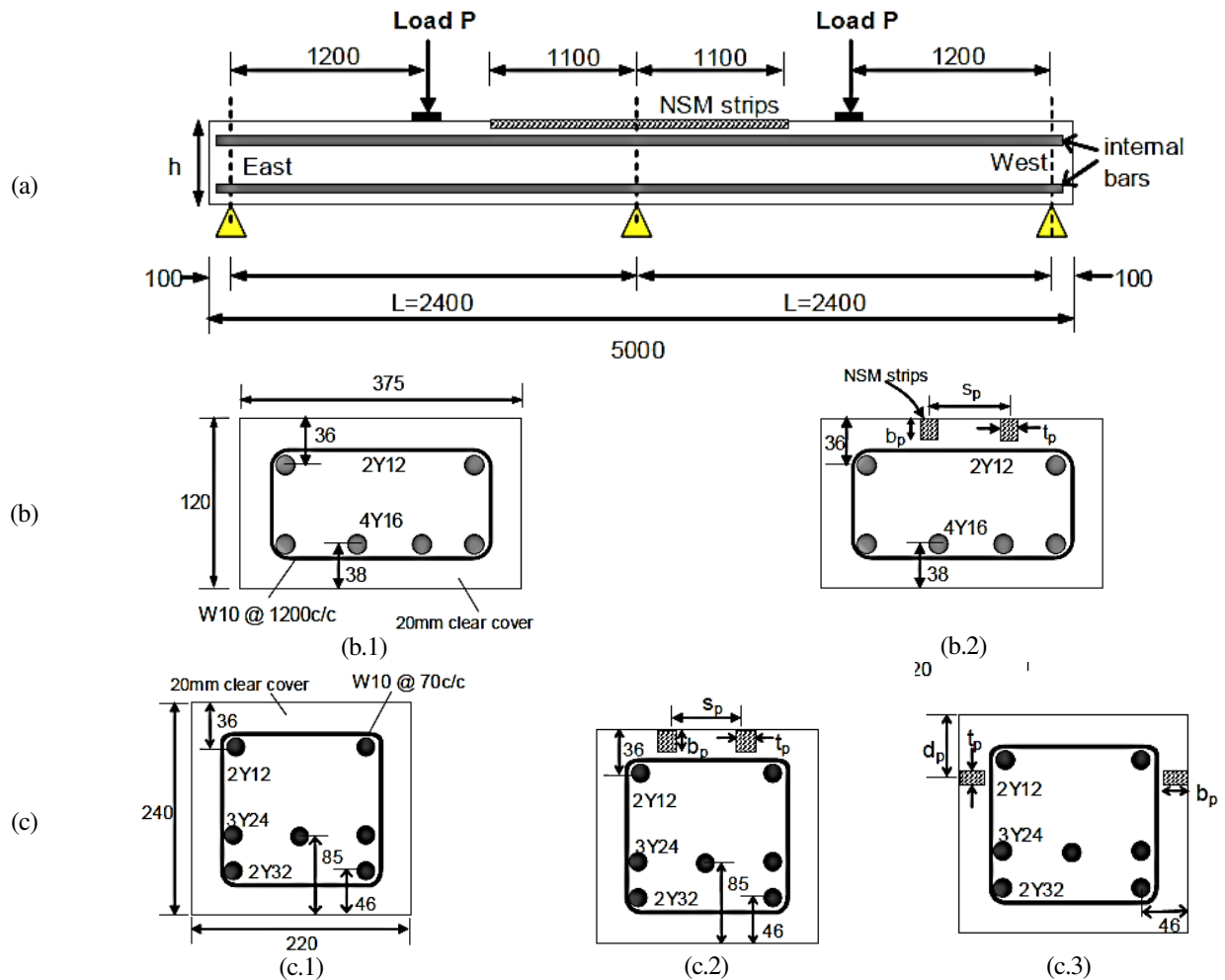
Figure 2.23: (a) Specimens, (b) cross-sectional details of the NS test series, where (b.1) is the sagging and (b.2) is the hogging region, (c) cross-sectional details of the NB test series, where (c.1) is the sagging, (c.2) is the hogging region for beams with tension face strips and (c.3) is the hogging region for beams with side face strips (Liu, 2005; Liu et al., 2006).

The results showed that the beams strengthened with NSM steel and NSM CFRP laminates achieved a moment redistribution percentage of 39% and 32%, respectively. Additionally, it was found that the debonding strains when using NSM technique were considerably larger than those associated with EB plates, which justifies the relatively high moment redistribution levels observed in the NSM strengthened beams.

Table 2.22: Properties of the NSM strips.

Material	Thickness (mm)	Yielding stress (MPa)	Ultimate tensile stress (MPa)	Young's Modulus (GPa)
Steel	0.89	837	933	182.94
Steel (double strip)	1.98	700	846	168.06
CFRP	1.23	-----	2796	173.50
CFRP (double strip)	2.80	-----	2331	140.14

Table 2.23: Strengthening details and main results obtained in the experimental program.

Specimens ID	Material	Number of CFRP sheets	Spacing (mm)	Thickness (mm)	Width (mm)	Ultimate load (kN)
NS_F1	CFRP	5	62	1.22	20.5	66.3
NS_F2	CFRP	2	125	1.24	15.5	63.0
NS_F3	CFRP	1	188	1.25	15.4	61.4
NS_F4	CFRP	2 (glued)	188	2.95	15.2	59.4
NS_S1	Steel	2	75	0.93	19.1	60.0
NS_F2	Steel	2 x 2 (glued)	125	2.05	19.1	60.0
NB_F1	CFRP	2	60	1.25	14.8	242.0
NB_F2	CFRP	2	73	1.24	1.2	244.0
NB_F3	Steel	2 x 2 (glued)	73	2.77	15.0	246.5

Bonaldo (2008)

An experimental program to analyse the moment redistribution capability of two-span continuous RC slab strips strengthened according to the NSM technique was carried by Bonaldo (2008). The experimental program was composed of three series of three slab strips of two equal span lengths, in order to verify the possibility of maintaining moment redistribution levels of 15%, 30% and 45% when the flexural resistance of the intermediate support region is increased in 25% and 50%. Though the flexural resistance of the NSM strengthened sections has exceeded the target values, the moment redistribution was relatively low, and the increase of the load carrying capacity of the strengthened slabs did not exceed 25%.

2.2 STATE-OF-THE-ART ON THE SHEAR STRENGTHENING

2.2.1 Introduction

Since the early 1990s, tests on a wide variety of shear strengthening schemes have been undertaken with the goal to increase shear capacity of reinforced concrete beams. Shear is actually a very complex problem and is not completely solved for simple reinforced-concrete (RC) beams. Due to its brittle nature and occurrence with no advance warning of distress, shear failure has been identified as the most disastrous failure mode for RC elements. Shear deficiency may occur due to many factors, such as: insufficient shear reinforcement; reduction in steel area due to corrosion; increased service load; and construction errors. In addition, there exist several RC structures of structural elements that do not have shear resistance in order to be in agreement with the requirements imposed by recent design guidelines.

There have been a number of studies on strengthening of RC beams in shear using different techniques. The several existing approaches often involves the use of strengthening materials fixed to the webs of the beams, such as concrete jacketing, external prestressing and steel plate bonding. Recently, experimental studies on shear strengthening of reinforced concrete beams with CFRP composites, according to the EBR (Externally Bonded Reinforcement) and Near-Surface Mounted (NSM), show that these techniques are good alternative of the traditional shear strengthening techniques. However, the EBR technique frequently fails by premature debonding of the external reinforcement, and EBR and NSM techniques have no applicability in the shear strengthening of RC slabs.

Concerning to the slabs, in general, the shear strengthening involves installing external shear reinforcement and/or collars in the slab-column connections to increase the critical shear perimeter, the use of steel bars introduced into inclined at 45-degree drilled holes and bonded with a grout adhesive (Hassanzadeh and Sundqvist 1998), bolts to act as shear reinforcement (El-Salakawy et al. 2003), and carbon fibre reinforced polymer stirrups (Binici, 2003). Figure 2.24 presents some of the shear strengthening methods.

This section provides a comprehensive review of some works related to reported experimental investigations on shear strengthening, and is divided in five parts:

i) Concrete jacketing;

ii) Externally bonded reinforcement (EBR) technique with FRP systems;

iii) Near-Surface Mounted (NSM) technique with FRP systems; and

iv) Embedded through-section (ETS) technique.

i) Concrete jacketing

One of the most commonly used rehabilitation techniques for poor detailed or damaged reinforced concrete (RC) members is the application of jackets around the structural elements. RC jacketing is a traditional and well-known upgrading technique to provide increased strength, stiffness, and overall enhancement of the structural performance. On this topic, five beams were constructed and subjected to monotonic loading in order to exhibit shear failure (Chalioris and Constantin, 2012). The damaged specimens were strengthened using reinforced jackets and retested by the same four-point bending loading.

(a)

SH-2SR

(a)

(b)

Specimen A4-1

Slab specimen

1 in.

Aramid cross fibers

Carbon fibers

d/2

Holes

Electrical Strain Gauges

2 CFRP Layers

Chamfered corners

r =1/2 in.

CFRP shear reinforcement leg

(c)
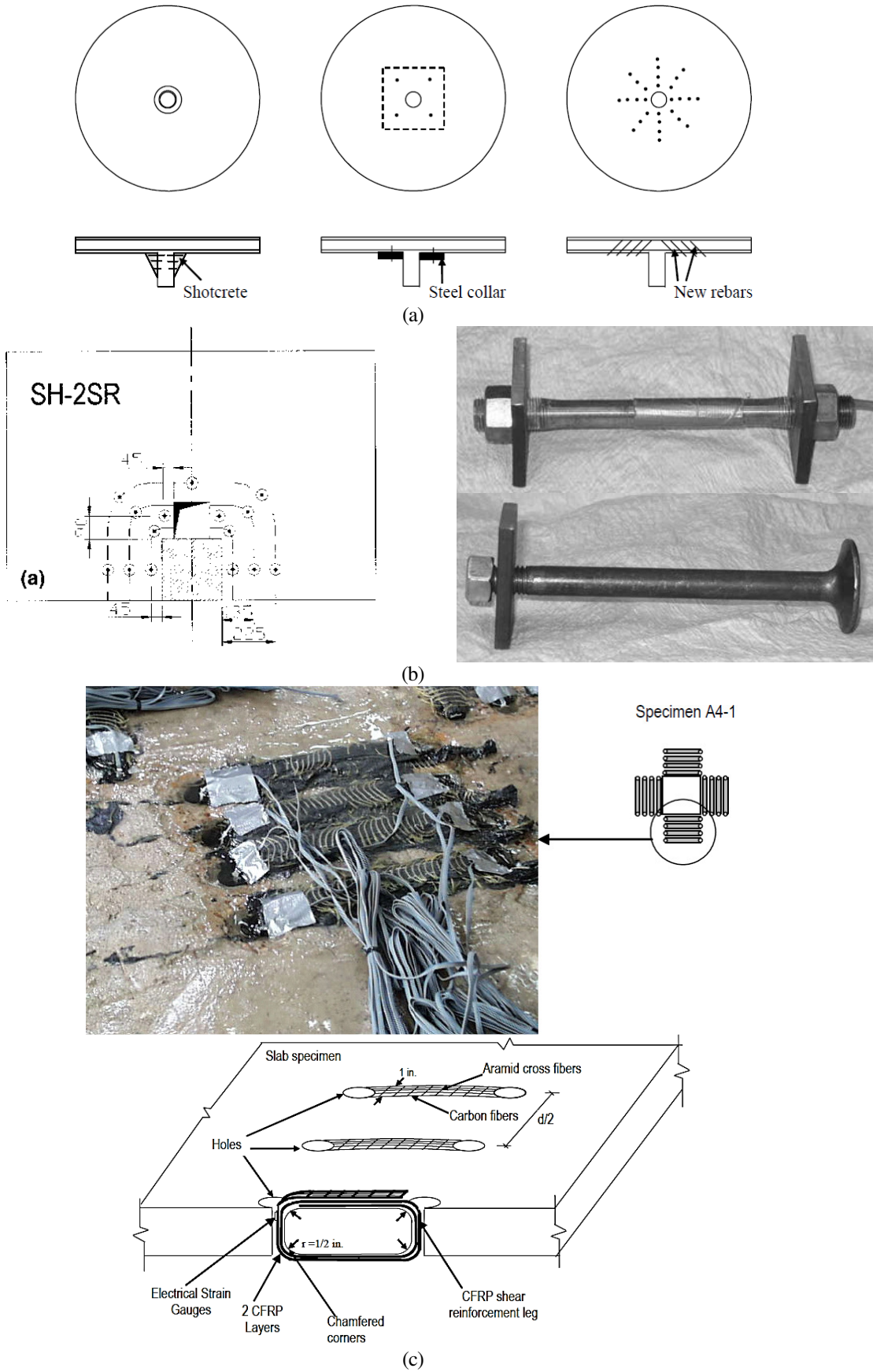
Figure 2.24: (a) Strengthening methods (Hassanzadeh and Sundqvist 1998 apud Binici, 2003), (b) Shear reinforcement: steel rods and shear bolts (El-Salakawy et al. 2003), and (c) application of CFRP Layers as Shear Reinforcement (Benici, 2003).

The self-compacting concrete jacket applied, encasing the bottom width and both vertical sides of the initially tested beams (U-formed jacketing), has a small thickness (25 mm) and includes small (Ø5 mm) steel bars and U-formed stirrups (see Figures 2.25 and 2.26). Table 2.24 presents the strengthening details and main results obtained in the experimental program.
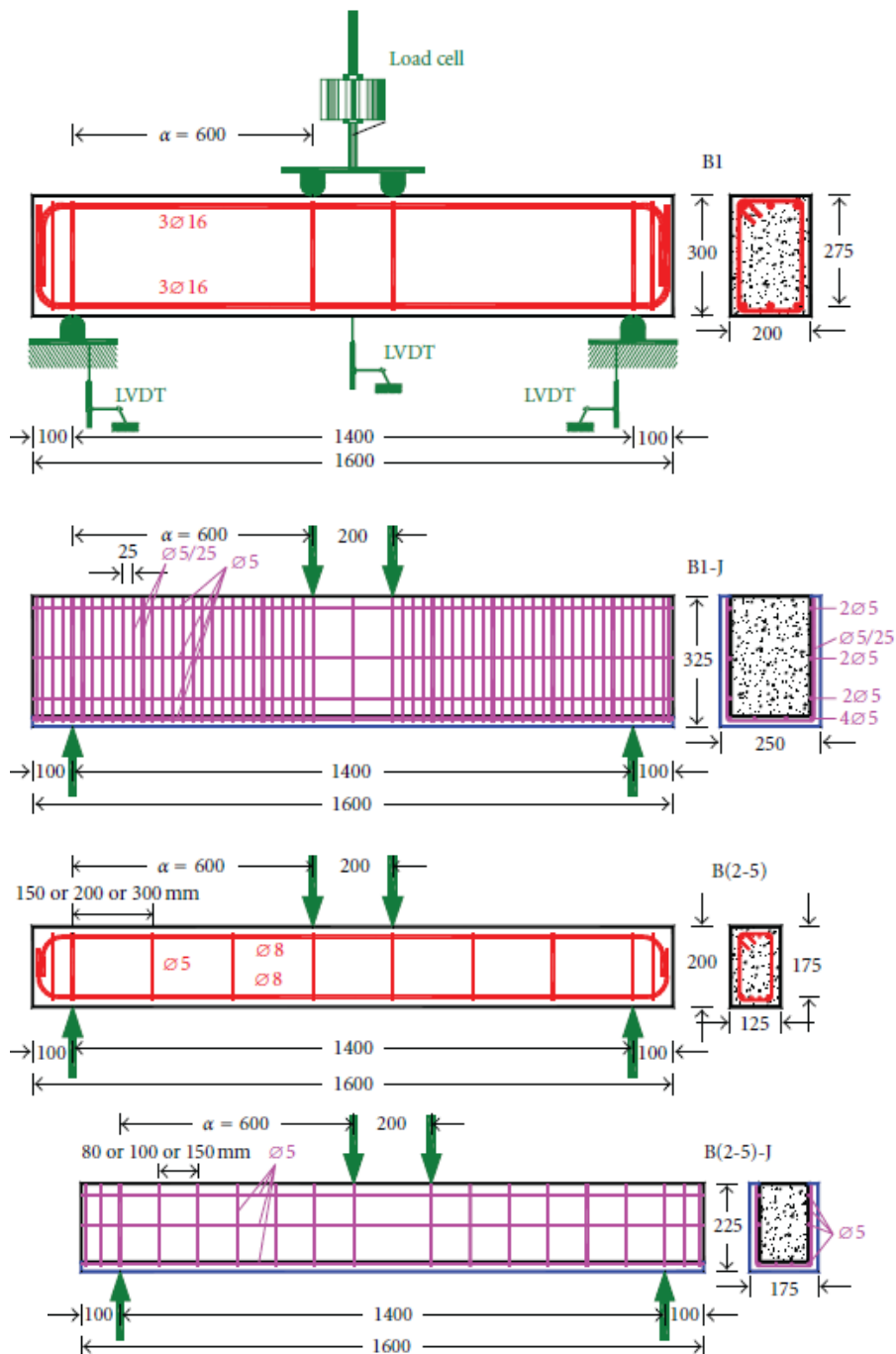
Figure 2.25: Geometry, test setup, and steel reinforcement arrangement of the tested beams (Chalioris and Constantin, 2012) - dimensions are given in mm.
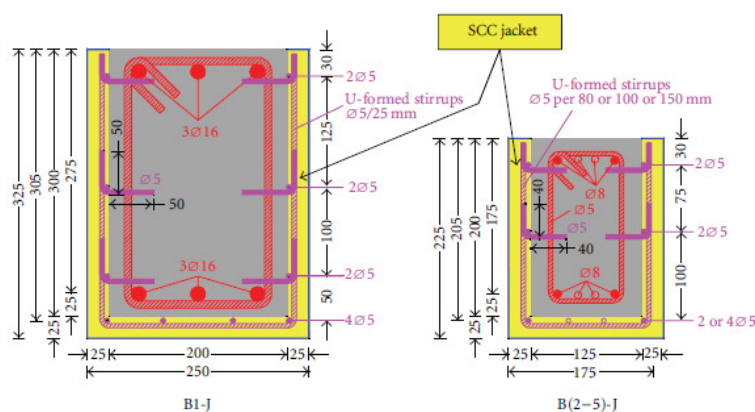
Figure 2.26: Cross-sectional dimensions and steel reinforcement arrangement of the jacketed beams (Chalioris and Constantin, 2012) - dimensions are given in mm.

Table 2.24: Strengthening details and main results obtained in the experimental program.

Specimens ID	b/h (mm)	Longitudinal bars of the jacket			U-formed stirrups of the jacket	Ultimate load (kN)	Failure mode
		Up	Middle	Bottom			
B1	250/325	-----	-----	-----	-----	-----	Shear
B1-J		2ϕ5	2ϕ5	2+4ϕ5	ϕ5/25	315.3	Shear
B2	175/225	-----	-----	-----	-----	29.9	Flexure-shear
B2-J		2ϕ5	2ϕ5	4ϕ5	ϕ5/150	41.5	Flexure-shear
B3	175/225	-----	-----	-----	-----	-----	Shear
B3-J		2ϕ5	2ϕ5	2ϕ5	ϕ5/80	69.8	Flexure
B4	175/225	-----	-----	-----	-----	-----	Shear
B4-J		2ϕ5	2ϕ5	2ϕ5	ϕ5/100	69.3	Flexure
B5	175/225	-----	-----	-----	-----	58.7	Shear
B5-J		2ϕ5	2ϕ5	2ϕ5	ϕ5/100	70.8	Flexure

Test results and comparisons between the experimental behaviour of the beams indicated that the examined jacketing technique is a reliable rehabilitation method since the capacity of the retrofitted beams was fully restored or ameliorated with respect to the initial specimens. A significant improvement of the loading bearing capacity of all the retrofitted beams with respect to the corresponding initially tested beams can be observed. This increase of the maximum applied load that varied approximately from 35% (in beam B5-J) to 200% (in beam B1-J).

ii) Shear Strengthening of RC Beams with Externally Bonded Reinforcement

Different shear strengthening schemes using FRP have consisted of: complete FRP wraps covering the whole cross section (i.e., complete wrapping, valid only for rectangular sections), FRP U-jackets covering the tensile face and the two faces that can be crossed by shear cracks (i.e., U-jacketing), and FRP sheets only glued onto the two faces that can be crossed by shear cracks (i.e., side bonding). Different orientations angles of the fibres and

different anchorage systems are used. An overview of the different EBR shear strengthening techniques based on the use of FRP materials is described in the next paragraphs.

Berset (1992)

The oldest known study on the shear strengthening with EBR FRP was carried out by Berset (1992). Six rectangular cross section beams with dimensions 102x114x600 mm^3 were tested, in which one of them was the reference (with no stirrups), one beam was reinforced with 4 mm diameter steel stirrups at 40 mm spacing, two beams were strengthened with GFRP sheets with fibres at 45º of 0.64 mm and 1.57 mm thickness, respectively, and also included 4 mm diameter steel stirrups at 40 mm spacing. Finally, two beams were only strengthened with GFRP sheets with fibres at 45º of 0.64 mm and 1.57 mm thickness, respectively. The longitudinal steel reinforcement was identical for all the beams and consisted of two 12.7 mm diameter bars. The description of the test specimen strengthening and main results are presented in Table 2.25.

Concerning to the properties of the materials, a concrete with an average compressive strength of 42.9 MPa was used. A tensile strength and young´s modulus of 413.7 MPa and 200 GPa, respectively, was obtained for the steel reinforcement. For the GFRP sheets, a tensile strength and young´s modulus of 344.7 MPa and 16.8 GPa, respectively, was obtained. The adhesive used to bond the GFRP sheets to the concrete was the Sikadur 31. The following two parameters were analysed: the thickness of the GFRP sheet and the effect of existing steel stirrups.

Table 2.25: Description of the test specimen strengthening and main results.

Specimens ID	GFRP thickness (mm)	Stirrups	Failure load (kN)	Failure mechanism
1	-----	-----	47.4	Shear
2	-----	Yes	78.9	Shear
3	0.64	-----	62.5	Shear-debonding
4	1.57	-----	78.9	Shear-debonding
5	0.64	Yes	94.2	Bending
6	1.57	Yes	94.7	Bending

According to the results, an increase of 66% was obtained in the shear capacity of the beams when comparing the reference beams with (2) and without stirrups (1). When comparing the reference beam without stirrups (1) and the strengthened beams with stirrups (3 and 4), an increase in the shear capacity of 32% to 66% was attained when using

the GFRP sheets of 0.64 mm and 1.57 mm thickness, respectively. For the beams with stirrups, a lower increase of the shear capacity (of about 19%) was obtained. The beams with steel stirrups failed in flexure, while the beams retrofitted only with GFRP have failed in shear with debonding of the GFRP composite.

Khalifa and Nanni (2002)

An experimental program with twelve, full-scale, RC beams were carried out by Khalifa and Nanni (2002). The specimens had the dimension 150x305x3050 mm^3 and were grouped into two main series designated SW and SO depending on the presence of steel stirrups in the shear span of interest. Series SW consisted of four specimens. The details and dimensions of the specimens designated series SW are illustrated in Figure 2.27.
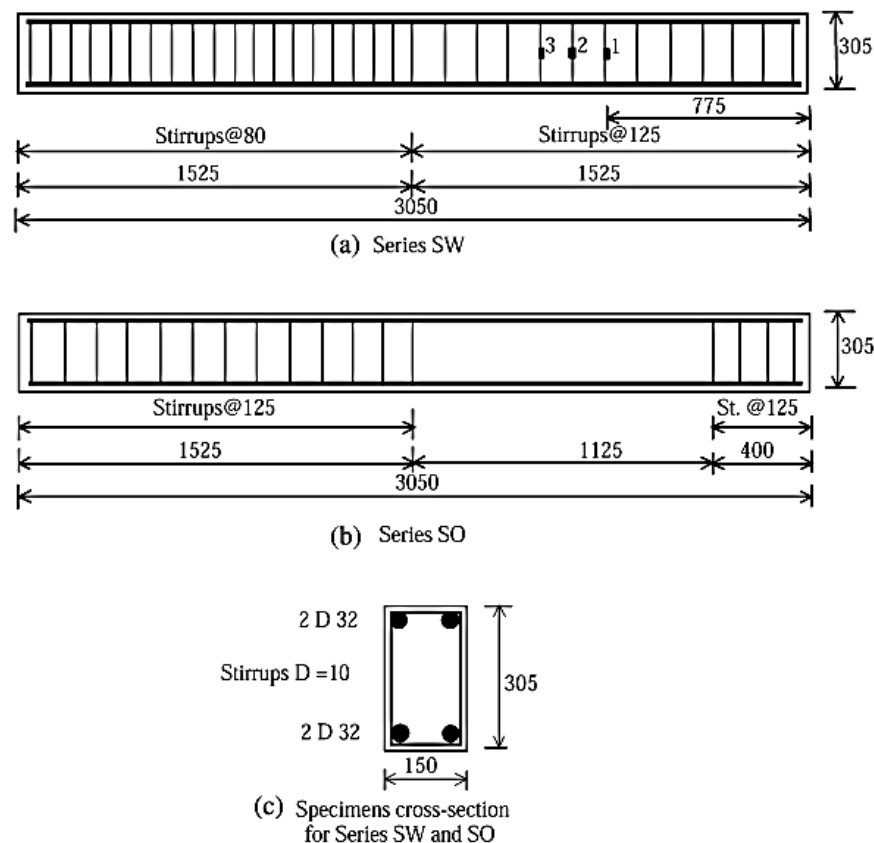
Figure 2.27: Configuration and reinforcement for beam specimens (Khalifa and Nanni, 2002).

In this series, four 32 mm steel bars were used as longitudinal reinforcement with two at top and two at bottom face of the cross-section to induce a shear failure. The specimens were reinforced with 10 mm steel stirrups throughout their entire span. The stirrups spacing in the shear span of interest, right half, was selected to allow failure in that span. Series SO consisted of eight beam specimens, which had the same cross-section dimension

and longitudinal steel reinforcement as for series SW. No stirrups were provided in the test half span as illustrated in Figure 2.28. Each main series (i.e., series SW and SO) was subdivided into two subgroups according to shear span to effective depth ratio, resulting in the following four subgroups: SW3; SW4; SO3; and SO4. One specimen from each series (SW3-1, SW4-1, SO3-1 and SO4-1) was left without strengthening as a control specimen, whereas eight beam specimens were strengthened with externally bonded CFRP sheets following three different schemes as illustrated in Figure 2.28. A resume of the experimental tests is presented in Table 2.26.

(a) One ply of CFRP U-wrap strips (specimens SO3-2, SO3-3 and SO4-2)

(b) One ply of continuous CFRP U-wrap, 90^0 (specimens SO3-4, and SO4-3)

(c) Two plies of CFRP, $90^0/0^0$ (specimens SW3-2, SW4-2, and SO3-5)
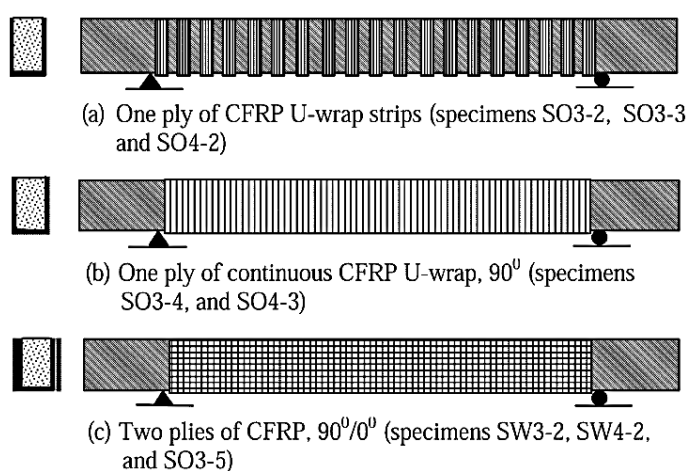
Figure 2.28: Schematic representation of CFRP strengthening schemes (Khalifa and Nanni, 2002).

Table 2.26: Test summary.

Specimens ID	Concrete Compressive strength (MPa)	Shear reinforcement		Ultimate load (kN)	Failure mechanism
		Steel stirrups	CFRP		
SW3-1	19.3	10mm at a spacing 125mm	-----	253	Shear
SW3-2	19.3	10mm at a spacing 125mm	2 plies 90°/0°	354	Splitting
SW4-1	19.3	10mm at a spacing 125mm	-----	200	Shear
SW4-2	19.3	10mm at a spacing 125mm	2 plies 90°/0°	361	Splitting
SO3-1	27.5	-----	-----	154	Shear
SO3-2	27.5	-----	Strips 50mm at a spacing 125mm	262	Debonding
SO3-3	27.5	-----	Strips 75mm at a spacing 125mm	266	Debonding
SO3-4	27.5	-----	1 ply 90°	289	Debonding
SO3-5	27.5	-----	2 plies 90°/0°	339	Splitting
SO4-1	27.5	-----	-----	130	Shear
SO4-2	27.5	-----	Strips 50mm at a spacing 125mm	255	Debonding
SO4-3	27.5	-----	1 ply 90°	310	Splitting

For the beams tested in this program, increases in shear strength of 40–138% were achieved. As expected, the test results indicated that contribution of CFRP benefits the shear capacity at a greater degree for beams without shear reinforcement than for beams with adequate shear reinforcement.

Al-Sulaimani et al. (1994)

To explore the effectiveness of GFRP materials for the shear strengthening of RC beams deficiently reinforced in shear, Al-Sulaimani et al. (1994) carried out an experimental program with sixteen beams with dimensions of 150 mmx150x1250 mm^3. Each beam's test had two phases. In the first phase the beams were damaged by applying a load level that was defined after the control beams have been tested. Then, in the second phase, the beams were repaired and tested up to failure. Different shear strengthening configurations were used: (a) strips or continuous fabric and (b) composite bonded on the sides or wrapped in a U-configuration. The results showed that the operations of repairing the preloaded beams have increased the shear capacity and restored the stiffness of the beams. It was observed that the beams retrofitted with GFRP strips or continuous GFRP fabric without additional strengthening in flexure failed by debonding, while the remaining beams failed in flexure. Finally, the authors concluded that the U-shaped wrap configuration is more effective in preventing debonding than the sided-bond technique.

Chajes et al. (1995)

An experimental program with 12 RC T cross-section beams was carried out by Chajes et al. (1995) to study the effectiveness of externally bonded composites for the shear strengthening. Woven composite fabrics made of aramid, E-glass, and graphite fibres were bonded to the web of the T-beams using an epoxy adhesive. The three different fabrics were chosen to assess influence on the strengthening effectiveness of using fabrics of different stiffness and strength. No internal steel shear reinforcement was used in any of the beams. The beams were tested in flexure, and the performance of eight beams with external FRP shear reinforcement was compared to the results of four control beams with no external reinforcement. All the beams failed in shear due to the diagonal tension of concrete followed by the rupture of FRP and no debonding of the fabric from concrete surface occurred. For the beams with external FRP reinforcement, increases in ultimate strength of 60 to 150 % were obtained.

Umezu et al. (1997)

Umezu et al. (1997) carried out an extensive experimental program to determine the effects of aramid (AFRP) and carbon (CFRP) sheets on the shear capacity of twenty six simply supported RC beams. A total wrap strengthening scheme was used in all the tested beams. Most of the specimens exhibited failure due to peeling of CFRP sheets around diagonal cracks when cracks appeared in the beams. A truss model was used to predict the contribution of AFRP to the shear capacity, based on an average stress of AFRP equal to the tensile strength of the sheet multiplied by a reduction coefficient determined from the test results. According to the results, the reduction factor of the ultimate FRP strength varies between 0.4 and 1.2.

Grace et. al (1999)

Grace et al. (1999) investigated the behaviour of fourteen RC beams simply supported, with rectangular cross section, strengthened with CFRP and GFRP sheets and laminates Figure 2.29 shows the dimensions and the combinations of strengthening materials and epoxies for the strengthening systems. The test program was divided in two phases: in the first, each beam was initially loaded up to a load level above its cracking load. Later, the cracked beams were strengthened with FRP laminates and then tested with a concentrated load applied at midspan until complete complete failure. Five strengthening systems of various types of CFRP/GFRP strengthening materials were used, namely: two types of CFRP sheets (Systems I and II), bi and unidirectional GFRP sheets (Systems III and IV), and CFRP plates (System V). Four types of epoxies, identified as Types 1-4, were used in these systems. Concrete with a compressive strength of 48.26 MPa and high-strength steel with a tensile strength of 650 MPa was used for reinforcement. The mechanical properties of the materials used in the experimental program are presented in Table 2.27.

The influence of different numbers of FRP layers, epoxy types and strengthening configuration on the behaviour of the strengthened beams was examined. Based on the experimental results presented in Table 2.28, the following observations were derived: (i) Reinforcing the bottom and lateral faces of the beam with CFRP plates was more effective than using CFRP plates only at the bottom of the beam; (ii) The use of FRP laminates has reduced the deflection performance and has increased the load carrying capacity of the beams. In addition to the longitudinal layers, the sheets oriented in the vertical direction forming a U-shape around the beam cross section have significantly reduced beam deflections and have increased the beam's load carrying capacity. Furthermore, the

presence of vertical sheets has also prevented the rupture of the FRP systems applied in the bottom face; (iii) By extending the vertical sheets over the entire span of the beam has reduced the diagonal cracks and the load carrying capacity of the beams was significantly increased; (iv) The combination of vertical and horizontal sheets, together with a proper epoxy, has lead to an increase of 100% in the load carrying capacity the strengthened beam. However, all the strengthened beams experienced brittle failure, which can pose some concerns on the design philosophy, since ductile failures should be a design target.

Table 2.27: Mechanical properties.

FRP Materials						
Strengthening system	Type of fibers	Fibers orientation	Tensile Strength (MPa)	Modulus of elasticity (GPa)	Thickness (mm)	Epoxy type
I	CFRP*	Unidirectional	2937	230	5	1
II	CFRP*	Unidirectional	758	62	13	2
III	GFRP*	Unidirectional	416	21	10	2
IV	GFRP*	Bidirectional	482 (x-direction) 310 (y-direction)	14 (x-direction) 11 (y-direction)	13	3
V	CFRP [†]	Unidirectional	2399	149	13	4
Adhesives						
Epoxy type		1	2	3	4	
Tensile strength (MPa)		29.8	66.5	95.0	24.8	
Modulus of elasticity (GPa)		-----	2.70	3.70	4.50	
*Sheets, [†]Plates.						

Table 2.28: Details and results of the experimental program.

Group	Beam ID	Strengthening system	Epoxy type	Remarks	Failure loads (kN)	Maximum deflection (mm)
1	CF-I	I	1	Strengthening for flexural only	104.5	82
	CFS-I			Strengthening for flexural and shear	110.3	74
2	CFS-II	II	2	One Hl† layer and 2 Vl‡ layers of 0.15L§ length	108.9	91
	UG1-III	III		Two Hl layers and 2 Vl layers of 0.15L§ length	164.5	119
	UG2-III			Two Hl layers and 2 Vl layers of 0.15L§ length	177.9	82
3	BG1-IV	IV	3	One layer	80.0	72
	BG2-IV			Two layers	94.7	96
	BG3-IV			Three layers	92.5	104
4	BG2-IV-E4	Combination‖	4	GFRP sheets of System IV with epoxy Type 4	142.2	139
	BG2-IV-E1		1	GFRP sheets of System IV with epoxy Type 1	129.0	114
5	CP1-V	V	4	Strengthening bottom only	110.3	81
	CP2-V			Strengthening bottom and 1/4 sides	120.1	93
	CP3-V			Strengthening bottom and 1/2 sides	131.2	109
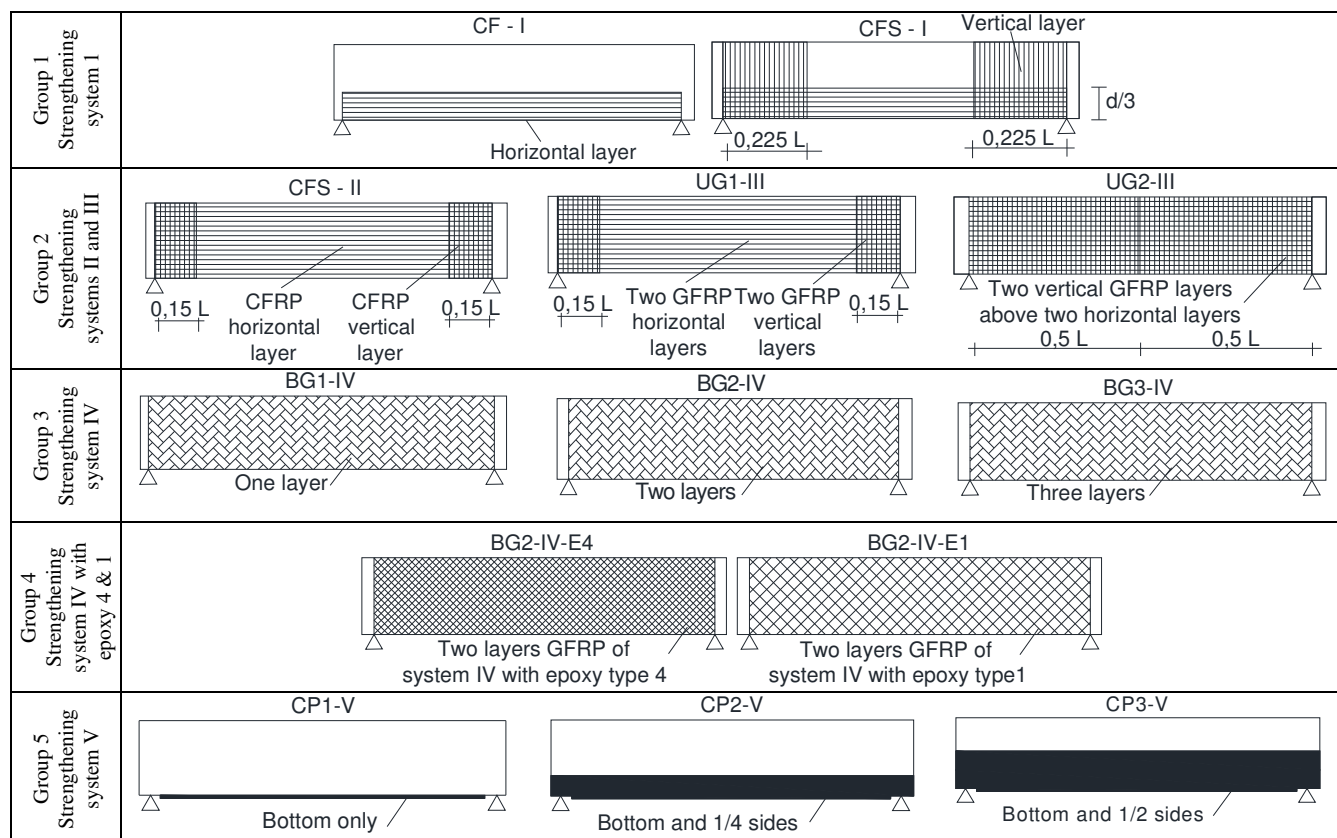
Figure 2.29: Dimensions and the combinations of strengthening materials
and epoxies for the strengthening systems (Grace et. al, 1999)

Grace et al. (2003)

The effectiveness of a triaxially braided ductile fabric for the strengthening of concrete beams was experimentally investigated by Grace et. al (2003). Twelve RC beams, divided into three different groups, were strengthened in flexure and shear by using the fabric applied according to the EBR technique. Groups A and B were used to investigate the fabric behaviour in flexural strengthening, while group C was used to investigate the fabric behaviour in shear strengthening. Only the results of the beams shear strengthened will be herein presented. The beams of the group C had the dimensions of 152x280x2744 mm³ and were deficient in shear. The beams were reinforced with two steel bars of 32 mm diameter (2ϕ32 mm) and two steel bars of 16 mm diameter (2ϕ16 mm) as tensile and compression reinforcement, respectively. Steel stirrups of 9.5 mm diameter, at spacing of 295 mm, were used throughout the length of the beams. Figure 2.30 shows the beam dimensions, reinforcement details, and loading setup for the beams of Group C. The mechanical properties of the materials can be found in 2.1.2.1. The details and results of the experimental program are presented in Table 2.29.

All dimensions in mm

(a) Cross Section for the beams strengthened at sides only

(b) Cross Section for the U-wrapped beam
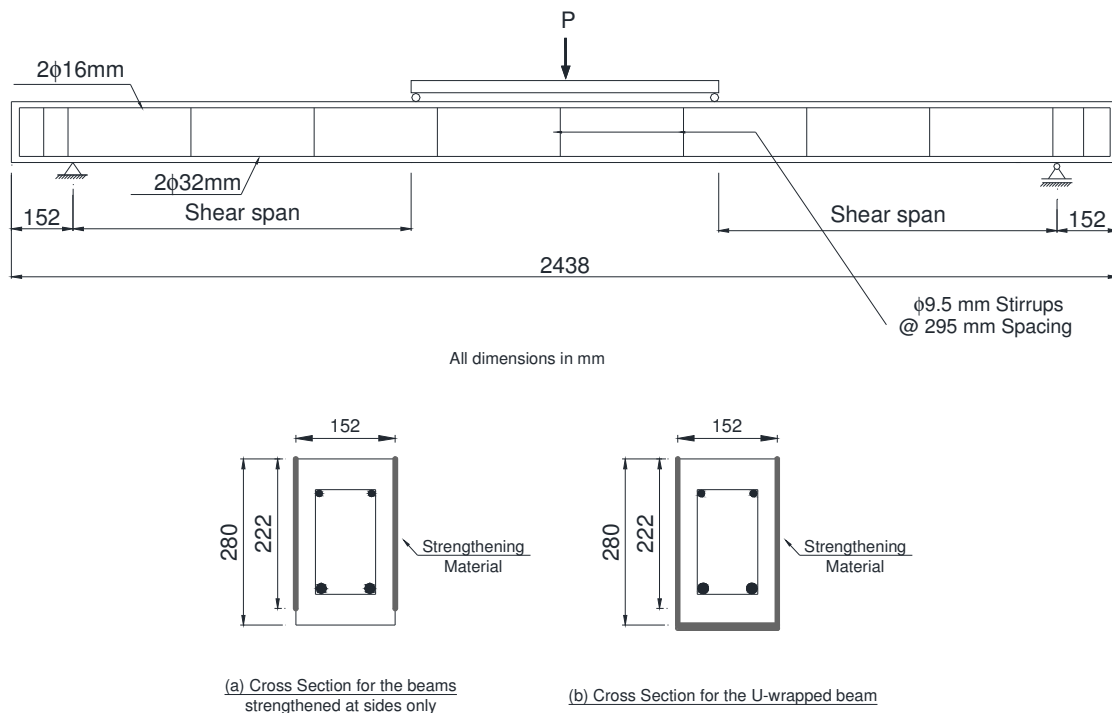
Figure 2.30: Details of test beams in Group C (Grace et al., 2003).

Table 2.29: Details and results of the experimental program.

Group	Beam ID	Strengthening squeme	Strengthening material	Failure Load (kN)	Type of failure
C	Control 3	-----	-----	101	Large diagonal cracks formed in the constant shear span, which led to shear failure of the beam
	S-S-1	Sides only	Triaxial fabric (one layer)	137	The beam failed in shear without rupture of the fabric
	S-S-2			137	The beam failed by concrete damage in the constant moment zone near the midspan causing lateral tensile stresses in the concrete leading to premature failure.
	S-S-3			141	The beam failed by debonding of the fabric
	S-U-1	U-wrap	Triaxial fabric (one layer at sides + two layers at bottom)	145	The beam failed due to damage of the concrete near the midspan, caused by buckling of the fabric.
	S-U-2			154	The beam it failed by debonding of the fabric
	S-CU45-1		Carbon fiber sheet (one layer) at 45 degrees	146	The beam failed in flexure.

The test results of the beams strengthened in shear demonstrate that the fabric demonstrated the capability of increasing the beam shear strength using only one layer. None of the beams strengthened with the fabric failed in flexure, while the beam strengthened with carbon fiber failed in flexure. The U-wrapped beams showed higher ultimate loads than those strengthened only on the sides. The difference in ultimate load, however, was in the range of 6% to 12%.

Carolin (2003)

Twenty three rectangular reinforced concrete beams were shear strengthened by using CFRP sheets. The beams were divided into two groups (type A and type B) according to the dimensions and presence of steel stirrups: The first group is formed of twenty beams without steel stirrups, with dimensions of 180x500x4500 mm^3; the second group is formed of three beams with steel stirrups and dimensions of 180x400x3500 mm^3 (Figure 2.31).

All beams were heavily reinforced in bending. The fibre direction has been varied, as well as the thickness of the fibre sheets used. Some beams were pre-cracked before have been strengthened. A group of beams were strengthened with sheets only applied on the lateral sides, and another group with sheets wrapping the entire beam in order to achieve better anchorage conditions. Some beams were subjected to fatigue loading after have been strengthened. All beams were tested up to failure by deflection controlled loading conditions. A concrete with an average compressive strength of 55 MPa was used in the experimental program. For strengthening in shear, the system BPE Composites consisting of low viscosity resin and unidirectional carbon fiber sheets has been used. When testing 290W the mode of failure changed from shear to bending. Therefore 290WR and 245W were strengthened in bending with one Sika Carbodur laminate over the whole length of the tension side of the beam. Table 2.30 shows the details and results of the experimental program.

According to the results, the bond of the CFRP sheets with an adhesive material to the concrete substrata is an effective method to increase the shear capacity of RC beams. A concrete beam may be strengthened so that the failure mode changes from shear to flexure. A damaged beam may be repaired with the proposed strengthened method, not only to get its original loading capacity, but also to exceed its original loading capacity.

(a)

(b)
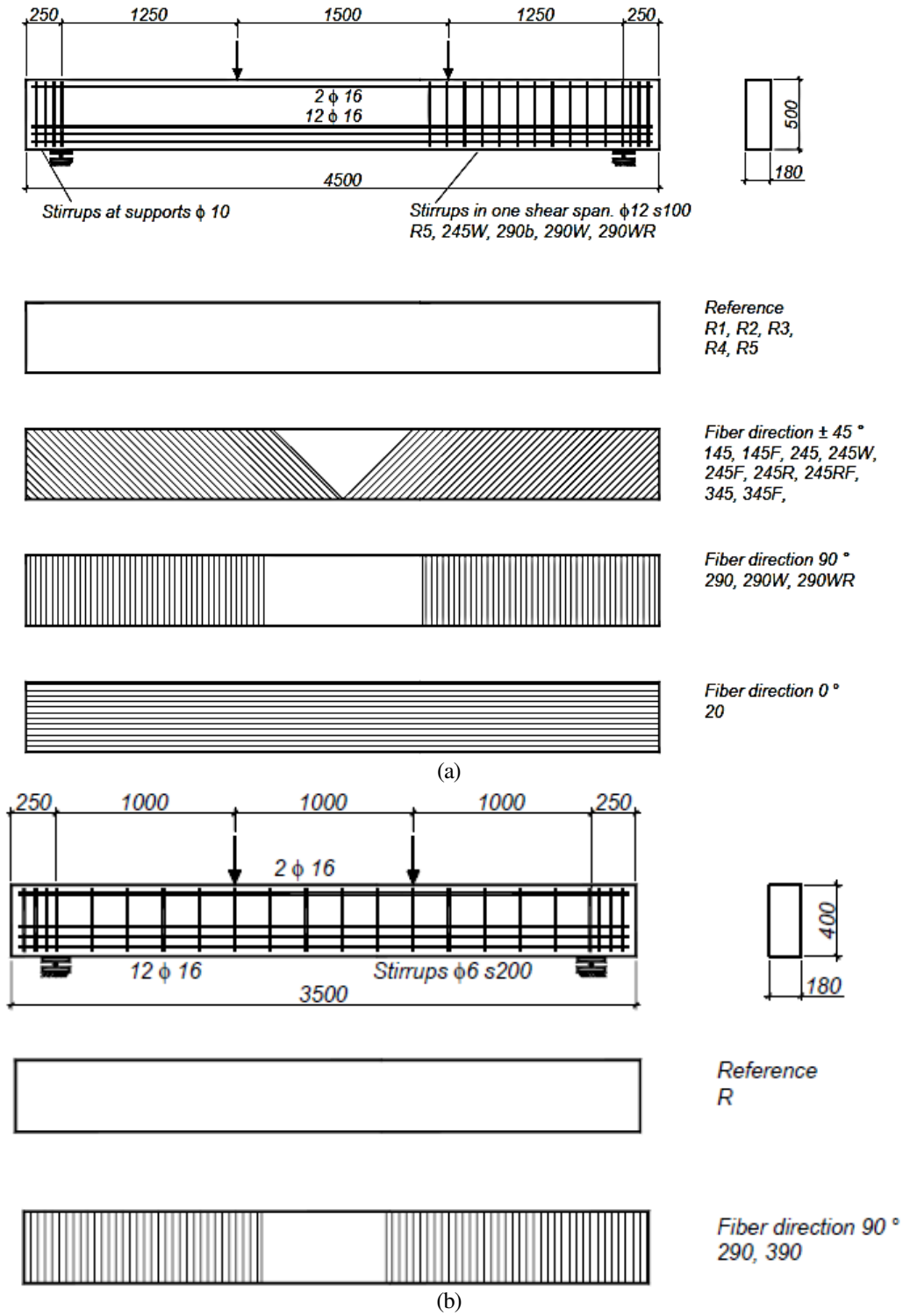
Figure 2.31: Strengthening scheme for type A (a) and type B (b) beams (Carolin, 2003).

Table 2.30: Details and results of the experimental program.

Group ID	Beam ID	Direction (º)	Comments	Ultimate shear Load (kN)	Type of failure
Type A	R1	-----	-----	126	S
	R2	-----	-----	124	S
	R3	-----	-----	103	S
	R4	-----	-----	119	S
	R5	-----	-----	125	S
	145	45	-----	247	R
	145F	-----	Fatigue loaded	338	R
	20	0	-----	154	S
	245a	45	-----	257	AR
	245b	-----		305	AR
	245W	-----	Wrapped	338	A+R
	245F	-----	Fatigue loaded	319	AR
	245Ra	-----	R2 repaired	306	AR
	245Rb	-----	R3 repaired	251	AR
	245RF	-----	R4 repaired, fatigue loaded	291	AR
	290a	90	-----	256	A
	290b	-----	-----	298	A
	290W	-----	Wrapped	367	C
	290WR	-----	R5 repaired, wrapped	388	A+R
	345	45	-----	334	A
	345F	-----	-----	344	A
Type B	R	-----	Steel stirrups	237	C
	290	90	Steel stirrups	298	A
	390	90	Steel stirrups	298	A

A: Anchorage, R: Fiber rupture; AR: anchorage and fiber rupture; A+R: fiber rupture after anchorage failure.

Lee et al. (2012)

The effective strains of the FRP used as shear strengthening material in RC beams evaluated experimentally by Lee et al. (2012). For this purpose, ten concrete beams strengthened in shear with FRP-wrap composites and reinforced internally with conventional steel stirrups were tested. The FRP reinforcement ratio, the type of fibre material (carbon or glass), and the strengthening configuration (continuous sheets or strips) were the parameters investigated in terms of shear strengthening effectiveness. The beams had the dimensions of 450x350x2800 mm^3. The longitudinal reinforcement was composed of 10ϕ25mm steel bars in the bottom and 5ϕ25 mm steel bars in the top. The shear reinforcement consisted of steel stirrups of ϕ10 mm at a spacing of 200 mm. The test results indicated that the effective strain of the FRP at shear failure has decreased with the increase of the percentage of FRP and with the decrease of the spacing of the FRP strips. An equation was proposed to predict the effective strain of the FRP. According to the

results, the proposed model was capable of predicting the effective strain of the FRP in the RC beams that fail due to crushing of the concrete or FRP rupture without debonding.

iii) Shear Strengthening of RC Beams using the Near Surface Mounted (NSM) Technique

The efficacy of the NSM technique for the shear strengthening of rectangular and T cross section RC beams has been intensively investigated in the last decade. FRP bars of circular, square and rectangular cross section have been used for the NSM shear strengthening of RC beams. Due to the largest bond area and higher confinement provided by the surrounding concrete, CFRP laminates of rectangular cross section are proved as being the most effective strengthening elements for the NSM shear strengthening of RC beams. NSM does not require surface preparation work and, after cutting the slit, requires minimal installation time compared to the EBR technique. A further advantage associated with NSM is its ability to significantly reduce the probability of harm resulting from acts of vandalism, mechanical damages and aging effects. When NSM is used, the appearance of a structural element is practically unaffected by the strengthening intervention.

De Lorenzis and Nanni (2001)

The performance of RC beams strengthened in shear with NSM CFRP rods was analysed by De Lorenzis and Nanni (2001). A total of eight beams with a T-shaped cross section, with dimensions of 152x355x3000 mm^3, were tested (Figure 2.32). The parameters studied were: (i) spacing of rods, (ii) inclination of rods, (iii) presence of an anchorage in the flange, and (iv) presence of internal steel stirrups. The average concrete strength was 31 MPa. The internal steel flexural and shear reinforcement had nominal yield strengths of 414 MPa and 345 MPa, respectively. CFRP deformed no. 3 rods, with a nominal diameter of 9.5 mm, were used in this program. Tensile strength and modulus of elasticity of the CFRP rods were determined from laboratory testing. The average resulting values were 1875 MPa and 104.8 GPa, respectively. A commercially available epoxy paste was used for embedding the rods. Their mechanical property, as specified by the manufacturer, was 13.8MPa tensile strength.

The specimens were tested under four-point loads with a shear span ratio (a/d) of 3. With the exception of the beam with steel stirrups that failed in flexure, all the beams strengthened in shear with FRP NSM rods failed in shear. One of the observed failure

modes was debonding of one or more FRP rods due to splitting of the epoxy cover. Test results seem to indicate that this mechanism can be prevented by providing a larger bond length by anchoring the NSM rods in the beam's flange or using 45° rods at a sufficiently close spacing. Table 2.31 presents the details and results of the experimental program.
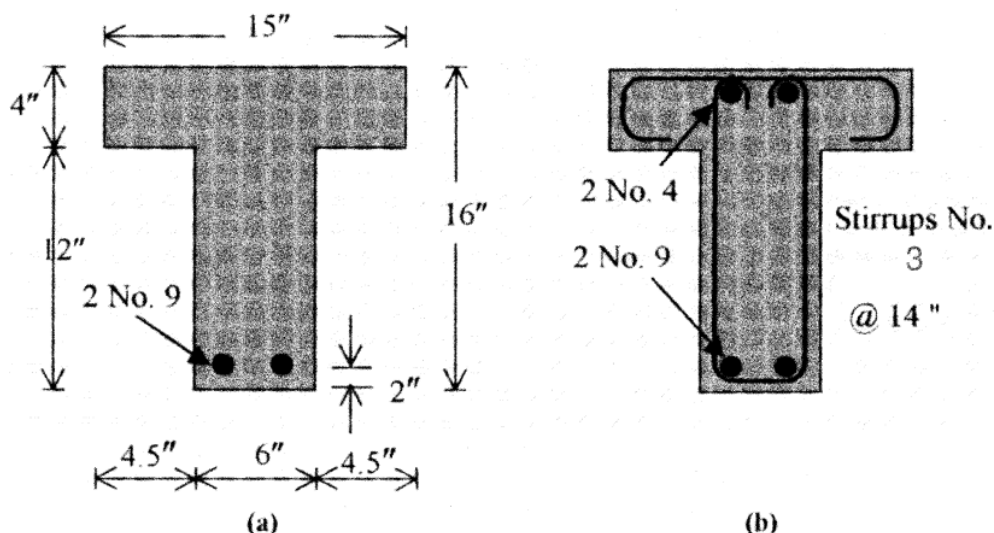
Figure 2.32: Cross section of beams: (a) beams without stirrups; and (b) beams with stirrups
(De Lorenzis and Nanni, 2001) - dimensions in inches.

Table 2.31: Details and results of the experimental program.

Beam ID	Steel stirrups		NSM FRP rods				Ultimate load (kips)	Failure mode
	Quantity	Spacing (in)	Quantity	Spacing (in)	Angle degrees	Anchorage in flange		
BV	-----	-----	-----	-----	-----	-----	40.6	SC
B90-7	-----	-----	2 no. 3	7	90	No	51.8	BF
B90-5	-----	-----	2 no. 3	5	90	No	57.4	BF
B90-5A	-----	-----	2 no. 3	5	90	Yes	83.5	SP
B45-7	-----	-----	2 no. 3	7	45	No	74.4	BF
B45-5	-----	-----	2 no. 3	5	45	No	80.0	SP
BSV	2 no. 3	14	-----	-----	-----	-----	68.9	SC
BS90-7A	2 no. 3	14	2 no. 3	7	90	Yes	93.0	SP+FF
Note: 1 kip = 4.448 kN; SC = shear compression; BF = bond failure of NSM rods; SP = splitting of concrete cover; and FF = flexural failure.								

The obtained results revealed that the NSM FRP rods are an effective technique to increase the shear capacity of RC beams. In the absence of steel stirrups, an increase in the load capacity of 106% with respect to the reference beam was obtained. The shear capacity of the strengthened beams can be increased by decreasing the spacing of the NSM rods, by anchoring the rods into the flange, or by changing the inclination of the rods from vertical to 45 degrees.

De Lorenzis and Nanni (2002)

De Lorenzis and Nanni (2002) investigated the bond between NSM FRP rods and concrete under the framework of the shear strengthening capacity these elements can provide to RC beams. The test variables were the bond length, diameter of the FRP rod, type of FRP material, surface finish of the rod, and size of the groove. Twenty two specimens were tested to investigate the effect of the mentioned factors on the bond behaviour. Concrete beams without steel stirrups, with an inverted T-shaped cross-section, were selected since they provide a larger tension area for concrete while minimizing the overall weight of the beam. Each beam had a NSM FRP rod applied on the tension face and oriented along the longitudinal axis of the beam. One side of the beam was the test region, with the NSM FRP rod having a limited bond length in order to evaluate the influence of this parameter on the bond behaviour. The rod was fully bonded on the other side of the beam, to cause bond failure to occur in the test region. According to the results, three different failure modes were experienced during the experimental tests, namely: splitting of the epoxy cover, cracking of the concrete surrounding the groove, and pull-out of the FRP rod. In some cases, combined failure modes were registered.

Barros et al. (2007)

The efficacy of the NSM and EBR techniques for the flexural and shear strengthening of reinforced concrete beams were compared by Barros et al. (2007) by carrying out two experimental groups of tests. For the flexural strengthening, the influence of the longitudinal equivalent reinforcement ratio on the strengthening effectiveness of both techniques was assessed. The experimental program was composed by four series of tests. Each series was constituted by a beam without any shear reinforcement (R) and a beam for each of the following shear reinforcing systems: steel stirrups (S), strips of CFRP sheet (M), laminate strips of CFRP at 90º with the beam axis (VL), and laminate strips of CFRP at 45º with the beam axis (IL). Two series of beams had the dimensions of 150x300x1600 mm^3, with longitudinal steel reinforcement composed of 2ϕ6 mm and 4ϕ10 mm at the top and bottom faces. The other two series of beams had the dimensions of 150x150x1000 mm^3, with longitudinal steel reinforcement composed of 2ϕ6 mm and 4ϕ10 mm at the top and bottom faces. The amount of shear reinforcement applied on the four reinforcing systems was evaluated in order to assure that all beams would fail in shear, at a similar load carrying capacity. For the shear strengthening, the influence of the longitudinal steel reinforcement ratio and the beam depth on the strengthening effectiveness of both NSM

and EBR techniques were evaluated. In the shear strengthening program, the influence of the inclination of the CFRP laminates in the NSM technique was also investigated. According to the results, the NSM was the most effective of the CFRP systems and was also the easiest and the fastest to apply. This efficacy was not only in terms of the beam load carrying capacity, but also in terms of ultimate deflection performance of the beams. Using the load carrying capacity of the unreinforced beams for comparison purposes, the beams strengthened by EBR and NSM techniques presented an average increase of 54% and 83%, respectively. Failure modes of the beams strengthened by the NSM technique were not as brittle as the ones observed in the beams strengthened by the EBR technique.

Lee and Lim (2008)

The effectiveness of reinforced concrete beams strengthened in shear with NSM CFRP strips was analysed by Lee and Lim (2008) testing nine concrete beams with dimensions of 200x300x3000 mm^3. The main test variables were the type of CFRP strengthening system, such as EBR and NSM reinforcement, the spacing of CFRP strips and the effect of existing steel stirrups. Three beams (SCF-15-NO, NSM-15-NO, NER-15-NO) were strengthened with different configurations of CFRP strips such as externally bonded reinforcement (EBR), near surface mounted (NSM) and a strengthening that combines EBR and NSM principles. Two beams were also tested to investigate the shear effect according to the spacing and layer numbers of EBR CFRP strips attached in the shear region (SCF-12.5-NO, SCF-25-NO), strengthened with EBR CFRP strips spacing of 125mm and 250mm, respectively. Three beams (SCF-25-A, SCF-25-B, NER-25-B) of different reinforcement ratio of steel sitrups were also additionally strengthened with EBR strips (SCF-25-A, SCF-25-B) and combined NSM and EBR strips (NER-25-B). Table 2.32 presents a summary of of the tested beams.

According to the results presented in Table 2.32, it was found that the stiffness and load carrying capacity of the beams strengthened with NSM strips were significantly increased compared to the control beam. A maximum increase in the shear capacity of about 154% was obtained when compared to the reference beam. The obtained results show that the NSM and EBR strips can be properly combined to be an effective shear strengthening method for RC beams, by exploring the reinforcing capabilities of each system (NSM and EBR reinforcements).

Table 2.32: Summary of the tested beams.

Specimens	CFRP strip			Steel bars		Shear Strength (kN)
	Configuration type	Spacing (mm)	Width (mm)	Longitudinal reinforcement	Stirrup	
Reference	-----	-----	-----	3ϕ22	-----	137.35
SCF-12.5-NO	EBR	125	50	3ϕ22	-----	253.21
SCF-15-NO	EBR	150	50	3ϕ22	-----	248.51
SCF-25-NO	EBR	250	50	3ϕ22	-----	223.62
SCF-25-A	EBR	250	50	3ϕ22	ϕ13 at a spacing of 150	366.78
SCF-25-B	EBR	250	50	3ϕ22	ϕ13 at a spacing of 150	362.73
NSM-15-NO	NSM	150	25	3ϕ22	-----	320.00
NER-15-NO	EBR+NSM	150	25+25	3ϕ22	-----	348.00
NER-25-B	EBR+NSM	250	25+25	3ϕ22	ϕ13 at a spacing of 150	350.00

Rizzo and De Lorenzis (2009)

An experimental program on shear strengthening of RC beams with NSM reinforcement was carried out by Rizzo and De Lorenzis (2009). A total of nine RC beams with dimensions of 200x210x2000 mm^3 were tested to analyse the influence on the structural behaviour and failure mode of selected test parameters: type of NSM reinforcement (round bars and strips), spacing and inclination of the NSM reinforcement, and mechanical properties of the groove-filling epoxy. The longitudinal reinforcement consisted of 4ϕ 22 mm and 2ϕ 22 mm at the bottom and top, respectively. The steel shear reinforcement consisted of closed double-legged stirrups. One half of each beam starting from midspan (side A in Figure 2.33) was taken as the ''test side'', while the other half (side B in Figure 2.33) was designed as the ''strong side''. As a result, side A had stirrups with 6 mm nominal diameter spaced at 160 mm (section A–A), and side B had stirrups with 10 mm nominal diameter spaced at 50 mm (section B–B). One beam strengthened in shear with externally bonded FRP laminates was also tested for comparison purposes. All beams had internal steel flexural and shear reinforcement designed to ensure that all beams would fail in shear. The concrete used in the experimental program had an average compressive strength of 29.3 MPa. The steel rebars with 22 mm diameter used as flexural tension and compression reinforcement had yield strength of 544.5 MPa and a modulus of elasticity of 211.3 GPa. The steel rebars with 6mm diameter used as stirrups had yield strength of 665.3 MPa and a modulus of elasticity of 251.5 GPa. The FRP round bars presented a tensile strength and the modulus of elasticity of the bars equal to 2214 MPa and 145.7 GPa, respectively. The CFRP strips presented a tensile strength of 2068 MPa and a yield an ultimate tensile strain of 1.70%. The CFRP laminate used as externally bonded

reinforcement, according to the manufacturer's values, presented a tensile strength and elastic modulus of 3430 MPa and 230 GPa, respectively. Finally, two types of epoxy paste were used for embedment of the NSM reinforcement. The direct tensile strength and secant tensile elastic modulus of type-a epoxy are 18.6 MPa and 4.15 GPa, respectively, while and secant tensile elastic modulus of 22.8 MPa and 12.87 GPa, respectively, was obtained for the type-b. Table 2.33 presents the details and results of the experimental program.
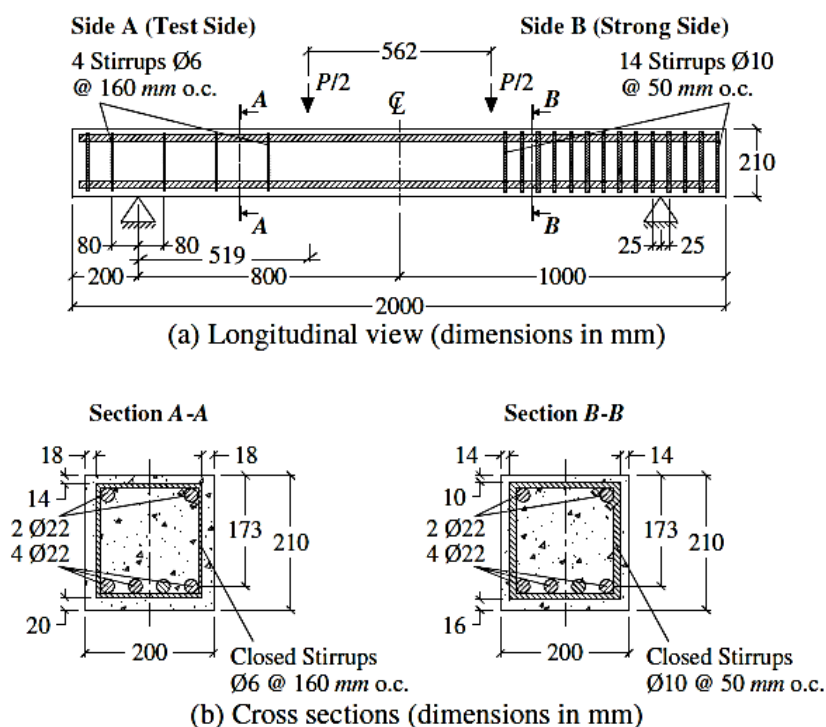
Figure 2.33: Geometrical details of the RC beams (Rizzo and De Lorenzis, 2009).

Table 2.33: Details and results of the experimental program.

Beam ID	Strengthening system	Type of groove-filling epoxy	Angle of the CFRP fibers to the beam axis (°)	Spacing of the strengthening system measured along the beam axis (mm)	Ultimate shear force (kN)
C	None (reference)	-----	------	------	244.3
UW90	Externally bonded CFRP laminate	-----	90	0 (continuous strengthening)	283.0
NB90-73-a	NSM CFRP round bars	a	90	73	352.8
NB90-73-b		b	90	73	297.1
NB90-45-b		b	90	45	301.5
NB45-146a		a	45	146	322.6
NB45-73a		a	45	73	300.3
NS90-73a	NSM CFRP strips	a	90	73	345.3
NS45-146a		a	45	146	309.7

According to the results, the FRP systems and, in particular, NSM FRP reinforcement can significantly enhance the shear capacity of RC beams also in presence of a limited amount of steel shear reinforcement. In this test program, the increase in shear capacity was about 16% for the beam strengthened with externally bonded U-wrapped laminate, and ranged between 22% and 44% for the beams strengthened with NSM reinforcement.

Dias and Barros (2012)

Dias and Barros (2012) executed an experimental program to evaluate the influence of the percentage and orientation of NSM CFRP strips for the shear strengthening of RC T-beams. The performance of this technique was evaluated by comparing the behaviour of the beams strengthened by the NSM technique with the behaviour of: (i) the unstrengthened reference beam; (ii) the homologous RC beams strengthened with U-shape CFRP wet lay-up sheets (discrete strips) applied according to the EBR technique; (iii) the homologous RC beam with an additional amount of vertical steel stirrups (beam with $\rho_{sw} = 0.28\%$). Furthermore, the influence of the percentage of existing steel stirrups in the performance of the NSM technique was also analysed. To localise the shear failure in only one of the beam shear spans, a three-point loading configuration with a distinct length for the beam shear spans was selected. This shear failure localization was also assured by applying steel stirrups with 6 mm of diameter at a spacing of 75 mm in the other shear span. The differences between the tested beams are restricted to the shear strengthening configurations applied in the critical shear span. The experimental program was composed of four reference beams and two groups of CFRP shear-strengthened beams. The reference beams consisted of one beam without any shear reinforcement (C-R); one beam with steel stirrups of ϕ6mm at a spacing of 300 mm (2S-R); one beam with steel stirrups ϕ6mm at a spacing of 180 mm (4S-R); one beam with steel stirrups ϕ6mm at a spacing of 112.5 mm (7S-R). For the CFRP shear-strengthened beams, the first group was composed of twelve beams with the percentage of stirrups adopted in the beam with ϕ6mm at a spacing of 300mm. Nine of these beams were strengthened according to the NSM technique, where three distinct percentages of CFRP laminates were considered and, for each CFRP percentage, three inclinations for the laminates are analysed: 90º, 60º and 45º. The other three beams were strengthened according to the EBR technique applying strips of unidirectional CFRP wet lay-up sheets of U configuration (see Figures 2.34 to 2.36).

A concrete with an average compressive strength of 31.7MPa at 28 days was used. CFRP laminates with a tensile strength and young´s modulus of 2741.7 MPa and 170.9 GPa, respectively, were used. The wet lay-up CFRP sheet used in the experimental program presented a tensile strength and young´s modulus of 2862.9 MPa and 218.4 GPa, respectively. Table 2.34 presents the details and results of the experimental program.

According to the results, the strengthening arrangements with NSM CFRP laminates provided an increase in terms of the maximum load that has ranged between 11.1% and 47.0%. From the results obtained in NSM and EBR beams, the following considerations can be pointed out: i) using the load-carrying capacity of the reference beam for comparison purposes, the beams strengthened by NSM and EBR solutions provided an average increase of 30.3% and 10.4%, respectively; and ii) in general, the NSM-strengthened beams were stiffer than the EBR-strengthened beams, which reflects the better performance of the NSM laminates in terms of controlling the shear cracks. These considerations indicate that NSM-strengthened beams had better structural behaviour than EBR-strengthened beams.
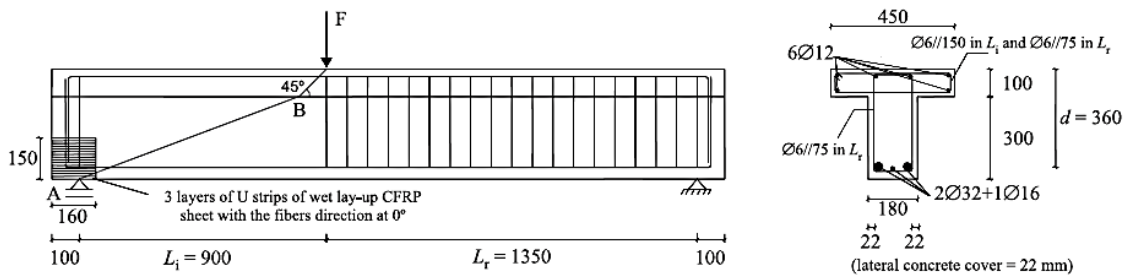
Figure 2.34: Geometry of the type of beam, steel reinforcements common to all beams, support and load conditions (Dias and Barros, 2012) - dimensions in mm.
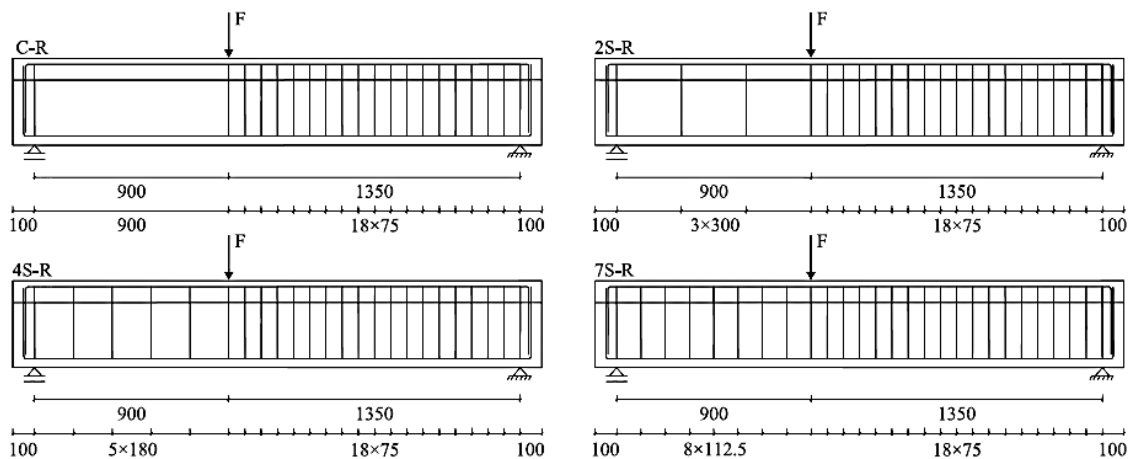
Figure 2.35: Details of the reference beams (Dias and Barros, 2012) - dimensions in mm.
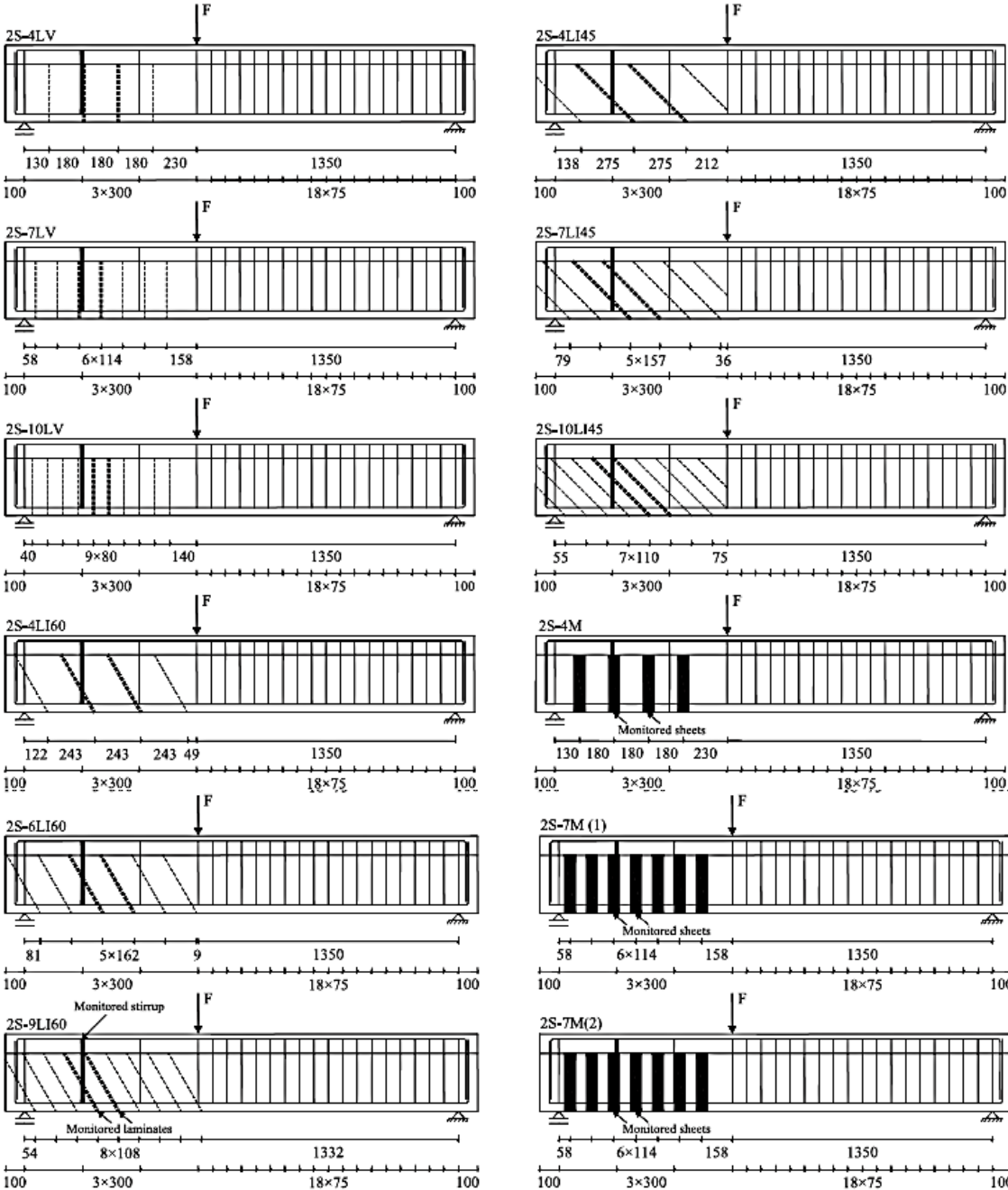
Figure 2.36: Shear strengthening arrangements
(Dias and Barros, 2012) - dimensions in mm.

Table 2.34: Details and results of the experimental program.

Beam ID	CFRP shear reinforcement system in the smaller beam shear span (L_i)					
	Shear strengthening	Quantify	Percentage (%)	Spacing (mm)	Angle (º)	Maximum load (kN)
C-R	-----	-----	-----	-----	-----	207.0
2S-R		-----	-----	-----	-----	303.8
7S-R		-----	-----	-----	-----	467.5
2S-4LV	NSM CFRP laminates	2x4 laminates (1.4x9.5mm^2)	0.08	180	90	337.4
2S-7LV		2x7 laminates (1.4x9.5mm^2)	0.13	114	90	374.1
2S-10LV		2x10 laminates (1.4x9.5mm^2)	0.18	80	90	397.5
2S-4LI45		2x4 laminates (1.4x9.5mm^2)	0.08	275	45	392.8
2S-7LI45		2x7 laminates (1.4x9.5mm^2)	0.13	157	45	421.7
2S-10LI45		2x10 laminates (1.4x9.5mm^2)	0.19	110	45	446.5
2S-4LI60		2x4 laminates (1.4x9.5mm^2)	0.07	243	60	386.4
2S-6LI60		2x6 laminates (1.4x9.5mm^2)	0.11	162	60	394.4
2S-9LI60		2x9 laminates (1.4x9.5mm^2)	0.16	108	60	412.7
2S-4M	EBR CFRP wet lay-up sheets	4 strips of CFRP wet lay-up sheets U configuration – 1 layer (0.176x60mm^2)	0.07	180	90	311.1
2S-7M(1)		7 strips of CFRP wet lay-up sheets U configuration – 1 layer (0.176x60mm^2)	0.10	114	90	325.1
2S-7M(2)		7 strips of CFRP wet lay-up sheets U configuration –2 layers (0.176x60mm^2)	0.21	114	90	370.1
4S-R	-----	-----	-----	-----	-----	371.4
4S-4LV	NSM CFRP laminates	2x4 laminates (1.4x9.5mm^2)	0.08	180	90	424.5
4S-7LV		2x7 laminates (1.4x9.5mm^2)	0.13	114	90	427.4
4S-4LI45		2x4 laminates (1.4x9.5mm^2)	0.08	275	45	442.5
4S-7LI45		2x7 laminates (1.4x9.5mm^2)	0.13	157	45	478.1
4S-4LI60		2x4 laminates (1.4x9.5mm^2)	0.07	243	60	443.8
4S-6LI60		2x6 laminates (1.4x9.5mm^2)	0.11	162	60	457.6

iv) Shear Strengthening of RC Beams using the Embedded Through-Section (ETS) Technique

A shear strengthening technique, designated by Embedded Through-Section (ETS) is briefly described in this section. According to this strengthening technique, holes are opened through the beam/slab's section, with the desired inclinations, and bars are introduced into these holes and bonded to the concrete substrate with adhesive materials. Limited researcher has been conducted on the use of embedded bars for shear strengthening. Chaalal et al. (2011) and Valerio et al. (2008, 2009) performed some tests and the results showed that this technique can be very effective for the shear strengthening of RC beams. The ETS shear strengthening technique is composed of the following steps: 1) Before drilling the holes, a rebar detector should be used to verify the position of the existing longitudinal bars and stirrups; 2) Afterward, the positions of the strengthening bars should be marked on the RC beams, and holes are made with the desired inclination through the core of the cross-section of the RC beams; 3) The holes should be cleaned with compressed air, and one extremity of the holes should be blocked before bonding the strengthening bars to the concrete; 4) The bars should be cleaned with acetone to remove any possible dirt; 5) The adhesive should be prepared according to the supplier recommendations, and the bars are introduced into the holes that should be previously filled with the adhesive (care should be taken to prevent air bubble formation in the adhesive layer during the application of the strengthening system); 6) Finally, the adhesive in excess should be removed.

Valerio et al. (2005, 2009)

Valerio et al. (2005, 2009) performed some tests on unstrengthened and ETS strengthened beams. They also executed pull-out tests on carbon, glass, aramid and steel bars embedded into concrete with different embedment lengths (15, 30, 45, 60 and 75 mm) and adhesive materials in order to assess the bond properties and select the most suitable strengthening bars for the ETS technique. These pull-out tests have shown that the ETS strengthening effectiveness relies on the bond between the embedded bar and the surrounding concrete, and also evidenced that the bond–slip response of the system is ductile when appropriate adhesives and bars with proper surface are used. Also, an experimental test program of ten FRP strengthened prestressed small-scale concrete bridges was performed by Valerio et al. (2009). The percentage of transverse reinforcement was 0.175% in the shear spans. The

beams were 110 mm wide, 190 mm deep and 3000 mm long (Figure 2.37). The longitudinal reinforcement consisted of four 7 mm wires (only the upper two were pre-tensioned) and 3 mm-diameter mild steel bars at 100 mm spacing in the shear zone as transverse steel reinforcement.
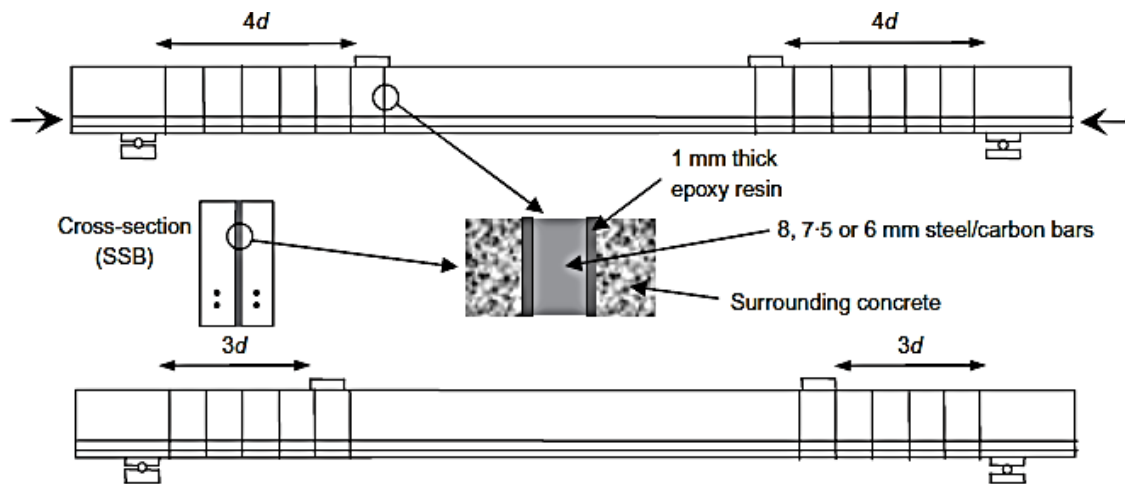
Figure 2.37: Test layout for the strengthened beams (Valerio et al., 2005)

The specimens were tested under four-point loading configuration. In the beams strengthened with ETS FRP bars a shear strengthening ratio of 0.24%, 0.36% and 0.48% has conducted to an increase of load carrying capacity of, respectively, 33%, 42% and 84% with respect to the reference beam. Thus it was concluded that the proposed shear strengthening method is feasible and effective for both pre-stressed and RC beams, even in the presence of transverse steel reinforcement.

Chaalal et al. (2011)

Chaalal et al. (2011) carried out some tests to assess the effectiveness of the ETS FRP technique, and to compare the performance of ETS, EBR and NSM shear strengthening techniques. The experimental program involves twelve tests performed RC T beams. The control specimens, not strengthened with Carbon FRP (CFRP), are identified as CON, whereas the specimens retrofitted with one layer of EB CFRP sheet are identified as EB. The specimens strengthened with NSM FRP rods are identified as NSM and the specimens strengthened with the ETS FRP method are identified as ETS. Series S0 consists of specimens with no internal transverse steel reinforcement (that is, no stirrups). Series S1 and S3 correspond to specimens with internal transverse steel stirrups. The T beams are 4520 mm long, with overall dimensions of 508 mm (width of flange) by 406 mm (total

depth). The longitudinal steel reinforcement consists of four bars with diameter of 25.2 mm laid in two layers at the bottom and six bars with diameter of 10.3 mm laid in one layer at the top. The internal steel stirrups (where applicable) are 8 mm in diameter (Figure 2.38).
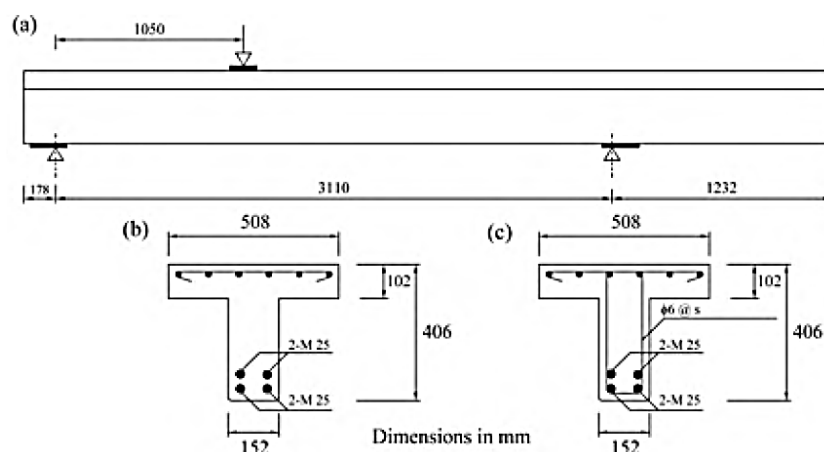
Figure 2.38: Details of concrete beams: (a) elevation, (b) cross section with no transverse steel and (c) cross section with transverse steel (Chaalal et al., 2011).

The average concrete strength is 25 MPa for S0 and S1 series and 35 MPa for S3 series, respectively. The internal flexural steel had yield strength of 470 MPa for S0 and S1 series and 650 MPa for S3 series. The shear reinforcement had yield strength of 540 MPa for S0 and S1 and 650 MPa for S3 series. Sand coated CFRP rods with nominal diameters of 9.5 mm and 12.7 mm are used for NSM and ETS strengthening methods, respectively. An average tensile strength and modulus of elasticity are 1870 MPa and 143.9 GPa, respectively, was obtained. A commercially available epoxy paste is used for embedding the rods. Its mechanical properties, as specified by the manufacturer, are 21 MPa bond strength, 1% elongation at break, 75MPa compressive strength and 3656 MPa compressive modulus. The CFRP sheet used for EB series is a unidirectional carbon fiber fabric (SikaWrap Hex 230C) that presents an ultimate stress and young´s modulus of 3650 MPa and 231 GPa, respectively. The main results of the experimental program are presented in Table 2.35.

The results shown that the techniques based on the use of EBR U-jacket sheet, NSM FRP rods, and ETS FRP rods have provided an average increase in shear capacity of, respectively, 23%, 31% and 60%. Additionally, the ETS technique was more efficient in terms of mobilizing the tensile capacity of FRP systems, since they have failed due to the attainment of their tensile strength when applied according to the ETS technique, while the

EBR systems failed by debonding, and the NSM rods by the separation of the concrete cover. At the failure of the FRP systems applied according to the EBR and NSM techniques, the maximum tensile strain was much lower than their ultimate tensile strain.

Table 2.35: Main results of the experimental program.

Strengthening Method	Series	Specimen	Load at rupture (kN)	Total shear resistance (kN)	Failure mode
Control	S0	S0-CON	122.7	81.3	Shear
	S1	S1-CON	350.6	232.2	Shear
	S2	S2-CON	294.0	194.7	Shear
EB	S0	S0-EB	181.2	120.0	Shear
	S1	S1-EB	378.5	250.7	Shear
	S2	S2-EB	335.2	222.0	Shear
NSM	S0	S0-NSM	198.0	131.1	Shear
	S1	S1-NSM	365.0	241.7	Shear
	S2	S2-NSM	380.0	251.6	Shear
ETS	S0	S0-ETS	273.0	180.8	Shear
	S1	S1-ETS	397.0	262.9	Flexure
	S2	S2-ETS	425.50	281.8	Flexure

2.3 CONCLUSIONS

A brief overview of the currently strengthening techniques, the development and applications of FRP materials was described in this chapter.

The findings concerning to the behaviour of the strengthened structures supported the initial theoretical basis for the investigation performed in this thesis. Concerning to the state-of-art presented throughout this chapter, it was identified the main contribution of this thesis, namely:

i) The strengthening techniques based on the use of fibre reinforced polymer (FRP) materials have been recognised as very effective to increase the load and deformational capacity of reinforced concrete members. The remarkable properties of FRP, such as high specific strength and stiffness, low thickness and weight, and immunity to corrosion, allow them to be applied in a construction site without serious difficulties;

ii) Based on the results, it was found that the NSM technique provides a higher ductility and load carrying capacity than the EBR technique;

iii) Most of the tests were carried out with NSM strengthened simply supported elements;

iv) Although many in situ RC strengthened elements are of continuous construction nature, there is a lack of experimental and theoretical studies in the behaviour of statically

indeterminate RC members strengthened with FRP materials. In addition, most design guidelines have been developed for simply supported beams with external FRP laminates;

v) The Externally Bonded Reinforcement (EBR) and the Near Surface Mounted (NSM) are the most used techniques for the strengthening of RC elements. However, when compared to EBR, the NSM technique is especially appropriate to increase the negative bending moments (in the intermediate supports, herein designated by hogging regions) of continuous RC slabs, since its strengthening process is simpler and faster to apply than other FRP-based techniques. Furthermore, since the laminates are inserted into thin slits open on the concrete cover, they are protected against external agents and do not create any type of obstacle to the normal functionality of the slab; and

vi) Limited information is available in literature dealing with the behaviour of continuous structures strengthened according to the NSM technique.

Concerning to the shear strengthening, there have been a number of studies on RC beams and slabs using different techniques. The several existing approaches often involves the use of strengthening materials fixed to the webs of the beams, such as concrete jacketing, external prestressing and steel plate bonding. Recently, experimental studies on shear strengthening of reinforced concrete beams with CFRP composites, according to the EBR (Externally Bonded Reinforcement) and Near-Surface Mounted (NSM) show that these techniques are good alternative of the traditional shear strengthening techniques. However, the EBR technique frequently fails by premature debonding of the external reinforcement, and EBR and NSM techniques have no applicability in the shear strengthening of RC slabs. In terms of shear strengthening, the above review of literature evidences that, although substantial research has been conducted on strengthening of RC elements, llimited research has been conducted on the use of embedded bars for the shear strengthening.

The knowledge derived in the ambit of this PhD Program can be of great way to obtain a better understanding of continuous RC structures flexurally strengthened with NSM CFRP laminates and shear strengthened with embedded bars, improving the quality of the design guidelines that fib and ACI are working.

2.4 Bibliography

Aiello, M. A., Valente, L., Rizzo, A., "Moment redistribution in continuous reinforced concrete beams with carbon-reinforced polymer laminates", Mechanics of Composite Materials, Vol. 43 (5), 2007.

Akbarzadeh, H., Maghsoudi, A.A., "Experimental and analytical investigation of reinforced high strength concrete continuous beams strengthened with fiber reinforced polymer", Materials and Design. 31 (3), pp. 1130-47, 2010.

Al-Sulaimani, G.J., Sharif, A.M., Basunbul, I.A., Baluch, M.H., Ghaleb, B.N., "Shear repair for reinforced concrete by fibreglass plate bonding", ACI Struct. J., 91(3), pp. 458–464, 1994.

Ashour, A.F., El-Refaie, S.A., Garrity, S.W., "Flexural Strengthening of RC Continuous Beams using CFRP Laminates", Cement & Concrete Composites, 26, 765-775, 2004.

Barros, J.A.O., Ferreira, D.R.S.M., Lourenço, P.B., "Comportamento de pilares de betão armado reforçados com laminados de fibras de carbono. Behaviour of reinforced concrete columns strengthened with CFRP laminate strips." Proceedings of Betão Estrutural 2000, J.A. Figueiras, A. Serra Neves, A.M. Bastos, E. Cansado de Carvalho, J. Almeida, and P.B. Lourenço (eds.), Porto, 393-402, 2000. [in Portuguese].

Barros, J.A.O., Fortes, A.S., "Flexural strengthening of concrete beams with CFRP laminates bonded into slits", Cement & Concrete Composites 27, pp. 471-480, 2005.

Barros, J.A.O., Dias, S.J.E., Lima, J.L.T., "Efficacy of CFRP-based techniques for the flexural and shear strengthening of concrete beams", Journal Cement and Concrete Composites, 29(3), 203-217, 2007.

Barros, J.A.O., Ferreira, D.R.S.M., "Assessing the efficiency of CFRP discrete confinement systems for concrete column elements", ASCE Journal of Composites for Construction, Vol. 12, No. 2, pp. 134-148, 2008.

Barros, J. A. O., "Pre-stress technique for the flexural strengthening with NSM-CFRP strips", Proceedings of the FRPRCS-9, Sydney, Australia, 2009.

Berset, J.D., "Strengthening of Reinforced Concrete Beams for Shear Using FRP Composites", MSc Thesis, Department of Civil and Environmental Engineering, Massachusetts Institute of Technology, Boston MA USA: 105 pp., 1992.

Binici, B., "Punching shear strengthening of reinforced concrete slabs using fiber reinforced Polymers." Ph.D. Dissertation, University of Texas at Austin, 2003.

Blaschko, M., Zilch, K., "Rehabilitation of concrete structures with CFRP strips glued into slits", Proceedings of the 12th International Conference on Composite Materials, Paris, France, 7 pp, 1999.

Bonaldo, E. Composite materials and discrete steel fibres for the strengthening of thin concrete structures" PhD Thesis, University of Minho, Guimarães, Portugal; 2008.

Carolin, A., "Carbon fibre reinforced polymers for strengthening of structural elements", PhD thesis, Lulea University of Technology, 2003.

Chaallal, O., Mofidi, A., Benmokrane, B., Neale, K., "Embedded Through-Section FRP Rod Method for Shear Strengthening of RC Beams: Performance and Comparison with Existing Techniques." Journal of Composites for Construction, May/June, pp. 374-383, 2011.

Chajes, M.J., Januszka, T.F., Mertz, D.R., Thomson, T.A. Jr., Finch W.W. Jr, "Shear strengthening of reinforced concrete beams using externally applied composite fabrics", ACI Struct. J. 92(3), pp. 295–303, 1995.

Chalioris, C. E., Constantin, N. P., "Rehabilitation of Shear-Damaged Reinforced Concrete Beams Using Self-Compacting Concrete Jacketing", International Scholarly Research Network ISRN Civil Engineering, 12 pages, 2012.

De Lorenzis, L., Nanni, A., "Shear Strengthening of Reinforced Concrete Beams with Near-Surface Mounted Fiber-Reinforced Polymer Rods", ACI Structural Journal, Vol. 98, Nº. 1, pp. 60-68, 2001.

De Lorenzis, L, Nanni, A., "Bond Between Near Surface Mounted FRP Rods and Concrete in Structural Strengthening," ACI Structures Journal, Vol. 99, No. 2, pp. 123-133, 2002.

Dias, S. J. E., Barros, J. A. O., "Experimental Behaviour of RC Beams Shear Strengthened with NSM CFRP Laminates", Strain, 48(1), pp. 88-100, 2012.

EI-Hacha, R., Rizkalla, S. H., "Near-Surface-Mounted Fiber-Reinforced Polymer Reinforcements for Flexural Strengthening of Concrete Structures", ACI Structural Journal, pp. 717-726, 2004.

El-Hacha, R., Gaafar, M., "Flexural strengthening of reinforced concrete beams using prestressed near-surface mounted CFRP bars", PCI Journal, Fall, pp. 134-151, 2011.

El-Refaie, S.A, Ashour, A.F., Garrity S.W, "CFRP strengthened continuous concrete beams", Proceedings of the ICE - Structures and Buildings, 156 (4), pp. 395-404, 2003.

El-Salakawy, E.F., Polak, M.A., Soudki, K.A., "New strengthening technique for concrete slab column Connections". ACI Structural Journal, 100(3), pp. 297-304, 2003.

Ferreira, D.R.S.M., Barros, J.A.O., "Confinement efficacy of partially and fully wrapped CFRP systems in RC column prototypes", 2nd International fib Congress, Naples, June 5-8, Article 10-20 in CD, 2006.

Grace, N.F., Sayed, G. A., Soliman, A. K., Saleh, K. R., "Strengthening Reinforced Concrete Beams Using Fiber Reinforced Polymer (FRP) Laminates", ACI Structural Journal, 96 (5), pp. 865-875, 1999.

Grace, N.F., Ragheb, W.F., Abdel-Sayed, G., "Flexural and shear strengthening of concrete beams using new triaxially braided ductile fabric", ACI Structural Journal, V. 100, nº 6, pp. 804-814, 2003.

Grace, N.F., Ragheb, W.F., Abdel-Sayed, G., "Innovative Triaxially Braided Ductile FRP Fabric for Strengthening Structures", Proceedings of the 7th International Symposium on Fiber Reinforced Polymer Reinforcement for Reinforced. Concrete Structures (FRPRCS-7) - New Orleans, Louisiana, USA, November, 2005.

Hassanzadeh, G., Sundqvist, H., "Strengthening of bridge slabs on columns", Nordic Concrete Research, 21, paper no.2, 1998.

Kaiser, H., "Strengthening of reinforced concrete with CFRP plates", Ph.D. dissertation, ETH Zürich, 1989.

Khalifa, A., Nanni, A., "Rehabilitation of rectangular simply supported RC beams with shear deficiencies using CFRP composites", Constr. and Building Materials. 16, pp. 135–146, 2002.

Lee, D. O., Lim, D. H., "Shear behavior of RC beams strengthened with NSM CFRP strips", Proceedings of the 3rd ACF International Conference, 2008.

Lee, J., Hwang, H., Doh, J., "Effective strain of RC beams strengthened in shear with FRP", Composites Part B: Engineering, Volume 43 (2), pp. 754–765, 2012.

Liu, I.S.T., "Intermediate crack debonding of plated reinforced concrete beams", PhD Thesis, School of Civil and Environmental Engineering, The University of Adelaide, Adelaide, Australia, 2005.

Liu, I.S.T., Oehlers, D.J., Seracino, R., "Tests on the ductility of reinforced concrete beams retrofitted with FRP and steel near-surface mounted plates", Journal of Composites for Construction, 10(2), pp. 106-114, 2006.

Mahdy, A. S, Seleem, M. H., Sallam, H.E.M., Abdin, E.M., El-Ghandour, N. A., "Flexural behaviour and mode of failure of jacketed RC beams", Scientific Bulletin, Ain Shams University, Vol. 39, No. 4, pp. 75-90, December, 2004.

Martin, J.A., Lamanna, A.J., "Performance of mechanically fastened FRP strengthened concrete beams in flexure." Journal of Composites for Construction, 12 (3), pp. 257-265, 2008,

Meier, U., "Bridge repair with high performance composite materials", Material & Technik, 4, 125-128, 1987.

Monti, G., "Seismic upgrade of reinforced concrete columns with FRP", Seismic upgrade of reinforced concrete columns with FRP, Teheran, July, 2003.

Oehlers, D. J., Ju, G., Liu, I. S. T., Seracino, R., "Moment redistribution in continuous plated RC flexural members. Part 1: neutral axis depth approach and tests", Engineering Structures, Vol. 26, No. 14, pp. 2197-2207, 2004.

Park, S. M., Oehlers, D. J., "Details of tests on steel and FRP plated continuous reinforced concrete beams", School of Civil and Environmental Engineering, University of Adelaide, Research Report R170, 2000.

Ray, J. C., Scott, D. W., Lamanna, A. J., Bank, L. C., "Flexural behavior of reinforced concrete members strengthened using mechanically fastened fiber reinforced polymer plates." Proc. 22nd Army Science Conf., The United States Army, Washington, D.C., pp. 556–560, 2000.

Rizzo, A., De Lorenzis, L., "Behavior and capacity of RCbeamsstrengthened in shear with NSM FRP reinforcement", Construction and Building Materials, 23(4), pp. 1555–1567, 2009.

Sena-Cruz, J. M., Barros, J. A. O., Coelho, M., "Bond between concrete multidirectional CFRP laminates." Advanced Materials Research, Vols. 133-134, pp. 917-922, 2010.

Sena-Cruz, J., Barros, J.A.O., Coelho, M., Silva, L. F.F.T., "Efficiency of different techniques in flexural strengthening of RC beams under monotonic and fatigue loading", Construction and Building Materials, 29, pp. 175-182, 2012.

Triantafillou, T. C., Deskovic, N., Deuring, M., "Strengthening of concrete structures with prestressed fiber reinforced plastic sheets", ACI Structural Journal, 89(3), pp. 235-244, 1992.

Umezu, K., Fujita, M., Nakai, H., Tamaki, K., "Shear Behavior of RC Beams with Aramid Fiber Sheets", Non-Metallic (FRP) Reinforcement for Concrete Structures, Proceedings of the Third Symposium, Vol. I, Japan, pp. 491-498, 1997.

Valerio, P., Ibell, T.J., Darby, A.P., "Shear Assessment and Strengthening of Continuous-Beam Concrete Bridges Using FRP Bars", Proceedings of the FRPRCS-7, 7th International Symposium on Fiber Reinforced Polymer Reinforcement for Reinforced Concrete Structures, Kansas City, EUA, pp. 825 – 848, 2005.

Valerio, P., Ibell, T. J., Darby, A. P., "Deep embedment of FRP for concrete shear strengthening", Proceedings of the Institution of Civil Engineers Structures and Buildings, 162, SB5, 311–321, 2009.

Vasseur, L., "Non-linear behavior of continuous concrete beams strengthened with externally bonded FRP reinforcement", PhD Thesis, University of Gent, 2009.

Wang, J. H., Kikuchi, K., Kuroki, M., "Seismic retrofit of existing RC rectangular columns with circular steel jackets", Proceedings of the 30th Conference on our world in concrete & structures, Singapore, August, 2005.

"Engineering is the art of modeling materials we do not wholly understand, into shapes we cannot precisely analyze so as to withstand forces we cannot properly assess, in such a way that the public has no reason to suspect the extent of our ignorance".
Dr. A.R. Dykes, 1976

Chapter 3

NSM TECHNIQUE TO INCREASE THE LOAD CARRYING CAPACITY OF CONTINUOUS RC SLAB STRIPS

In this chapter, the results of an experimental research program on the use of the near surface mounted (NSM) Carbon Fibre Reinforced Polymer (CFRP) laminates for the flexural strengthening of continuous reinforced concrete (RC) slabs are presented.

The experimental program is formed by slab strips of two equal span lengths, and has the main purpose of verifying the possibility of maintaining moment redistribution levels of 15%, 30% and 45% when applying NSM strengthening configurations designed with the aim of increasing the load carrying capacity to 25% and 50%. So, in the present work, the strengthening arrangements with CFRP laminates applied in both the hogging and sagging regions (HS series). Additionally, the results obtained in this work are compared to the ones obtained by Bonaldo (2008).

3.1 PRELIMINARY EXPERIMENTAL PROGRAM

Bonaldo (2008) carried out an experimental program to assess the moment redistribution capacity of two-span RC slabs flexural strengthened with NSM CFRP laminates. In this section, this experimental program is analysed in depth in order to assess the possibilities and challenges of the NSM technique in terms of flexural strengthening effectiveness, moment redistribution and ductility performance of continuous RC slabs.

According to the CEB-FIB Model Code (1993), the coefficient of moment redistribution, $\delta = M_{red}/M_{elas}$, is defined as the relationship between the moment at the critical section after redistribution (M_{red}) and the elastic moment (M_{elas}) at the same section calculated according to the theory of elasticity, while $\eta = (1-\delta) \cdot 100$ is the moment redistribution percentage.

To assess the influence of NSM flexural strengthening technique, using CFRP laminates, on the moment redistribution capability of continuous RC slabs, an experimental program composed of nine 120×375×5875 mm³ RC two-span slabs was carried out (Figure 3.1).

Three of the RC slabs were unstrengthened, forming a control set (SL15-H, SL30-H and SL45-H), and six slabs were strengthened with CFRP laminates according to the NSM technique (SL15s25-H, SL15s50-H, SL30s25-H, SL30s50-H, SL45s25-H and SL45s50-H, Figure 3.2).
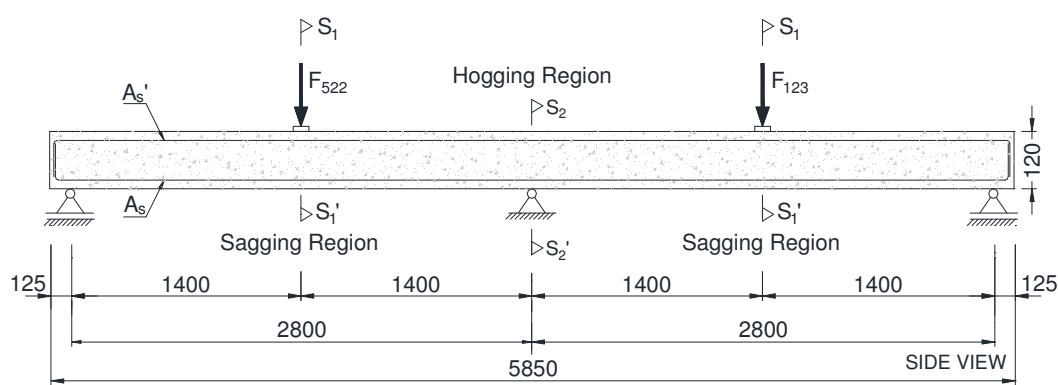
Figure 3.1: Geometry of the slit and CFRP strip (dimensions in mm).

The notation adopted to identify each slab specimen is SLxsy-z, where SL is the slab strip base, x is the moment redistribution percentage, η (15%, 30% or 45%), s means that the slab is strengthened, y is the increase of the load carrying capacity of the slab strip in 25% or 50 and z=H when the slab is strengthened in the hogging region (H), respectively. The concrete cover thickness for both the top and bottom reinforcements is about 26 mm. The

values of the properties evaluated for the concrete, steel bars and CFRP laminates are included in Annex 3.1. Details of how these properties were characterized can be found elsewhere (Bonaldo 2008).

Figures 3.2 to 3.4 and Table 3.1 show the geometry and the reinforcement and strengthening details of the cross sections of the slabs of the experimental program. These reinforcement arrangements were designed for a load of F=50.82 kN, which is 10% higher the load for the verification of deflection service limit state according to ACI 318 (2008).

The steel reinforcement was designed according to the Eurocode 2 (2010) recommendations, while the NSM CFRP strips were designed following the suggestions of ACI 440 (2008), taking for effective strain, ε_{fd}, 70% the ultimate strain obtained in uniaxial tensile tests, ε_{fu}. The design details of these slabs can be found in Annex 3.2.
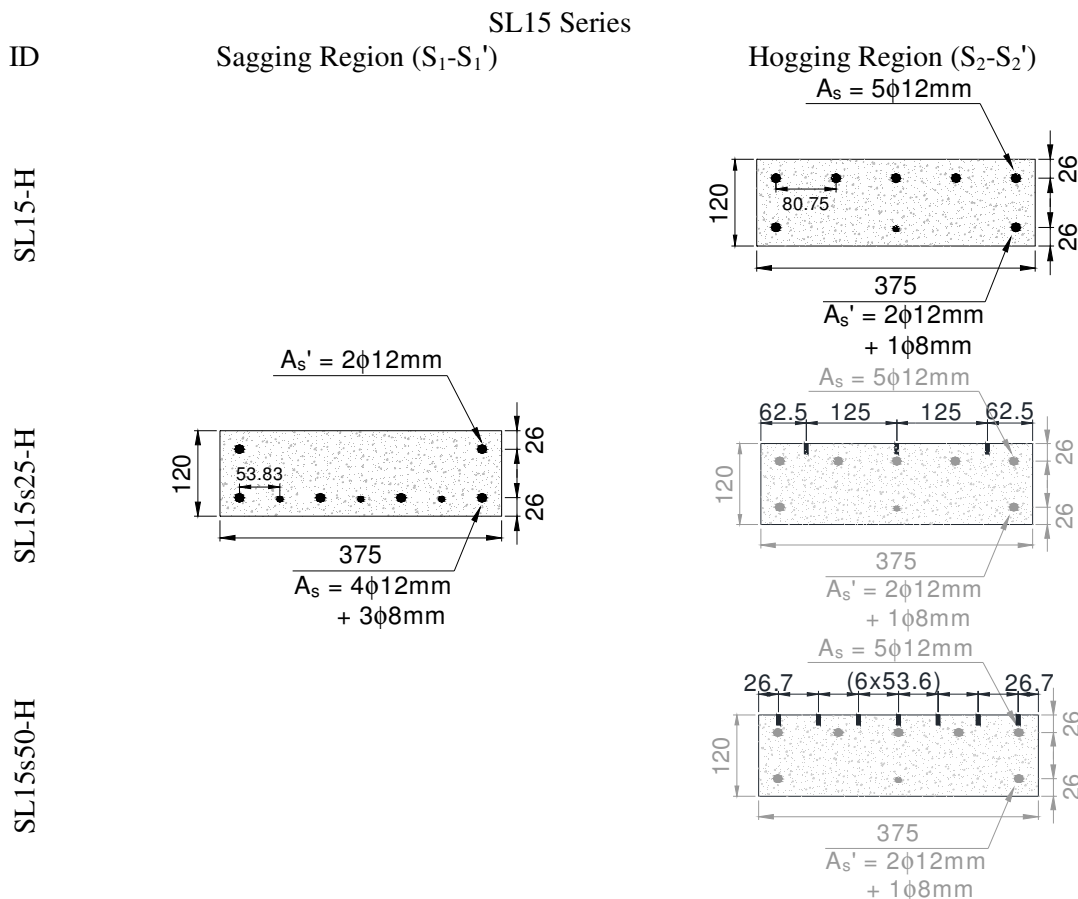
Figure 3.2: Slab strips of SL15-H Series: specimen's cross-sectional dimensions, reinforcement and strengthening of sagging (S1-S1') and hogging regions (S2-S2'). Dimensions in mm.

SL30 Series

ID	Sagging Region (S₁-S₁')	Hogging Region (S₂-S₂')

SL30-H

$A_s = 4\phi12mm$

120

107.67

26

26

375

$A_s' = 2\phi10mm$
$+ 1\phi12mm$

SL30s25-HS

$A_s' = 2\phi12mm$

120

53.83

26

26

375

$A_s = 3\phi12mm$
$+ 4\phi10mm$

$A_s = 4\phi12mm$

94   187   94

120   26   26

375

$A_s' = 2\phi10mm$
$+ 1\phi12mm$

SL30s50-HS

$A_s = 4\phi12mm$

37.5   (4x75)   37.5

120   26   26

375

$A_s' = 2\phi10mm$
$+ 1\phi12mm$
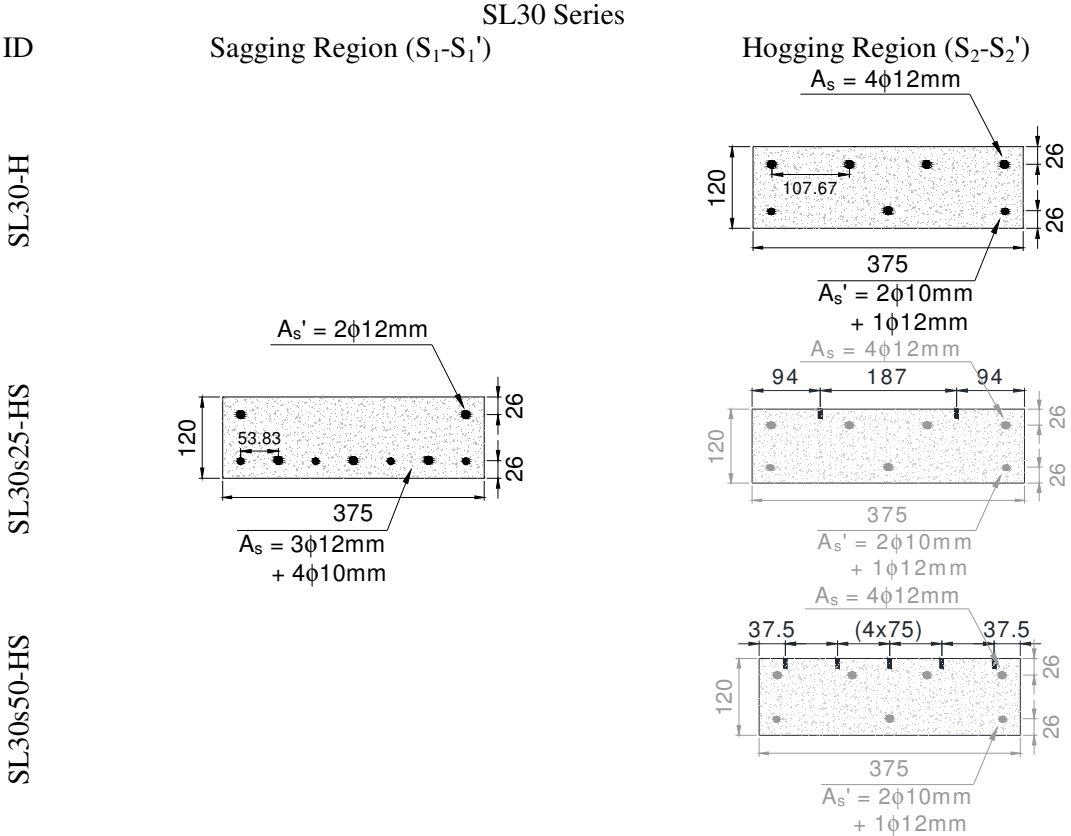
Figure 3.3: Slab strips of SL30-H Series: specimen's cross-sectional dimensions, reinforcement and strengthening of sagging (S1-S1') and hogging regions (S2-S2'). Dimensions in mm.

SL 45 Series

ID	Sagging Region (S₁-S₁')	Hogging Region (S₂-S₂')

SL45-H

$A_s' = 3\phi10mm$
$+ 2\phi8mm$

120   81.25   26   26

375

$A_s = 2\phi12mm$
$+ 1\phi8mm$

SL45s25-H

$A_s' = 2\phi10mm$

120   53.83   26   26

375

$A_s = 6\phi12mm$
$+ 1\phi8mm$

$A_s' = 3\phi10mm$
$+ 2\phi8mm$

187.5   187.5

120   26   26

375

$A_s = 2\phi12mm$
$+ 1\phi8mm$

SL45s50-H

$A_s' = 3\phi10mm$
$+ 2\phi8mm$

62.5   125   125   62.5

120   26   26

375

$A_s = 2\phi12mm$
$+ 1\phi8mm$
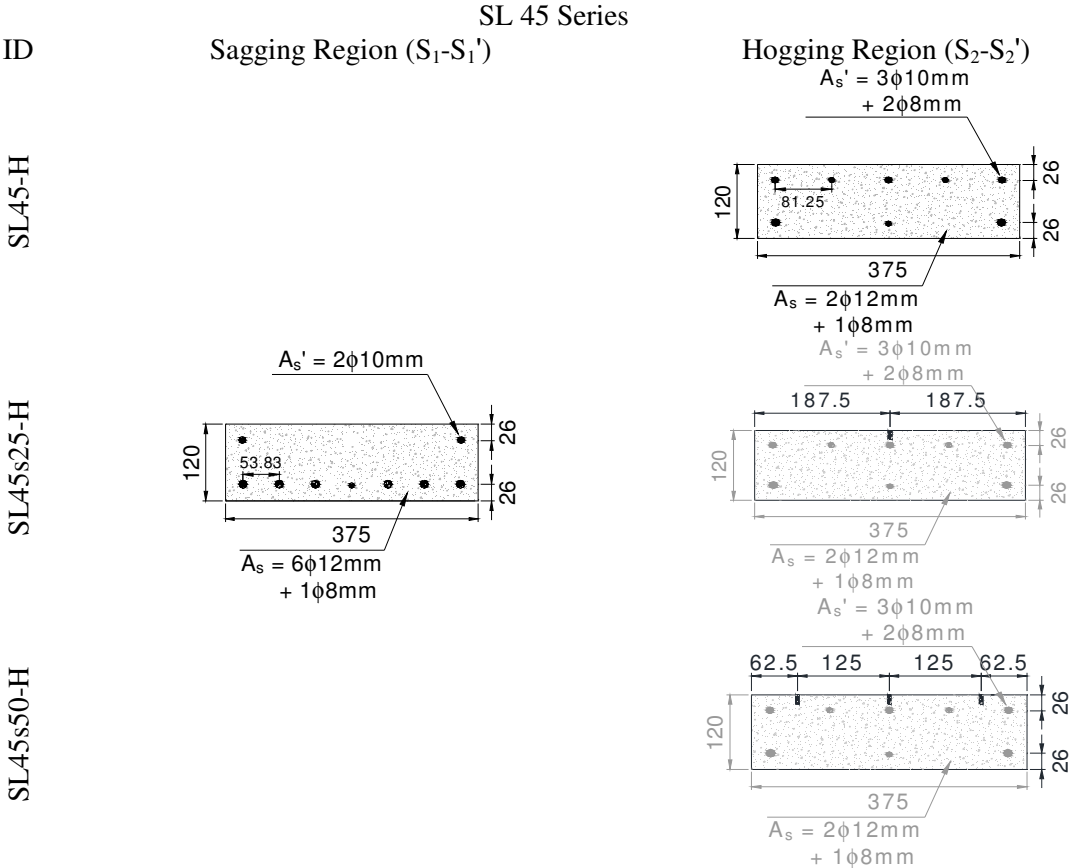
Figure 3.4: Slab strips of SL45-H Series: specimen's cross-sectional dimensions, reinforcement and strengthening of sagging (S1-S1') and hogging regions (S2-S2'). Dimensions in mm

The average load ($\overline{F} = (F_{522} + F_{123})/2$) versus deflection curves of the tested slab strips are presented in Figure 3.5. For all the slabs, flexural cracks were first observed at a $\overline{F}$ of about 6 kN. Four phases occurred during each test in the following sequence: a) the uncracked elastic response; b) crack propagation in the hogging and sagging regions with steel bars in elastic stage; c) yielding of the steel reinforcement in the hogging region and crack propagation in the sagging regions with steel bars in elastic stage; and d) yielding of the steel reinforcement in the hogging and sagging regions.

Reference slabs:

As expected, the unstrengthened control slab strips behaved in a perfectly plastic manner in the post-yielding phase (after the formation of plastic hinges in the hogging and sagging regions), whereas the strengthened slab strips exhibited continuous hardening up to failure. The reference slabs failed in bending, i.e., by yielding of internal reinforcements, with extensive concrete cracking in both hogging and sagging regions, followed by concrete crushing in compression parts.

H series:

The slab strips strengthened to increase in 25% the loading carrying capacity (SL15s25-H, SL30s25-H and SL45s25-H) were also governed by flexural failure: yielding of the internal steel reinforcements followed by the concrete crushing and CFRP rupture after high deflection values. In the slab strips strengthened to increase in 50% the loading carrying capacity, all slab strips (SL15s50-H, SL30s50-H and SL45s50-H) failed in shear, by intermediate shear crack mechanism with extensive cracking in the zones. In these strengthened slabs, neither the CFRP laminate cover separation nor the full debond of the CFRP laminates failure mode has occurred.

As previously mentioned, six arrangements of CFRP laminates were applied in the hogging region with the purpose of increasing the load carrying capacity of the reference slab in 25% and 50%. However, it is verified that an average increase of 6% and 13% was obtained for the load carrying capacity of these strengthened slabs (see Table 3.2). This can be justified by the analysis of the graphics of Figure 3.6 (also see Annex 3.3) and values of Table 3.3. In this table, for each slab, the following data is supplied: the moment at loaded section (M_{static}^+) and at intermediate support (M_{static}^-) obtained by static equilibrium, the corresponding variation of negative bending moment (ΔM^-) and applied load (ΔF), the

total load (F=50.82 kN+ΔF), the positive (M_{Rd}^{S}, at Section S_1-$S_1^{'}$, see Figure 3.1) and negative (M_{Rd}^{H}, at Section S_2-$S_2^{'}$, see Figure 3.1) resisting bending moments, the last one calculated according to the recommendations of ACI 440 (2008), see Annex 3.2. For the series SL15-H, to assure an increase of 25% and 50% of the negative resisting bending moment and, consequently, the load carrying capacity, the applied load should increases 12.71 kN and 25.41 kN, respectively, leading to a final values of positive bending moment of 30.29 and 36.35 kN.m (see also Figure 3.6).

However, according to the reinforcement arrangement of section S_1-$S_1^{'}$ (Figures 3.2 to 3.4), the maximum load when the concrete crushing at the sagging region (H) was attained $\varepsilon_c^{H} = -3.5‰$ is 49.22 kN and corresponds to a resisting bending moment of 22.47kN.m, which means that, the contribution of the laminates for the load carrying capacity of the slab is

$$\left[\frac{49.22[kN]+\Delta F[kN]}{2} + \frac{22.47[kN.m]+5.91[kN.m]}{2.8[m]}\right]\times1.4[m] = 22.47[kN.m] \Rightarrow \Delta F = 3.30\ kN \tag{3.1}$$

which corresponds to an increase (IR) of 6.71%, similar to the one obtained experimentally (8.02%). Performing similar analysis for the SL15s50-H slab,

$$\left[\frac{49.22[kN]+\Delta F[kN]}{2} + \frac{22.47[kN.m]+11.64[kN.m]}{2.8[m]}\right]\times1.4[m] = 22.47[kN.m] \Rightarrow \Delta F = 7.39\ kN \tag{3.2}$$

which corresponds to an increase of 15.02%. In case of SL30s25-H and SL30s50-H slabs the CFRP laminates can provide an increase of 4.69% and 11.89% in the load carrying capacity of these slabs that are similar to the obtained values (5.93% and 9.15%, respectively). Finally, for SL45s25-H and SL45s50-H slabs an increase of 1.00% and 8.67% in the load carrying capacity of these slabs are determined, which are similar to the obtained values (2.89% and 8.46%).

Therefore, to increase significantly the load carrying capacity of this type of slabs, the positive resisting bending moments need also to be increased, using, for instance, NSM CFRP laminates in the bottom tensile surface of the two spans of the slab.

Table 3.4 resumes the results obtained experimentally for two scenarios: when a plastic hinge formed at the hogging region (at intermediate support zone, H); when a plastic hinge formed at the sagging region (at loaded sections, S).

In this Table, $\overline{F}_y^{H}$ and $\overline{F}_y^{S}$ are the average loads at the formation of the plastic hinge at H and S, respectively, $\overline{u}_y^{H}$ and $\overline{u}_y^{S}$ are the average deflection for $\overline{F}_y^{H}$ and $\overline{F}_y^{S}$, respectively,

$\varepsilon_{c,max}^{H}$ and $\varepsilon_{c,max}^{S}$ are the maximum concrete strains at H and S, $\varepsilon_{s,max}^{H}$ and $\varepsilon_{s,max}^{S}$ are the maximum strains in steel bars at H and S, respectively, $\varepsilon_{f,max}$ is the maximum strain in the CFRP laminates, $\overline{F}$ is the average load when a concrete compressive strain of 3.5‰ was recorded at the IS ($\varepsilon_{c}^{H} = -3.5‰$), and $\varepsilon_{f,max}^{\overline{F}}$ and $\varepsilon_{s,max}^{\overline{F}}$ are the maximum strains in the CFRP laminates and in steel bars at $\overline{F}$. It was assumed that a plastic hinge has formed when yield strain was attained at the steel bars of this region. In this table, *IR* represents the increase of load carrying capacity provided by the strengthening technique, calculated according to the following equation:

$$IR = \frac{F_{cu}^{CFRP} - F_{cu}^{REF}}{F_{cu}^{CFRP}} 100 \qquad (3.3)$$

where F_{cu}^{CFRP} and F_{cu}^{REF} are the loads of, respectively, the strengthened and reference slabs when the maximum compressive strain in the sagging regions attained 3.5 ‰.

The following remarks can be pointed out:

(i) After concrete crack initiation, the slab stiffness decreased significantly, but the elasto-cracked stiffness was almost maintained up to the formation of the plastic hinge at the hogging region;

(ii) Up to the formation of the plastic hinge at the hogging region, the tensile strains in the laminates are far below their ultimate tensile strain.

At concrete crushing (assumed as -3.5‰) the maximum tensile strain in the laminates did not exceed 60% of their ultimate tensile strain;

(iii) The force-deflection relationship evidences that, up to the formation of the plastic hinge at the hogging region, the laminates had a marginal contribute for the slabs load carrying capacity. The deflection at $\overline{F}_{y}^{S}$, $\overline{u}_{y}^{H}$, was not significantly affected by the presence of the laminates.

At the formation of the plastic hinge in the hogging region, the maximum strains in the steel bars at the loaded sections, $\varepsilon_{s,max}^{S}$, are as nearest the yield strain as smaller is the level of moment redistribution. Therefore, the increment of load between the formation of the plastic hinge at hogging and at sagging regions decreased with the decrease of moment redistribution and, for each series, in general, this increment decreased with the increase of the percentage of laminates;

(iv) As expected, $\overline{F}_{y}^{S}$ was almost equal for all series because the M_{Rd}^{+} of all the slabs is similar (7th column of Table 3.3);

(v) At $\overline{F}_y^S$, $\varepsilon_{c,\max}^H$ and $\varepsilon_{c,\max}^S$ were as higher as larger was the moment redistribution. For the SL30-H and SL45-H series the $\varepsilon_{c,\max}^H$ exceeded the strain at uniaxial concrete compressive strength, *i.e.,* the concrete is in its compressive softening phase, while $\varepsilon_{c,\max}^S$ was almost attaining the compressive strain in the concrete at the peak stress (ε_{c1}). This also collaborates for the small contribution of the laminates for the slab load carrying capacity.

Figure 3.7 depicts the relationship between the average applied load and the moment redistribution percentage for the three tested series of slabs.

It is visible that, in general, after the cracking load ($\overline{F}_{cr}$), the moment redistribution decreases up to the formation of the plastic hinge in the hogging region ($\overline{F}_y^H$), followed by an increase of η up to the formation of the plastic hinge in the sagging regions ($\overline{F}_y^S$). The decrease of η is due to the decrease of stiffness in the sagging regions due to the crack formation and propagation in these zones. When the plastic hinge formed at the hogging region, the consequent loss of stiffness forced a migration of moments from the hogging to the sagging regions resulting an increase of η. The graphs of Figure 3.7 also show that η decreases with the increase of the percentage of CFRP laminates.

At the formation of the plastic hinge in the sagging region the following η values were obtained: 18.8%, 4.6%, -1.8% for SL15-H, SL15s25-H, SL15s50-H; 38.4%, 26.0%, 18.7% for SL30-H, SL30s25-H, SL30s50-H, 52.9%, 42.9%, 35.7% for SL45-H, SL45s25-H, SL45s50-H. For a compressive strain of 3.5 ‰ in the concrete surface at loaded sections, the following values of η were obtained: 17.5%, -3.9%, -14.8% for SL15-H, SL15s25-H, SL15s50-H; 36.4%, 25.3%, 14.9% for SL30-H, SL30s25-H, SL30s50-H, 53.0%, 42.8%, 30.8% for SL45-H, SL45s25-H, SL45s50-H.
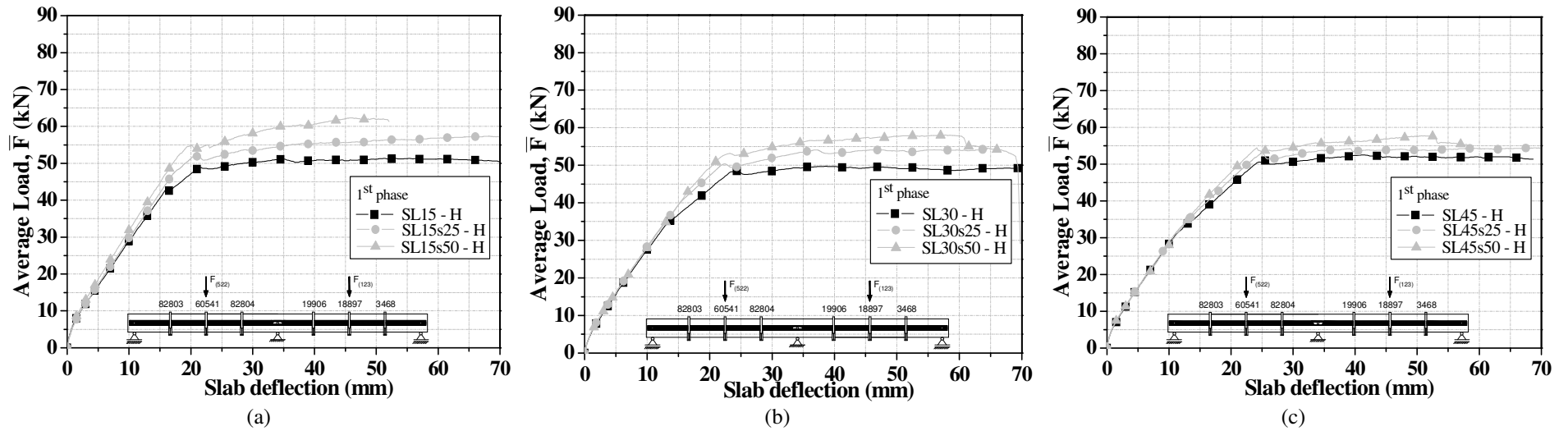
Figure 3.5: Load-midspan deflection of the tested slab strips Series: (a) SL15-H, (b) SL30-H and (c) SL45-H.

Table 3.1: Geometry, reinforcement and strengthening details of the cross sections of the slab strips.

ID	η	Increase of the loading carrying capacity	Cross-Section S_1-S_1'	Number of CFRP laminates at S	$\rho_{l,eq}^{S}$ (%)	Cross-Section S_2-S_2'	Number of CFRP Laminates at H	$\rho_{l,eq}^{H}$ (%)
H Series	15%	0%	$A_s' = 2\phi12mm$ $A_s = 4\phi12mm + 3\phi8mm$	0	1.71	$A_s = 5\phi12mm$ $A_s' = 2\phi12mm + 1\phi8mm$	0	1.60
		25%		0	1.71		3 x 1.4 x 10 mm^2	1.68
		50%		0	1.71		7 x 1.4 x 10 mm^2	1.80
	30%	0%	$A_s' = 2\phi12mm$ $A_s = 3\phi12mm + 4\phi10mm$	0	1.85	$A_s = 4\phi12mm$ $A_s' = 2\phi10mm + 1\phi12mm$	0	1.28
		25%		0	1.85		2 x 1.4 x 10 mm^2	1.34
		50%		0	1.85		5 x 1.4 x 10 mm^2	1.42
	45%	0%	$A_s' = 2\phi10mm$ $A_s = 6\phi12mm + 1\phi8mm$	0	2.07	$A_s = 3\phi10mm + 2\phi8mm$ $A_s' = 2\phi12mm + 1\phi8mm$	0	0.95
		25%		0	2.07		1 x 1.4 x 10 mm^2	0.98
		50%		0	2.07		3 x 1.4 x 10 mm^2	1.03
$\rho_{l,eq} = A_s / (bd_s) + (A_f E_f / E_s) / (bd_f)$								

Table 3.2: Main results when $\varepsilon_c^H = -3.5\%o$.

Slab strip ID	ΔF_{Tar} (%)	$\overline{F}_{max}$ (kN)	IR (%)
SL15-H	----	49.22	----
SL15s25-H	25	53.17	8.02
SL15s50-H	50	58.95	19.76
SL30-H	----	48.51	----
SL30s25-H	25	51.39	5.93
SL30s50-H	50	52.95	9.15
SL45-H	-----	50.89	----
SL45s25-H	25	52.35	2.86
SL45s50-H	50	55.20	8.46

Table 3.3: Elastic redistribution of bending moments and the corresponding variation of the applied load for the series of slabs.

Slab strip ID	M_{static}^+ (kN.m)	M_{static}^- (kN.m)	ΔM^- (kN.m)	ΔF (kN)	F (kN)	M_{Rd}^{+} (1) (kN.m)	M_{Rd}^{-} (1) (kN.m)
SL	22.24	26.68	-----	-----	50.82	-----	-----
SL15-H	24.24	22.68	-----	-----	50.82	22.47	-----
SL15s25-H	30.29	28.35	5.67	12.71	63.53	22.47	28.59
SL15s50-H	36.35	34.02	11.34	25.41	76.23	22.47	34.32
SL30-H	26.23	18.68	-----	-----	50.82	24.18	-----
SL30s25-H	32.79	23.35	4.67	12.71	63.53	24.18	22.74
SL3050-H	39.35	28.02	9.34	25.41	76.23	24.18	27.63
SL45-H	28.23	14.68	-----	-----	50.82	26.89	-----
SL45s25-H	35.29	18.35	3.67	12.70	63.53	26.89	17.99
SL45s50-H	42.35	22.02	7.34	25.41	76.23	26.89	23.64

(1) Obtained using the formulation proposed by Eurocode 2 and ACI 440.

Table 3.4: Main results – Experimental program.

Series		Hinge at hogging region (H)						Hinge at sagging region (S)						$\varepsilon_c^H = -3.5\%o$		
		$\overline{F}_y^H$ (kN)	$\overline{u}_y^H$ (mm)	$\varepsilon_{c,max}^H$ (‰)	$\varepsilon_{c,max}^S$ (‰)	$\varepsilon_{s,max}^S$ (‰)	$\varepsilon_{s,max}^H$ (‰)	$\varepsilon_{f,max}$ (‰)	$\overline{F}_y^S$ (kN)	$\overline{u}_y^S$ (mm)	$\varepsilon_{c,max}^H$ (‰)	$\varepsilon_{c,max}^S$ (‰)	$\varepsilon_{s,max}^S$ (‰)	$\varepsilon_{s,max}^H$ (‰)	$\varepsilon_{f,max}$ (‰)	$\overline{F}$ (kN)	$\overline{\varepsilon}_{f,max}^F$ (‰)	$\overline{\varepsilon}_{s,max}^F$ (‰)
SL15-H	Reference	42.67	15.86	-1.38	-1.13	2.04	2.40	------	46.99	19.80	-1.71	-1.38	2.45	2.91	------	49.22	------	2.46
SL15-H	SL15s25-H	49.13	18.52	-1.74	-1.29	2.32	2.42	3.19	51.36	20.09	-1.93	-1.60	2.40	2.73	3.47	53.17	7.82	2.87
SL15-H	SL15s50-H	54.33	21.77	-1.97	-1.48	2.70	2.41	4.06	54.38	19.67	-1.71	-1.31	2.40	2.21	3.36	58.95	7.64	2.75
SL30-H	Reference	31.52	11.82	-1.15	-0.90	1.32	2.40	------	48.48	24.07	-3.38	-1.82	2.70	4.38	------	48.51	------	4.44
SL30-H	SL30s25-H	43.66	17.63	-1.54	-1.25	1.78	2.30	2.77	49.90	24.98	-2.80	-1.77	2.50	2.60	5.90	51.39	7.35	2.64
SL30-H	SL30s50-H	42.39	16.26	-1.83	-1.31	2.17	2.40	4.13	51.96	21.63	-2.70	-1.76	2.77	2.74	6.25	52.95	8.13	2.88
SL45-H	Reference	32.50	12.16	-1.01	-0.97	1.15	m.d.	------	50.20	27.88	-4.05	-2.11	2.77	m.d.	------	50.89	------	0.80
SL45-H	SL45s25-H	33.59	12.27	-1.08	-0.86	1.11	m.d.	2.97	53.42	33.57	-5.15	-3.54	2.40	2.38	11.95	52.35	9.65	1.66
SL45-H	SL45s50-H	38.00	14.45	-1.22	-1.06	1.62	m.d.	2.93	53.00	23.19	-2.35	-1.64	2.40	1.78	6.44	55.20	9.34	2.12

m.d.: The gauge may have been mechanically damaged
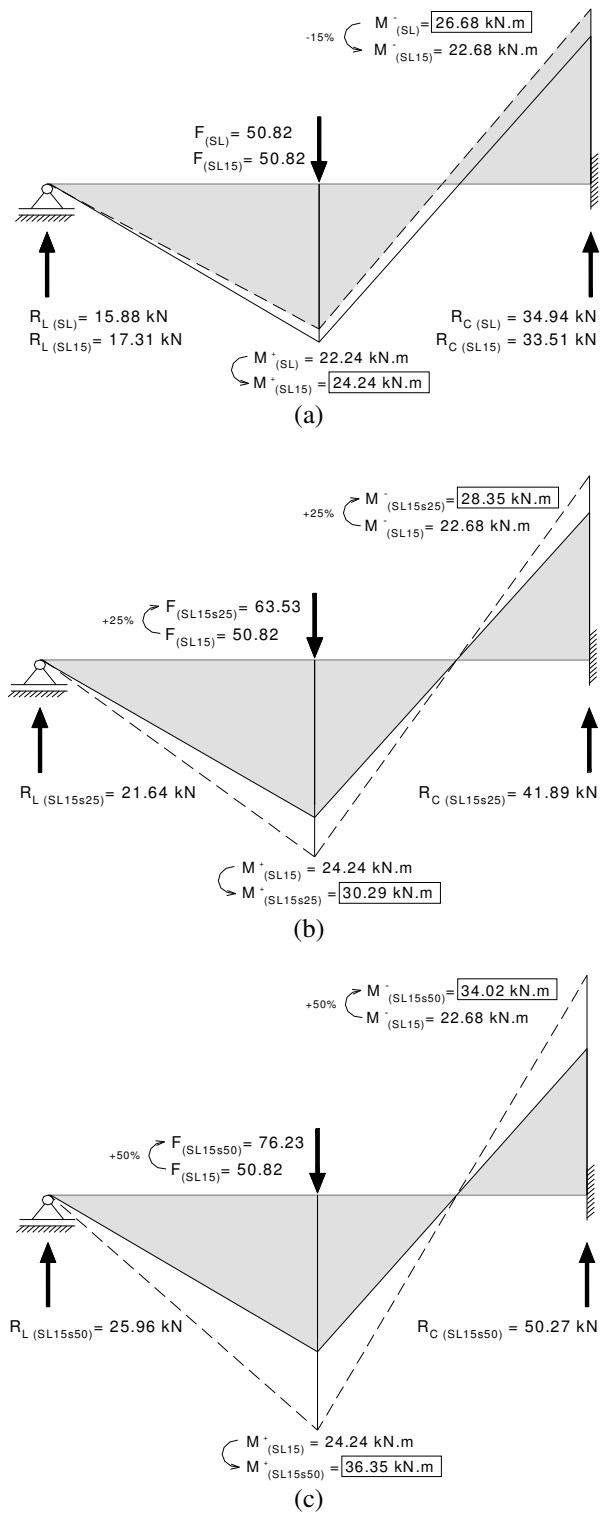
Figure 3.6: Elastic bending moments of SL15 series: (a) SL15-H, (b) SL15s25-H, (c) SL15s50-H.
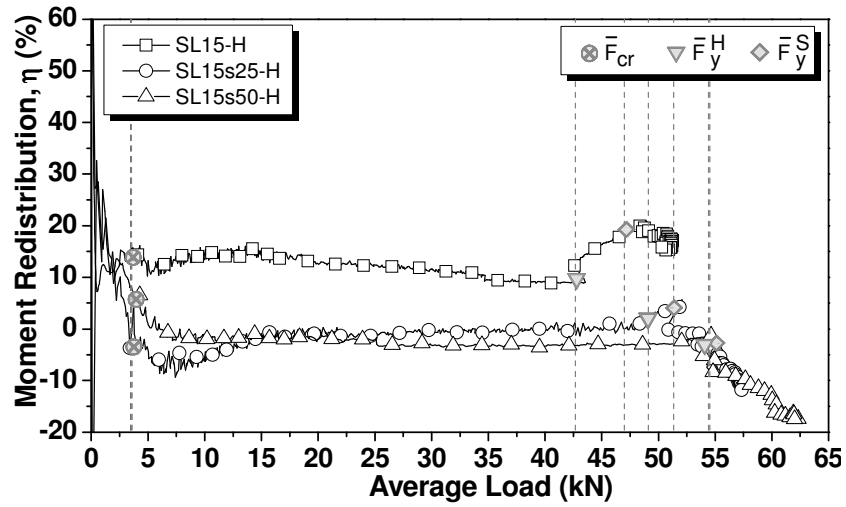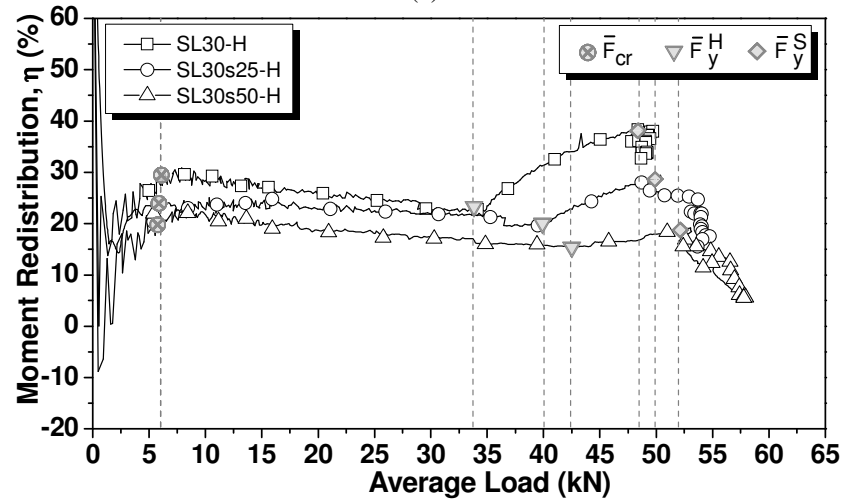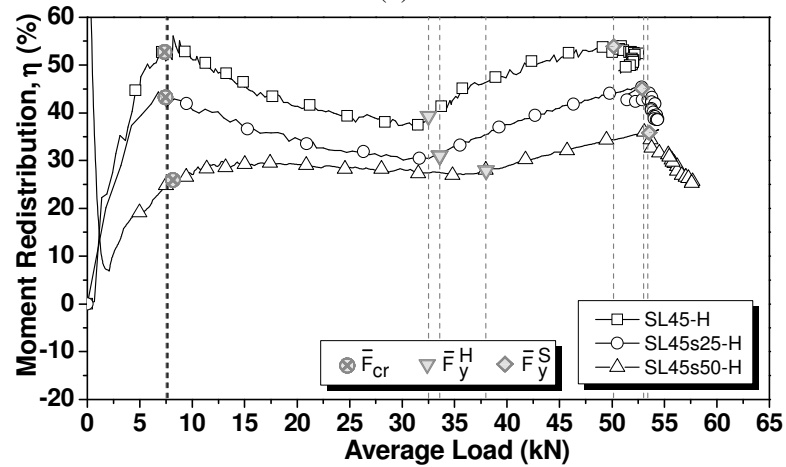
Figure 3.7: Degree of moment redistribution, η, for the slab strips series: (a) SL15-H, (b) SL30-H, (c) SL45-H.

3.2 PROPOSED EXPERIMENTAL PROGRAM

According to the results obtained in the experimental program carried out by Bonaldo (2008), to increase significantly the load carrying capacity of the slab strips, it is necessary to strengthen both sagging and hogging regions, using, for instance, NSM CFRP laminates. Thus, a new experimental program is proposed. The experimental program is composed of eight 120×375×5875 mm^3 RC slab strips (Figure 3.8). This figure also represents the geometry, support and load conditions of the tested slab strips.

Three of them were unstrengthened RC slabs forming a control set (SL15-HS, SL30-HS and SL45-HS), and the other five slabs were strengthened with CFRP strips according to the NSM technique (SL15s25-HS, SL30s25-HS, SL30s50-HS, SL45s25-HS and SL45s50-HS). The notation adopted to identify each slab specimen is the same presented in previous section, but now z=HS, indicating that the slabs were strengthened in both hogging and sagging regions (HS). According to CEB-FIP Model Code (1990), the moment redistribution for RC slabs should be limited to 25%, but the possibility of attaining a η of 30 and 45% was also explored in the present work.

The reinforcement and strengthening arrangements of the slab strips composing this experimental program are represented in Figures 3.9 to 3.11. Additionally, the details of the cross sections of the slab strips are presented in Table 3.5, where $\rho_{l,eq}^{H}$ and $\rho_{l,eq}^{S}$ are the equivalent steel reinforcement ratio [$\rho_{l,eq} = A_s/(bd_s) + (A_f E_f/E_s)/(bd_f)$] of the hogging and sagging regions, respectively, where b is the width of the slab's cross section and d_s and d_f are the effective depth of the longitudinal steel bars and CFRP laminates, respectively, and E_s and E_f are the Young's modulus of the longitudinal tensile steel bars and CFRP laminates.

3.2.1 Slab specimens and test configuration

The steel reinforcement arrangements in the reference slabs (with the designations of SL15-HS, SL30-HS and SL45-HS) were designed in compliance with ACI 318 (2008). Taking into account the concrete compressive strengths obtained in the experimental program, design loads of 44.92 kN, 45.45 kN and 47.93 kN were obtained for the SL15-HS, SL30-HS and SL45-HS series. Furthermore, in the evaluation of the reinforcement

percentages a coefficient of moment redistribution (η) equal to 15, 30 or 45% was considered, and a strain limit of 3.5‰ for the concrete crushing was assumed. Thus, the δ parameter was evaluated when the maximum strain at extreme concrete compression fibre has attained the value of 3.5‰.

The NSM flexurally strengthened slabs had the same steel reinforcement arrangements adopted in the reference slabs of the corresponding series. The number of CFRP laminates was designed to increase the load carrying capacity of the reference slabs (REF) in 25% and 50%.

The design of cross sections subject to flexure was based on force and moment equilibriums, as well as in strain compatibility. The design details of these slabs can be found in Annex 3.2.

If only laminates of 1.4x10 mm^2 cross section had been selected to increase the load carrying capacity of the sagging regions, the number of laminates would have been relatively high in these regions, leading to a small distance between laminates, which could favor the occurrence of group effect, with an eventual premature detachment of the concrete cover that includes the laminates (Bianco et. al, 2010).
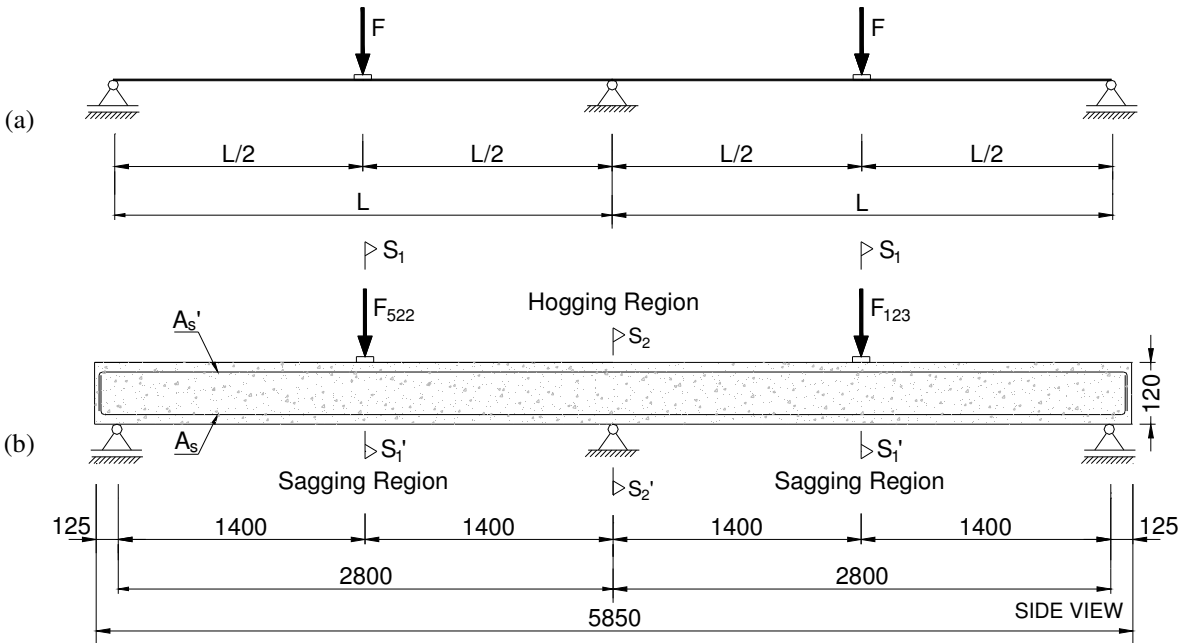
Figure 3.8: Slab strips: (a) test configuration and (b) specimens dimensions (in mm).

SL15 Series

ID	Sagging Region (S_1-S_1')	Hogging Region (S_2-S_2')
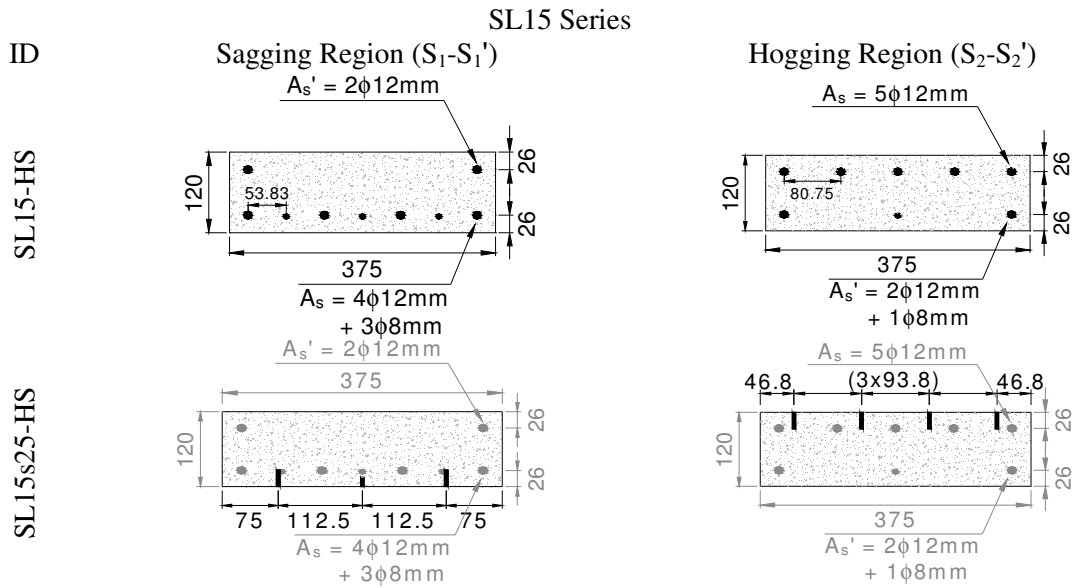
Figure 3.9: Slab strips of the SL15-HS series: specimen's cross-sectional dimensions, reinforcement and strengthening of sagging (S1-S1') and hogging regions (S2-S2'). Dimensions in mm

SL30 Series

ID	Sagging Region (S_1-S_1')	Hogging Region (S_2-S_2')
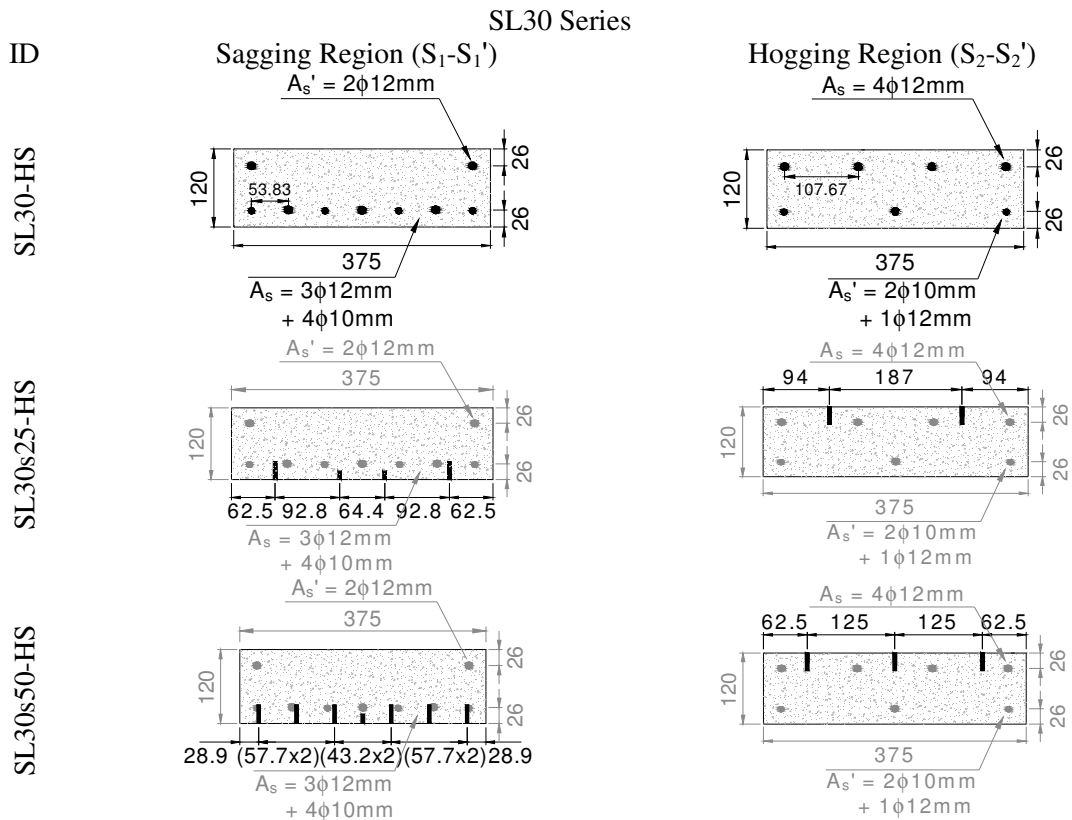
Figure 3.10: Slab strips of the SL30-HS series: specimen's cross-sectional dimensions, reinforcement and strengthening of sagging (S1-S1') and hogging regions (S2-S2'). Dimensions in mm
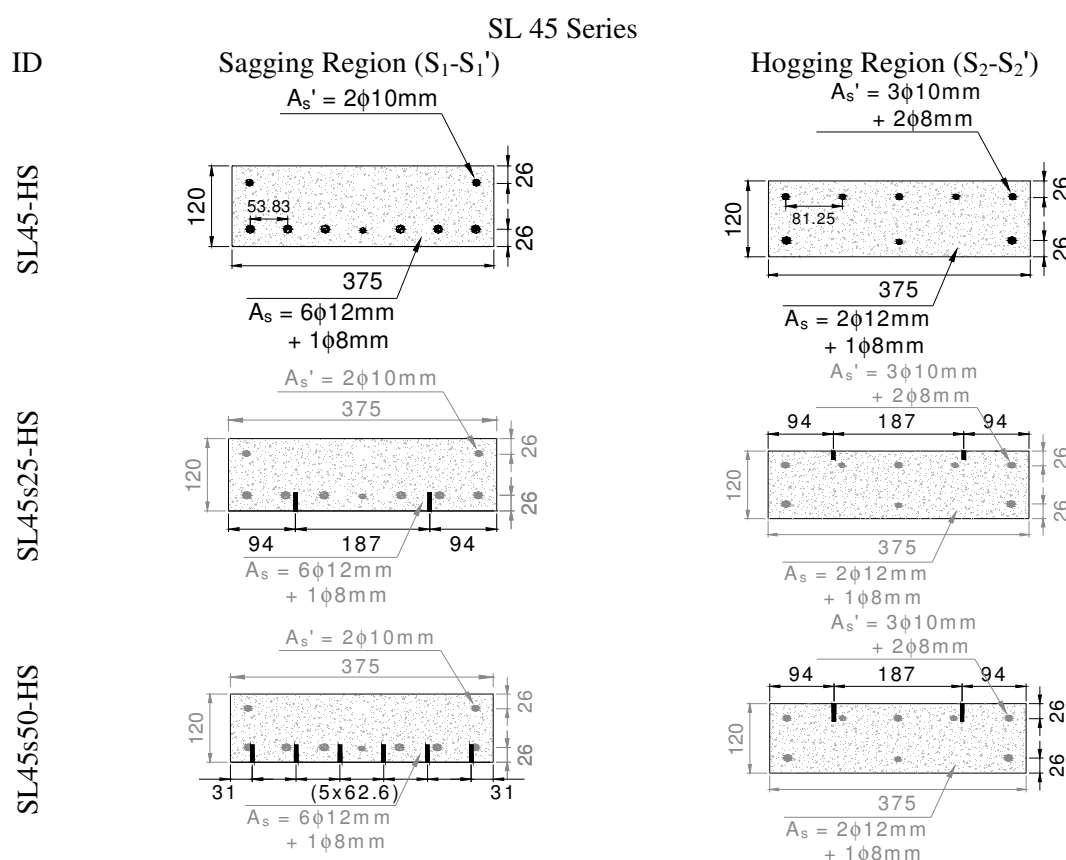
Figure 3.11: Slab strips of the SL45-HS series: specimen's cross-sectional dimensions, reinforcement and strengthening of sagging (S1-S1') and hogging regions (S2-S2'). Dimensions in mm

Therefore, for this series, CFRP laminates of 1.4x20mm^2 cross section were preferentially selected. However, in the SL30s25-HS, to avoid the placement of a laminate coinciding with the position of an existing longitudinal steel bar that previous research has indicated to be an unfavourable arrangement (Barros and Kotynia, 2008), two laminates of 1.4x10mm^2 cross section were applied instead of one 1.4x20 mm^2 laminate.

Each test of the slab strips of HS series had two phases. In the first testing phase the slab was loaded up to attain, in the loaded sections, a deflection corresponding to 50% of the deflection measured in the reference slab when the steel reinforcement in the hogging region has reached its yield strain. When attained this deflection level (a value that varied between 5.4 mm and 5.7 mm), a temporary reaction system was applied (Figure 3.12) in order to maintain this deformability during the period necessary to strengthen the slab. To control the maintenance of this deflection, dial gauges were used to adjust the temporary reaction system when necessary. Therefore, the strengthening process was applied to the slab that has a damage level that can be representative of real slabs requiring structural

rehabilitation. After the curing time of the adhesive used to bond the NSM CFRP strips (which in general took about two weeks), the temporary reaction system was removed, while the load was transferred to the slab. This stress transfer process was governed by the criteria of maintaining the deflection level that corresponds to the initiation of the second phase of the test. This second phase of the test ended when the strengthened slab strip has ruptured.
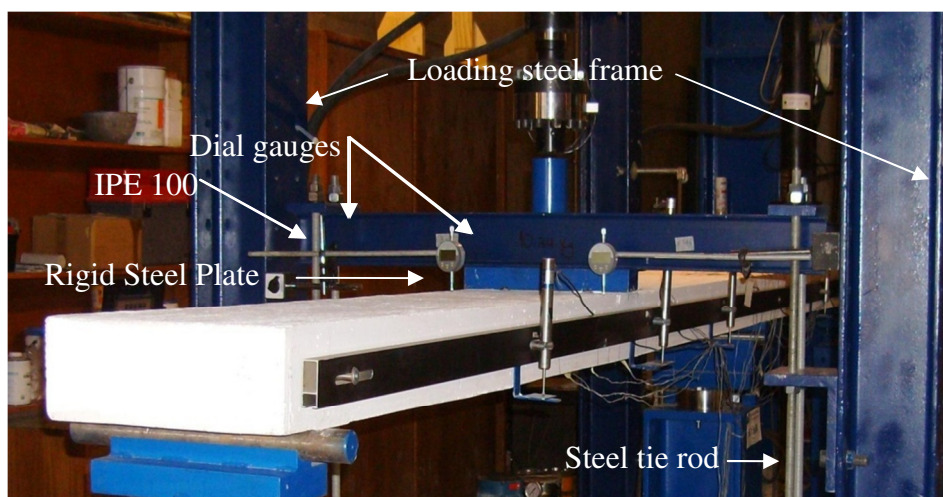
Figure 3.12: Apparatus to sustain and to control the mid-span deflection
applied in the slab strips to be strengthened.

3.2.2 Measuring devices

Figure 3.12 shows the arrangement of the test set up of the continuous RC slabs simply supported with two equal spans and two concentrated loads applied at the middle of each span. A servo-controlled test equipment with two independent actuators was used in the experimental program. Six linear voltage differential transducers supported on a suspension yoke (LVDT 82803, LVDT 60541, LVDT 82804, LVDT 19906, LVDT 18897 and LVDT 3468) were used to measure the vertical deflection of a slab strip (see Figure 3.13). The LVDTs 60541 and 18897, placed at the slab midspan, were also used to control the test at a displacement rate of 10 µm/s up to the deflection of 50 mm. After this deflection, the internal LVDTs of the actuators were used to control the test at a displacement rate of 20 µm/s up to the failure of the slab strip.

The force (F_{522}) applied at the left span was measured using a load cell of ±200 kN and accuracy of ±0.03% (designated as Ctrl_1), placed between the loading steel frame and the actuator of 150 kN load capacity and 200 mm stroke. In the right span, the load (F_{123}) was applied with an actuator of 100 kN and 200 mm stroke, and the corresponding force was measured using a load cell of ±250 kN and accuracy of ±0.05% (designated as Ctrl_2). To transfer uniformly each

applied vertical load (F) to the entire width of the slab strip, a rigid steel plate (375 mm x 70 mm x 40 mm) was placed in between the load cells and the slab specimen.

To monitor the reaction forces, load cells were installed in three supports. One load cell (AEP_200) was positioned at the central support (nonadjustable support), placed between the reaction steel frame and the slab's support device. The other load cells (MIC_200) were positioned in-between the reaction steel frame and the apparatus of the adjustable right support of the slab. These cells have a load capacity of 200 kN and accuracy of ±0.05%. Unfortunately, due to a deficient functioning of the data acquisition device, the signals in these last two load cells were not registered in the test of the SL15-HS reference slab.

The translational movements in the vertical and horizontal (longitudinal axis of the slab strip) directions, and the rotations along these axes were restrained in the central support. In the other two supports only the translational movements and the rotation along the vertical axis were restrained. To evaluate the rotation of the supports in which the load cells were installed, two linear displacement transducer were used, LVDT 61531 and LVDT 50855 at the central support, and LVDT 31923 and LVDT 47789, at the right support, respectively (see Figure 3.13).

To monitor the strain variation in the steel bars, concrete and CFRP laminates, the arrangements of strain gauges (SGs) represented in Figures 3.14 to 3.16 were adopted. Eleven SGs were installed in steel bars, seven of them in steel bars at top surface in the hogging region (SG1 to SG7), and the other four in steel bars at bottom surface in the sagging regions (SG8 to SG11). Six SGs were applied at the concrete surface in the compression regions (SG12 to SG17). Finally, three SGs were installed along one CFRP laminate in both sagging regions (SG18 to SG20 and SG21 to SG23), and three SGs (SG24 to SG26) were bonded along one CFRP laminate in the hogging region. In this experimental program FLA-3-11, BFLA-5-3 and PFL-30-11 strain gauges from TML (TML, 2004) were used in steel bars, CFRP laminates and concrete, respectively. The main technical characteristics of the used displacement transducers are indicated in Table 3.6.

3.2.3 Materials characterization

3.2.3.1 Concrete ready-mixes

Further details regarding the compressive strength of the manufactured concretes and the detailed concrete mix proportions and the main properties of the ordinary ready-mix

concretes used in the construction of the slab strips can be found in Annex 3.4. Cylinder specimens with a diameter of 150 mm and a height of 300 mm were used to obtain the compressive strength and the Young's modulus according to LNEC-E397 (1993). Table 3.7 shows detailed information regarding the compressive properties of the three concrete mixes at the age of 28 days and at the testing age of the slab strips.

3.2.3.2 Reinforcing steel

To characterize the steel reinforcement bars, uniaxial tensile tests were conducted according to the standard procedures of ASTM A370 (2002). The mechanical properties of the steel reinforcement bars, obtained from three coupon specimens for each bar diameter, are indicated in Table 3.8. More details can be found in Bonaldo (2008).

3.2.3.3 CFRP laminates

The results for the ultimate tensile stress and tensile strain, as well as the modulus of elasticity of the CFRP samples tested are included in Table 3.9. Unidirectional pultruded CFRP laminates, supplied by "S&P Clever Reinforcement Ibérica Company", were used in this study, and their tensile behaviour was assessed by performing uniaxial tensile tests carried out according to ISO 527-1 (1993) and ISO 527-5 (1993) recommendations.
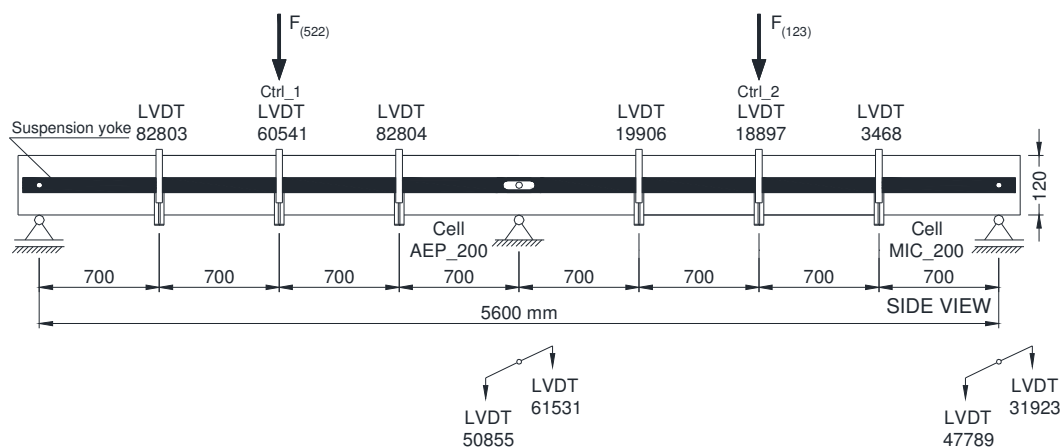
Figure 3.13: Displacement transducers (LVDTs). Dimensions in mm.

Table 3.5: Geometry, reinforcement and strengthening details of the cross sections of the slab strips.

ID	η	Increase of the loading carrying capacity	Cross-Section S_1-S_1'	Number of CFRP laminates at S	$\rho_{l,eq}^{S}$ (%)	Cross-Section S_2-S_2'	Number of CFRP Laminates at H	$\rho_{l,eq}^{H}$ (%)
HS Series	15%	0%	A_s' = 2ϕ12mm A_s = 4ϕ12mm + 3ϕ8mm	0	1.71	A_s = 5ϕ12mm A_s' = 2ϕ12mm + 1ϕ8mm	0	1.60
		25%		1 x 1.4 x 10 mm^2 + 2 x 1.4 x 20 mm^2	1.85		4 x 1.4 x 20 mm^2	1.83
	30%	0%	A_s' = 2ϕ12mm A_s = 3ϕ12mm + 4ϕ10mm	0	1.85	A_s = 4ϕ12mm A_s' = 2ϕ10mm + 1ϕ12mm	0	1.28
		25%		2 x 1.4 x 10 mm^2 + 2 x 1.4 x 20 mm^2	2.02		2 x 1.4 x 20 mm^2	1.39
		50%		1 x 1.4 x 10 mm^2 + 6 x 1.4 x 20 mm^2	2.22		3 x 1.4 x 20 mm^2	1.45
	45%	0%	A_s' = 2ϕ10mm A_s = 6ϕ12mm + 1ϕ8mm	0	2.07	A_s = 3ϕ10mm + 2ϕ8mm A_s' = 2ϕ12mm + 1ϕ8mm	0	0.95
		25%		2 x 1.4 x 20 mm^2	2.20		2 x 1.4 x 10 mm^2	1.00
		50%		6 x 1.4 x 20 mm^2	2.43		2 x 1.4 x 20 mm^2	1.06

$\rho_{l,eq} = A_s / (bd_s) + (A_f E_f / E_s) / (bd_f)$

Table 3.6: Technical characteristics of the LVDTs, extracted from technical datasheet (RDP, 1995).

LVDT device	Linear range (mm)	Linearity deviation (%)
82803	±25	±0.09
60541[a]	±50	±0.31
82804	±25	±0.10
19906	±25	±0.07
18897[b]	±50	±0.08
3468	±25	±0.08
47789	±2.5	±0.06
61531	±2.5	±0.09
50855	±2.5	±0.09
31923	±2.5	±0.16

[a] Control the actuator placed at the left span (F_{522})

[b] Control the actuator placed at the right span (F_{123})
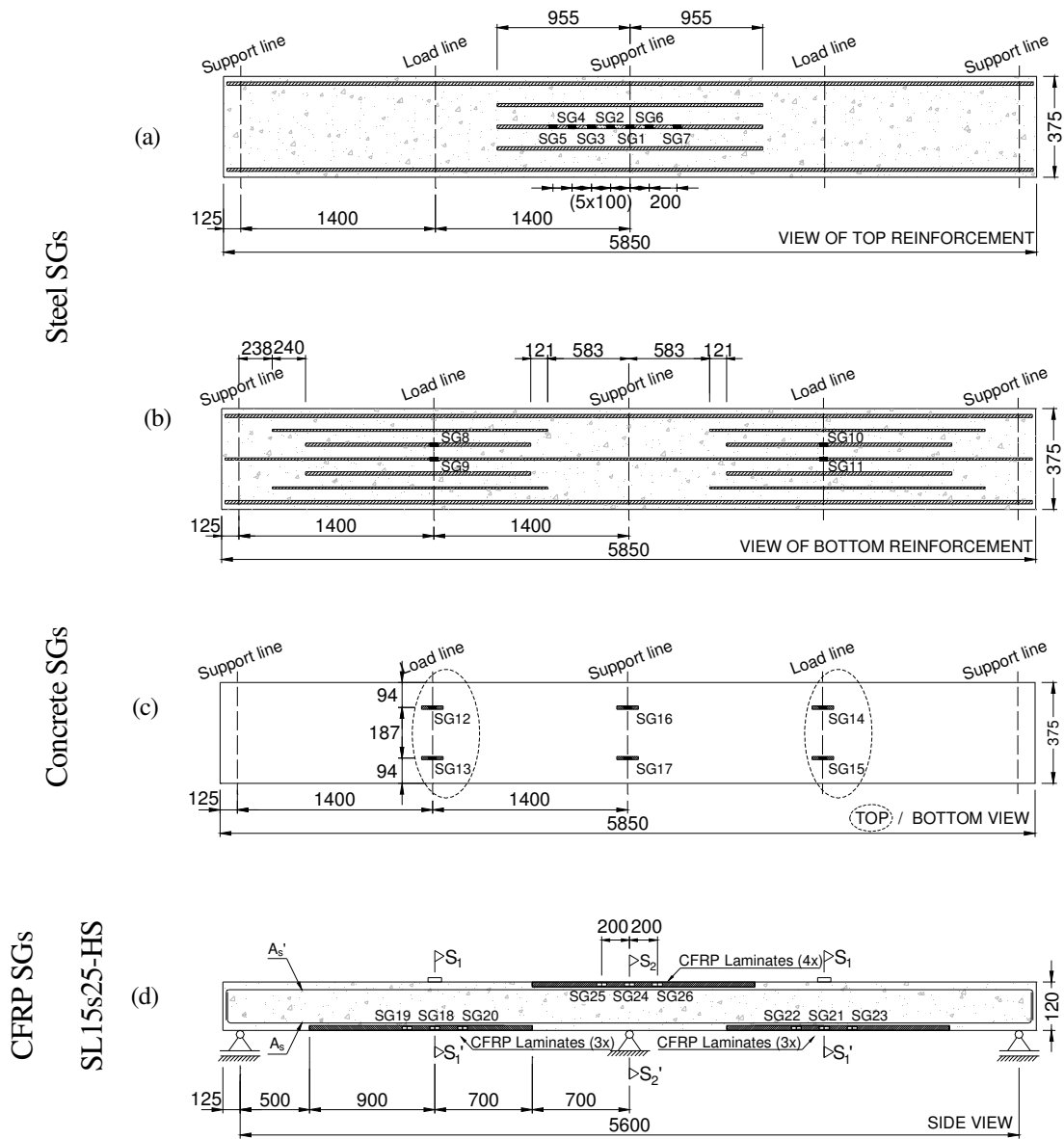
Figure 3.14: Arrangement of strain gages in: (a) steel bars at hogging region and (b) steel bars at sagging region; (c) concrete slab surfaces and (d) CFRP laminates for SL15s25-HS.
Dimensions in mm.
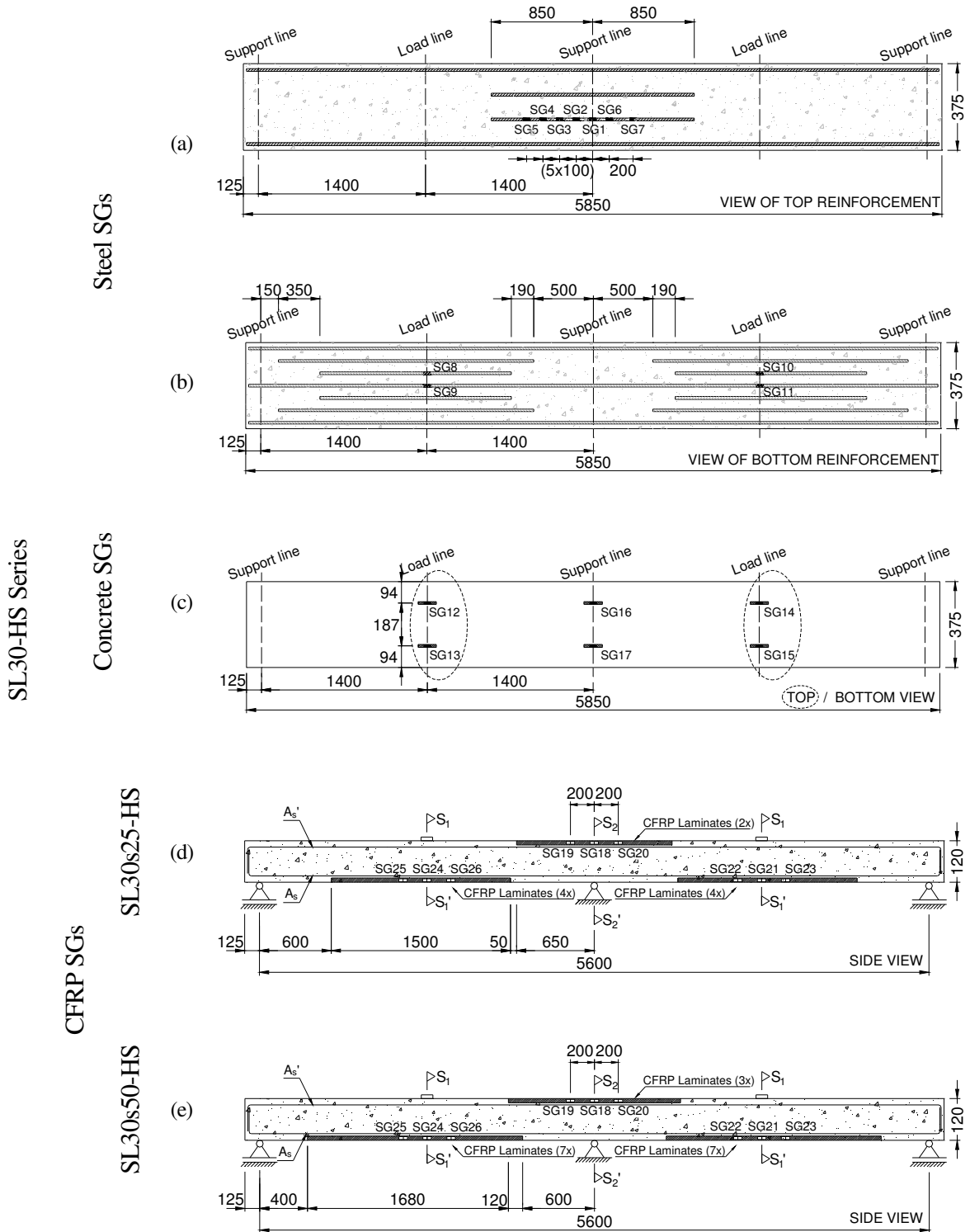
Figure 3.15: Arrangement of strain gages in: (a) steel bars at hogging region and (b) steel bars at sagging region; (c) concrete slab surfaces; CFRP laminates for (d) SL30s25-HS and (e) SL30s50-HS. Dimensions in mm.
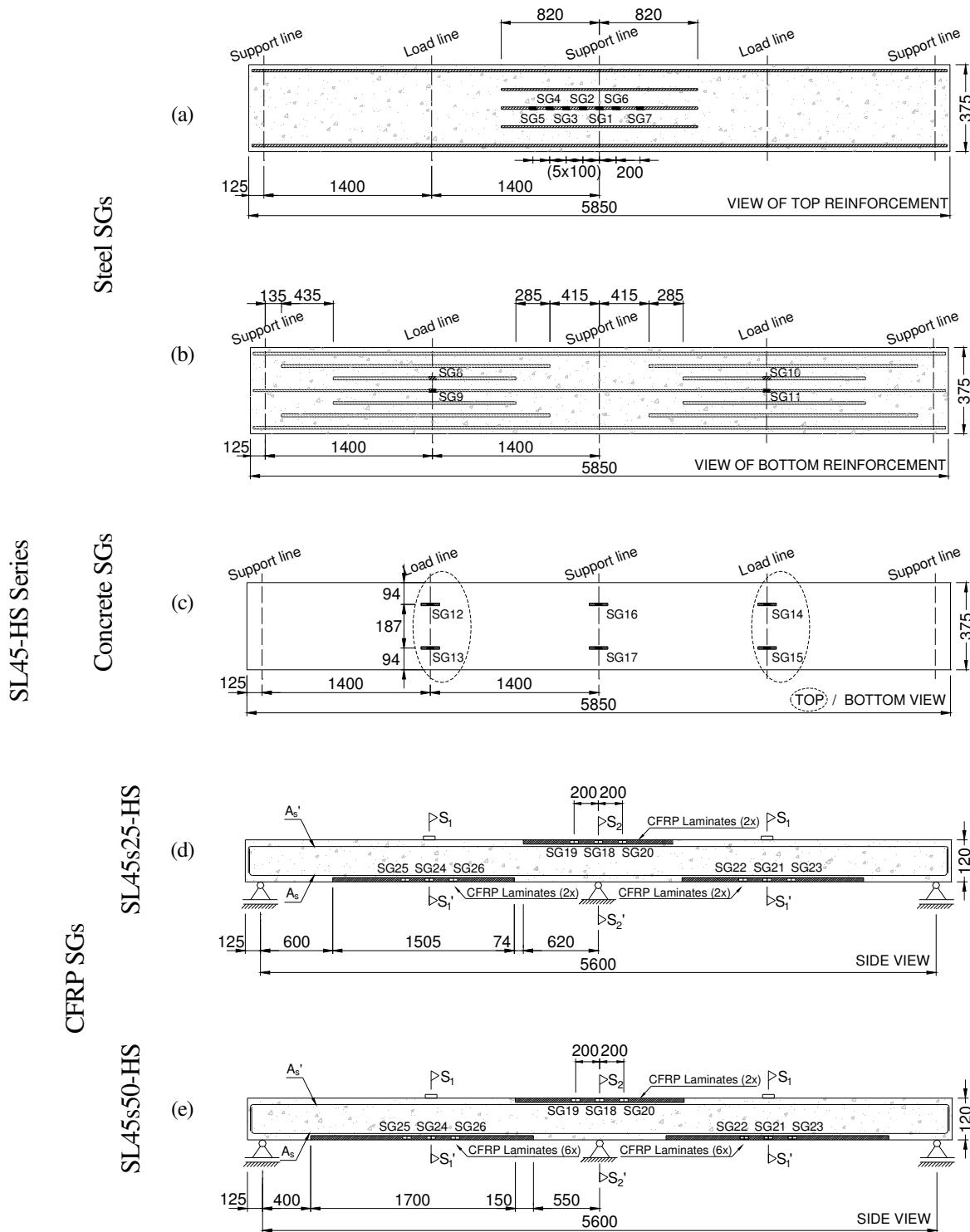
Figure 3.16: Arrangement of strain gages in: (a) steel bars at hogging region and (b) steel bars at sagging region; (c) concrete slab surfaces; CFRP laminates for (d) SL45s25-HS and (e) SL45s50-HS. Dimensions in mm.

Table 3.7: Properties of concrete.

At 28 days			At the slabs testing age			
Slab ID	f_{cm} (N/mm^2)	E_{cm} (kN/mm^2)	Slab ID	Age (days)	f_{cm} (N/mm^2)	E_{cm} (kN/mm^2)
SL15-HS	26.37 (1.06)	24.29 (1.18)	SL15-HS	56	30.36 (0.33)	24.54 (0.83)
			SL15s25-HS	99	32.64 (1.24)	25.89 (1.12)
SL30-HS	28.40 (1.61)	29.83 (0.29)	SL30-HS	34	30.10 (1.08)	31.52 (0.86)
			SL30s25-HS	98	32.59 (1.15)	30.62 (2.42)
			SL30s50-HS	112	32.90 (0.80)	31.22 (1.44)
SL45-HS	42.38 (0.03)	28.32 (1.54)	SL45-HS	35	42.25 (1.12)	27.97 (1.12)
			SL45s25-HS	434	45.14 (1.28)	30.10 (1.30)
			SL45s50-HS	514	44.80 (0.89)	31.05 (0.80)
(value) = Standard deviation in MPa, f_{cm} = mean cylinder compressive strength, E_{cm} = modulus of elasticity						

Table 3.8: Mechanical properties of the reinforcing steel.

Steel bar diameter (ϕs)	Sample ID	Modulus of elasticity (kN/mm^2)	Yield stress (0.2 %)[a] (N/mm^2)	Strain at yield stress[b]	Tensile strength (N/mm^2)
8 mm	1	195.40	423.93	0.0024	578.30
	2	203.16	420.29	0.0023	576.93
	3	203.84	419.83	0.0023	581.03
	Average Std. Dev.	200.80 (2.33 %)	421.35 (0.53 %)	0.0023 (2.65 %)	578.75 (0.36 %)
10 mm	1	183.33	463.37	0.0027	576.44
	2	175.86	441.80	0.0027	573.82
	3	175.52	435.68	0.0027	577.61
	Average Std. Dev.	178.23 (2.48 %)	446.95 (3.25 %)	0.0027 (0.45 %)	575.95 (0.34 %)
12 mm	1	192.20	427.83	0.0024	528.41
	2	200.11	449.69	0.0024	545.41
	3	202.76	449.89	0.0024	545.82
	Average Std. Dev.	198.36 (2.77 %)	442.47 (2.87 %)	0.0024 (0.19%)	539.88 (1.84%)

[a] Yield stress determined by the "Offset Method", according to ASTM 370 (2002)
[b] Strain at yield point, for the 0.2 % offset stress
(value) Coefficient of Variation (COV) = (Standard deviation/Average) x 100

Table 3.9: Mechanical properties of the CFRP laminates.

CFRP laminate cross section height	Sample ID	Ultimate tensile stress (N/mm^2)	Ultimate tensile strain (‰)	Modulus of Elasticity a (kN/mm^2)
10 mm	1	2879.13	18.45	156.100
	2	2739.50	17.00	158.800
	3	2952.00	17.70	166.600
	4	2942.32	17.81	153.620
	5	2825.20	17.40	161.400
	Average	2867.63	17.67	159.304
	Std. Dev.	88.10 (3.07%)	0.54 (3.04%)	5.01 (3.15%)
20 mm	1	2858.799	18.37303	155.5976
	2	2782.862	17.6256	157.8875
	3	2706.926	17.28808	156.5775
	Average	2782.86	17.76	156.69
	Std. Dev.	75.94 (2.73%)	0.56 (3.13%)	1.15 (0.73%)

[a]According to ISO 527-1 and ISO 527-5 (1993)
(value) Coefficient of Variation (COV) = (Standard deviation/Average) x 100

3.2.3.4 Epoxy adhesive

For the characterization of the tensile behaviour of the epoxy adhesive, uniaxial tensile tests were performed complying with the procedures outlined in ISO 527-2 (1993). For the elasticity modulus and tensile strength of the adhesive the values of, respectively, 7.91 GPa (5.16%) and 19.19 MPa (15.59%) were obtained, where the values between round brackets correspond to the coefficient of variation. More details about the specimen's dimensions and test procedures of the used epoxy adhesive can be found in Bonaldo (2008).

3.2.4 Specimens preparation and strengthening

Eight reinforced concrete slab strips were grouped in three series of two slabs for the SL15-HS series and three slabs for the SL30-HS and SL45-HS series. Each series was cast at distinct periods. For each concrete batch, sixteen cylindrical concrete specimens, of 150 mm diameter and 300 mm depth were cast, four for compressive strength control at 28 days of age and twelve for compressive strength control at the slabs testing age. The moulds used for casting the slabs are shown in Figure 3.17a. For each concrete batch, the slabs were cast in two layers (Figure 3.17b), each one vibrated using an electrical concrete poker vibrator with a 25 mm tip and 50 Hz frequency (Figure 3.17c).

After casting the slabs and the cylinder concrete specimens, their top surfaces were immediately finished manually using a smooth plastic float and were covered with wet

burlap sacks, which were kept wet for two days. After this curing period, the slabs and the cylinders specimens were removed from the moulds and maintained in natural laboratory environmental conditions up to 28 days. Concerning to the NSM strengthening, the first step of the process consisted in opening the slits for the installation of the CFRP laminates, by using a conventional diamond saw cut machine (Figure 3.18).

The slits had a width that varied between 4.5 and 4.6 mm and a depth of 15 mm or 27 mm, depending on the depth of the cross section of the used CFRP laminate, 10 or 20 mm, respectively. To eliminate the dust resultant from the sawing process, the slits were cleaned using compressed air before bonding the laminates to the concrete into the slits. The CFRP laminates were cleaned with acetone to remove any possible dirt. Finally, the slits were filled with the epoxy adhesive using a spatula, and the CFRP laminates were introduced into the slits.

| (a) | (b) |
| (c) | (d) |

Figure 3.17: Slab strips specimens: formwork setup (a), concrete casting (b), concrete vibration (c) and final aspect of the slab strips (d).

(a)

(b)

(c)

(d)

(e)

(f)

Figure 3.18: Strengthening procedures.

3.2.5 Results and discussion

The results and discussion of the eight tested slab strips are presented in this chapter, focusing on the load-displacement response, load carrying capacity, failure mode, slab's ductility and moment redistribution capacity.

3.2.5.1 Unstrengthened slab strips

<u>**SL15-HS**</u>

The unstrengthened SL15-HS slab strip is shown in Figure 3.19 before and after having been tested. The span deflections, steel reinforcement strains, concrete strains, support reactions, and rotation of the reaction devices are shown in Figures 3.20 to 3.25, respectively.

<div align="center">(a)   (b)</div>

Figure 3.19: SL15-HS specimen before (a) and after having been tested (b).
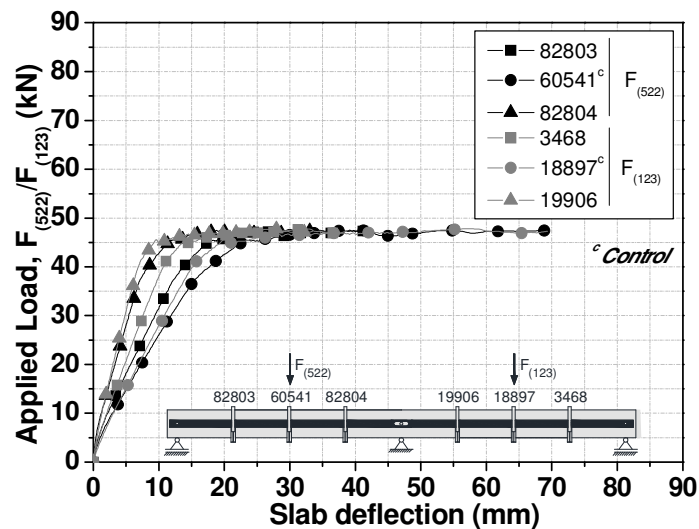
Figure 3.20: Relationship between applied load and deflections at spans of the SL15-HS.
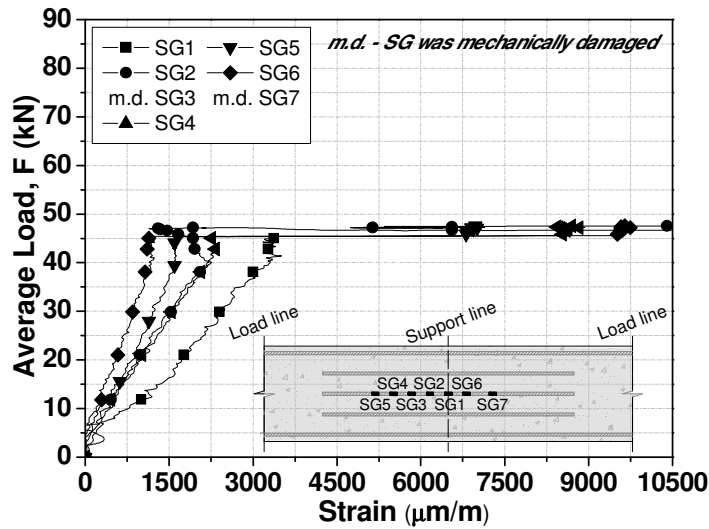
Figure 3.21: Relationship between average load and tensile strains on the negative longitudinal steel reinforcement for the SL15-HS slab strip.
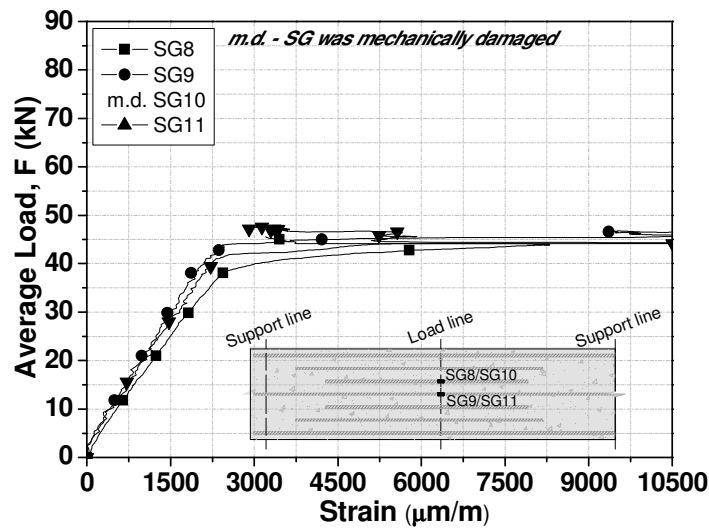
Figure 3.22: Relationship between average load and tensile strain on the positive longitudinal steel reinforcement for the SL15-HS slab strip.
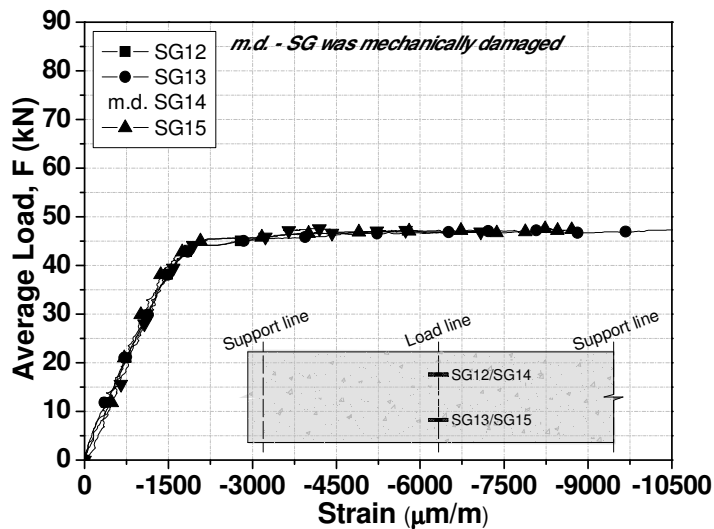
Figure 3.23: Relationship between average load and compressive strain on the concrete at sagging region for the SL15-HS slab strip.
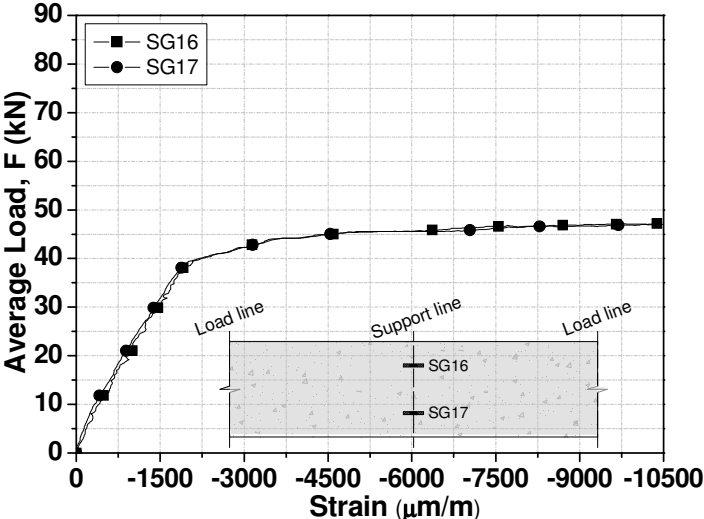
Figure 3.24: Relationship between average load and compressive strain
on the concrete at hogging region for the SL15-HS slab strip.
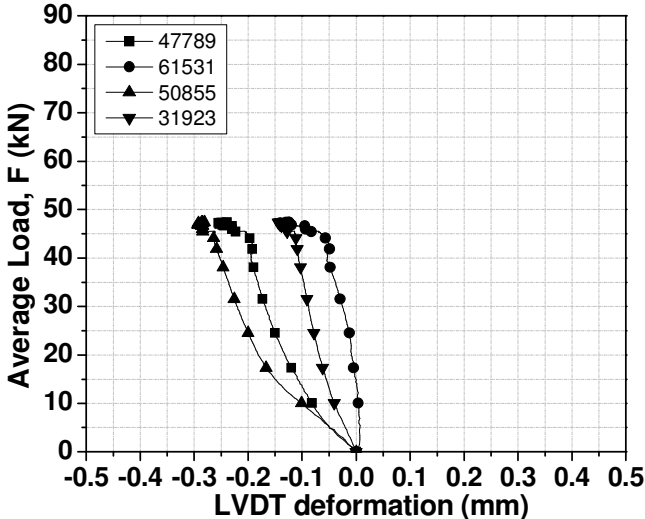
Figure 3.25: Relationship between average load and support devices rotation for the SL15-HS slab strip.

SL30-HS

The unstrengthened SL30-HS slab strip is shown in Figure 3.26 before and after having been tested. The span deflections, steel reinforcement strains, concrete strains, support reactions, and rotation of the reaction devices are shown in Figures 3.27 to 3.33, respectively

(a)   (b)

Figure 3.26: SL30-HS specimen before (a) and after having been tested (b).
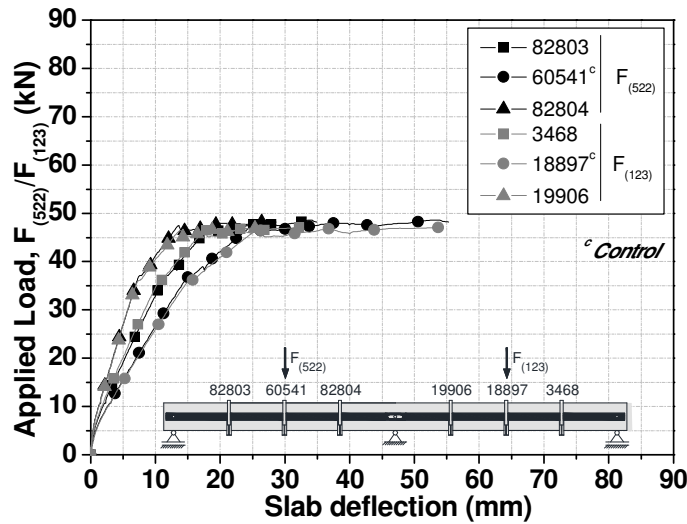
Figure 3.27: Relationship between applied load and deflections at spans of the SL30-HS.
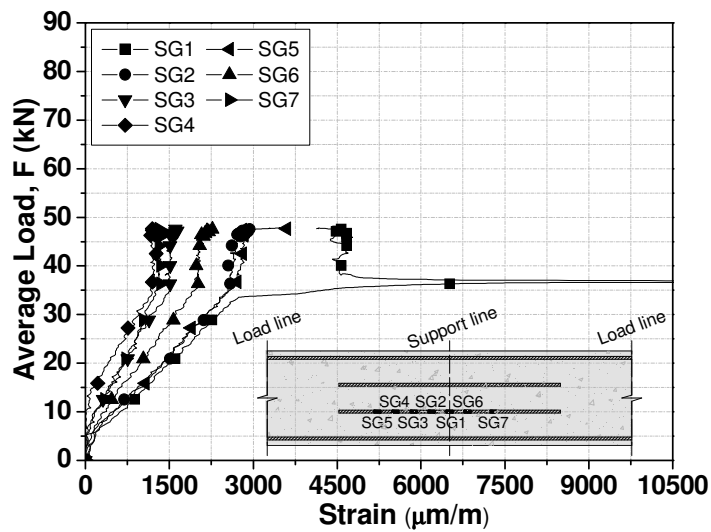
Figure 3.28: Relationship between average load and tensile strain on the
negative longitudinal steel reinforcement for the SL30-HS slab strip.
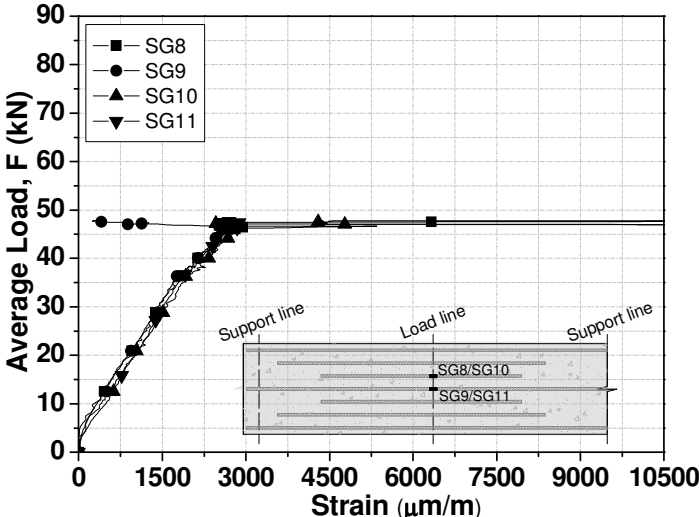
Figure 3.29: Relationship between average load and tensile strain on the positive longitudinal steel reinforcement for the SL30-HS slab strip
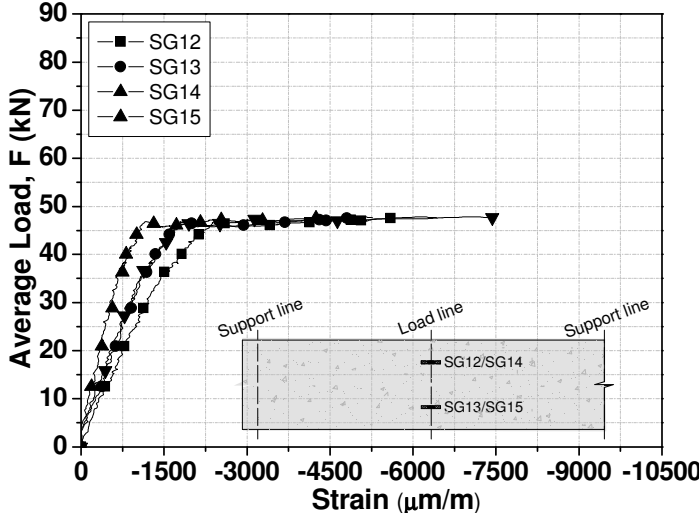
Figure 3.30: Relationship between average load and compressive strain on the concrete at sagging region for the SL30-HS slab strip.
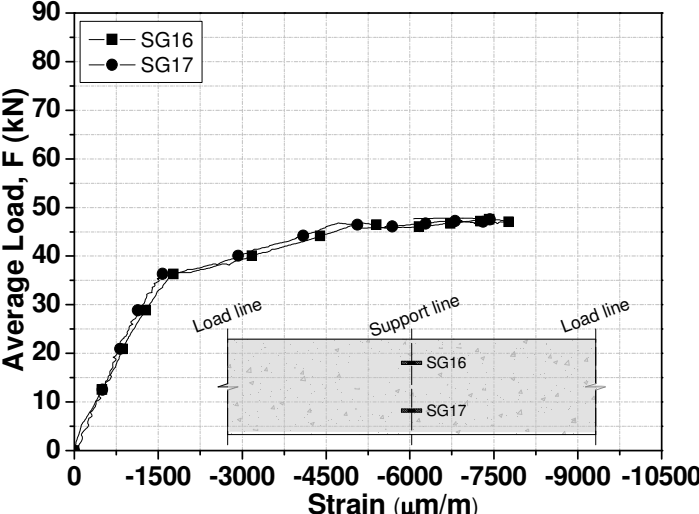
Figure 3.31: Relationship between average load and compressive strain on the concrete at hogging region for the SL30-HS slab strip.
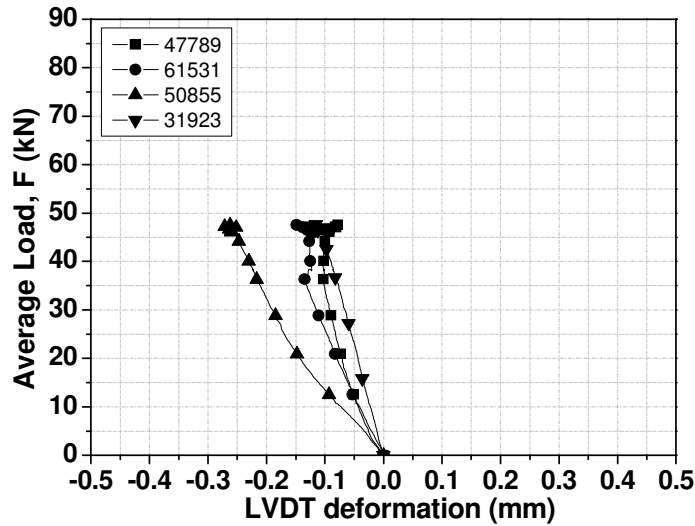
Figure 3.32: Relationship between average load and support devices rotation for the SL30-HS slab strip.
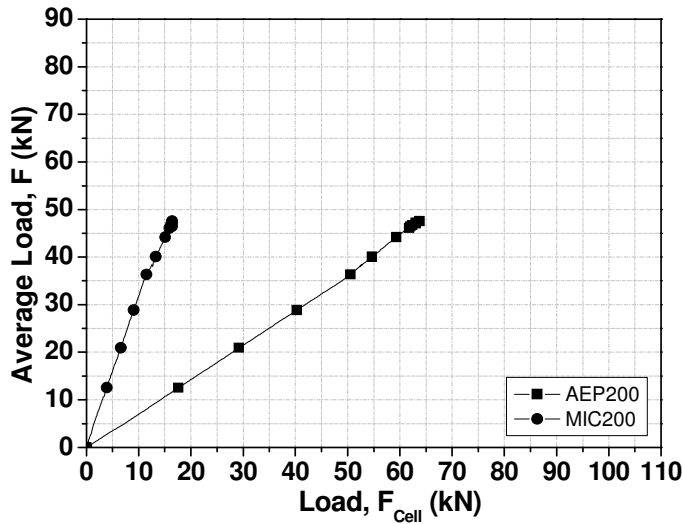
Figure 3.33: Relationship between the applied load and support reaction for the SL30-HS slab strip.

SL45-HS

The unstrengthened SL45-HS slab strip is shown in Figure 3.34 before and after having been tested. The span deflections, steel reinforcement strains, concrete strains, support reactions, and rotation of the reaction devices are shown in Figures 3.35 to 3.41, respectively.

(a)   (b)
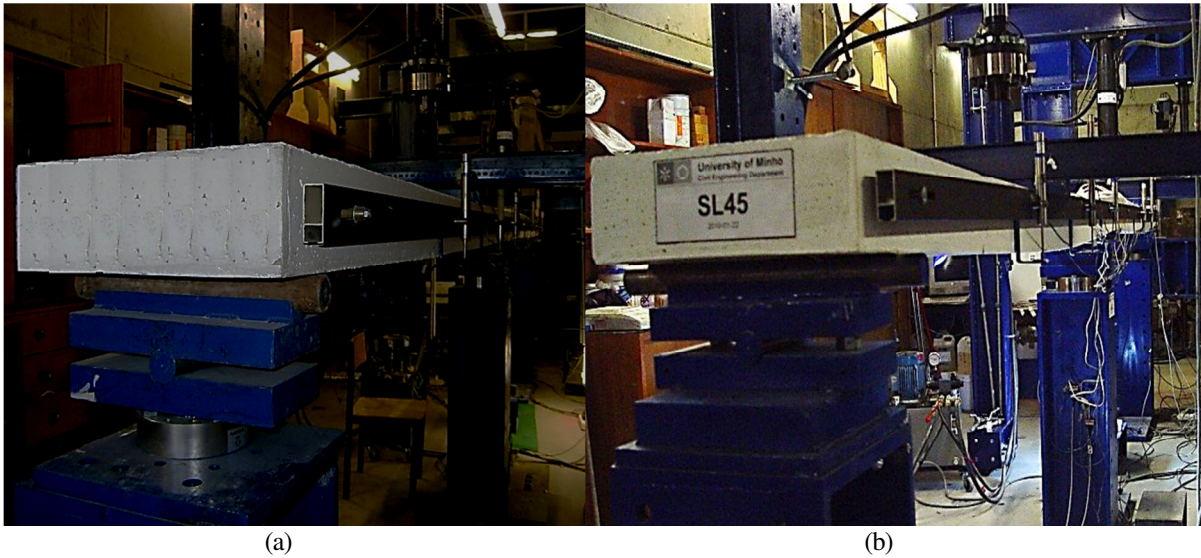
Figure 3.34: SL45-HS specimen before (a) and after having been tested (b).
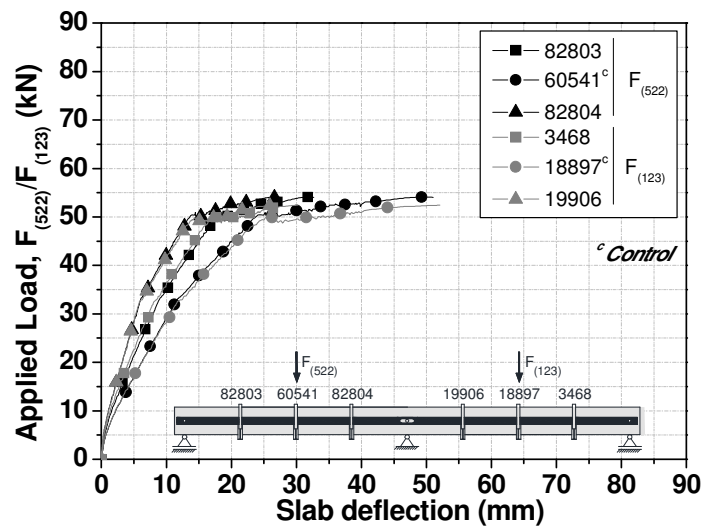
Figure 3.35: Relationship between applied load and deflections at spans of the SL45-HS.
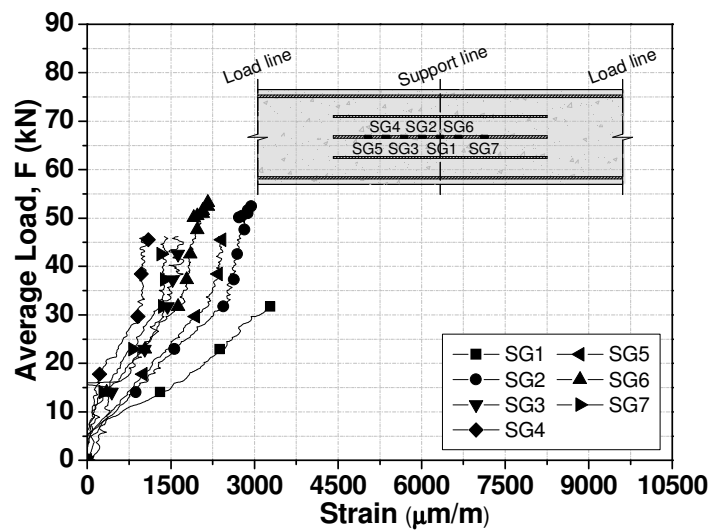
Figure 3.36: Relationship between average load and tensile strain on the
negative longitudinal steel reinforcement for the SL45-HS slab strip.
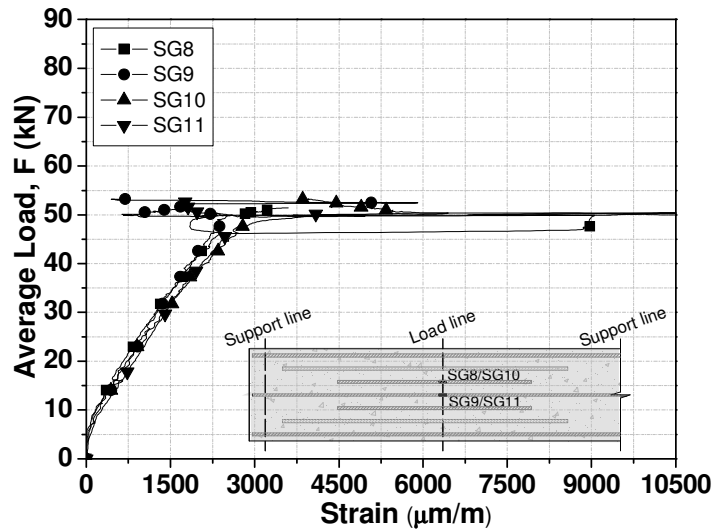
Figure 3.37: Relationship between average load and tensile strain on the positive longitudinal steel reinforcement for the SL45-HS slab strip.
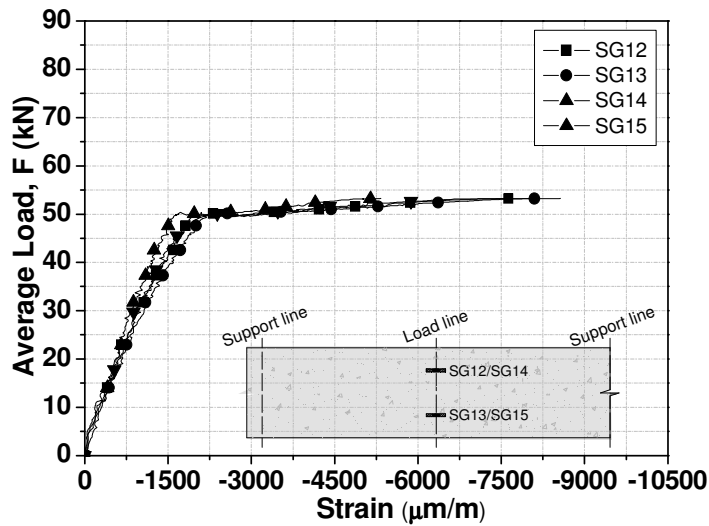
Figure 3.38: Relationship between average load and compressive strain on the concrete at sagging region for the SL45-HS slab strip.
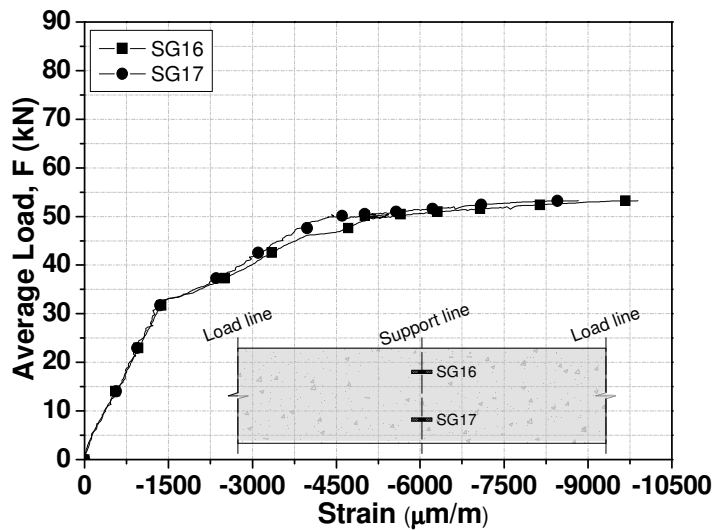
Figure 3.39: Relationship between average load and compressive strain on the concrete at hogging region for the SL45-HS slab strip.
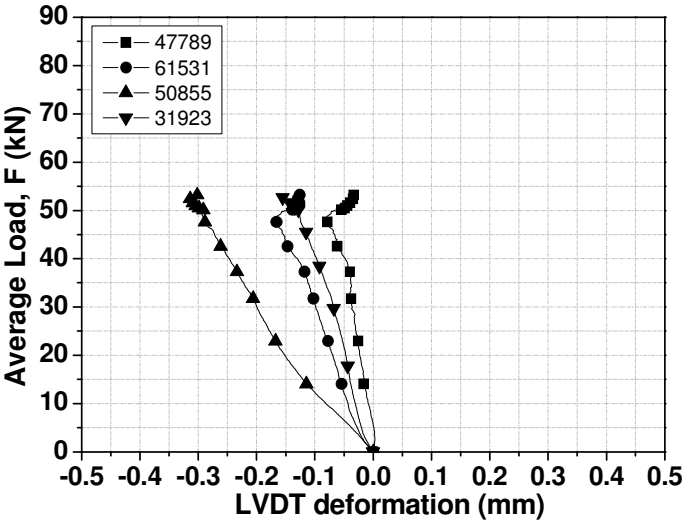
Figure 3.40: Relationship between average load and support devices rotation for the SL45-HS slab strip.
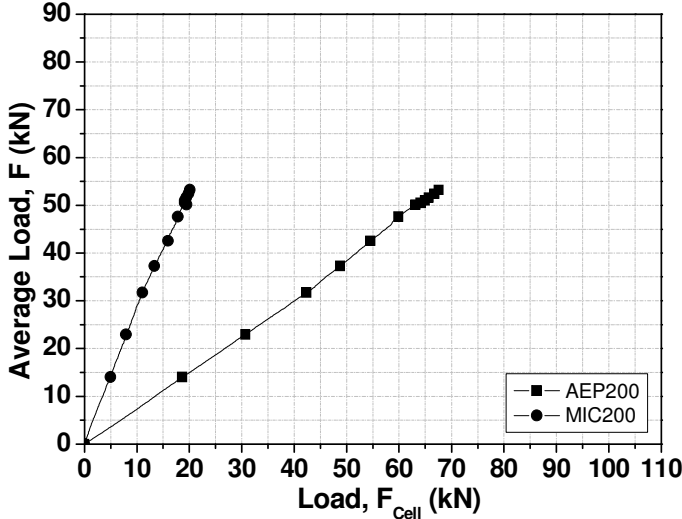
Figure 3.41: Relationship between the applied load and support reaction for the SL45-HS slab strip.

3.2.5.2 Strengthened slab strips

SL15s25-HS

The strengthened SL15s25-HS slab strip is shown in Figure 3.42 before and after having been tested. The span deflections, steel reinforcement strains, concrete strains, support reactions, and rotation of the reaction devices are shown in Figures 3.43 to 3.51, respectively.

(a)   (b)

Figure 3.42: SL15s25-HS specimen before (a), and after having been tested (b).
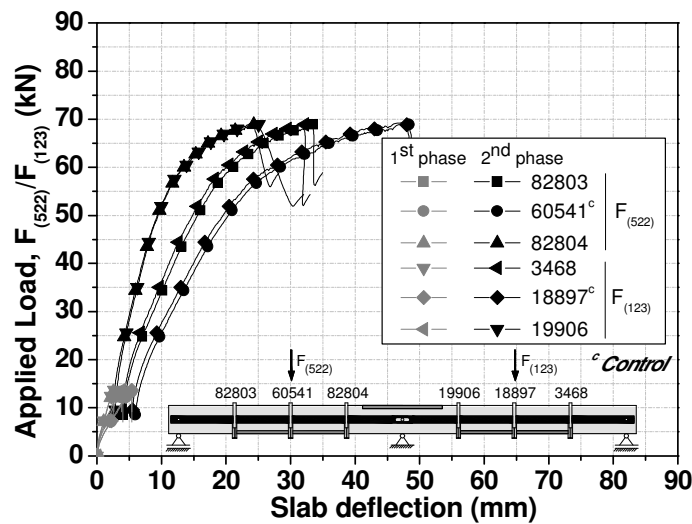
Figure 3.43: Relationship between applied load and deflections at spans of the SL15s25-HS.
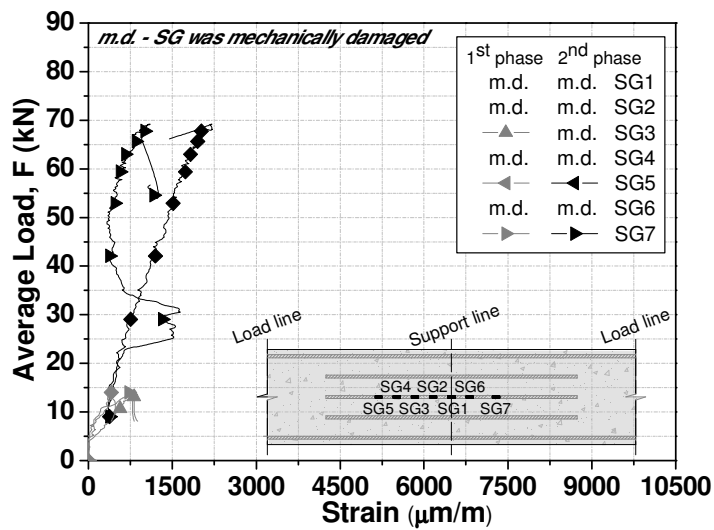
Figure 3.44: Relationship between average load and tensile strain on the
negative longitudinal steel reinforcement for the SL15s25-HS slab strip.
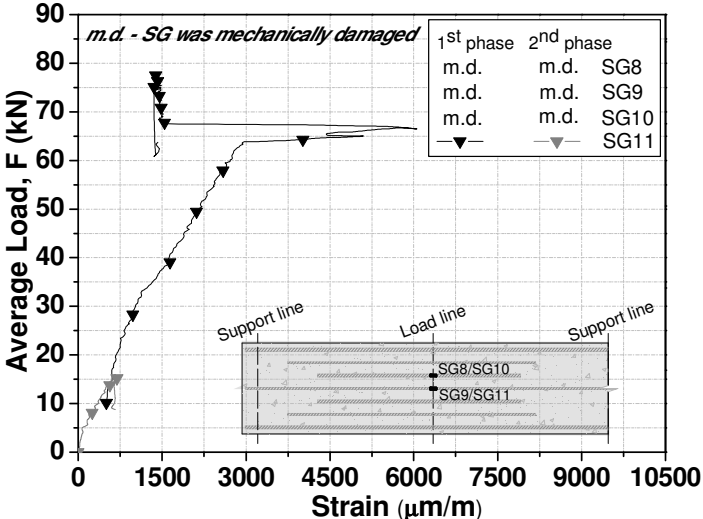
Figure 3.45: Relationship between average load and tensile strain on the positive longitudinal steel reinforcement for the SL15s25-HS slab strip.
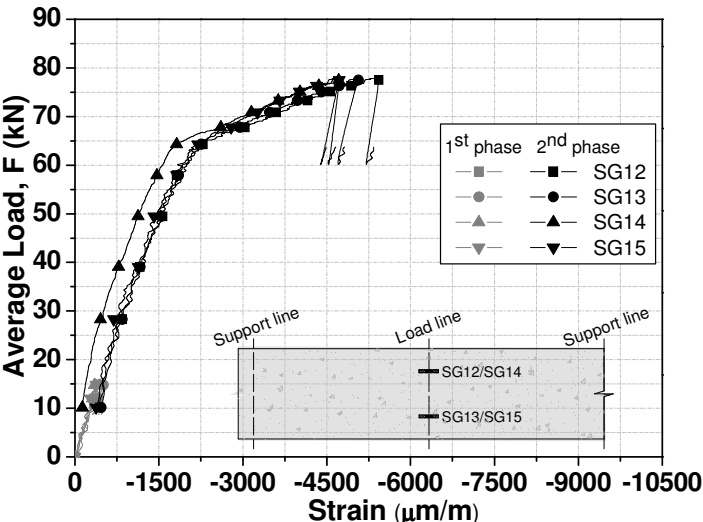
Figure 3.46: Relationship between average load and compressive strain on the concrete at sagging region for the SL15s25-HS slab strip.
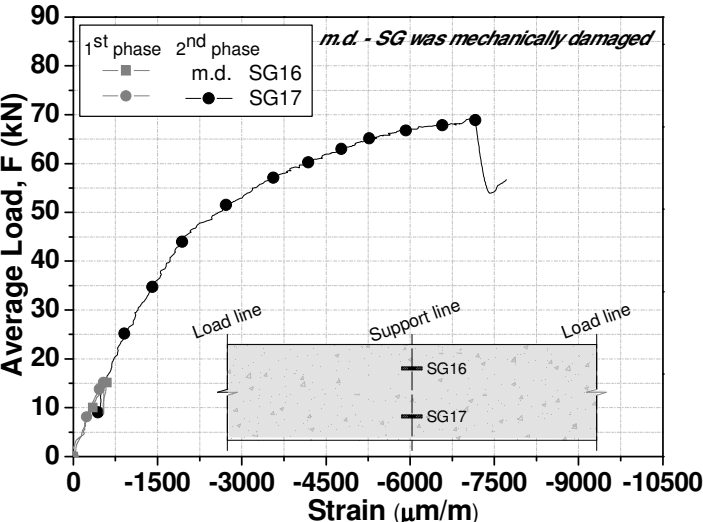
Figure 3.47: Relationship between average load and compressive strain on the concrete at hogging region for the SL15s25-HS slab strip.
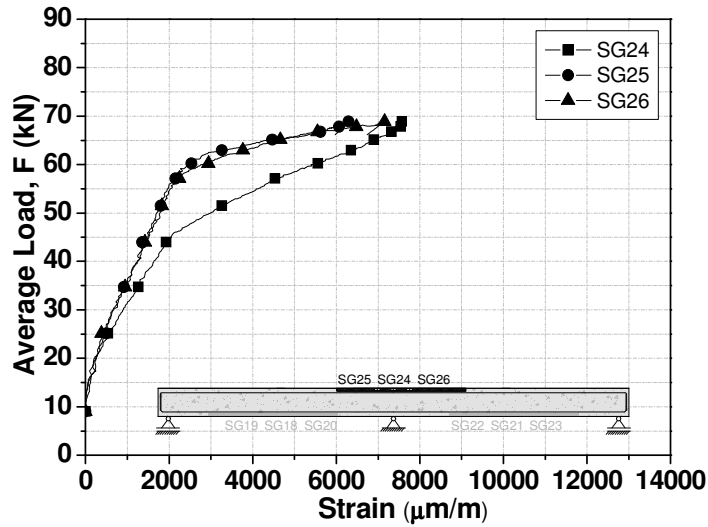
Figure 3.48: Relationship between average load and tensile strain
on the CFRP laminate at hogging region for the SL15s25-HS slab strip.
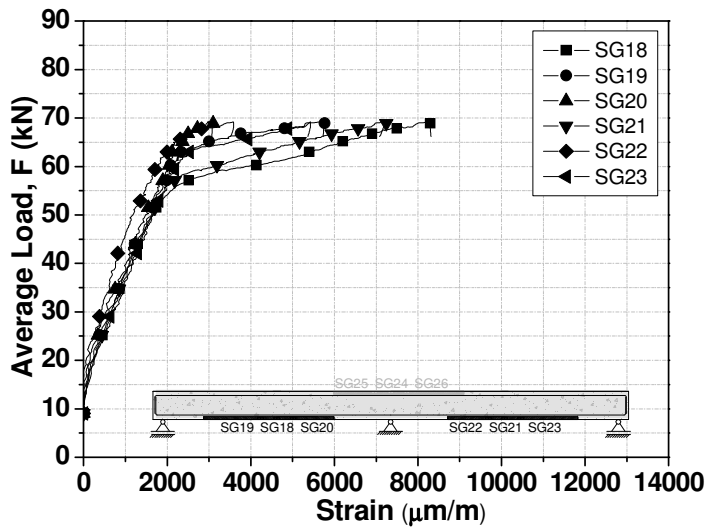
Figure 3.49: Relationship between average load and tensile strain
on the CFRP laminate at sagging regions for the SL15s25-HS slab strip.
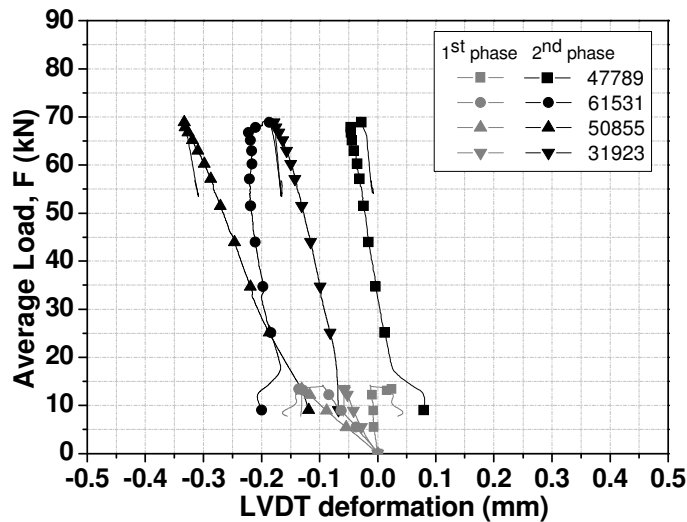
Figure 3.50: Relationship between average load and support devices rotation for the SL15s25-HS slab strip.
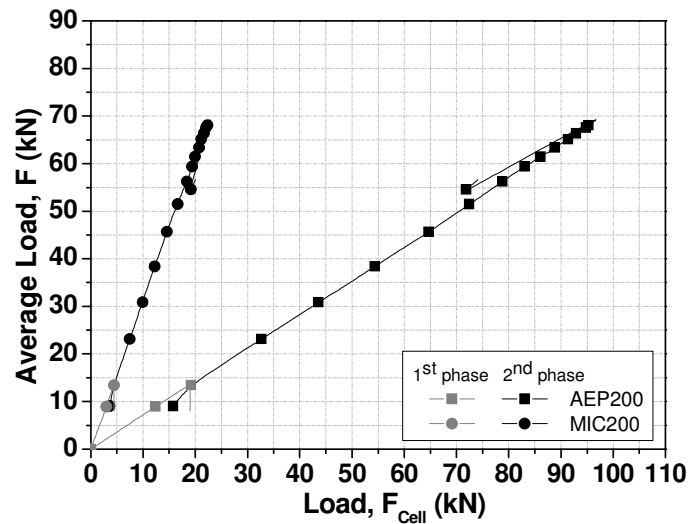
Figure 3.51: Relationship between the applied load and support reaction for the SL15s25-HS slab strip.

SL30s25-HS

The strengthened SL30s25-HS slab strip is shown in Figure 3.52 before and after having been tested. The deflections, steel reinforcement strains, concrete strains, support reactions, and rotation of the reaction devices are shown in Figures 3.53 to 3.61, respectively.span

(a)   (b)

Figure 3.52: SL30s25-HS specimen before (a) and after having been tested (b).
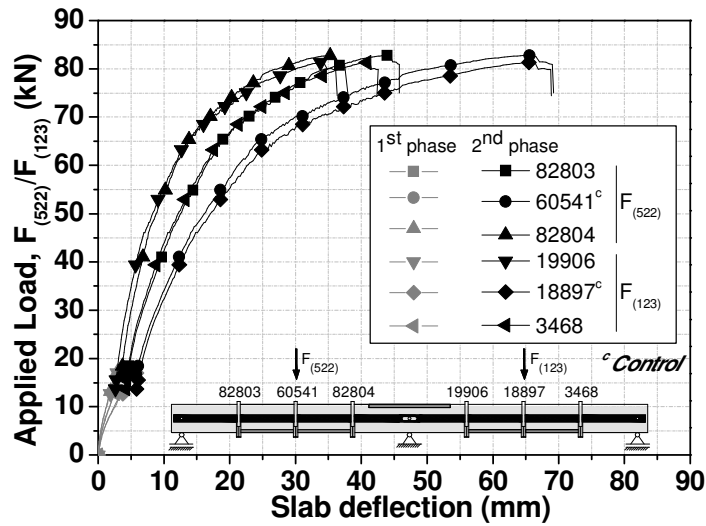
Figure 3.53: Relationship between applied load and deflections at spans of the SL30s25-HS.
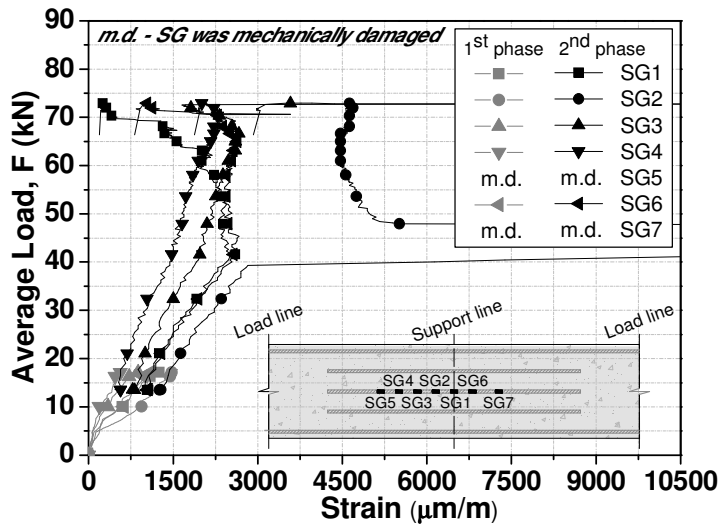
Figure 3.54: Relationship between average load and tensile strain on the
negative longitudinal steel reinforcement for the SL30s25-HS slab strip.
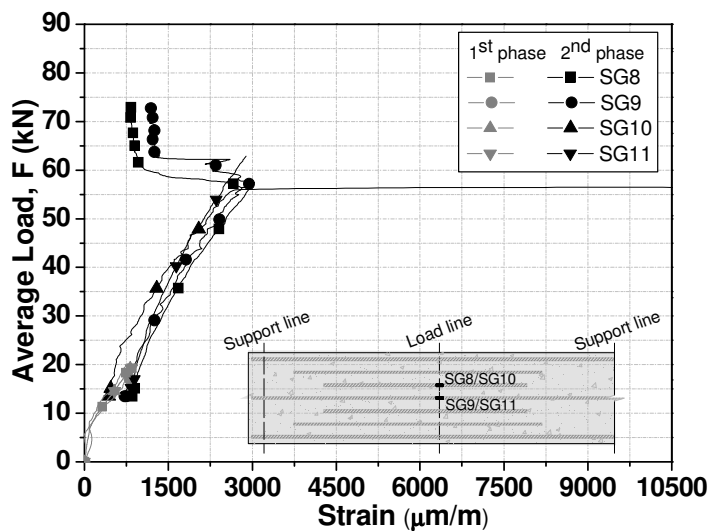
Figure 3.55: Relationship between average load and tensile strain on the
positive longitudinal steel reinforcement for the SL30s25-HS slab strip.
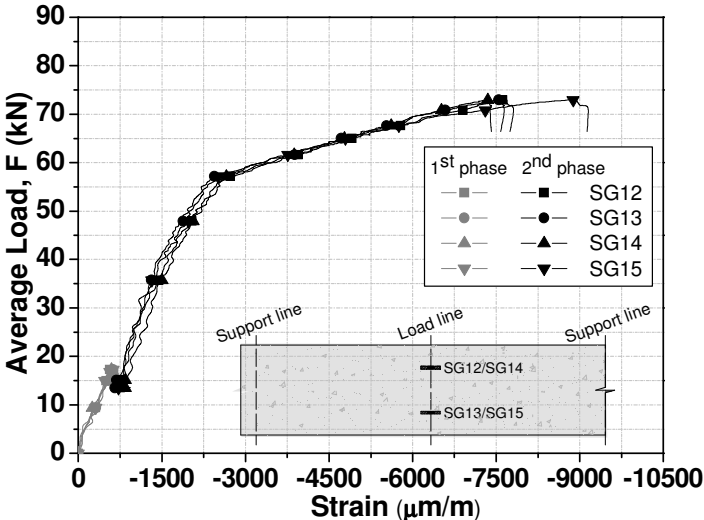
Figure 3.56: Relationship between average load and compressive strain on the concrete at sagging region for the SL30s25-HS slab strip.
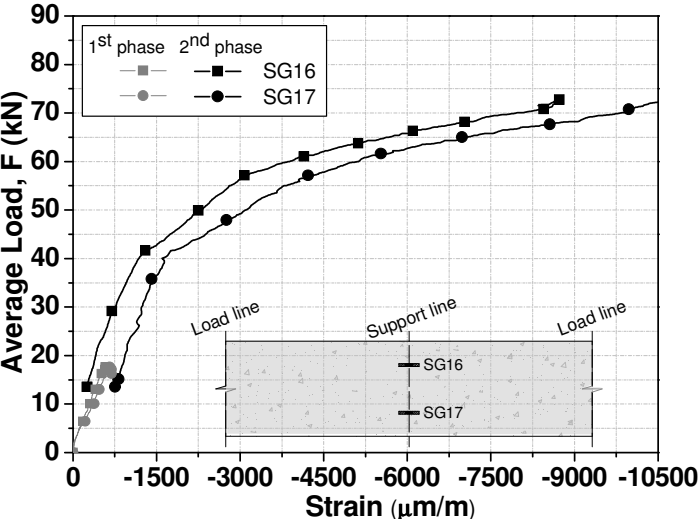
Figure 3.57: Relationship between average load and compressive strain on the concrete at hogging region for the SL30s25-HS slab strip.
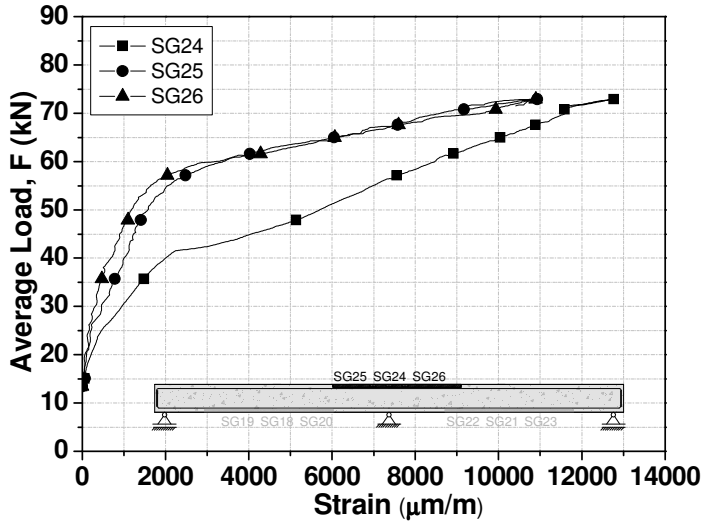
Figure 3.58: Relationship between average load and tensile strain on the CFRP laminate at hogging region for the SL30s25-HS slab strip.
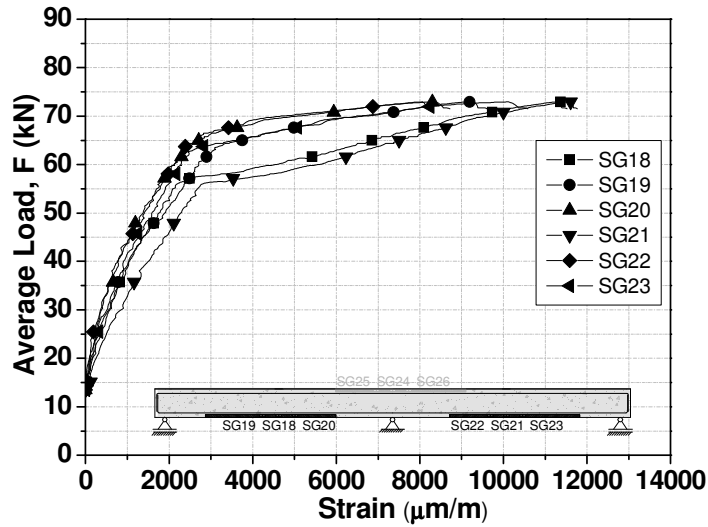
Figure 3.59: Relationship between average load and tensile strain on the
CFRP laminate at sagging regions for the SL15s30-HS slab strip.
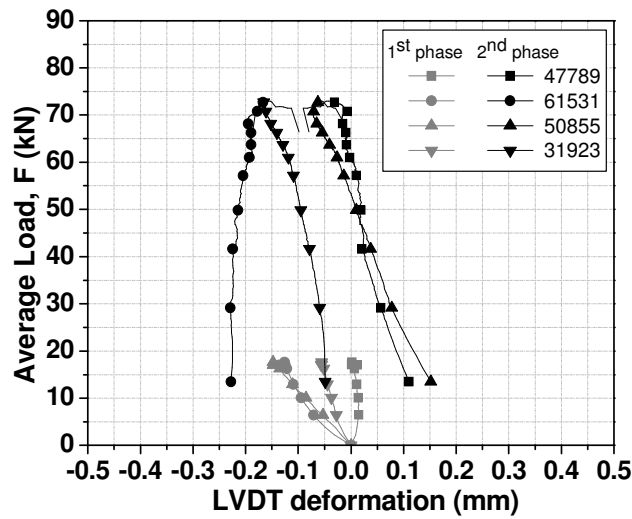
Figure 3.60: Relationship between average load and support devices rotation for the SL30s25-HS slab strip.
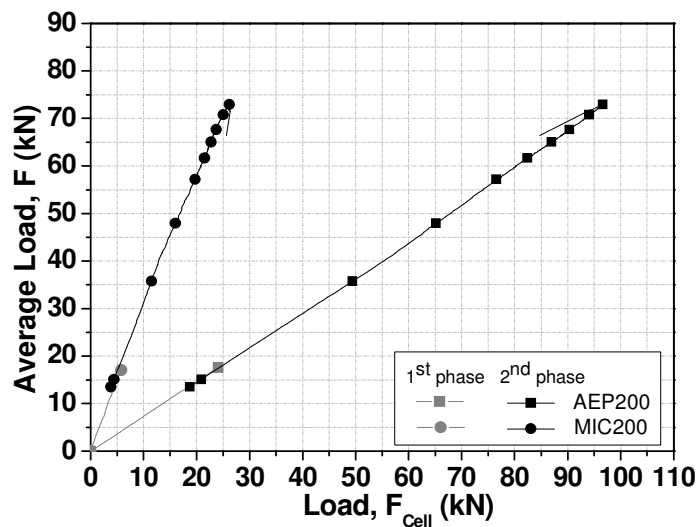
Figure 3.61: Relationship between the applied load and support reaction for the SL30s25-HS slab strip.

SL30s50-HS

The strengthened SL30s50-HS slab strip is shown in Figure 3.62 before and after having been tested. The span deflections, steel reinforcement strains, concrete strains, support reactions, and rotation of the reaction devices are shown in Figures 3.63 to 3.71, respectively.

(a) (b)

Figure 3.62: SL30s50-HS specimen before (a) and after having been tested (b).
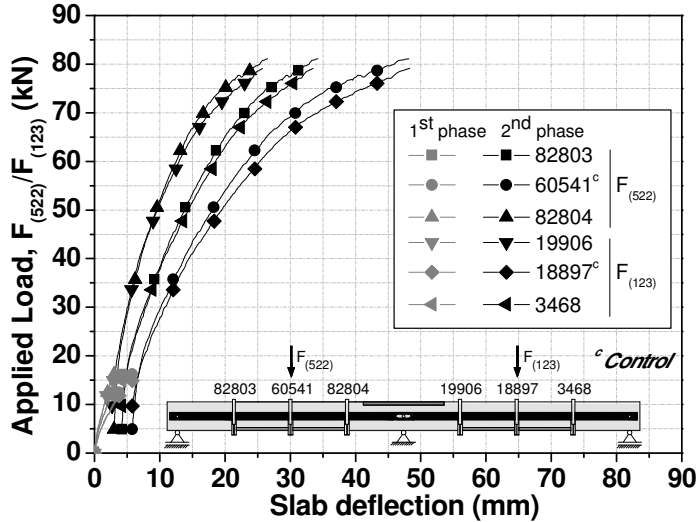
Figure 3.63: Relationship between applied load and deflections at spans of the SL30s50-HS.
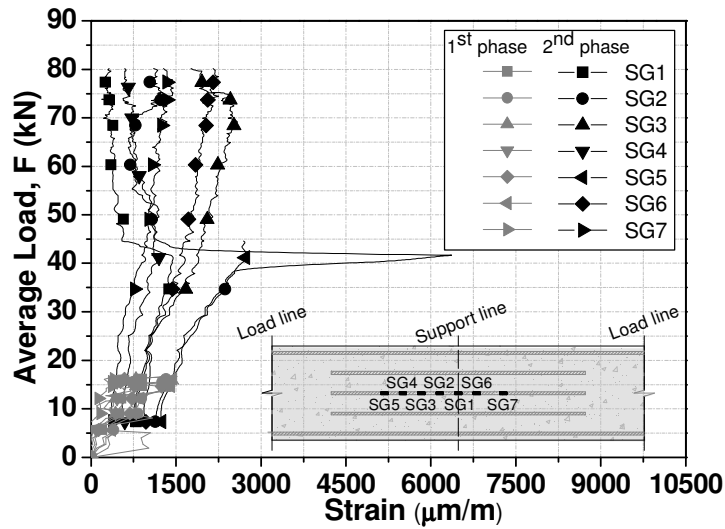
Figure 3.64: Relationship between average load and tensile strain
on the negative longitudinal steel reinforcement for the SL30s50-HS slab strip.
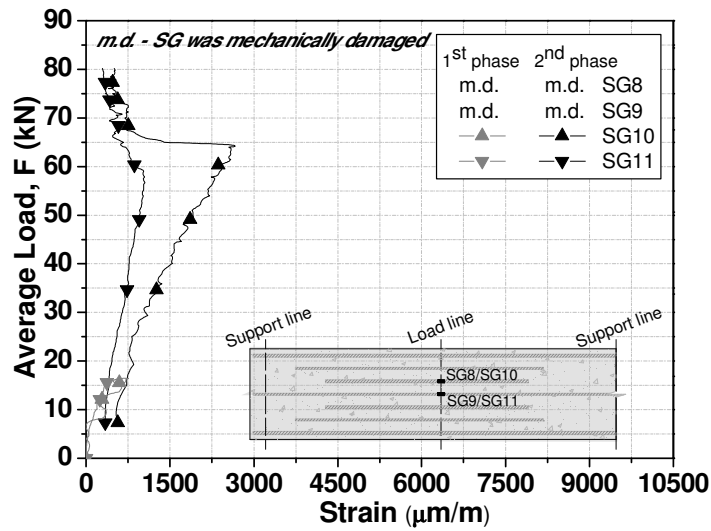
Figure 3.65: Relationship between average load and tensile strain
on the positive longitudinal steel reinforcement for the SL30s50-HS slab strip.
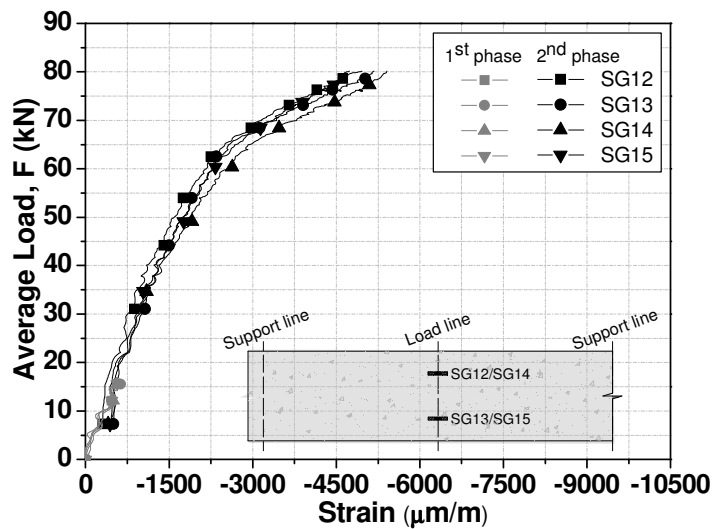
Figure 3.66: Relationship between average load and compressive strain
on the concrete at sagging region for the SL30s50-HS slab strip.
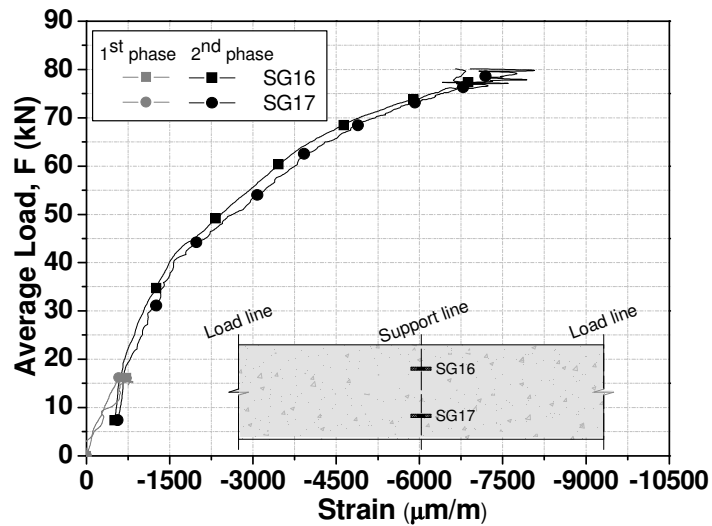
Figure 3.67: Relationship between average load and compressive strain
on the concrete at hogging region for the SL30s50-HS slab strip.
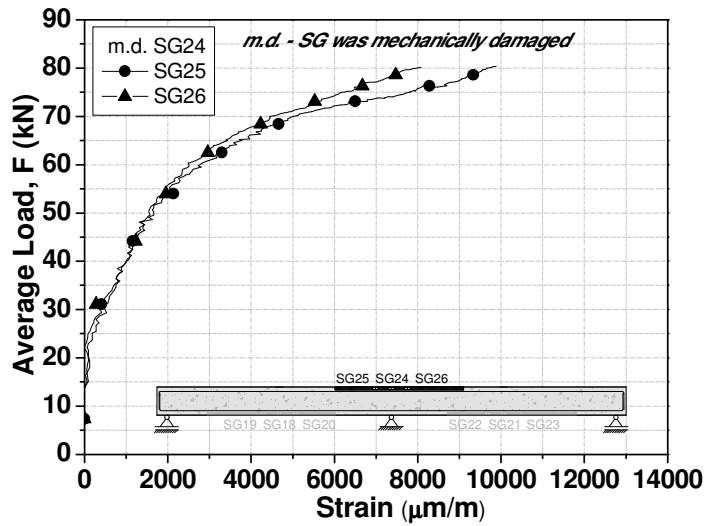
Figure 3.68: Relationship between average load and tensile strain
on the CFRP laminate at hogging region for the SL30s50-HS slab strip.
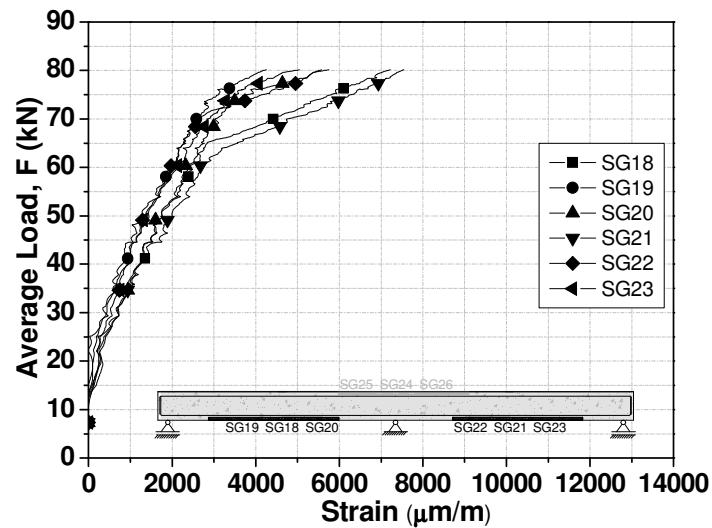
Figure 3.69: Relationship between average load and tensile strain
on the CFRP laminate at sagging regions for the SL30s50-HS slab strip.
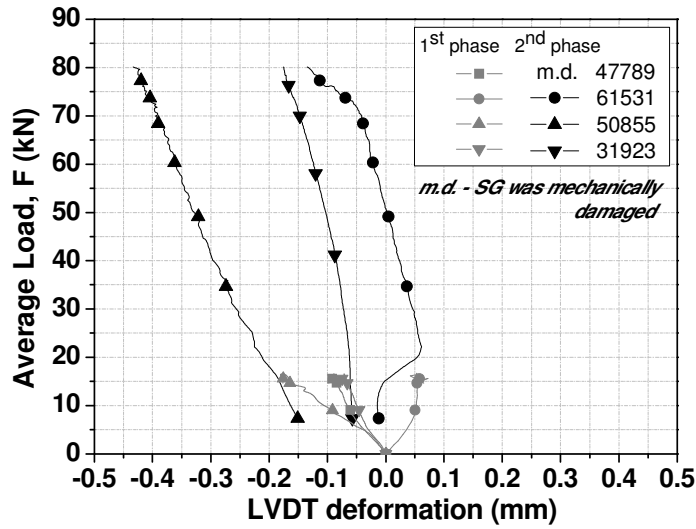
Figure 3.70: Relationship between average load and support devices rotation for the SL30s50-HS slab strip.
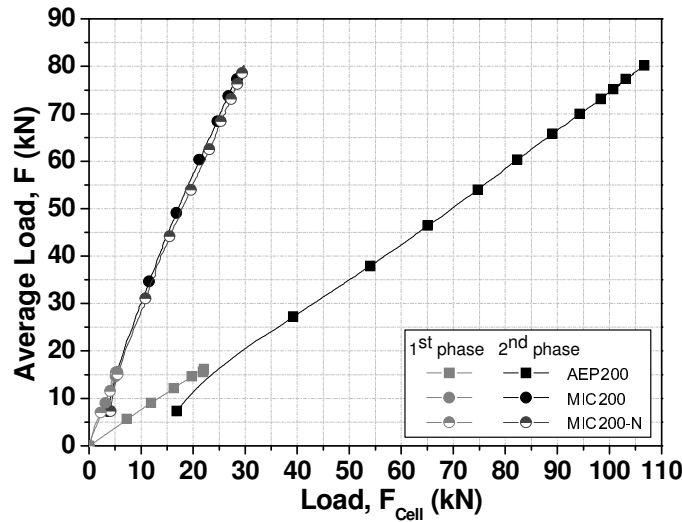
Figure 3.71: Relationship between the applied load and support reaction for the SL30s50-HS slab strip.

SL45s25-HS

The strengthened SL45s25-HS slab strip is shown in Figure 3.72 before and after having been tested. The span deflections, steel reinforcement strains, concrete strains, support reactions, and rotation of the reaction devices are shown in Figures 3.73 to 3.81, respectively.

<p align="center">(a)   (b)</p>

Figure 3.72: SL45s25-HS specimen before (a) and after having been tested (b).
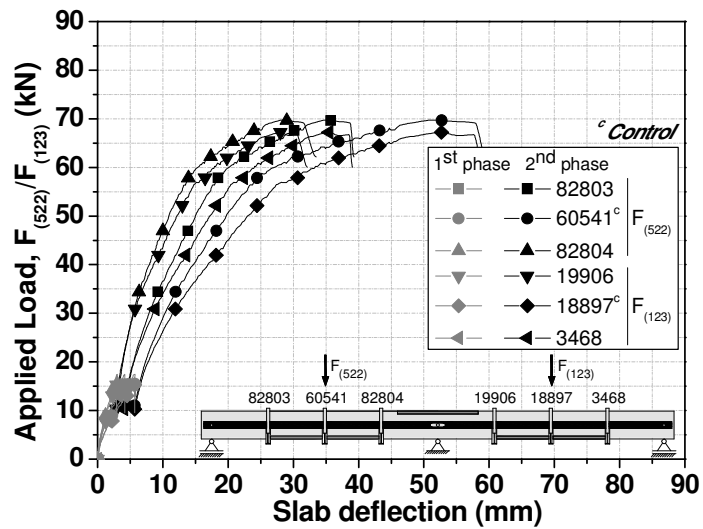
Figure 3.73: Relationship between applied load and deflections at spans of the SL45s25-HS.
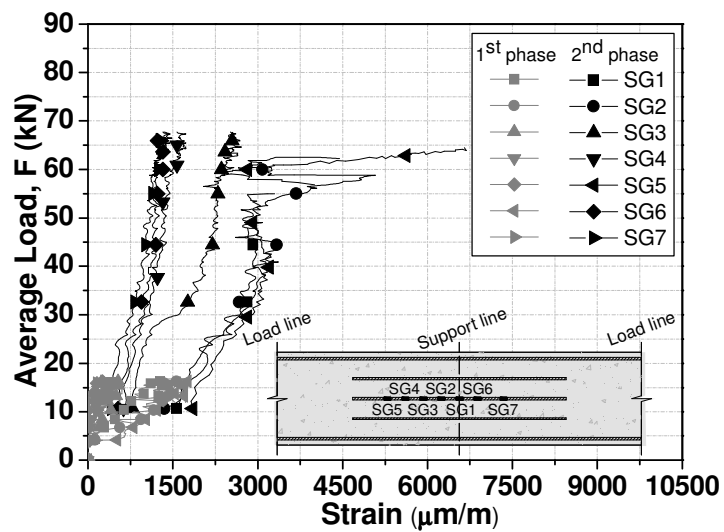
Figure 3.74: Relationship between average load and tensile strain on the negative longitudinal steel reinforcement for the SL45s25-HS slab strip.
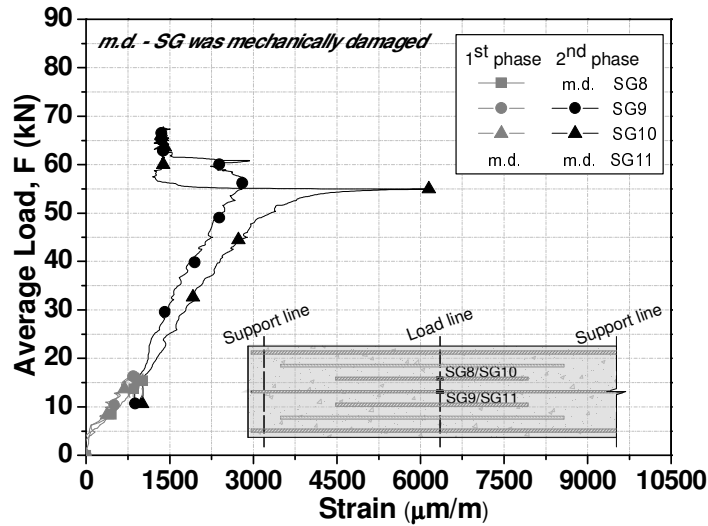
Figure 3.75: Relationship between average load and tensile strain on the
positive longitudinal steel reinforcement for the SL45s25-HS slab strip.
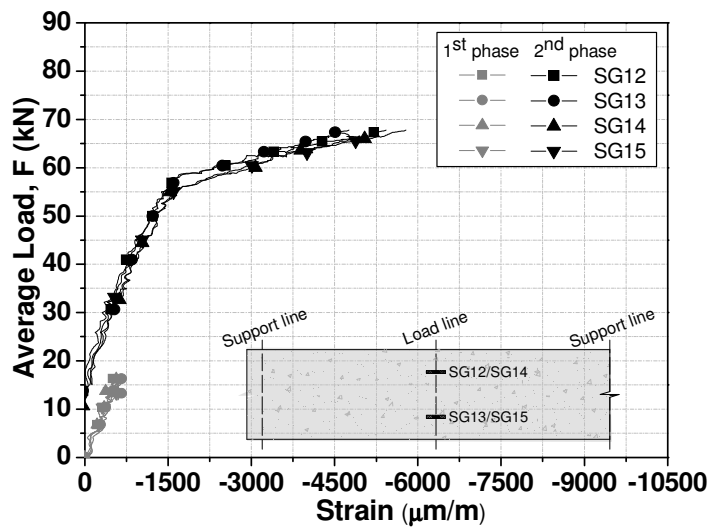
Figure 3.76: Relationship between average load and compressive strain on the
concrete at sagging region for the SL45s25-HS slab strip.
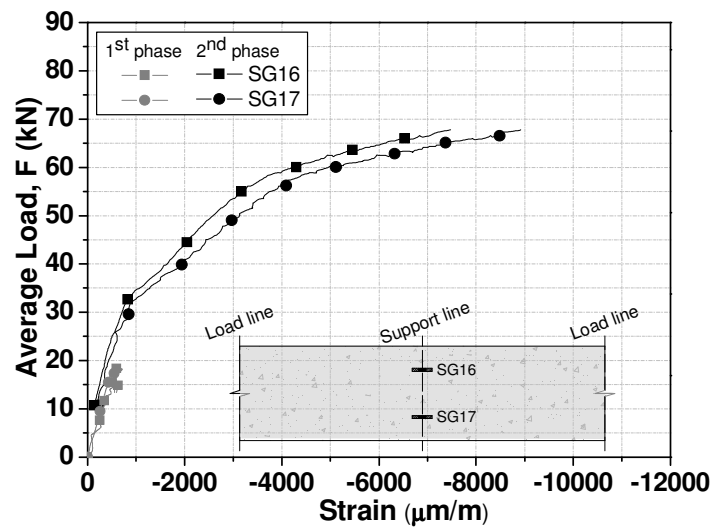
Figure 3.77: Relationship between average load and compressive strain on the
concrete at hogging region for the SL45s25-HS slab strip.
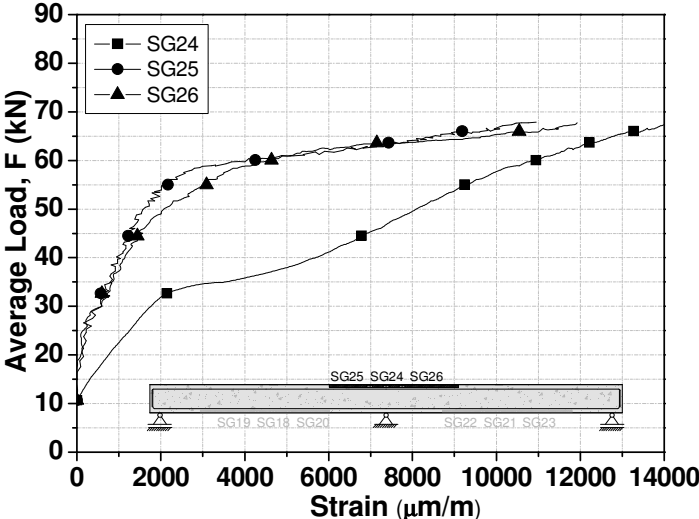
Figure 3.78: Relationship between average load and tensile strain on the CFRP laminate at hogging region for the SL45s25-HS slab strip.
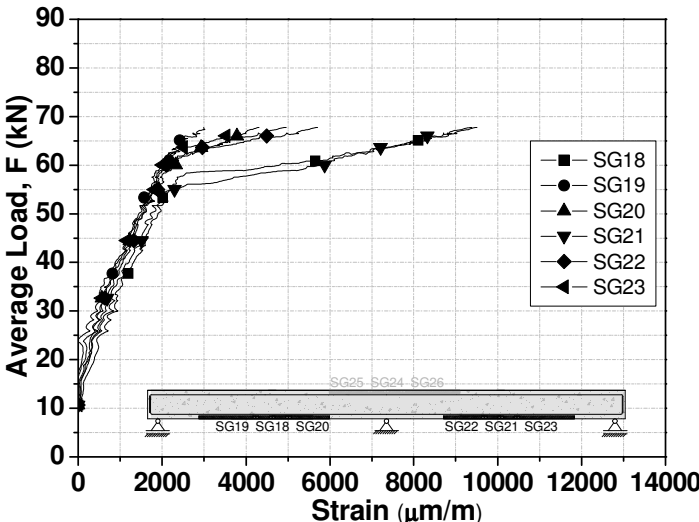
Figure 3.79: Relationship between average load and tensile strain on the CFRP laminate at sagging regions for the SL45s25-HS slab strip.
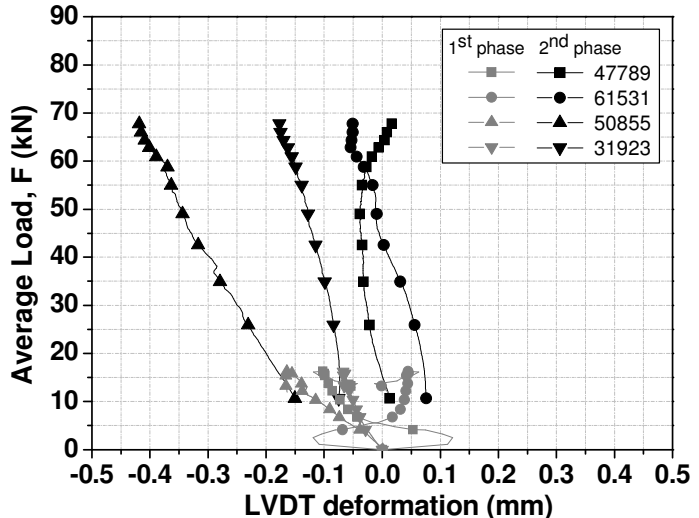
Figure 3.80: Relationship between average load and support devices rotation for the SL45s25-HS slab strip.
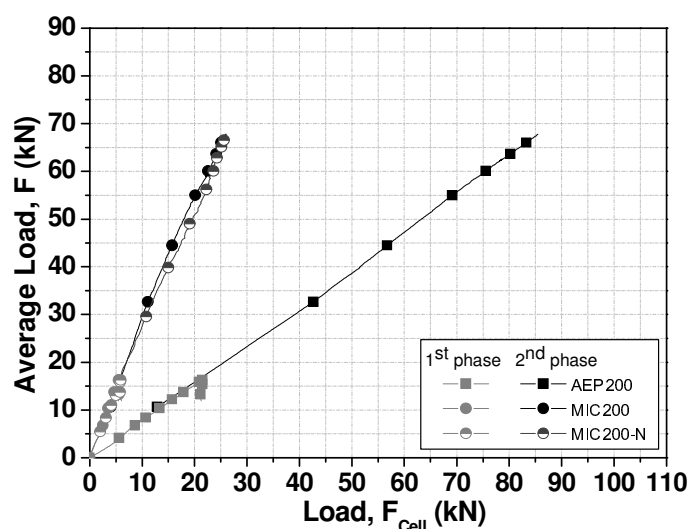
Figure 3.81: Relationship between the applied load and support reaction for the SL45s25-HS slab strip.

SL45s50-HS

The strengthened SL45s50-HS slab strip is shown in Figure 3.82 before and after having been tested. The span deflections, steel reinforcement strains, concrete strains, support reactions, and rotation of the reaction devices are shown in Figures 3.83 to 3.91, respectively.

(a)   (b)
Figure 3.82: SL45s50-HS specimen before (a), and after having been tested (b).
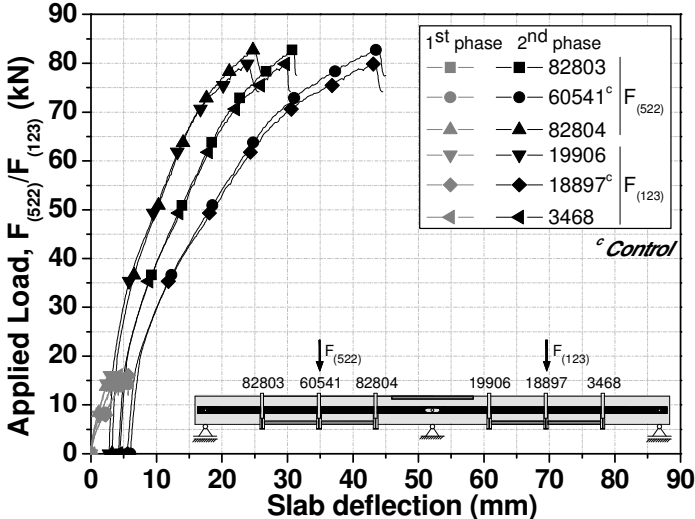
Figure 3.83: Relationship between applied load and deflections at spans of the SL45s50-HS.
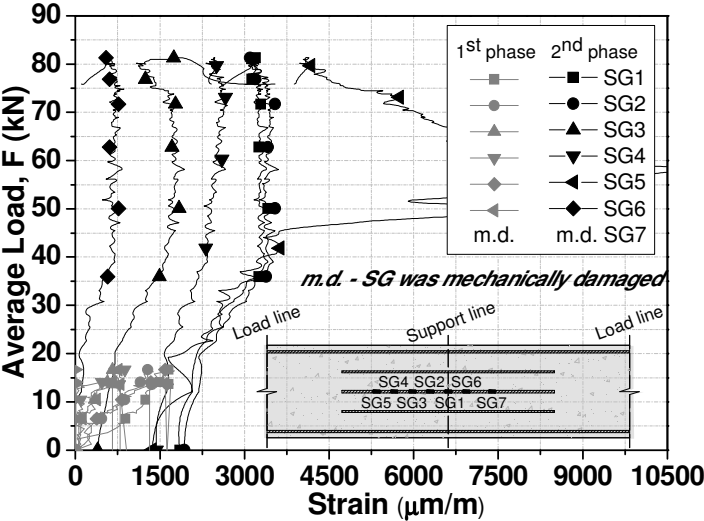
Figure 3.84: Relationship between average load and tensile strain
on the negative longitudinal steel reinforcement for the SL45s50-HS slab strip.
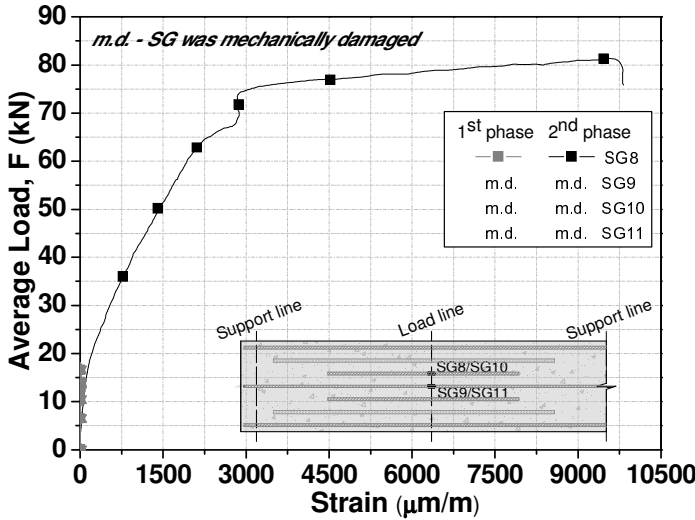
Figure 3.85: Relationship between average load and tensile strain
on the positive longitudinal steel reinforcement for the SL45s50-HS slab strip.
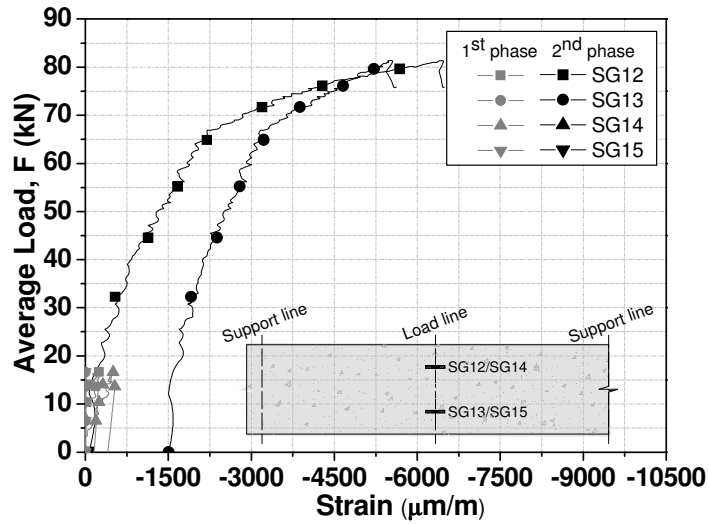
Figure 3.86: Relationship between average load and tensile strain
on the positive longitudinal steel reinforcement for the SL45s50-HS slab strip.
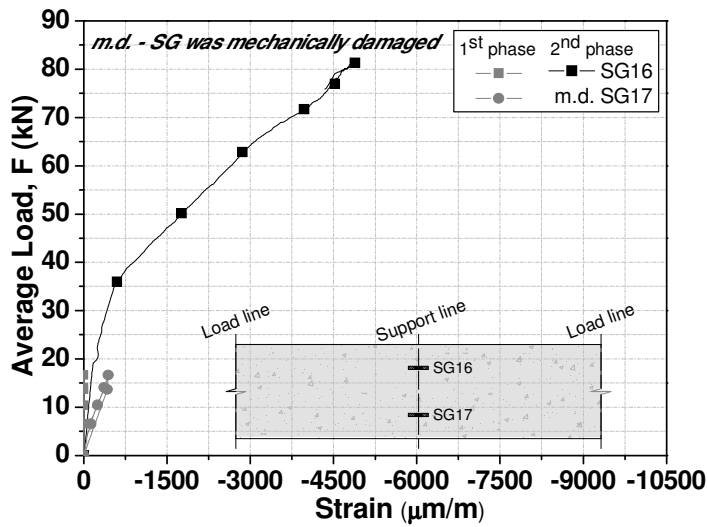
Figure 3.87: Relationship between average load and compressive strain
on the concrete at hogging region for the SL45s50-HS slab strip.
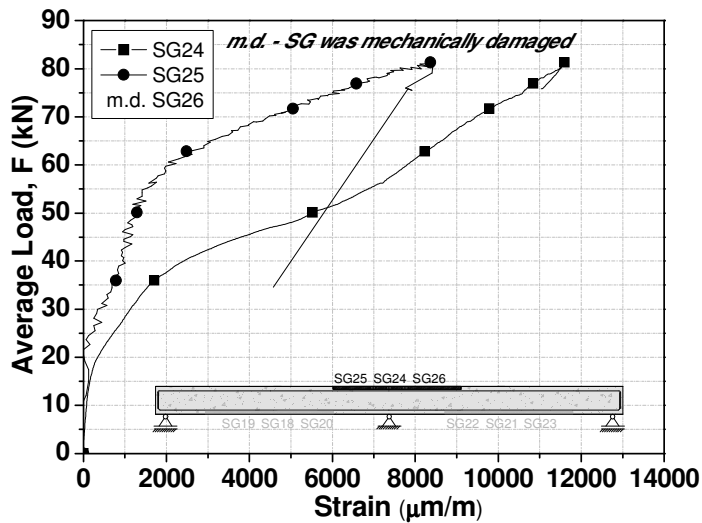
Figure 3.88: Relationship between average load and tensile strain on the CFRP laminate
at hogging region for the SL45s50-HS slab strip.
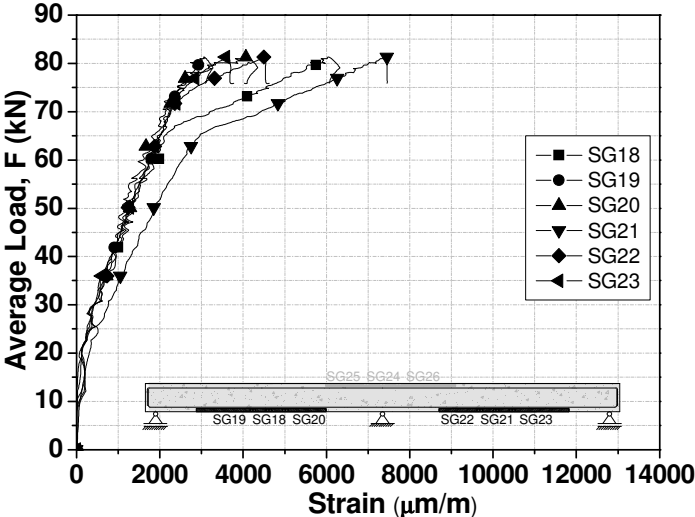
Figure 3.89: Relationship between average load and tensile strain on the CFRP laminate
at sagging regions for the SL45s50-HS slab strip.
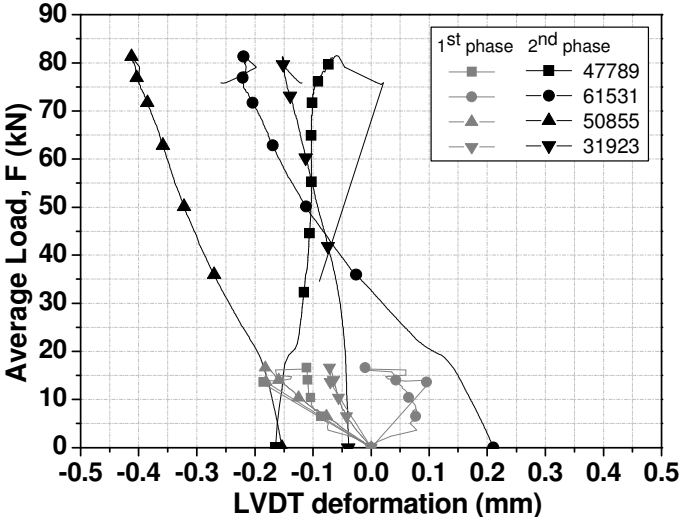
Figure 3.90: Relationship between average load and support devices rotation for the SL45s50-HS slab strip.
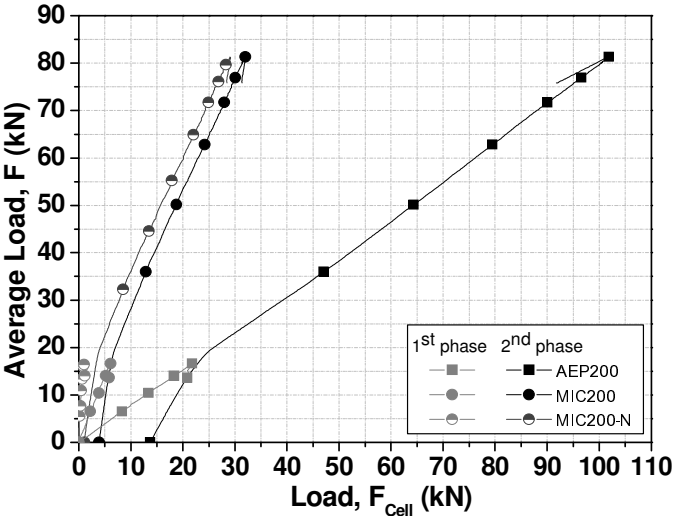
Figure 3.91: Relationship between the applied load and support reaction for the SL45s50-HS slab strip.

The average load ($\overline{F}=\left(F_{522}+F_{123}\right)/2$) versus deflection curves of the tested slab strips are presented in Figure 3.92. This figure reveals that the adopted NSM HS strengthening configurations have provided a significant increase of the load carrying capacity in the second phase of the test loading process.

Table 3.10 summarizes the results obtained experimentally for two scenarios: when a plastic hinge formed at the hogging region (superscript H); when a plastic hinge formed at the sagging regions (superscript S). Plastic hinge was assumed formed when the steel tensile reinforcement attained its yield strain (ε_{sy}). In this table, F_y^H and F_y^S are the average loads ($\overline{F}=\left(F_{522}+F_{123}\right)/2$) at the formation of the plastic hinge at hogging and sagging regions, respectively, u_y^H and u_y^S are the average deflections corresponding to F_y^H and F_y^S, respectively, ε_c^H and ε_c^S are the maximum concrete strains registered at H and S regions, ε_s^H and ε_s^S are the maximum strains in steel bars at H and S regions, respectively, ε_f^H and ε_f^S are the maximum strains in the CFRP laminates at the hogging and sagging regions, and, finally, ΔF_y^H and ΔF_y^S are the increase of the loading carrying capacity when a plastic hinge was formed at the H and S regions. Unfortunately, for the SL15-HS, due to a deficient functioning of the data acquisition system, the forces in the AEP_200 and MIC_200 load cells were not recorded, thus impeding the moment redistribution calculation for this slab.

Table 3.11 presents the relevant results when the maximum concrete compressive strain attained 3.5 ‰ (assumed to be the concrete crushing strain) in the hogging and sagging regions (symbols with subscript "*cu*"). In this table *IR* represents the increase of load carrying capacity provided

$$IR = \frac{F_{cu}^{CFRP} - F_{cu}^{REF}}{F_{cu}^{CFRP}} 100 \qquad (3.4)$$

where F_{cu}^{CFRP} and F_{cu}^{REF} are the loads of, respectively, the strengthened and reference slabs when the maximum compressive strain in the sagging regions attained 3.5 ‰ .

According to results obtained in the tests, for all the slabs, flexural cracks were first observed at a *F* of about 6 kN. Four phases occurred during each test in the following sequence: a) the uncracked elastic response; b) crack propagation in the hogging and sagging regions with steel bars in elastic stage; c) yielding of the steel reinforcement in the hogging region and crack propagation in the sagging regions with steel bars in elastic stage; and d) yielding of the steel reinforcement in the hogging and sagging regions.

Reference slabs:

As expected, the unstrengthened control slab strips behaved in a perfectly plastic manner in the post-yielding phase (after the formation of plastic hinges in the hogging and sagging regions), whereas the strengthened slab strips exhibited continuous hardening up to failure. The reference slabs failed in bending, i.e. by yielding of internal reinforcements, with extensive concrete cracking in both hogging and sagging regions, followed by concrete crushing in compression parts, as shown in Figures 3.93 and 3.94.

Strengthened slab strips:

The first phase of the loading process of the SL15s25-HS slab strip ended at a deflection of 5.40 mm, when a load of 14 kN was recorded. This slab strip failed by the detachment of the top concrete cover that includes the laminates in the hogging region.

At the end of the first phase of the test of SL30s25-HS slab strip a deflection of 5.80 mm and a load 17 kN were registered. From the analysis of the results of Table 3.11, it can be noted that, for a concrete compressive strain of 3.5‰, the increase of the load carrying capacity provided by the strengthening system was of about 29%, which exceeded the target value. This slab strip failed by the detachment of the top concrete cover that included the laminates in the hogging region (Figure 3.94).

The SL30s50-HS failed by the detachment of the bottom concrete cover that includes the laminates in sagging region (left span, Figure 3.95). In the first phase of the test, the strengthened slab strip was loaded up to a deflection of 5.80 mm, which corresponds to a load of 14 kN. From the analysis of the results presented in Table 3.11, it can be noted that, for a concrete compressive strain of 3.5‰, the increase of the load carrying capacity provided by the strengthening system was about 49%, very close to the target value.

The SL45s25-HS failed by shear in the intermediate support (Figures 3.93 and 3.94). In the first phase of the test this slab strip was loaded up to a deflection of 5.70 mm, which corresponds to a load of 16.7 kN. From the analysis of the results shown in Table 3.11, it can be noted that, for a compressive strain of 3.5‰, the increase of the load carrying capacity provided by the strengthening system was about the target value (24.42%).

The SL45s50-HS also failed by shear in the intermediate support, followed by the detachment of the top concrete cover that includes the laminates in the hogging region (Figure 3.95). In the first phase of the test this slab strip was loaded up to a deflection of 5.70 mm, which corresponds to a load of 17.10 kN. From the analysis of the results, it can be noted that, for a compressive strain of 3.5‰, the increase of the load carrying capacity provided by the strengthening system was about 37.24%.

From the analysis of the results included in Tables 3.10 and 3.11 and represented in Figure 3.91 the following observations can be outlined for the HS Series:

(i) Up to the formation of the plastic hinge in the hogging region the strains in the laminates have ranged from 0.88‰ to 1.94‰, which justifies the relative low contribution of the laminates to the load carrying capacity of the slabs up to this load level. At the formation of the plastic hinge in the sagging regions the strains in the laminates have increased, having been in the range 2.69‰ to 9.66‰. However, at concrete crushing in the sagging regions, the maximum strain in the CFRP laminates has varied between 4.03‰ and 11.78‰, which is 23% to 67% of the CFRP laminate ultimate strain.

(ii) The deflection at F_y^S, u_y^S, was not significantly affected by the presence of the CFRP laminates, which means that ductility was preserved.

(iii) The contribution of the CFRP laminates for the slab's maximum load carrying capacity was limited by the occurrence of concrete crushing, the detachment of the concrete cover layer that includes the laminates or the shear capacity of the slabs.

Figure 3.96 depicts the relationship between the average applied load and the moment redistribution percentage for the tested slabs. Between cracking load ($\overline{F}_{cr}$) and the formation of the plastic hinge in the hogging region ($\overline{F}_y^H$) no clear tendency is observed for the moment redistribution, but after $\overline{F}_y^H$ the η has a tendency to increase up to the formation of the plastic hinge in the sagging regions ($\overline{F}_y^S$). Adopting a flexural strengthening strategy composed of CFRP laminates applied in both hogging and sagging regions, the moment redistribution capacity was not significantly affected by the presence of the laminates and, in some cases, higher values were obtained in comparison to the reference slab strips. For the HS series, the following values of η were obtained: 6.10% for SL15s25-HS; 19.94%, 21.45%, 29.89% for SL30-HS, SL30s25-HS, SL30s50-HS; 39.21%, 41.69%, 44.10% for SL45-HS, SL45s25-HS, SL45s50-HS.
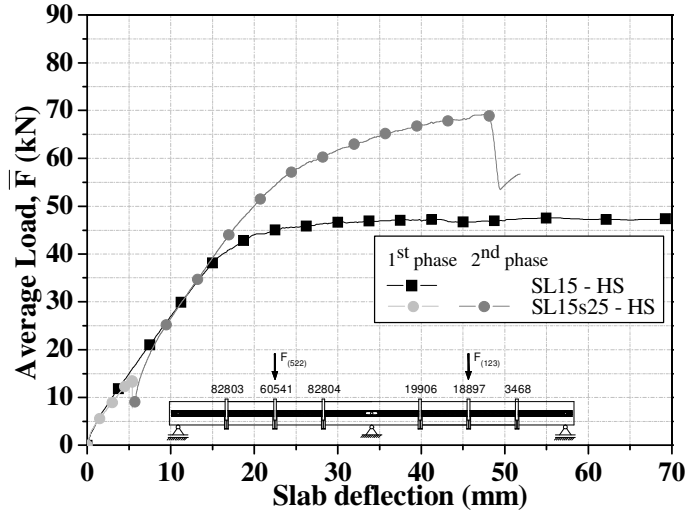
(a)
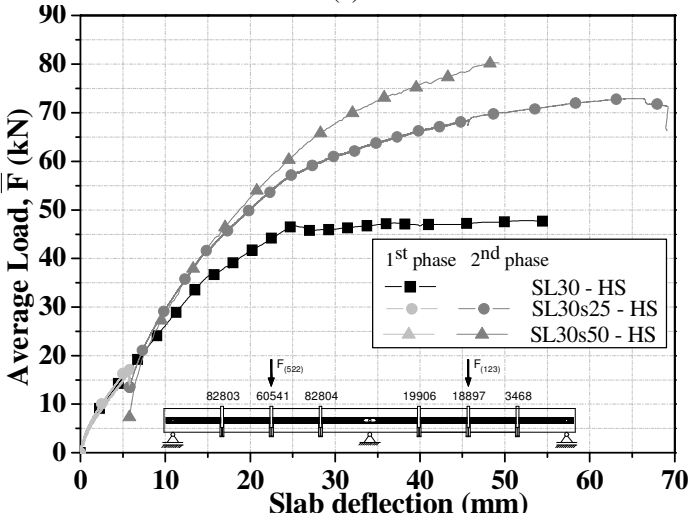
(b)
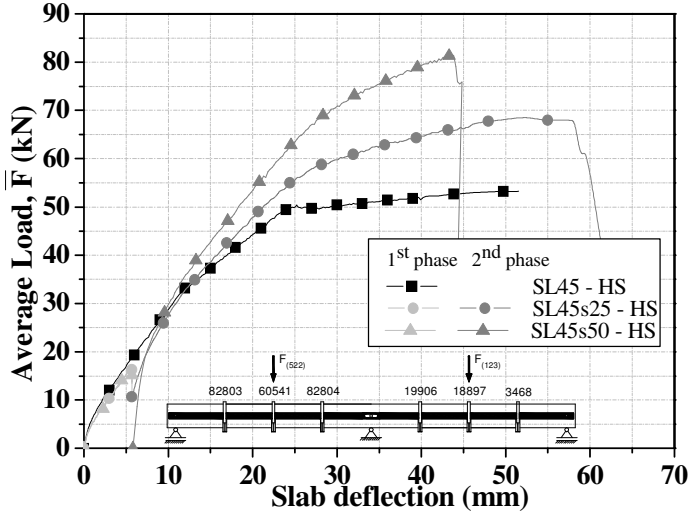
(c)

Figure 3.92: Load-midspan deflection of the tested slab strips Series: (a) SL15-HS, (b) SL30-HS and (c) SL45-HS.
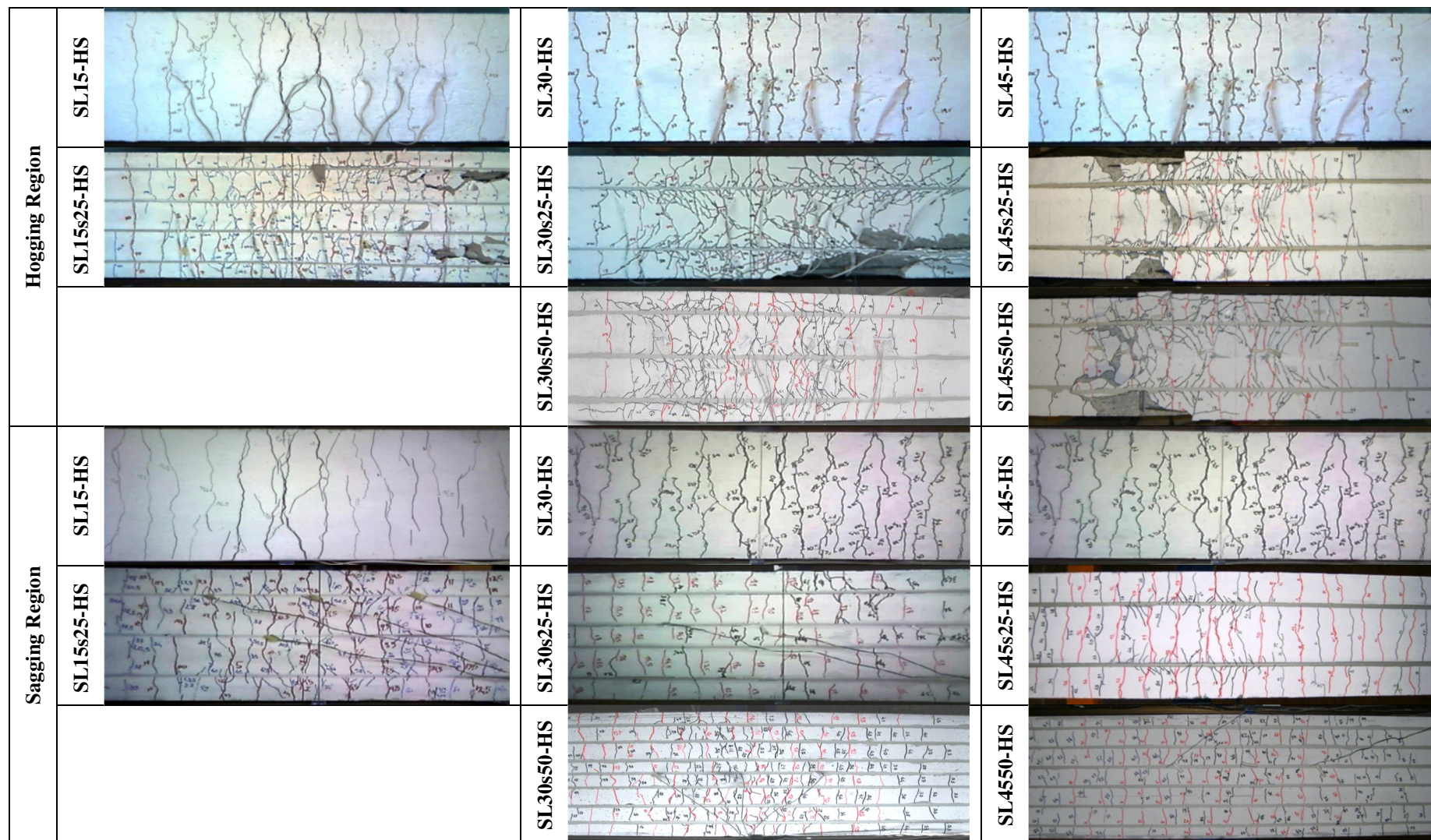
Figure 3.93: Crack patterns of HS series: view of sagging and hogging regions.
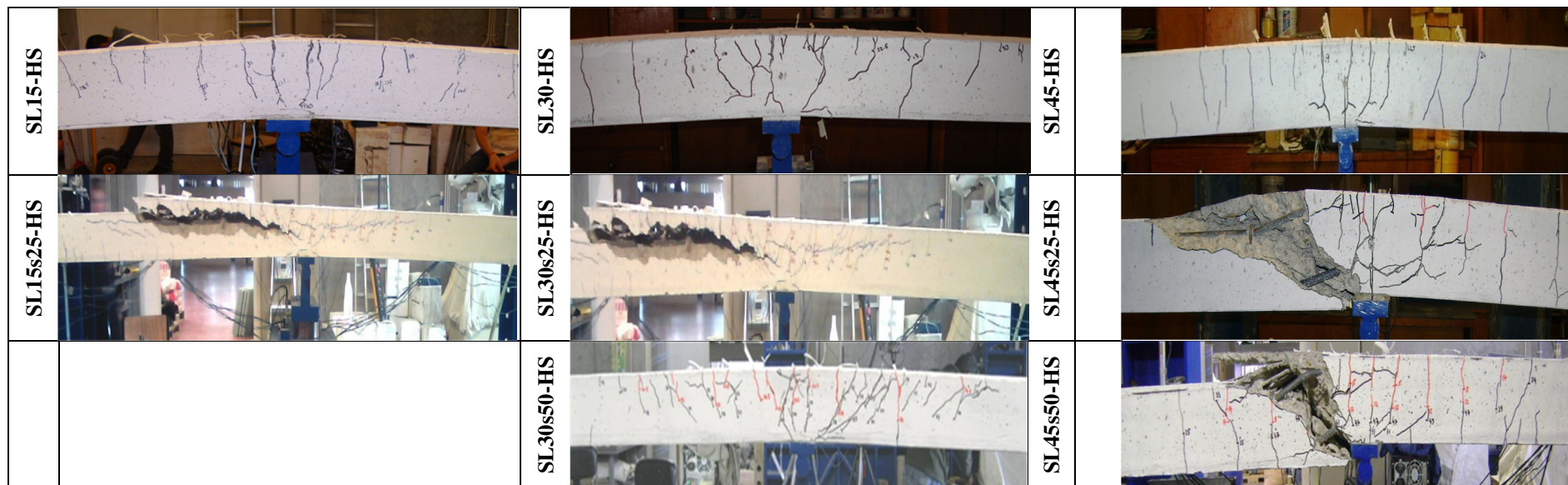
Figure 3.94: Crack patterns of HS series: side view of hogging region.

Figure 3.95: Side view of the left span of SL30s50-HS.
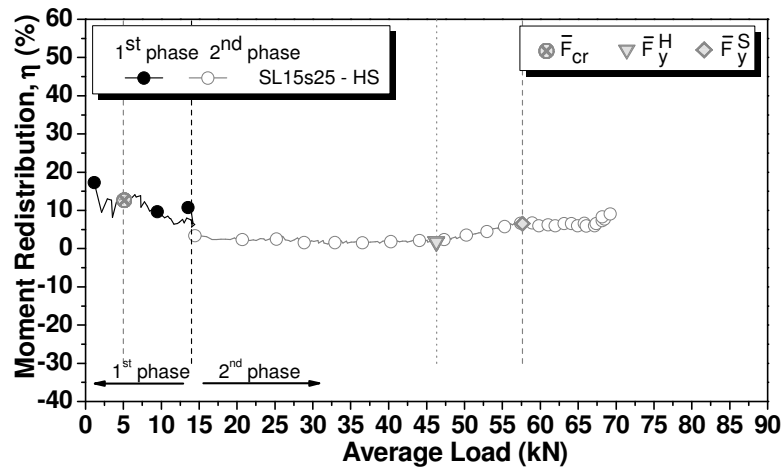
(a)
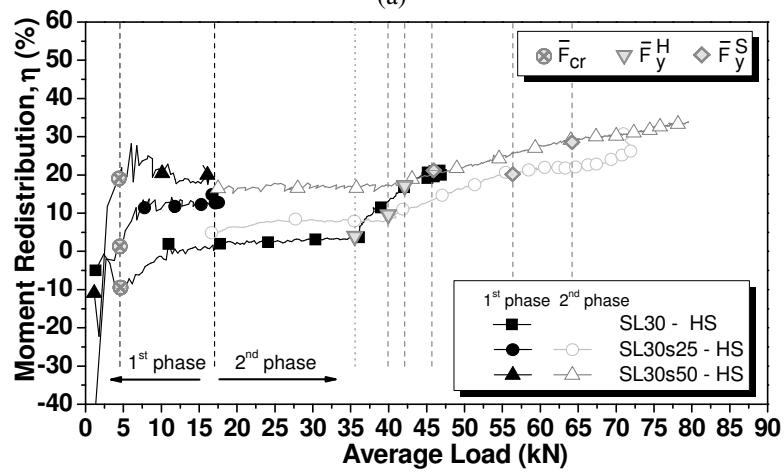
(b)
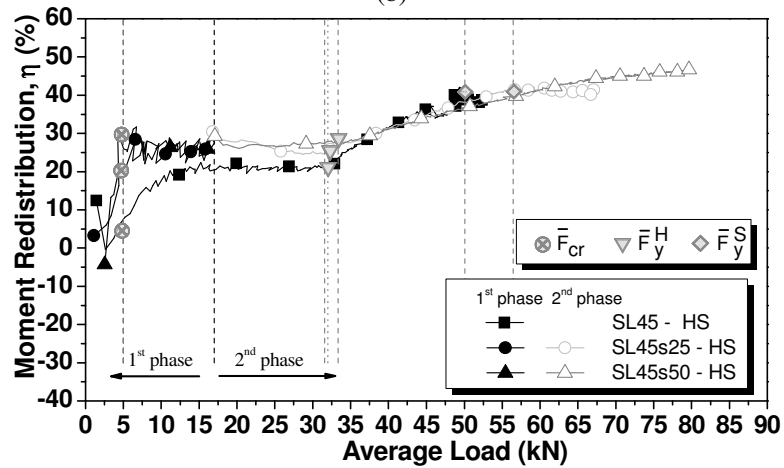
(c)

Figure 3.96: Degree of moment redistribution, η, for the slab strips series strengthened in both hogging and sagging regions (HS): (a) SL15-HS, (b) SL30-HS, (c) SL45-HS Series.

Table 3.10: Main results obtained in the experimental program in the formation of the hinges.

Slab strip ID	Hinge at hogging region (H)								Hinge at sagging region (S)							
	F_y^H (kN)	u_y^H (mm)	ε_c^H (‰)	ε_c^S (‰)	ε_s^H (‰)	ε_s^S (‰)	ε_f^H (‰)	ε_f^S (‰)	F_y^S (kN)	u_y^S (mm)	ε_c^H (‰)	ε_c^S (‰)	ε_s^H (‰)	ε_s^S (‰)	ε_f^H (‰)	ε_f^S (‰)
SL15-HS	39.24	15.66	-2.07	-1.58	2.10	2.30	-----	-----	44.24	20.22	-3.68	-2.01	2.30	3.37	-----	-----
SL15s25-HS	46.32	18.06	-2.10	-1.63	m.d	m.d	2.18	1.45	57.67	24.93	-3.62	-2.38	m.d	m.d	4.75	2.69
SL30-HS	35.58	14.53	-1.70	-1.48	1.85	2.61	-----	-----	45.70	23.92	-4.80	-2.29	2.65	2.90	-----	-----
SL30s25-HS	39.94	14.04	-1.63	-1.66	1.81	2.51	1.92	1.00	56.38	24.26	-4.15	-2.69	2.77	2.25	7.33	2.93
SL30s50-HS	42.13	14.92	-1.83	-1.51	1.45	2.66	1.25	0.88	64.20	27.09	-4.20	-2.88	2.68	2.40	3.65	3.41
SL45-HS	31.99	11.35	-1.38	-1.10	1.52	2.37	-----	-----	50.07	25.00	-5.26	-2.25	2.67	2.76	-----	-----
SL45s25-HS	31.56	11.50	-0.88	-0.57	1.85	2.51	1.94	0.88	56.44	25.76	-4.06	-1.95	2.77	4.06	9.66	3.12
SL45s50-HS	33.33	11.18	-0.91	-2.10	m.d.	2.73	1.42	0.96	(a)	(a)	(a)	(a)	(a)	(a)	(a)	(a)

[a] The forces in the AEP_200 and MIC_200 load cells were not recorded, thus impeding the moment redistribution calculation for this slab; m.d.: The gauge may have been mechanically damaged

Table 3.11: Main results obtained in the experimental program at the concrete crushing initiation.

Slab strip ID	Concrete crushing initiation at hogging region ($\varepsilon_{cu}^H = 3.5‰$)									Concrete crushing initiation at sagging regions ($\varepsilon_{cu}^S = 3.5‰$)								
	F_{cu}^H (kN)	u_{cu}^H (mm)	$\varepsilon_{c,max}^S$ (‰)	$\varepsilon_{s,max}^S$ (‰)	$\varepsilon_{s,max}^H$ (‰)	$\varepsilon_{f,max}^H$ (‰)	$\varepsilon_{f,max}^S$ (‰)	η (%)	IR (%)	F_{cu}^S (kN)	u_{cu}^S (mm)	$\varepsilon_{c,max}^H$ (‰)	$\varepsilon_{s,max}^S$ (‰)	$\varepsilon_{s,max}^H$ (‰)	$\varepsilon_{f,max}^H$ (‰)	$\varepsilon_{f,max}^S$ (‰)	η (%)	IR (%)
SL15-HS	43.81	19.70	-1.95	2.43	3.40	-----	-----	(na)	-----	45.55	24.69	-6.53	14.63	9.51	-----	-----	(na)	-----
SL15s25-HS	56.72	24.04	-2.25	m.d.	m.d.	4.47	2.38	6.76	29.47	62.00	30.35	-4.59	m.d.	m.d.	6.10	5.07	6.10	36.11
SL30-HS	41.28	19.74	-1.88	2.37	2.84	-----	-----	13.99	-----	46.14	30.51	-6.25	2.84	2.87	-----	-----	19.94	-----
SL30s25-HS	53.06	21.88	-2.38	2.75	2.42	6.52	2.52	18.21	28.54	59.91	28.54	-5.09	4.42	2.51	8.46	5.59	21.45	29.84
SL30s50-HS	57.77	22.85	-2.35	2.40	2.24	2.39	2.58	24.98	39.95	68.95	30.94	-4.98	0.82	2.06	4.69	4.61	29.89	49.44
SL45-HS	43.52	19.42	-1.82	2.35	2.66	-----	-----	34.17	-----	50.24	29.87	-5.61	2.29	2.85	-----	-----	39.21	-----
SL45s25-HS	52.48	23.06	-1.48	3.77	6.52	8.74	2.04	38.18	20.59	62.51	34.56	-6.04	1.47	5.20	11.78	6.83	41.69	24.42
SL45s50-HS	65.18	25.92	-3.25	m.d.	6.65	8.64	2.97	42.89	49.77	68.95	28.33	-3.95	m.d.	6.10	9.25	4.03	44.10	37.24

m.d.: The gauge may have been mechanically damaged

3.2.5.3 Analytical Prediction of Ultimate Loads

A simplified analytical model for the evaluation of the resisting bending moment of a flexural strengthened RC slab was used (see details in Annex 3.2). In this model η is the ratio of the average concrete stress to the concrete compressive strength, λ is the ratio of the depth of the equivalent rectangular stress block to the depth of the neutral axis according to the Eurocode 2 (2010).

Assuming for these two parameters the values of 1.00 and 0.80, and for the remaining materials properties of the analytical model the values included in Tables 3.7 to 3.9, the results indicated in Table 3.12 were obtained, where M_{rd}^{S} and M_{rd}^{H} are the resisting bending moments in the sagging and hogging regions, respectively, n_{f}^{S} and n_{f}^{H} are the number of laminates at sagging and hogging regions, F_{cu}^{ana} is the force predicted by the analytical model and $\bar{F}_{cu}^{S}$ is the force registered experimentally when concrete crushes at the sagging regions. From the comparison of the values it can be concluded that this model predicts with good accuracy the load level at concrete crushing.

3.6 CONCLUSIONS

In this work an experimental program with statically indeterminate (two equal spans) reinforced concrete (RC) slab strips was carried out to assess the effectiveness of the Near Surface Mounted (NSM) technique for the increase of the load carrying capacity and moment redistribution capability of this type of structures. Carbon fiber reinforced polymer (CFRP) laminates of rectangular cross section were used. The experimental program was composed of eight 120×375×5875 mm^3 RC slab strips. Three of them were unstrengthened RC slabs forming a control set (SL15-HS, SL30-HS and SL45-HS), and the other five slabs were strengthened with CFRP strips according to the NSM technique (SL15s25-HS, SL30s25-HS, SL30s50-HS, SL45s25-HS and SL45s50-HS) applied in both sagging and hogging regions (HS Series).

The results obtained from this experimental program were compared to the ones obtained by Bonaldo (2008), in which the experimental program was composed of nine 120×375×5875 mm^3 RC slab strips. Three of them were unstrengthened RC slabs forming a control set (SL15-H, SL30-H and SL45-H), and the other six slabs were strengthened with CFRP strips, applied only in the hogging region (H Series), according to the NSM technique (SL15s25-H, SL15-50-H, SL30s25-H, SL30s50-H, SL45s25-H and SL45s50-H).

Table 3.12: Theoretical calculations of the load capacity and the experimental loads at concrete crushing.

Slabs ID	Theoretical					Experimental
	M_{rd}^{S} (kN·m)	n_{f}^{S}	M_{rd}^{H} (kN·m)	n_{f}^{H}	F_{cu}^{ana} (kN)	$\overline{F}_{cu}^{S}$ (kN)
SL15-H	22.47	-----	21.44	-----	47.41	50.60
SL15s25-H	22.47	-----	28.42	3 [a]	52.40	54.43
SL15s50-H	22.47	-----	34.02	7 [a]	56.40	60.36
SL15-HS	21.27	-----	20.35	-----	44.92	45.55
SL15s25-HS	26.36	1 [a]/2 [b]	27.84	4 [b]	57.54	62.00
SL30-H	24.18	-----	17.33	-----	46.92	48.89
SL30s25-H	24.18	-----	22.74	2 [a]	50.78	52.63
SL30s50-H	24.18	-----	27.63	5 [a]	54.28	54.31
SL30-HS	23.35	-----	16.93	-----	45.45	46.14
SL30s25-HS	29.79	2 [a]/2 [b]	24.10	2 [b]	59.77	59.91
SL30s50-HS	34.06	1 [a]/6 [b]	26.31	3 [b]	67.45	68.95
SL45-H	26.89	-----	13.18	-----	47.83	51.31
SL45s25-H	26.89	-----	17.99	1 [a]	51.26	53.38
SL45s50-H	26.89	-----	23.64	3 [a]	55.30	55.77
SL45-HS	26.96	-----	13.19	-----	47.93	50.24
SL45s25-HS	33.67	2 [b]	20.96	2 [a]	63.07	62.51
SL45s50-HS	41.28	6 [b]	25.37	2 [b]	77.09	68.95

[a]: CFRP laminates of 1.4x10 mm^2 cross section; [b]: CFRP laminates of 1.4x20 mm^2 cross section

The amount and disposition of the steel bars were designed to assure a moment redistribution percentages of 15%, 30% and 45%. The NSM CFRP systems applied in the flexurally strengthened RC slabs were designed to increase in 25% and 50% the load carrying capacity of the reference slab. From the obtained results the following conclusions can be pointed out:

1) For the H Series, when the concrete compressive strain attained 3.5‰ in the hogging region, the increase of slab's load carrying capacity (ΔF) varied between 2.86% and 19.76%. According to the obtained results, the strengthening configurations composed by laminates only applied in the hogging region did not attain the target increase of the load carrying capacity.

2) For the HS series, when the concrete compressive strain attained 3.5‰ in the hogging region, the increase of ΔF has varied between 24.42% and 49.44%, while an increase of ΔF between 29.84 and 49.44% was registered when a concrete compressive strain of 3.5‰

was recorded in the sagging regions. When applying CFRP laminates in both sagging and hogging regions (HS series), the target increase of the load carrying capacity was attained.

3) Moment redistribution percentage (η) lower than the predicted one was determined in the slabs strengthened with CFRP laminates in the hogging region (H). For this strengthening configuration the η has decreased with the increase of the CFRP percentage. However, adopting a flexural strengthening strategy composed of CFRP laminates applied in both hogging and sagging regions, the moment redistribution capacity was not significantly affected. For this configuration of NSM laminates, the flexural strengthening performance was limited by the detachment of the concrete cover that includes the laminates or by the formation of a shear crack in the hogging region.

3.7 BIBLIOGRAPHY

ACI Committee 318, "Building code requirements for structural concrete (ACI 318-08) and Commentary", ACI 318R-08, Reported by ACI Committee 318, American Concrete Institute, Farmington Hills, Mich, 471 pp., 2008.

ACI Committee 440, "Guide for the design and construction of externally bonded FRP systems for strengthening concrete structures", ACI440.2R-08, Reported by ACI Committee 440, American Concrete Institute, Farmington Hills, Mich, 80 pp., 2008.

ASTM A370, "Standard test methods and definitions for mechanical testing of steel products", American Society for Testing and Materials, 52pp., 2002.

Barros, J.A.O., Kotynia, R., "Possibilities and challenges of NSM for the flexural strengthening of RC structures", Fourth International Conference on FRP Composites in Civil Engineering (CICE2008), Zurich, Switzerland, 22-24 July, 2008.

Bianco, V., Barros, J.A.O., Monti, G., "New approach for modeling the contribution of NSM FRP strips for shear strengthening of RC beams", ASCE Composites for Construction Journal, 14(1): 36-48, 2010.

Bonaldo, E., "Composite materials and discrete steel fibres for the strengthening of thin concrete structures" PhD Thesis, University of Minho, Guimarães, Portugal, 2008.

CEB-FIP Model Code 1990, "Design Code", Thomas Telford, Lausanne, Switzerland, 1993.

EN 1992-1-1, "Eurocode 2: Design of Concrete Structures-Part 1-1: General Rules and Rules for Buildings", CEN, Brussels, 2010.

ISO 527-1, "Plastics - Determination of tensile properties - Part 1: General principles", International Organization for Standardization (ISO), Genèva, Switzerland, 9 pp., 1993.

ISO 527-2, "Plastics - Determination of Tensile Properties - Part 2: Test Conditions for Moulding and Extrusion Plastics", International Organization for Standardization (ISO), Geneva, Switzerland, 5 pp., 1993.

ISO 527-5, "Plastics - Determination of tensile properties - Part 5: Test conditions for unidirectional fibre-reinforced plastic composites", International Organization for Standardization (ISO), Genèva, Switzerland, 9 pp, 1993.

LNEC-E397, "Concrete-Assessment of the elasticity modulus under uniaxial compression", Laboratório Nacional de Engenharia Civil (in Portuguese), 1993.

RDP, "LVDTs calibration certificates", RDP Group, October, 1995.

TML, Tokyo Sokki Kenkyujo Co., Ltd., http://www.tokyosokki.co.jp/e/index.html, Japan, 2004. (available on September 24, 2004)
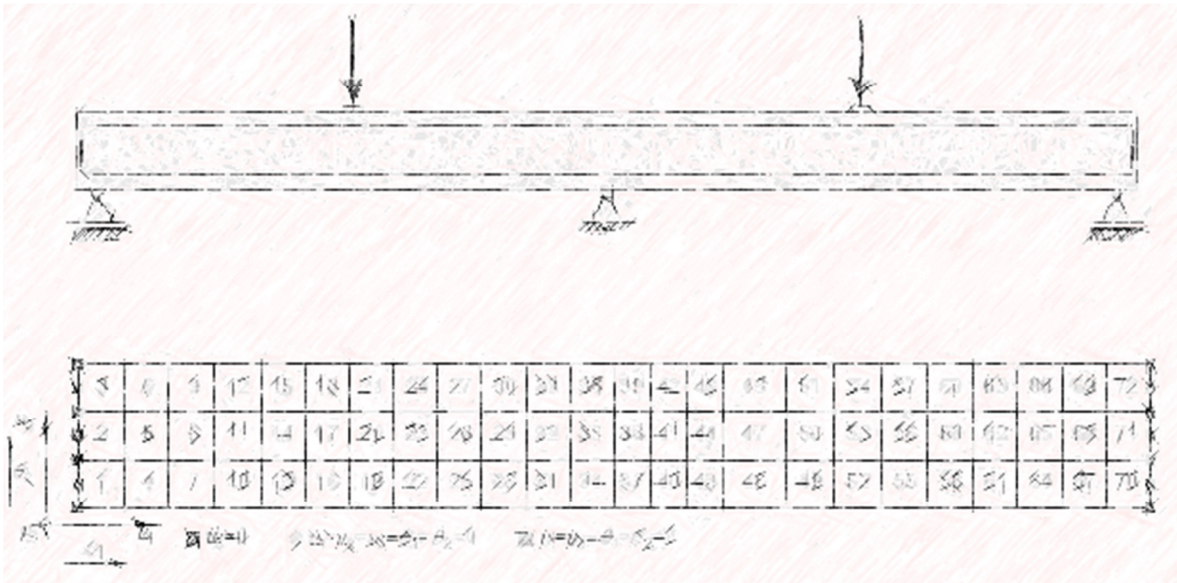
Chapter 4
SIMULATION OF RC SLAB STRIPS STRENGTHENED WITH NSM CFRP LAMINATES

In this chapter, numerical simulations of the experimental program described in previous chapter were performed. For assessing the predictive performance of a FEM-based computer program (FEMIX V4.0), the experimental results are compared with values predicted by this software. Then, a parametric study with 144 numerical models is carried out to investigate the influence of the strengthening arrangement and CFRP percentage in terms of load carrying capacity and moment redistribution capacity of continuous RC slab strips flexurally strengthened by the NSM technique.

4.1 Assessment of the behaviour of continuous NSM flexurally strengthened RC slabs by FEM-based material nonlinear analysis

To simulate the tests of the experimental program corresponding to the slab strips NSM flexurally strengthened in both the hogging and sagging regions, described in the previous chapter, the values of the material properties tested experimentally were used to characterize the parameters of the constitutive models adopted in the FEM-based material nonlinear simulations. The finite element mesh, support and load conditions are also assumed equal in all the simulations of the experimentally tested slabs.

4.1.1 Simulation of the continuous slab strips strengthened in both sagging and hogging regions with NSM CFRP laminates

The main objective of the present research is to simulate the behavior of the slab strips presented in the experimental program. The reliability of this study requires the use of a computational tool capable of simulating the relevant aspects of this structural system. For this purpose, the version 4.0 of FEMIX computer program was used. FEMIX 4.0 is a computer code whose purpose is the analysis of structures by the Finite Element Method (FEM). This code is based on the displacement method, being a large library of types of finite elements already available, namely 3D frames and trusses, plane stress elements, flat or curved elements for shells and 3D solid elements. Linear elements may have two or three nodes, plane stress and shell elements may be of 4, 8 or 9 nodes, and 8 or 20-noded hexahedra may be used in 3D solid analyses. This library of finite elements is complemented by a set of point, line and surface springs that model elastic contact with the supports, and also a few types of interface elements to model inter-element contact. Embedded line elements can be added to other types of elements in order to model reinforcement bars. All these types of elements can be simultaneously included in the same analysis, with the exception of some incompatible combinations. The analysis may be static or dynamic and the material behaviour may be linear or nonlinear. In the same nonlinear analysis several nonlinear models may be simultaneously considered, allowing, for instance, the combination of reinforced concrete with strengthening components, which exhibit distinct nonlinear constitutive laws. Interface elements with appropriate friction

laws and nonlinear springs may also be simultaneously considered. The global response history is recorded in all the sampling points for selected post processing. Advanced numerical techniques are available, such as the Newton Raphson method combined with arc length techniques and path dependent or independent algorithms. When the size of the systems of linear equations is very large, a preconditioned conjugate gradient method can be advantageously used (Breveglieri et al., 2012).

The predictive performance of FEMIX to simulate the behaviour of several type of NSM strengthened RC columns (Barros et al. 2008a), beams (Barros et al. 2011) and statically determinate slabs (Bonaldo, 2008) was already assessed, and in this chapter it will be extended to statically indeterminate RC slabs by simulating the tests carried out in the experimental program previously presented.

For the numerical simulations a constitutive model able to simulate the concrete crack initiation and crack propagation, the nonlinear concrete compression behaviour, the elasto-plastic behaviour of steel reinforcements and the elastic-brittle failure behaviour of FRP elements was selected. According to the selected model, a concrete slab is considered as a plane shell formulated under the Reissner Mindlin theory (Barros et al. 2001). In this numerical approach the shell element is discretized in layers and each layer is considered in plane stress state. A detailed description of this model can be found elsewhere (Barros et al. 2008b).

4.1.1.1 Materials properties and finite element mesh

Due to the structural symmetry, only half of the slab is considered in the numerical simulations. Figure 4.1 shows the eight node finite element mesh adopted and the support conditions. The slab thickness is discretized in 20 layers.
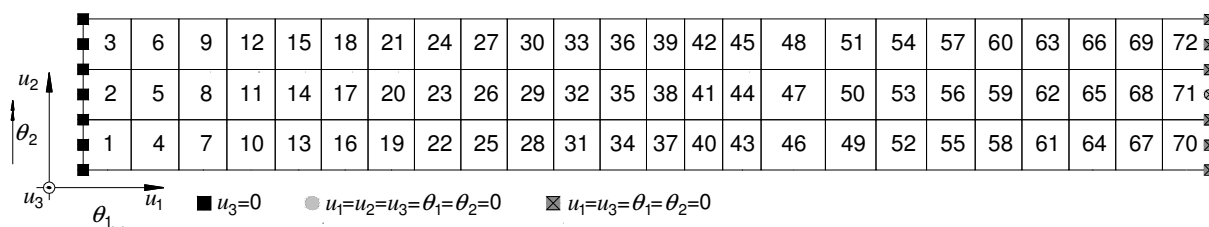
Figure 4.1: Finite element mesh adopted to discretize the half part of a RC slab.

The values of the parameters of the constitutive model are indicated in Tables 4.1 to 4.3 (see also Figures 4.2 and 4.3 for the comprehension of the physical meaning of some parameters of the model). To take into account that at the cracked section the stress in the steel reinforcement is higher than between cracks, and considering that the model evaluates the average strains in the steel, the stress reduction factors for σ_{sy}, σ_{sh} and σ_{su} (Figure 4.3) proposed by Stevens (1987) were adopted:

$$\sigma_{sy} = \sigma_{sy}^{exp} - 3\Delta\sigma_{ycr} \; ; \; \sigma_{sh} = \sigma_{sh}^{exp} - \Delta\sigma_{ycr} \; ; \; \sigma_{su} = \sigma_{su}^{exp} - \Delta\sigma_{ycr} \; ; \; \Delta\sigma_{ycr} = 75\phi_s / f_{ct} \qquad (4.1)$$

where σ_{sy}^{exp}, σ_{sh}^{exp} and σ_{su}^{exp} are the values registered experimentally, f_{ct} is the concrete tensile strength in MPa, and ϕ_s is the bar diameter (or equivalent bar diameter) in mm. The values in Table 4.1 are already affected by these reduction factors.

For the numerical simulations, the CFRP laminates of $1.4 \times 20 \text{mm}^2$ cross sectional area were assumed as an isotropic material of an elasticity modulus of 160 GPa and null value for the Poisson's coefficient, since the consideration of their real orthotropic properties has marginal influence in terms of their contribution for the behaviour of NSM strengthened RC slabs.

4.1.1.2 Predictive performance of the model

Figure 4.4 compares the numerical and experimental load-deflection curves for the slabs of SL15-HS and SL15s25-HS, where the good predictive performance of the adopted model is visible. The effectiveness of the model is also visible on the evaluation of the strains in the steel bars, concrete and CFRP strips, as shown in Figures 4.5 to 4.9.

The SL15-HS Series is analysed in this chapter, but similar predictive performance was obtained for all the tested slabs. These simulations are indicated in the Annex 4.

Table 4.1: Values of the parameters of the steel constitutive model (see Figure 4.3).

Steel bar diameter	$P_1(\varepsilon_{sy}[-]; \sigma_{sy}[\text{MPa}])$	$P_2(\varepsilon_{sh}[-]; \sigma_{sh}[\text{MPa}])$	$P_3(\varepsilon_{su}[-]; \sigma_{su}[\text{MPa}])$	E_s [GPa]
$\varnothing$ 8mm	$(1.90 \times 10^{-3}; 379.16)$	$(4.42 \times 10^{-2}; 512.19)$	$(8.85 \times 10^{-2}; 541.66)$	200.80
$\varnothing$ 10mm	$(2.32 \times 10^{-3}; 413.20)$	$(3.07 \times 10^{-2}; 434.75)$	$(1.31 \times 10^{-1}; 546.25)$	178.23
$\varnothing$ 12mm	$(2.09 \times 10^{-3}; 414.35)$	$(3.05 \times 10^{-2}; 435.63)$	$(1.02 \times 10^{-1}; 537.98)$	198.36

Table 4.2 Mechanical properties of the CFRP laminates.

Property	Value
E_f	160 GPa
$\varepsilon_{fu}{}^{*}$	17.70 ‰
b_f	1.4 mm
h_f	20. mm
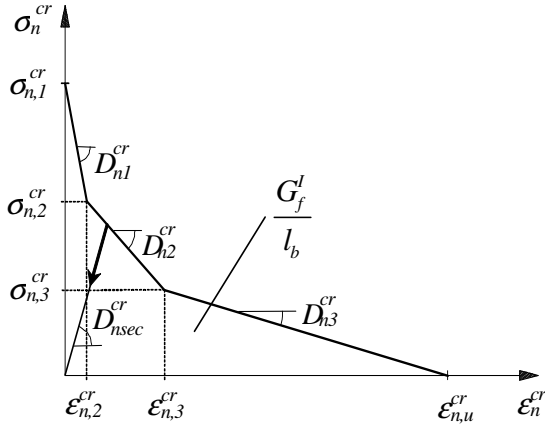
Figure 4.2: Crack normal stress *vs* crack normal strain diagram for modelling the concrete tensile-softening behaviour.
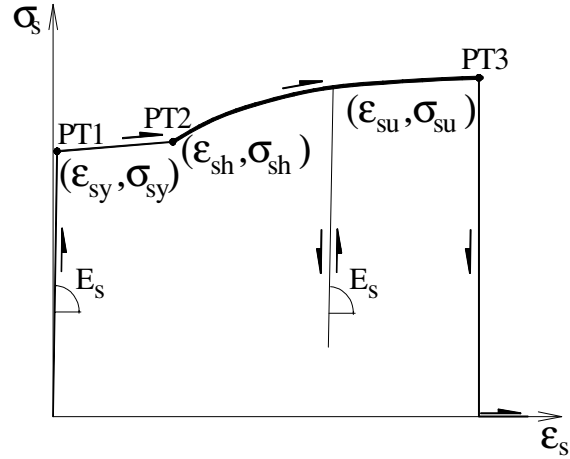
Figure 4.3: Uniaxial constitutive model of the steel bars.

Table 4.3: Concrete properties used in the FEM simulations (Sena-Cruz, 2004).

Parameters	SL15-HS	SL30-HS	SL45-HS
Compressive strength	$f_{cm} = 26.37$ N/mm^2	$f_{cm} = 28.40$ N/mm^2	$f_{cm} = 42.38$ N/mm^2
Initial Young's modulus	$E_c = 29.43$ N/mm^2	$E_c = 30.09$ N/mm^2	$E_c = 33.93$ N/mm^2
Poisson's ratio	$\nu_c = 0.0$		
Strain at peak compression stress	$\varepsilon_{c1} = 2.80 \times 10^{-3}$	$\varepsilon_{c1} = 2.80 \times 10^{-3}$	$\varepsilon_{c1} = 2.80 \times 10^{-3}$
Tri-linear tension softening [(1)]	$f_{ct} = 1.39$ N/mm^2 $G_f = 0.049$ N/mm	$f_{ct} = 1.49$ N/mm^2 $G_f = 0.052$ N/mm	$f_{ct} = 2.11$ N/mm^2 $G_f = 0.069$ N/mm
	$\xi_1 = 0.015$; $\alpha_1 = 0.6$; $\xi_2 = 0.2$; $\alpha_2 = 0.25$		
Parameter defining the initial yield surface	$\alpha_0 = 0.0$		
Parameter defining the mode I fracture energy to the new crack	n=2		
Parameter defining the evolution of the shear retention factor	$p_1 = 2$		
Crack band-width	Square root of the area of Gauss integration point		
Threshold angle	$\alpha_{th} = 30°$		
Maximum numbers of cracks per integration point	1		

[(1)] $f_{ct} = \sigma_{n,1}^{cr}$; $\xi_1 = \varepsilon_{n,2}^{cr} / \varepsilon_{n,u}^{cr}$; $\alpha_1 = \sigma_{n,2}^{cr} / \sigma_{n,1}^{cr}$; $\xi_2 = \varepsilon_{n,3}^{cr} / \varepsilon_{n,u}^{cr}$; $\alpha_2 = \sigma_{n,3}^{cr} / \sigma_{n,1}^{cr}$ (see Figure 4.2)

4.2 PARAMETRIC STUDY

The computer program, which good predictive performance on the simulation of the behaviour of the type of structures in analysis was confirmed in the previous section, was adopted to execute a parametric study for the evaluation of the influence of relevant parameters on the load carrying capacity, moment redistribution level and ductility performance of statically indeterminate RC slabs strengthened according to the NSM technique. These parameters are: concrete strength class, percentage of existing longitudinal tensile reinforcement, strengthening configuration, and percentage of CFRP laminates.

4.2.1 Mechanical properties and strengthening arrangements

In the parametric study, the mechanical properties adopted for the concrete strength classes (C12/15, C25/30 or C35/45) were determined following the recommendations of Eurocode 2 (2010) and CEB-FIP Model Code (1993) and are presented in Table 4.4. The values of the parameters adopted for the constitutive model used to simulate the behaviour of the steel bars are those included in Table 4.1.

The arrangements of the steel reinforcement, dimensions of the cross section, support and load conditions are the same adopted in the experimental/numerical program for the reference slab strip of SL15-H/HS, SL30-H/HS and SL45-H/HS series. However, distinct strengthening arrangements were applied in the hogging (H) and sagging regions (S), as shown in Figure 4.10 and Tables 4.5 to 4.10. The details of the cross sections of the slab strips are presented in these Tables, where $\rho_{l,eq}^{H}$ and $\rho_{l,eq}^{S}$ are the percentage of equivalent steel reinforcement (equivalent reinforcement ratio) [$\rho_{l,eq} = A_s / (bd_s) + (A_f E_f / E_s) / (bd_f)$] of the hogging and sagging regions, respectively, where b is the width of the slab's cross section and d_s and d_f are the effective depth of the longitudinal steel bars and CFRP laminates, respectively, and E_s and E_f are the Young's modulus of the longitudinal tensile steel bars and CFRP laminates. Additionally, ρ_f^{H} and ρ_f^{S} are the percentage of CFRP laminates in the hogging [$\rho_f^{S} = A_f^{S} / (bd_f^{S})$] and sagging regions [$\rho_f^{H} = A_f^{H} / (bd_f^{H})$], respectively.

4.2.2 Results and discussion

The slab strips can be classified in three different groups, due to the distinct adopted strengthening arrangements: (a) applied in the hogging region, (b) applied in the sagging regions and (c) applied in both hogging and sagging regions. The notation adopted to identify a slab strip is SLx_y_w_z, where x is the moment redistribution percentage, η (15%, 30% and 45%), y is the concrete strength class (C12/15, C25/30 or C35/45), and w and z indicate the number of NSM CFRP laminates applied in the sagging or hogging regions, respectively. Therefore, SL15_30_4_2 represents a slab with a moment redistribution target of η=15%, made by a concrete of f_{ck}=30 MPa (in cubic specimens), and strengthened with 4 and 2 laminates in the sagging and hogging regions, respectively.

(a)

(b)
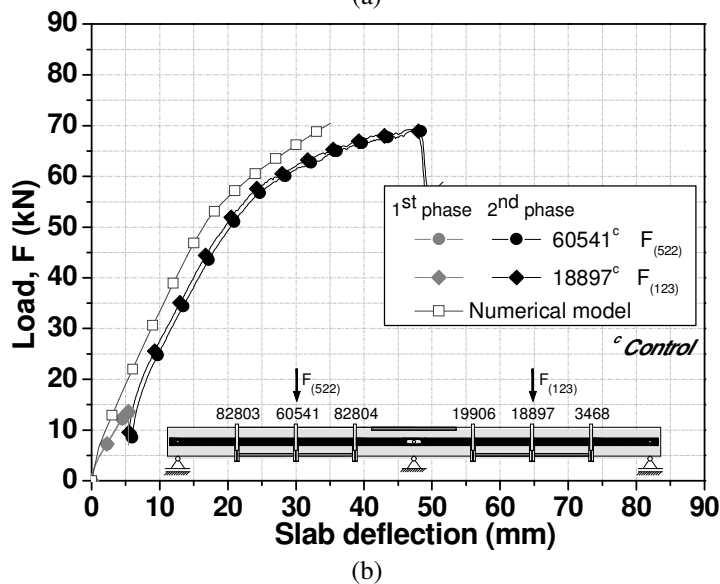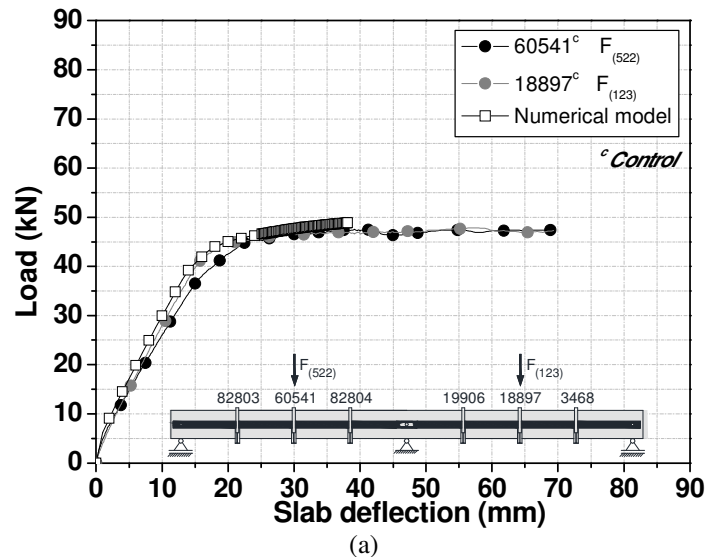
Figure 4.4: Relationship between applied load and deflections at spans of the (a) SL15-HS and (b) SL15s25-HS.

(a)
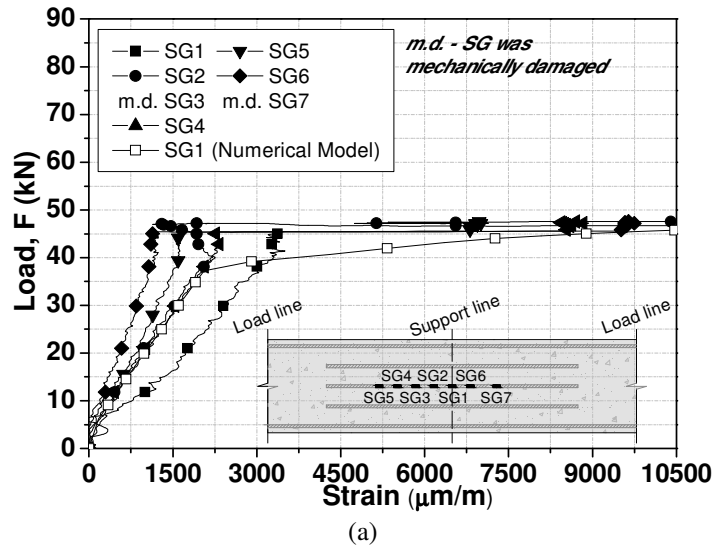
Figure 4.5: Relationship between average load and tensile strain on the negative longitudinal steel reinforcement for the (a) SL15-HS.

(a)

(b)
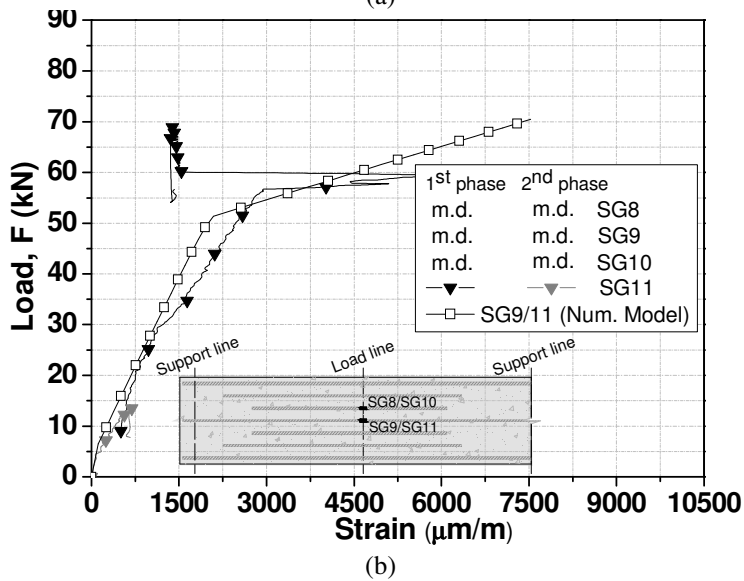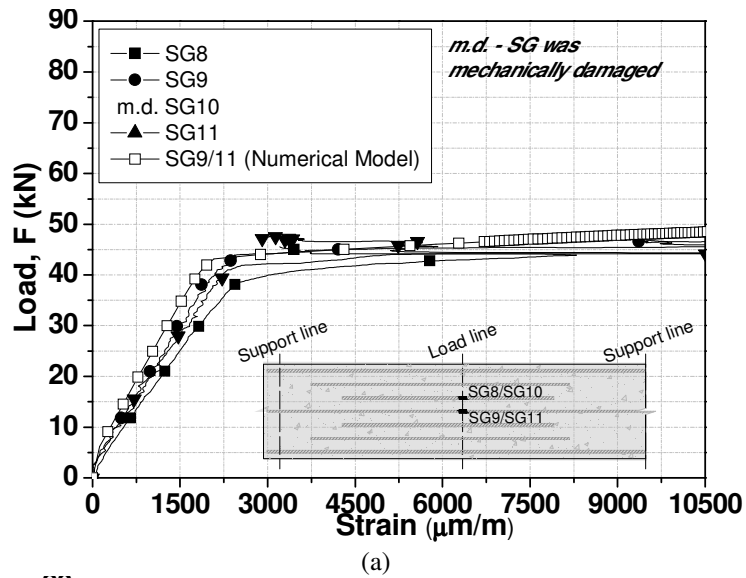
Figure 4.6: Relationship between average load and tensile strain on the positive longitudinal steel reinforcement for the (a) SL15-HS and (b) SL15s25-HS slab strips.

(a)

(b)
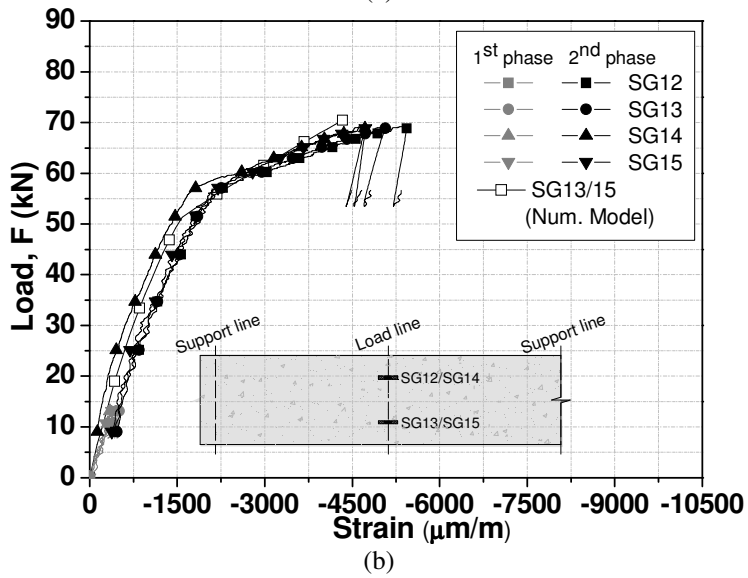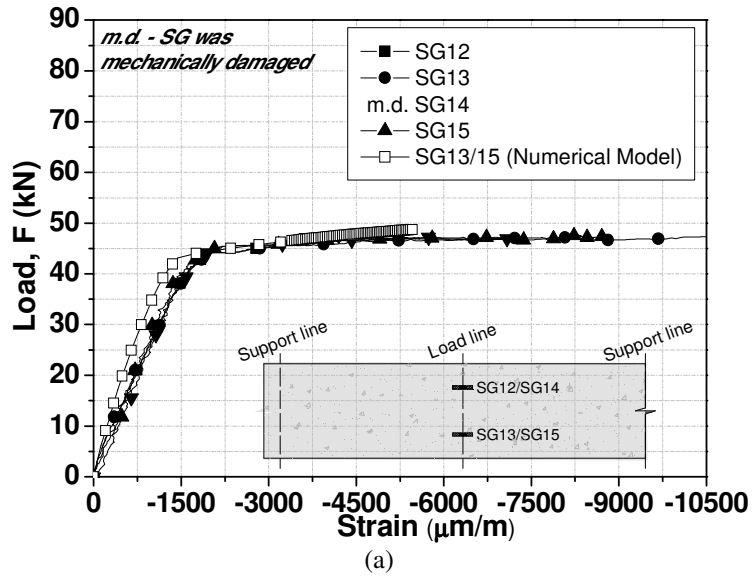
Figure 4.7: Relationship between average load and compressive strain on the concrete at sagging region for the (a) SL15-HS and (b) SL15s25-HS slab strips.
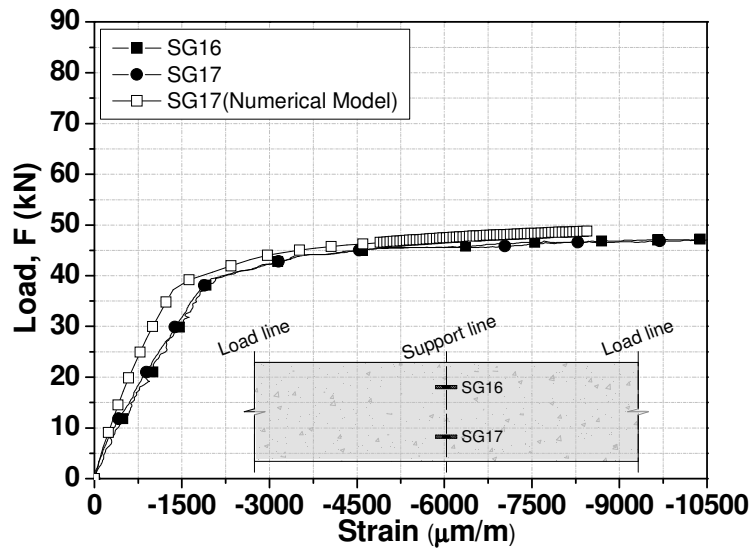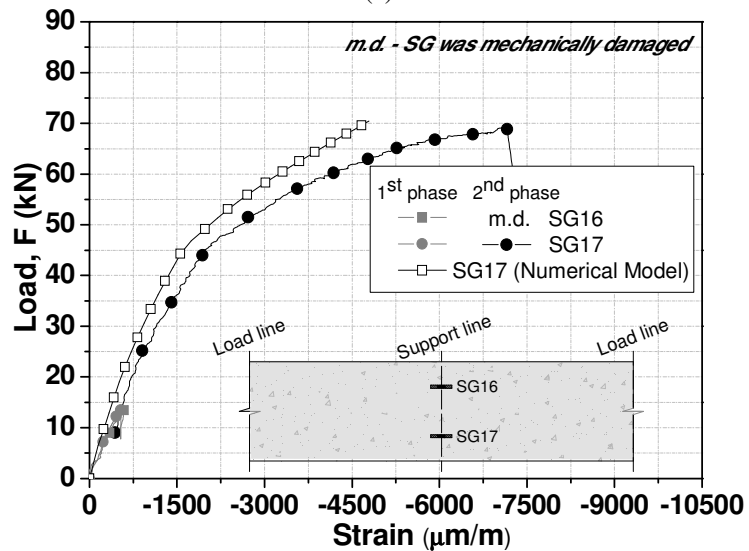
Figure 4.8: Relationship between average load and compressive strain on the concrete at hogging region for the (a) SL15-HS and (b) SL15s25-HS slab strips.
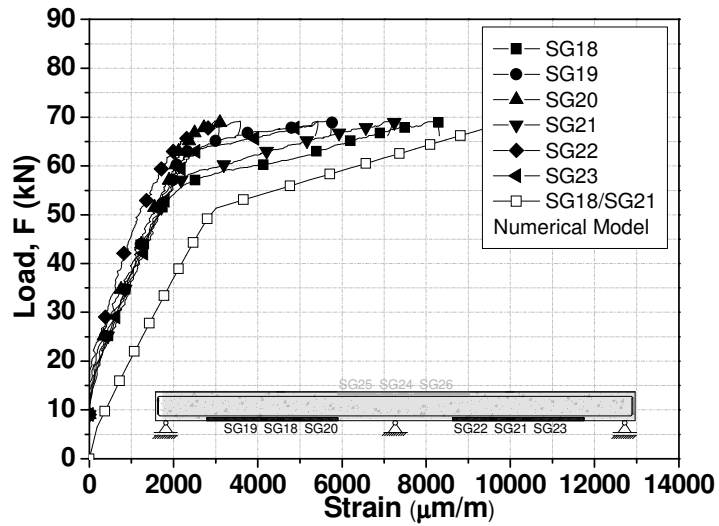
(a)
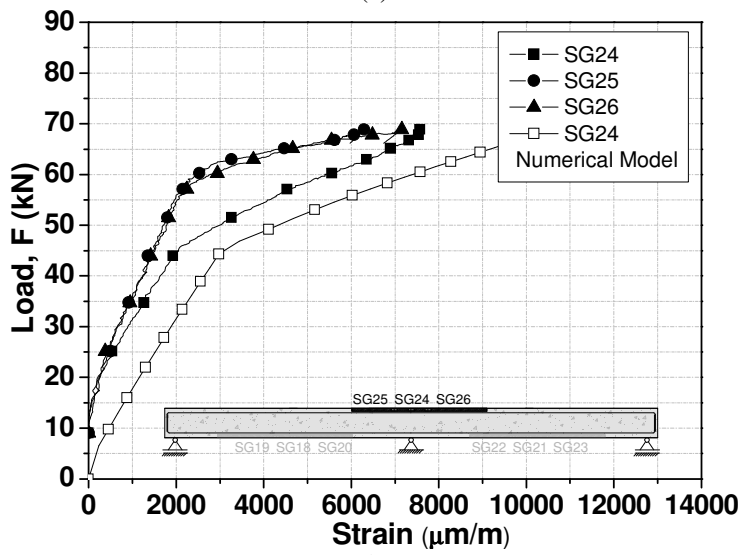
(b)

Figure 4.9: Relationship between average load and tensile strain on the CFRP laminate at (a) sagging and (b) hogging regions for the SL15s25-HS slab strip.
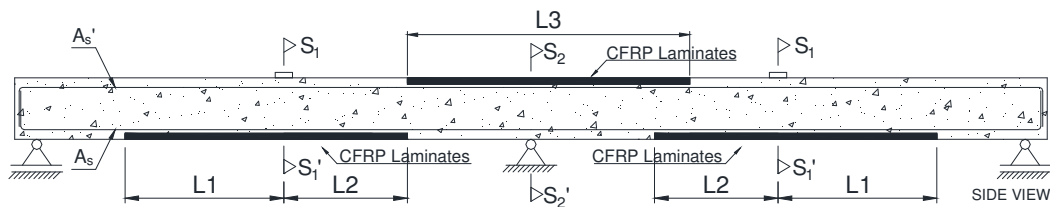
Figure 4.10: Length of the NSM CFRP laminates for the slab strips
(see Tables 4.6, 4.8 and 4.10).

Table 4.4: Concrete properties used for the FEM simulations
(Eurocode 2, 2010; CEB-FIP Model Code, 1993; Sena-Cruz, 2004).

Parameters	C12/15	C25/30	C35/45
Compressive strength	f_{cm} = 20 N/mm^2	f_{cm} = 33 N/mm^2	f_{cm} = 43 N/mm^2
Initial Young's modulus	E_c = 22.85 N/mm^2	E_c = 27.21 N/mm^2	E_c = 30.82 N/mm^2
Poisson's ratio	ν_c =0.00		
Strain at peak compression stress	ε_{c1} = 2.80 × 10^{-3}	ε_{c1} = 2.80 × 10^{-3}	ε_{c1} = 2.80 × 10^{-3}
Tri-linear tension softening [(1)]	f_{ct} = 1.10 N/mm^2 G_f = 0.041 N/mm	f_{ct} = 1.75 N/mm^2 G_f = 0.058 N/mm	f_{ct} = 2.14 N/mm^2 G_f = 0.070 N/mm
	ξ_1= 0.015; α_1= 0.6; ξ_2= 0.2; α_2=0.25		
Parameter defining the initial yield surface	α_0 =0.4		
Parameter defining the mode I fracture energy to the new crack	n=2		
Parameter to define the evolution of the shear retention factor	p_1= 2		
Crack band-width	Square root of the area of Gauss integration point		
Threshold angle	α_{th}= 30°		
Maximum numbers of cracks per integration point	2		

[(1)] $f_{ct} = \sigma_{n,1}^{cr}$; $\xi_1 = \varepsilon_{n,2}^{cr}/\varepsilon_{n,u}^{cr}$; $\alpha_1 = \sigma_{n,2}^{cr}/\sigma_{n,1}^{cr}$; $\xi_2 = \varepsilon_{n,3}^{cr}/\varepsilon_{n,u}^{cr}$; $\alpha_2 = \sigma_{n,3}^{cr}/\sigma_{n,1}^{cr}$ (see Figure 4.2)

In the numerical simulations, the analyses were assumed ended when one of the following two considered failure conditions was attained: (i) when the concrete crushing strain was reached in the sagging region (ε_c^s =3.5‰); (ii) when the effective strain in the CFRP laminates, ε_{fd} , was attained in the sagging or in the hogging region. This ε_{fd} is the maximum tensile strain that can be applied in order to prevent a failure controlled by FRP debonding, also designated by effective failure strain. According to the ACI 440 (2008), for NSM FRP applications $\varepsilon_{fd} = 0.7\varepsilon_{fu}$, where ε_{fu} is the ultimate strain obtained from uniaxial tensile tests.

Tables 4.11 to 4.19 summarize the results obtained in the numerical simulations for the three concrete strength classes, respectively. In these tables, F_y and F_u are, respectively, the load at the formation of the plastic hinge in the hogging region (the first hinge to be formed in all the simulations) and the load when the failure condition has occurred (ε_c^s or ε_{fd} in hogging or sagging regions); Δ_y and Δ_u are the deflections corresponding to F_y and F_u , respectively, ε_c^H and ε_c^s are the maximum concrete compressive strains at H and S, ε_s^H and ε_s^s are the maximum tensile strains in steel bars at H and S, respectively, ε_f^H and ε_f^s are the maximum tensile strains in the CFRP laminates at H and S, and η is the moment redistribution percentage at F_u .

Table 4.5: Resume of the strengthening arrangements of the SL15 Series.

Concrete strength class	Number of laminates		ρ_f^S	ρ_f^H	$\rho_{l,eq}^S$	$\rho_{l,eq}^H$	F.E.M. ID
	S [a]	H [b]	(%)	(%)	(%)	(%)	
C12/15	0	0	0	0	1.71	1.60	SL15_15 [c]
	0	2	0	0.14	1.71	1.72	SL15_15_0_2
	0	4	0	0.27	1.71	1.83	SL15_15_0_4
	0	7	0	0.48	1.71	2.00	SL15_15_0_7
	2	0	0.14	0	1.82	1.60	SL15_15_2_0
	4	0	0.27	0	1.94	1.60	SL15_15_4_0
	7	0	0.48	0	2.10	1.60	SL15_15_7_0
	2	2	0.14	0.14	1.82	1.72	SL15_15_2_2
	2	4	0.14	0.27	1.82	1.83	SL15_15_2_4
	2	7	0.14	0.48	1.82	2.00	SL15_15_2_7
	4	2	0.27	0.14	1.94	1.72	SL15_15_4_2
	4	4	0.27	0.27	1.94	1.83	SL15_15_4_4
	4	7	0.27	0.48	1.94	2.00	SL15_15_4_7
	7	2	0.48	0.14	2.10	1.72	SL15_15_7_2
	7	4	0.48	0.27	2.10	1.83	SL15_15_7_4
	7	7	0.48	0.48	2.10	2.00	SL15_15_7_7
C25/30	0	0	0	0	1.71	1.60	SL15_30 [c]
	0	2	0	0.14	1.71	1.72	SL15_30_0_2
	0	4	0	0.27	1.71	1.83	SL15_30_0_4
	0	7	0	0.48	1.71	2.00	SL15_30_0_7
	2	0	0.14	0	1.82	1.60	SL15_30_2_0
	4	0	0.27	0	1.94	1.60	SL15_30_4_0
	7	0	0.48	0	2.10	1.60	SL15_30_7_0
	2	2	0.14	0.14	1.82	1.72	SL15_30_2_2
	2	4	0.14	0.27	1.82	1.83	SL15_30_2_4
	2	7	0.14	0.48	1.82	2.00	SL15_30_2_7
	4	2	0.27	0.14	1.94	1.72	SL15_30_4_2
	4	4	0.27	0.27	1.94	1.83	SL15_30_4_4
	4	7	0.27	0.48	1.94	2.00	SL15_30_4_7
	7	2	0.48	0.14	2.10	1.72	SL15_30_7_2
	7	4	0.48	0.27	2.10	1.83	SL15_30_7_4
	7	7	0.48	0.48	2.10	2.00	SL15_30_7_7
C35/45	0	0	0	0	1.71	1.60	SL15_45 [c]
	0	2	0	0.14	1.71	1.72	SL15_45_0_2
	0	4	0	0.27	1.71	1.83	SL15_45_0_4
	0	7	0	0.48	1.71	2.00	SL15_45_0_7
	2	0	0.14	0	1.82	1.60	SL15_45_2_0
	4	0	0.27	0	1.94	1.60	SL15_45_4_0
	7	0	0.48	0	2.10	1.60	SL15_45_7_0
	2	2	0.14	0.14	1.82	1.72	SL15_45_2_2
	2	4	0.14	0.27	1.82	1.83	SL15_45_2_4
	2	7	0.14	0.48	1.82	2.00	SL15_45_2_7
	4	2	0.27	0.14	1.94	1.72	SL15_45_4_2
	4	4	0.27	0.27	1.94	1.83	SL15_45_4_4
	4	7	0.27	0.48	1.94	2.00	SL15_45_4_7
	7	2	0.48	0.14	2.10	1.72	SL15_45_7_2
	7	4	0.48	0.27	2.10	1.83	SL15_45_7_4
	7	7	0.48	0.48	2.10	2.00	SL15_45_7_7

[a] *Sagging region;* [b] *Hogging region;* [c] *Reference slab strip*

Table 4.6: Length of the NSM CFRP laminates for the SL15 Series (see Figure 4.10).

Concrete strength class	F.E.M. ID	S (a)				H (b)	
		Number of CFRP laminates	L1 Length (mm)	L2 Length (mm)	Total length (mm)	Number of CFRP laminates	L3 Total length (mm)
C12/15	SL15_15 (c)	0	-----	-----	-----	0	-----
	SL15_15_0_2	0	-----	-----	-----	2	637.07
	SL15_15_0_4	0	-----	-----	-----	4	701.03
	SL15_15_0_7	0	-----	-----	-----	7	760.73
	SL15_15_2_0	2	721.17	630.11	1351.28	0	-----
	SL15_15_4_0	4	822.06	691.88	1513.94	0	-----
	SL15_15_7_0	7	910.36	750.10	1660.46	0	-----
	SL15_15_2_2	2	721.17	621.57	1342.74	2	628.57
	SL15_15_2_4	2	721.17	616.86	1338.03	4	688.51
	SL15_15_2_7	2	721.17	612.43	1333.6	7	744.83
	SL15_15_4_2	4	822.06	679.14	1501.2	2	623.76
	SL15_15_4_4	4	822.06	672.07	1494.13	4	681.37
	SL15_15_4_7	4	822.06	665.39	1487.45	7	735.73
	SL15_15_7_2	7	910.36	733.80	1644.16	2	619.19
	SL15_15_7_4	7	910.36	724.69	1635.05	4	674.57
	SL15_15_7_7	7	910.36	716.07	1626.43	7	727.01
C25/30	SL15_30 (c)	0	-----	-----	-----	0	-----
	SL15_30_0_2	0	-----	-----	-----	2	727.55
	SL15_30_0_4	0	-----	-----	-----	4	822.87
	SL15_30_0_7	0	-----	-----	-----	7	906.45
	SL15_30_2_0	2	865.77	720.47	1586.24	0	-----
	SL15_30_4_0	4	1000.66	814.54	1815.2	0	-----
	SL15_30_7_0	7	1108.62	897.84	2006.46	0	-----
	SL15_30_2_2	2	865.77	694.45	1560.22	2	701.69
	SL15_30_2_4	2	865.77	682.12	1547.89	4	787.80
	SL15_30_2_7	2	865.77	671.10	1536.87	7	864.74
	SL15_30_4_2	4	1000.66	778.92	1779.58	2	689.16
	SL15_30_4_4	4	1000.66	761.80	1762.46	4	770.56
	SL15_30_4_7	4	1000.66	746.36	1747.02	7	843.97
	SL15_30_7_2	7	1108.62	855.24	1963.86	2	677.85
	SL15_30_7_4	7	1108.62	834.46	1943.08	4	754.84
	SL15_30_7_7	7	1108.62	815.56	1924.18	7	824.86
C35/45	SL15_45 (c)	0	-----	-----	-----	0	-----
	SL15_45_0_2	0	-----	-----	-----	2	793.81
	SL15_45_0_4	0	-----	-----	-----	4	906.31
	SL15_45_0_7	0	-----	-----	-----	7	1001.15
	SL15_45_2_0	2	961.58	789.01	1750.59	0	-----
	SL15_45_4_0	4	1109.15	901.89	2011.04	0	-----
	SL15_45_7_0	7	1220.83	997.41	2218.24	0	-----
	SL15_45_2_2	2	961.58	742.52	1704.1	2	750.29
	SL15_45_2_4	2	961.58	723.52	1685.1	4	850.15
	SL15_45_2_7	2	961.58	707.03	1668.61	7	936.87
	SL15_45_4_2	4	1109.15	841.43	1950.58	2	730.94
	SL15_45_4_4	4	1109.15	816.12	1925.27	4	824.60
	SL15_45_4_7	4	1109.15	793.83	1902.98	7	907.04
	SL15_45_7_2	7	1220.83	927.89	2148.72	2	714.03
	SL15_45_7_4	7	1220.83	898.15	2118.98	4	801.96
	SL15_45_7_7	7	1220.83	871.66	2092.49	7	880.29

(a) Sagging region; (b) Hogging region; (c) Reference slab strip

Table 4.7: Resume of the strengthening arrangements of the SL30 Series.

Concrete strength class	Number of laminates		ρ_f^S (%)	ρ_f^H (%)	$\rho_{l,eq}^S$ (%)	$\rho_{l,eq}^H$ (%)	F.E.M. ID
	S [a]	H [b]					
C12/15	0	0	0	0	1.85	1.28	SL30_15 [c]
	0	2	0	0.14	1.85	1.40	SL30_15_0_2
	0	4	0	0.27	1.85	1.51	SL30_15_0_4
	0	7	0	0.48	1.85	1.68	SL30_15_0_7
	2	0	0.14	0	1.97	1.28	SL30_15_2_0
	4	0	0.27	0	2.08	1.28	SL30_15_4_0
	7	0	0.48	0	2.25	1.28	SL30_15_7_0
	2	2	0.14	0.14	1.97	1.40	SL30_15_2_2
	2	4	0.14	0.27	1.97	1.51	SL30_15_2_4
	2	7	0.14	0.48	1.97	1.68	SL30_15_2_7
	4	2	0.27	0.14	2.08	1.40	SL30_15_4_2
	4	4	0.27	0.27	2.08	1.51	SL30_15_4_4
	4	7	0.27	0.48	2.08	1.68	SL30_15_4_7
	7	2	0.48	0.14	2.25	1.40	SL30_15_7_2
	7	4	0.48	0.27	2.25	1.51	SL30_15_7_4
	7	7	0.48	0.48	2.25	1.68	SL30_15_7_7
C25/30	0	0	0	0	1.85	1.28	SL30_30 [c]
	0	2	0	0.14	1.85	1.40	SL30_30_0_2
	0	4	0	0.27	1.85	1.51	SL30_30_0_4
	0	7	0	0.48	1.85	1.68	SL30_30_0_7
	2	0	0.14	0	1.97	1.28	SL30_30_2_0
	4	0	0.27	0	2.08	1.28	SL30_30_4_0
	7	0	0.48	0	2.25	1.28	SL30_30_7_0
	2	2	0.14	0.14	1.97	1.40	SL30_30_2_2
	2	4	0.14	0.27	1.97	1.51	SL30_30_2_4
	2	7	0.14	0.48	1.97	1.68	SL30_30_2_7
	4	2	0.27	0.14	2.08	1.40	SL30_30_4_2
	4	4	0.27	0.27	2.08	1.51	SL30_30_4_4
	4	7	0.27	0.48	2.08	1.68	SL30_30_4_7
	7	2	0.48	0.14	2.25	1.40	SL30_30_7_2
	7	4	0.48	0.27	2.25	1.51	SL30_30_7_4
	7	7	0.48	0.48	2.25	1.68	SL30_30_7_7
C35/45	0	0	0	0	1.85	1.28	SL30_45 [c]
	0	2	0	0.14	1.85	1.40	SL30_45_0_2
	0	4	0	0.27	1.85	1.51	SL30_45_0_4
	0	7	0	0.48	1.85	1.68	SL30_45_0_7
	2	0	0.14	0	1.97	1.28	SL30_45_2_0
	4	0	0.27	0	2.08	1.28	SL30_45_4_0
	7	0	0.48	0	2.25	1.28	SL30_45_7_0
	2	2	0.14	0.14	1.97	1.40	SL30_45_2_2
	2	4	0.14	0.27	1.97	1.51	SL30_45_2_4
	2	7	0.14	0.48	1.97	1.68	SL30_45_2_7
	4	2	0.27	0.14	2.08	1.40	SL30_45_4_2
	4	4	0.27	0.27	2.08	1.51	SL30_45_4_4
	4	7	0.27	0.48	2.08	1.68	SL30_45_4_7
	7	2	0.48	0.14	2.25	1.40	SL30_45_7_2
	7	4	0.48	0.27	2.25	1.51	SL30_45_7_4
	7	7	0.48	0.48	2.25	1.68	SL30_45_7_7

[a] *Sagging region;* [b] *Hogging region;* [c] *Reference slab strip*

Table 4.8: Length of the NSM CFRP laminates for the SL30 Series (see Figure 4.10).

Concrete strength class	F.E.M. ID	S (a)				H (b)	
		Number of CFRP laminates	L1 Length (mm)	L2 Length (mm)	Total length (mm)	Number of CFRP laminates	L3 Total length (mm)
C12/15	SL30_15 [c]	0	-----	-----	-----	0	-----
	SL30_15_0_2	0	-----	-----	-----	2	671.29
	SL30_15_0_4	0	-----	-----	-----	4	744.47
	SL30_15_0_7	0	-----	-----	-----	7	809.79
	SL30_15_2_0	2	713.29	637.77	1351.06	0	-----
	SL30_15_4_0	4	760.02	668.49	1428.51	0	-----
	SL30_15_7_0	7	839.76	723.15	1562.91	0	-----
	SL30_15_2_2	2	713.29	626.01	1339.30	2	659.84
	SL30_15_2_4	2	713.29	620.24	1333.53	4	728.40
	SL30_15_2_7	2	713.29	615.05	1328.34	7	790.12
	SL30_15_4_2	4	760.02	653.98	1414.00	2	656.82
	SL30_15_4_4	4	760.02	646.84	1406.86	4	724.14
	SL30_15_4_7	4	760.02	640.40	1400.42	7	784.87
	SL30_15_7_2	7	839.76	704.08	1543.84	2	651.40
	SL30_15_7_4	7	839.76	694.64	1534.40	4	716.47
	SL30_15_7_7	7	839.76	686.09	1525.85	7	775.41
C25/30	SL30_30 [c]	0	-----	-----	-----	0	-----
	SL30_30_0_2	0	-----	-----	-----	2	764.49
	SL30_30_0_4	0	-----	-----	-----	4	864.13
	SL30_30_0_7	0	-----	-----	-----	7	948.99
	SL30_30_2_0	2	807.33	702.64	1509.97	0	-----
	SL30_30_4_0	4	933.68	794.29	1727.97	0	-----
	SL30_30_7_0	7	1039.46	877.35	1916.81	0	-----
	SL30_30_2_2	2	807.33	674.26	1481.59	2	737.55
	SL30_30_2_4	2	807.33	662.31	1469.64	4	829.15
	SL30_30_2_7	2	807.33	651.95	1459.28	7	908.56
	SL30_30_4_2	4	933.68	754.41	1688.09	2	723.55
	SL30_30_4_4	4	933.68	737.34	1671.02	4	810.71
	SL30_30_4_7	4	933.68	722.39	1656.07	7	886.97
	SL30_30_7_2	7	1039.46	828.70	1868.16	2	710.58
	SL30_30_7_4	7	1039.46	804.55	1844.01	4	793.45
	SL30_30_7_7	7	1039.46	788.88	1828.34	7	866.60
C35/45	SL30_45 [c]	0	-----	-----	-----	0	-----
	SL30_45_0_2	0	-----	-----	-----	2	818.87
	SL30_45_0_4	0	-----	-----	-----	4	930.12
	SL30_45_0_7	0	-----	-----	-----	7	1022.26
	SL30_45_2_0	2	883.87	758.07	1641.94	0	-----
	SL30_45_4_0	4	1023.95	868.88	1892.83	0	-----
	SL30_45_7_0	7	1135.63	959.72	2095.35	0	-----
	SL30_45_2_2	2	883.87	714.30	1598.17	2	777.39
	SL30_45_2_4	2	883.87	697.15	1581.02	4	878.23
	SL30_45_2_7	2	883.87	682.58	1566.45	7	963.94
	SL30_45_4_2	4	1023.95	807.19	1831.14	2	757.56
	SL30_45_4_4	4	1023.95	783.64	1807.59	4	852.89
	SL30_45_4_7	4	1023.95	763.36	1787.31	7	934.95
	SL30_45_7_2	7	1135.63	890.71	2026.34	2	739.73
	SL30_45_7_4	7	1135.63	862.41	1998.04	4	829.81
	SL30_45_7_7	7	1135.63	837.78	1973.41	7	908.26

[a] *Sagging region;* [b] *Hogging region;* [c] *Reference slab strip*

Table 4.9: Resume of the strengthening arrangements of the SL45 Series.

Concrete strength class	Number of laminates		ρ_f^S (%)	ρ_f^H (%)	$\rho_{l,eq}^S$ (%)	$\rho_{l,eq}^H$ (%)	F.E.M. ID
	S [a]	H [b]					
C12/15	0	0	0	0	0.95	2.07	SL45_15 [c]
	0	2	0	0.14	0.95	2.18	SL45_15_0_2
	0	4	0	0.27	0.95	2.29	SL45_15_0_4
	0	7	0	0.48	0.95	2.46	SL45_15_0_7
	2	0	0.14	0	1.07	2.07	SL45_15_2_0
	4	0	0.27	0	1.18	2.07	SL45_15_4_0
	7	0	0.48	0	1.35	2.07	SL45_15_7_0
	2	2	0.14	0.14	1.07	2.18	SL45_15_2_2
	2	4	0.14	0.27	1.07	2.29	SL45_15_2_4
	2	7	0.14	0.48	1.07	2.46	SL45_15_2_7
	4	2	0.27	0.14	1.18	2.18	SL45_15_4_2
	4	4	0.27	0.27	1.18	2.29	SL45_15_4_4
	4	7	0.27	0.48	1.18	2.46	SL45_15_4_7
	7	2	0.48	0.14	1.35	2.18	SL45_15_7_2
	7	4	0.48	0.27	1.35	2.29	SL45_15_7_4
	7	7	0.48	0.48	1.35	2.46	SL45_15_7_7
C25/30	0	0	0	0	0.95	2.07	SL45_30 [c]
	0	2	0	0.14	0.95	2.18	SL45_30_0_2
	0	4	0	0.27	0.95	2.29	SL45_30_0_4
	0	7	0	0.48	0.95	2.46	SL45_30_0_7
	2	0	0.14	0	1.07	2.07	SL45_30_2_0
	4	0	0.27	0	1.18	2.07	SL45_30_4_0
	7	0	0.48	0	1.35	2.07	SL45_30_7_0
	2	2	0.14	0.14	1.07	2.18	SL45_30_2_2
	2	4	0.14	0.27	1.07	2.29	SL45_30_2_4
	2	7	0.14	0.48	1.07	2.46	SL45_30_2_7
	4	2	0.27	0.14	1.18	2.18	SL45_30_4_2
	4	4	0.27	0.27	1.18	2.29	SL45_30_4_4
	4	7	0.27	0.48	1.18	2.46	SL45_30_4_7
	7	2	0.48	0.14	1.35	2.18	SL45_30_7_2
	7	4	0.48	0.27	1.35	2.29	SL45_30_7_4
	7	7	0.48	0.48	1.35	2.46	SL45_30_7_7
C35/45	0	0	0	0	0.95	2.07	SL45_45 [c]
	0	2	0	0.14	0.95	2.18	SL45_45_0_2
	0	4	0	0.27	0.95	2.29	SL45_45_0_4
	0	7	0	0.48	0.95	2.46	SL45_45_0_7
	2	0	0.14	0	1.07	2.07	SL45_45_2_0
	4	0	0.27	0	1.18	2.07	SL45_45_4_0
	7	0	0.48	0	1.35	2.07	SL45_45_7_0
	2	2	0.14	0.14	1.07	2.18	SL45_45_2_2
	2	4	0.14	0.27	1.07	2.29	SL45_45_2_4
	2	7	0.14	0.48	1.07	2.46	SL45_45_2_7
	4	2	0.27	0.14	1.18	2.18	SL45_45_4_2
	4	4	0.27	0.27	1.18	2.29	SL45_45_4_4
	4	7	0.27	0.48	1.18	2.46	SL45_45_4_7
	7	2	0.48	0.14	1.35	2.18	SL45_45_7_2
	7	4	0.48	0.27	1.35	2.29	SL45_45_7_4
	7	7	0.48	0.48	1.35	2.46	SL45_45_7_7

[a] *Sagging region;* [b] *Hogging region;* [c] *Reference slab strip*

Table 4.10: Length of the NSM CFRP laminates for the SL45 Series (see Figure 4.10).

Concrete strength class	F.E.M. ID	S (a)				H (b)	
		Number of CFRP laminates	L1 Length (mm)	L2 Length (mm)	Total length (mm)	Number of CFRP laminates	L3 Total length (mm)
C12/15	SL45_15 (c)	0	-----	-----	-----	0	-----
	SL45_15_0_2	0	-----	-----	-----	2	730.88
	SL45_15_0_4	0	-----	-----	-----	4	814.94
	SL45_15_0_7	0	-----	-----	-----	7	885.64
	SL45_15_2_0	2	639.36	600.97	1240.33	0	-----
	SL45_15_4_0	4	712.00	652.67	1364.67	0	-----
	SL45_15_7_0	7	782.28	704.55	1486.83	0	-----
	SL45_15_2_2	2	639.36	589.38	1228.74	2	720.43
	SL45_15_2_4	2	639.36	584.70	1224.06	4	801.31
	SL45_15_2_7	2	639.36	580.74	1220.10	7	869.78
	SL45_15_4_2	4	712.00	634.32	1346.32	2	713.66
	SL45_15_4_4	4	712.00	626.85	1338.85	4	792.43
	SL45_15_4_7	4	712.00	620.51	1332.51	7	859.39
	SL45_15_7_2	7	782.28	679.93	1462.21	2	706.79
	SL45_15_7_4	7	782.28	669.83	1452.11	4	783.38
	SL45_15_7_7	7	782.28	661.21	1443.49	7	848.76
C25/30	SL45_30 (c)	0	-----	-----	-----	0	-----
	SL45_30_0_2	0	-----	-----	-----	2	823.68
	SL45_30_0_4	0	-----	-----	-----	4	927.60
	SL45_30_0_7	0	-----	-----	-----	7	1012.88
	SL45_30_2_0	2	761.35	691.94	1453.29	0	-----
	SL45_30_4_0	4	878.47	783.02	1661.49	0	-----
	SL45_30_7_0	7	980.29	866.76	1847.05	0	-----
	SL45_30_2_2	2	761.35	658.32	1419.67	2	793.68
	SL45_30_2_4	2	761.35	646.40	1407.75	4	890.80
	SL45_30_2_7	2	761.35	636.44	1397.79	7	971.88
	SL45_30_4_2	4	878.47	734.72	1613.19	2	777.11
	SL45_30_4_4	4	878.47	717.24	1595.71	4	870.17
	SL45_30_4_7	4	878.47	702.50	1580.97	7	948.63
	SL45_30_7_2	7	980.29	806.96	1787.25	2	761.44
	SL45_30_7_4	7	980.29	784.91	1765.20	4	850.47
	SL45_30_7_7	7	980.29	766.14	1746.43	7	926.22
C35/45	SL45_45 (c)	0	-----	-----	-----	0	-----
	SL45_45_0_2	0	-----	-----	-----	2	876.59
	SL45_45_0_4	0	-----	-----	-----	4	989.14
	SL45_45_0_7	0	-----	-----	-----	7	1079.91
	SL45_45_2_0	2	833.58	748.66	1582.24	0	-----
	SL45_45_4_0	4	967.57	857.64	1825.21	0	-----
	SL45_45_7_0	7	1078.15	953.42	2031.57	0	-----
	SL45_45_2_2	2	833.58	697.82	1531.40	2	831.30
	SL45_45_2_4	2	833.58	680.84	1514.42	4	935.24
	SL45_45_2_7	2	833.58	666.80	1500.38	7	1021.20
	SL45_45_4_2	4	967.57	788.11	1755.68	2	808.30
	SL45_45_4_4	4	967.57	764.23	1731.80	4	907.30
	SL45_45_4_7	4	967.57	744.23	1711.80	7	990.23
	SL45_45_7_2	7	1078.15	870.68	1948.83	2	787.27
	SL45_45_7_4	7	1078.15	841.54	1919.69	4	881.39
	SL45_45_7_7	7	1078.15	816.83	1894.98	7	961.20

(a) *Sagging region;* (b) *Hogging region;* (c) *Reference slab strip*

The failure mode governed the interruption of an analysis is also indicated in these tables (last column). The results obtained allow pointing out the following observations:

1. When the NSM CFRP laminates are applied only in the hogging region, regardless of the concrete strength class, the first plastic hinge (coinciding with the yield initiation of tensile steel bars) occurred at the hogging region, followed by the formation of a plastic hinge in the sagging regions, and the analysis ended due to the concrete crushing occurrence in the sagging regions.

2. For any value of ρ_f^H, regardless the concrete strength class, the increase of ρ_f^S provided an increase of Δ_u and a small decrease of Δ_y, leading to an increase of the deflection amplitude between the formation of the plastic hinges in the hogging and sagging regions (Δ_u - Δ_y), which contributes to better performances of the corresponding strengthening configurations in terms of load-carrying and deflection capacities, as will be observed in next section. In contrast, for any value of ρ_f^S and regardless the concrete strength class, the increase of ρ_f^H provided a decrease of Δ_u and an increase of Δ_y, resulting a decrease of (Δ_u - Δ_y), with a detrimental consequence in terms of load-carrying and deflection capacities.

3. The aforementioned tendencies in terms Δ_y and Δ_u were also observed for the load-carrying capacity (F_y and F_u). In fact, for all the concrete strength classes considered, the increase of F_u with ρ_f^H was much smaller than with the increase of ρ_f^S, which is in agreement with the experimental results presented in Chapter 3.

4. The increase of the concrete strength class led to a higher probability of the failure condition to be governed by the attainment of the effective failure strain, ε_{fd}.

4.2.2.1   The load carrying capacity index

The load carrying capacity index (λ) is defined as the ratio between the load carrying capacity of the strengthened $\left(F_{streng}\right)$ and the corresponding reference slab $\left(F_{ref}\right)$, $\lambda = F_{streng} / F_{ref}$, where F is the force at the initiation of the second plastic hinge. The relationships between λ and $\rho_{s,eq}$ in the hogging ($\rho_{s,eq}^H$) and sagging ($\rho_{s,eq}^S$) regions are represented in Figures 4.11 to 4.13 and Tables 4.20 to 4.22. In these graphs, the results obtained in the experimental programs are also indicated (see also Table 4.23, where the

relevant results of these experimental programs are indicated). In these figures the relationships $\lambda - \rho_f^S$ and $\lambda - \rho_f^H$ are also indicated, where ρ_f^S and ρ_f^S is the percentage of CFRP in the sagging and hogging regions, respectively. As expected, the load carrying capacity of the strengthened slabs increases with $\rho_{s,eq}^S$ and $\rho_{s,eq}^H$, but the increase of λ is more pronounced with $\rho_{s,eq}^S$. For the slabs only strengthened in the hogging region, the increase of λ is less than 19%, 22% and 23% for the SL15, SL30 and SL45 series, which is in agreement to the experimental results presented in Chapter 3. In the slab strips only strengthened in the sagging region, a maximum increase of 67%, 58% and 39% for the SL15, SL30 and SL45 series was obtained. As expected, to increase significantly the load carrying capacity of this type of slabs, a flexural strengthening strategy composed by CFRP laminates applied in both hogging and sagging regions should be adopted. According to the results, a maximum increase of 108%, 103% and 97% for the SL15, SL30 and SL45 series was obtained. Additionally, the analysis of the results and the observations of Barros and Kotynia (2008) indicate that the increase of the load carrying capacity with the increase of ρ_f^S and ρ_f^H would be even higher if smaller values of ρ_s^H and ρ_s^S have been used (the values adopted in this parametric study were relatively high for RC slabs).

However, the failure mode of the slab strips can affect the increase of the load carrying capacity, mainly in the cases where the CFRP laminates placed in the hogging region have reached their effective strain before the concrete crushing has occurred (these cases are represented by black circles in Figure 4.11 to 4.13). The experimental results obtained in previous chapter are also indicated in Figures 4.11 to 4.13, and they are in good agreement with the data obtained from the parametric study. It should be noted that the red circles indicate the numerical simulations where at the last converged load level neither the concrete crushing in the sagging region (ε_c^S =3.5‰) nor the effective strain in the CFRP laminates in both sagging and hogging regions was attained.

4.2.2.2 Displacement Ductility Index

The displacement ductility (Δ) is defined as the ratio between the displacements of the loaded section at the formation of the second and the first hinges ($\Delta = \Delta_{2nd} / \Delta_{1st}$). The displacement ductility index (μ_Δ) is expressed as the ratio between the displacement ductility of the strengthened (Δ_{streng}) and the reference (Δ_{ref}) slab strips ($\mu_\Delta = \Delta_{streng} / \Delta_{ref}$).

The relationships $\mu_\Delta - \rho_{s,eq}^S$ and $\mu_\Delta - \rho_{s,eq}^H$ are represented in Figures 4.14 to 4.16, while the corresponding obtained values are included in Tables 4.20 to 4.22. In these figures it is also indicated the relationships $\mu_\Delta - \rho_f^S$ and $\mu_\Delta - \rho_f^H$. From the results it can be noted that the displacement ductility index decreases with the increase of the percentage of the CFRP laminates in the hogging region. In fact, values of μ_Δ smaller than 1 were obtained for some strengthening configurations, which means that these configurations have a detrimental influence in terms of deflection ductility performance. However, the displacement ductility increases with ρ_f^S, and values of μ_Δ higher than 1 are obtained for the configurations with $\rho_f^H = 0$.

Figures 4.14 to 4.16 also evidences concordance between the results of this parametric study and the data obtained in the experimental programs described in Chapter 3.

4.2.2.3 Rotational Ductility Index

The rotational ductility (ν) is defined as the ratio between the curvatures of the loaded section at the formation of the second and the first hinges ($\nu = \chi_{2nd} / \chi_{1st}$). The rotational ductility index (μ_χ) is expressed as the ratio between the rotational ductility of the strengthened (ν_{streng}) and the reference (ν_{ref}) slab strips ($\mu_\chi = \nu_{streng} / \nu_{ref}$). The relationships $\mu_\chi - \rho_{s,eq}^S$ and $\mu_\chi - \rho_{s,eq}^H$ are represented in Figures 4.17 to 4.19, while the corresponding obtained values are included in Tables 4.20 to 4.22. In these figures it is also indicated the relationships $\mu_\chi - \rho_f^S$ and $\mu_\chi - \rho_f^H$.

In the hogging region, the rotational ductility decreases with the increase of the percentage of the CFRP laminates in this region. In fact, values of μ_χ smaller than 1 were obtained for some strengthening configurations, which means that these configurations have a detrimental influence in terms of rotational ductility performance. However, the rotational ductility increases with ρ_f^S, and values of μ_χ higher than 1 are obtained for the configurations with $\rho_f^H = 0$.

In the slab strips strengthened in both sagging and hogging regions, $\mu_\chi < 1$, which means that the strengthened sections of a strengthened slab have a considerable lower rotational capacity than the corresponding sections of its reference slab.

4.2.2.4   Moment redistribution analysis

The moment redistribution index (*MRI*) is defined as the ratio between the η of a strengthened slab, η_{streng}, and the η of its reference slab, η_{ref}, ($MRI = \eta_{streng}/\eta_{ref}$), where η is the moment redistribution percentage at the formation of the second hinge (in the sagging region).

The relationships $MRI - \rho_{s,eq}^{S}$ and $MRI - \rho_{s,eq}^{H}$ are shown in Figures 4.20 to 4.22, while the corresponding obtained values are included in Tables 4.20 to 4.22. In these figures it is also indicated the relationships $MRI - \rho_{f}^{S}$ and $MRI - \rho_{f}^{H}$.

It is observed that the *MRI* depends strongly on the strengthening arrangement. In the slab strips only strengthened in the hogging region η_{streng} is less than η_{ref}. Increasing the percentage of laminates in the sagging region, *MRI* increases, regardless the $\rho_{s,eq}^{H}$.

For slabs only strengthened in the sagging regions, *MRI*>1.0, which means that this type of slabs has higher moment redistribution capacity than its reference slab. However, with the increase of the percentage of laminates in the hogging region the *MRI* decreases. Figures 4.20 to 4.22 show a good agreement between the results of the parametric study and the values obtained in the experimental programs described in Chapter 3.

To avoid a decrease in the moment redistribution capacity, CFRP laminates strips should be applied in both sagging and hogging regions, in appropriate percentages. Figure 4.23 shows that the moment redistribution index increases with $\rho_{s,eq}^{S}/\rho_{s,eq}^{H}$. For $\rho_{s,eq}^{S}/\rho_{s,eq}^{H}$ >1.09, $\rho_{s,eq}^{S}/\rho_{s,eq}^{H}$ >1.49 and $\rho_{s,eq}^{S}/\rho_{s,eq}^{H}$ >2.27 the *MRI* is positive for η equal to 15%, 30% and 45%, respectively.

Table 4.11: Main results of the numerical simulations – concrete strength class C12/15 – SL15.

Concrete strength class C12/15	When the first hinge was formed								Failure									Failure mode
	F_y	Δ_y	ε_c^H	ε_s^H	ε_f^H	ε_c^S	ε_s^S	ε_f^S	F_u	Δ_u	ε_c^H	ε_s^H	ε_f^H	ε_c^S	ε_s^S	ε_f^S	η	
	(kN)	(mm)	(‰)	(‰)	(‰)	(‰)	(‰)	(‰)	(kN)	(mm)	(‰)	(‰)	(‰)	(‰)	(‰)	(‰)	(%)	
Reference	36.83	14.38	-1.76	2.40	----	-1.36	1.70	----	44.31	23.08	-4.76	9.25	----	-3.50	6.26	----	9.78	Concrete crushing at S
SL15_15_0_2	40.37	15.55	-1.91	2.40	3.49	-1.51	1.85	----	46.87	21.98	-3.23	5.13	7.25	-3.50	6.26	----	0.16	Concrete crushing at S
SL15_15_0_4	43.63	16.46	-2.07	2.40	3.54	-1.65	2.00	----	48.58	21.37	-2.92	3.95	5.69	-3.50	6.26	----	-5.71	Concrete crushing at S
SL15_15_0_7	47.91	18.12	-2.32	2.40	3.60	-2.36	3.65	----	50.42	20.83	-2.73	3.03	4.50	-3.50	6.26	----	-11.59	Concrete crushing at S
SL15_15_2_0	38.18	14.21	-1.77	2.40	----	-1.37	1.61	2.36	51.89	28.53	-6.86	13.68	----	-3.50	5.39	7.63	19.56	Concrete crushing at S
SL15_15_2_2	41.67	15.24	-1.92	2.40	3.50	-1.51	1.74	2.56	55.25	26.54	-4.30	7.17	10.08	-3.50	5.25	7.43	7.09	Concrete crushing at S
SL15_15_2_4	50.00	16.18	-2.08	2.40	3.54	-1.64	1.86	2.74	57.86	26.21	-3.84	5.54	7.92	-3.50	5.38	7.61	0.26	Concrete crushing at S
SL15_15_2_7	49.87	17.56	-2.32	2.40	3.60	-1.81	2.14	3.00	59.10	24.14	-3.38	4.00	5.88	-3.50	4.97	7.62	-6.31	Concrete crushing at S
SL15_15_4_0	39.43	14.01	-1.77	2.40	----	-1.38	1.53	2.26	57.62	30.67	-8.01	16.04	----	-3.50	4.70	6.76	26.10	Concrete crushing at S
SL15_15_4_2	42.73	14.91	-1.92	2.40	3.50	-1.51	1.64	2.43	61.87	28.98	-4.92	8.33	11.70	-3.50	4.70	6.76	12.88	Concrete crushing at S
SL15_15_4_4	46.09	15.83	-2.07	2.40	3.54	-1.64	1.75	2.61	64.46	28.11	-4.31	6.31	9.00	-3.50	4.70	6.76	5.66	Concrete crushing at S
SL15_15_4_7	51.32	17.26	-2.32	2.40	3.60	-1.85	1.93	2.88	67.33	27.29	-3.97	4.85	7.09	-3.50	4.70	6.76	-1.68	Concrete crushing at S
SL15_15_7_0	40.33	13.43	-1.75	2.40	----	-1.36	1.39	2.08	64.00	31.43	-8.84	17.72	----	-3.50	3.93	5.80	32.63	Concrete crushing at S
SL15_15_7_2	44.15	14.47	-1.91	2.40	3.49	-1.51	1.51	2.27	67.82	28.95	-5.19	8.84	12.40	-3.41	3.80	5.62	18.83	FRP maximum strain at H
SL15_15_7_4	47.82	15.94	-2.07	2.40	3.54	-1.65	1.62	2.45	71.43	28.78	-4.64	6.86	9.78	-3.50	3.93	5.80	11.68	Concrete crushing at S
SL15_15_7_7	53.10	16.79	-2.32	2.40	3.60	-1.85	1.78	2.69	74.53	27.94	-4.26	5.26	7.68	-3.50	3.93	5.80	4.39	Concrete crushing at S

Table 4.12: Main results of the numerical simulations – concrete strength class C25/30 – SL15.

Concrete strength class C25/30	When the first hinge was formed								Failure									Failure mode
	F_y	Δ_y	ε_c^H	ε_s^H	ε_f^H	ε_c^S	ε_s^S	ε_f^S	F_u	Δ_u	ε_c^H	ε_s^H	ε_f^H	ε_c^S	ε_s^S	ε_f^S	η	
	(kN)	(mm)	(‰)	(‰)	(‰)	(‰)	(‰)	(‰)	(kN)	(mm)	(‰)	(‰)	(‰)	(‰)	(‰)	(‰)	(%)	
Reference	38.69	13.42	-1.38	2.40	----	-1.09	1.68	----	46.61	24.82	-4.04	13.25	----	-3.50	10.23	----	11.51	Concrete crushing at S
SL15_30_0_2	42.53	14.49	-1.52	2.40	3.39	-1.20	1.83	----	50.30	23.07	-2.78	6.17	8.44	-3.50	10.22	----	-1.65	Concrete crushing at S
SL15_30_0_4	46.11	15.44	-1.65	2.40	3.43	-1.31	1.98	----	52.33	22.33	-2.52	4.55	6.34	-3.50	10.27	----	-8.31	Concrete crushing at S
SL15_30_0_7	49.34	16.00	-1.71	2.40	3.16	-1.40	2.40	----	54.48	21.65	-2.39	3.45	4.94	-3.50	10.27	----	-14.41	Concrete crushing at S
SL15_30_2_0	40.12	13.25	-1.40	2.40	----	-1.10	1.60	2.28	58.01	36.73	-7.48	25.41	----	-3.50	7.79	10.63	25.98	Concrete crushing at S
SL15_30_2_2	43.98	14.27	-1.53	2.40	3.40	-1.20	1.73	2.48	61.95	30.35	-3.91	9.10	12.40	-3.15	6.85	9.37	7.16	FRP maximum strain at H
SL15_30_2_4	47.53	15.16	-1.65	2.40	3.43	-1.30	1.86	2.65	67.58	32.73	-3.87	7.49	10.38	-3.50	7.81	10.65	-1.38	Concrete crushing at S
SL15_30_2_7	52.45	16.33	-1.82	2.40	3.47	-1.45	2.09	2.98	71.15	31.67	-3.73	5.69	8.09	-3.50	7.80	10.65	-9.72	Concrete crushing at S
SL15_30_4_0	41.71	13.11	-1.41	2.40	----	-1.11	1.54	2.20	64.61	37.18	-8.15	27.53	----	-3.50	5.96	8.35	33.20	Concrete crushing at S
SL15_30_4_2	45.43	14.03	-1.54	2.40	3.40	-1.21	1.66	2.38	66.36	28.58	-3.91	9.10	12.40	-2.91	4.84	6.79	13.26	FRP maximum strain at H
SL15_30_4_4	48.74	14.80	-1.65	2.40	3.43	-1.30	1.76	2.53	74.97	33.07	-4.13	8.04	11.13	-3.50	5.97	8.35	5.61	Concrete crushing at S
SL15_30_4_7	53.92	15.99	-1.82	2.40	3.47	-1.44	1.92	2.77	78.91	32.13	-3.99	6.11	8.68	-3.50	6.04	8.44	-2.66	Concrete crushing at S
SL15_30_7_0	42.43	12.46	-1.38	2.40	----	-1.09	1.40	2.03	72.78	37.84	-8.91	29.95	----	-3.50	5.10	7.27	40.43	Concrete crushing at S
SL15_30_7_2	46.65	13.48	-1.52	2.40	3.39	-1.20	1.53	2.21	71.07	27.00	-3.91	9.10	12.40	-2.68	3.78	5.41	18.88	FRP maximum strain at H
SL15_30_7_4	50.60	14.40	-1.65	2.40	3.43	-1.31	1.64	2.38	84.10	33.68	-4.47	8.72	12.06	-3.50	5.11	7.27	12.59	Concrete crushing at S
SL15_30_7_7	55.86	15.54	-1.82	2.40	3.47	-1.44	1.79	2.60	88.17	32.59	-4.30	6.58	9.34	-3.50	5.10	7.27	4.37	Concrete crushing at S

Table 4.13: Main results of the numerical simulations – concrete strength class C35/45 - SL15.

Concrete strength class C35/45	When the first hinge was formed								Failure									Failure mode
	F_y	Δ_y	ε_c^H	ε_s^H	ε_f^H	ε_c^S	ε_s^S	ε_f^S	F_u	Δ_u	ε_c^H	ε_s^H	ε_f^H	ε_c^S	ε_s^S	ε_f^S	η	
	(kN)	(mm)	(‰)	(‰)	(‰)	(‰)	(‰)	(‰)	(kN)	(mm)	(‰)	(‰)	(‰)	(‰)	(‰)	(‰)	(%)	
Reference	40.32	13.15	-1.25	2.40	----	-1.00	1.71	----	47.77	26.05	-3.73	14.89	----	-3.50	13.48	----	11.61	Concrete crushing at S
SL15_45_0_2	43.96	14.06	-1.34	2.40	3.35	-1.08	1.84	----	52.03	24.09	-2.54	6.74	9.09	-3.50	13.51	----	-3.03	Concrete crushing at S
SL15_45_0_4	47.14	14.80	-1.44	2.40	3.38	-1.15	1.97	----	54.27	23.24	-2.32	4.95	6.80	-3.50	13.52	----	-9.74	Concrete crushing at S
SL15_45_0_7	52.02	16.20	-1.61	2.40	3.42	-1.54	3.47	----	56.74	22.45	-2.20	3.81	5.33	-3.50	13.53	----	-16.60	Concrete crushing at S
SL15_45_2_0	41.47	12.84	-1.25	2.40	----	-1.00	1.60	2.26	61.69	42.67	-8.07	32.52	----	-3.50	8.98	12.12	28.44	Concrete crushing at S
SL15_45_2_2	44.77	13.59	-1.34	2.40	3.35	-1.08	1.71	2.41	63.57	29.77	-3.26	9.23	12.40	-2.74	6.83	9.24	6.99	FRP maximum strain at H
SL15_45_2_4	48.56	14.49	-1.45	2.40	3.38	-1.16	1.84	2.59	73.41	37.52	-3.83	8.70	11.88	-3.50	9.08	12.24	-2.41	Concrete crushing at S
SL15_45_2_7	53.81	15.68	-1.61	2.40	3.42	-1.28	2.04	2.87	77.82	36.18	-3.64	6.77	9.42	-3.50	9.09	12.25	-11.67	Concrete crushing at S
SL15_45_4_0	42.03	12.37	-1.24	2.40	----	-0.99	1.50	2.13	70.57	45.52	-9.73	36.88	----	-3.50	7.67	10.49	37.77	Concrete crushing at S
SL15_45_4_2	46.17	13.36	-1.34	2.40	3.35	-1.08	1.64	2.32	68.13	27.93	-3.25	9.23	12.40	-2.44	5.07	6.97	13.10	FRP maximum strain at H
SL15_45_4_4	50.10	14.26	-1.46	2.40	3.38	-1.17	1.76	2.50	81.14	36.76	-4.00	9.08	12.40	-3.26	7.10	9.71	5.30	FRP maximum strain at H
SL15_45_4_7	55.39	15.40	-1.61	2.40	3.42	-1.28	1.92	2.73	88.78	38.26	-4.07	7.56	10.52	-3.50	7.67	10.49	-4.11	Concrete crushing at S
SL15_45_7_0	44.11	12.17	-1.25	2.40	----	-1.00	1.42	2.03	79.90	44.54	-10.72	38.46	----	-3.50	6.23	8.69	45.42	Concrete crushing at S
SL15_45_7_2	48.53	13.18	-1.36	2.40	3.35	-1.10	1.55	2.22	73.21	26.29	-3.25	9.23	12.40	-2.31	3.86	5.42	19.00	FRP maximum strain at H
SL15_45_7_4	51.68	13.79	-1.44	2.40	3.38	-1.16	1.63	2.34	88.32	34.30	-4.00	9.08	12.40	-3.09	5.46	7.62	12.85	FRP maximum strain at H
SL15_45_7_7	57.40	14.97	-1.61	2.40	3.42	-1.28	1.79	2.57	99.25	34.64	-4.28	7.93	11.03	-3.50	6.23	8.69	4.17	Concrete crushing at S

Table 4.14: Main results of the numerical simulations – concrete strength class C12/15 – SL30.

Concrete strength class C12/15	When the first hinge was formed								Failure									Failure mode
	F_y (kN)	Δ_y (mm)	ε_c^H (‰)	ε_s^H (‰)	ε_f^H (‰)	ε_c^S (‰)	ε_s^S (‰)	ε_f^S (‰)	F_u (kN)	Δ_u (mm)	ε_c^H (‰)	ε_s^H (‰)	ε_f^H (‰)	ε_c^S (‰)	ε_s^S (‰)	ε_f^S (‰)	η (%)	
Reference	32.62	13.20	-1.47	2.40	----	-1.18	1.51	----	43.44	26.14	-6.80	17.88	----	-3.50	5.96	---	25.93	Concrete crushing at S
SL30_30_0_2	36.33	14.41	-1.66	2.40	3.42	-1.34	1.67	----	47.61	24.18	-3.48	6.13	8.55	-3.50	5.95	----	9.04	Concrete crushing at S
SL30_30_0_4	39.77	15.46	-1.81	2.40	3.46	-1.48	1.80	----	49.60	23.46	-3.07	4.69	6.64	-3.50	5.96	----	1.97	Concrete crushing at S
SL30_30_0_7	44.89	16.98	-2.05	2.40	3.52	-1.68	2.00	----	51.91	22.81	-2.86	3.65	5.29	-3.50	5.97	----	-5.36	Concrete crushing at S
SL30_30_2_0	33.29	12.82	-1.46	2.40	----	-1.17	1.41	2.05	50.30	31.34	-9.70	25.36	----	-3.50	5.11	7.26	35.42	Concrete crushing at S
SL30_30_2_2	37.39	14.13	-1.65	2.40	3.42	-1.33	1.56	2.28	55.81	28.68	-4.36	7.81	10.87	-3.50	5.11	7.26	15.53	Concrete crushing at S
SL30_30_2_4	40.94	15.17	-1.81	2.40	3.46	-1.47	1.69	2.48	58.36	27.79	-3.81	5.96	8.42	-3.50	5.11	7.26	7.65	Concrete crushing at S
SL30_30_2_7	46.15	16.67	-2.05	2.40	3.52	-1.68	1.88	2.77	61.18	26.90	-3.53	4.62	6.68	-3.50	5.11	7.26	-0.36	Concrete crushing at S
SL30_30_4_0	34.52	12.68	-1.47	2.40	3.37	-1.18	1.34	1.98	55.59	33.21	-11.14	28.95	----	-3.50	4.46	6.45	41.54	Concrete crushing at S
SL30_30_4_2	38.43	13.87	-1.66	2.40	3.42	-1.33	1.48	2.18	61.84	30.35	-4.83	8.68	12.08	-3.50	4.46	6.45	20.52	Concrete crushing at S
SL30_30_4_4	42.04	14.90	-1.81	2.40	3.46	-1.47	1.60	2.37	64.62	29.41	-4.19	6.60	9.31	-3.50	4.46	6.45	12.52	Concrete crushing at S
SL30_30_4_7	47.37	16.38	-2.05	2.40	3.52	-1.68	1.78	2.64	67.70	28.47	-3.87	5.11	7.38	-3.50	4.46	6.45	4.31	Concrete crushing at S
SL30_30_7_0	35.63	12.32	-1.47	2.40	----	-1.18	1.24	1.84	61.52	33.99	-12.21	31.54	----	-3.50	3.72	5.53	47.21	Concrete crushing at S
SL30_30_7_2	39.78	13.52	-1.66	2.40	3.42	-1.34	1.37	2.04	66.71	29.59	-4.96	8.91	12.40	-3.33	3.48	5.18	25.45	FRP maximum strain at H
SL30_30_7_4	43.56	14.54	-1.81	2.40	3.46	-1.48	1.48	2.22	71.31	29.99	-4.48	7.07	9.98	-3.50	3.72	5.53	17.91	Concrete crushing at S
SL30_30_7_7	49.08	16.00	-2.05	2.40	3.52	-1.69	1.64	2.47	74.62	29.06	-4.13	5.47	7.90	-3.50	3.72	5.53	9.73	Concrete crushing at S

Table 4.15: Main results of the numerical simulations – concrete strength class C25/30 – SL30.

Concrete strength class C25/30	When the first hinge was formed								Failure									Failure mode
	F_y (kN)	Δ_y (mm)	ε_c^H (‰)	ε_s^H (‰)	ε_f^H (‰)	ε_c^S (‰)	ε_s^S (‰)	ε_f^S (‰)	F_u (kN)	Δ_u (mm)	ε_c^H (‰)	ε_s^H (‰)	ε_f^H (‰)	ε_c^S (‰)	ε_s^S (‰)	ε_f^S (‰)	η (%)	
Reference	33.97	12.27	-1.18	2.40	----	-0.96	1.48	----	46.25	26.52	-5.21	20.61	----	-3.50	9.07	----	26.29	Concrete crushing at S
SL30_30_0_2	37.89	13.37	-1.30	2.40	3.32	-1.07	1.64	----	50.82	24.45	-2.71	7.01	9.46	-3.50	9.08	----	8.87	Concrete crushing at S
SL30_30_0_4	41.58	14.36	-1.42	2.40	3.36	-1.17	1.77	----	53.15	23.56	-2.47	5.15	7.08	-3.50	9.11	----	1.18	Concrete crushing at S
SL30_30_0_7	47.07	15.79	-1.62	2.40	3.41	-1.32	1.98	----	55.79	22.89	-2.38	3.96	5.57	-3.50	9.10	----	-6.76	Concrete crushing at S
SL30_30_2_0	35.16	12.08	-1.18	2.40	----	-0.96	1.42	2.00	56.43	36.57	-9.28	34.95	----	-3.50	6.60	9.12	38.88	Concrete crushing at S
SL30_30_2_2	39.00	13.10	-1.29	2.40	3.33	-1.06	1.55	2.20	61.10	29.85	-3.44	9.22	12.40	-3.10	5.75	7.96	16.25	FRP maximum strain at H
SL30_30_2_4	42.80	14.08	-1.42	2.40	3.36	-1.16	1.68	2.39	66.77	31.97	-3.47	7.42	10.16	-3.50	6.60	9.12	7.11	Concrete crushing at S
SL30_30_2_7	48.43	15.49	-1.62	2.40	3.41	-1.32	1.87	2.66	70.50	30.82	-3.33	5.70	7.98	-3.50	6.60	9.13	-2.00	Concrete crushing at S
SL30_30_4_0	36.01	11.79	-1.18	2.40	----	-0.95	1.33	1.91	62.94	39.10	-11.11	40.05	----	-3.50	5.75	8.06	46.34	Concrete crushing at S
SL30_30_4_2	40.07	12.83	-1.29	2.40	3.33	-1.06	1.47	2.10	64.91	28.43	-3.43	9.22	12.40	-2.76	4.37	6.15	21.00	FRP maximum strain at H
SL30_30_4_4	43.98	13.80	-1.42	2.40	3.86	-1.16	1.60	2.29	78.86	33.96	-3.86	8.24	9.00	-3.50	5.75	8.06	12.51	Concrete crushing at S
SL30_30_4_7	49.73	15.19	-1.62	2.40	3.41	-1.31	1.78	2.55	78.93	32.76	-3.70	6.33	8.86	-3.50	5.75	8.06	3.28	Concrete crushing at S
SL30_30_7_0	37.49	11.48	-1.18	2.40	----	-0.96	1.25	1.80	70.36	39.92	-12.63	43.55	----	-3.50	4.93	7.04	53.86	Concrete crushing at S
SL30_30_7_2	41.63	12.48	-1.29	2.40	3.33	-1.06	1.37	1.98	69.19	26.98	-3.44	9.22	12.40	-2.56	3.41	4.91	25.75	FRP maximum strain at H
SL30_30_7_4	45.67	13.43	-1.41	2.40	3.36	-1.17	1.49	2.16	83.75	34.53	-4.15	8.85	12.12	-3.50	4.93	7.04	18.68	Concrete crushing at S
SL30_30_7_7	51.59	14.79	-1.62	2.40	3.41	-1.32	1.66	2.40	88.09	33.35	-3.98	6.79	9.50	-3.50	4.93	7.04	9.57	Concrete crushing at S

Table 4.16: Main results of the numerical simulations – concrete strength class C35/45 – SL30.

Concrete strength class C35/45	When the first hinge was formed								Failure									Failure mode
	F_y (kN)	Δ_y (mm)	ε_c^H (‰)	ε_s^H (‰)	ε_f^H (‰)	ε_c^S (‰)	ε_s^S (‰)	ε_f^S (‰)	F_u (kN)	Δ_u (mm)	ε_c^H (‰)	ε_s^H (‰)	ε_f^H (‰)	ε_c^S (‰)	ε_s^S (‰)	ε_f^S (‰)	η (%)	
Reference	34.70	11.83	-1.07	2.40	----	-0.87	1.49	----	47.85	28.48	-4.67	21.86	----	-3.50	12.64	----	24.58	Concrete crushing at S
SL30_45_0_2	38.76	12.90	-1.16	2.40	3.30	-0.96	1.64	----	52.60	26.35	-2.47	7.74	10.31	-3.50	12.70	----	7.32	Concrete crushing at S
SL30_45_0_4	42.39	13.78	-1.25	2.40	3.32	-1.04	1.77	----	55.26	25.34	-2.33	5.65	7.66	-3.50	12.68	----	-1.15	Concrete crushing at S
SL30_45_0_7	47.89	15.10	-1.41	2.40	3.36	-1.16	1.97	----	58.22	24.48	-2.23	4.39	6.06	-3.50	12.69	----	-9.55	Concrete crushing at S
SL30_45_2_0	35.46	11.46	-1.06	2.40	----	-0.86	1.39	1.95	60.58	44.07	-9.51	45.16	----	-3.50	8.66	11.69	41.25	Concrete crushing at S
SL30_45_2_2	39.72	12.56	-1.16	2.40	3.30	-0.96	1.54	2.16	62.38	29.19	-2.91	9.32	12.40	-2.60	6.10	8.28	16.02	FRP maximum strain at H
SL30_45_2_4	43.71	13.52	-1.26	2.40	3.32	-1.05	1.67	2.35	73.34	37.91	-3.51	8.84	11.96	-3.50	8.66	11.69	5.15	Concrete crushing at S
SL30_45_2_7	49.30	14.80	-1.41	2.40	3.36	-1.17	1.86	2.61	77.82	36.45	-3.41	6.84	9.42	-3.50	8.66	11.69	-4.76	Concrete crushing at S
SL30_45_4_0	36.96	11.39	-1.07	2.40	----	-0.88	1.34	1.89	67.43	47.62	-15.48	53.05	----	-3.50	7.41	10.13	54.79	Concrete crushing at S
SL30_45_4_2	41.05	12.37	-1.16	2.40	3.30	-0.96	1.47	2.08	66.60	27.63	-2.91	9.32	12.40	-2.35	4.58	6.31	21.20	FRP maximum strain at H
SL30_45_4_4	44.93	13.25	-1.26	2.40	3.32	-1.05	1.59	2.25	80.82	37.04	-3.65	9.17	12.40	-3.25	6.83	9.35	12.07	FRP maximum strain at H
SL30_45_4_7	50.63	14.48	-1.41	2.40	3.36	-1.17	1.77	2.50	88.59	38.45	-3.79	7.57	10.43	-3.50	7.41	10.43	1.96	Concrete crushing at S
SL30_45_7_0	38.42	11.07	-1.07	2.40	----	-0.87	1.25	1.79	75.69	44.74	-14.99	51.68	----	-3.50	5.68	7.98	59.39	Concrete crushing at S
SL30_45_7_2	42.59	12.02	-1.16	2.40	3.30	-0.96	1.38	1.96	71.21	26.14	-2.91	9.32	12.40	-2.25	3.45	4.88	26.16	FRP maximum strain at H
SL30_45_7_4	46.60	12.87	-1.26	2.40	3.32	-1.04	1.49	2.12	87.77	34.58	-3.65	9.17	12.40	-3.17	5.12	7.19	18.82	FRP maximum strain at H
SL30_45_7_7	52.51	14.10	-1.41	2.40	3.36	-1.17	1.65	2.36	97.20	36.67	-3.87	7.70	10.61	-3.50	5.68	7.98	9.50	Concrete crushing at S

Table 4.17: Main results of the numerical simulations – concrete strength class C12/15 – SL45.

Concrete strength class C12/15	When the first hinge was formed								Failure									Failure mode
	F_y	Δ_y	ε_c^H	ε_s^H	ε_f^H	ε_c^S	ε_s^S	ε_f^S	F_u	Δ_u	ε_c^H	ε_s^H	ε_f^H	ε_c^S	ε_s^S	ε_f^S	η	
	(kN)	(mm)	(‰)	(‰)	(‰)	(‰)	(‰)	(‰)	(kN)	(mm)	(‰)	(‰)	(‰)	(‰)	(‰)	(‰)	(%)	
Reference	27.66	10.93	-1.17	2.35	----	-1.01	1.15	----	42.90	25.34	-10.96	36.00	----	-3.50	5.25	----	41.95	Concrete crushing at S
SL45_15_0_2	31.47	12.13	-1.32	2.35	3.31	-1.16	1.29	----	47.48	23.17	-3.32	7.39	10.01	-3.50	5.25	----	21.81	Concrete crushing at S
SL45_15_0_4	35.16	13.24	-1.48	2.35	3.35	-1.31	1.42	----	49.75	22.37	-2.91	5.38	7.41	-3.50	5.25	----	13.21	Concrete crushing at S
SL45_15_0_7	40.73	14.89	-1.76	2.35	3.42	-1.55	1.62	----	52.22	21.64	-2.76	4.05	5.72	-3.50	5.25	----	4.68	Concrete crushing at S
SL45_15_2_0	27.50	10.36	-1.14	2.35	----	-0.97	1.05	1.56	48.05	30.53	-18.37	54.54	----	-3.50	4.43	6.45	52.44	Concrete crushing at S
SL45_15_2_2	32.29	11.95	-1.32	2.35	3.31	-1.16	1.22	1.83	54.66	27.20	-4.06	9.05	12.27	-3.50	4.43	6.46	26.00	Concrete crushing at S
SL45_15_2_4	36.17	13.09	-1.49	2.35	3.35	-1.32	1.35	2.03	57.42	26.21	-3.53	6.57	9.05	-3.50	4.43	6.46	16.84	Concrete crushing at S
SL45_15_2_7	41.78	14.68	-1.76	2.35	3.42	-1.55	1.52	2.31	60.45	25.31	-3.34	4.95	6.99	-3.50	4.44	6.47	7.74	Concrete crushing at S
SL45_15_4_0	28.18	10.19	-1.14	2.35	----	-0.97	0.99	1.49	52.26	32.02	-21.33	61.69	----	-3.50	3.67	5.50	57.42	Concrete crushing at S
SL45_15_4_2	32.65	11.57	-1.31	2.35	3.31	-1.14	1.14	1.72	57.51	26.39	-4.11	9.15	12.40	-3.15	3.16	4.78	29.27	FRP maximum strain at H
SL45_15_4_4	37.04	12.87	-1.48	2.35	3.35	-1.32	1.28	1.94	62.67	27.39	-3.82	7.12	9.81	-3.50	3.67	5.50	20.39	Concrete crushing at S
SL45_15_4_7	42.74	14.45	-1.76	2.35	3.42	-1.55	1.45	2.22	65.90	26.42	-3.62	5.35	7.56	-3.50	3.67	5.50	11.27	Concrete crushing at S
SL45_15_7_0	30.03	10.33	-1.17	2.35	----	-1.00	0.96	1.46	57.39	33.03	-23.59	67.55	----	-3.50	3.19	4.90	61.47	Concrete crushing at S
SL45_15_7_2	33.65	11.30	-1.31	2.35	3.31	-1.14	1.06	1.63	60.09	25.37	-4.11	9.15	12.40	-2.87	2.40	3.76	32.24	FRP maximum strain at H
SL45_15_7_4	37.80	12.45	-1.48	2.35	3.35	-1.30	1.18	1.82	68.54	28.20	-4.11	7.64	10.52	-3.50	3.19	4.90	24.32	Concrete crushing at S
SL45_15_7_7	44.00	14.13	-1.76	2.35	3.42	-1.54	1.35	2.10	71.97	27.22	-3.88	5.73	8.09	-3.50	3.19	4.90	15.25	Concrete crushing at S

Table 4.18: Main results of the numerical simulations – concrete strength class C25/30 – SL45.

Concrete strength class C25/30	When the first hinge was formed								Failure									Failure mode
	F_y (kN)	Δ_y (mm)	ε_c^H (‰)	ε_s^H (‰)	ε_f^H (‰)	ε_c^S (‰)	ε_s^S (‰)	ε_f^S (‰)	F_u (kN)	Δ_u (mm)	ε_c^H (‰)	ε_s^H (‰)	ε_f^H (‰)	ε_c^S (‰)	ε_s^S (‰)	ε_f^S (‰)	η (%)	
Reference	28.77	10.07	-0.97	2.35	----	-0.82	1.13	----	47.29	27.48	-7.46	34.84	----	-3.50	6.99	----	42.94	Concrete crushing at S
SL45_30_0_2	33.08	11.32	-1.09	2.35	3.26	-0.93	1.28	----	52.34	24.76	-2.67	8.34	11.04	-3.50	7.07	----	22.23	Concrete crushing at S
SL45_30_0_4	37.04	12.38	-1.20	2.35	3.28	-1.04	1.42	----	55.04	23.85	-2.51	5.99	8.07	-3.50	7.07	----	12.99	Concrete crushing at S
SL45_30_0_7	42.75	13.83	-1.37	2.35	3.33	-1.20	1.61	----	57.80	22.86	-2.38	4.55	6.26	-3.50	7.20	----	4.13	Concrete crushing at S
SL45_30_2_0	29.91	10.04	-0.98	2.35	----	-0.83	1.07	1.58	53.44	35.30	-19.41	65.50	----	-3.50	5.93	8.33	58.22	Concrete crushing at S
SL45_30_2_2	34.41	11.30	-1.10	2.35	3.26	-0.95	1.24	1.80	58.77	26.49	-2.99	9.37	12.40	-2.87	4.65	6.57	26.97	FRP maximum strain at H
SL45_30_2_4	38.11	12.22	-1.20	2.35	3.28	-1.05	1.35	1.97	65.60	29.73	-3.21	7.66	10.33	-3.50	5.93	8.34	16.62	Concrete crushing at S
SL45_30_2_7	43.66	13.55	-1.36	2.35	3.32	-1.20	1.52	2.22	69.28	28.62	-3.08	5.87	8.07	-3.50	5.93	8.34	6.90	Concrete crushing at S
SL45_30_4_0	31.08	10.02	-1.00	2.35	----	-0.84	1.05	1.54	59.21	37.76	-24.35	76.26	----	-3.50	5.24	7.48	64.10	Concrete crushing at S
SL45_30_4_2	35.21	11.08	-1.10	2.35	3.26	-0.95	1.18	1.72	61.64	25.34	-2.99	9.37	12.40	-2.55	3.49	5.04	30.33	FRP maximum strain at H
SL45_30_4_4	39.21	12.06	-1.20	2.35	3.28	-1.05	1.30	1.90	72.97	31.63	-3.57	8.45	11.40	-3.50	5.24	7.48	20.64	Concrete crushing at S
SL45_30_4_7	44.97	13.40	-1.37	2.35	3.33	-1.21	1.46	2.14	77.05	30.49	-3.42	6.48	8.91	-3.50	5.25	7.49	10.87	Concrete crushing at S
SL45_30_7_0	32.03	9.72	-0.99	2.35	----	-0.83	0.98	1.44	73.52	35.82	-14.31	50.28	----	-3.50	4.16	6.12	49.93	Concrete crushing at S
SL45_30_7_2	35.86	10.61	-1.09	2.35	3.26	-0.93	1.08	1.60	64.81	24.21	-2.99	9.37	12.40	-2.36	2.64	3.92	33.68	FRP maximum strain at H
SL45_30_7_4	40.12	11.62	-1.19	2.35	3.28	-1.04	1.20	1.78	81.03	32.27	-3.86	9.05	12.22	-3.50	4.45	6.49	25.47	Concrete crushing at S
SL45_30_7_7	46.43	13.07	-1.37	2.35	3.33	-1.21	1.37	2.03	85.30	31.10	-3.68	6.93	9.53	-3.50	4.45	6.49	15.88	Concrete crushing at S

Table 4.19: Main results of the numerical simulations – concrete strength class C35/45 – SL45.

Concrete strength class C35/45	When the first hinge was formed								Failure									Failure mode
	F_y (kN)	Δ_y (mm)	ε_c^H (‰)	ε_s^H (‰)	ε_f^H (‰)	ε_c^S (‰)	ε_s^S (‰)	ε_f^S (‰)	F_u (kN)	Δ_u (mm)	ε_c^H (‰)	ε_s^H (‰)	ε_f^H (‰)	ε_c^S (‰)	ε_s^S (‰)	ε_f^S (‰)	η (%)	
Reference	29.69	9.74	-0.89	2.35	----	-0.76	1.13	----	47.98	26.23	-5.30	29.26	----	-3.50	11.69	----	41.75	Concrete crushing at S
SL45_45_0_2	34.47	11.10	-1.00	2.35	3.24	-0.87	1.30	----	53.13	24.23	-2.33	8.28	10.88	-3.50	11.53	----	21.80	Concrete crushing at S
SL45_45_0_4	38.50	12.11	-1.10	2.35	3.26	-0.96	1.44	----	55.90	23.38	-2.14	6.04	8.05	-3.50	11.49	----	12.49	Concrete crushing at S
SL45_45_0_7	43.97	13.37	-1.23	2.35	3.29	-1.08	1.61	----	58.93	22.53	-2.10	4.58	6.22	-3.50	11.56	----	3.36	Concrete crushing at S
SL45_45_2_0	29.58	9.24	-0.88	2.35	----	-0.73	1.04	1.49	56.65	35.53	-14.24	62.02	----	-3.07	6.77	9.29	55.00	The numerical model reached the maximum convergence
SL45_45_2_2	35.35	10.90	-1.01	2.35	3.24	-0.86	1.24	----	60.74	26.14	-2.64	9.44	12.40	-2.50	5.17	7.13	27.31	FRP maximum strain at H
SL45_45_2_4	39.32	11.84	-1.09	2.35	3.26	-0.95	1.36	1.95	71.84	34.41	-3.10	8.90	11.85	-3.50	7.99	10.93	15.39	Concrete crushing at S
SL45_45_2_7	45.10	13.15	-1.23	2.35	3.29	-1.08	1.54	2.21	76.22	32.98	-3.13	6.77	9.20	-3.50	7.97	10.91	4.90	Concrete crushing at S
SL45_45_4_0	30.46	9.13	-0.88	2.35	----	-0.73	1.00	1.44	61.52	33.92	-14.10	62.00	----	-2.82	4.94	6.93	58.18	The numerical model reached the maximum convergence
SL45_45_4_2	35.62	10.48	-0.99	2.35	3.23	-0.85	1.16	1.68	64.01	24.87	-2.64	9.44	12.40	-2.26	3.67	5.18	30.97	FRP maximum strain at H
SL45_45_4_4	40.00	11.52	-1.09	2.35	3.26	-0.94	1.29	1.87	78.90	34.06	-3.26	9.31	12.40	-3.33	6.10	8.52	20.73	FRP maximum strain at H
SL45_45_4_7	46.07	12.86	-1.23	2.35	3.29	-1.08	1.47	2.12	85.37	34.33	-3.43	7.37	10.03	-3.50	6.46	9.00	10.10	Concrete crushing at S
SL45_45_7_0	32.05	9.06	-0.89	2.35	----	-0.75	0.96	----	66.54	32.56	-14.15	62.24	----	-2.70	3.90	----	61.95	The numerical model reached the maximum convergence
SL45_45_7_2	37.48	10.43	-1.01	2.35	3.24	-0.87	1.11	1.62	67.41	23.70	-2.64	9.44	12.40	-2.08	2.79	4.04	34.37	FRP maximum strain at H
SL45_45_7_4	41.45	11.27	-1.09	2.35	3.26	-0.95	1.22	1.77	84.58	31.98	-3.26	9.31	12.40	-3.11	4.63	6.61	25.97	FRP maximum strain at H
SL45_45_7_7	47.72	12.58	-1.23	2.35	3.29	-1.08	1.38	2.01	94.58	34.39	-3.65	7.78	10.59	-3.50	5.28	7.53	15.74	Concrete crushing at S
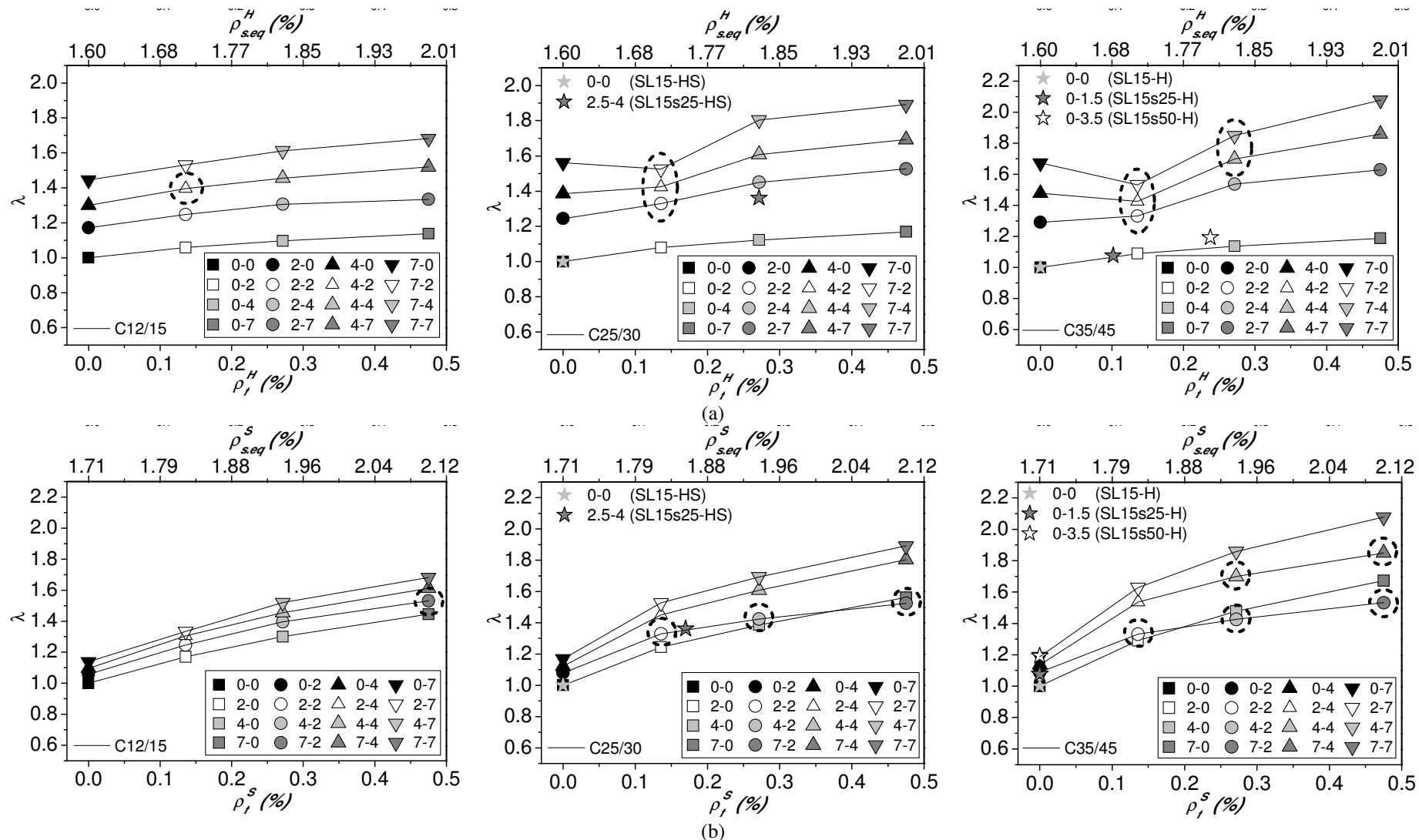
Figure 4.11: Relationship between the load carrying capacity index, λ, and the CFRP strengthening ratio /equivalent reinforcement ratio in the (a) hogging and (b) sagging regions for the SL15 Series.
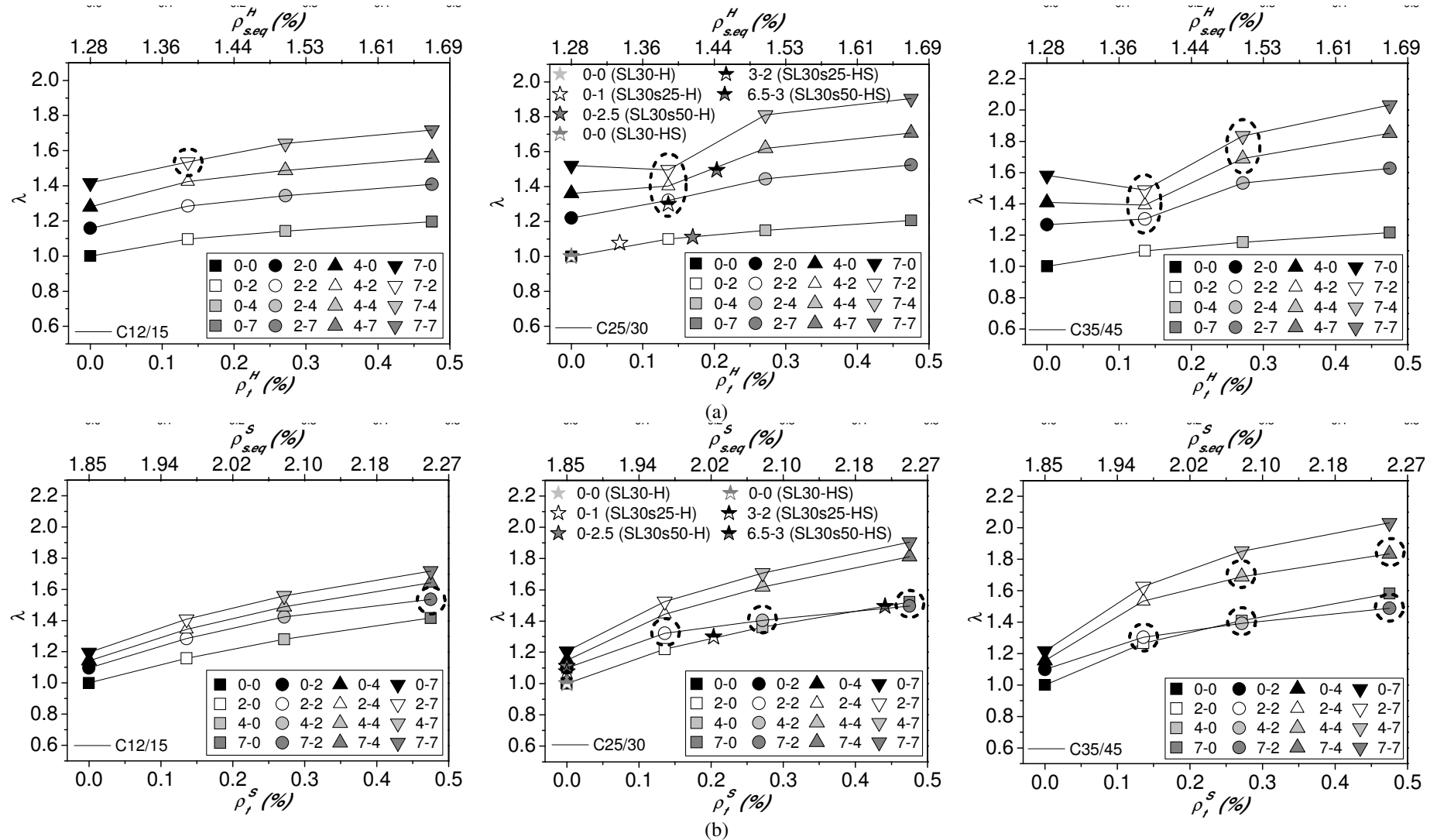
Figure 4.12: Relationship between the load carrying capacity index, λ, and the CFRP strengthening ratio /equivalent reinforcement ratio in the (a) hogging and (b) sagging regions for the SL30 Series.
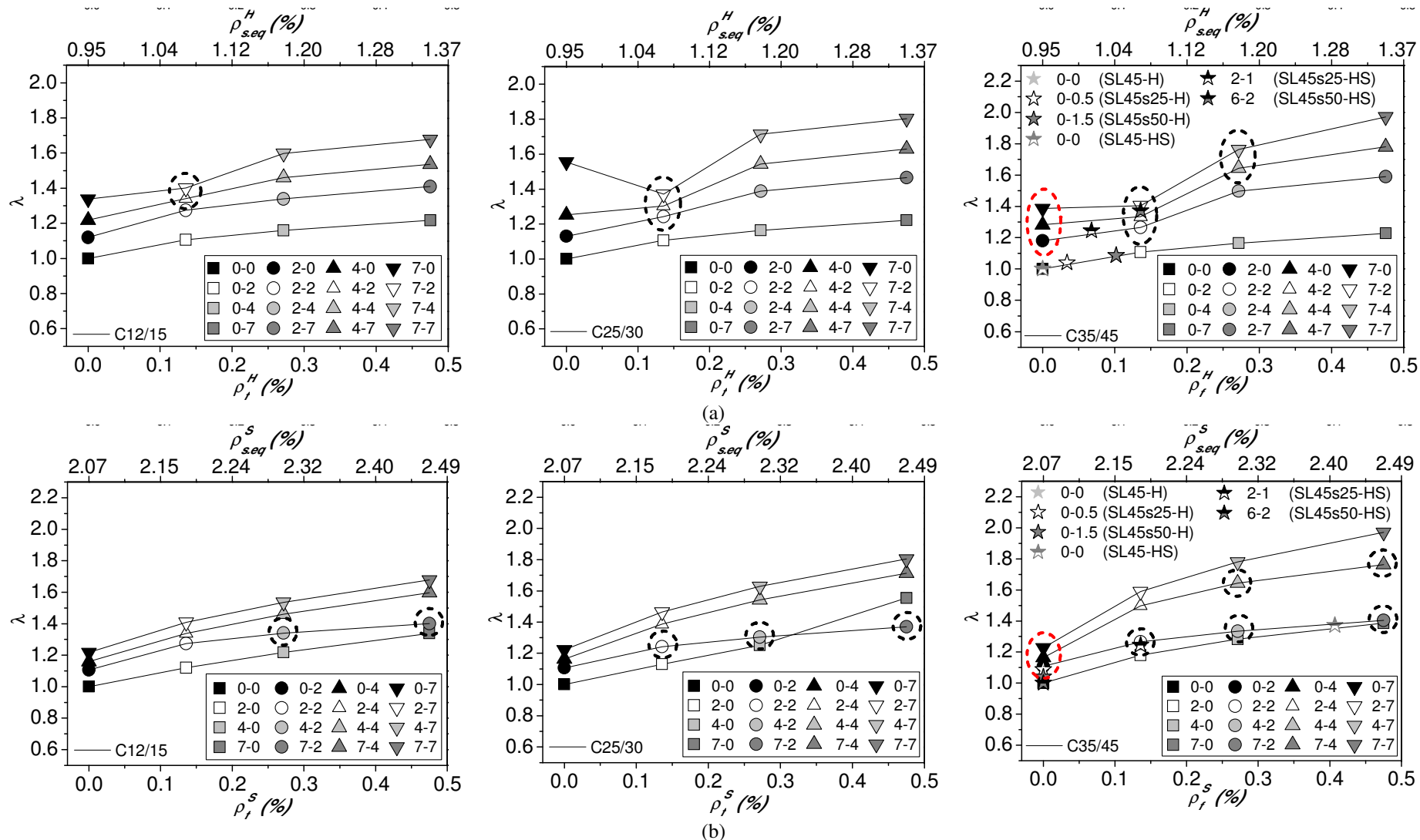
Figure 4.13: Relationship between the load carrying capacity index, λ, and the CFRP strengthening ratio /equivalent reinforcement ratio in the (a) hogging and (b) sagging regions for the SL45 Series.
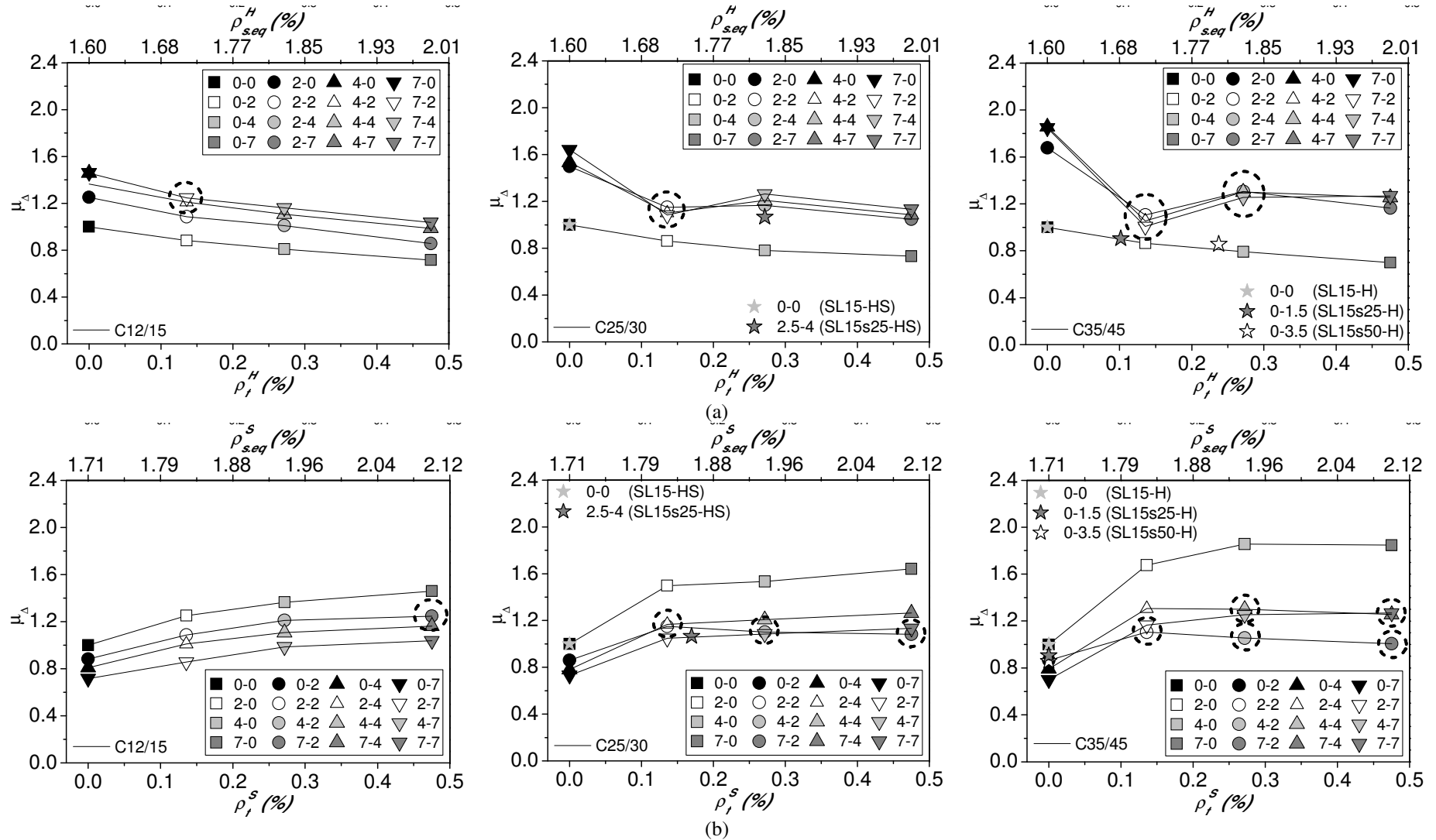
Figure 4.14: Relationship between the deflection ductility index, μ_Δ, and the CFRP strengthening ratio/equivalent reinforcement ratio in the (a) hogging and (b) sagging regions for the SL15 Series.
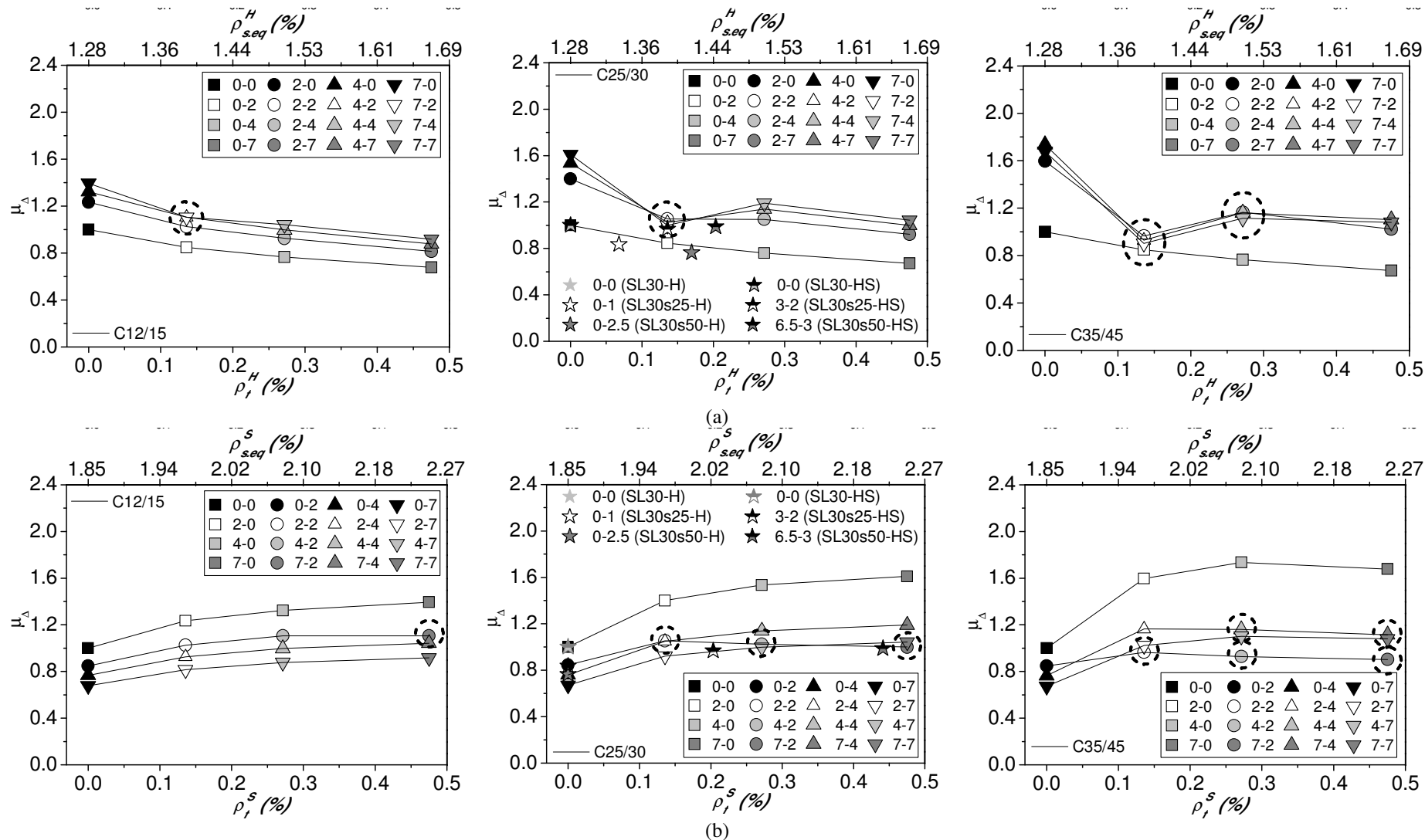
Figure 4.15: Relationship between the deflection ductility index, μ_Δ, and the CFRP strengthening ratio/equivalent reinforcement ratio in the (a) hogging and (b) sagging regions for the SL30 Series.
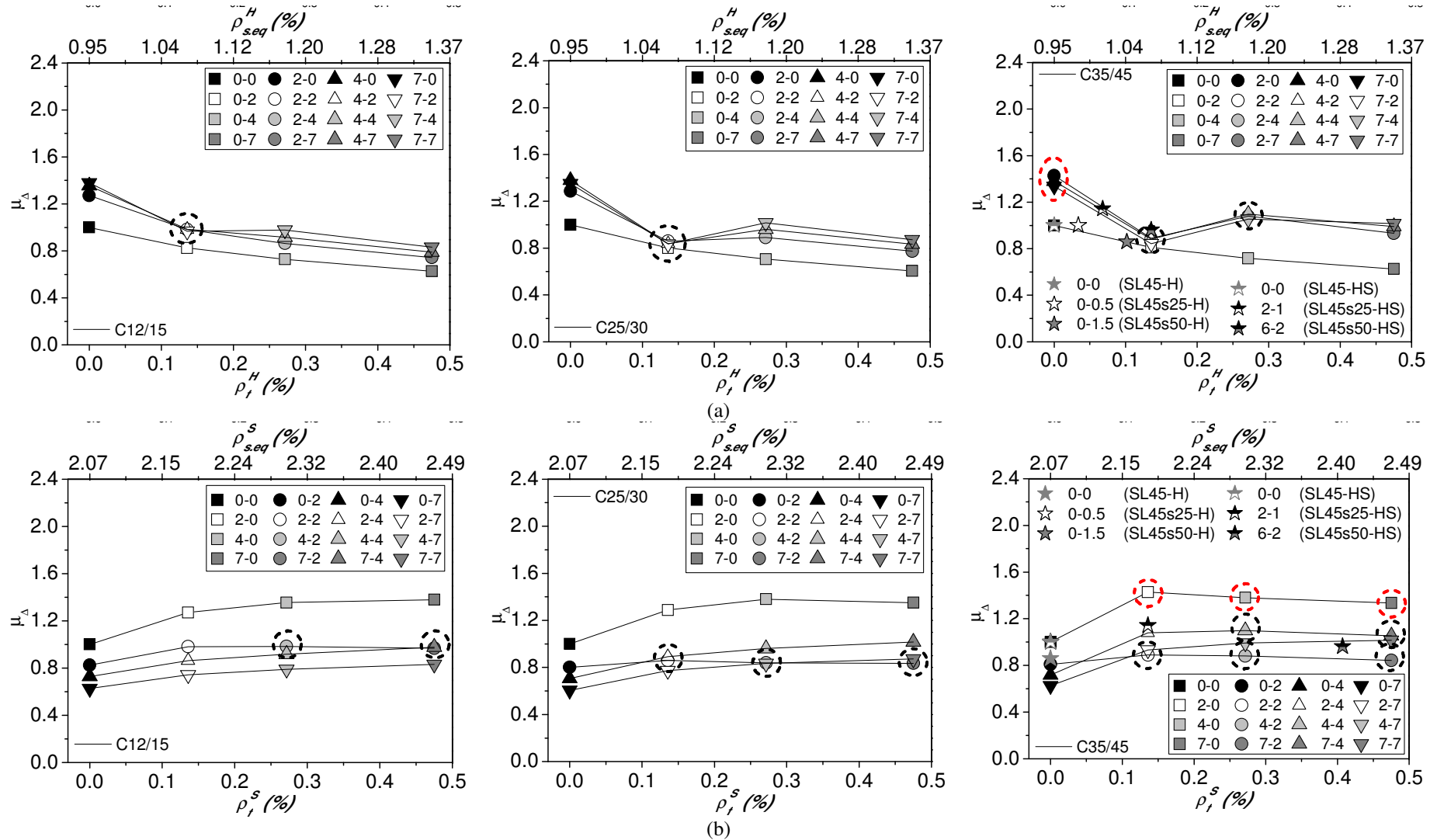
Figure 4.16: Relationship between the deflection ductility index, μ_Δ, and the CFRP strengthening ratio/equivalent reinforcement ratio in the (a) hogging and (b) sagging regions for the SL45 Series.
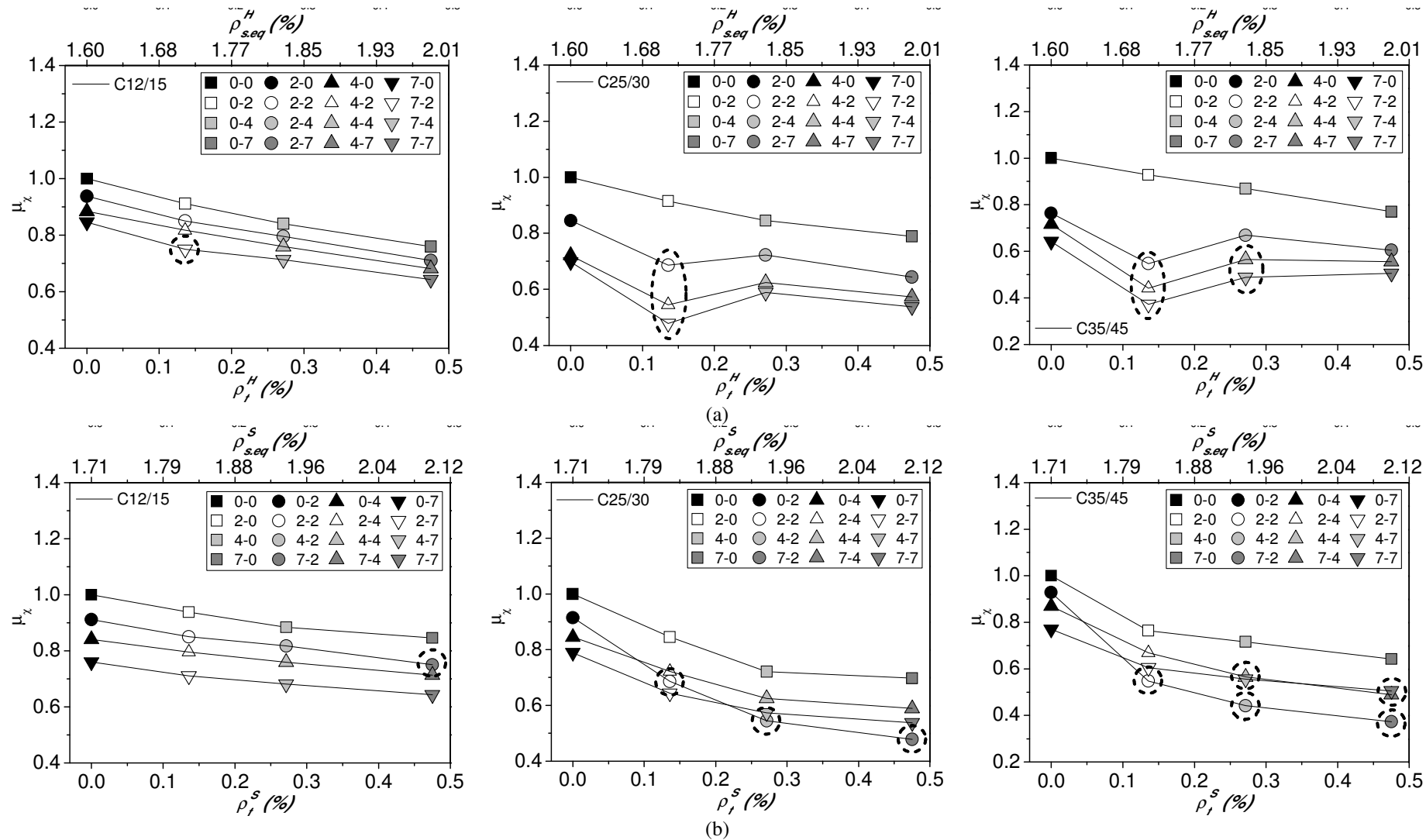
Figure 4.17: Relationship between the rotational ductility index, μ_χ, and the CFRP strengthening ratio/equivalent reinforcement ratio in the (a) hogging and (b) sagging regions for the SL15 Series.
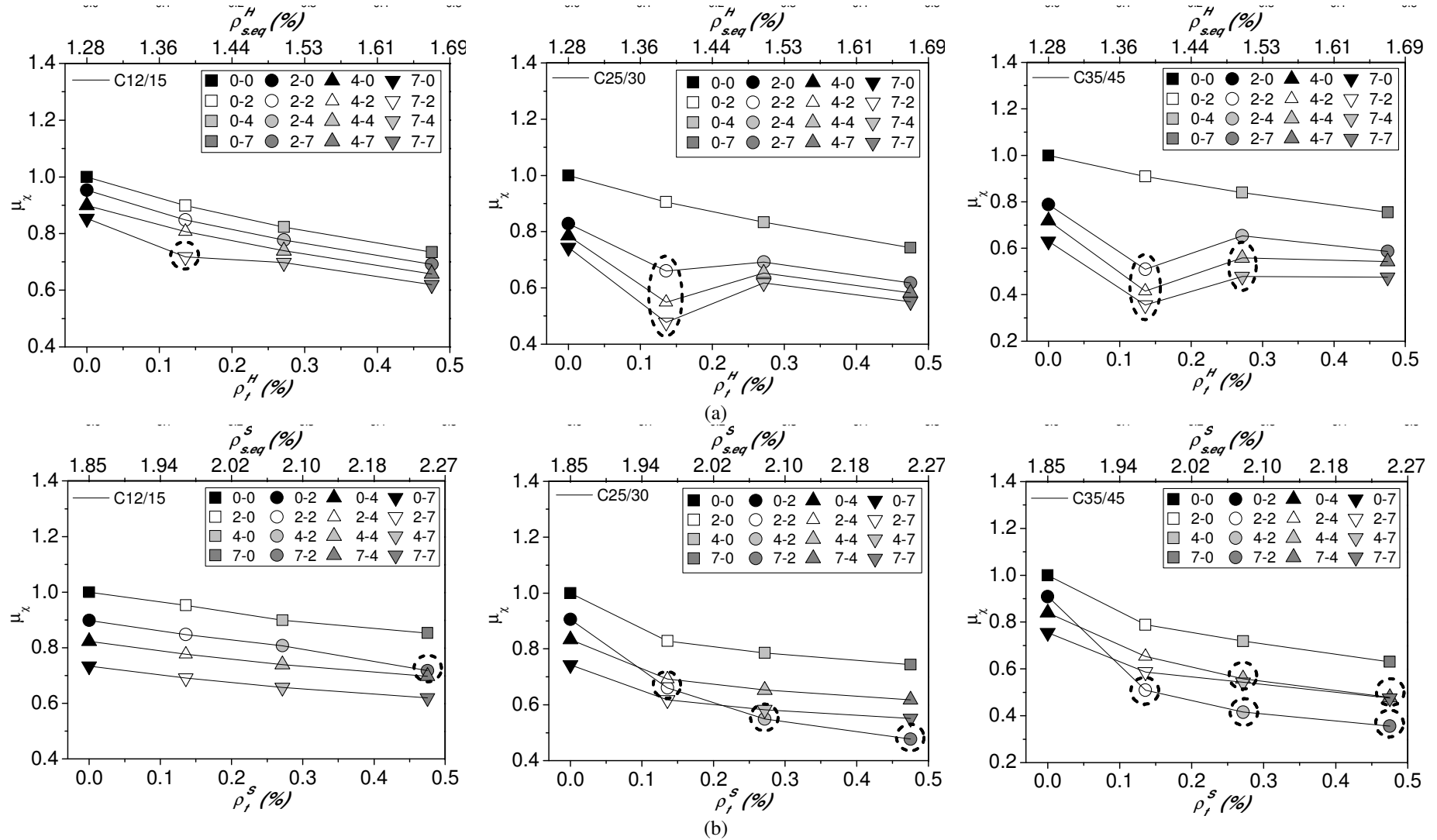
Figure 4.18: Relationship between the rotational ductility index, μ_χ, and the CFRP strengthening ratio/equivalent reinforcement ratio in the (a) hogging and (b) sagging regions for the SL30 Series.
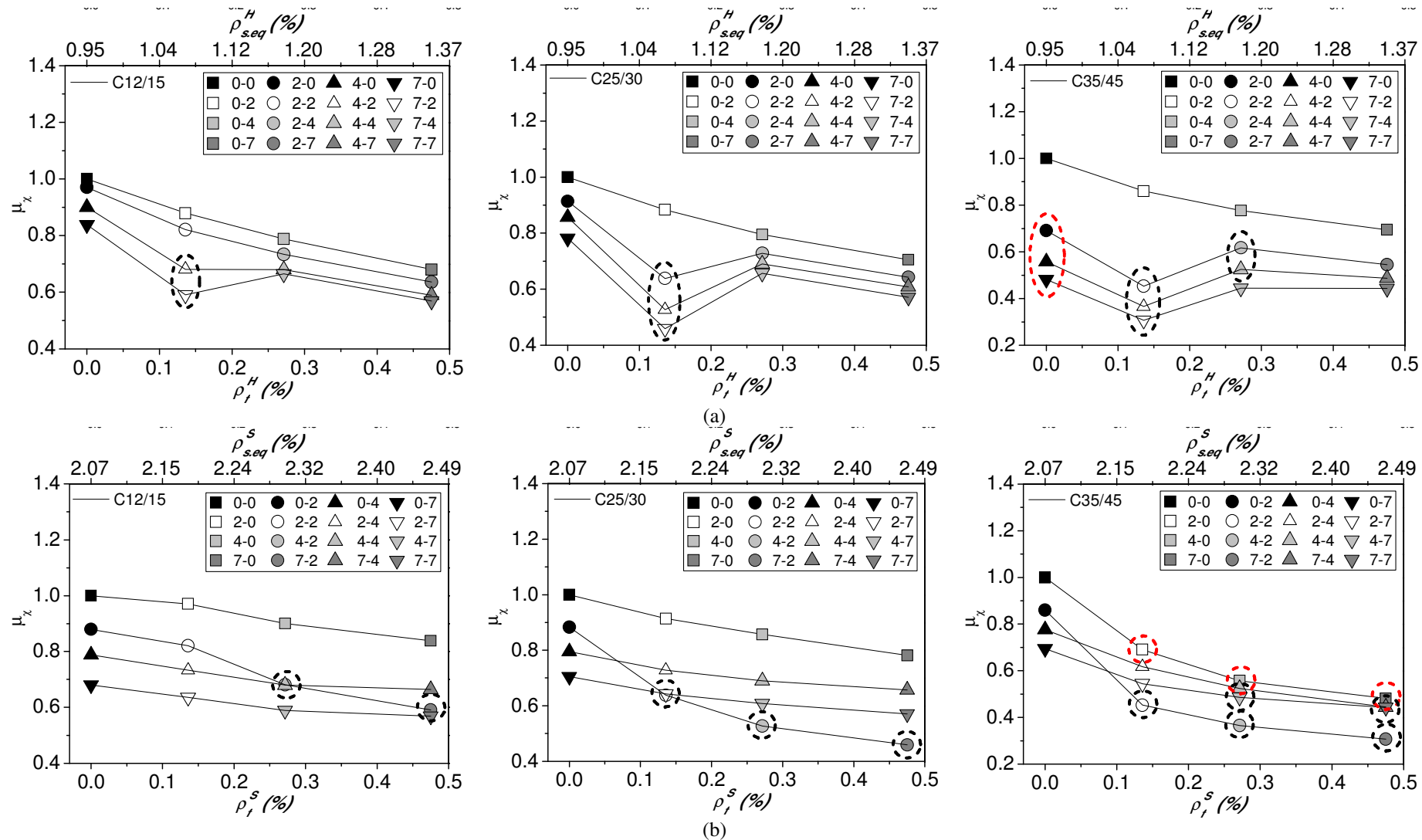
Figure 4.19: Relationship between the rotational ductility index, μ_χ, and the CFRP strengthening ratio/equivalent reinforcement ratio in the (a) hogging and (b) sagging regions for the SL45 Series.

(a)

(b)
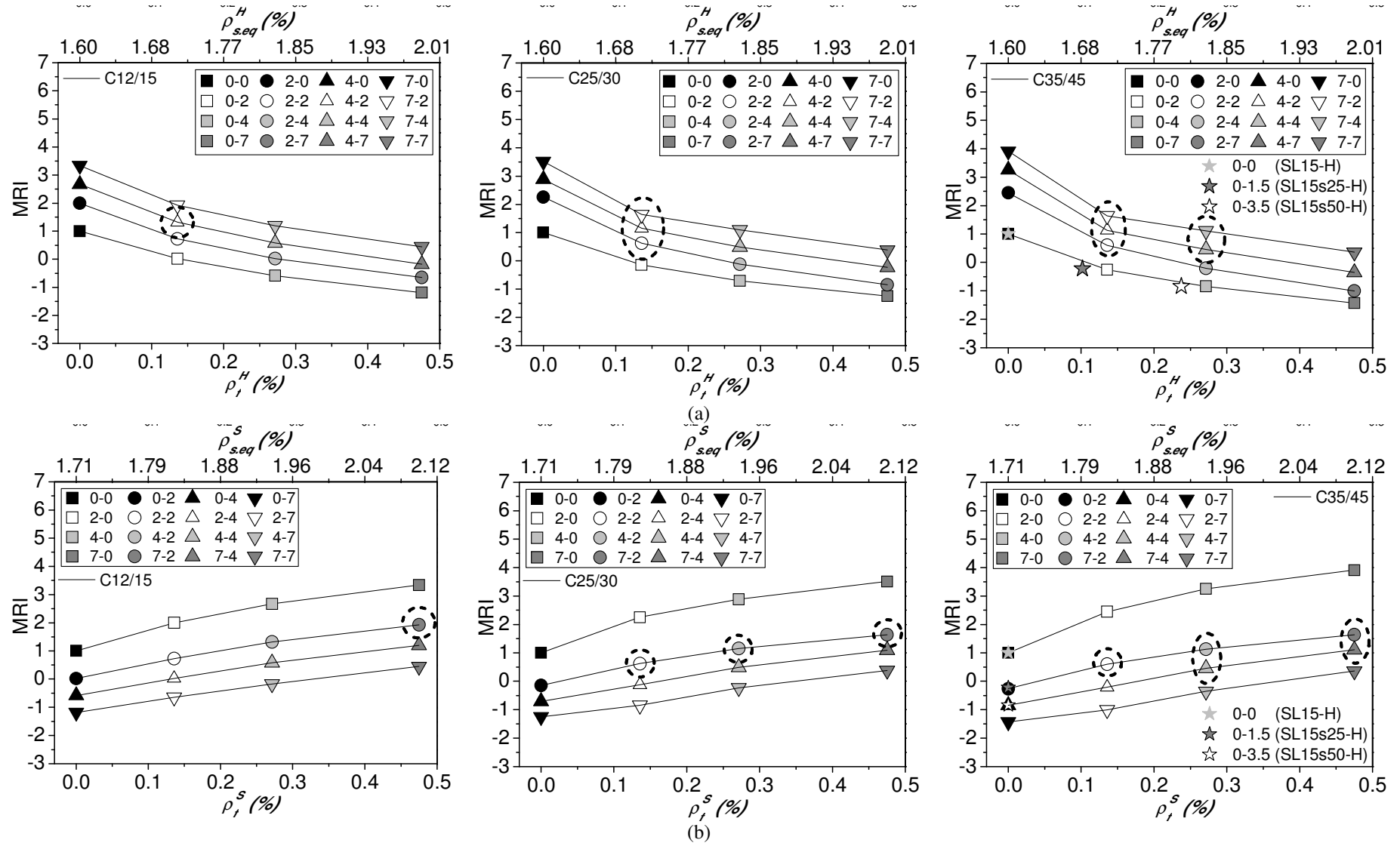
Figure 4.20: Relationship between the moment redistribution index, *MRI*, and the CFRP strengthening ratio/equivalent reinforcement ratio in the (a) hogging and (b) sagging regions for the SL15 Series.
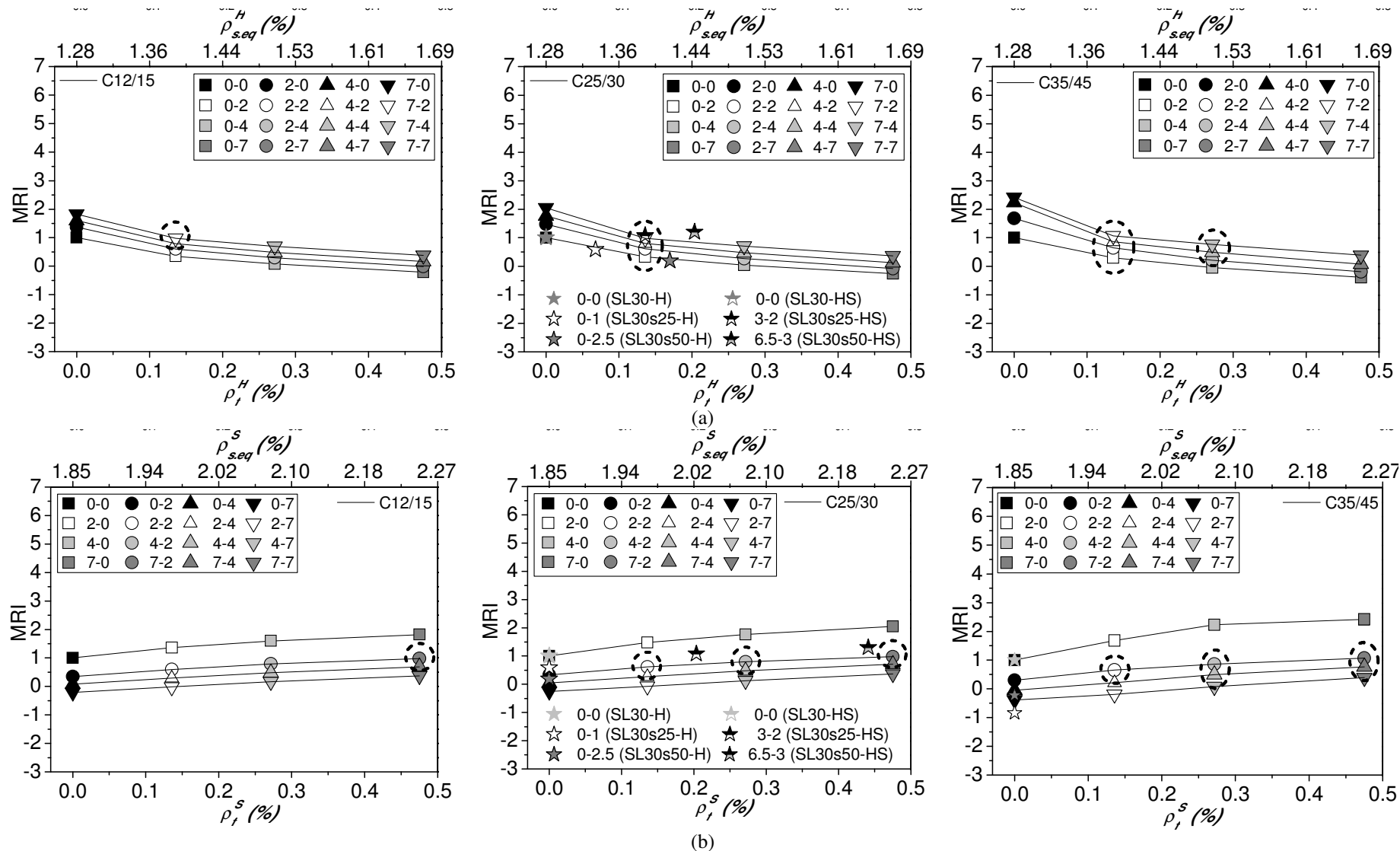
Figure 4.21: Relationship between the moment redistribution index, *MRI*, and the CFRP strengthening ratio/equivalent reinforcement ratio in the (a) hogging and (b) sagging regions for the SL30 Series.
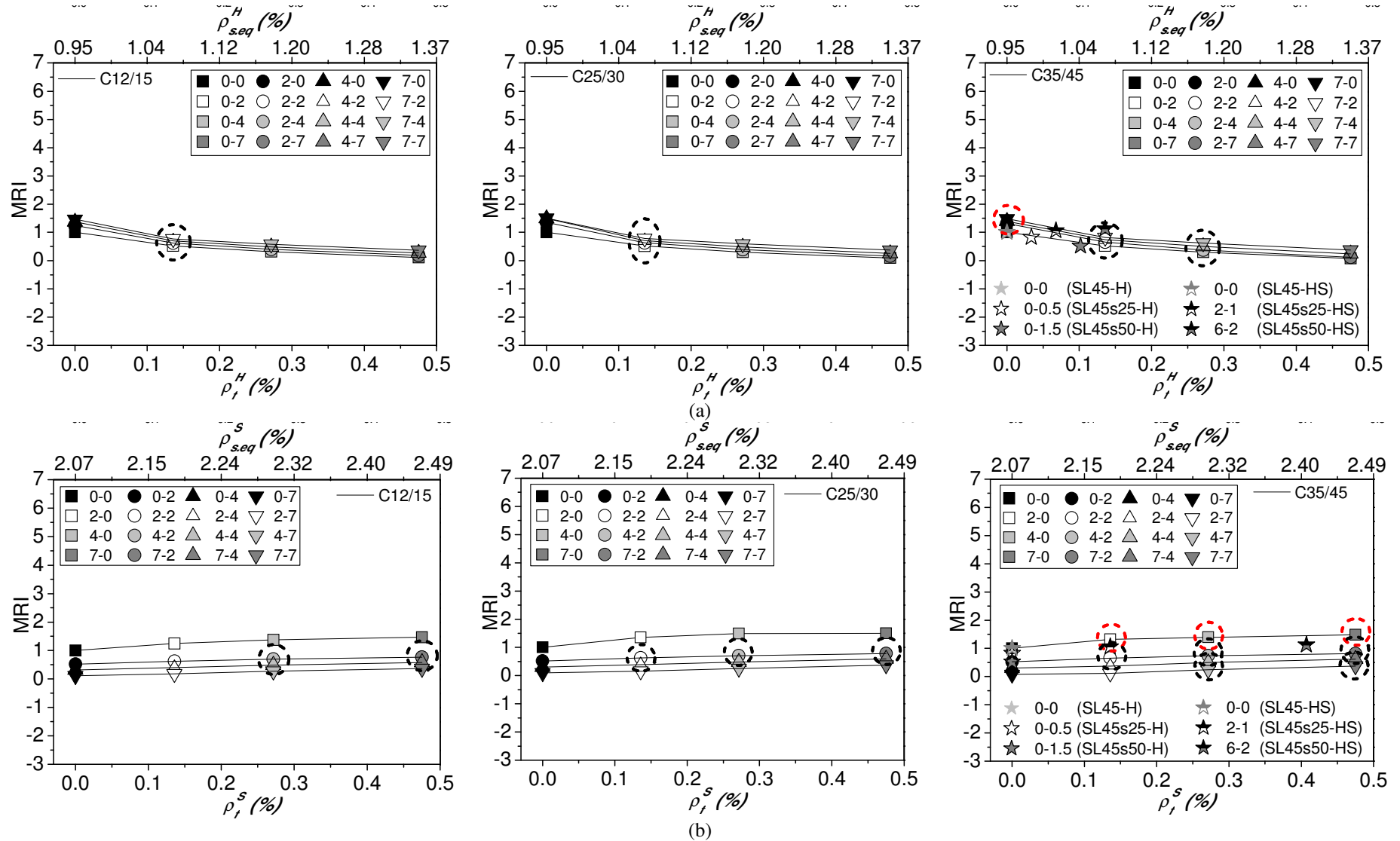
Figure 4.22: Relationship between the moment redistribution index, *MRI*, and the CFRP strengthening ratio/equivalent reinforcement ratio in the (a) hogging and (b) sagging regions for the SL45 Series.
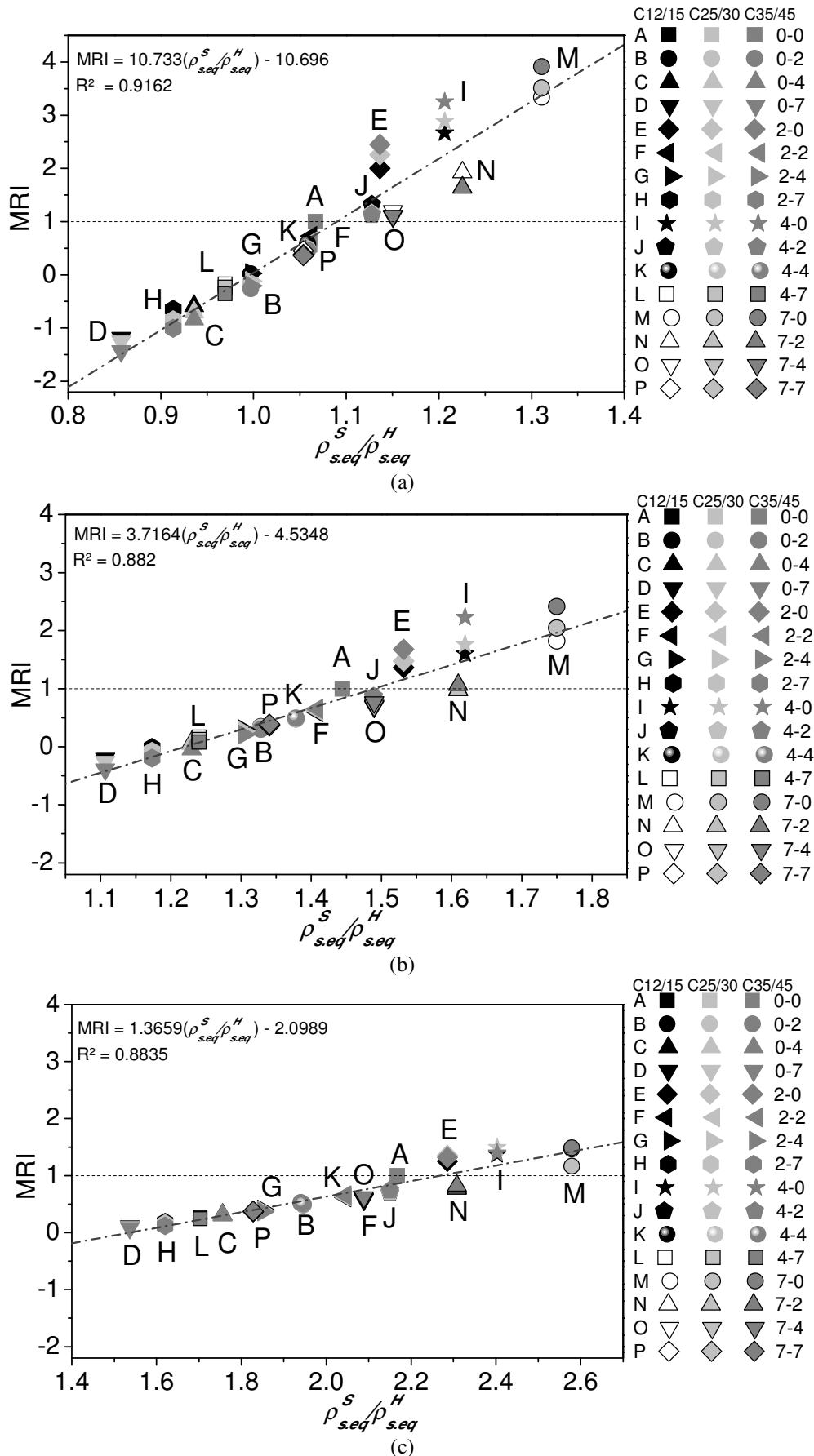
Figure 4.23: Relationship between the moment redistribution index and $\rho_{s,eq}^{S}/\rho_{s,eq}^{H}$ for series: (a) SL15, (b), SL30, and (c) SL45.

Table 4.20: Load carrying capacity, displacement ductility, rotational ductility
and moment redistribution indexes for the SL15 Series.

Concrete strength class	F.E.M. ID	S (a) Number of CFRP laminates	H (b) Number of CFRP laminates	λ	μ_Δ	μ_χ	MRI
C12/15	SL15_15 [c]	0	0	1.00	1.00	1.00	1.00
	SL15_15_0_2	0	2	1.06	0.88	0.91	0.02
	SL15_15_0_4	0	4	1.10	0.81	0.84	-0.58
	SL15_15_0_7	0	7	1.14	0.72	0.76	-1.18
	SL15_15_2_0	2	0	1.17	1.25	0.94	2.00
	SL15_15_2_2	2	2	1.25	1.09	0.85	0.72
	SL15_15_2_4	2	4	1.31	1.01	0.80	0.03
	SL15_15_2_7	2	7	1.33	0.86	0.71	-0.65
	SL15_15_4_0	4	0	1.30	1.36	0.88	2.67
	SL15_15_4_2	4	2	1.40	1.21	0.82	1.32
	SL15_15_4_4	4	4	1.45	1.11	0.76	0.58
	SL15_15_4_7	4	7	1.52	0.99	0.68	-0.17
	SL15_15_7_0	7	0	1.44	1.46	0.85	3.33
	SL15_15_7_2	7	2	1.53	1.25	0.75	1.92
	SL15_15_7_4	7	4	1.61	1.16	0.71	1.19
	SL15_15_7_7	7	7	1.68	1.04	0.64	0.45
C25/30	SL15_30 [c]	0	0	1.00	1.00	1.00	1.00
	SL15_30_0_2	0	2	1.08	0.86	0.91	-0.14
	SL15_30_0_4	0	4	1.12	0.78	0.85	-0.71
	SL15_30_0_7	0	7	1.17	0.73	0.79	-1.25
	SL15_30_2_0	2	0	1.24	1.50	0.85	2.26
	SL15_30_2_2	2	2	1.33	1.15	0.69	0.62
	SL15_30_2_4	2	4	1.45	1.17	0.72	-0.12
	SL15_30_2_7	2	7	1.53	1.05	0.64	-0.84
	SL15_30_4_0	4	0	1.39	1.53	0.72	2.88
	SL15_30_4_2	4	2	1.42	1.10	0.54	1.15
	SL15_30_4_7	4	4	1.61	1.21	0.62	0.49
	SL15_30_4_7	4	7	1.69	1.09	0.57	-0.23
	SL15_30_7_0	7	0	1.56	1.64	0.70	3.51
	SL15_30_7_2	7	2	1.52	1.08	0.48	1.64
	SL15_30_7_4	7	4	1.80	1.26	0.59	1.09
	SL15_30_7_7	7	7	1.89	1.13	0.54	0.38
C35/45	SL15_45 [c]	0	0	1.00	1.00	1.00	1.00
	SL15_45_0_2	0	2	1.09	0.86	0.93	-0.26
	SL15_45_0_4	0	4	1.14	0.79	0.87	-0.84
	SL15_45_0_7	0	7	1.19	0.70	0.77	-1.43
	SL15_45_2_0	2	0	1.29	1.68	0.76	2.45
	SL15_45_2_2	2	2	1.33	1.11	0.55	0.60
	SL15_45_2_4	2	4	1.54	1.31	0.67	-0.21
	SL15_45_2_7	2	7	1.63	1.16	0.61	-1.01
	SL15_45_4_0	4	0	1.48	1.86	0.72	3.25
	SL15_45_4_2	4	2	1.43	1.05	0.44	1.13
	SL15_45_4_4	4	4	1.70	1.30	0.57	0.46
	SL15_45_4_7	4	7	1.86	1.25	0.56	-0.35
	SL15_45_7_0	7	0	1.67	1.85	0.64	3.91
	SL15_45_7_2	7	2	1.53	1.01	0.37	1.64
	SL15_45_7_4	7	4	1.85	1.26	0.49	1.11
	SL15_45_7_7	7	7	2.08	1.27	0.51	0.36

[a] *Sagging region;* [b] *Hogging region;* [c] *Reference slab strip*

Table 4.21: Load carrying capacity, displacement ductility, rotational ductility
and moment redistribution indexes for the SL30 Series.

Concrete strength class	F.E.M. ID	S (a) Number of CFRP laminates	H (b) Number of CFRP laminates	λ	μ_Δ	μ_χ	MRI
C12/15	SL30_15 (c)	0	0	1.00	1.00	1.00	1.00
	SL30_15_0_2	0	2	1.10	0.85	0.90	0.35
	SL30_15_0_4	0	4	1.14	0.77	0.82	0.08
	SL30_15_0_7	0	7	1.20	0.68	0.73	-0.21
	SL30_15_2_0	2	0	1.16	1.23	0.95	1.37
	SL30_15_2_2	2	2	1.28	1.03	0.85	0.60
	SL30_15_2_4	2	4	1.34	0.92	0.78	0.30
	SL30_15_2_7	2	7	1.41	0.81	0.69	-0.01
	SL30_15_4_0	4	0	1.28	1.32	0.90	1.60
	SL30_15_4_2	4	2	1.42	1.11	0.81	0.79
	SL30_15_4_4	4	4	1.49	1.00	0.74	0.48
	SL30_15_4_7	4	7	1.56	0.88	0.66	0.17
	SL30_15_7_0	7	0	1.42	1.39	0.85	1.82
	SL30_15_7_2	7	2	1.54	1.11	0.72	0.98
	SL30_15_7_4	7	4	1.64	1.04	0.70	0.69
	SL30_15_7_7	7	7	1.72	0.92	0.62	0.38
C25/30	SL30_30 (c)	0	0	1.00	1.00	1.00	1.00
	SL30_30_0_2	0	2	1.10	0.85	0.91	0.34
	SL30_30_0_4	0	4	1.15	0.76	0.83	0.04
	SL30_30_0_7	0	7	1.21	0.67	0.74	-0.26
	SL30_30_2_0	2	0	1.22	1.40	0.83	1.48
	SL30_30_2_2	2	2	1.32	1.05	0.66	0.62
	SL30_30_2_4	2	4	1.44	1.05	0.69	0.27
	SL30_30_2_7	2	7	1.52	0.92	0.62	-0.08
	SL30_30_4_0	4	0	1.36	1.53	0.79	1.76
	SL30_30_4_2	4	2	1.40	1.02	0.55	0.80
	SL30_30_4_4	4	4	1.62	1.14	0.65	0.48
	SL30_30_4_7	4	7	1.71	1.00	0.58	0.12
	SL30_30_7_0	7	0	1.52	1.61	0.74	2.05
	SL30_30_7_2	7	2	1.50	1.00	0.48	0.98
	SL30_30_7_4	7	4	1.81	1.19	0.62	0.71
	SL30_30_7_7	7	7	1.90	1.04	0.55	0.36
C35/45	SL30_45 (c)	0	0	1.00	1.00	1.00	1.00
	SL30_45_0_2	0	2	1.10	0.85	0.91	0.30
	SL30_45_0_4	0	4	1.16	0.76	0.84	-0.05
	SL30_45_0_7	0	7	1.22	0.67	0.75	-0.39
	SL30_45_2_0	2	0	1.27	1.60	0.79	1.68
	SL30_45_2_2	2	2	1.30	0.96	0.51	0.65
	SL30_45_2_4	2	4	1.53	1.16	0.65	0.21
	SL30_45_2_7	2	7	1.63	1.02	0.59	-0.19
	SL30_45_4_0	4	0	1.41	1.74	0.72	2.23
	SL30_45_4_2	4	2	1.39	0.93	0.42	0.86
	SL30_45_4_7	4	4	1.69	1.16	0.56	0.49
	SL30_45_4_7	4	7	1.85	1.10	0.54	0.08
	SL30_45_7_0	7	0	1.58	1.68	0.63	2.42
	SL30_45_7_2	7	2	1.49	0.90	0.36	1.06
	SL30_45_7_4	7	4	1.83	1.12	0.48	0.77
	SL30_45_7_7	7	7	2.03	1.08	0.48	0.39

(a) *Sagging region;* (b) *Hogging region;* (c) *Reference slab strip*

Table 4.22: Load carrying capacity, displacement ductility, rotational ductility
and moment redistribution indexes for the SL45 Series.

Concrete strength class	F.E.M. ID	S (a) Number of CFRP laminates	H (b) Number of CFRP laminates	λ	μ_Δ	μ_χ	MRI
C12/15	SL45_15 [c]	0	0	1.00	1.00	1.00	1.00
	SL45_15_0_2	0	2	1.11	0.82	0.88	0.52
	SL45_15_0_4	0	4	1.16	0.73	0.79	0.31
	SL45_15_0_7	0	7	1.22	0.63	0.68	0.11
	SL45_15_2_0	2	0	1.12	1.27	0.97	1.25
	SL45_15_2_2	2	2	1.27	0.98	0.82	0.62
	SL45_15_2_4	2	4	1.34	0.86	0.73	0.40
	SL45_15_2_7	2	7	1.41	0.74	0.64	0.18
	SL45_15_4_0	4	0	1.22	1.35	0.90	1.37
	SL45_15_4_2	4	2	1.34	0.98	0.68	0.70
	SL45_15_4_4	4	4	1.46	0.92	0.68	0.49
	SL45_15_4_7	4	7	1.54	0.79	0.59	0.27
	SL45_15_7_0	7	0	1.34	1.38	0.84	1.47
	SL45_15_7_2	7	2	1.40	0.97	0.59	0.77
	SL45_15_7_4	7	4	1.60	0.98	0.66	0.58
	SL45_15_7_7	7	7	1.68	0.83	0.57	0.36
C25/30	SL45_30 [c]	0	0	1.00	1.00	1.00	1.00
	SL45_30_0_2	0	2	1.11	0.80	0.88	0.52
	SL45_30_0_4	0	4	1.16	0.71	0.80	0.30
	SL45_30_0_7	0	7	1.22	0.61	0.70	0.10
	SL45_30_2_0	2	0	1.13	1.29	0.91	1.36
	SL45_30_2_2	2	2	1.24	0.86	0.64	0.63
	SL45_30_2_4	2	4	1.39	0.89	0.73	0.39
	SL45_30_2_7	2	7	1.46	0.77	0.64	0.16
	SL45_30_4_0	4	0	1.25	1.38	0.86	1.49
	SL45_30_4_2	4	2	1.30	0.84	0.53	0.71
	SL45_30_4_7	4	4	1.54	0.96	0.69	0.48
	SL45_30_4_7	4	7	1.63	0.83	0.61	0.25
	SL45_30_7_0	7	0	1.55	1.35	0.78	1.50
	SL45_30_7_2	7	2	1.37	0.84	0.46	0.78
	SL45_30_7_4	7	4	1.71	1.02	0.66	0.59
	SL45_30_7_7	7	7	1.80	0.87	0.57	0.37
C35/45	SL45_45 [c]	0	0	1.00	1.00	1.00	1.00
	SL45_45_0_2	0	2	1.11	0.81	0.86	0.52
	SL45_45_0_4	0	4	1.17	0.72	0.78	0.30
	SL45_45_0_7	0	7	1.23	0.63	0.69	0.08
	SL45_45_2_0	2	0	1.18	1.43	0.69	1.32
	SL45_45_2_2	2	2	1.27	0.89	0.45	0.65
	SL45_45_2_4	2	4	1.50	1.08	0.62	0.37
	SL45_45_2_7	2	7	1.59	0.93	0.54	0.12
	SL45_45_4_0	4	0	1.28	1.38	0.56	1.39
	SL45_45_4_2	4	2	1.33	0.88	0.37	0.74
	SL45_45_4_4	4	4	1.64	1.10	0.52	0.50
	SL45_45_4_7	4	7	1.78	0.99	0.49	0.24
	SL45_45_7_0	7	0	1.39	1.33	0.48	1.48
	SL45_45_7_2	7	2	1.40	0.84	0.31	0.82
	SL45_45_7_4	7	4	1.76	1.05	0.44	0.62
	SL45_45_7_7	7	7	1.97	1.02	0.44	0.38

[a] *Sagging region;* [b] *Hogging region;* [c] *Reference slab strip*

Table 4.23: Load carrying capacity, displacement ductility
and moment redistribution indexes – Experimental program.

Experimental program	Slab strips ID	λ	μ_Δ	MRI	f_{cm} (MPa)
H Series	Reference	1.00	1.00	1.00	
	SL15_0_1.5*	1.08	0.90	-0.22	40.07
	SL15_0_3.5*	1.19	0.86	-0.84	
	Reference	1.00	1.00	1.00	
	SL30_0_1*	1.08	0.83	0.58	35.99
	SL30_0_2.5*	1.11	0.76	0.19	
	Reference	1.00	1.00	1.00	
	SL45_0_0.5*	1.04	1.00	0.83	41.41
	SL45_0_1.5*	1.09	0.86	0.52	
HS Series	Reference	1.00	1.00	(na)	26.37
	SL15_2.5_4	1.36	1.06		
	Reference	1.00	1.00	1.00	
	SL30_3_2	1.30	0.97	1.07	28.40
	SL30_6.5_3	1.49	0.98	1.20	
	Reference	1.00	1.00	1.00	
	SL45_2_1	1.24	1.14	1.06	42.38
	SL45_6_2	1.37	0.96	1.12	

(na): The results are not presented due to a deficient functioning of the data acquisition system during the test of this slab; *Area equivalent to a CFRP laminate of 20 mm height.

4.3 CONCLUSIONS

To evaluate the influence of the concrete strength class, the percentage of existing longitudinal tensile reinforcement and the percentage of CFRP on the strengthening effectiveness, moment redistribution capacity and ductility performance, a parametric study was carried out by executing material nonlinear analysis with a FEM-based computer program, which predictive performance was calibrated using the results of the experimental programs described in Chapter 3. From the obtained results it can be pointed out the following main observations:

(i) The overall behaviour of the strengthened slab strips is not significantly affected by the concrete strength class, as long as structural concrete strength classes, according the Model Code classification, are used;

(ii) The load carrying and the moment redistribution capacities strongly depend on the flexural strengthening arrangement;

(iii) The load carrying capacity of the strengthened slabs increases with $\rho_{s,eq}^{S}$ and $\rho_{s,eq}^{H}$, but the increase is much more pronounced with $\rho_{s,eq}^{S}$, specially up to the formation of the plastic hinge in the hogging region ($\rho_{s,eq} = A_{sl}/bd_{s} + (A_{f}E_{f}/E_{s})/(bd_{f})$ is the equivalent reinforcement ratio);

(vi) The moment redistribution decreases with the increase of $\rho_{s,eq}^{H}$, and increases with $\rho_{s,eq}^{S}$;

(v) The moment redistribution increases with $\rho_{s,eq}^{S}/\rho_{s,eq}^{H}$ and positive values (which means that the moment redistribution of the strengthened slab is higher than its corresponding reference slab) are positive when $\rho_{s,eq}^{S}/\rho_{s,eq}^{H}$ >1.09, $\rho_{s,eq}^{S}/\rho_{s,eq}^{H}$ >1.49 and $\rho_{s,eq}^{S}/\rho_{s,eq}^{H}$ >2.27 for η equal to 15%, 30% and 45%, respectively. Additionally, when considering all the series analysed in this work, a good fit for a linear model was obtained for $\eta - \rho_{s,eq}^{S}/\rho_{s,eq}^{H}$. Thus, the moment redistribution percentage can be estimated by using the parameter $\rho_{s,eq}^{S}/\rho_{s,eq}^{H}$;

(vi) A flexural strengthening strategy composed of CFRP laminates applied in both hogging and sagging regions has a deflection ductility performance similar to its corresponding RC slab.

(vii) The rotational capacity of the strengthened slab strips decreases with the increase of $\rho_{s,eq}^{H}$, and increases with $\rho_{s,eq}^{S}$. In the slab strips strengthened in both sagging and hogging regions, a rotational capacity lower than its reference slabs was obtained.

In conclusion, the obtained results evidence that the use of efficient strengthening strategies can provide adequate level of ductility and moment redistribution in statically indeterminate structures, with a considerable increase in the load carrying capacity.

4.4 BIBLIOGRAPHY

ACI Committee 440, "Guide for the design and construction of externally bonded FRP systems for strengthening concrete structures", ACI440.2R-08, Reported by ACI Committee 440, American Concrete Institute, Farmington Hills, Mich, 80 pp, 2008.

Barros J.A.O, Figueiras, J.A., "Nonlinear analysis of steel fibre reinforced concrete slabs on grade", Computers & Structures Journal, 79(1), pp. 97-106, 2001.

Barros J.A.O, Varma, R.K., Sena-Cruz, J.M., Azevedo, A.F.M., "Near surface mounted CFRP strips for the flexural strengthening of RC columns - experimental and numerical research", Engineering Structures Journal, 30(12), pp. 3412-3425, 2008a.

Barros J.A.O, Dalfré, G.M, Dias, J.P., "Numerical Simulation of Continuous RC Slabs Strengthened using NSM Technique", Proceedings of 2nd International Conference on Concrete Repair, Rehabilitation and Retrofitting, Cape Town, South Africa, 2008b.

Barros, J.A.O., Kotynia, R., "Possibilities and challenges of NSM for the flexural strengthening of RC structures", Fourth International Conference on FRP Composites in Civil Engineering (CICE2008), Zurich, Switzerland, 22-24 July, 2008.

Barros J.A.O, Costa, I.G., Ventura-Gouveia, A., "CFRP flexural and shear strengthening technique for RC beams: experimental and numerical research", Advances in Structural Engineering Journal, 14(3), pp. 551-573, 2011.

Breveglieri, M., Barros, J., Dalfré, G., Aprile, A., "A parametric study on the effectiveness of the NSM technique for the flexural strengthening of continuous RC slabs", Composites: Part B 43 (2012) 1970–1987, 2012.

Bonaldo, E., "Composite materials and discrete steel fibres for the strengthening of thin concrete structures", PhD Thesis, University of Minho, Guimarães, Portugal, 2008.

CEB-FIP Model Code 1990, "Design Code". Thomas Telford, Lausanne, Switzerland, 1993.

EN 1992-1-1, "Eurocode 2: Design of Concrete Structures-Part 1-1: General Rules and Rules for Buildings", CEN, Brussels, 2010.

Sena-Cruz, J.M., "Strengthening of concrete structures with near-surface mounted CFRP laminate strips", PhD Thesis, Department of Civil Engineering, University of Minho, Portugal, 2004.

Stevens N.J., "Analytical modelling of reinforced concrete subjected to monotonic and reversed loadings", Publication No. 87-1, ISBN 0-7727-7088-3, University of Toronto, January, 1987.

"We can't solve problems by using the same kind of
thinking we used when we created them".
Albert Einstein
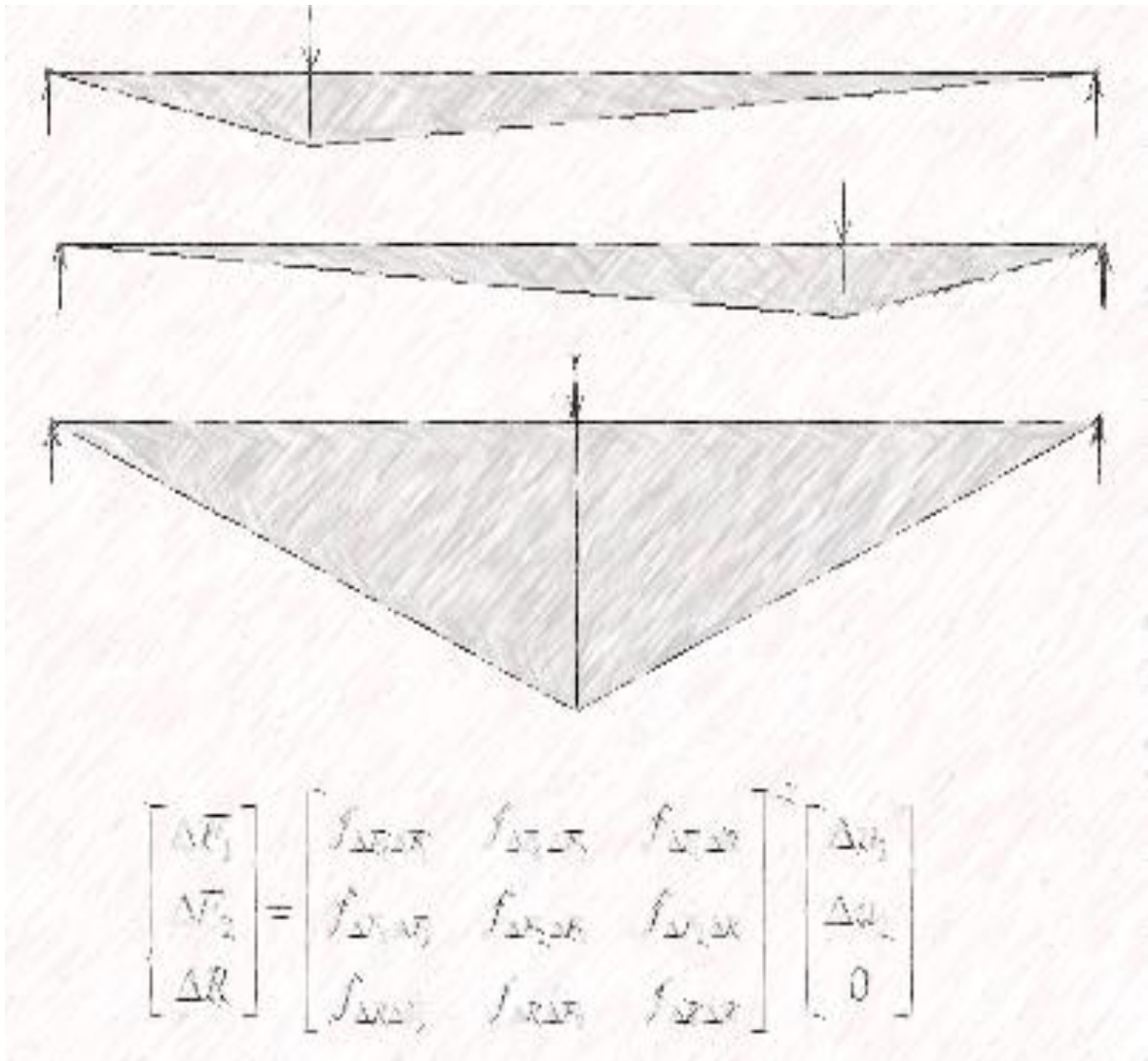
Chapter 5

DESCRIPTION OF THE ANALYTICAL STRATEGY

To predict the load-deflection response of statically indeterminate structures up to its collapse, an analytical model was developed and its performance was appraised by using the data obtained in the experimental program described in Chapter 3. The proposed approach is based on the force method by establishing the displacement compatibility equations from that the unknown variables are determined. To determine the tangential flexural stiffness making part of these equations, moment-curvature relationship is determined for the cross sections representative of the structure by using constitutive models for the intervening materials, strain compatibility and force-equilibrium. This model can be easily implemented according to a design format, and is applicable in statically determinate or indeterminate reinforced concrete structures strengthened according to the NSM or EBR techniques. The predictive performance of the model was appraised by simulating two series of tests composed of seventeen RC slab strips strengthening with NSM CFRP laminates.

5.1. MODEL IDEALISATION

Indeterminate structures are being widely used since they can be more economic, safer and develop more ductile behaviour than statically determinate structures. In the case of indeterminate structures either the reactions or the internal forces cannot be determined from equations of statics alone. In such structures, the number of reactions or the number of internal forces exceeds the number of static equilibrium equations. There are two methods of analysis for statically indeterminate structure depending on the approach selected to establish the system of equations that can derive the unknown variables (Ghali et al. 2003):

1. Force method (also known as flexibility method, method of consistent deformation, flexibility matrix method), where a system of displacement compatibility equations is established, whose number is equal to the unknown redundant supports (extra equations corresponding to selected displacements can also be added).

2. Displacement method (also known as stiffness matrix method), where a system of equilibrium equations is established, whose number is equal to the degrees of freedom of the structure.

In this work, an analytical model based on the force method is proposed. In this method, primary unknown are forces corresponding to selected redundant supports. To determine simultaneously, not only these forces but also the deflections at the loaded sections, extra displacement compatibility equations are established solving these equations, the redundant forces and the displacement at the loaded sections are determined. Once the redundant forces are calculated, the remaining reactions are evaluated by equations of equilibrium, as well as the internal forces in the elements forming the structure (Barros 2004).

5.2 FORCE METHOD APPLIED TO STATICALLY INDETERMINATE SLAB STRIP OF TWO SPANS

Figure 5.1 presents the slab strip used in the experimental program, which is statically indeterminate of one degree, e.g., a displacement compatibility equation corresponding to a reaction support should be established to determine the value of this reaction force.

Assuming the principle of superposition of effects can be applied for each relatively small load increment, ΔF , the structure is decomposed into a number of equilibrium configurations. In the present case, three compatibility equations will be established, corresponding to the loaded sections and to the intermediate support, in order to obtain the incremental displacements (Δu_1 and Δu_2) and the incremental reaction (ΔR) due to ΔF (Figure 5.2).

(a)

(b)
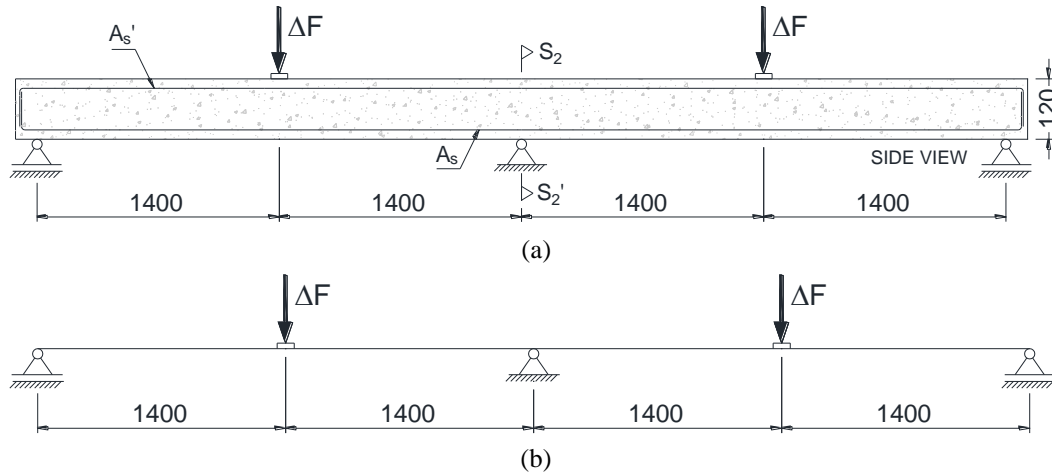
Figure 5.1: Actual continuous beam (Original)
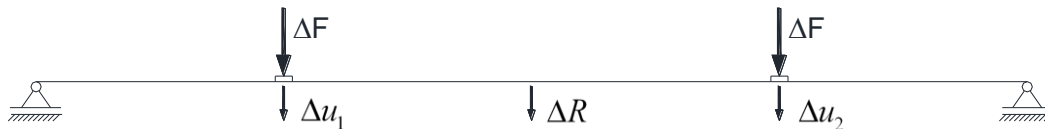
Figure 5.2: Basic determinate beam (primary structure) , redundant displacements Δu_1 , Δu_2 and the reaction ΔR .

For each configuration it is determined the deflections corresponding to the applied forces (fictitious ΔF_1 and ΔF_2 forces and unknown reaction ΔR , Figure 5.3). The terms of the flexibility matrix, $f_{\Delta F_1 \Delta F_1}$, $f_{\Delta R \Delta F_1}$, $f_{\Delta F_2 \Delta F_1}$, $f_{\Delta F_1 \Delta F_2}$, $f_{\Delta R \Delta F_2}$, $f_{\Delta F_2 \Delta F_2}$, $f_{\Delta F_1 \Delta R}$, $f_{\Delta R \Delta R}$ and $f_{\Delta F_2 \Delta R}$, is presented with a generic representation, f_{ij} , that means the displacement in generalized X_i force direction due to the application of an unit load in the X_j direction, is obtained by applying the principle of virtual work to the external and internal forces of the configuration of the X_i forces in the external and internal displacements of the configuration of the X_j forces (Barros 2004). The diagrams of bending moments (in the present work it is neglected the work due to axial and shear forces) for the three configurations of Figure 5.3 are represented in Figure 5.4.
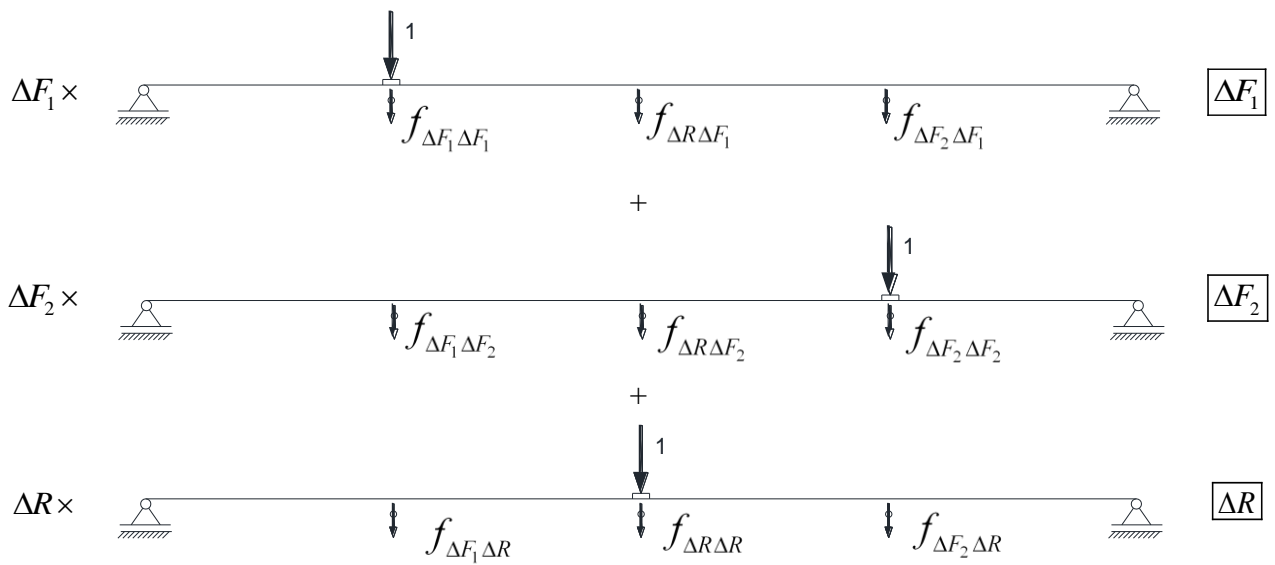
Figure 5.3: Physical meaning of the terms of the flexibility matrix, based on the displacements for each equilibrium configuration: a) $\Delta F_1 = 1$, b) $\Delta F_2 = 1$, and c) $\Delta R = 1$.
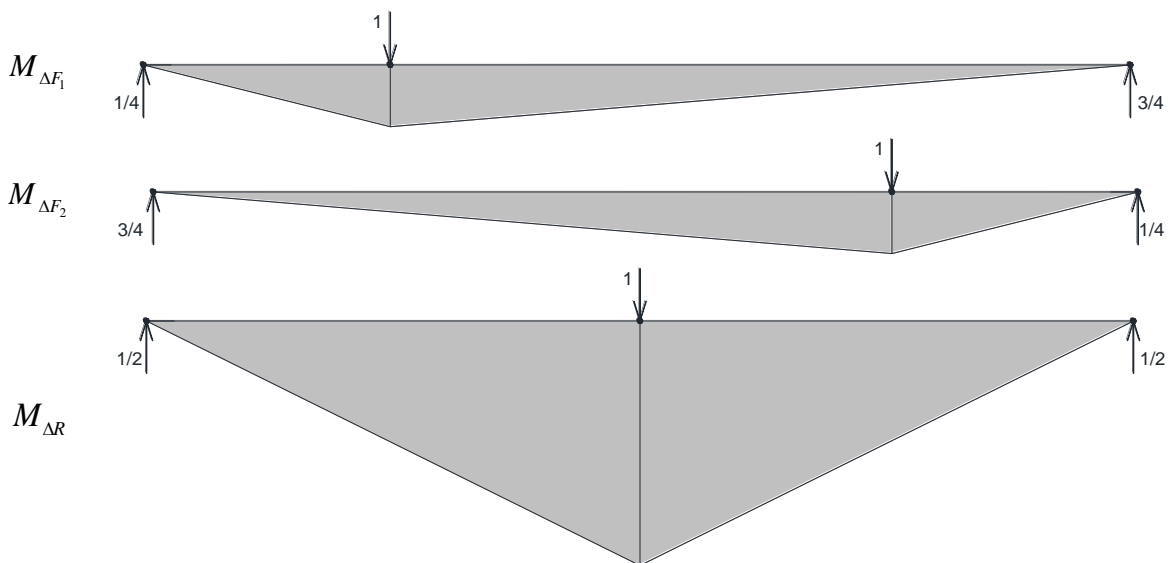
Figure 5.4: Diagrams of bending moments for the three equilibrium configurations of Figure 5.3.

The evaluation of each term of the flexibility matrix (only considering the internal work due to bending) is executed by Ghali et al. 2003:

$$f_{ij} = \int_a^b \frac{M_i M_j}{(EI)_{element}} ds = \frac{\Omega \lambda}{(EI)_{element}} \tag{5.1}$$

where Ω is the area of the diagram M_i, λ corresponds to the ordinate of the diagram M_j and the centre of gravity of M_i (see Figure 5.5) and EI is the tangential flexural stiffness of the element between $s=a$ and $s=b$, where s represents the axis of the slab.
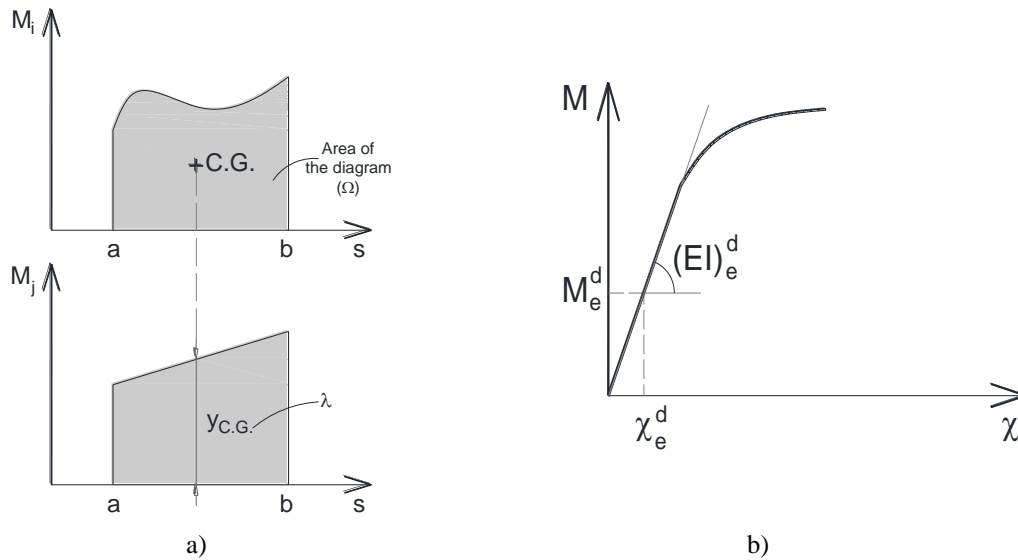
Figure 5.5: a) Principle of Bonfim Barreiros's method, and b) moment-curvature relationship.

From Figure 5.3 the following three equations of displacements compatibility can be established by applying the principle of superposition effects:

$$\Delta u_1 = f_{\Delta F_1 \Delta F_1} \times \Delta F_1 + f_{\Delta F_1 \Delta F_2} \times \Delta F_2 + f_{\Delta F_1 \Delta R} \times \Delta R$$
$$\Delta u_2 = f_{\Delta F_2 \Delta F_1} \times \Delta F_1 + f_{\Delta F_2 \Delta F_2} \times \Delta F_2 + f_{\Delta F_2 \Delta R} \times \Delta R$$
$$0 = f_{\Delta R \Delta F_1} \times \Delta F_1 + f_{\Delta R \Delta F_2} \times \Delta F_2 + f_{\Delta R \Delta R} \times \Delta R$$

(5.2)

or

$$\begin{bmatrix} f_{\Delta F_1 \Delta F_1} & f_{\Delta F_1 \Delta F_2} & f_{\Delta F_1 \Delta R} \\ f_{\Delta F_2 \Delta F_1} & f_{\Delta F_2 \Delta F_2} & f_{\Delta F_2 \Delta R} \\ f_{\Delta R \Delta F_1} & f_{\Delta R \Delta F_2} & f_{\Delta R \Delta R} \end{bmatrix} \begin{bmatrix} \Delta F_1 \\ \Delta F_2 \\ \Delta R \end{bmatrix} = \begin{bmatrix} \Delta u_1 \\ \Delta u_2 \\ 0 \end{bmatrix}$$

(5.3)

that can get the following format:

$$[f][F] = [D]$$

(5.4)

where f is the flexibility matrix, F is the vector of applied forces (ΔF_1, ΔF_2 and ΔR are unknown, since the experimental tests were displacement controlled, therefore Δu_1 and Δu_2 are the imposed displacements), and D is the vector of the displacements in the directions of ΔF_1, ΔF_2 and ΔR (where the displacement corresponding to ΔR is null).

By solving Equation (5.3) in terms of the vector of the unknown incremental forces:

$$[F] = [f]^{-1}[D]$$
(5.5)

or

$$
\begin{bmatrix} \Delta F_1 \\ \Delta F_2 \\ \Delta R \end{bmatrix} = \begin{bmatrix} f_{\Delta F_1 \Delta F_1} & f_{\Delta F_1 \Delta F_2} & f_{\Delta F_1 \Delta R} \\ f_{\Delta F_2 \Delta F_1} & f_{\Delta F_2 \Delta F_2} & f_{\Delta F_2 \Delta R} \\ f_{\Delta R \Delta F_1} & f_{\Delta R \Delta F_2} & f_{\Delta R \Delta R} \end{bmatrix}^{-1} \begin{bmatrix} \Delta u_1 \\ \Delta u_2 \\ 0 \end{bmatrix}
$$
(5.6)

Therefore, imposing for each loading step the increment of displacements adopted in the experimental tests (Δu_1 and Δu_2, where $\Delta u_1 = \Delta u_2$), and solving the Equation (5.6), the unknown incremental forces ΔF_1, ΔF_2 and ΔR are obtained. Knowing these values, the updated diagrams of internal resultant stresses are determined for each loading step by applying fundamental statics principles.

5.3 CASE STUDY – SL15-H

To assess the influence of CFRP NSM flexural strengthening technique, the experimental program described in Chapter 3, composed of seventeen $120 \times 375 \times 5875$ mm^3 RC two-span slabs, was simulated.

5.3.1 Brief description of the slab strip

The SL15-H is a statically indeterminate RC slab strip designed to assure a moment redistribution percentage, η, of 15% (Bonaldo, 2008). The arrangement of the positive and negative longitudinal steel reinforcement is presented in Figure 5.6. To evaluate correctly the flexural stiffness of this slab, it is necessary to determine the moment-curvature relationship, $M - \chi$, for each cross section that has distinct reinforcement arrangement. Therefore, each span of the slab strip was discretized in eight different cross-sections, as shown in Figures 5.7 and 5.8.

The $M - \chi$ of the cross sections was evaluated with the DOCROS computer program (Basto and Barros, 2008; Varma, 2013). According to the model implemented in DOCROS, a cross section is discretized in layers that can have distinct constitutive laws for the characterization of the behaviour of the materials that constitute these layers. It should be noted that the cross section

can be composed of plain concrete and can include steel and FRP laminates/bars. A detailed description of DOCROS can be found elsewhere (Varma, 2013).
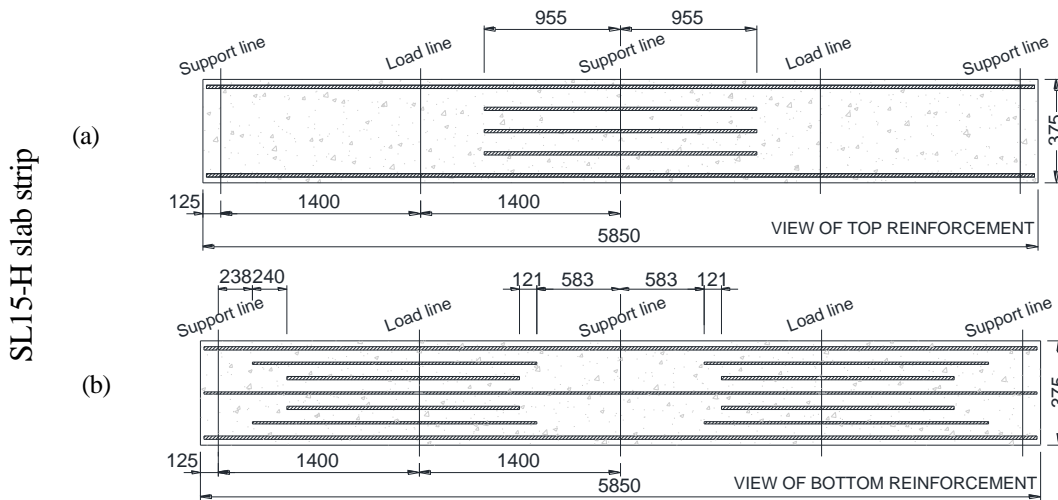
Figure 5.6: Arrangement of the longitudinal steel reinforcement of the SL15-H slab strip.
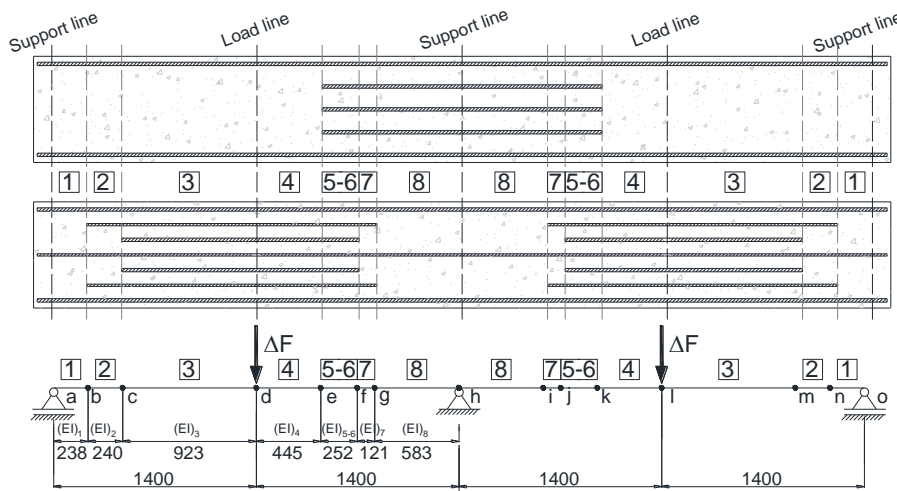
Figure 5.7: Discretization of the slab strip.
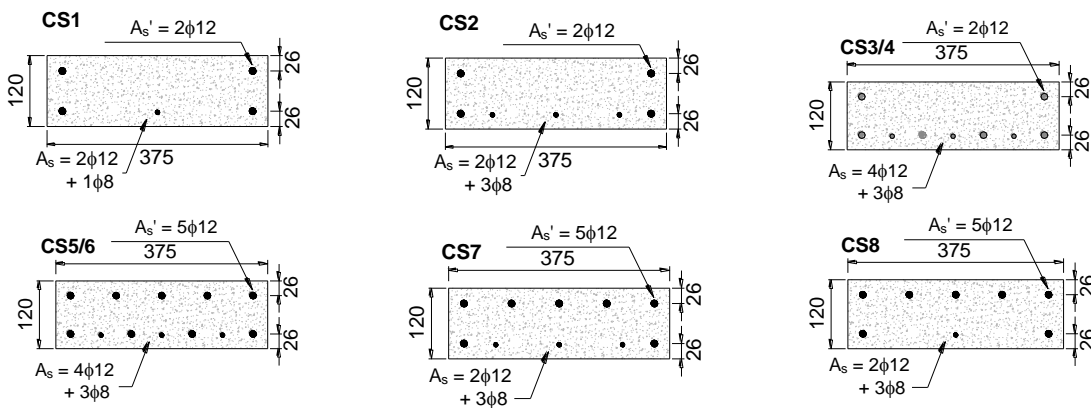
Figure 5.8: Resume of the cross-section according to the longitudinal steel reinforcement.

Table 5.1 presents a brief resume with the values of the material parameters adopted for the assessment of the predictive performance of the developed formulation. The ultimate tensile strain, as well as the modulus of elasticity of the CFRP laminates, is included in Table 3.9.

It should be noted that only the description of the slab strip SL15-H is shown in this chapter, but more details regarding the other slabs can be found in Annex 5. The values that define $M - \chi$ relationship of the cross sections of the SL15-H slab strip are presented in Table 5.2.

The moment diagrams due to the unit loads corresponding to ΔF_1, ΔF_2 and ΔR are represented in Figure 5.9. Applying the principle of virtual work it is obtained the terms of the flexibility matrix, whose equations are included in Table 5.3 (see also Annex 5).

Table 5.1: Mechanical properties of the materials used in the analytical model.

	Concrete		Steel reinforcement		
ID	Compressive strength (f_{cm}) MPa	Initial Young's modulus (E_c) GPa	Steel bar diameter (ϕs)	Modulus of elasticity (kN/mm^2)	Yield stress (0.2 %)[a] (N/mm^2)
SL15-H	40.07	33.36	8 mm	200.80	421.35
SL15-HS	26.37	29.43			
SL30-H	35.99	32.31	10 mm	178.23	446.95
SL30-HS	28.40	30.09			
SL45-S	41.41	33.69	12 mm	198.36	442.47
SL45-HS	42.38	33.93			
f_{cm} = mean cylinder compressive strength at 28 days, see Tables 3.7 and A3.1.1; E_c = determined following the recommendations of Eurocode 2 (2010), see Table 4.3; see Table 3.8.					

Using Equation (5.6) and applying determined displacements (Δu_1 and Δu_2, where $\Delta u_1 = \Delta u_2$), the ΔF_1, ΔF_2 and ΔR are obtained, and, by equilibrium (or applying the principle of superposition effects), the reactions in the other supports can be determined, as well as the updated diagrams of resultant stresses in the statically indeterminate structure.

5.3.2 Force-Deformation Response

Figures 5.10 to 5.12 compare the analytical and experimental load-deflection curves for the slabs of SL15-H/HS, SL30-H/HS and SL45-H/HS series, where the good predictive performance of the adopted formulation is visible.

Table 5.2: Values that define the M−χ relationship of the cross sections of the SL15-H slab strip.

Element 1		Element 2		Element 3		Element 4		Element 5/6		Element 5/6		Element 7		Element 7		Element 8	
M^+	χ	M^+	χ	M^+	χ	M^+	χ	M^+	χ	M^-	χ	M^+	χ	M^-	χ	M^+	χ
0.00	1.89E+12	0.00	1.91E+12	0.00	1.95E+12	0.00	1.95E+12	0.00	2.02E+12	0.00	2.02E+12	0.00	1.98E+12	0.00	1.98E+12	0.00	1.96E+12
2.91	1.69E+12	2.93	1.72E+12	2.97	1.77E+12	2.97	1.77E+12	3.13	1.82E+12	3.14	1.82E+12	3.08	1.76E+12	3.04	1.79E+12	2.99	1.77E+12
4.95	1.23E+12	5.09	1.30E+12	5.34	1.42E+12	5.34	1.42E+12	5.52	1.42E+12	5.49	1.39E+12	5.21	1.27E+12	5.39	1.40E+12	5.33	1.40E+12
4.58	5.20E+11	5.25	6.64E+11	6.23	9.06E+11	6.23	9.06E+11	6.33	8.75E+11	6.19	8.33E+11	5.26	6.29E+11	6.13	8.54E+11	6.11	8.64E+11
5.30	3.68E+11	6.05	4.77E+11	7.31	6.92E+11	7.31	6.92E+11	7.51	6.82E+11	7.33	6.46E+11	6.18	4.71E+11	7.21	6.52E+11	7.15	6.55E+11
6.59	3.42E+11	7.45	4.40E+11	8.85	6.30E+11	8.85	6.30E+11	9.15	6.29E+11	8.95	5.97E+11	7.61	4.38E+11	8.77	5.98E+11	8.69	5.99E+11
7.92	3.32E+11	8.92	4.26E+11	10.53	6.07E+11	10.53	6.07E+11	10.90	6.08E+11	10.67	5.78E+11	9.11	4.26E+11	10.46	5.78E+11	10.35	5.78E+11
9.20	3.26E+11	10.40	4.19E+11	12.22	5.95E+11	12.22	5.95E+11	12.66	5.98E+11	12.40	5.69E+11	10.60	4.19E+11	12.15	5.68E+11	12.02	5.67E+11
10.35	3.15E+11	11.83	4.13E+11	13.89	5.88E+11	13.89	5.88E+11	14.40	5.91E+11	14.11	5.63E+11	12.03	4.13E+11	13.82	5.61E+11	13.67	5.61E+11
11.18	2.89E+11	13.15	4.04E+11	15.53	5.82E+11	15.53	5.82E+11	16.10	5.86E+11	15.78	5.58E+11	13.33	4.02E+11	15.45	5.56E+11	15.28	5.55E+11
11.48	2.43E+11	14.23	3.86E+11	17.11	5.77E+11	17.11	5.77E+11	17.75	5.80E+11	17.40	5.51E+11	14.35	3.81E+11	17.03	5.51E+11	16.84	5.50E+11
11.60	2.08E+11	14.91	3.54E+11	18.63	5.71E+11	18.63	5.71E+11	19.33	5.72E+11	18.91	5.42E+11	14.95	3.48E+11	18.54	5.43E+11	18.33	5.43E+11
11.71	1.83E+11	15.23	3.14E+11	20.05	5.62E+11	20.05	5.62E+11	20.76	5.60E+11	20.24	5.26E+11	15.21	3.07E+11	19.90	5.30E+11	19.70	5.32E+11
11.82	1.63E+11	15.32	2.67E+11	21.33	5.47E+11	21.33	5.47E+11	21.94	5.37E+11	21.24	4.99E+11	15.33	2.69E+11	21.02	5.08E+11	20.87	5.12E+11
11.91	1.46E+11	15.40	2.35E+11	22.37	5.24E+11	22.37	5.24E+11	22.73	5.02E+11	21.80	4.61E+11	15.45	2.42E+11	21.73	4.71E+11	21.67	4.78E+11
12.00	1.33E+11	15.49	2.12E+11	23.03	4.85E+11	23.03	4.85E+11	23.13	4.60E+11	22.10	4.22E+11	15.56	2.21E+11	22.08	4.31E+11	22.06	4.37E+11
12.09	1.22E+11	15.58	1.93E+11	23.33	4.41E+11	23.33	4.41E+11	23.35	4.22E+11	22.29	3.87E+11	15.67	2.04E+11	22.28	3.94E+11	22.28	3.99E+11
12.17	1.13E+11	15.66	1.78E+11	23.50	4.04E+11	23.50	4.04E+11	23.51	3.89E+11	22.43	3.56E+11	15.77	1.90E+11	22.43	3.63E+11	22.43	3.66E+11
12.24	1.06E+11	15.74	1.65E+11	23.63	3.72E+11	23.63	3.72E+11	23.63	3.59E+11	22.52	3.26E+11	15.86	1.78E+11	22.54	3.35E+11	22.54	3.38E+11
12.31	1.00E+11	15.81	1.54E+11	23.73	3.45E+11	23.73	3.45E+11	23.72	3.33E+11	22.58	3.00E+11	15.95	1.68E+11	22.62	3.08E+11	22.63	3.13E+11
12.37	9.48E+10	15.86	1.44E+11	23.82	3.22E+11	23.82	3.22E+11	23.78	3.08E+11	22.63	2.78E+11	16.02	1.59E+11	22.66	2.83E+11	22.69	2.88E+11
12.43	9.01E+10	15.91	1.36E+11	23.89	3.01E+11	23.89	3.01E+11	23.82	2.86E+11	22.67	2.60E+11	16.09	1.51E+11	22.69	2.62E+11	22.71	2.65E+11
12.48	8.60E+10	15.95	1.28E+11	23.93	2.81E+11	23.93	2.81E+11	23.85	2.67E+11	22.72	2.45E+11	16.15	1.44E+11	22.72	2.45E+11	22.73	2.46E+11
12.52	8.22E+10	15.99	1.21E+11					23.88	2.52E+11	22.75	2.31E+11	16.20	1.37E+11	22.75	2.31E+11	22.75	2.31E+11
12.55	7.89E+10	16.02	1.16E+11					23.90	2.39E+11	22.78	2.20E+11	16.23	1.32E+11	22.77	2.18E+11	22.77	2.18E+11
12.58	7.59E+10	16.04	1.11E+11					23.92	2.27E+11	22.80	2.10E+11	16.26	1.26E+11	22.79	2.08E+11	22.78	2.07E+11
12.63	6.65E+10																

M (N.mm); χ (1/mm); M^+ (Positive bending moment); M^- (Negative bending moment)

$M_{\Delta F_1}$

a)

$M_{\Delta F_2}$

b)

$M_{\Delta R}$

c)

Figure 5.9: Moment diagrams due to: a) $\Delta F_1 = 1$, b) $\Delta F_2 = 1$, and c) $\Delta R = 1$.

Table 5.3: Equations for the evaluation of the terms of the flexibility matrix of the structure.

$$
f_{\Delta F_1 \Delta F_1} = \sum \left(
\begin{array}{l}
\int_a^b \dfrac{M_{\Delta F_1} M_{\Delta F_1}}{(EI)_1} ds + \int_b^c \dfrac{M_{\Delta F_1} M_{\Delta F_1}}{(EI)_2} ds + \int_c^d \dfrac{M_{\Delta F_1} M_{\Delta F_1}}{(EI)_3} ds + \int_d^e \dfrac{M_{\Delta F_1} M_{\Delta F_1}}{(EI)_4} ds + \\[2ex]
\int_e^f \dfrac{M_{\Delta F_1} M_{\Delta F_1}}{(EI)_{5-6}} ds + \int_f^g \dfrac{M_{\Delta F_1} M_{\Delta F_1}}{(EI)_7} ds + \int_g^h \dfrac{M_{\Delta F_1} M_{\Delta F_1}}{(EI)_8} ds + \int_h^i \dfrac{M_{\Delta F_1} M_{\Delta F_1}}{(EI)_8} ds + \\[2ex]
\int_i^j \dfrac{M_{\Delta F_1} M_{\Delta F_1}}{(EI)_7} ds + \int_j^k \dfrac{M_{\Delta F_1} M_{\Delta F_1}}{(EI)_{5-6}} ds + \int_k^l \dfrac{M_{\Delta F_1} M_{\Delta F_1}}{(EI)_4} ds + \int_l^m \dfrac{M_{\Delta F_1} M_{\Delta F_1}}{(EI)_3} ds + \\[2ex]
\int_m^n \dfrac{M_{\Delta F_1} M_{\Delta F_1}}{(EI)_2} ds + \int_n^o \dfrac{M_{\Delta F_1} M_{\Delta F_1}}{(EI)_1} ds
\end{array}
\right)
$$

$$
f_{\Delta F_1 \Delta F_2} = \sum \left(
\begin{array}{l}
\int_a^b \dfrac{M_{\Delta F_1} M_{\Delta F_2}}{(EI)_1} ds + \int_b^c \dfrac{M_{\Delta F_1} M_{\Delta F_2}}{(EI)_2} ds + \int_c^d \dfrac{M_{\Delta F_1} M_{\Delta F_2}}{(EI)_3} ds + \int_d^e \dfrac{M_{\Delta F_1} M_{\Delta F_2}}{(EI)_4} ds + \\[2ex]
\int_e^f \dfrac{M_{\Delta F_1} M_{\Delta F_2}}{(EI)_{5-6}} ds + \int_f^g \dfrac{M_{\Delta F_1} M_{\Delta F_2}}{(EI)_7} ds + \int_g^h \dfrac{M_{\Delta F_1} M_{\Delta F_2}}{(EI)_8} ds + \int_h^i \dfrac{M_{\Delta F_1} M_{\Delta F_2}}{(EI)_8} ds + \\[2ex]
\int_i^j \dfrac{M_{\Delta F_1} M_{\Delta F_2}}{(EI)_7} ds + \int_j^k \dfrac{M_{\Delta F_1} M_{\Delta F_2}}{(EI)_{5-6}} ds + \int_k^l \dfrac{M_{\Delta F_1} M_{\Delta F_2}}{(EI)_4} ds + \int_l^m \dfrac{M_{\Delta F_1} M_{\Delta F_2}}{(EI)_3} ds + \\[2ex]
\int_m^n \dfrac{M_{\Delta F_1} M_{\Delta F_2}}{(EI)_2} ds + \int_n^o \dfrac{M_{\Delta F_1} M_{\Delta F_2}}{(EI)_1} ds
\end{array}
\right)
$$

Table 5.3 (continued)

$$f_{\Delta F_2 \Delta F_1} = \sum \left(\begin{array}{l} \int_a^b \dfrac{M_{\Delta F_2} M_{\Delta F_1}}{(EI)_1}ds + \int_b^c \dfrac{M_{\Delta F_2} M_{\Delta F_1}}{(EI)_2}ds + \int_c^d \dfrac{M_{\Delta F_2} M_{\Delta F_1}}{(EI)_3}ds + \int_d^e \dfrac{M_{\Delta F_2} M_{\Delta F_1}}{(EI)_4}ds + \\[3mm] \int_e^f \dfrac{M_{\Delta F_2} M_{\Delta F_1}}{(EI)_{5-6}}ds + \int_f^g \dfrac{M_{\Delta F_2} M_{\Delta F_1}}{(EI)_7}ds + \int_g^h \dfrac{M_{\Delta F_2} M_{\Delta F_1}}{(EI)_8}ds + \int_h^i \dfrac{M_{\Delta F_2} M_{\Delta F_1}}{(EI)_8}ds + \\[3mm] \int_i^j \dfrac{M_{\Delta F_2} M_{\Delta F_1}}{(EI)_7}ds + \int_j^k \dfrac{M_{\Delta F_2} M_{\Delta F_1}}{(EI)_{5-6}}ds + \int_k^l \dfrac{M_{\Delta F_2} M_{\Delta F_1}}{(EI)_4}ds + \int_l^m \dfrac{M_{\Delta F_2} M_{\Delta F_1}}{(EI)_3}ds + \\[3mm] \int_m^n \dfrac{M_{\Delta F_2} M_{\Delta F_1}}{(EI)_2}ds + \int_n^o \dfrac{M_{\Delta F_2} M_{\Delta F_1}}{(EI)_1}ds \end{array} \right)$$

$$f_{\Delta F_2 \Delta F_2} = \sum \left(\begin{array}{l} \int_a^b \dfrac{M_{\Delta F_2} M_{\Delta F_2}}{(EI)_1}ds + \int_b^c \dfrac{M_{\Delta F_2} M_{\Delta F_2}}{(EI)_2}ds + \int_c^d \dfrac{M_{\Delta F_2} M_{\Delta F_2}}{(EI)_3}ds + \int_d^e \dfrac{M_{\Delta F_2} M_{\Delta F_2}}{(EI)_4}ds + \\[3mm] \int_e^f \dfrac{M_{\Delta F_2} M_{\Delta F_2}}{(EI)_{5-6}}ds + \int_f^g \dfrac{M_{\Delta F_2} M_{\Delta F_2}}{(EI)_7}ds + \int_g^h \dfrac{M_{\Delta F_2} M_{\Delta F_2}}{(EI)_8}ds + \int_h^i \dfrac{M_{\Delta F_2} M_{\Delta F_2}}{(EI)_8}ds + \\[3mm] \int_i^j \dfrac{M_{\Delta F_2} M_{\Delta F_2}}{(EI)_7}ds + \int_j^k \dfrac{M_{\Delta F_2} M_{\Delta F_2}}{(EI)_{5-6}}ds + \int_k^l \dfrac{M_{\Delta F_2} M_{\Delta F_2}}{(EI)_4}ds + \int_l^m \dfrac{M_{\Delta F_2} M_{\Delta F_2}}{(EI)_3}ds + \\[3mm] \int_m^n \dfrac{M_{\Delta F_2} M_{\Delta F_2}}{(EI)_2}ds + \int_n^o \dfrac{M_{\Delta F_2} M_{\Delta F_2}}{(EI)_1}ds \end{array} \right)$$

$$f_{\Delta F_1 \Delta R} = \sum \left(\begin{array}{l} \int_a^b \dfrac{M_{\Delta F_1} M_{\Delta R}}{(EI)_1}ds + \int_b^c \dfrac{M_{\Delta F_1} M_{\Delta R}}{(EI)_2}ds + \int_c^d \dfrac{M_{\Delta F_1} M_{\Delta R}}{(EI)_3}ds + \int_d^e \dfrac{M_{\Delta F_1} M_{\Delta R}}{(EI)_4}ds + \\[3mm] \int_e^f \dfrac{M_{\Delta F_1} M_{\Delta R}}{(EI)_{5-6}}ds + \int_f^g \dfrac{M_{\Delta F_1} M_{\Delta R}}{(EI)_7}ds + \int_g^h \dfrac{M_{\Delta F_1} M_{\Delta R}}{(EI)_8}ds + \int_h^i \dfrac{M_{\Delta F_1} M_{\Delta R}}{(EI)_8}ds + \\[3mm] \int_i^j \dfrac{M_{\Delta F_1} M_{\Delta R}}{(EI)_7}ds + \int_j^k \dfrac{M_{\Delta F_1} M_{\Delta R}}{(EI)_{5-6}}ds + \int_k^l \dfrac{M_{\Delta F_1} M_{\Delta R}}{(EI)_4}ds + \int_l^m \dfrac{M_{\Delta F_1} M_{\Delta R}}{(EI)_3}ds + \\[3mm] \int_m^n \dfrac{M_{\Delta F_1} M_{\Delta R}}{(EI)_2}ds + \int_n^o \dfrac{M_{\Delta F_1} M_{\Delta R}}{(EI)_1}ds \end{array} \right)$$

$$f_{\Delta R \Delta F_1} = \sum \left(\begin{array}{l} \int_a^b \dfrac{M_{\Delta R} M_{\Delta F_1}}{(EI)_1}ds + \int_b^c \dfrac{M_{\Delta R} M_{\Delta F_1}}{(EI)_2}ds + \int_c^d \dfrac{M_{\Delta R} M_{\Delta F_1}}{(EI)_3}ds + \int_d^e \dfrac{M_{\Delta R} M_{\Delta F_1}}{(EI)_4}ds + \\[3mm] \int_e^f \dfrac{M_{\Delta R} M_{\Delta F_1}}{(EI)_{5-6}}ds + \int_f^g \dfrac{M_{\Delta R} M_{\Delta F_1}}{(EI)_7}ds + \int_g^h \dfrac{M_{\Delta R} M_{\Delta F_1}}{(EI)_8}ds + \int_h^i \dfrac{M_{\Delta R} M_{\Delta F_1}}{(EI)_8}ds + \\[3mm] \int_i^j \dfrac{M_{\Delta R} M_{\Delta F_1}}{(EI)_7}ds + \int_j^k \dfrac{M_{\Delta R} M_{\Delta F_1}}{(EI)_{5-6}}ds + \int_k^l \dfrac{M_{\Delta R} M_{\Delta F_1}}{(EI)_4}ds + \int_l^m \dfrac{M_{\Delta R} M_{\Delta F_1}}{(EI)_3}ds + \\[3mm] \int_m^n \dfrac{M_{\Delta R} M_{\Delta F_1}}{(EI)_2}ds + \int_n^o \dfrac{M_{\Delta R} M_{\Delta F_1}}{(EI)_1}ds \end{array} \right)$$

Table 5.3 (continued)

$$
f_{\Delta F_2 \Delta R} = \sum \left(\begin{array}{l}
\displaystyle\int_a^b \frac{M_{\Delta F_2} M_{\Delta R}}{(EI)_1}ds + \int_b^c \frac{M_{\Delta F_2} M_{\Delta R}}{(EI)_2}ds + \int_c^d \frac{M_{\Delta F_2} M_{\Delta R}}{(EI)_3}ds + \int_d^e \frac{M_{\Delta F_2} M_{\Delta R}}{(EI)_4}ds + \\[12pt]
\displaystyle\int_e^f \frac{M_{\Delta F_2} M_{\Delta R}}{(EI)_{5-6}}ds + \int_f^g \frac{M_{\Delta F_2} M_{\Delta R}}{(EI)_7}ds + \int_g^h \frac{M_{\Delta F_2} M_{\Delta R}}{(EI)_8}ds + \int_h^i \frac{M_{\Delta F_2} M_{\Delta R}}{(EI)_8}ds + \\[12pt]
\displaystyle\int_i^j \frac{M_{\Delta F_2} M_{\Delta R}}{(EI)_7}ds + \int_j^k \frac{M_{\Delta F_2} M_{\Delta R}}{(EI)_{5-6}}ds + \int_k^l \frac{M_{\Delta F_2} M_{\Delta R}}{(EI)_4}ds + \int_l^m \frac{M_{\Delta F_2} M_{\Delta R}}{(EI)_3}ds + \\[12pt]
\displaystyle\int_m^n \frac{M_{\Delta F_2} M_{\Delta R}}{(EI)_2}ds + \int_n^o \frac{M_{\Delta F_2} M_{\Delta R}}{(EI)_1}ds
\end{array} \right)
$$

$$
f_{\Delta R \Delta F_2} = \sum \left(\begin{array}{l}
\displaystyle\int_a^b \frac{M_{\Delta R} M_{\Delta F_2}}{(EI)_1}ds + \int_b^c \frac{M_{\Delta R} M_{\Delta F_2}}{(EI)_2}ds + \int_c^d \frac{M_{\Delta R} M_{\Delta F_2}}{(EI)_3}ds + \int_d^e \frac{M_{\Delta R} M_{\Delta F_2}}{(EI)_4}ds + \\[12pt]
\displaystyle\int_e^f \frac{M_{\Delta R} M_{\Delta F_2}}{(EI)_{5-6}}ds + \int_f^g \frac{M_{\Delta R} M_{\Delta F_2}}{(EI)_7}ds + \int_g^h \frac{M_{\Delta R} M_{\Delta F_2}}{(EI)_8}ds + \int_h^i \frac{M_{\Delta R} M_{\Delta F_2}}{(EI)_8}ds + \\[12pt]
\displaystyle\int_i^j \frac{M_{\Delta R} M_{\Delta F_2}}{(EI)_7}ds + \int_j^k \frac{M_{\Delta R} M_{\Delta F_2}}{(EI)_{5-6}}ds + \int_k^l \frac{M_{\Delta R} M_{\Delta F_2}}{(EI)_4}ds + \int_l^m \frac{M_{\Delta R} M_{\Delta F_2}}{(EI)_3}ds + \\[12pt]
\displaystyle\int_m^n \frac{M_{\Delta R} M_{\Delta F_2}}{(EI)_2}ds + \int_n^o \frac{M_{\Delta R} M_{\Delta F_2}}{(EI)_1}ds
\end{array} \right)
$$

$$
f_{\Delta R \Delta R} = \sum \left(\begin{array}{l}
\displaystyle\int_a^b \frac{M_{\Delta R} M_{\Delta R}}{(EI)_1}ds + \int_b^c \frac{M_{\Delta R} M_{\Delta R}}{(EI)_2}ds + \int_c^d \frac{M_{\Delta R} M_{\Delta R}}{(EI)_3}ds + \int_d^e \frac{M_{\Delta R} M_{\Delta R}}{(EI)_4}ds + \\[12pt]
\displaystyle\int_e^f \frac{M_{\Delta R} M_{\Delta R}}{(EI)_{5-6}}ds + \int_f^g \frac{M_{\Delta R} M_{\Delta R}}{(EI)_7}ds + \int_g^h \frac{M_{\Delta R} M_{\Delta R}}{(EI)_8}ds + \int_h^i \frac{M_{\Delta R} M_{\Delta R}}{(EI)_8}ds + \\[12pt]
\displaystyle\int_i^j \frac{M_{\Delta R} M_{\Delta R}}{(EI)_7}ds + \int_j^k \frac{M_{\Delta R} M_{\Delta R}}{(EI)_{5-6}}ds + \int_k^l \frac{M_{\Delta R} M_{\Delta R}}{(EI)_4}ds + \int_l^m \frac{M_{\Delta R} M_{\Delta R}}{(EI)_3}ds + \\[12pt]
\displaystyle\int_m^n \frac{M_{\Delta R} M_{\Delta R}}{(EI)_2}ds + \int_n^o \frac{M_{\Delta R} M_{\Delta R}}{(EI)_1}ds
\end{array} \right)
$$
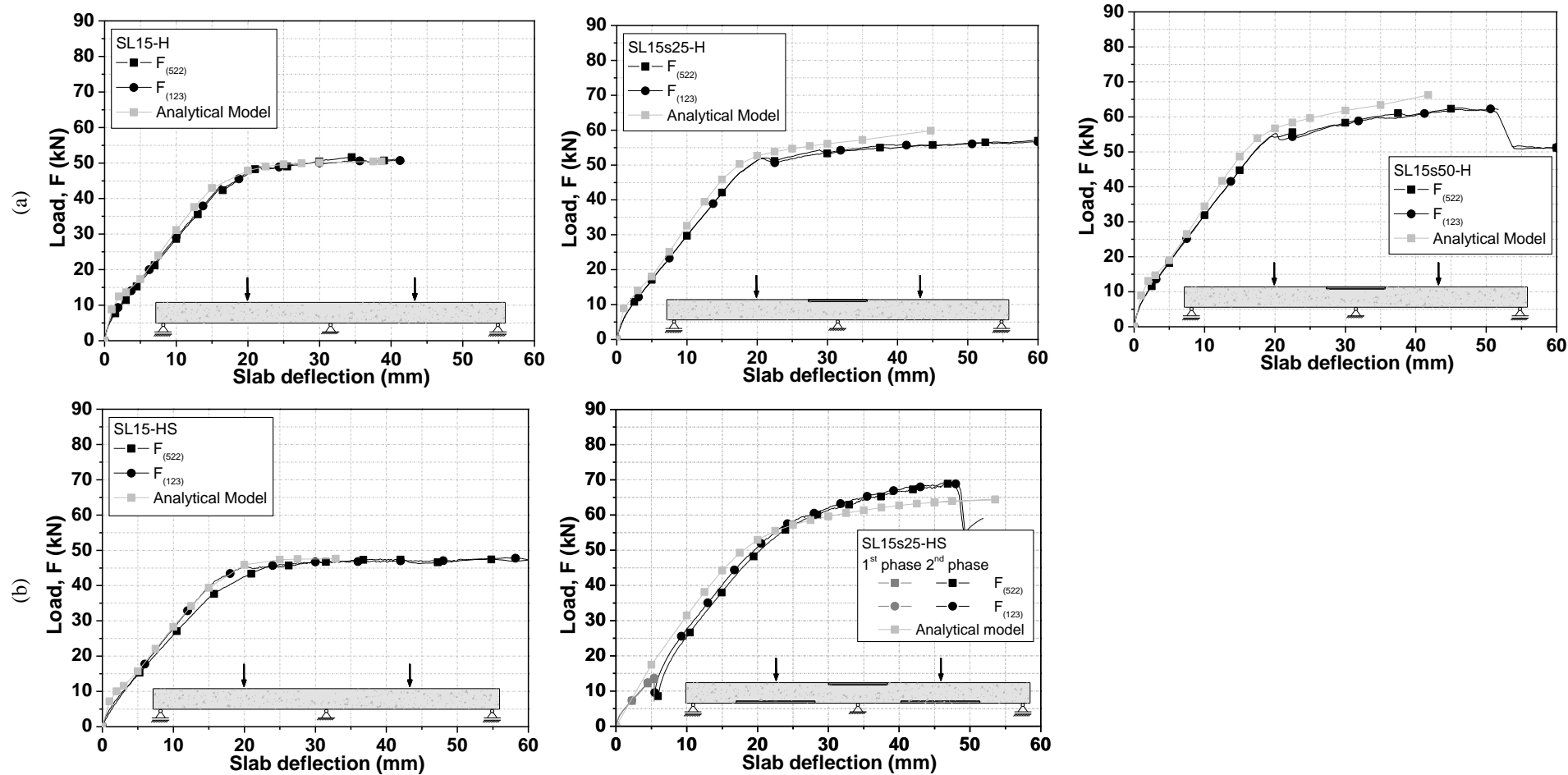
Figure 5.10: Relationship between applied load and deflections at spans of the (a) SL15-H and (b) SL15-HS Series.
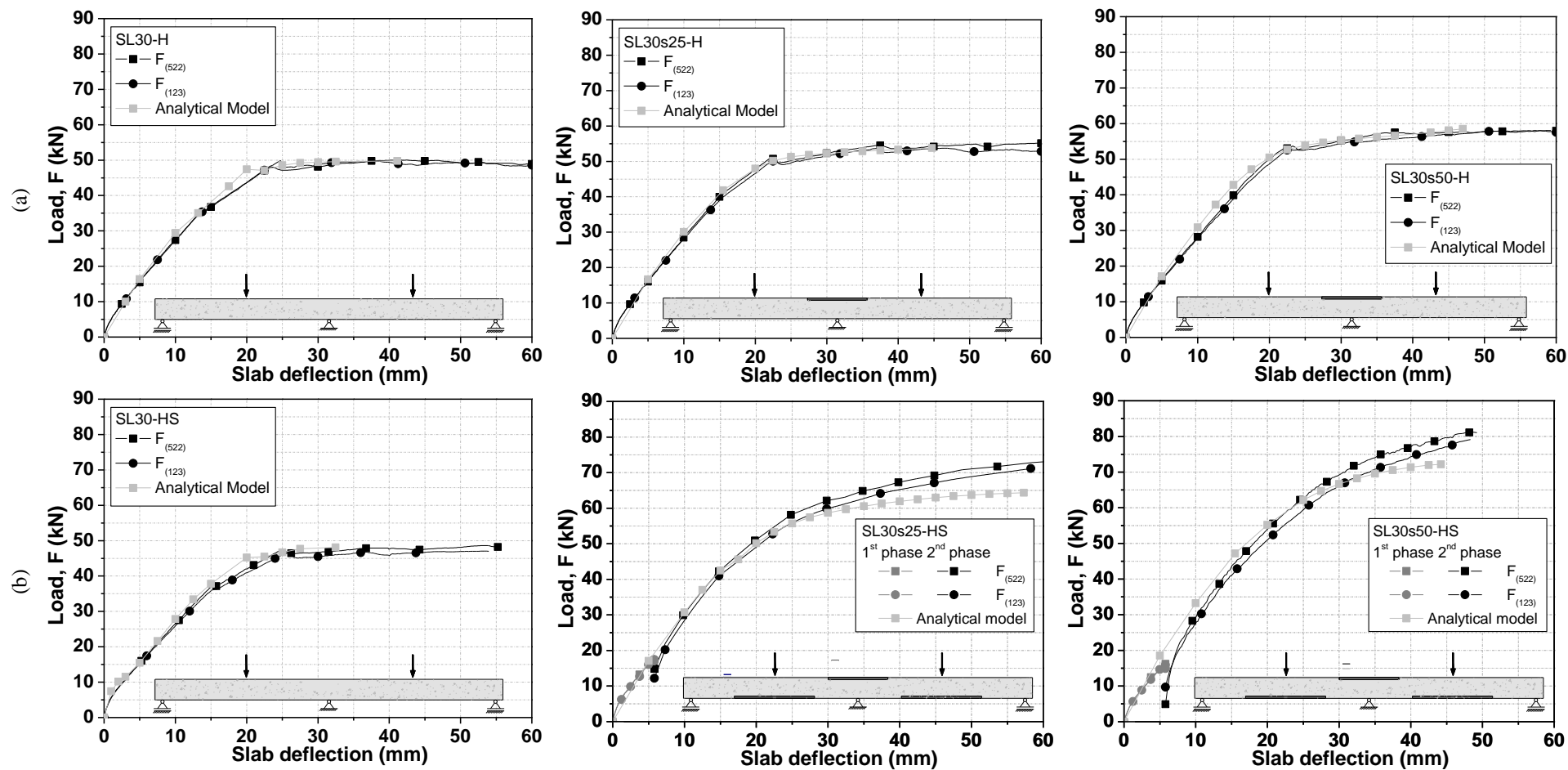
Figure 5.11: Relationship between applied load and deflections at spans of the (a) SL30-H and (b) SL30-HS Series.
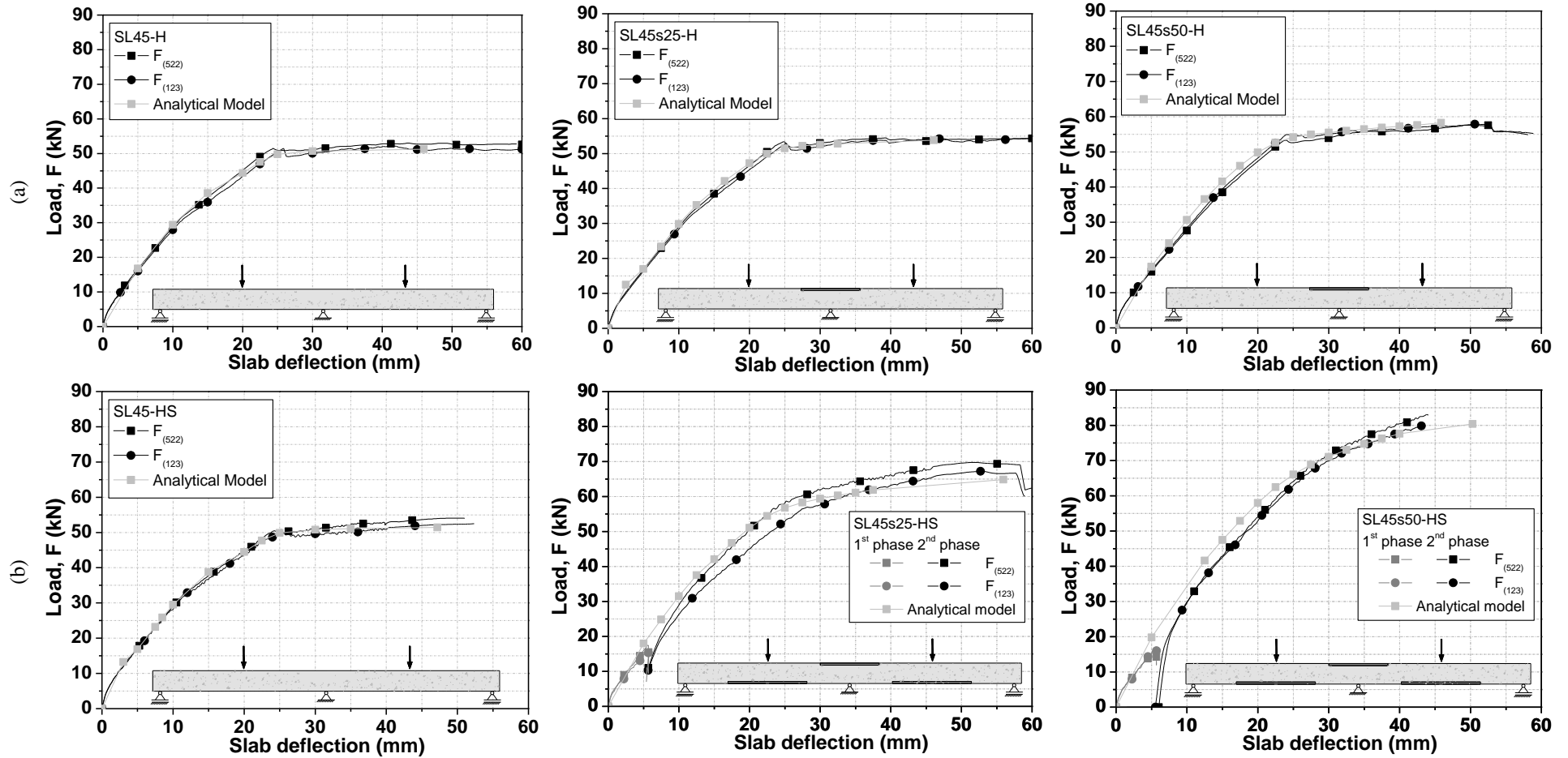
Figure 5.12: Relationship between applied load and deflections at spans of the (a) SL45-H and (b) SL45-HS Series.

5.4 CONCLUSIONS

In this chapter an analytical model based on the force method, and using the moment-curvature relationship ($M-\chi$) to determine the actual flexural stiffness, was proposed to evaluate the force deflection relationship of the statically indeterminate RC strips described in Chapter 3. To correctly evaluate the actual flexural stiffness of a certain slab strip, by taking into account the different arrangements of steel and CFRP reinforcements applied in the simulated slab strips, a slab strip was discretized in several types of cross section according to its reinforcement specificities. The software DOCROS was used to determine the $M-\chi$ of these cross sections.

The predictive performance of the developed model was assessed by simulating seventeen slab strips of the experimental programs described in chapter 3. The results showed that the developed numerical strategy fits with enough accuracy the registered experimental load-deflection curves of the tested slab strips.

5.5 BIBLIOGRAPHY

Ghali, A., Neville, A. M., Brown T. G., "Structural Analysis – a unified classical and matrix approach", Fifth edition, Spon Press, 2003.

Barros, J.A.O., "Formulação directa do método das forças", Technical report 04-DEC/E-25, Department of Civil Engineering, School Engineering, University of Minho, 25 pp., April 2004. http://hdl.handle.net/1822/12986.

Basto C.A.A, Barros J.A.O., "Numeric simulation of sections submitted to bending", Technical report 08-DEC/E-46, Department of Civil Engineering, School Engineering, University of Minho, 73 p., 2008.

Bonaldo, E., "Composite materials and discrete steel fibres for the strengthening of thin concrete structures", PhD Thesis, University of Minho, Guimarães, Portugal, 2008.

Rajendra K. Varma, "Numerical models for the simulation of the cyclic behaviour of RC structures incorporating new advanced materials", PhD Thesis, University of Minho, 2013. (in press)

Chapter 6

STEEL BAR - CONCRETE BOND BEHAVIOUR IN THE CONTEXT OF THE ETS SHEAR STRENGTHENING TECHNIQUE FOR RC BEAMS

The use of near-surface mounted (NSM) technique is a promising technology to increase the flexural and shear strength of deficiently reinforced concrete (RC) members. Chapter 3 showed that, in some cases, the effectiveness of the NSM technique for the flexural strengthening of statically indeterminate slab strips was limited due to the occurrence of shear failure at the hogging region. In case of slabs, the NSM shear strengthening technique is not applicable, which has motivated the development of a new shear strengthening technique that can be suitable for RC slabs and beams. This technique consists in opening holes across the slab thickness in the shear zone, where bars are introduced and embedded with an adhesive material (embedded through section, ETS, technique).

Since the strengthening bars are inserted into holes open through the cross section, they are much better protected from fire, environmental aggressive agents and vandalism acts than externally bonded reinforcement (EBR) and near surface mounted (NSM) techniques based on the use of fibre reinforced polymer (FRP) systems. This research program has started in 2007, where the use of FRP and steel bars, applied according to a technique that was originally designated by Core Drilled Mounted (CDM), was explored for the shear strengthening of concrete elements. In this context, direct shear tests were executed with the purpose of capturing the main features of FRP/Steel CDM bars for the shear resistance, and to provide data for a rational decision about the most effective bars and adhesives for this type of application (Barros et al., 2008). From the results, a significant increase in shear strength was obtained with a relatively low reinforcement ratio, and it was verified that steel bars were very effective.

To assess the bond contribution mechanisms for the shear strengthening effectiveness of this technique, an experimental program of pullout tests was carried out, where the influence on the bond behaviour of the adhesive type (two epoxy-based adhesives) and the thickness layer of the adhesive (2 mm and 5 mm when using strengthening bars of 8 mm; 2 mm, 4 mm and 6 mm for the 12 mm diameter steel bars) was assessed. The experimental program is described and the obtained results are presented and analysed in this chapter.

6.1 SPECIMENS

The geometry of the pull out test specimens is shown in Figure 6.1 and was based on recommendations given by RILEM/CEB/FIP (1973) and on experimental programs described in other publications (Pilakoutas et al. 1994, Cook et al. 1993, Bakis et al. 1998). The typical test specimen consisted of a concrete block with 15x15x20 cm^3 in which a steel anchor bar was embedded in its centre.

The specimens were divided into two series, S1 and S2, in correspondence to diameter of the steel bar, 8 mm and 12 mm, respectively. Each series includes two groups, one for each adhesive type. Since adhesives have an important role on the effectiveness of this strengthening technique, specimens strengthened with two different adhesives were tested, namely two distinct types of epoxy-based bond agents (S&P Resin 50 and Sikadur 32N).

The test specimens in each group have two different embedment lengths: 50 mm and 75 mm. Table 6.1 resume the full experimental program. Each specimen is designated by a set of symbols and numbers to be uniquely identified. The notation adopted to identify the specimens is AX_DY_LZ_TW-N, where X is the type of adhesive (X=K for Sikadur and X=S for S&P; Y is the diameter in mm: Y=8 or 12; Z is the bond length in mm: Z=50 or 75; W is the thickness of the adhesive layer in mm: W=2, 4, 5 or 6 and N is number of sample: 1 or 2). Therefore, AK_D8_L50_T6-1 denotes the type of adhesive (Sikadur), D8 represents the steel bar diameter (8 mm), L50 indicates the embedded length of 50 mm, T6 corresponds to a layer thickness of 6 mm and 1 denotes the first specimen out of the two replicates.

6.2 TEST SETUP AND MONITORING SYSTEM

The tests were executed according to RILEM/CEB/FIP (1973) recommendations. The pull-out test setup is shown in Figure 6.2. The tests were performed using a servo-hydraulic testing machine with a capacity of 1000 kN. Displacement control was selected to capture the full response of the specimen up to an aimed slip between the bar and the surrounding concrete. The load was applied to the reinforcement bar in order to accomplish a displacement rate of 0.6 mm/min, and was measured with the electronic load cell of the testing machine, with ±200 kN and accuracy of ±0.05 %. The loaded and free end slips were measured with two linear variable differential transformers (LVDTs). An automatic data acquisition system was used to record the data.

 The bond length was localized at the loaded end, in order to reproduce, as much as possible, the real conditions of an ETS bars crossing a shear crack. In these conditions, three types of failure modes can occur (Bianco et al. 2009a): debond; concrete fracture with the formation of a concrete failure cone; yielding of the steel bar.
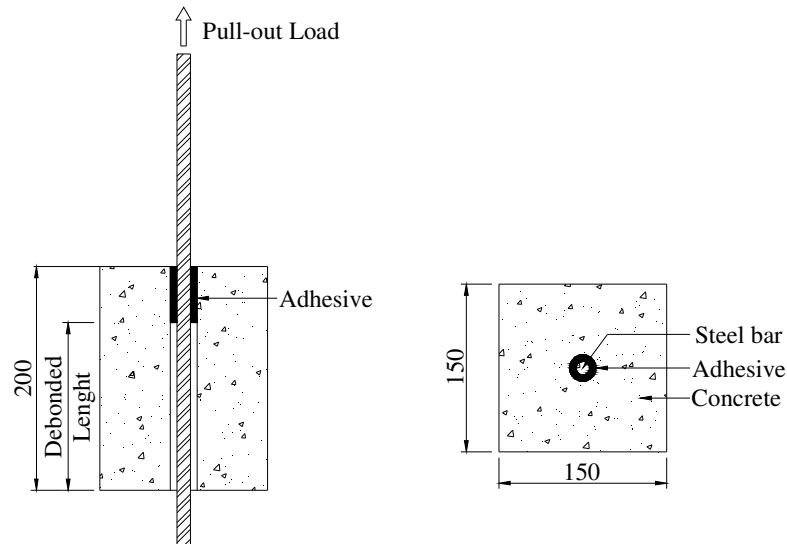
Figure 6.1: Geometry of the specimens (all dimensions in mm).
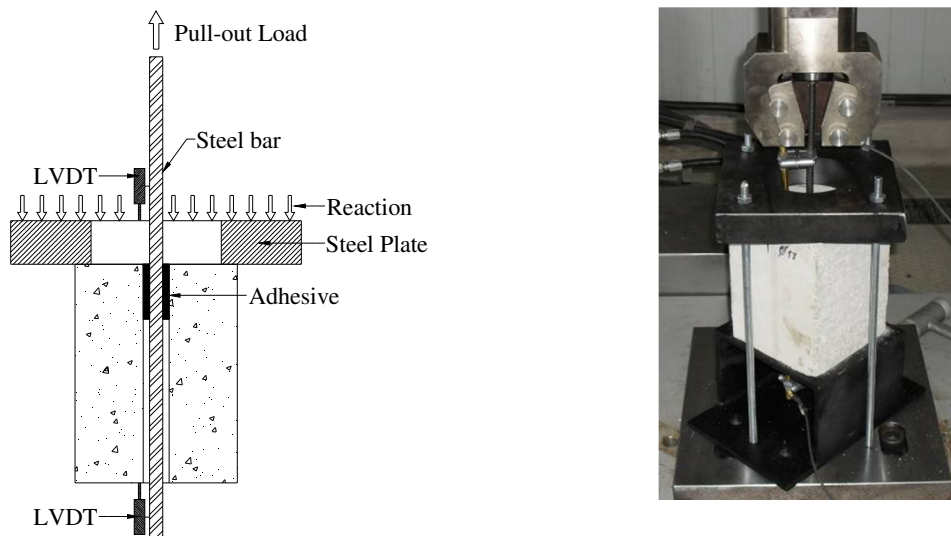
Figure 6.2: Pull-out test setup.

6.3 MATERIALS PROPERTIES

Table 6.2 includes values obtained from experimental tests for the characterization of the main properties of the materials used in the present work.

Table 6.1: Details of the experimental program.

Adhesive Type	Series					
	S1 (8 mm)			S2 (12 mm)		
	Hole diameter (mm)	Layer thickness (mm)	Embedment length (mm)	Hole diameter (mm)	Layer thickness (mm)	Embedment length (mm)
Sikadur 32N (S)	12	2	50	16	2	50	75
				20	4		
	18	5		24	6		
S&P Resin 50 (E)	12	2		16	2		
				20	4		
	18	5		24	6		

Table 6.2: Summary of the properties of steel bars and epoxy adhesives.

Steel bars					Epoxy Adhesive			
					Sikadur 32N		S&P Resin 50	
Diameter (ϕs)	Modulus of elasticity (GPa)	Yield stress (0.2 %)[a] (MPa)	Strain at yield stress[b]	Tensile strength (MPa)	Tensile strength (MPa)	Modulus of elasticity (GPa)	Tensile strength (MPa)	Modulus of elasticity (GPa)
8 mm	200.80 (2.33%)	421.35 (0.53%)	0.0023 (2.65%)	578.75 (0.36%)	26.29 (10.62)	3.94 (9.82)	26.83 (4.62)	1.60 (4.64)
12 mm	200.46 (0.75%)	449.44 (1.06%)	0.0022 (1.72%)	589.62 (0.77%)				

[a]Yield stress determined by the "Offset Method", according to ASTM A370 (2002)
[b]Strain at yield point, for the 0.2 % offset stress
(value) Coefficient of Variation (COV) = (Standard deviation/Average) x 100

Cylinder specimens with a diameter of 150 mm and a height of 300 mm were used to obtain the compressive strength and the Young's modulus according to LNEC-E397 (1993). Further details regarding the compressive strength of the manufactured concrete, the detailed concrete mix proportion and the main properties of the ordinary ready-mix concrete can be found in Annex 3.4 (see the information regarding to the slab strip SL30-HS). The average compressive strength (f_{cm}) and the static modulus of elasticity in compression (E_c) were determined according to LNEC-E397 (1993) at the age of 28 days. For the concrete, an elasticity modulus and average compressive strength of 29.83 (0.29) GPa and 28.40 (1.61) MPa were obtained, respectively, where the values between round brackets correspond to the standard deviation.

To characterize the steel bars, uniaxial tensile tests were conducted according to the standard procedures of ASTM A370 (2002). For the characterization of the tensile behaviour of the epoxy adhesive, uniaxial tensile tests were performed complying with the procedures outlined in ISO 527-1 (1993) and ISO 527-2 (1993). Two types of epoxy adhesive were used: Sikadur 32N and S&P Resin 50, formed by two components. Additional information concerning to the adhesives used in this work can be found in Annex 6.

6.4 SPECIMENS PREPARATION AND STRENGTHENING

The first step of the strengthening process consisted in opening the holes for the installation of the steel bars, by using a conventional diamond-coated drill. Compressed air was used to remove the dust generated during drilling. The anchors were made of 8 mm or 12 mm diameter steel bars. These bars were cut to the desired length, wire brushed and wiped clean with a cloth saturated with acetone to remove any residue.

The holes had a diameter that varied between 12 mm and 24 mm. The drilled holes were filled with the epoxy adhesives (Sikadur and S&P Resin 50) and then the steel bars were installed. The adhesive thickness was 2 mm and 5 mm for the steel bars with 8 mm diameter and 2 mm, 4 mm and 6 mm for the steel bars with 12 mm diameter (Table 6.1). The embedment lengths were 50 mm and 75 mm.

To ensure that any adhesive flowing down did not form an extra bond between the steel and concrete, a plastic tube was applied over the part of the bar to be unbounded length (Figure 6.3). The pull-out tests were executed when the adhesives have been cured at least 16 days. The pull-out tests were executed at the laboratory environmental conditions, according to the set-up illustrated in Figure 6.2.

Figura 6.3: Jacketing of the steel bar with a plastic tube to obtain the unbounded length.

6.5 RESULTS AND DISCUSSION

The strengthening or rehabilitation of structures by adding glue between reinforcing steel bars and the concrete requires special attention to the interface between these materials. The influence of the adhesive layer thickness and the bond length on the behaviour of the strengthened specimens is analysed in this section. During the pull-out test the bond stress profile changes along the embedment length (Bianco et al. 2009b), but the main focus of the present research was not to assess the local bond law and its dependence on the parameters investigated. To derive a practical design indicator, the influence of the parameters analysed was restricted to the average bond stress that is defined as (it is assumed that the bond strength is constant along the bond length):

$$\tau = \frac{F}{\pi d_b l_b} \tag{6.1}$$

where F is the tensile load applied to the bar, d_b is the bar diameter and l_b is the embedment length. The variability of the results can be attributed to the small size of the specimens and the adhesive bond length, since a minor variation in their length may lead to a large variation in the results. Thus, the measurement of the bond length of each specimen was performed after each test. It should be noted that the specimen AS_D8_L50_T5-1 presented a bond length lower than expected due to poor positioning of the steel bar.

The relationship between the average bond stress and the slip between the bar and the concrete (at loaded and free ends) is used to analyze the bond behaviour. The experimental results obtained from the bond tests are indicated in Table 6.3. In this table, F_{max} is the maximum pull-out force, τ_{max} is the bond strength (bond stress at F_{max}), ε_s is the strain in the steel bar at F_{max}, and $s_{m,l}$ and $s_{m,f}$ are the loaded and free end slip at F_{max}, respectively. The average value of the bond strength for the replicated specimens ($\overline{\tau}_{max}$) is also indicated.

The global behavior of the bond stress–slip relationship is characterized by an initial ascending part with an almost linear response, followed by a nonlinear branch with slippage amplitude that increases with the layer thickness of the adhesive. After bond strength has been attained a softening regime occurs with a decrease of the bond strength with the increase of the slip. The relationships between the bond stress and the slip at the loaded and free ends for each tested specimen are shown in Figures 6.4 to 6.6. A resume of the tests is also presented in Figure 6.7.

Table 6.3: Results from the experimental program.

Specimen	At the specimens testing age (days)		l_b	Adhesive layer thickness	F_{max}	τ_{max}	ε_s	$\overline{\tau}_{max}$	$s_{m,l}$	$s_{m,f}$
	Specimens	Adhesive	(mm)	(mm)	(kN)	(MPa)	(‰)	(MPa)	(mm)	(mm)
S1 (8 mm) AK_D8_L50_T2-1	190	23	50	2	21.79	17.34	0.09	-----	3.14	1.53
AK_D8_L50_T5-1	195	28	48	5	20.19	16.74	0.08	-----	1.67	-----
AS_D8_L50_T2-1	188	21	50	2	15.89	12.64	0.06	-----	1.91	1.36
AS_D8_L50_T5-1*	184	17	28	5	9.43	13.40	0.07	-----	2.23	1.63
S2 (12 mm) AK_D12_L50_T2-1	223	21	48	2	29.78	16.46	0.07	14.40	0.38	0.15
AK_D12_L50_T2-2	223	21	52		24.18	12.33			0.33	0.11
AK_D12_L50_T4-1	223	21	50	4	23.74	12.59	0.06	11.40	1.83	1.35
AK_D12_L50_T4-2	223	21	51		19.63	10.21			0.23	0.12
AK_D12_L50_T6-1	223	21	51	6	30.19	15.70	0.07	14.85	0.75	0.35
AK_D12_L50_T6-2	223	21	52		27.42	13.99			0.92	0.73
AK_D12_L75_T2-1	223	21	75	2	46.42	16.42	0.07	14.45	0.63	0.12
AK_D12_L75_T2-2	223	21	76		35.75	12.48			0.40	0.13
AK_D12_L75_T4-1	223	21	73	4	42.02	15.26	0.07	14.81	0.70	0.53
AK_D12_L75_T4-2	223	21	76		41.16	14.36			0.16	0.09
AK_D12_L75_T6-1	223	21	76	6	39.93	13.94	0.07	14.32	1.80	1.25
AK_D12_L75_T6-2	223	21	75		41.53	14.69			1.33	0.98
AS_D12_L75_T2-1	220	18	53	2	19.28	9.65	0.06	13.01	2.60	2.00
AS_D12_L75_T2-2	220	18	50		30.86	16.37			2.51	1.63
AS_D12_L75_T4-1	218	16	53	4	26.07	13.04	0.06	12.59	0.60	0.72
AS_D12_L75_T4-2	218	16	56		25.62	12.13			0.62	0.49
AS_D12_L75_T6-1	220	18	56	6	28.59	13.54	0.07	13.40	1.09	0.75
AS_D12_L75_T6-2	220	18	60		30.02	13.27			1.28	0.05
AS_D12_L75_T2-1	220	18	72	2	28.59	10.53	0.06	11.18	0.61	0.51
AS_D12_L75_T2-2	220	18	77		34.29	11.82			3.24	2.32
AS_D12_L75_T4-1	218	16	75	4	37.77	13.36	0.06	12.75	0.72	0.43
AS_D12_L75_T4-2	225	23	82		37.50	12.13			0.94	0.80
AS_D12_L75_T6-1	220	18	76	6	40.49	14.13	0.07	13.47	1.49	1.00
AS_D12_L75_T6-2	220	18	78		37.63	12.80			0.43	0.40

* Bond length lower than expected due to poor positioning of the steel bar
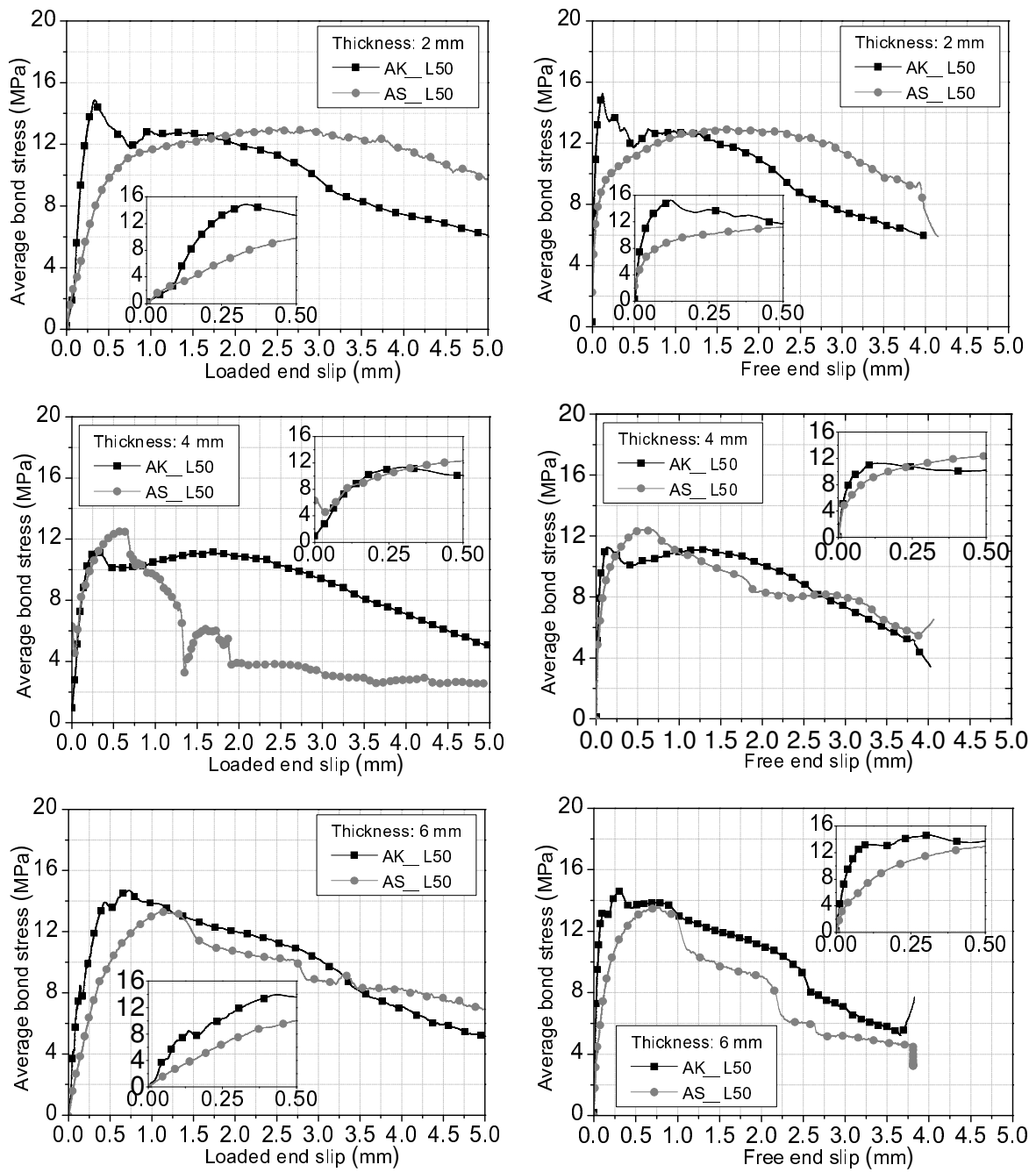
Figure 6.4: Influence of the type of adhesive on the average bond stress vs slip at the loaded and free ends for the specimens with a bond length of 50 mm and bar diameter of 12 mm.
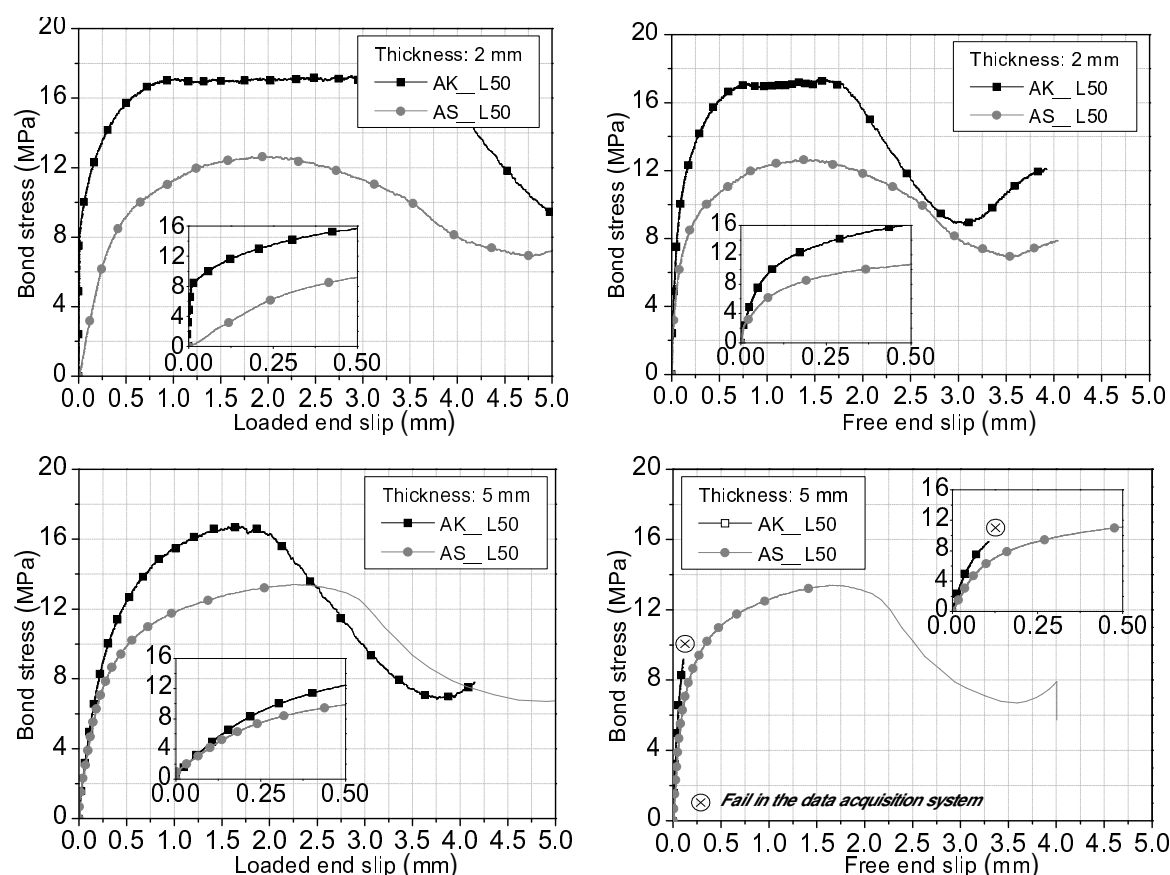
Figure 6.5: Influence of the type of adhesive on the average bond stress vs slip at the loaded and free ends for the specimens with a bond length of 50 mm and bar diameter of 8 mm.

6.5.1 Influence of the type of adhesive on the average bond strength

For the strengthening of RC structures by bonding the concrete substrata to an intervening material, it is necessary to choose the best type of adhesive that suits the aimed goal. Thus, there is a large number of formulations on the market in order to obtain the better response of the adhesive according to its mechanical properties and specifications of application. As aforementioned, two types of epoxy adhesive were used: Sikadur 32N (K) and S&P Resin 50 (S), formed by two components.

The relationship between the average bond stress and the slip up to bond strength is stiffer for the K bond adhesive than for the S adhesive, which is justified by the higher elasticity modulus of the former adhesive.

Apart the $\overline{\tau}_{max}$ obtained for the specimens AK_D12_L50_T4-1 and AK_D12_L50_T4-2, the specimens bonded with K bond adhesive developed higher F_{max}, and consequently, higher $\overline{\tau}_{max}$. Since both K and S adhesives have similar tensile strength, this feature provided by

the adhesive is justified by the larger elasticity modulus of the S adhesive. In fact, this particularity of this adhesive has provided larger resistance to the sliding process of the bar due to the higher confinement provided by the micro-compressive-adhesive struts formed during the pullout process (Barros and Fortes 2005).
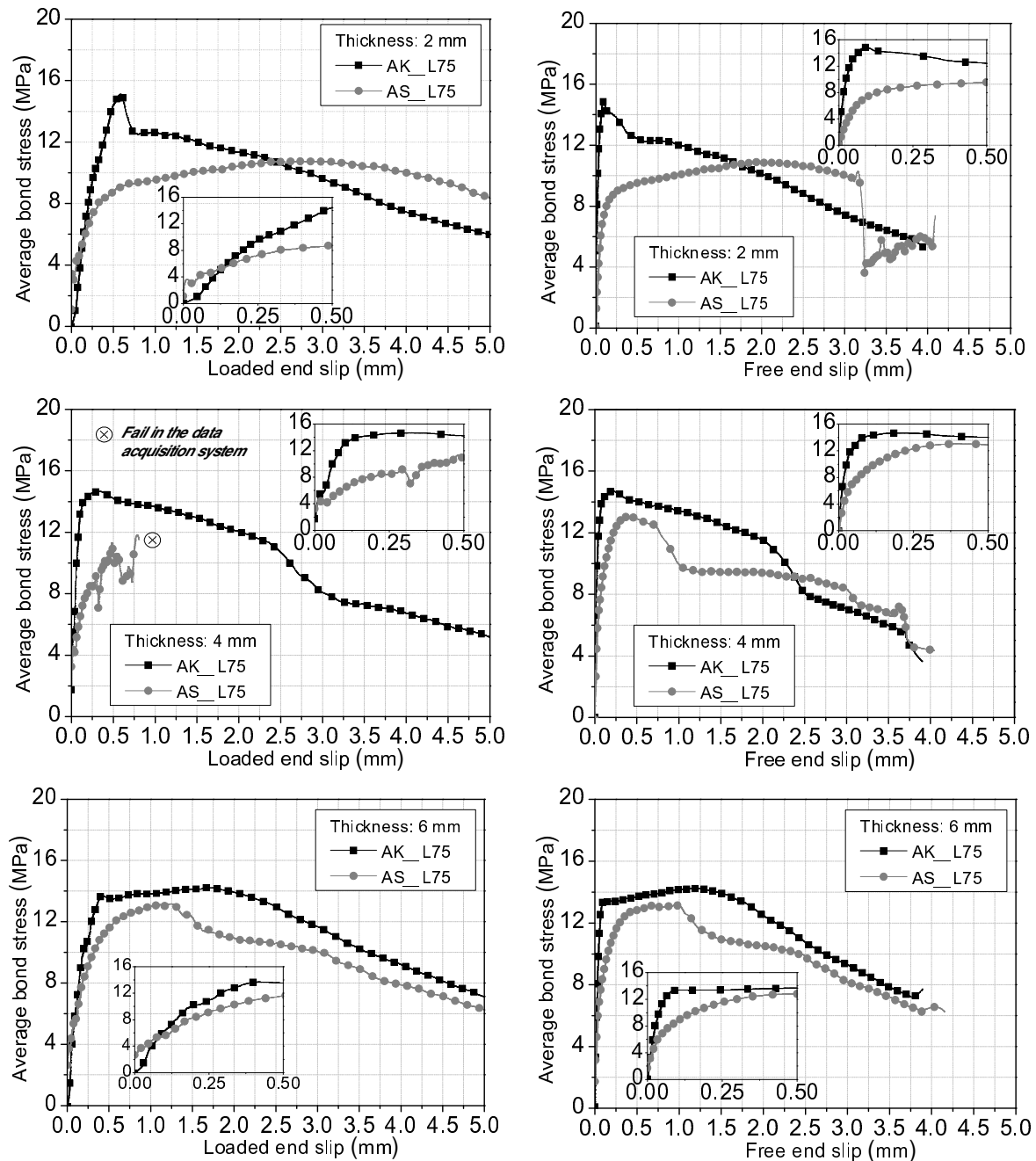
Figure 6.6: Influence of the type of adhesive on the average bond stress vs slip at the loaded and free ends for the specimens with a bond length of 75 mm and bar diameter of 12 mm.
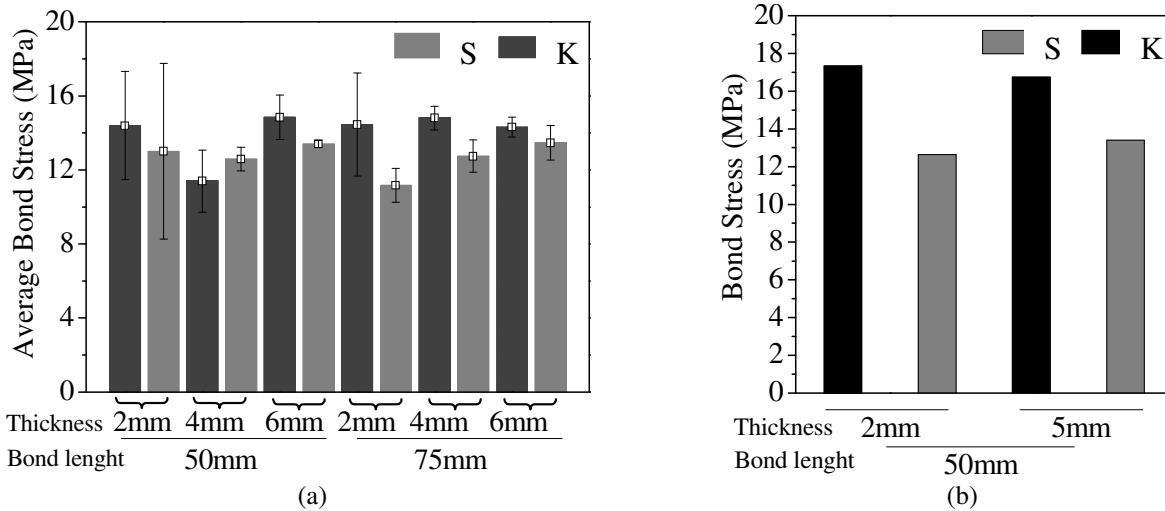
Figure 6.7: Resume of the tested specimens: (a) S1 and (b) S2.

6.5.2 Influence of the strengthening bar diameter on the average bond strength

The results presented in Figures 6.4 to 6.7 and in Table 6.3 indicate that, in most of the tested specimens, the bond stress decreased with the increasing of the strengthening bar diameter. Tests conducted by Meszaros (*apud* Cook et al. 2007) also showed similar behavior to the ones obtained in this experimental program.

6.5.3   The effect of adhesive layer thickness on the bond strength

The bond stress in the interface between concrete/epoxy and adhesive/strengthening bars was investigated as a function of adhesive thickness. Two different adhesive thicknesses were adopted to the strengthening of the specimens with bars of 8 mm diameter: 2 mm and 5 mm. Concerning to the specimens strengthened with bars of 12 mm, three adhesive thickness were tested: 2 mm, 4mm and 6mm (Table 6.1).

According to the results, the specimens strengthened with a steel bar of 8 mm diameter (S1) exhibited similar behavior regardless the thickness of the adhesive. An average bond stress of 13.02 MPa and 17.04 MPa were obtained for the S and K bond adhesives, respectively.

In general, when using a steel bar with 12 mm diameter (S2), the maximum bond stress did not present an evident variation when increasing the adhesive layer thickness. For a very thin adhesive thickness, 2 mm, epoxy systems has provided average shear stress values of 14.04 MPa (1.31) and 12.74 MPa (0.87) for K and S bond adhesives, respectively, where the values between round brackets correspond to the standard deviation. As the adhesive thickness increases, the average bond stress of both systems is similar to the results

obtained for the adhesive thickness of 2 mm, except for the AK_D12_L50_T4 specimens, which presented a lower bond stress (11.40 MPa). Resuming, for the considered thickness values of the adopted adhesives, the adhesive shear strength was not significantly affected by the layer thickness of the adhesive.
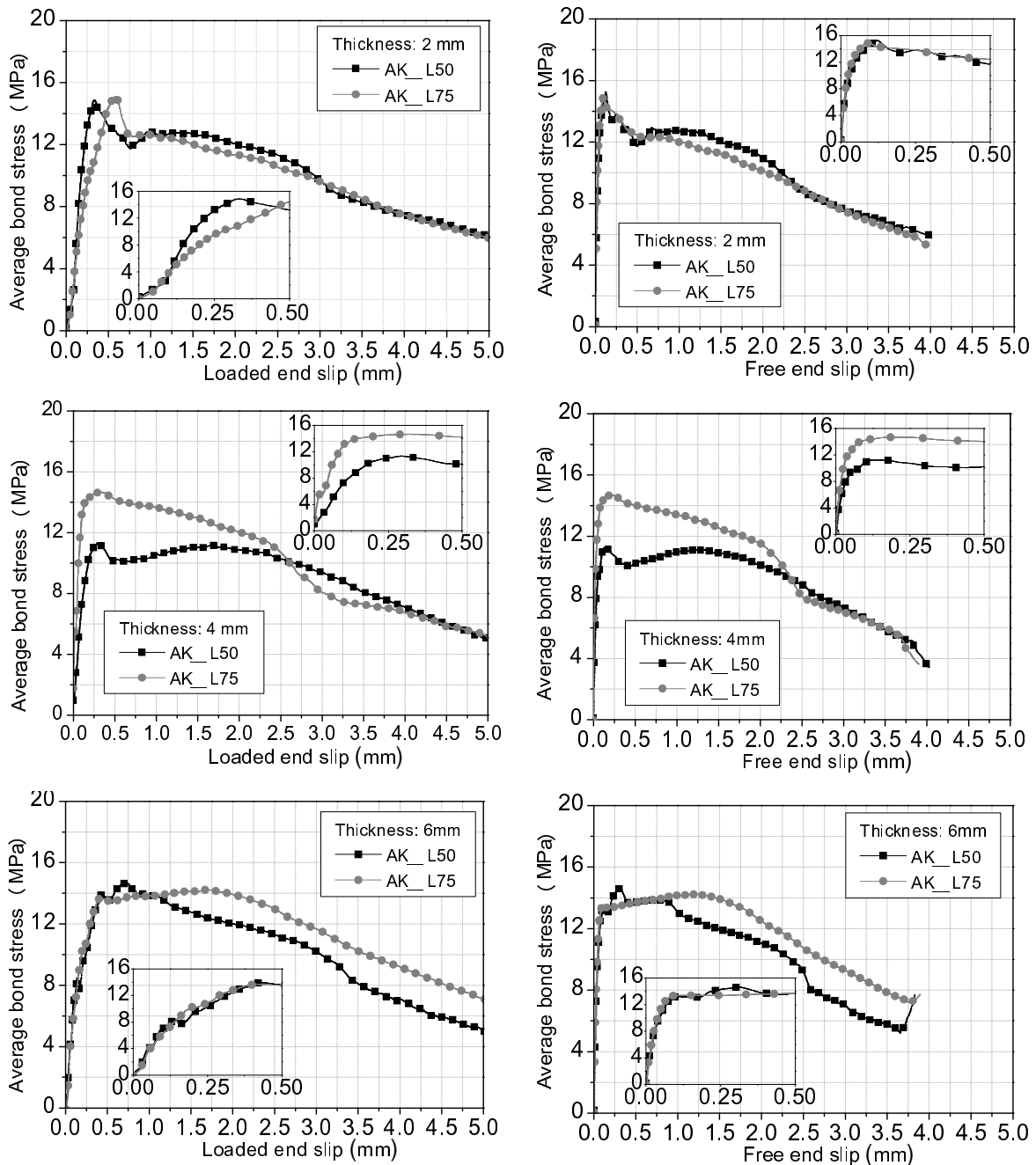
Figure 6.8: Influence of the bond length on the average bond stress vs slip at the loaded and free ends for the specimens with Sikadur adhesive and bar diameter of 12 mm.
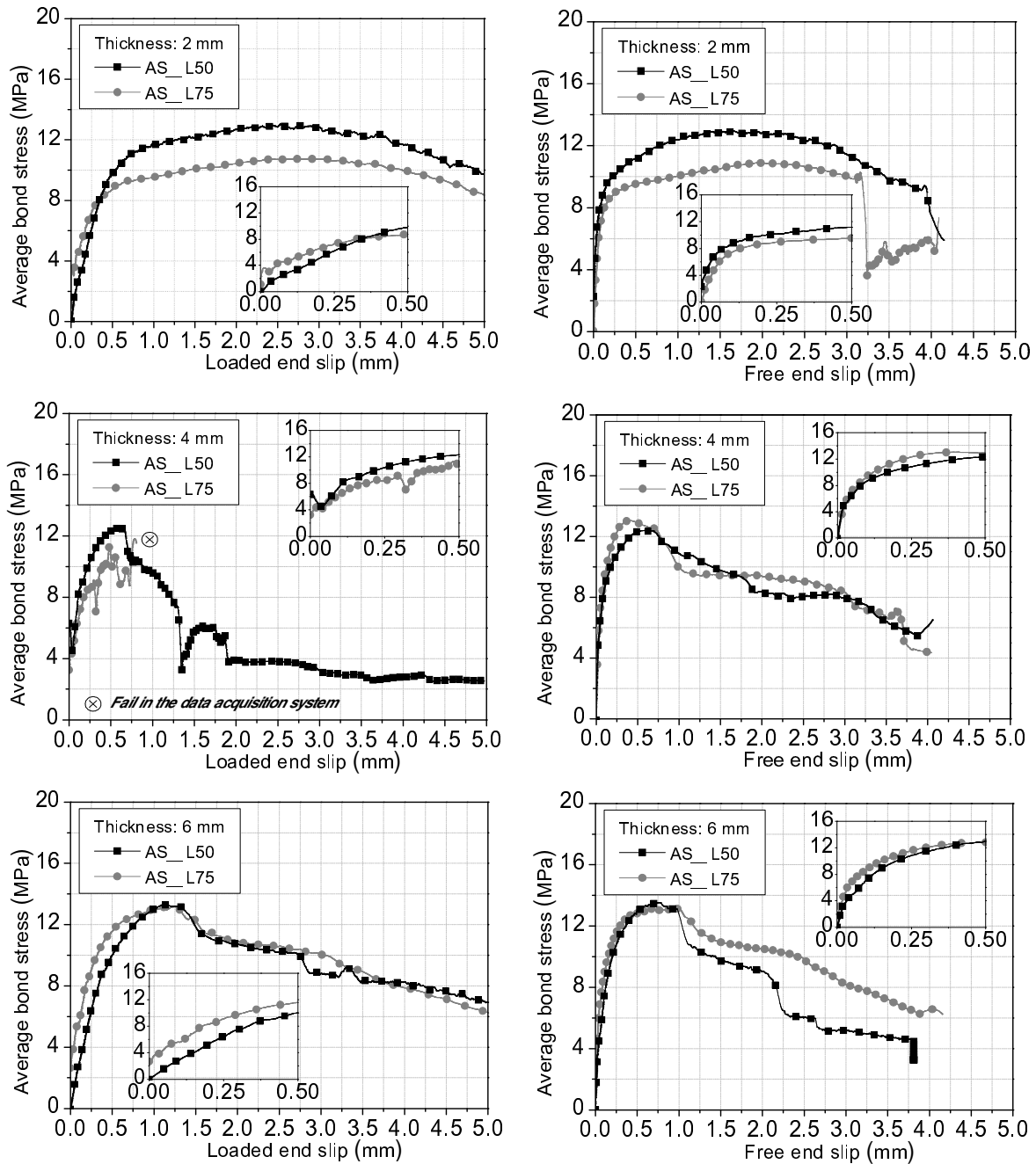
Figure 6.9: Influence of the bond length on the average bond stress vs slip at the loaded and free ends for the specimens with S&P adhesive and bar diameter of 12 mm.

6.5.4   The effect of embedment length on the bond stress

To assess the influence of the embedment length on the maximum bond stress, two different embedment lengths were tested: 50 mm and 75 mm. The relationship between the average bond stress and the embedment length is represented in Figures 6.4 to 6.9. It was expected an increase of load with the embedment length. However, in general, the strengthened specimens reached similar average bond stress. From these data, no influence of the embedment length was noticeable.

6.5.5 Crack evolution on concrete and failure modes

No visible cracks were observed until the specimen lost its ability to support any additional load (F_{max}). After peak load the specimens presented a softening sliding response. The specimens strengthened with a steel bar of 8 mm diameter (S1) presented bond failure at the steel/adhesive interface. For the specimens with a steel bar of 12 mm diameter (S2), at peak load, some radial and circumferential cracks started being visible due to concrete fracture, followed by a decrease of the pull-out force with the increase of the pullout displacement of the steel bar. All the specimens of this series presented a mixed failure mode composed of debond at adhesive/concrete or steel/adhesive interfaces and concrete fracture due to the formation of a concrete cone. The typical failure mode is shown in Figure 6.10. Details of the specimens after loading can be found in Annex 6.

(a)

(b.1)

(b.2)
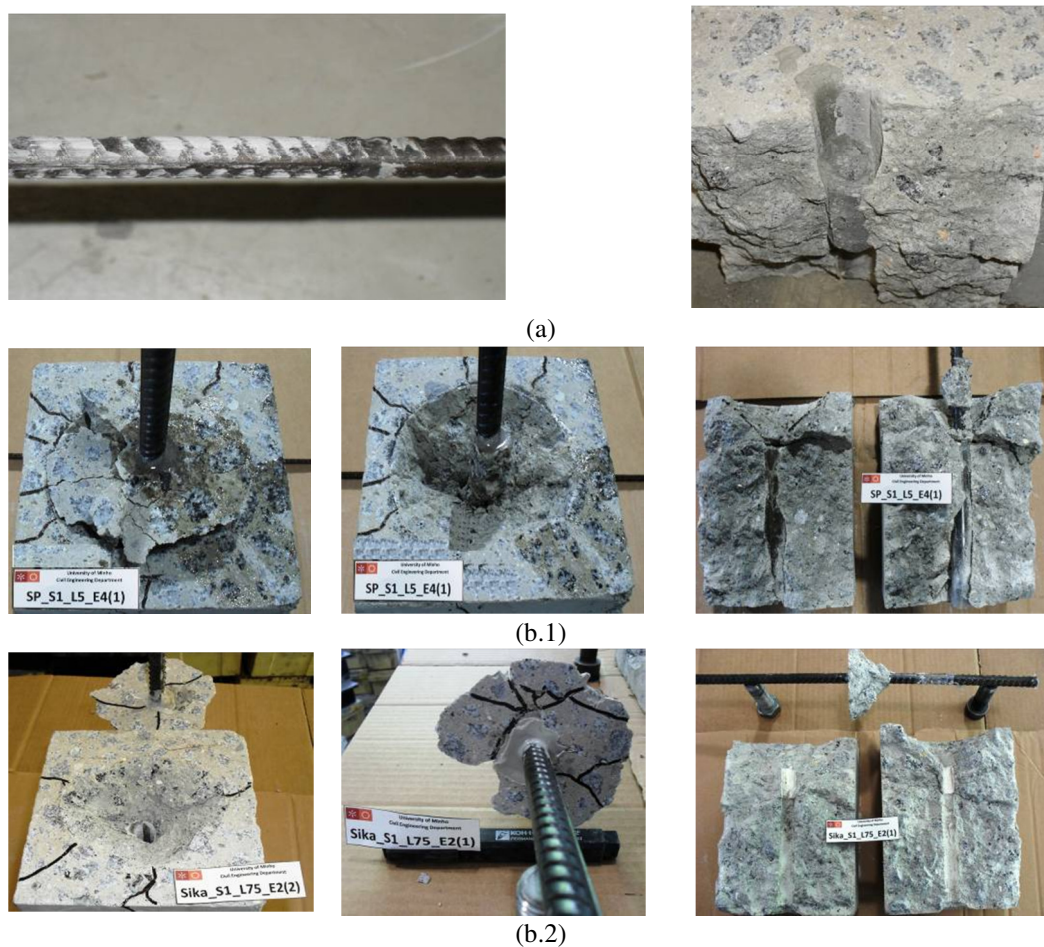
Figure 6.10: Typical bond failure in the steel/adhesive interface (a) and mixed bond failure for E (b.1) and S (b.2) bond adhesives.

6.6 CONCLUSIONS

In the present chapter, a comprehensive experimental program of pullout tests was carried out, where the influence on the bond behaviour of the following parameters was assessed: modulus of elasticity of types of epoxy-based adhesives; layer thickness (2 mm and 5 mm when using strengthening bars of 8 mm diameter; 2 mm, 4 mm, and 6 mm for the steel bars of 12 mm diameter) and the adhesive bond lengths (50 mm and 75 mm). Based on the results of this experimental program the following conclusions can be drawn:

(i) The bond behavior between bars and concrete depends on the type of adhesive chosen for the strengthening system;

(ii) With the values adopted for the anchorage length and for the adhesive layer thickness, the bond strength is marginal affected, but this last property has increased with the Young's modulus of the adhesive; and

(iii) From the obtained results it seems that for the interval of values considered for the adhesive thickness, this thickness has no significant influence on the type of failure mode and on the average bond strength.

6.7 BIBLIOGRAPHY

ASTM A370, "Standard test methods and definitions for mechanical testing of steel products", American Society for Testing and Materials, 52pp, 2002.

Barros, J.A.O., Fortes, A. S., "Flexural strengthening of concrete beams with CFRP laminates bonded into slits", Journal Cement and Concrete Composites, 27(4), pp. 471-480, 2005.

Barros, J.A.O., Dalfré, G.M., Trombini, E., Aprile, A., "Exploring the possibilities of a new technique for the shear strengthening of RC elements", Proceedings of the International Conference Challenges for Civil Construction, University of Porto, Portugal, 2008.

Bakis. C. E., Uppuluri. V.S., Nanni. A., Boothby. T.E., "Analysis of Bonding Mechanisms of Smooth and Lugged FRP Rods Embedded in Concrete", Composites Science and Technology, 58, pp. 1307-1319, 1998.

Bianco, V., Barros, J.A.O., Monti, G., "Three dimensional mechanical model for simulating the NSM FRP strips shear strength contribution to RC beams", Engineering Structures Journal, 31 (4), pp. 815-826, 2009a.

Bianco, V., Barros, J.A.O., Monti, G., "Bond model of NSM CFRP in the context of the shear strengthening of RC beams", ASCE Structural Engineering Journal, 135(6), pp. 619-631, 2009b.

Cook, R. A., Doerr, G. T., and Klingner, R. E., "Bond stress model for design of adhesive anchors", ACI Structural Journal., 90 (5), pp. 514–524, 1993.

Cook, R.A., Eligehausen, R., Appl., J., "Overview - Behavior of Adhesive Bonded Anchors", Beton- und Stahlbetonbau, Ernst & Sohn, V. 102, Issue S1, pp.16-21, 2007.

ISO 527-1, "Plastics - Determination of tensile properties - Part 1: General principles", International Organization for Standardization (ISO), International Organization for Standardization (ISO), Geneva, Switzerland, 9 pp, 1993.

ISO 527-2, "Plastics - Determination of Tensile Properties - Part 2: Test Conditions for Moulding and Extrusion Plastics", International Organization for Standardization (ISO), Geneva, Switzerland, 5 pp, 1993.

LNEC-E397, "Concrete-Assessment of the elasticity modulus under uniaxial compression", Laboratório Nacional de Engenharia Civil, 1993 (in Portuguese).

Pilakoutas. K., Hafeez. S., Dritsos. S., "Residual bond strength of polymer adhesive anchored reinforcement subjected to high temperatures", Materials and Structures, 27, pp. 527-531, 1994.

RILEM/FIP/CEB, "Bond Test for Reinforcing Steel – 1. Beam Test (7 – II – 28 D). 2. Pull-Out Test (7 – II – 128), Tentative Recommendations", RILEM Journal Materials and Structures, v. 6, n. 32, pp. 96-105, 1973.

"It's fine to celebrate success but it is more important to
heed the lessons of failure".
Bill Gates
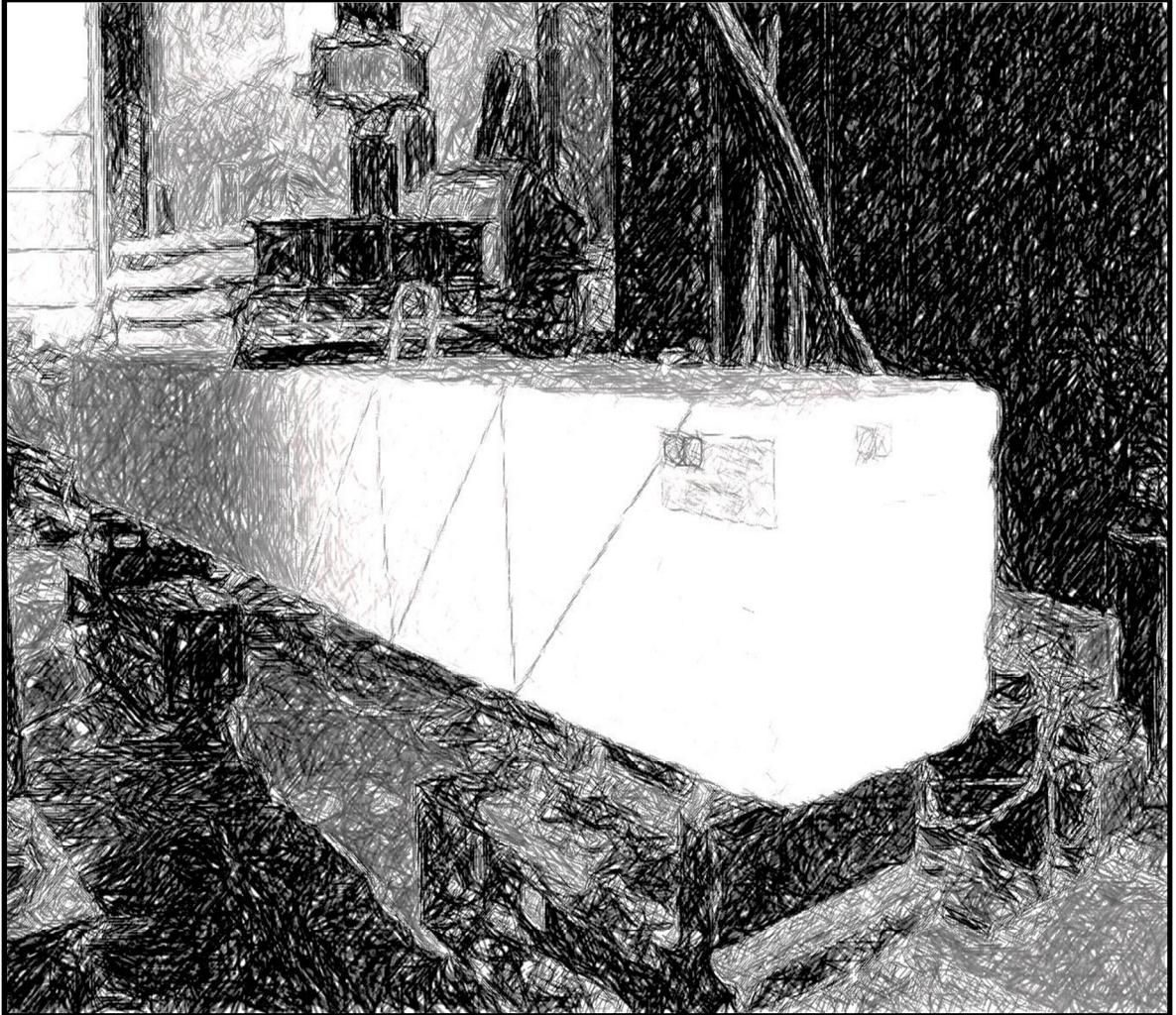
Chapter 7

ASSESSMENT OF THE EFFECTIVENESS OF THE EMBEDDED THROUGH-SECTION TECHNIQUE FOR THE SHEAR STRENGTHENING OF RC BEAMS

In this chapter, an experimental research program was carried out to evaluate the performance of the Embedded Through-Section (ETS) technique to increase the shear resistance of RC beams. This technique consists on opening holes across the beam thickness, with the desired inclinations, where bars are introduced and are bonded to the concrete substrate with an adhesive material. To assess the effectiveness of this technique, an experimental program composed of 14 RC beams was carried out. The applicability of the ACI 318 (2008) and Eurocode 2 (2004) standard specifications for shear resistance was also investigated.

Finally, to have a better assessment of the contribution of the ETS bars for the shear resistance of RC beams, material nonlinear analysis were performed with a FEM-based computer program.

7.1 EXPERIMENTAL PROGRAM

7.1.1 SPECIMENS

The experimental program is formed by two series, A and B, composed of beams with a cross section of 150x300 mm^2 and 300x300mm^2, respectively, with a total length of 2450 mm and a shear span length of 900 mm (Figures 7.1 to 7.3 and Table 7.1). The longitudinal tensile steel reinforcement of A and B series consists of two and three steel bars of 25 mm diameter ($\varnothing$ 25 mm), respectively. The longitudinal compressive steel reinforcement was composed of two and three steel bars of 12 mm diameter ($\varnothing$ 12 mm) in the A and B series, respectively. Steel stirrups of two vertical arms and 6 mm diameter were used. The concrete clear cover for the top, bottom and lateral faces of the beams was 20 mm.

Each series is made up of a beam without any shear reinforcement (reference beam) and a beam for each of the following shear reinforcing systems: (i) steel stirrups of $\varnothing$6 mm at a spacing of 300 mm, (ii) ETS strengthening bars at 45º or at 90º in relation to the beam axis, with a spacing of 300 mm, (iii) steel stirrups of $\varnothing$6 mm at a spacing of 300 mm and ETS strengthening bars at 45º or at 90º, with a spacing of 300 mm. Additionally, for the A Series, two other shear reinforcing systems were also tested: (iv) steel stirrups of $\varnothing$6 mm at a spacing of 225 mm and (v) steel stirrups of $\varnothing$6 mm at a spacing of 225 mm and ETS strengthening bars at 90º, with a spacing of 225 mm. For the series A and B, ETS bars of $\varnothing$10 mm and $\varnothing$8 mm were used, respectively. It should be noted that an ETS bar was designed as a stirrup of one arm, following the design recommendations of ACI Code (2008) for the steel stirrups in the context of shear reinforcement or RC beams.
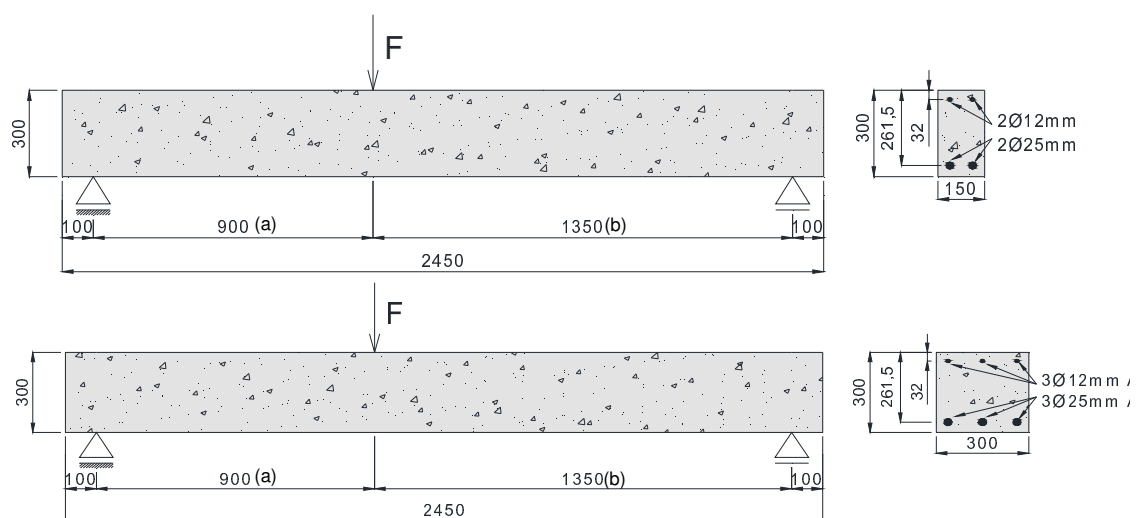
Figure 7.1: Test configuration. All dimensions are in mm.

Beam´s designation		Shear strengthening system	Shear strengthening arrangements	Shear span reinforcement/ strengthening
A Series Beams	A.1 Reference	-----------		
	A.2 S300.90	Stirrups at 90° (2ϕ6 mm, 2 arms, 300 mm spacing)		
	A.3 E300.90	ETS strengthening bars at 90° (3ϕ10 mm, 300 mm spacing)		
	A.4 E300.45	ETS strengthening bars at 45° (3ϕ10 mm, 300 mm spacing)		
	A.5 S300.90/ E300.90	Stirrups at 90° (2ϕ6 mm, 2 arms, 300 mm spacing) ETS strengthening bars at 90° (3ϕ10 mm, 300 mm spacing)		
	A.6 S300.90/ E300.45	Stirrups at 90° (2ϕ6 mm, 2 arms, 300 mm spacing) ETS strengthening bars at 45° (3ϕ10 mm, 300 mm spacing)		
	A.7 S225.90	Stirrups at 90° (3ϕ6 mm, 2 arms, 225 mm spacing)		
	A.8 S225.90/ E225.90	Stirrups at 90° (3ϕ6 mm, 2 arms, 225 mm spacing) ETS strengthening bars at 90° (4ϕ10 mm, 225 mm spacing)		

Figure 7.2: General information about A series.

Beam's designation		Shear strengthening system	Shear strengthening arrangements	Shear span reinforcement/ strengthening
B Series	B.1	Reference	-----------	
	B.2	S300.90	Stirrups at 90° (2ϕ6 mm, 2 arms, 300 mm spacing)	
	B.3	E300.90	ETS strengthening bars at 90° (2 x 3ϕ8 mm, 300 mm spacing)	
	B.4	E300.45	ETS strengthening bars at 45° (2 x 3ϕ8 mm, 300 mm spacing)	
	B.5	S300.90/ E300.90	Stirrups at 90° (2ϕ6 mm, 2 arms, 300 mm spacing) ETS strengthening bars at 90° (2 x 3ϕ8 mm, 300 mm spacing)	
	B.6	S300.90/ E300.45	Stirrups at 90° (2ϕ6 mm, 2 arms, 300 mm spacing) ETS strengthening bars at 45° (2 x 3ϕ8 mm, 300 mm spacing)	

Figure 7.3: General information about B series.

Table 7.1 includes general information of the beams composing the two series, where ρ_{sl} is the longitudinal steel reinforcement ratio [$\rho_{sl} = (A_{sl}/b_w \cdot d) \times 100$, where A_{sl} is the cross sectional area of the longitudinal steel bars, b_w is the web width and d is the distance from the extreme compression fibre of the cross section to the centroid of the longitudinal reinforcement]. In this Table, the shear reinforcement ratio (ρ_{sw}) is given by $\rho_{sw} = (A_{sw}/b_w \cdot s_w) \times 100$, where A_{sw} is the cross sectional area of the two arms of a steel stirrup and s_w is the spacing between stirrups. Finally, the ρ_f indicated in Table 7.1 is the ETS strengthening ratio,

$\rho_f = (A_f / b_w \cdot s_f \cdot sin\theta_f) \times 100$, where A_f is the cross sectional area of a ETS shear strengthening bar, s_f is the spacing between these bars and θ_f is the inclination of the strengthening bars with respect to the longitudinal axis of the beam. The number of days between the strengthening intervention and the test is indicated in Table 7.1. Since the beams were not cast in the same batch, the corresponding batch is also indicated in this Table.

Table 7.1: General information of the beams.

Beams ID	150 x 300 mm^2					300 x 300 mm^2				
	Age of the strengthening when the beam was tested (days)	ρ_{sl} (%)	ρ_{sw} (%)	ρ_f (%)	Batch	Age of the strengthening when the beam was tested (days)	ρ_{sl} (%)	ρ_{sw} (%)	ρ_f (%)	Batch
Reference	------	2.50	0.00	0.00	1	------	1.88	0.00	0.00	1
S300.90	------	2.50	0.13	0.00	1	------	1.88	0.06	0.00	1
E300.90	34	2.50	0.00	0.17	1	65	1.88	0.00	0.11	1
E300.45	34	2.50	0.00	0.25	2	64	1.88	0.00	0.16	2
S300.90/ E300.90	33	2.50	0.13	0.17	1	69	1.88	0.06	0.11	1
S300.90/ E300.45	29	2.50	0.13	0.25	2	68	1.88	0.06	0.16	2
S225.90	------	2.50	0.17	0.00	2					
S225.90/ E225.90	35	2.50	0.17	0.23	2					

7.1.2 TEST SETUP AND MONITORING SYSTEM

Figure 7.4 depicts the positioning of the sensors for data acquisition. To measure the deflection of a beam, four linear voltage differential transducers (LVDTs) were supported in a suspension yoke (see Figure 7.4a). The LVDT 3558 was also used to control the test at a displacement rate of 20 µm/s up to the failure of the beams. The beams were loaded under three-point bending with a shear span of 900 mm. This corresponds to a a/d ratio equal to 3.44, where a is the shear span and d is the depth of the longitudinal reinforcement (Figure 7.1). The applied load (F) was measured using a load cell of ±500 kN and accuracy of ±0.05%. Two or three electrical resistance strain gauges (S1 to S3), depending on the shear reinforcing arrangement, were installed in the steel stirrups to measure the strains. Additionally, six or eight SGs (1 to 8) were bonded on the ETS strengthening bars according to the strengthening arrangement represented in Figure 7.4(b).

(a)

(b1)

(b2)
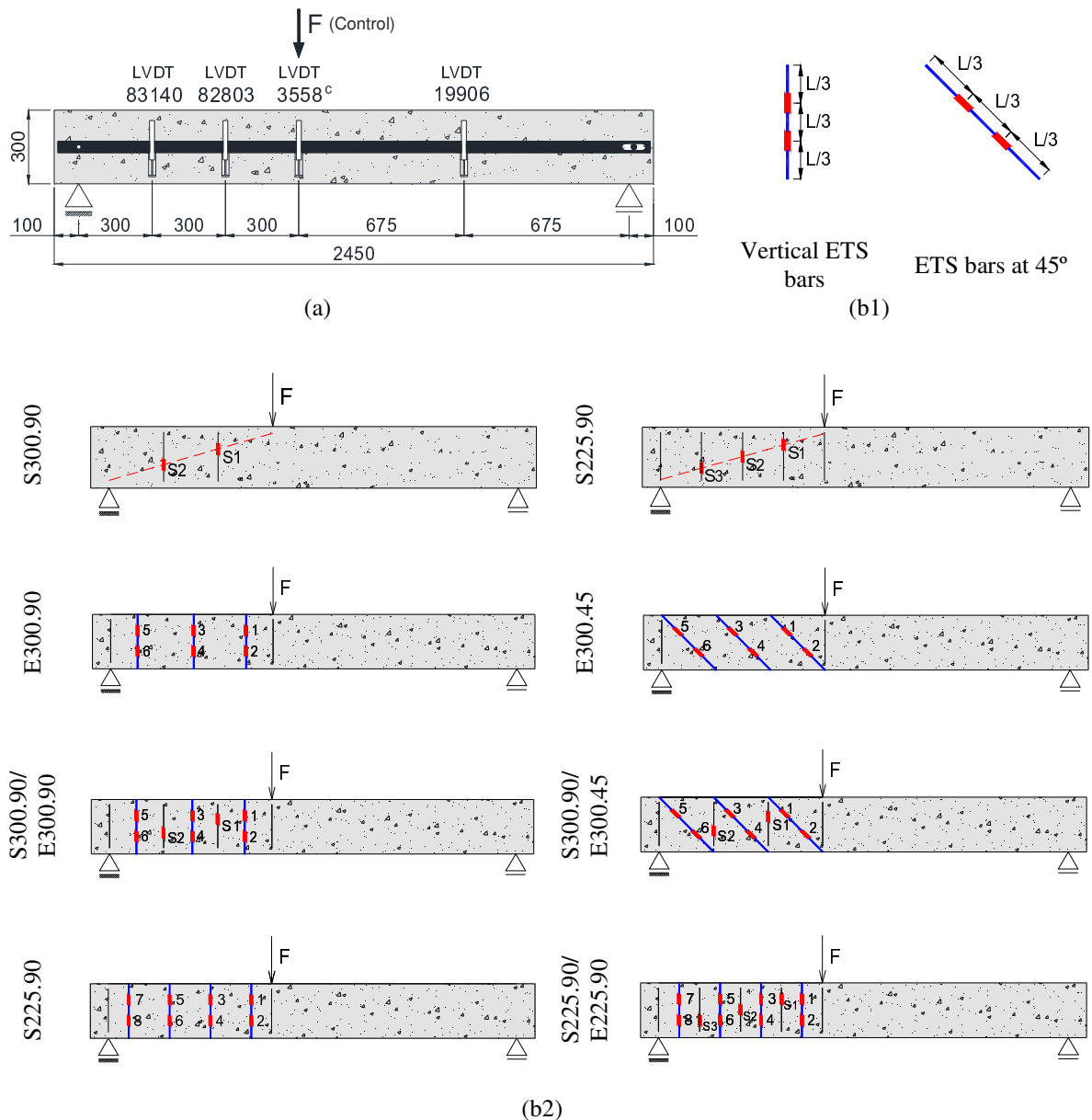
Figure 7.4: Monitoring system: (a) arrangement of the displacement transducers and (b1-b2) positions of the strain gauges in the monitored stirrups and ETS bars. All dimensions are in mm.

7.1.3 MATERIALS CHARACTERIZATION

Table 7.2 includes the values obtained from the experimental tests for the characterization of the main properties of the materials used in the present work. The average compressive strength (f_{cm}) was determined according to NP-E397 (1993). To characterize the tensile behaviour of the steel bars, uniaxial tensile tests were conducted according to the standard procedures of ASTM 370 (2002). Taking into account the results obtained in the experimental program with pull-out tests described in previous chapter, the Sikadur 32N

structural epoxy-based adhesive was selected to bond the ETS steel bars to the concrete. For the characterization of the tensile behaviour of this adhesive, uniaxial tensile tests were performed according to the procedures outlined in ISO 527-2 (1993). The results corresponding to the tensile strength and modulus of elasticity of this adhesive are included in Table 6.2.

Table 7.2: Materials properties.

Steel Reinforcement						Concrete	
Steel bar diameter (∅s)	Modulus of elasticity (GPa)	Yield stress (MPa)	Strain at yield stress (‰)	Tensile strength (MPa)	Bars ID	Batch ID	f_{cm} (MPa)
12 mm	206.62 (1.84)	484.68 (1.26)	2.35 (3.21)	655.53 (0.91)	Longitudinal reinforcement	1	30.78 (4.90)
25 mm	216.19 (9.83)	507.68 (0.96)	2.27 (4.76)	743.41 (1.31)	Longitudinal reinforcement	2	27.81 (4.55)
6 mm	206.07 (6.72)	559.14 (1.00)	2.75 (6.54)	707.93 (1.44)	Stirrups		
8 mm	212.36 (4.29)	566.50 (4.17)	2.66 (6.97)	675.73 (2.03)	ETS strengthening bar		
10 mm	205.16 (3.25)	541.60 (0.91)	2.66 (3.98)	643.23 (0.39)	ETS strengthening bar		
(value) Coefficient of Variation (COV) = (Standard deviation/Average) x 100; f_{cm} = mean cylinder concrete compressive strength							

7.1.4 SPECIMENS PREPARATION AND STRENGTHENING

The main steps for the execution of the ETS shear strengthening technique are represented in Figure 7.5. Before drilling the holes, a rebar detector was used to verify the position of the existing longitudinal bars and stirrups. Afterward, the positions of the strengthening bars were marked on the RC beams and holes were made with the desired inclinations through the core of the cross-section of the RC beams. These holes had 16 mm or 18 mm of diameter, where bars of 8 mm or 10 mm diameter were introduced, respectively, resulting in an adhesive layer of about 4 mm thickness. The holes were cleaned with compressed air, and one extremity of the holes was blocked before bonding the strengthening bars to the concrete. The bars were cleaned with acetone to remove any possible dirt. The adhesive was prepared according to the supplier recommendations, and the bars were introduced into the holes that were filled with the adhesive (care was taken to prevent air bubble formation in the adhesive layer during the application of the strengthening system). Finally, the adhesive in excess was removed. A period of 15 days was dedicated to cure the adhesive (in laboratory environmental conditions) prior to testing the beams.

<p align="center">(a)   (b)   (c)</p>
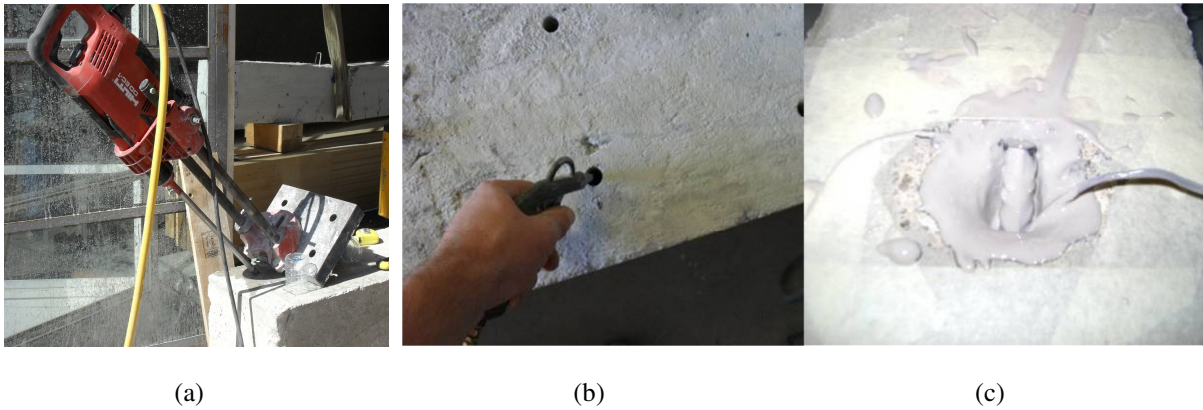
Figure 7.5: ETS strengthening technique: (a) drilling the holes, (b) compressed air to clean the holes and (c) the hole is filled with adhesive and the ETS strengthening bar.

7.1.5 RESULTS AND DISCUSSION

Figures 7.6a and 7.6b show the relationship between the total applied load and the deflection of the loaded section, *F-u*, of the beams of A and B Series, respectively.

<p align="center">(a)   (b)</p>
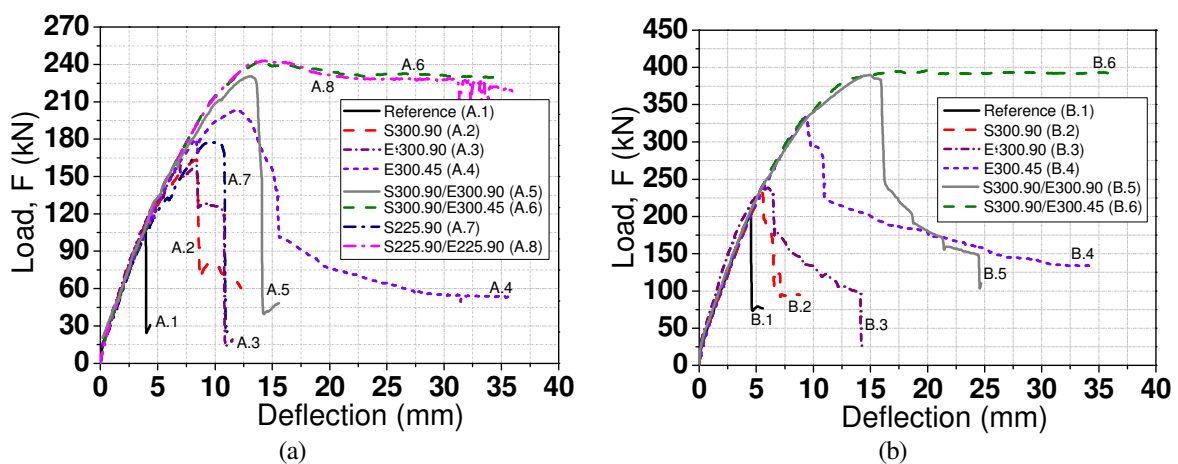
<p align="center">Figure 7.6 – Relationship between the load versus the loaded section deflection for
A (a) and B (b) Series.</p>

Two phases occurred during each test in the following sequence: 1st) the reference and the strengthened beams show similar response up to a deflection corresponding to the formation of the shear failure crack in the reference beam; 2nd) after the shear crack initiation, the stirrups and/or strengthening bars are effectively activated, providing an increase of load carrying and deflection capacities of a level that depends on the shear reinforcement arrangements. In fact, the ETS bars have started to strain at an applied load of approximately 90 kN and 200 kN for the A and B Series, respectively.

For similar ρ_{sw} and ρ_f the RC beams reinforced with steel stirrups or strengthened with ETS bars have identical behaviour (S300.90 and E300.90 beams). For the beams with ETS bars of

equal spacing but different inclination (which means different shear strengthening ratio, ρ_f), ETS bars applied at 45-degrees have provided a higher increase in terms of load carrying capacity and deflection at peak load (E300.90 versus E300.45 beams of both series). In series B, similar stiffness was observed in all beams up to their peak load, which indicate a prevalent influence of the concrete aggregate interlock for the stiffness due to the larger width of the cross section of the beams of this series. Due to the significant increase provided by the ETS bars for the shear resistance, the beams reinforced with steel stirrups and strengthened with ETS bars collapsed by the yielding of the longitudinal steel bars, followed by concrete crushing. In the design phase of the ETS strengthening systems it was not expected a so high shear strengthening effectiveness for these systems. This means that if a higher ρ_{sl} was adopted, from the theoretical point of view, the increased level of the ultimate load would have been even higher than the ones registered in this experimental program, as long as the concrete crushing could be avoided. However, for the geometry and concrete compressive strength of the beams adopted in this experimental programme, the ρ_{sl} was designed to occur concrete crushing just after the yield initiation of longitudinal reinforcement, as recommended by good design practice of RC elements.

Table 7.3 presents the main results obtained in the experimental tests. In this Table, F_{max} is the maximum value of the load registered in the load cell during the test, $\Delta F_{max}/F_{max}^{REF}$ is the ratio between the increase in terms of load carrying capacity provided by the shear reinforcing system, ΔF_{max}, and the maximum load supported by the reference beam, F_{max}^{REF}, $\delta_{F\,max}$ is the deflection of the loaded section at F_{max} and $\Delta \delta_{F\,max}/\delta_{F\,max}^{REF}$ is the ratio between the increase in terms of deflection capacity provided by the shear reinforcing system, $\Delta \delta_{F\,max}$, and the deflection at F_{max}^{REF}, $\delta_{F\,max}^{REF}$. Additionally, $V_n = 0.6 F_{max}$ is the shear resistance of the beam, and V_c, V_s and V_f are the shear resistance attributable to the concrete, steel stirrups and ETS strengthening bars, respectively ($V_n = V_c + V_s + V_f$). Finally, $\varepsilon_{s,F\,max}$ and $\varepsilon_{f,F\,max}$ are the maximum strains in the steel stirrups and in the ETS strengthening bars at F_{max}, while $\varepsilon_{s,max}$ and $\varepsilon_{f,max}$ are the maximum strains in the stirrups and ETS bars up to the failure of the corresponding beams. It is noted that the values indicated in Table 7.3 were obtained based on the following assumptions: a) the shear resistance due to concrete is the same regardless the beam is reinforced with steel stirrups or/and strengthened with ETS bars; and b) the contribution of steel stirrups for the shear resistance is the same in strengthened and unstrengthened beams.

Table 7.3: Experimental results.

Specimen			F_{max} (kN)	$\dfrac{\Delta F_{max}}{F_{max}^{REF}}$ (%)	$\delta_{,Fmax}$ (mm)	$\dfrac{\Delta\delta_{Fmax}}{\delta_{Fmax}^{REF}}$ (%)	V_n (kN)	V_c (kN)	V_s (kN)	V_f (kN)	$\varepsilon_{s,Fmax}$ (‰)	$\varepsilon_{f,Fmax}$ (‰)	$\varepsilon_{s,max}$ (‰)	$\varepsilon_{f,max}$ (‰)
Series A	A.1	Reference	107.86	------	4.01	------	65.32		--------	--------	------	------	--------	--------
	A.2	S300.90	164.67	51.27	7.40	109.58	98.80		33.48	--------	2.73 (S2)	--------	2.95 (S2)	--------
	A.3	E300.90	160.78	47.69	6.97	73.96	96.47		--------	31.15	--------	2.15 (1)	--------	7.38 (3)
	A.4	E300.45	203.98	87.38	12.04	200.25	122.39	65.32	--------	57.07	--------	2.07 (4)	--------	4.12 (4)
	A.5	S300.90/ E300.90	231.83	112.96	13.12	227.18	139.10		33.48	40.30	2.44 (S2)	2.57 (1)	3.08 (S2)	2.68 (1)
	A.6	S300.90/ E300.45	244.41	124.52	14.00	249.21	146.65		33.48	47.85	2.41 (S1)	15.64 (4)	2.70 (S1)	17.29 (4)
	A.7	S225.90	180.31	65.63	9.92	147.32	108.19		42.87	--------	4.27 (S2)	--------	4.56 (S2)	--------
	A.8	S225.90/ E225.90	244.17	124.30	14.44	260.10	146.50		42.87	38.31	2.08 (S3)	2.60 (1)	2.31 (S2)	4.70 (5)
Series B	B.1	Reference	203.36	------	4.45	------	122.02		--------	--------	------	------	--------	--------
	B.2	S300.90	232.31	14.24	5.56	24.94	139.39		17.37	--------	1.66 (S2)	--------	17.70 (S2)	--------
	B.3	E300.90	237.88	17.47	6.06	36.18	143.33	122.02	--------	21.31	--------	0.53 (1)	--------	1.13 (4)
	B.4	E300.45	336.19	65.32	9.42	111.68	201.71		--------	79.69	--------	1.97 (4)	--------	3.20 (4)
	B.5	S300.90/ E300.90	390.11	91.83	15.01	237.30	234.07		17.37	94.68	2.91 (S1)	2.54 (3)	3.27 (S2)	4.53 (1)
	B.6	S300.90/ E300.45	396.51	94.97	20.18	353.48	237.91		17.37	98.52	14.63 (S1)	4.77 (1)	29.09 (S1)	4.99 (1)

(value) = SG that registered the maximum strain at F_{max}.

257

From the obtained results, included in Table 7.3, it can be pointed out the following main observations:

(i) The use of steel ETS bars for the shear strengthening provided significant increase of the load carrying capacity of RC beams for the both bar orientations considered. The effectiveness is also significant in terms of the deflection performance.

(ii) Based on the results of the unstrengthened beams (Reference), it was found that the beams reinforced with steel stirrups (S300.90) and the beam strengthened according to the ETS technique (E300.90) presented an increase in the load carrying capacity of 51 % and 48 % (A Series), and of 14 % and 17% (B Series), respectively. In terms of deflection capacity ($\delta_{F\max}$), an increase of 110 % and 74 % (A Series) and of 25 % and 36 % (B Series), respectively, was obtained.

(iii) The shear reinforcing system composed by inclined ETS strengthening bars was more effective than vertical ETS bars, assuring a better performance in terms of load and deflection capacities. This is justified by the orientation of the shear failure cracks that had a tendency to be almost orthogonal to inclined ETS bars. Furthermore, for vertical ETS bars, the total resisting bond length is lower than that of inclined ETS bars, and ρ_f of vertical ETS bars is lower than ρ_f of inclined ETS bars for the same spacing. Based on the results of the E300.90 beams, it was found that the E300.45 beams presented an increase in the load carrying capacity of 27 % and 41% for A and B Series, respectively. The deflection capacity has also increased in 72 % and 55 % for A and B Series, respectively.

(iv) Since the strains recorded by strain gauges (SGs) are quite dependent of the relative position between the SGs and the shear failure crack, remarks based on these values should not be regarded as conclusions. However, since ETS shear strengthening systems have increased significantly the load carrying capacity of the RC beams, the increase of the maximum strains in both stirrups and ETS bars was expected, and, in general, they have exceeded the yield strain of the stirrups and ETS bars. The maximum strains in the ETS bars, $\varepsilon_{f,\max}$, are particularly high in the bars positioned at 45-degrees.

7.1.5.1 Analysis of the beams of A series (150x300 mm^2 cross section)

a) Reference beam

Figure 7.7 represents the total load versus the deflection, $F-u$, registered in the LVDTs of the A.1 beam, as well as the schematic representation of the crack pattern at failure. During

loading of A.1 reference beam, visible diagonal shear cracks formed at a load of 42 kN. With the increase of the load, the shear failure crack has widen and an abrupt failure has occurred at a load of 108.86 kN. The maximum deflection recorded in the loaded section was 4.01 mm. After the development of a reduced number of flexural cracks, this beam has failed by the occurrence of a unique shear crack at the smaller shear span (a).
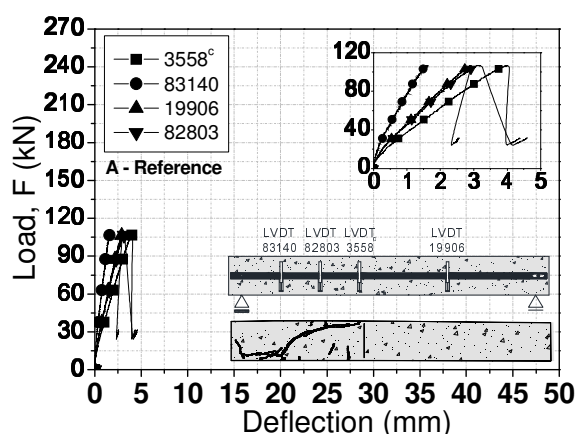
Figure 7.7: Relationship between the applied load and the deflections of the Reference beam of Series A.

b) Beams with steel stirrups

Figure 7.8a represents the $F - u$ registered in the LVDTs of the A.2 beam, as well as the schematic representation of the crack pattern at failure. In the A.2 and A.7 beams, a brittle shear failure has occurred at a maximum load (F_{max}) of 164.67 kN and 180.31 kN, respectively, which correspond to an increase of 51.27% and 65.63% with respect to the carrying capacity of the A.1 reference beam. At first, flexural cracks were formed near the loaded section, and with the increase of the load, other flexural cracks have propagated along the shear span. Some of these flexural cracks have degenerated in shear cracks during the subsequent loading stages. Finally, the beams have abruptly failed with the formation of a shear crack at the shear span (see Figure 7.16). In the beam with stirrups at a spacing of 300 mm (A.2), the first visible crack was formed at a load of 77 kN. In Figure 7.8c is represented the load versus the strains recorded in the strain gauges (SG) installed in the stirrups, $F - \varepsilon_s$, (see also Table 7.3).The maximum strain in the stirrups, $\varepsilon_{s,max}$, was recorded in the S2 strain gauge (SG), in the second stirrup, at 600 mm from the applied load (Figure 7.4), close to the zone crossed by the diagonal crack, and was approximately equal to 2953 $\mu\varepsilon$, indicating that the stirrup has yielded (Table 7.3).

Figure 7.8b represents the $F-u$ registered in the LVDTs of the A.7 beam, as well as the schematic representation of the crack pattern at failure. In this beam, the first visible crack was formed at a load of 37 kN. The $F-\varepsilon_s$ of the stirrups of A.7 beam is represented in Figure 7.8d. The maximum strain was recorded in the S2 SG of stirrup number 2 (450 mm from the applied load) and was equal to 4555 $\mu\varepsilon$. It must be pointed out that these strain values and all those reported herein are not necessarily the maximum values installed in the stirrups and ETS bars. They only represent the strains in the regions where the strain gauges are bonded. The A.2 and A.7 beams presented a deflection of 7.40 mm and 9.92 mm at F_{max} ($\delta_{,F max}$), respectively, which corresponds to an increase of 109.47% and 147.38% with respect to the reference beam.

Figure 7.16 shows that the first stirrup from the support has ruptured in A.2 beam, while in the A.7 beam the first two stirrups from the support have ruptured.

Figure 7.8: Relationship between applied load and deflections (a-b) and relationship between applied load and tensile strain in the steel stirrups (c-d) for the specimens A.2 and A.7, respectively (m.d.=mechanically damaged).

c) Beams without steel stirrups and strengthened according to the ETS technique

Two different inclinations of the ETS bars with respect to the longitudinal axis of the beams were used, vertical (A.3 beam) and at 45-degrees (A.4), maintaining the same spacing between bars (300 mm). Figure 7.9a represents the $F-u$ registered in the LVDTs of the A.3 beam, as well as the schematic representation of the crack pattern at failure. In the A.3 beam, the first visible crack was registered at a load of 36 kN. The maximum load of 160.78 kN was attained at a deflection of 6.97 mm. In Figure 7.9c is represented the load versus the strains recorded in the strain gauges (SG) installed in the ETS bars of A.3 beam, $F-\varepsilon_f$ (see also Table 7.3). The maximum strain was recorded in the strain gage 3 installed in the ETS bar number 3 (450 mm from the applied load) and was equal to 8379 $\mu\varepsilon$.

Figure 7.9b represents the $F-u$ registered in the LVDTS of the A.4 beam, as well as the schematic representation of the crack pattern at failure. The A.4 beam has presented a maximum load of 203.98 kN for a deflection of 12.04 mm. The first visible crack was registered at a load of 38 kN. The $F-\varepsilon_f$ of the ETS bars of A.4 beam is represented in Figure 7.9d. The maximum strain was recorded in the SG number 4 placed in the ETS bar 4 (600 mm from the applied load) and was equal to 4124 $\mu\varepsilon$.

Figure 7.16 shows that in the A.3 beam the stirrups have not ruptured and two shear cracks were formed. In A.4 beam two shear failure cracks were also formed, but involved with a much diffuse crack pattern. One crack has developed at the level just above the longitudinal reinforcement, and the other with an inclination of around 30 degrees.

The analysis of these results prompts the following conclusions:

i) The maximum carrying capacity of the beam strengthened with vertical ETS bars (A.3) was almost the same of the beam with steel stirrups (A.2). Moreover, a reduction on the $\delta_{,F\max}$ of about 17% was observed in the strengthened beams.

ii) The beams strengthened with ETS bars at 45-degrees (A.4) presented an increase of 23.87% and 43.33% in terms of $F_{\max}$ and $\delta_{,F\max}$ respectively, when the beam reinforced with steel stirrups (A.2) is taken for comparison purposes. When compared with the A.3 beam, the A.4 beam presented an increase of 26.87% and 72.74% in terms of $F_{\max}$ and $\delta_{,F\max}$, respectively, was obtained. The more ductile response of A.4 beam, when compared to A.2 and A.3, is evident in Figure 7.6.
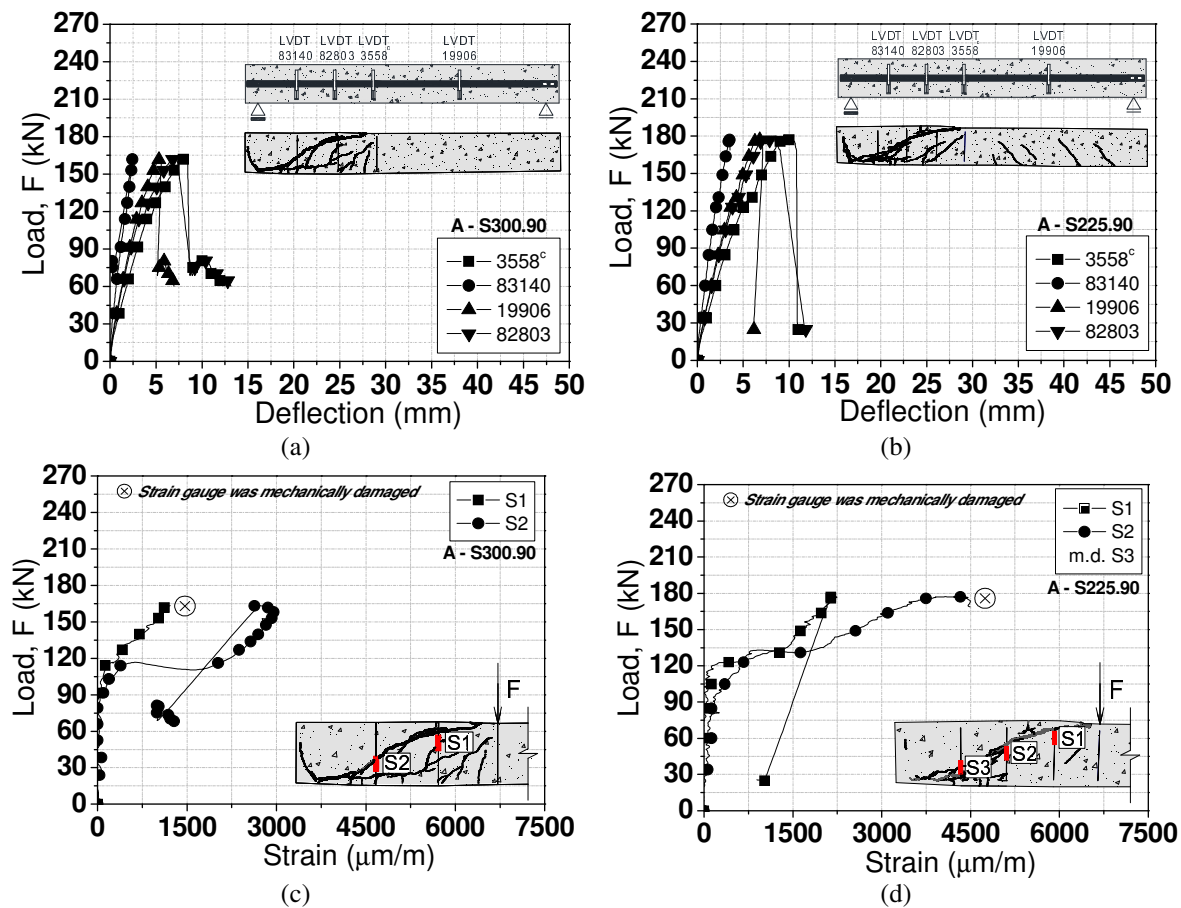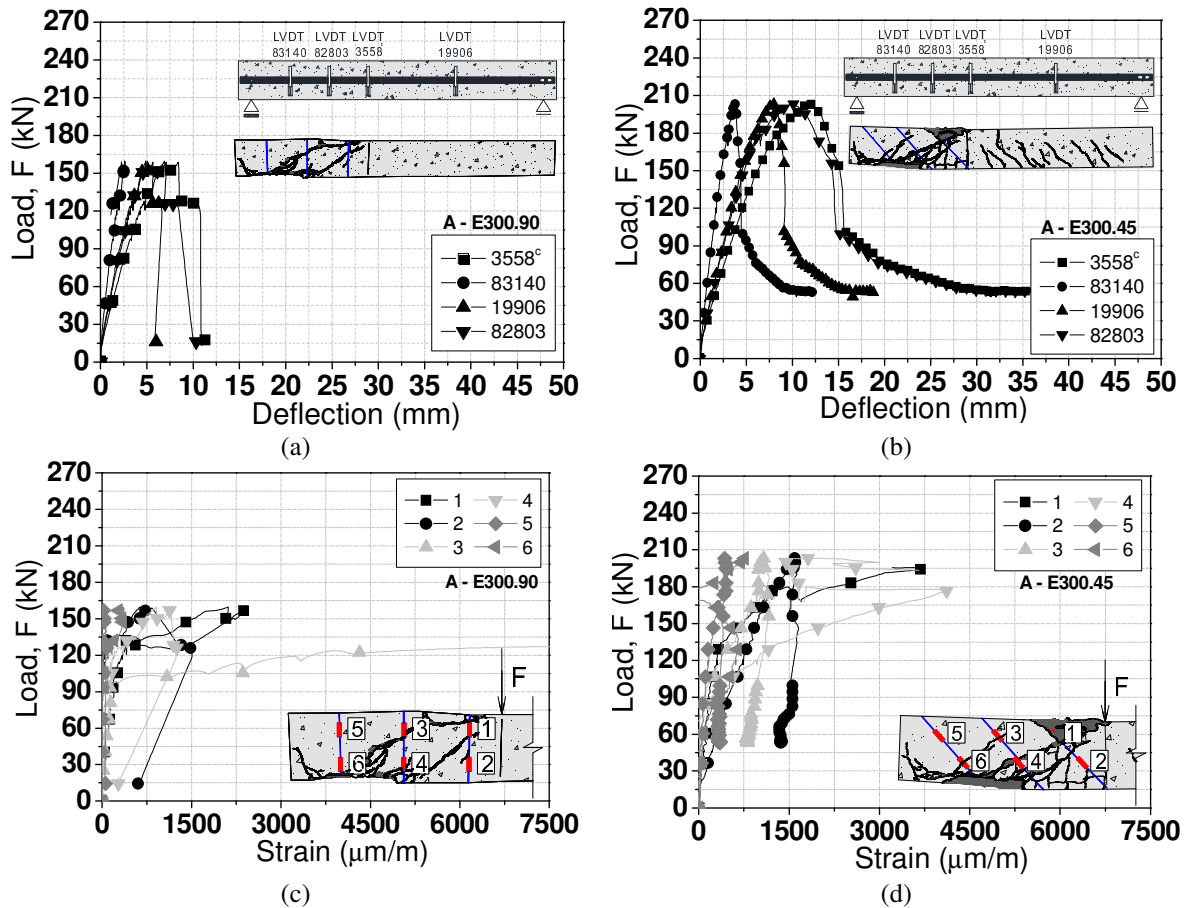
Figure 7.9: Relationship between applied load and deflections (a-b) and relationship between applied load and tensile strain in the ETS strengthening bars (c-d) for the specimens A.3 and A.4, respectively.

d) Beams with steel stirrups and strengthened according to the ETS technique

Three beams were strengthened according to different arrangements of stirrups and ETS bars in order to assess the ETS shear strengthening effectiveness for distinct percentages of existing stirrups, as well as the influence of the percentage and inclination of ETS bars on this effectiveness. Two of these beams were strengthened with steel stirrups and ETS bars at a spacing of 300 mm, one with vertical ETS bars (A.5), and the other at 45-degrees (A.6). The third beam (A.8) was strengthened with stirrups and vertical ETS bars at a spacing of 225 mm.

Figures 7.10a-b represent the $F-u$ registered in the LVDTs of the A.5 and A.6 beams, as well as the schematic representation of the crack pattern at failure. When using vertical stirrups at a spacing of 300 mm, failure occurred at a load of 231.83 kN and 244.41 kN for the A.5 and A.6 beams, respectively, which correspond to an increase of 40.78% and 48.42% with respect to the load carrying capacity of the beam shear strengthened only with steel stirrups at a spacing of 300 mm (A.2). In terms of deflection capacity, the A.5 and A.6 beams presented a deflection of 13.12 mm and 14.00 mm at F_{max}, corresponding to an

increase of 56.19% and 66.67% with respect to the beam with steel stirrups at a spacing of 300 mm (A.2).

In the beam strengthened with vertical ETS bars (A.5) the first visible crack was registered at a load of 58 kN.

In Figure 7.10c is represented the $F - \varepsilon_s$ recorded in the SG installed in the stirrups of A.5 beam, while the $F - \varepsilon_f$ registered in the SG applied in the ETS bars of this beam is shown in Figure 7.10e. The maximum strain was recorded in the stirrup number 2 (600 mm from the applied load) and was equal to 3080 µε. In this beam the maximum strain in ETS bars was recorded in the strain gauge number 1 (150 mm from the applied load) and was equal to 2683 µε.

In the beam strengthened with 45-degree ETS bars (A.6), the first visible crack was registered at a load of 30 kN. In Figures 7.10d and 7.10f are represented the $F - \varepsilon_s$ and $F - \varepsilon_f$ for beam A.6. The maximum strain was recorded in the stirrup number 1 (300 mm from the applied load) and was equal to 2696 µε. The maximum strain in the ETS bars was recorded in the strain gauge number 4 and was equal to 17297 µε.

Figure 7.11a represents the $F - u$ registered in the LVDTS of the beam reinforced with vertical stirrups and strengthened with vertical ETS bars at a spacing of 225 mm (A.8), as well as the schematic representation of the crack pattern at failure. In this beam, the first visible crack was formed at a load of 28 kN. This beam reached a maximum load of 244.17 kN, which corresponds to an increase of 35.42% with respect to the load carrying capacity of the beam with steel stirrups at a spacing of 225 mm (A.7). In Figure 7.11b is represented the $F - \varepsilon_s$ recorded in the SG installed in the stirrups of A.8 beam, while the $F - \varepsilon_f$ registered in the SG applied in the ETS bars of this beam is shown in Figure 7.11c. The maximum strain was recorded in the SG 2 on the stirrup number 3 (675 mm from the applied load) and was equal to 2309 µε. The maximum strain in the vertical ETS bars was recorded in the strain gauge number 5 (562.50 mm from the applied load) and was equal to 4695 µε. The A.8 beam presented a deflection of 14.44 mm at F_{max}, which corresponds to an increase of 45.56% with respect to the deflection capacity of the beam with steel stirrups at a spacing of 225 mm (A.7).

Figure 7.16 shows that in the A.5 and A.6 beams a quite diffuse crack pattern has formed. In A.5 beam the intermediate stirrup, which was crossed by the widened shear crack, has ruptured.

7.1.5.2 Analysis of the beams of B series (300x300 mm^2 cross section)

a) Reference Beam

Figure 7.12 represents the total load versus the deflection, $F - u$, registered in the LVDTs of the B.1 beam, as well as the schematic representation of the crack pattern at failure. The crack pattern during the loading process of this beam (B.1) was similar to the A.1 beam, but due to the larger width of the cross section the maximum shear failure load (F_{max}) was higher, equal to 203.36 kN. At F_{max} the deflection recorded under the applied load was equal to 4.45 mm, a little bit higher the value measured in A.1 beam. As Figure 7.16 shows, the crack pattern of B.1 beam was quite similar to the one registered in A.1 beam.

b) Beams with steel stirrups

Figure 7.13a represents the $F - u$ registered in the LVDTs of the B.2 beam, as well as the schematic representation of the crack pattern at failure. In the B.2 beam with vertical stirrups at a spacing of 300 mm also a brittle shear failure occurred at a F_{max} of 232.31 kN, corresponding to an increase of 14.24 % with respect to the carrying capacity of the B.1 reference beam. The crack propagation process during loading was similar to the one of the homologous beam of A series (A.2).

In the B.2 beam with stirrups at a spacing of 300 mm, the first visible crack was formed at a load of 47 kN. In Figure 7.13b is represented the load versus the strains recorded in the strain gauges (SG) installed in the stirrups, $F - \varepsilon_s$, (see also Table 7.3). Such in the homologous A.2 beam of series A, the maximum strain in the stirrups was recorded in the S2 strain gage, which is positioned close to the zone crossed by the diagonal crack, and a strain of 18696 µε was measured. This B.2 beam presented a deflection of 5.56 mm at F_{max}, which corresponds to an increase of 24.94 % with respect to the deflection capacity of the B.1 reference beam, but smaller than the deflection registered in A.2 beam.

Figure 7.16 shows that, like in the A.2 beam, in the B.2 beam the first stirrup from the support has ruptured, however, the shear crack formed just above the longitudinal bars in the A.2 beam has not occurred in the B.2 beam.

c) Beams without steel stirrups and strengthened according to the ETS technique

Figure 7.14a represents the $F-u$ registered in the LVDTs of the B.3 beam strengthened with vertical ETS bars, as well as the schematic representation of the crack pattern at failure. In this beam, the first visible crack was registered at a load of 54 kN. The maximum load of 238.88 kN was attained at a deflection of 6.06 mm. In Figure 7.14c is represented the load versus the strains recorded in the strain gauges (SG) installed in the ETS bars of B.3 beam, $F-\varepsilon_f$ (see also Table 3). The maximum strain was recorded in the SG 4 installed in the ETS bar 4 at 450 mm from the applied load, and was equal to 1133 µε.

Figure 7.14b represents the $F-u$ registered in the LVDTs of the B.4 beam strengthened with ETS bars at 45-degrees. The schematic representation of the crack pattern at failure is also included. The first visible crack in the B.4 beam was registered at a load of 69 kN. This beam presented a maximum load of 336.19 kN at a deflection of 9.42 mm. The $F-\varepsilon_f$ of the ETS bars of A4 beam is represented in Figure 7.14d. The maximum strain was recorded in the SG 4 installed in the ETS bars from 300 mm of the applied load, and was equal to 3200 µε.

As Figure 7.16 shows, the failure crack patterns of B.3 and B.4 beams were similar to those registered in the A.3 and A.4 beams.

The analysis of the obtained results prompts the following conclusions:

i) The B.3 beam strengthened with vertical ETS bars presented a load-carrying capacity and a deflection performance that was 2.83 and 9.00% higher than the corresponding values registered in the B.2 beam reinforced with stirrups.

ii) When also compared to the B.2 beam, the B.4 beam strengthened with ETS bars at 45-degrees presented an increase of 44.72% and 69.42% for the load carrying and deflection capacity, respectively.

iii) A comparison between B.4 and B.3 beams reveals that applying ETS bars at 45 degrees conducted to an increase of 40.74 % on the load carrying capacity and an increase of 55.44 % on the deflection performance.

d) Beams with conventional steel stirrups and strengthened according to the ETS technique

Figures 7.15a-b represent the $F-u$ registered in the LVDTs of the B.5 and B.6 beams, as well as the schematic representation of the crack pattern at failure. For the beam with vertical (B.5) and 45-degrees ETS bars (B.6), failure occurred at a load of 390.11 kN and 396.51 kN, respectively, which correspond to an increase of 67.93% and 70.68% with respect to the carrying capacity of the B.2 beam with steel stirrups at a spacing of 300 mm. The deflection at F_{max} of B.5 and B.6 beams was 15.01 mm and 20.18 mm, which corresponds to an increase of 169.96 % and 262.95 % with respect to the deflection capacity of B.2 beam. In the B.5 beam, the first visible crack was registered at a load of 58 kN. In Figure 7.15c is represented the $F-\varepsilon_s$ recorded in the SG installed in the stirrups of B.5 beam, while the $F-\varepsilon_f$ registered in the SG applied in the ETS bars of this beam is shown in Figure 7.15e. The maximum strain was recorded in the SG 2 of the stirrup at 600 mm from the applied load and was equal to 3267 µε, while in the ETS bars a maximum strain of 4530 µε was registered in the strain gauge number 1.

In the B.6 beam the first visible crack was registered at a load of 69 kN. In Figures 7.15d and 7.10f are represented the $F-\varepsilon_s$ and $F-\varepsilon_f$ for beam B.6. The maximum strain in the stirrups was recorded in the SG 1, and was equal to 29090µε, while in the ETS bars at 45-degrees, the maximum strain was recorded in the strain gauge number 1 and was equal to 4992 µε.

Figure 7.16 shows that while A.5 beam failed in bending, with the yielding of the longitudinal reinforcement followed the concrete crushing, in the B.5 beam, just after the yield initiation of the longitudinal reinforcement, the beam has failed by the formation of a shear failure crack. Like in the A.5 beam, in the B.5 beam the second stirrup from the support of the beam has ruptured. The crack pattern of B.6 was quite similar to the one of A.6, and both beams have failed in bending.

7.2 PREDICTION OF EXPERIMENTAL RESULTS

The applicability of the ACI 318 (2008) and Eurocode 2 (2004) standard specifications for shear resistance was also investigated and the results are presented in the following sections.

Figure 7.10: Relationship between applied load and deflections (a-b), relationship between applied load and tensile strain in the steel stirrup (c-d) and ETS strengthening bars (e-f) for the specimens A.5 and A.6, respectively.

(a)

(b)

(c)
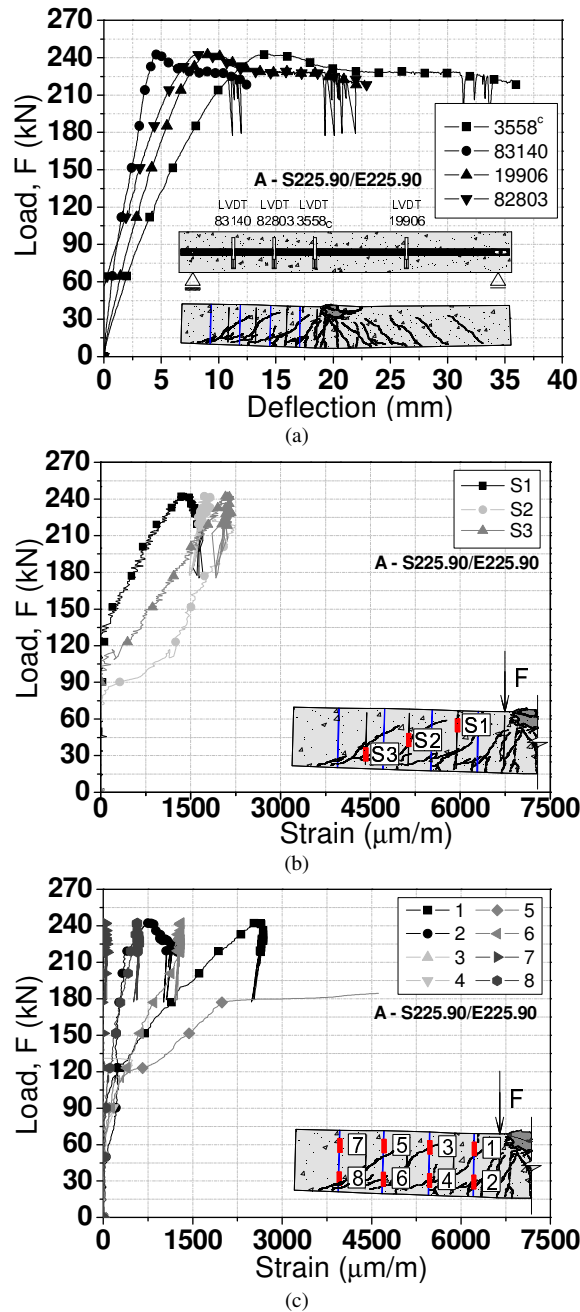
Figure 7.11: Relationship between applied load and deflections (a), relationship between applied load and tensile strain in the steel stirrup (b) and ETS strengthening bars (c) for the specimen A.7.
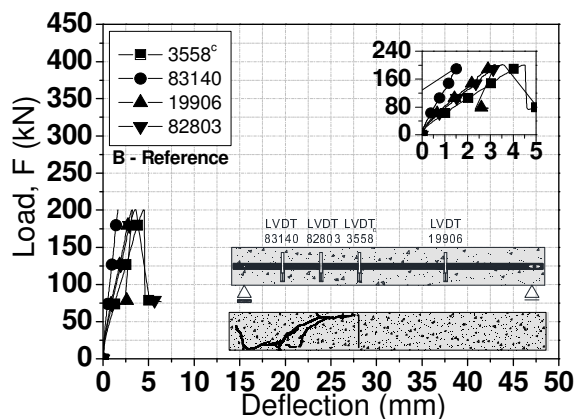
Figure 7.12: Relationship between the applied load and the deflections of the Reference beam (B.1) of B Series.
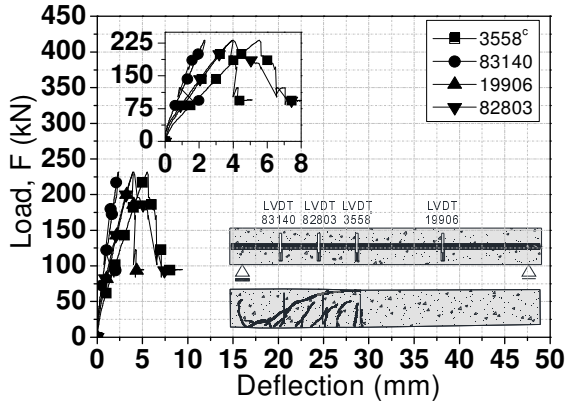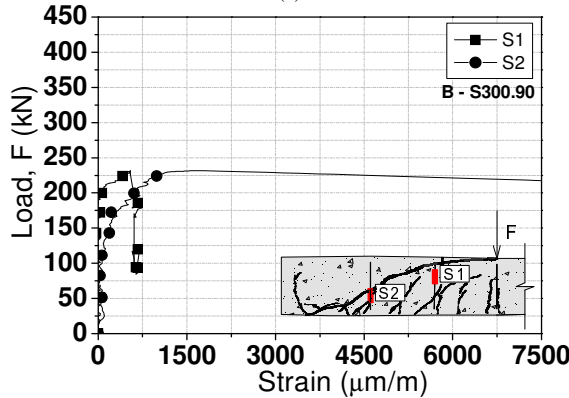
Figure 7.13: Relationship between the applied load and the deflections (a) and relationship between the applied load and tensile strain in the steel stirrups (b) for the specimens B.2.
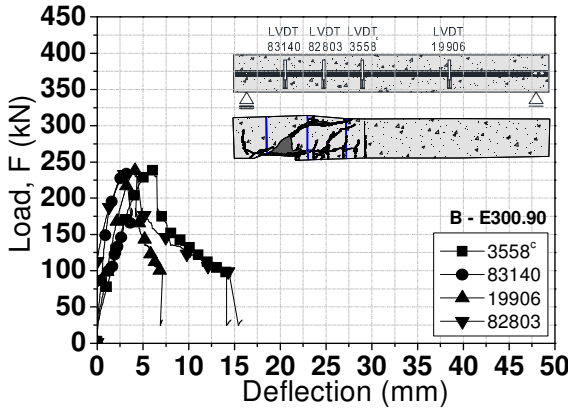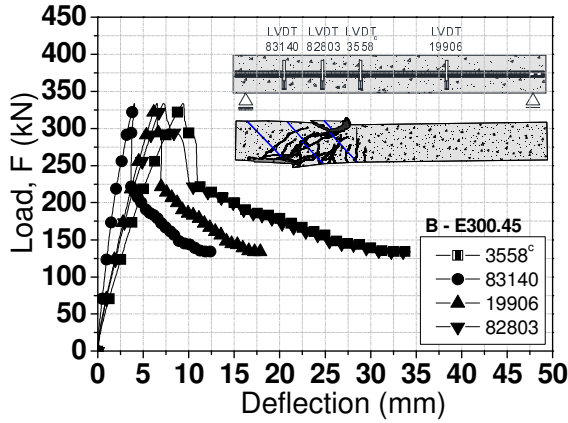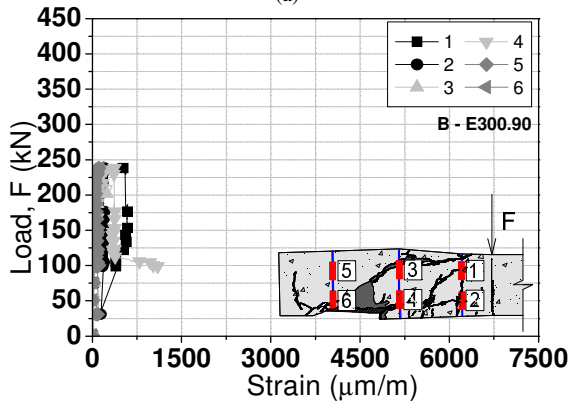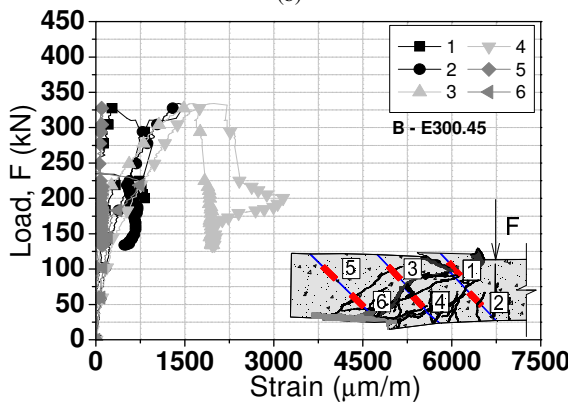
Figure 7.14: Relationship between applied load and deflections (a-b) and relationship between applied load and tensile strain in the ETS strengthening bars (c-d) for the specimens B.3 and B.4, respectively.
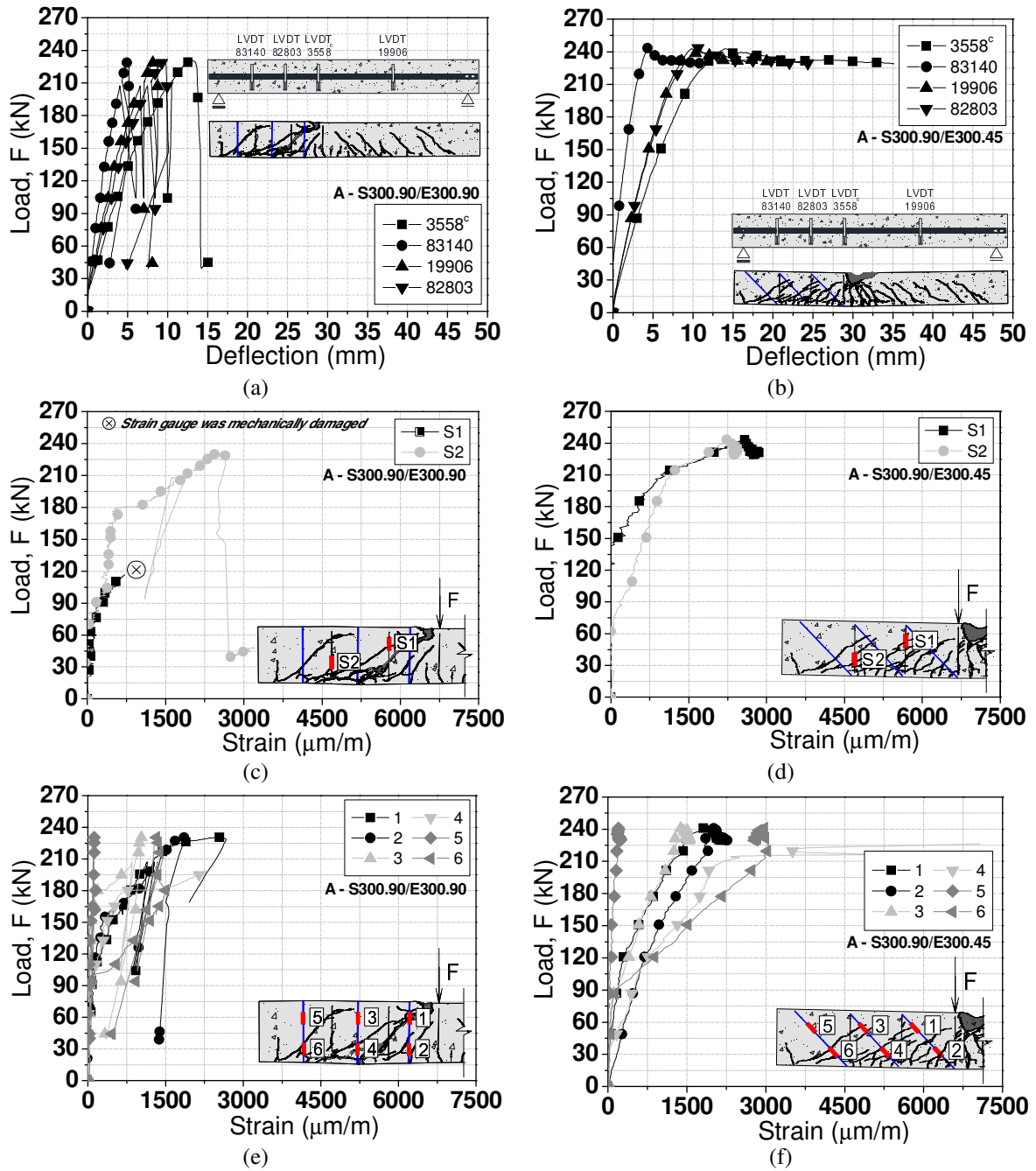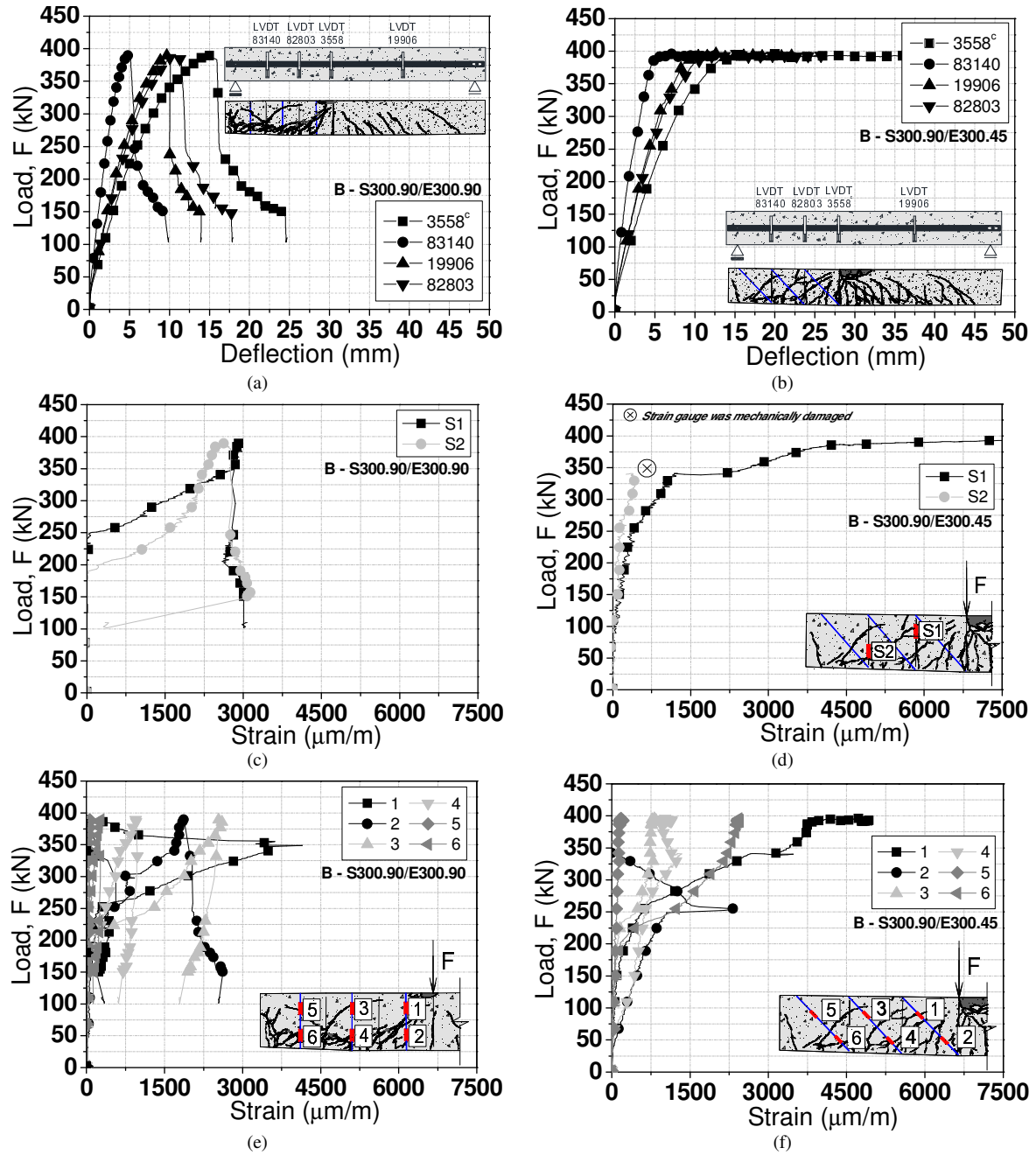
Figure 7.15: Relationship between applied load and deflections (a-b), relationship between applied load and tensile strain in the steel stirrup (c-d) and ETS strengthening bars (e-f) for the specimens B.5 and B.6, respectively.
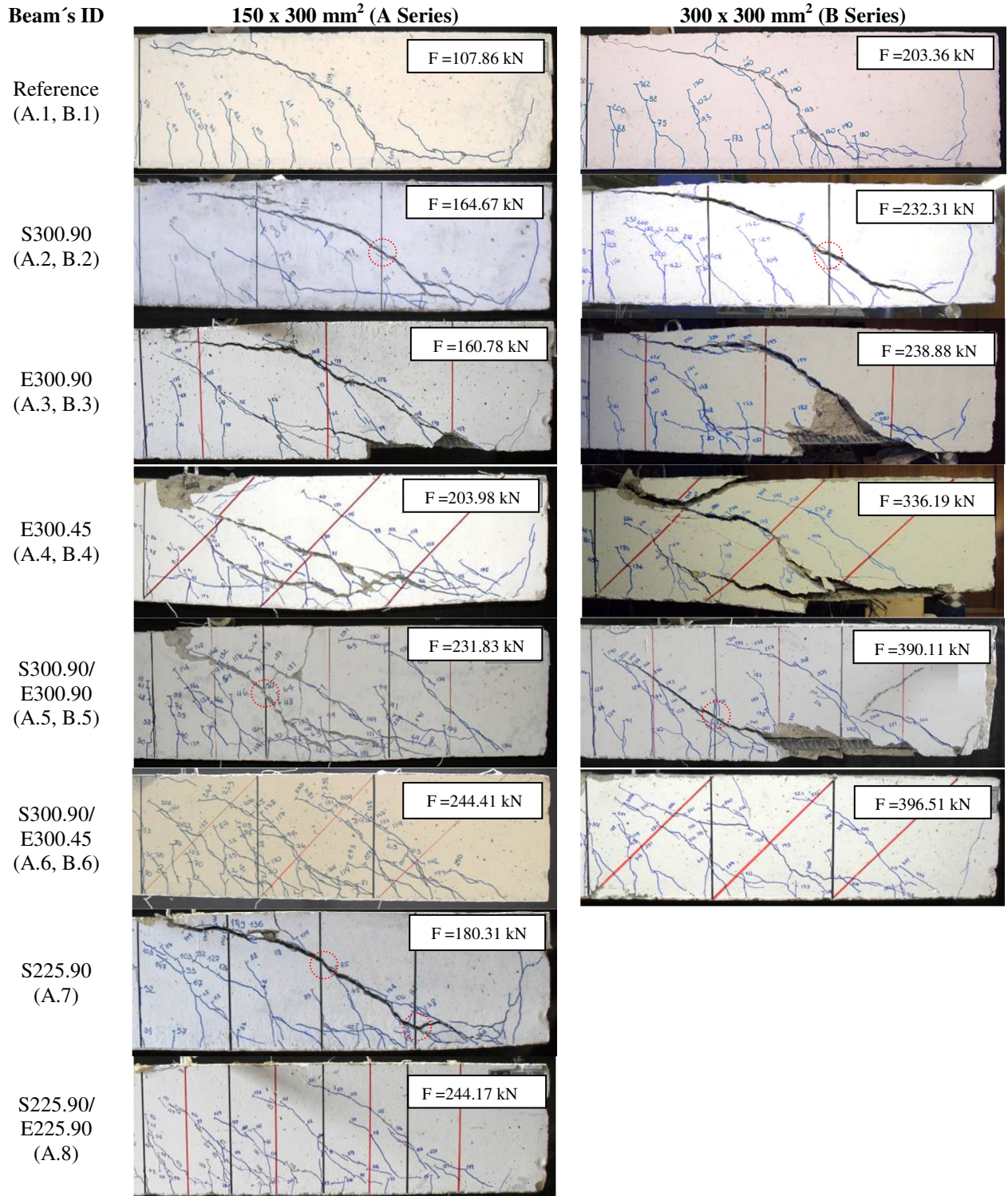
Figure 7.16: Crack pattern.

7.2.1 Shear resistance of RC beams according to ACI 440 and ACI318

To evaluate the nominal shear resistance of the tested beams (V_n), the recommendations of the ACI 440 (2008) were adopted by assuming that ETS bars can be regarded, from the strengthening point-of-view, like a fiber reinforced polymer (FRP) system. Therefore,

$$\phi V_n = \phi(V_c + V_s + \psi_f V_f) \tag{7.1}$$

where V_c, V_s and V_f are the contributions from the concrete, steel stirrups and ETS bars, respectively, ψ_f is a reduction applied to the contribution of the shear strengthening system, and ϕ is the strength-reduction factor required by ACI 318 (2008) that, for shear strengthening of concrete elements, has a value of 0.85. Since ETS bars have, in general, exceeded its yield strain and did not debond, a ψ_f value of 0.95, typical of FRP systems applied in order to guarantee full wrapped conditions for the section, is assumed in the present work (ACI 440, 2008). In equation (7.1), V_c has been computed using the upper limit indicated in Section 11.2.2.1 of the ACI 318 (2008), given by $V_c = 3.5\sqrt{f_c'} \cdot b_w \cdot d$, where f_c' is the concrete compressive strength, b_w is the web width, and d is the distance from the extreme compression fiber of the cross section to the centroid of the longitudinal reinforcement.

The contribution of the vertical steel stirrups has been computed according to Section 11.4.7.2 of the ACI 318 Code, by applying the equation

$$V_s = \frac{A_v \cdot f_{yt} \cdot d}{s} \tag{7.2}$$

where A_v is the cross sectional area of steel stirrups of spacing s, and f_{yt} is the yield stress of the steel stirrup. When inclined bars are used as shear reinforcement,

$$V_s = \frac{A_v \cdot f_{yt} \cdot (\sin\alpha + \cos\alpha) \cdot d}{s} \tag{7.3}$$

where α is the angle between inclined stirrups and longitudinal axis of the member, and s is measured in direction parallel to longitudinal reinforcement. The contribution of ETS bars is evaluated by introducing convenient adjustments in equations (7.2) and (7.3):

$$V_f = \frac{A_f \cdot f_{yt} \cdot d}{s_f} \tag{7.4}$$

and

$$V_f = \frac{A_f \cdot f_{yt} \cdot (\sin\alpha + \cos\alpha) \cdot d}{s_f} \tag{7.5}$$

where A_f is the cross sectional area of the ETS bars of spacing s_f and f_{yt} is the yield stress of the ETS bar.

7.2.2 Shear resistance of RC beams according to the Eurocode 2 (2004)

In the case of the reference beams, the design value for the shear resistance, $V_{Rd,c}$, for members not requiring shear reinforcement is determined from:

$$V_{Rd,c} = [C_{Rd,c} k (100\rho_l f_{ck} + k_1\sigma_{cp})^{1/3}] b_w d \geq (V_{min} + k_1\sigma_{cp}) b_w d \tag{7.6}$$

where f_{ck} is the characteristic value of concrete compressive strength, $k = 1 + \sqrt{200/d} \leq 2.0$ (width d in mm), $\rho_l = A_{sl}/b_w d \leq 0.02$ being A_{sl} the cross sectional area of the tensile reinforcement. The recommended value for $C_{Rd,c}$ is $0.18/\gamma_c$, where γ_c is the partial safety factor for concrete. Additionally, σ_{cp} is the stress due to the axial load, $k_1 = 0.15$ (recommended value) and $V_{min} = 0.035 k^{3/2} f_{ck}^{1/2}$.

The shear resistance of a member with shear reinforcement is equal to:

$$V_{Rd} = V_{Rd,s} + V_{cdd} + V_{td} \tag{7.7}$$

where $V_{Rd,s}$ is the design value of the shear force that is sustained by the steel stirrups, V_{cdd} and V_{td} are the design values of the shear components of the force in the compression area and in the tensile reinforcement, respectively, in the case of an inclined compression chord. In the present work, rectangular cross-sections, with no inclined chords, were considered, since the depth of the beam's cross section is constant. For reinforced concrete members with vertical steel stirrups, the $V_{Rd,s}$ is the smaller value between

$$V_{Rd,s} = \frac{A_{sw}}{s} \cdot z \cdot f_{ywd} \cdot \cot\theta \tag{7.8}$$

and

$$V_{Rd,max} = \alpha_{cw} b_w z \nu_1 f_{cd} / (\cot\theta + \tan\theta) \tag{7.9}$$

For members with inclined shear reinforcement, the $V_{Rd,s}$ is the smaller value between

$$V_{Rd,s} = \frac{A_{sw}}{s} \cdot z \cdot f_{ywd} \cdot (\cot\theta + \cot\alpha)\sin\alpha \tag{7.10}$$

and

$$V_{Rd,\max} = \alpha_{cw} b_w z \nu_1 f_{cd} (\cot\theta + \tan\alpha)/(1+\cot^2\theta) \tag{7.11}$$

where $V_{Rd,\max}$ is the design value of the maximum shear force that can be sustained by the member, limited by crushing of the compression struts; A_{sw} is the cross-sectional area of the shear reinforcement; s is the spacing of the stirrups; z is the lever arm (that may be considered as $z = 0.9 \cdot d$), f_{ywd} is the design value of the yield stress of the shear reinforcement; θ is the angle of the inclined struts ($1 \le \cot\theta \le 2.5$), α is the angle between the inclined bars and the axis of the beam, ν_1 is a strength reduction factor to take into account that concrete is cracked in the shear region (considered as 0.6 for $f_{ck} < 60\,\mathrm{MPa}$) ; α_{cw} is a coefficient to take into account the stress state in the compression chord (recommended values of 1 for non-prestressed structures) and f_{cd} is the design value of concrete compressive strength.

To take into account the contribution of the ETS bars ($V_{Rd,f}$) for the shear strengthening of a shear reinforced element, in equation (7.7), the term $V_{Rd,f}$ was also added:

$$V_{Rd} = V_{Rd,s} + V_{Rd,f} \tag{7.12}$$

where $V_{Rd,f}$ is the design value of the maximum shear force that can be sustained by the ETS bars:

$$V_{Rd,f} = \frac{A_{sf}}{s_f} \cdot z \cdot f_{ywd} \cdot (\cot\theta + \cot\alpha)\sin\alpha \tag{7.13}$$

being A_{sf} and f_{ywd} the cross-sectional area and the design value of the yield stress of a ETS bar ($f_{ywd} = f_{ym}/\gamma_s$), and s_f is the spacing of ETS bars.

The shear resistance of the beams tested in the experimental program ($V^{\exp}$) is compared to the nominal shear resistance (V_n) given by ACI 318 (2008) and Eurocode 2 (2004) formulations, and the results are presented in Table 7.4. For calculating the nominal shear resistance, the average materials properties presented in Table 7.2 were taken into consideration. More details on the calculations can be found in the Annex 7. Since the contribution of the stirrups and ETS bars depends on the inclination of the shear failure crack, the two extreme limits are considered: $\cot\theta = 2.5 \Rightarrow \theta = 21.8°$ and $\cot\theta = 1.0 \Rightarrow \theta = 45°$. According to the formulations of the ACI 318 (2008) and ACI 440 (2008), most of the values of $V^{\exp}/V_n$ were higher than one (safety condition) and an average value of about 1.22 for $V^{\exp}/V_n$ was obtained. The unsafe factor $\left(V^{\exp}/V_n < 1.0\right)$ of 0.97 was obtained in B.3 beam.

Following the recommendations of Eurocode 2 (2004) design values should be adopted for the properties of the intervening materials, and for the safety factors γ_c and γ_s the values of 1.5 and 1.15 are proposed. Taking into account these suggestions, the application of the Eurocode 2 formulation has conducted to 1.63 and 3.34 for $V^{\exp}/V_{Rd}$, respectively, for $\theta = 21.8°$ and $\theta = 45°$. Therefore, it can be concluded that, in general, ACI and Eurocode have predicted a shear resistance lower than the one registered experimentally, but ACI has conducted to more uniform values of $V^{\exp}/V_n$ than Eurocode 2 in terms of $V^{\exp}/V_{Rd}$.

7.3 ASSESSMENT OF THE BEHAVIOUR OF THE STRENGTHENED BEAMS BY FEM-BASED MATERIAL NONLINEAR ANALYSIS

7.3.1 Predictive performance of the model

For the prediction of the behavior of RC beams strengthened with the ETS technique, the version 4.0 of FEMIX computer program, based on the finite element method (FEM), was used. This program includes constitutive models able of simulating the concrete crack initiation and crack propagation, the nonlinear concrete compression behaviour and the elasto-plastic behaviour of steel reinforcements.

In this chapter, the performance of the adopted numerical model is assessed in terms of predicting the force-deflection response and crack pattern of RC beams shear strengthened according to the ETS technique. For this purpose, the tests of the experimental program described in section 7.1 are simulated. For the numerical simulations a constitutive model able to simulate the concrete crack initiation and crack propagation, the softening of both fracture mode I and fracture mode II of concrete, and the elasto-plastic behavior of steel reinforcements was selected.

7.3.2 Materials properties

7.3.2.1 Constitutive laws for the steel bars

For modeling the behavior of the longitudinal steel bars, stirrups and ETS bars, the stress-strain relationship represented in Figure 4.3 is adopted.

Table 7.4: Analytical vs experimental results for ETS technique.

Specimen			Experimental				Analytical									
			V_c (kN)	V_s (kN)	V_f (kN)	V^{exp} (kN)	ACI				$\dfrac{V^{exp}}{V_n}$	Eurocode 2				$\dfrac{V^{exp}}{V_{Rd}}$
							V_c (kN)	V_s (kN)	V_f (kN)	V_n (kN)		$V_{Rd,c}$ (kN)	$V_{Rd,s}$ (kN)	$V_{Rd,f}$ (kN)	V_{Rd} (kN)	
Series A	A.1	Reference	65.32	--------	--------	65.32	53.77	--------	--------	53.77	1.21	31.51	--------	--------	31.51	2.07
	A.2	S300.90		33.48	--------	98.80	53.77	23.42	--------	77.19	1.28	0.00	(53.93) [21.58]	--------	(53.93) [21.58]	(1.83) [4.58]
	A.3	E300.90		--------	31.15	96.47	53.77	--------	29.93	83.70	1.15	0.00	--------	(72.55) [29.04]	(72.55) [29.04]	(1.33) [3.32]
	A.4	E300.45		--------	57.07	122.39	52.02	--------	42.32	94.34	1.30	0.00	--------	(71.82) [41.06]	(71.82) [41.06]	(1.70) [2.98]
	A.5	S300.90/ E300.90		33.48	40.30	139.10	53.77	23.42	29.93	107.12	1.30	0.00	(53.93) [21.58]	(72.55) [29.04]	(126.48) [50.62]	(1.10) [2.75]
	A.6	S300.90/ E300.45		33.48	47.85	146.65	52.02	23.42	42.32	117.76	1.25	0.00	(53.93) [21.58]	(71.82) [41.06]	(125.75) [62.64]	(1.17) [2.34]
	A.7	S225.90		42.87	--------	108.19	52.02	31.21	--------	83.23	1.30	0.00	(71.90) [27.78]	--------	(71.90) [27.78]	(1.50) [3.76]
	A.8	S225.90/ E225.90		42.87	37.31	146.50	52.02	31.21	39.89	123.12	1.19	0.00	(71.90) [27.78]	(96.73) [37.72]	(167.63) [67.50]	(0.87) [2.17]
Series B	B.1	Reference	122.02	--------	--------	122.02	107.45	--------	--------	107.45	1.14	61.70	--------	--------	61.70	1.98
	B.2	S300.90		17.37	--------	139.39	107.45	23.42	--------	130.87	1.07	0.00	(53.93) [21.58]	--------	(53.93) [21.58]	(2.58) [6.46]
	B.3	E300.90		--------	21.31	143.33	107.45	--------	40.07	147.52	0.97	0.00	--------	(97.13) [37.88]	(97.13) [37.88]	(1.48) [3.69]
	B.4	E300.45		--------	79.69	201.71	103.96	--------	56.66	160.62	1.26	0.00	--------	(96.15) [54.98]	(96.15) [54.98]	(2.10) [3.67]
	B.5	S300.90/ E300.90		17.37	94.68	234.07	107.45	23.42	40.07	170.94	1.37	0.00	(53.93) [21.58]	(97.13) [37.88]	(151.06) [60.46]	(1.55) [3.87]
	B.6	S300.90/ E300.45		17.37	97.52	237.91	103.96	23.42	56.66	184.04	1.29	0.00	(53.93) [21.58]	(96.15) [54.98]	(150.08) [76.56]	(1.58) [3.11]

() values determined with $\cot\theta = 2.5 \Rightarrow \theta = 21.8°$; [ ]values determined with $\cot\theta = 1.0 \Rightarrow \theta = 45°$; Analytical predictions: (i) the average materials properties presented in Table 7.2 were taken into consideration; (ii) ACI: $\phi = 0.85$ and $\psi_f = 0.95$ and (iii) Eurocode 2: $f_{ck} = f_{cm} - 8(MPa)$, $\gamma_c = 1.50$ and $\gamma_s = 1.15$

The curve (under compressive or tensile loading) is defined by the points PT1=($\varepsilon_{sy}, \sigma_{sy}$), PT2=($\varepsilon_{sh}, \sigma_{sh}$) and PT3=($\varepsilon_{su}, \sigma_{su}$), and a parameter p that defines the shape of the last branch of the curve. Unloading and reloading linear branches with slope $E_s = \left(\sigma_{sy} / \varepsilon_{sy} \right)$ are assumed in the present approach. The values of the parameters of the constitutive model for the steel are indicated in Table 7.5.

7.3.2.2 Constitutive laws for the concrete

In order to simulate the crack initiation and the fracture mode I propagation of reinforced concrete, the tri-linear tension-softening diagram represented in Figure 4.2 was adopted. To distinguish concrete elements in tension softening and in tension stiffening, distinct values were considered for the concrete of the elements in the first two rows of finite element mesh (elements considered in tension stiffening). The values that define these diagrams are indicated in Table 7.6. Since the predictive performance of structures failing in shear is quite dependent on the constitutive model adopted to simulate the shear stress transfer in the cracked concrete, the shear-softening diagram represented in Figure 7.17 was adopted to reproduce the degradation of crack shear stress transfer after crack initiation. The data necessary to describe the constitutive model are the crack shear strength ($\tau_{t,p}^{cr}$), the shear fracture energy ($G_{f,s}$), and a constant shear retention factor (in the presented case a value β=0.2 was used). More details regarding the used constitutive model can be found in Rots and Borst (1987) and Ventura-Gouveia et.al (2008).

Table 7.5: Values of the parameters of the steel constitutive model (see Figure 4.3).

Steel bar diameter (mm)	PT1 $\varepsilon_{sy}[-]$ $\sigma_{sy}(MPa)$	PT2 $\varepsilon_{sh}[-]$ $\sigma_{sh}(MPa)$	PT3 $\varepsilon_{su}[-]$ $\sigma_{su}(MPa)$	p
6	2.750×10-3 559.14	2.000×10-2 707.14	5.000×10-2 707.93	1
8	2.660×10-3 566.50	2.533×10-2 675.73	5.000×10-2 675.73	1
10	2.660×10-3 541.60	2.405×10-2 643.23	5.000×10-2 643.23	1
12	2.350×10-3 484.68	2.302×10-2 655.00	5.000×10-2 655.53	1
25	2.270×10-3 507.68	3.450×10-3 607.75	2.052×10-2 743.41	1

Table 7.6: Values of the parameters of the concrete constitutive model.

Poisson's ratio (ν_c)	0.15
Initial Young's modulus (E_c)	31100 N/mm^2 (Batch 1) 30590 N/mm^2 (Batch 2)
Compressive strength (f_c)	30.78 N/mm^2 (Batch 1) 28.81 N/mm^2 (Batch 2)
Tri-linear tension-stiffening diagram (1)	fct = 2.0 N/mm^2 ; G$_f$ = 0.06 N/mm ξ1 = 0.01; α1 = 0.5; ξ2 = 0.5; α2 = 0.2
Tri-linear tension-softening diagram (1)	fct = 1.8 N/mm^2 ; G$_f$ = 0.05 N/mm ξ1 = 0.01; α1 = 0.4; ξ2 = 0.5; α2 = 0.2
Parameter defining the mode I fracture energy available to the new crack (Sena-Cruz, 2004)	n = 2
Parameter for defining the softening crack shear stress-strain diagram in the tension-stiffening concrete	$\tau_{t,p}^{cr}$ = 1.38 N/mm^2; $G_{f,s}$ =0.5 N/mm; β=0.2
Parameter for defining the Softening crack shear stress-strain diagram in the tension-softening concrete	$\tau_{t,p}^{cr}$ = 1.38 N/mm^2; $G_{f,s}$ =0.7 N/mm; β=0.2
Crack band-width, *lb*	Square root of the area of Gauss integration point
Threshold angle (Sena-Cruz, 2004)	αth = 30º
Maximum number of cracks per integration point	2

(1) $f_{ct} = \sigma_{n,1}^{cr}$; $\xi_1 = \varepsilon_{n,2}^{cr}/\varepsilon_{n,u}^{cr}$; $\alpha_1 = \sigma_{n,2}^{cr}/\sigma_{n,1}^{cr}$; $\xi_2 = \varepsilon_{n,3}^{cr}/\varepsilon_{n,u}^{cr}$; $\alpha_2 = \sigma_{n,3}^{cr}/\sigma_{n,1}^{cr}$ (see Figure 4.2)

7.3.2.3 Finite element meshes and integration schemes

An example of a finite element mesh used for the simulation of the E300.90 beam is represented in Figure 7.18. The beams are modeled with a mesh of 8-noded serendipity plane stress finite elements. A Gauss-Legendre integration scheme with 3×3 IP is used in all concrete elements. The longitudinal steel bars, stirrups and the ETS strengthening bars are modeled with 3-noded perfect bonded embedded cables (one degree-of-freedom per each node) and a Gauss-Legendre integration scheme with 3 IP (integration point) is used.

7.3.3 Results and discussion

The predictive performance of this model is assessed by simulating the tested beams. The experimental and the numerical relationships between the applied load and the deflection at the loaded section for the tested beams are compared in Figures 7.19 and 7.20. In these figures a horizontal line corresponding to the maximum experimental load (in dash) is also included. The crack patterns of these beams at the end of the analysis (at the end of the last converged load increment) are represented in Figures 7.21 and 7.22. The cracks are represented by quadrilateral 4-node finite elements.
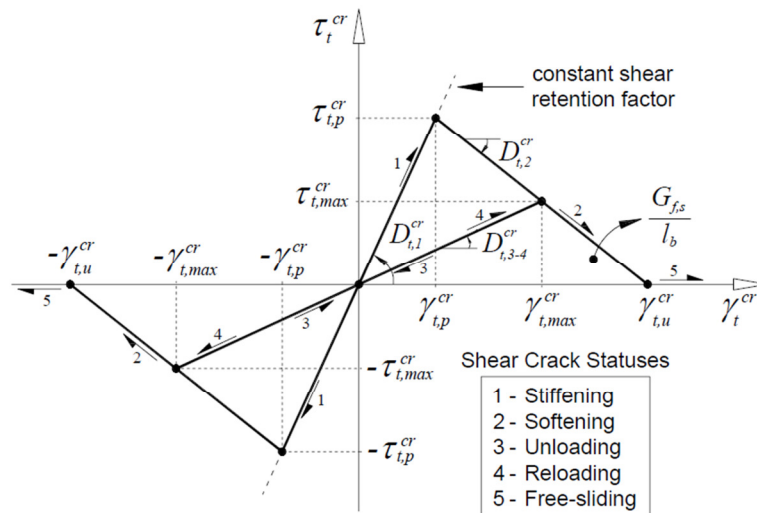
Figure 7.17: Generic crack shear stress and crack shear strain diagram and the adopted shear crack statuses (Ventura-Gouveia, 2012).
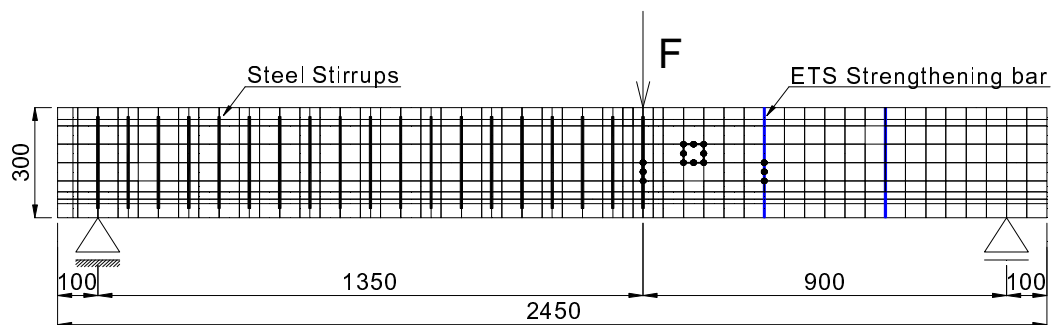
Figure 7.18: Finite element mesh (dimensions are in mm).

These figures show that the numerical model is able to capture with good accuracy the deformational response of the beams, and has also captured with good precision the localization and profile of the shear failure crack. Figures 7.23 and 7.24 also show that the numerical simulations fit with good accuracy the average strains measured in the steel stirrups and ETS strengthening bars, which means that the assumption of perfect bond between composite materials and surrounding concrete is acceptable, at least in the design point of view for the serviceability and ultimate limit states. More results can be found in the Annex 7.

The shear resistance of the beams tested in the experimental program (V^{exp}) is compared to the results obtained in the numerical simulations (V^{FEM}), and the results are presented in Table 7.7. It is possible to notice that the numerical predictions of the ultimate load are in good agreement with the experimental results. In fact, V^{exp}/V^{FEM} presented an average value of about 1.03 and 0.99 for the A and B Series, respectively.
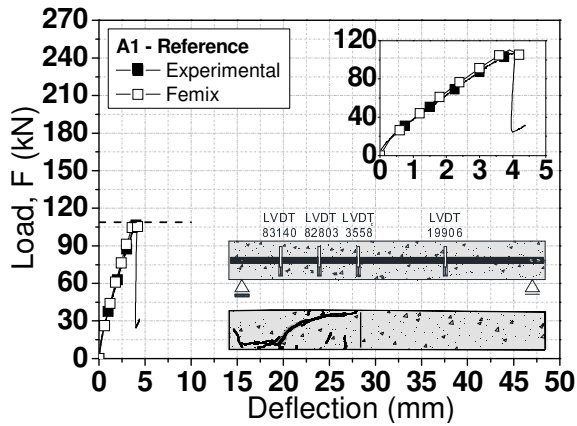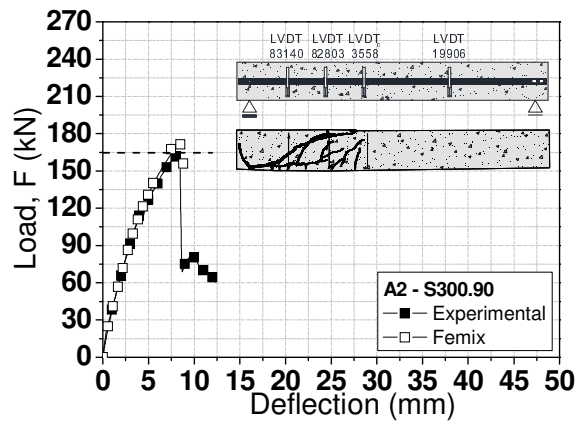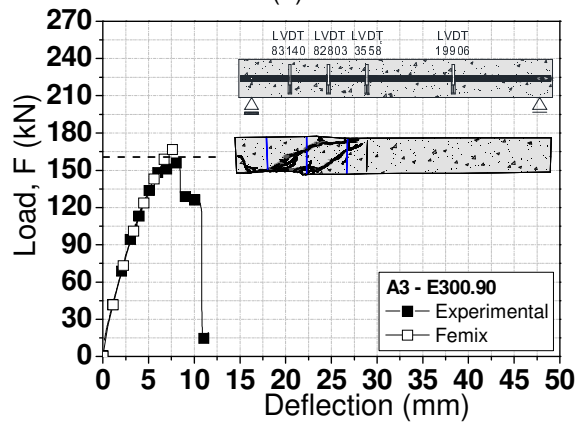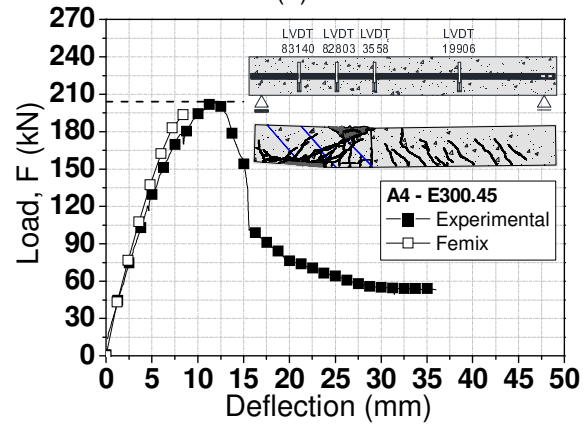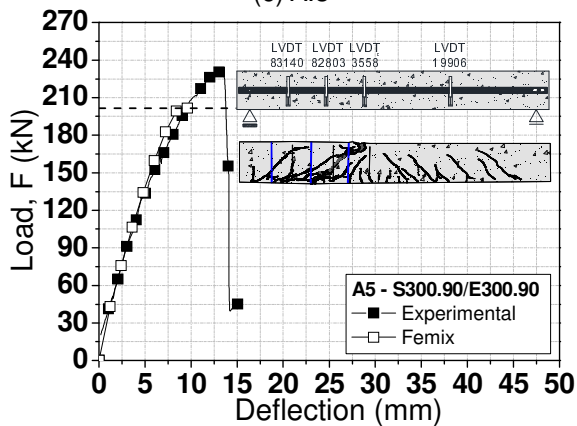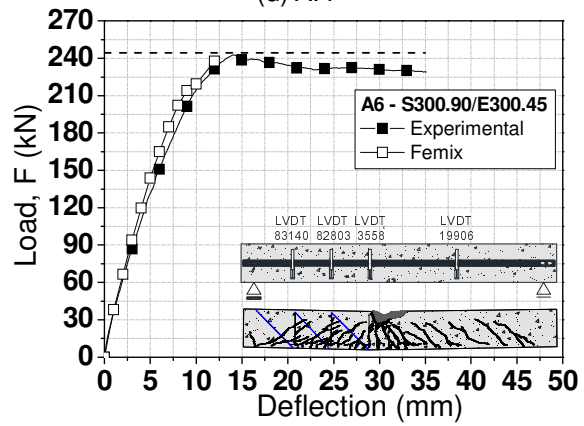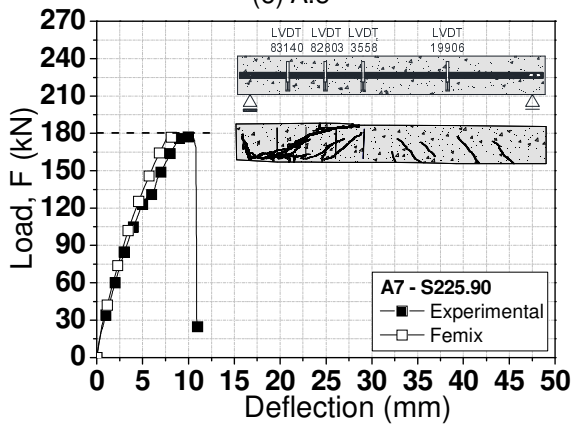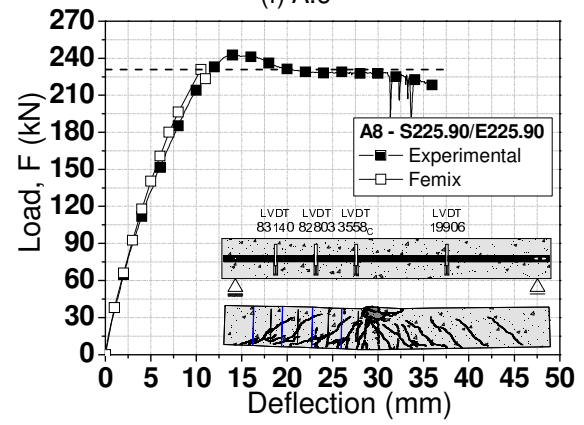
Figure 7.19: Load-deflection at the loaded section for the beams of A Series.
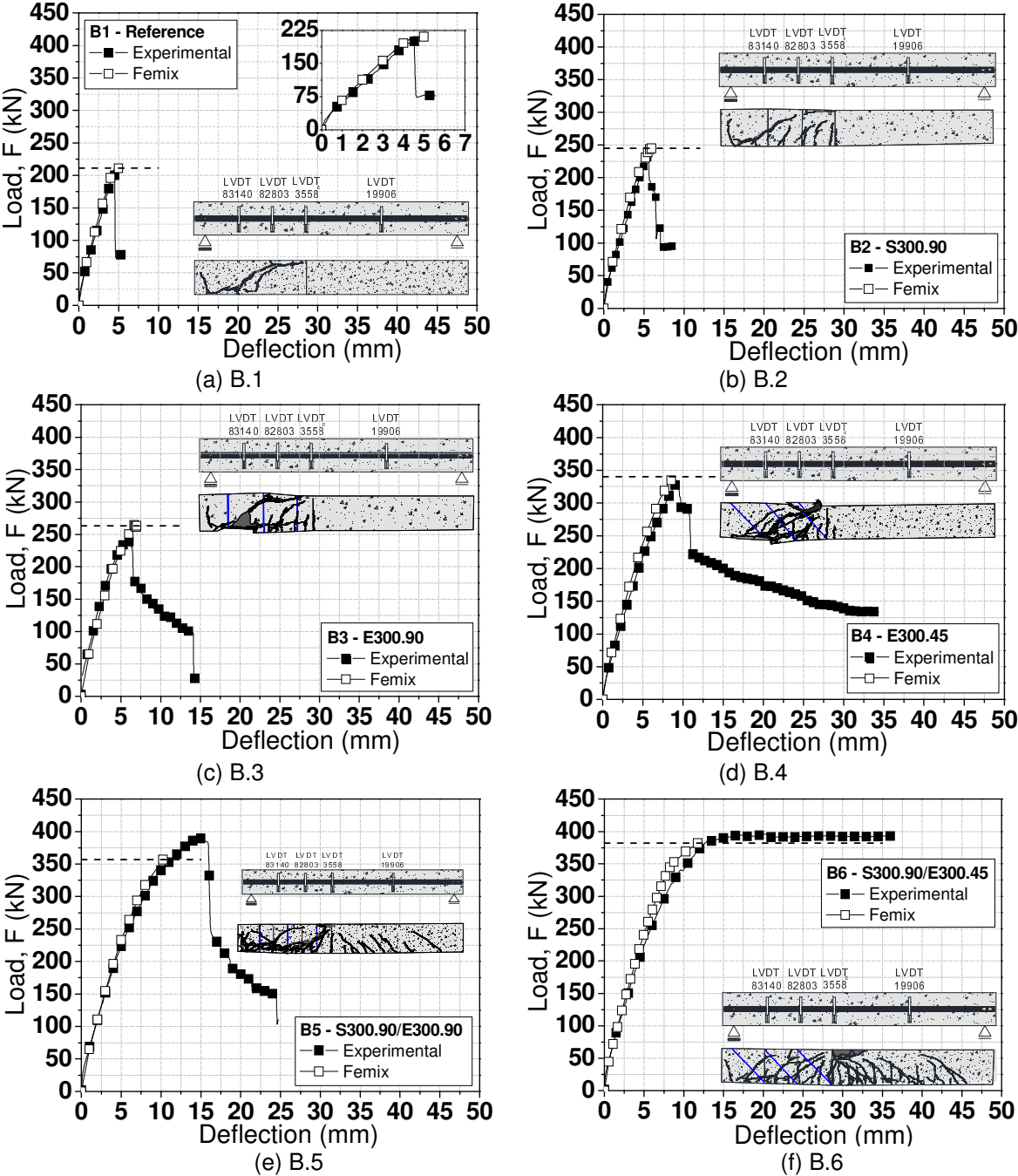
Figure 7.20: Load-deflection at the loaded section for the beams of B Series.
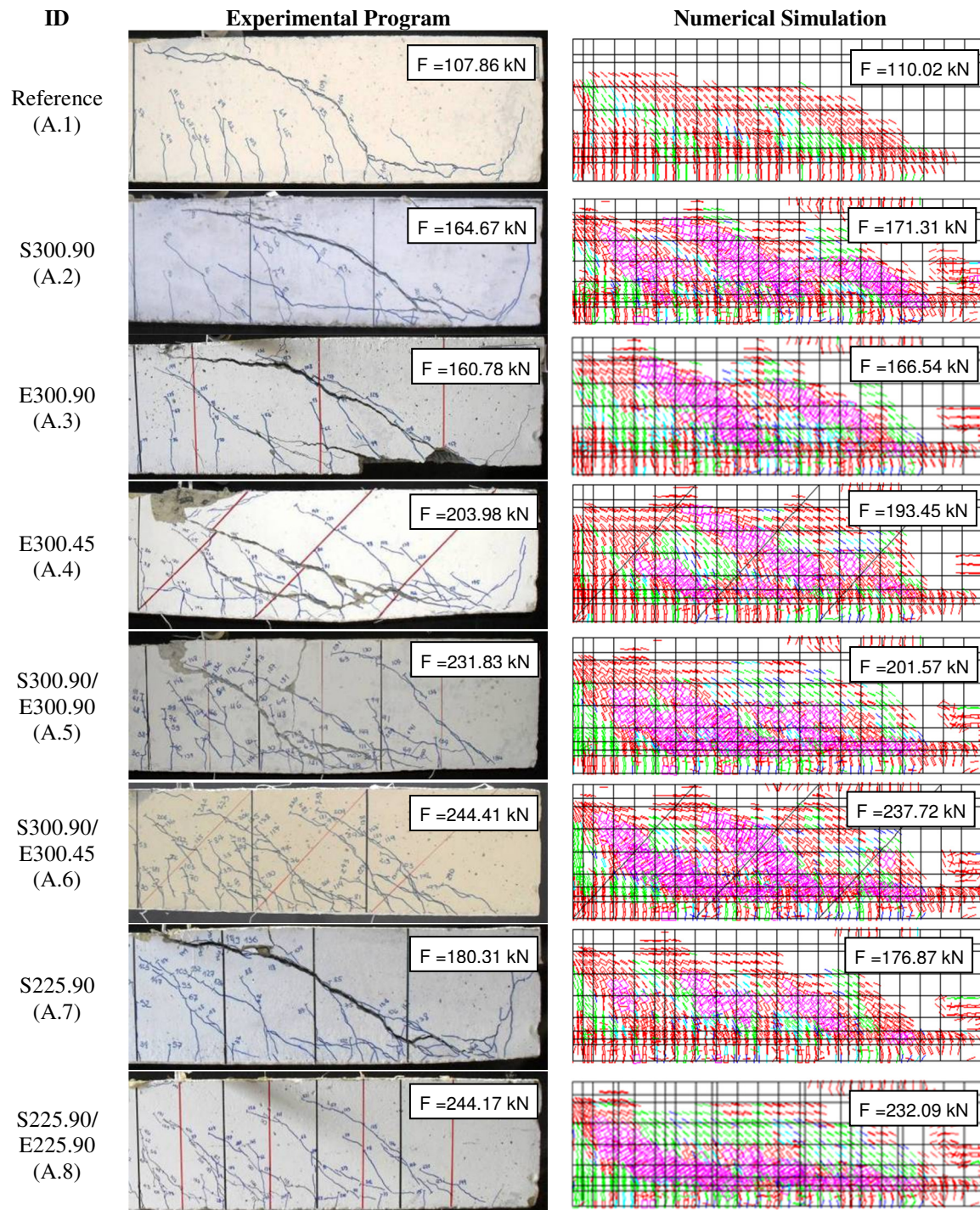
Figure 7.21: Crack patterns of the beams of A Series (in pink colour: crack completely open; in red colour: crack in the opening process; in cyan colour: crack in the reopening process; in green colour: crack in the closing process; in blue colour: closed crack).

ID	Experimental Program	Numerical Simulation
Reference (B.1)	F = 203.36kN	F = 211.14kN
S300.90 (B.2)	F = 232.31kN	F = 244.97 kN
E300.90 (A.3)	F = 237.88 kN	F = 264.80 kN
E300.45 (A.4)	F = 336.19 kN	F = 339.95 kN
S300.90/ E300.90 (A.5)	F = 390.11 kN	F = 356.60 kN
S300.90/ E300.45 (A.6)	F = 396.51 kN	F =381.95 kN
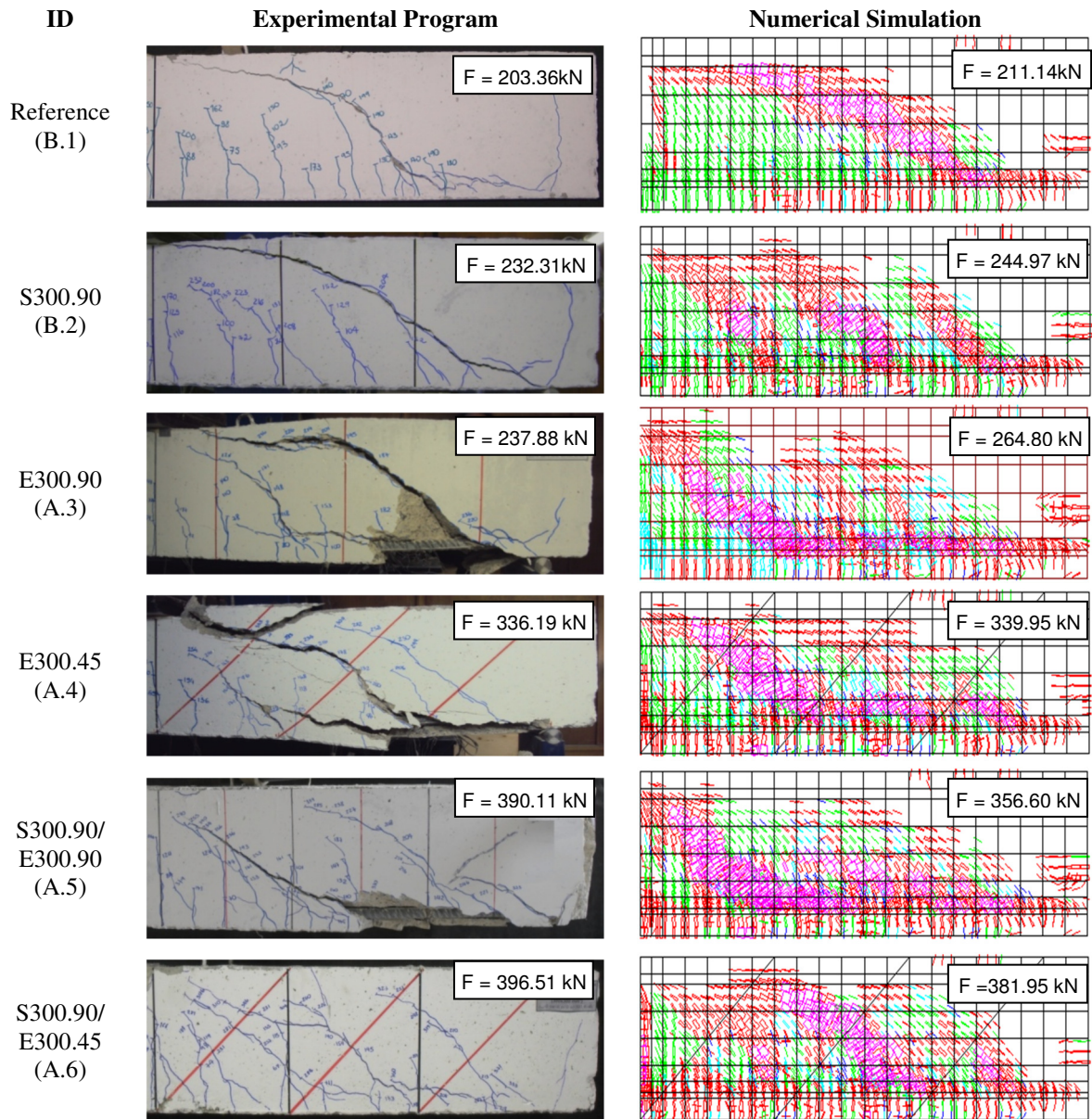
Figure 7.22: Crack patterns of the beams of B Series (in pink colour: crack completely open; in red colour: crack in the opening process; in cyan colour: crack in the reopening process; in green colour: crack in the closing process; in blue colour: closed crack).
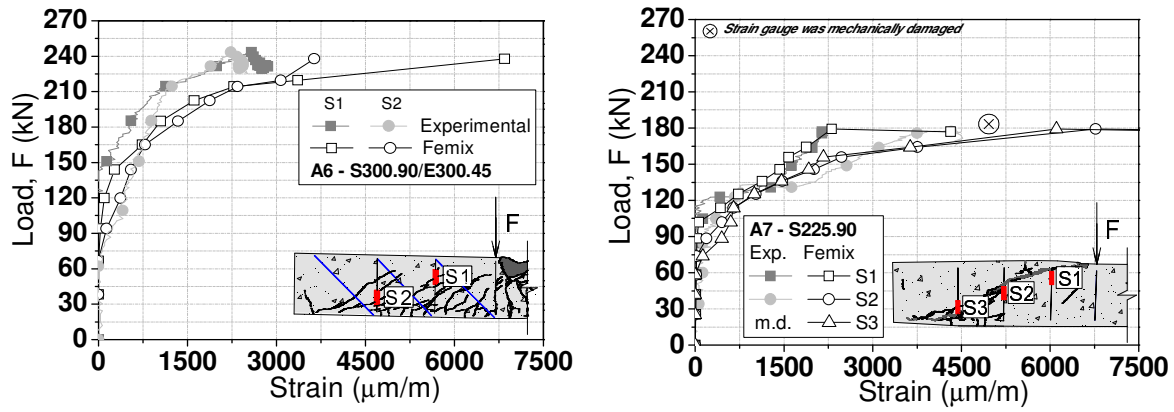
Figure 7.23: Relationship between Load-Strain in the steel stirrups for the beams A.6 and A.7.
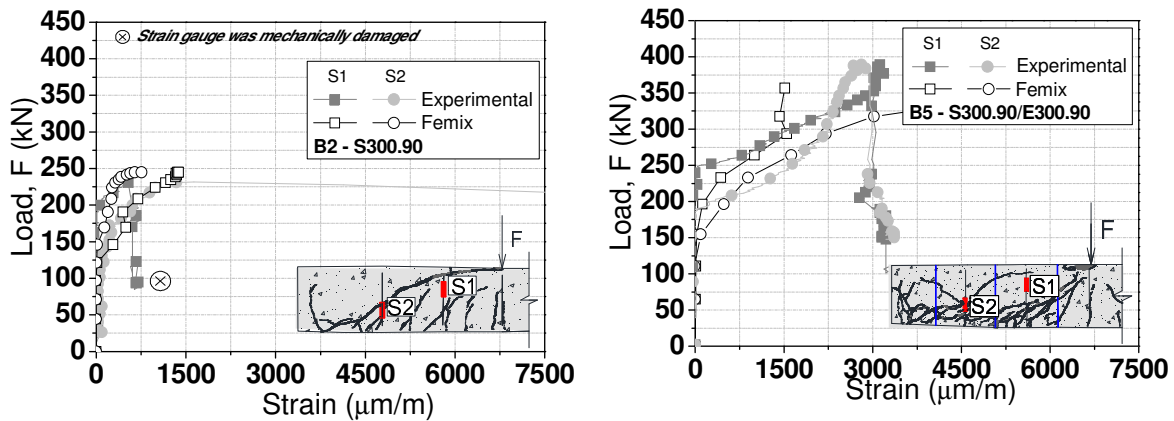
Figure 7.24: Relationship between Load-Strain in the steel stirrups for the beams B.2 and B.5.

Table 7.7: Numerical *vs* experimental results for ETS technique.

Specimen		Experimental				Femix		
		V_c (kN)	V_s (kN)	V_f (kN)	V^{exp} (kN)	F_{FEM} (kN)	V_{FEM} * (kN)	$\dfrac{V^{exp}}{V^{FEM}}$
A.1	Reference		-------	-------	65.32	110.02	66.01	0.99
A.2	S300.90		33.48	-------	98.80	171.31	102.79	0.96
A.3	E300.90		-------	31.15	96.47	166.54	99.92	0.96
A.4	E300.45		-------	57.07	122.39	193.45	116.07	1.05
A.5	S300.90/ E300.90	65.32	33.48	40.30	139.10	201.57	120.94	1.15
A.6	S300.90/ E300.45		33.48	47.85	146.65	237.72	142.63	1.03
A.7	S225.90		42.87	-------	108.19	176.87	106.12	1.02
A.8	S225.90/ E225.90		42.87	37.31	146.50	232.09	139.25	1.05
B.1	Reference		--------	--------	122.02	211.14	126.68	0.96
B.2	S300.90		17.37	--------	139.39	244.97	146.98	0.95
B.3	E300.90		--------	21.31	143.33	264.80	157.88	0.90
B.4	E300.45	122.02	--------	79.69	201.71	339.95	203.97	0.99
B.5	S300.90/ E300.90		17.37	94.68	234.07	356.60	213.96	1.09
B.6	S300.90/ E300.45		17.37	97.52	237.91	381.95	229.17	1.04
* The numerical models reached their maximum convergence								

7.4 CONCLUSIONS

This chapter presented the relevant results of an experimental program for the assessment of the effectiveness of the Embedded Through-Section (ETS) technique for the shear strengthening of reinforced concrete beams. The influence of the following parameters was investigated: spacing of the existing steel stirrups (225 and 300 mm), spacing (225 and 300 mm) and inclination of the strengthening bars (vertical and 45-degree), width of the cross section of the beam. When available experimental data on the use of EBR and NSM technique for the shear resistance of RC beams is considered (Dias and Barros, 2012), the obtained results show that, for the same shear strengthening ratio, ETS technique provides higher increase in terms of load carrying and deflection capacity than FRP-based shear strengthening techniques. The ETS technique can be used to avoid the occurrence of shear failure in RC beams, by converting this brittle failure mode in a ductile bending failure mode. Furthermore, in the ETS technique conventional steel bars are used instead of FRP reinforcements that are much more expensive. These steel bars can be bonded to concrete with cement based matrix that incorporates a small percentage of resin based-component. Since ETS steel bars have a relatively thick concrete cover, corrosion and injuries due to vandalism acts are not a concern.

The capability of the ACI and Eurocode 2 design guidelines to evaluate the shear resistance of the tested beams was appraised by using the experimental results. A good agreement between the experimental and analytical values was obtained, mainly when using the ACI 318 approach.

Using the obtained experimental results, the capability of a FEM-based computer program to predict with high accuracy the behavior of this type of structures up to its collapse was highlighted. Quite good predictions of the deformational behavior and crack pattern of the tested beams were obtained, even when the values of the parameters of the constitutive model are directly determined from the results obtained in experimental tests with specimens of the involved materials, which is the current source of data that a designer has in structural strengthening practice.

7.5 BIBLIOGRAPHY

ACI Committee 318, "Building code requirements for structural concrete and Commentary (ACI 318-08)", Reported by committee 318, American Concrete Institute, Detroit, 2008.

ACI Committee 440, "Guide for the design and construction of externally bonded FRP systems for strengthening concrete structures", American Concrete Institute; 2008, 80 pp., 2008.

ASTM 370, "Standard test methods and definitions for mechanical testing of steel products", American Society for Testing and Materials, 2002.

Dias, S.J.E., Barros, J.A.O., "Experimental behaviour of RC beams shear strengthened with NSM CFRP laminates", Strain - An International Journal for Experimental Mechanics, 48(1), 88-100, 2012.

"Eurocode 2: Design of concrete structures - part 1: General rules and rules for buildings EN 1992-1-1:2004:E", European Committee for Standardization, Brussels, December, 2004.

ISO 527-2, "Plastics - Determination of Tensile Properties - Part 2: Test Conditions for Moulding and Extrusion Plastics", International Organization for Standardization (ISO), Geneva, Switzerland, 1993.

LNEC NP-E397, "Concrete - Assessment of the elasticity modulus under uniaxial compression", Laboratório Nacional de Engenharia Civil (in Portuguese), 1993.

Rots J.G., de Borst R., "Analysis of mixed-mode fracture in concrete", Journal of Engineering Mechanics, ASCE, 113(11), pp. 1739-1758, 1987.

Sena-Cruz, J. M., "Strengthening of concrete structures with near-surface mounted CFRP laminate strips", PhD Thesis, Department of Civil Engineering, University of Minho, Guimarães, Portugal, 2004.

Ventura-Gouveia, A., Barros, J. A. O., Azevedo, A., Sena-Cruz, J. M., "Multi-fixed smeared 3D crack model to simulate the behavior of fiber reinforced concrete structures", CCC 2008 - Challenges for Civil Construction, 2008.

Ventura-Gouveia, A., "Constitutive models for the material nonlinear analysis of concrete structures including time-dependent effects", PhD thesis, University of Minho, Portugal, 2012.

"One day you will look back and see that your problems
were, in fact, the steps that led you to victory"
Unknown author

Chapter 8
SUMMARY, CONCLUSIONS AND FUTURE WORKS

8.1 SUMMARY AND CONCLUSIONS

In this doctoral thesis the potentialities of the Near Surface Mounted (NSM) technique for the increase of the load carrying capacity of two spans continuous RC slabs are explored. Carbon fiber reinforced polymer (CFRP) laminates of rectangular cross section were used. The experimental program was composed of eight $120\times375\times5875$ mm^3 RC slab strips. Three of them were unstrengthened RC slabs forming a control set (SL15-HS, SL30-HS and SL45-HS), and the other five slabs were strengthened with CFRP strips according to the NSM technique (SL15s25-HS, SL30s25-HS, SL30s50-HS, SL45s25-HS and SL45s50-HS) applied in both sagging and hogging regions (HS Series). The results obtained in this work were compared to the ones obtained by Bonaldo (2008). The amount and disposition of the steel bars were designed to assure a moment redistribution percentages of 15%, 30% and 45%. The NSM CFRP systems applied in the flexurally strengthened RC slabs were designed to increase in 25% and 50% the load carrying capacity of the reference slab. From the obtained results, it was verified that the strengthening configurations composed by laminates only applied in the hogging region did not attain the target increase of the load carrying capacity. In fact, when the CFRP laminates were applied in the hogging region, an increase of the load carrying capacity of 8.02%, 19.76%, 5.93%, 9.15%, 2.86% and 8.46% was registered for the slab strips SL15s25-H, SL15s50-H, SL30s25-H, SL30s50-H, SL45s25-H and SL45s50-H, respectively. These values were obtained when a concrete compressive strain of 3.5‰ was recorded in the sagging regions. When applying CFRP laminates in both sagging and hogging regions (HS series), an increase of the load carrying capacity of 36.11%, 29.84%, 49.44%, 24.42% and 37.24% was attained for the slab strips SL15s25-HS, SL30s25-HS, SL30s50-HS, SL45s25-HS and SL45s50-HS, respectively. Thus, the target increase of the load carrying capacity was attained.

A moment redistribution percentage (η) lower than the predicted one was determined in the slabs strengthened with CFRP laminates in the hogging region (H). For this strengthening configuration the η has decreased with the increase of the CFRP percentage. However, adopting a flexural strengthening strategy composed of CFRP laminates applied in both hogging and sagging regions, the target values for the moment redistribution capacity was attained, and the influence of the percentage of CFRP is marginal on the η. For this configuration of NSM laminates, the flexural strengthening performance was limited by

the detachment of the concrete cover that includes the laminates or by the formation of a shear crack in the hogging region.

Numerical analyses were carried out to simulate the load-deflection relationship of concrete elements reinforced with conventional steel bars and strengthened by NSM CFRP laminate strips. In general, the numerical simulations have reproduced with high accuracy the behavior of the carried out tests.

A parametric study composed of 144 numerical simulations was carried out to investigate the influence of the strengthening arrangement and CFRP percentage in terms of load carrying capacity and moment redistribution capacity of continuous RC slab strips flexurally strengthened by the NSM technique. According to the results, the load carrying and the moment redistribution capacities strongly depend on the flexural strengthening arrangement. The load carrying capacity of the strengthened slabs increases with $\rho_{s,eq}^{S}$ and $\rho_{s,eq}^{H}$, but the increase is much more pronounced with $\rho_{s,eq}^{S}$, specially up to the formation of the plastic hinge in the hogging region ($\rho_{s,eq} = A_{sl}/bd_{s} + (A_{f}E_{f}/E_{s})/(bd_{f})$ is the equivalent reinforcement ratio. The moment redistribution has increased with $\rho_{s,eq}^{S}/\rho_{s,eq}^{H}$, and positive values (*MRI*>0, which means that the moment redistribution of the strengthened slab was higher than its corresponding reference slab) were obtained when $\rho_{s,eq}^{S}/\rho_{s,eq}^{H}$ >1.09, $\rho_{s,eq}^{S}/\rho_{s,eq}^{H}$ >1.49 and $\rho_{s,eq}^{S}/\rho_{s,eq}^{H}$ >2.27 for η equal to 15%, 30% and 45%, respectively. Thus, the moment redistribution percentage can be estimated if $\rho_{s,eq}^{S}/\rho_{s,eq}^{H}$ is known. The results evidenced that the use of efficient strengthening strategies can provide adequate level of ductility and moment redistribution in statically indeterminate structures, with a considerable increase in the load carrying capacity.

An analytical model was developed and its performance was appraised by using the data obtained from the experimental program in order to predict the load-deflection response of continuous RC slabs up to its collapse. The proposed model is based on the constitutive laws for the intervening materials, strain compatibility and equilibrium of the cross sections representative of the structure. The predictive performance of the model was appraised by simulating two series of tests composed of seventeen RC slab strips strengthened with NSM CFRP laminates, grouped in two series that are different in terms of strengthening configuration: H series, where H is the notation to identify the slabs

strengthened with NSM CFRP laminates exclusively applied in the hogging region; HS series, where HS is the notation to identify the slabs strengthened with NSM CFRP laminates applied in both hogging and sagging regions. The results showed that the developed numerical strategy is capable of capturing with enough accuracy the relevant features observed experimentally.

The effectiveness of the NSM technique can be compromised by the formation of shear cracks in the hogging region of the flexural strengthened elements. Moreover, in some cases, the failure mode shifts from ductile flexural failure to brittle shear failure after a flexural strengthening. The shear failure of the retrofitted system should be avoided, once this failure is often brittle and occur with little or no visible warnings. In this context, an innovative technique herein designated as Embedded Through-Section (ETS) was developed for the shear strengthening of RC beams. To assess the contribution of the bond mechanism of the ETS bars in the context of the shear strengthening, and to better select the type of strengthening bars and adhesive materials, a comprehensive pull-out program was firstly executed. Based on the results, it was noted that the bond behavior between bars and concrete depends on the type of adhesive chosen for the strengthening system. With the values adopted for the anchorage length and for the adhesive layer thickness, the bond strength is marginal affected, but this last property has increased with the Young's modulus of the adhesive. Additionally, from the obtained results, it seems that for the interval of values considered for the adhesive thickness, this thickness has no significant influence on the type of failure mode and on the average bond strength.

Finally, the influence of the following parameters on the shear strengthening effectiveness of the ETS technique was investigated: spacing of the existing steel stirrups (225 and 300 mm), spacing (225 and 300 mm) and inclination of the strengthening bars (vertical and 45-degree), width of the cross section of the beam. When available experimental data on the use of EBR and NSM technique for the shear resistance of RC beams is considered, the obtained results show that, for the same shear strengthening ratio, ETS technique provides increase levels of load carrying and deflection capacities higher than those guaranteed by FRP-based shear strengthening techniques. The ETS technique can be used to avoid the occurrence of shear failure in RC beams. Furthermore, in the ETS technique it can be used low cost steel bars bonded to concrete with cement based matrix that incorporates a small

percentage of resin based-component. Since ETS steel bars have a relatively thick concrete cover, corrosion and injuries due to vandalism acts are not a concern.

The capability of the ACI and Eurocode 2 design guidelines to evaluate the shear resistance of the tested beams was appraised by using the experimental results. A good agreement between the experimental and analytical values was obtained, mainly when using the ACI 318 approach. Using the obtained experimental results, the capability of a FEM-based computer program to predict with high accuracy the behavior of this type of structures up to its collapse was highlighted. Quite good predictions of the deformational behavior and crack pattern of the tested beams were obtained, even when the values of the parameters of the constitutive model are directly determined from the results obtained in experimental tests with specimens of the involved materials, which is the current source of data that a designer has in structural strengthening practice.

8.2 SUGGESTIONS FOR FUTURE WORKS

Once NSM strengthening can increase the flexural capacity up to a level higher than the shear capacity of the member, the load carrying capacity of the strengthened slabs can be limited by the detachment of the strengthened concrete cover layer at the intermediate support or due to the formation of a shear failure crack in the hogging region. Therefore, to increase the effectiveness of this NSM flexural strengthening technique by avoiding shear failure, a hybrid strengthening strategy should be developed by combining NSM laminates for the flexural resistance and ETS steel bars for the shear resistance.

To increase the flexural and shear capacity, and simultaneously avoiding premature detachment of the concrete cover that includes the NSM laminates, the NSM/ETS technique schematically represented in Figure 8.1 is proposed. A FRP strand is proposed to stitch the ETS strengthening bars and the CFRP laminates, which provides a supplementary confinement to the concrete surrounding the laminates. As previously mentioned in the ETS technique, holes are opened through the slab thickness. Additionally, before the installation of the CFRP laminates, notches are executed in the top surface of the element, with a depth between 3 and 5 mm in order that the FRP strands stay above the

laminates in the critical detachment region. The FRP strands and the strengthening bars are positioned and, finally, bonded to concrete with an adhesive material.
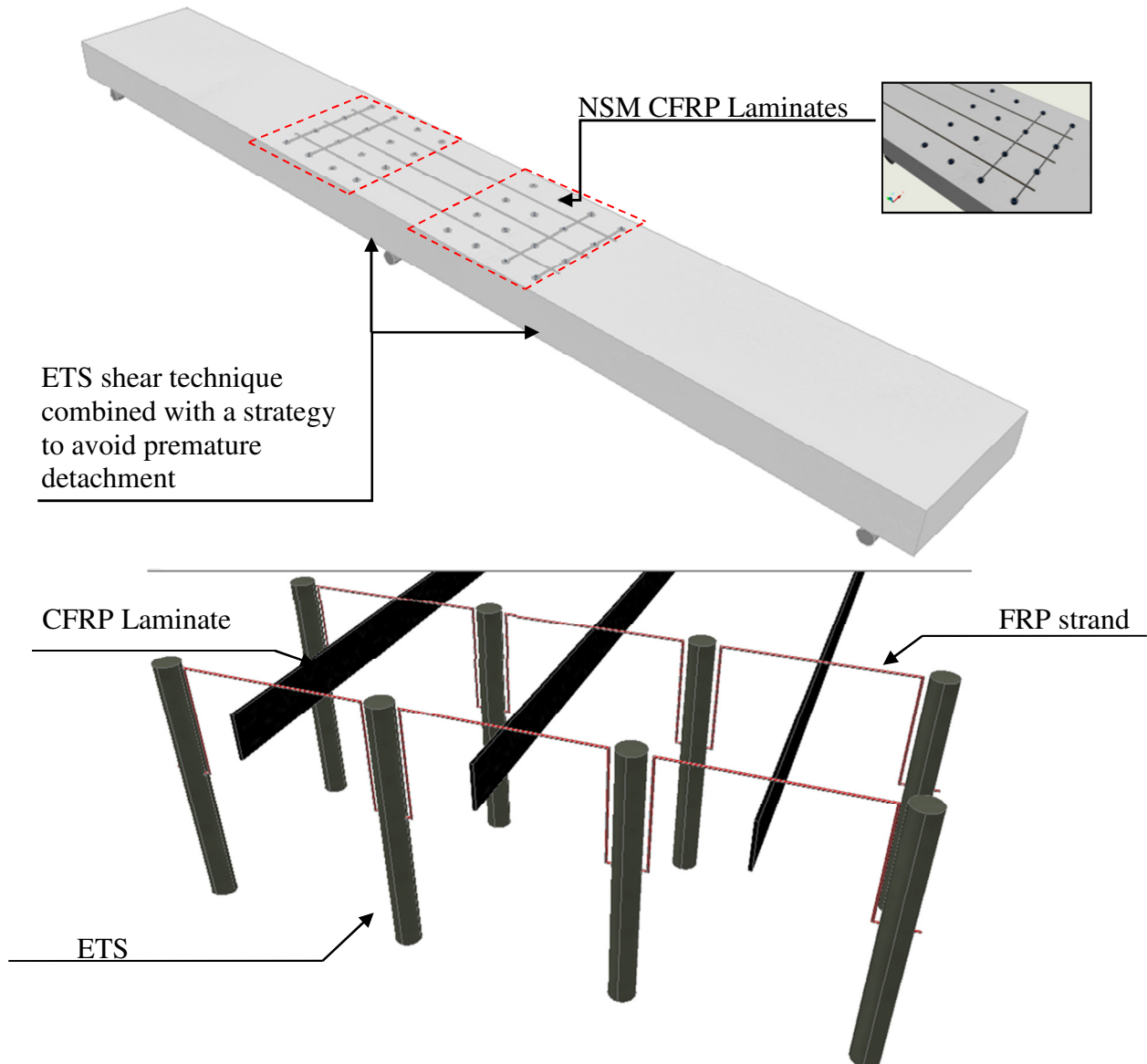
Figure 8.1: NSM/hybrid strengthening strategy: Slab strip strengthened according to the proposed techniques (ETS shear technique and a strategy to avoid the premature detachment of the concrete cover that includes the NSM bars).

A comprehensive experimental program to evaluate the influence of relevant parameters on the effectiveness of the NSM/ETS strengthening technique should be carried out, by considering: (i) pre-cracked members prior the application of NSM strengthening; (ii) ratio of NSM strengthening area to internal steel reinforcement area; (iii) arrangement of the NSM strengthening system (i.e., distribution of the FRP strengthening in the hogging and/or sagging regions, etc.); (iv) influence of the concrete compressive strength; (v) type

of strengthening bars in terms of material, diameter and surface treatment; and (vi) type of adhesives in terms of materials and layer thickness and position of the strengthening systems.

Additional investigations are needed concerning the ETS technique. An analytical model could be developed in order to predict the shear resistance provided by a certain ETS configuration, taking into account the geometry and the properties of the existing materials, the load configuration and the properties of the strengthening materials.

Finally, an analytical model to design the NSM/ETS strengthening technique for continuous RC beams/slabs should be developed. This analytical model should take into account the geometry and the properties of the existing materials, the positioning of NSM/ hybrid systems, load configuration and the properties of the strengthening materials.

ANNEXES

Chapter 3
ANNEXES

ANNEX 3.1 - MATERIALS PROPERTIES

Table A3.1.1: Concrete average compressive strength (Bonaldo, 2008).

At 28 days		At the slabs testing age	
Slab ID	f_{cm} (N/mm^2)	Age (days)	f_{cm} (N/mm^2)
SL15-H	40.07 (0.59)	126	44.38 (1.06)
SL30-H	35.99 (0.51)	105	44.91 (1.33)
SL45-H	41.41 (0.22)	204	49.29 (1.76)
(value) = Standard deviation in MPa, f_{cm} = mean cylinder compressive strength, E_{cm} = modulus of elasticity			

Table A3.1.2: Mechanical properties of the reinforcing steel (Bonaldo, 2008).

Steel bar diameter (ϕs)	Sample ID	Modulus of elasticity (kN/mm^2)	Yield stress (0.2 %)[a] (N/mm^2)	Strain at yield stress[b]	Tensile strength (N/mm^2)
6 mm	1	187.22	449.28	0.0026	568.28
	2	206.37	449.28	0.0024	569.09
	3	187.82	444.42	0.0026	562.61
	Average	193.80	447.66	0.0025	566.66
	Std. Dev.	10.890 (5.62%)	2.81 (0.63%)	0.0001 (4.68%)	3.53 (0.62%)
8 mm	1	195.40	423.93	0.0024	578.30
	2	203.16	420.29	0.0023	576.93
	3	203.84	419.83	0.0023	581.03
	Average	200.80	421.35	0.0023	578.75
	Std. Dev.	4.69 (2.33 %)	2.25 (0.53 %)	0.0001 (2.65 %)	2.09 (0.36 %)
10 mm	1	183.33	463.37	0.0027	576.44
	2	175.86	441.80	0.0027	573.82
	3	175.52	435.68	0.0027	577.61
	Average	178.23	446.95	0.0027	575.95
	Std. Dev.	4.42 (2.48 %)	14.55 (3.25 %)	0.0000 (0.45 %)	1.94 (0.34 %)
12 mm	1	192.20	427.83	0.0024	528.41
	2	200.11	449.69	0.0024	545.41
	3	202.76	449.89	0.0024	545.82
	Average	198.36	442.47	0.0024	539.88
	Std. Dev.	5.49 (2.77 %)	12.68 (2.87 %)	0.0000 (0.19%)	9.93 (1.84%)

[a] Yield stress determined by the "Offset Method", according to ASTM 370 (2002)
[b] Strain at yield point, for the 0.2 % offset stress
(value) Coefficient of Variation (COV) = (Standard deviation/Average) x 100

Table A3.1.3: Mechanical properties of the CFRP laminates (Bonaldo, 2008).

CFRP laminate cross section height	Sample ID	Ultimate tensile stress (N/mm^2)	Ultimate tensile strain (‰)	Modulus of Elasticity [a] (kN/mm^2)
10 mm	1	2879.13	18.45	156.100
	2	2739.50	17.00	158.800
	3	2952.00	17.70	166.600
	4	2942.32	17.81	153.620
	5	2825.20	17.40	161.400
	Average	2867.63	17.67	159.304
	Std. Dev.	88.10 (3.07%)	0.54 (3.04%)	5.01 (3.15%)

[a]According to ISO 527-1 and ISO 527-5 (1993)

(value) Coefficient of Variation (COV) = (Standard deviation/Average) x 100

ANNEX 3.2 - PREDICTION OF THE SLAB STRIP FLEXURAL CAPACITY

Figure A3.2.1 illustrates the internal strain and stress distribution for the CFRP strengthened sections under flexure at the ultimate limit state. The abovementioned assumptions were used to determine the nominal flexural strength of a section strengthened with an externally FRP system:

(a) Design calculations are based on the dimensions, internal reinforcing steel arrangement and material properties of the existing member being strengthened;

(b) The strains in the steel reinforcement and concrete are directly proportional to the distance from the neutral axis. That is, a plane section before loading remains plane after loading;

(c) There is no relative slip between the FRP reinforcement, the adhesive and the concrete substrata;

(d) The shear deformation within the adhesive layer is neglected because the adhesive layer is very thin with slight variations in its thickness;

(e) The maximum usable compressive strain in the concrete is 0.0035;

(f) The tensile strength of concrete is neglected; and

(g) The FRP reinforcement has a linear elastic stress-strain relationship to failure.
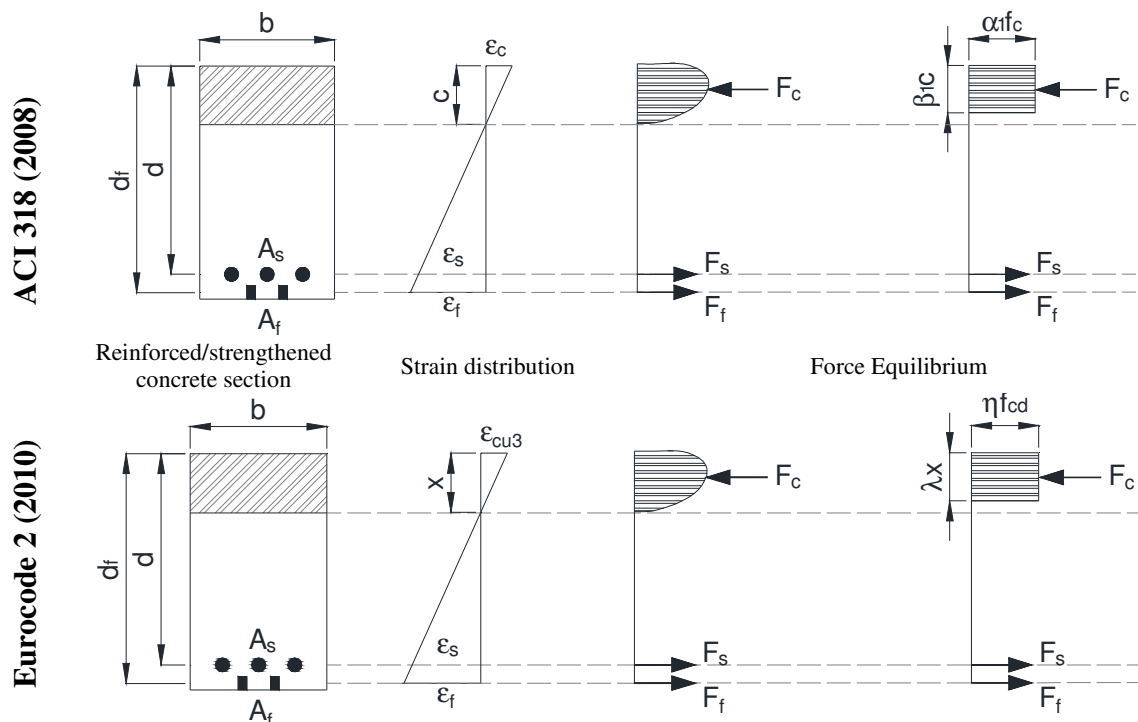
Figure A3.2.1: Internal strain and stress distribution for a rectangular section under flexure at ultimate limit state.

A3.2.1 H series

The terms α_1 and β_1 are parameters defining a rectangular stress block in the concrete equivalent to the nonlinear distribution of stress. If concrete crushing is the controlling mode of failure (before or after steel yielding), α_1 and β_1 can be taken as the values associated with the Whitney stress block. In the calculations of the slab strips flexural capacity according to the ACI 318 (2008), the following parameters were taken:

$\beta_1 =$ is the ratio of the depth of the equivalent rectangular stress block to the depth of the neutral axis [according to ACI 318 (2008, Section R10.2.7)], β_1 factor is 0.85 for concrete strength, f_c (herein considered as f_{cm}), up to 27.57 N/mm². For concretes of a compressive strength above 27.57 N/mm², β_1 is reduced continuously at a rate of 0.05 for each 6.89 N/mm² of strength in excess of 27.57 N/mm², but β_1 shall not be taken less than 0.65. Therefore, according to the concrete average compressive strength at 28 days presented in Table A3.1.1, β_1 is herein taken equal to 0.75, 0.79 and 0.75 for SL15-H, SL30-H and SL45-H series, respectively;

$\alpha_1 = 0.85$;

f_{cm} = value corresponding to each slab at 28 days (Annex 3.1, Table A.3.1.1);

f_s = 421.35 N/mm² for ϕ_s = 8mm; 446.95 N/mm² for ϕ_s = 10mm and 442.47 N/mm² for ϕ_s = 12mm (Bonaldo, 2008); and

E_f = 159.30 kN/mm² (Bonaldo, 2008).

For the calculations according to the Eurocode 2 (2010), the factor λ, defining the effective height of the compression zone and the factor η, defining the effective strength, follow from:

$$\lambda = 0.8 \text{ for } f_{ck} \leq 50\text{MPa}$$
$$\lambda = 0.8 - (f_{ck} - 50)/400 \text{ for } 50 \leq f_{ck} \leq 90\text{MPa}$$
(A3.1)

and

$$\eta = 1.0 \text{ for } f_{ck} \leq 50\text{MPa}$$
$$\eta = 1.0 - (f_{ck} - 50)/200 \text{ for } 50 \leq f_{ck} \leq 90\text{MPa}$$
(A3.2)

Considering the failure mode controlled by crushing of the concrete in compression and the yielding of the steel reinforcement, the internal forces are calculated as follows:

- Compressive force (F_c):

$$F_c = \beta_1 \cdot c \cdot b \cdot \alpha_1 \cdot f_{cm} \text{ (ACI 318, 2008)}$$ (A3.3)

$$F_c = \lambda \cdot x \cdot b \cdot \eta \cdot f_{cm} \text{ (Eurocode 2, 2010)}$$

- Tensile Force (F_s):

$$F_s = A_s \cdot f_y$$ (A3.4)

Due to the determination of the strain distribution, the neutral axis depth, x, is initially assumed and the correct value is iteratively determined when the equilibrium of internal forces is satisfied. Strains and stresses in different materials can be calculated.

$$\sum F_i = 0 \rightarrow F_c = F_s$$ (A3.5)

Consequently, the flexural strength, M_{rd}, is calculated by taking moments of internal forces about the level of tensile steel as follows:

$$M_{rd} = F_c \cdot z = F_s \cdot z$$ (A3.6)

where:

$$z = d_s - \frac{\lambda x}{2} \text{ (Eurocode 2)}$$

$$z = d_s - \frac{\beta_1 c}{2} \text{ (ACI R318-08)}$$

It should be noted that all the slabs strips have a concrete cover of 26 mm thickness.

When introducing the CFRP laminate a similar approach is used to calculate the flexural resistance of a strengthened section. In this way, a term concerning to force developed by the FRP material is added and the internal forces equilibrium is given by:

- Tensile force at CFRP laminate strips (F_f):

$$F_f = A_f \cdot \varepsilon_f \cdot E_f \tag{A3.7}$$

$$\sum F_i = 0 \rightarrow F_c = F_s + F_f \tag{A3.8}$$

The maximum strain level that can be achieved in the FRP reinforcement is governed by either of the following conditions: (i) the strain level developed in the FRP at the point at which concrete crushes, (ii) the strain level when the FRP ruptures, or (iii) the strain level when the FRP debonds from the substrate (ACI 440, 2008). For each internal arrangement, based on the theory of elasticity, the bending capacities of sagging and hogging regions were calculated, as well as the strains at the laminates when reaching a compressive strain of $\varepsilon_c = 3.5\%_0$. The elastic bending at sagging and hogging regions are presented in Tables A3.2.1 to A.3.2.3. In these Tables, n_f is the number of CFRP laminates applied at the sagging or hogging regions, A_s is the cross sectional area of the steel bars in tension, x or c are the neutral axis depth, M_{rd} is the elastic bending in the analysed section.

Table A3.2.1: Elastic bending at sagging and hogging regions – SL15-H Series.

Slab strip ID		n_f	A_s (mm²)	x (mm)	$M_{rd\,(1)}$ (kN·m)	c (mm)	$M_{rd\,(2)}$ (kN·m)	$M_{rd\,(3)}$ (kN·m)	$M_{rd\,(4)}$ (kN·m)
S1-S1´	SL15-H	----	603.19	27.53	22.07	21.94	22.47	23.68	24.24
	SL15s25-H	-----	603.19	27.53	22.07	21.94	22.47		30.29
	SL15s50-H	-----	603.19	27.53	22.07	21.94	22.47		36.35
S2-S2´	SL15-H	-----	565.49	26.12	21.07	20.81	21.44	22.57	22.68
	SL15s25-H	3	565.49	31.96	26.01	26.87	28.42	29.19	28.35
	SL15s50-H	7	565.49	37.10	30.14	31.96	34.02	35.32	34.02

(1) Calculated according to the recommendations of ACI 318; (2) Calculated according to the recommendations of Eurocode 2; (3) Docros, (4) See Chapter 3, Figure 3.6.

Table A3.2.2: Elastic bending at sagging and hogging regions – SL30-H Series.

Slab strip ID		n_f	A_s (mm²)	x (mm)	$M_{rd\,(1)}$ (kN·m)	c (mm)	$M_{rd\,(2)}$ (kN·m)	$M_{rd\,(3)}$ (kN·m)	$M_{rd\,(4)}$ (kN·m)
S1-S1´	SL30-H	----	653.45	32.06	23.63	26.91	24.18	25.26	26.23
	SL30s25-H	-----	653.45	32.06	23.63	26.91	24.18		32.79
	SL30s50-H	-----	653.45	32.06	23.63	26.91	24.18		39.35
S2-S2´	SL30-H	-----	452.39	22.09	17.07	18.54	17.33	18.39	18.68
	SL30s25-H	2	452.39	27.46	21.48	23.93	22.74	23.88	23.35
	SL30s50-H	5	452.39	32.70	25.57	29.02	27.63	28.65	28.02

(1) Calculated according to the recommendations of ACI318; (2) Calculated according to the recommendations of Eurocode 2; (3) Docros; (4) Figure A3.3.1.

Table A3.2.3: Elastic bending at sagging and hogging regions – SL45-H Series.

Slab strip ID		n_f	A_s (mm^2)	x (mm)	$M_{rd\,(1)}$ (kN·m)	c (mm)	$M_{rd\,(2)}$ (kN·m)	$M_{rd\,(3)}$ (kN·m)	$M_{rd\,(4)}$ (kN·m)
S1-S1`	SL45-H	-----	728.85	32.47	26.30	25.87	26.89		28.23
	SL45s25-H	-----	728.85	32.47	26.30	25.87	26.89	28.15	35.29
	SL45s50-H	-----	728.85	32.47	26.30	25.87	26.89		42.35
S2-S2`	SL45-H	-----	336.15	14.92	13.05	11.89	13.18	14.85	14.68
	SL45s25-H	1	336.15	18.69	16.88	15.61	17.99	18.64	18.35
	SL45s50-H	3	336.15	23.46	21.56	20.13	23.64	24.46	22.02

[1] Calculated according to the recommendations of ACI318; [2] Calculated according to the recommendations of Eurocode 2; [3] Docros; [4] See Figure 3.3.2.

A3.2.2 HS series

Concerning to the slab strips of the HS series, the following parameters were taken:

According to the concrete average compressive strength at 28 days, presented in Table 3.7, β_1 is herein taken equal to 0.85, 0.84 and 0.74 for SL15-HS, SL30-HS and SL45-HS series, respectively;

$\alpha_1 = 0.85$;

f_{cm} = value corresponding to each slab at 28 days (Chapter 3, Table 3.7);

f_s = 421.35 N/mm^2 for ϕ_s = 8mm; 446.95 N/mm^2 for ϕ_s = 10mm and 442.47 N/mm^2 for ϕ_s = 12mm (Bonaldo, 2008); and

E_f = 159.30 kN/mm^2 for the CFRP laminate with cross section height of 10mm (Bonaldo, 2008) and 156.69 kN/mm^2 for the CFRP laminate with cross section height of 20mm.

For the calculations according to the Eurocode 2 (2010), the factor λ, defining the effective height of the compression zone and the factor η, defining the effective strength, follow from:

$$\lambda = 0.8 \text{ for } f_{ck} \leq 50\text{MPa}$$
$$\lambda = 0.8 - (f_{ck} - 50)/400 \text{ for } 50 \leq f_{ck} \leq 90\text{MPa}$$
and
$$\eta = 1.0 \text{ for } f_{ck} \leq 50\text{MPa}$$
$$\eta = 1.0 - (f_{ck} - 50)/200 \text{ for } 50 \leq f_{ck} \leq 90\text{MPa}$$

(A3.9)

(A3.10)

The elastic bending at sagging and hogging regions are presented in Tables A3.2.4 to A.3.2.6. In these Tables, n_f is the number of CFRP laminates applied at the sagging or hogging regions, A_s is the cross sectional area of the steel bars in tension, x or c are the neutral axis depth, M_{rd} is the elastic bending in the analysed section.

Table A3.2.4: Elastic bending at sagging and hogging regions – SL15-HS Series.

Slab strip ID		n_f	A_s (mm^2)	x (mm)	$M_{rd\,(1)}$ (kN·m)	c (mm)	$M_{rd\,(2)}$ (kN·m)	$M_{rd\,(3)}$ (kN·m)
S1-S1´	SL15-HS	----	603.19	36.91	20.65	33.33	21.27	22.38
	SL15s25-HS	2.5	603.19	44.72	24.85	41.35	26.36	28.10
S2-S2´	SL15-HS	-----	565.49	35.02	19.80	31.63	20.35	21.37
	SL15s25-HS	4	565.49	46.65	26.05	43.46	27.84	30.19

[1] Calculated according to the recommendations of ACI 318; [2] Calculated according to the recommendations of Eurocode 2; [3] Docros.

Table A3.2.5: Elastic bending at sagging and hogging regions – SL30-HS Series.

Slab strip ID		n_f	A_s (mm^2)	x (mm)	$M_{rd\,(1)}$ (kN·m)	c (mm)	$M_{rd\,(2)}$ (kN·m)	$M_{rd\,(3)}$ (kN·m)
S1-S1´	SL30-HS	----	653.45	38.21	22.65	34.10	23.35	24.44
	SL30s25-HS	3	653.45	46.95	27.92	43.09	29.79	30.87
	SL30s50-HS	6.5	653.45	53.32	31.45	49.52	34.06	35.16
S2-S2´	SL30-HS	----	452.39	26.32	16.60	23.49	16.93	17.85
	SL30s25-HS	2	452.39	35.37	22.73	32.57	24.10	24.58
	SL30s50-HS	3	452.39	38.37	24.65	35.53	26.31	27.00

[1] Calculated according to the recommendations of ACI318; [2] Calculated according to the recommendations of Eurocode 2; [3] Docros.

Table A3.2.6: Elastic bending at sagging and hogging regions – SL45-HS Series.

Slab strip ID		n_f	A_s (mm^2)	x (mm)	$M_{rd\,(1)}$ (kN·m)	c (mm)	$M_{rd\,(2)}$ (kN·m)	$M_{rd\,(3)}$ (kN·m)
S1-S1´	SL45-HS	-----	728.85	32.15	26.39	25.28	26.96	
	SL45s25-HS	2	728.85	37.96	31.56	31.32	33.67	28.15
	SL45s50-HS	6	728.85	45.27	37.71	38.62	41.28	
S2-S2´	SL45-HS	-----	336.15	14.77	13.07	11.61	13.19	14.85
	SL45s25-HS	1	336.15	21.18	19.59	17.83	20.96	18.64
	SL45s50-HS	3	336.15	25.11	23.43	21.51	25.37	24.46

[1] Calculated according to the recommendations of ACI318; [2] Calculated according to the recommendations of Eurocode 2; [3] See Figure A.3.2.2; [4] Docros

ANNEX 3.3

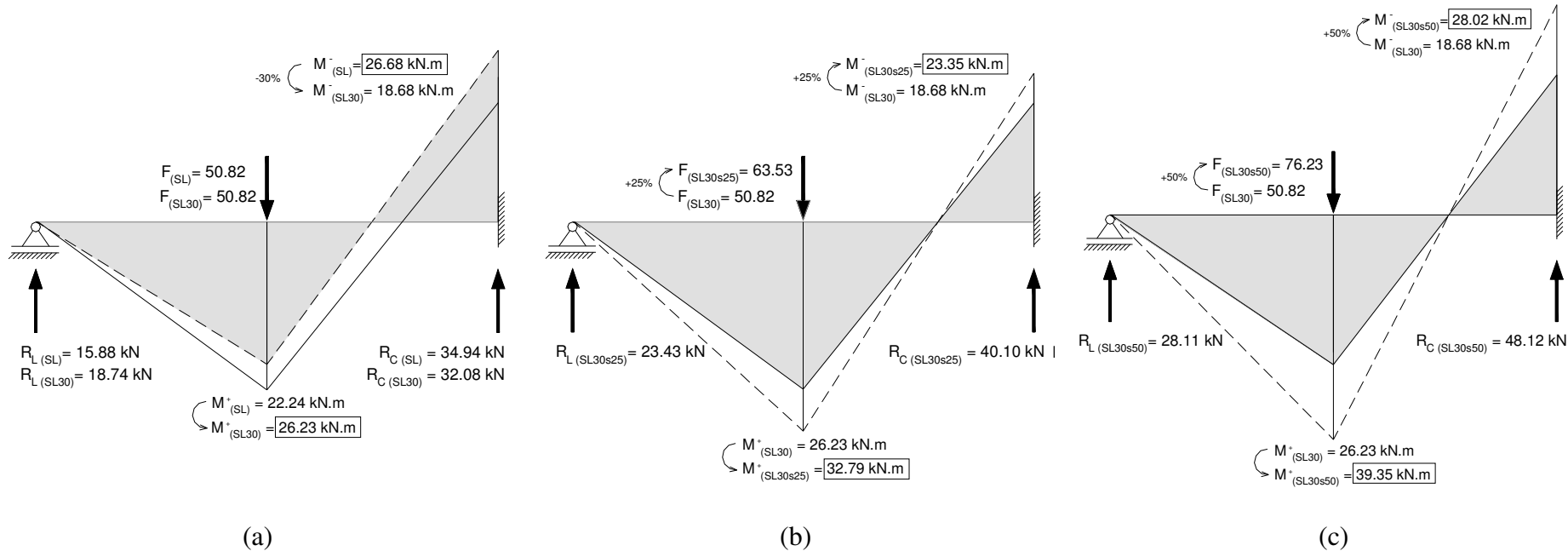### Elastic bending moments of SL30-H series

Figure A3.3.1: Elastic bending moments of SL30 series: (a) SL30-H, (b) SL30s25-H, (c) SL30s50-H.

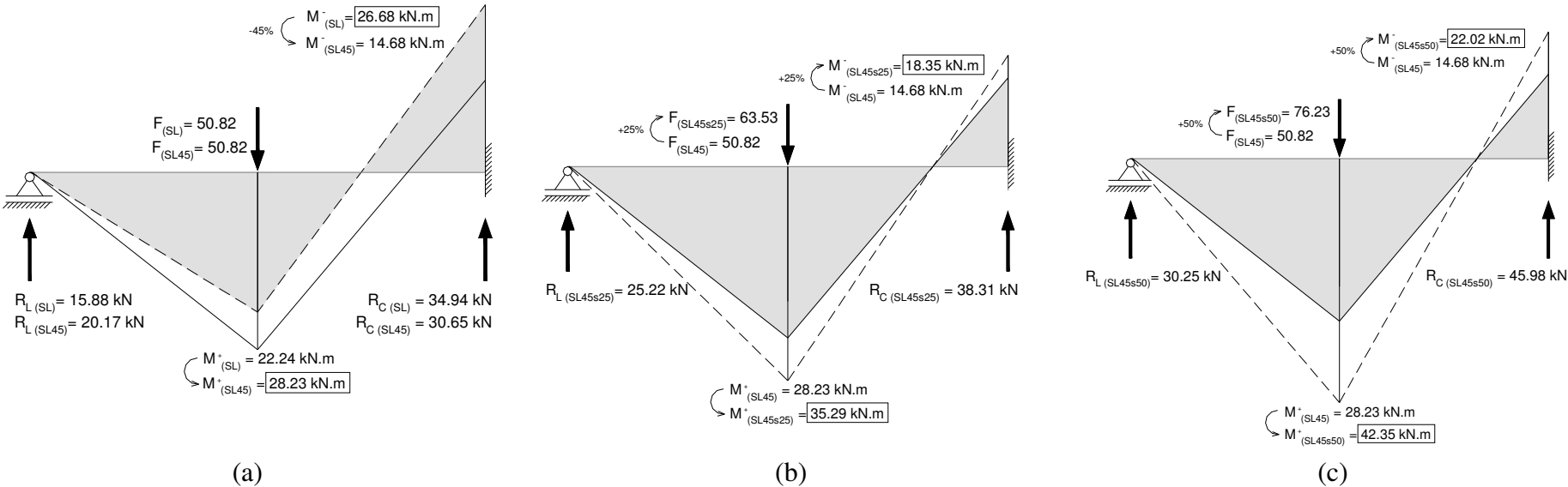**Elastic bending moments of SL45-H series**

Figure A3.3.2: Elastic bending moments of SL45 series: (a) SL45-H, (b) SL45s25-H, (c) SL45s50-H.

ANNEX 3.4 - MIXTURE PROPORTIONS AND MAIN PROPERTIES OF THE READY-MIX CONCRETES

Table A3.4.1: Mixture proportions and main properties of the ready-mix concretes.

Components	Mixture designation		
	SL15-HS	SL30-HS	SL45-HS
Cement II 42.5 R (kg/m^3)	200	215	340
Fly ash (kg/m^3)	110	112	--------
Fine river sand (kg/m^3)	320	339	354
Coarse river sand (kg/m^3)	640	639	--------
Brita 1 – 4 to 10mm	440	465	430
Course aggregate (kg/m^3)	456	466	721
W/B Ratio	0.52	0.53	0.47
Plasticizer (kg)	--------	--------	4.08
CHRYSOPLAST Superplasticizer (kg)	2.50	2.53	1.02
fc$_{28d}$ (MPa)	26.37	28.40	42.38
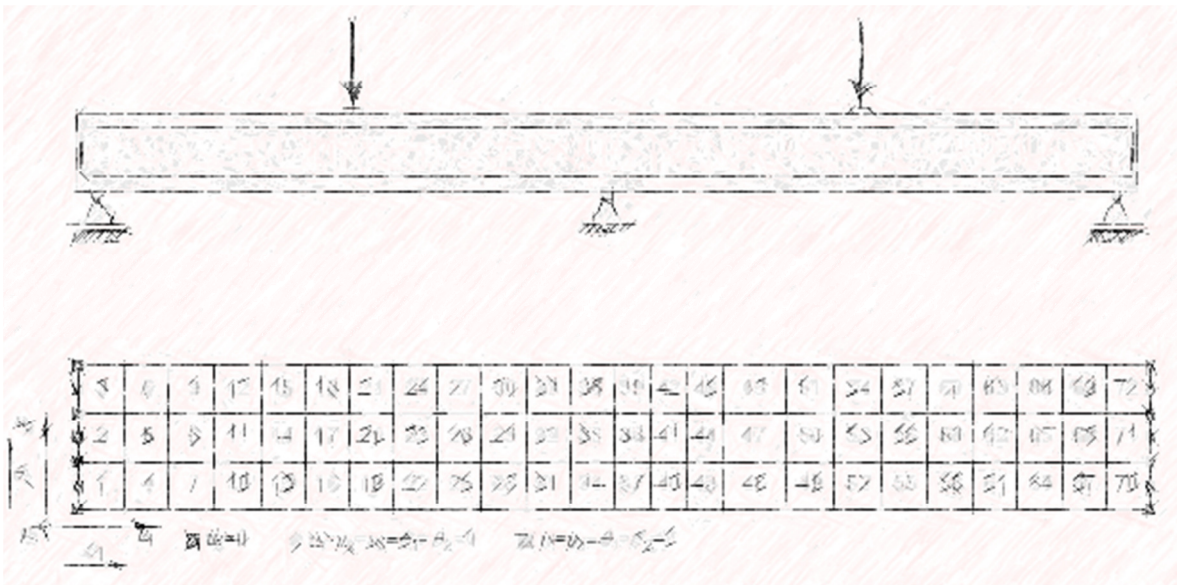
Chapter 4
ANNEXES

Data of the numerical simulations of the SL30-HS series
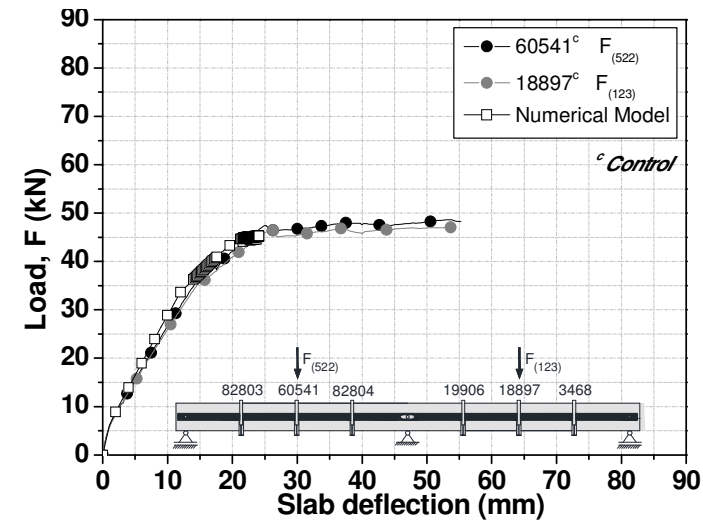
(a)
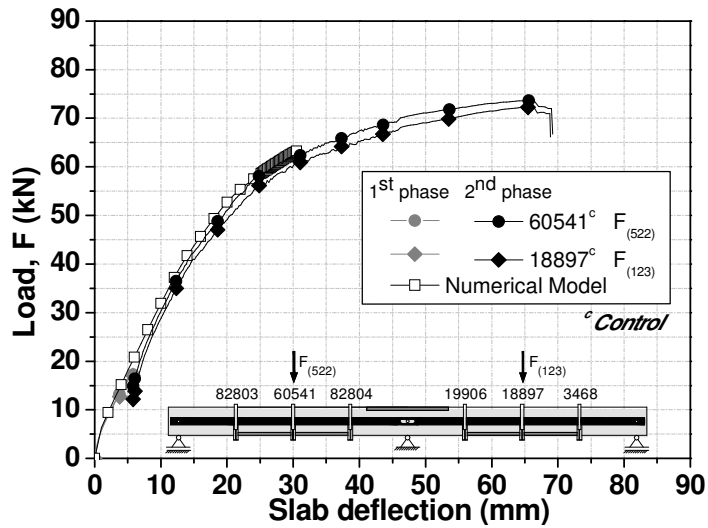
(b)
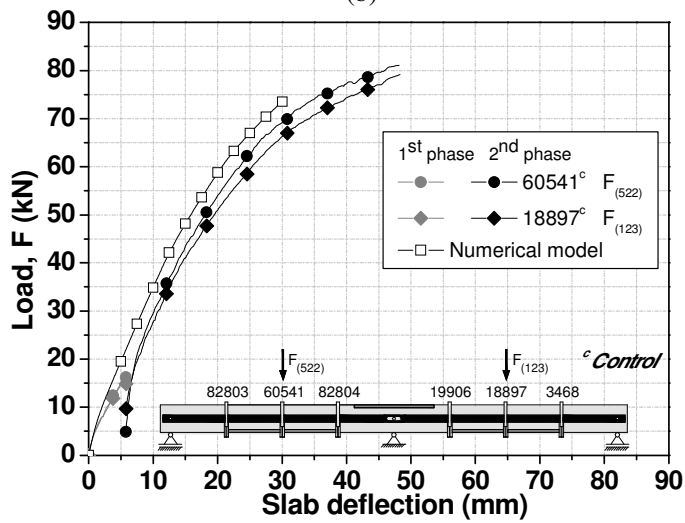
(c)

Figure A4.1: Relationship between applied load and deflections at spans of the (a) SL30-HS, (b) SL30s25-HS and (c) SL30s50-HS slab strips.
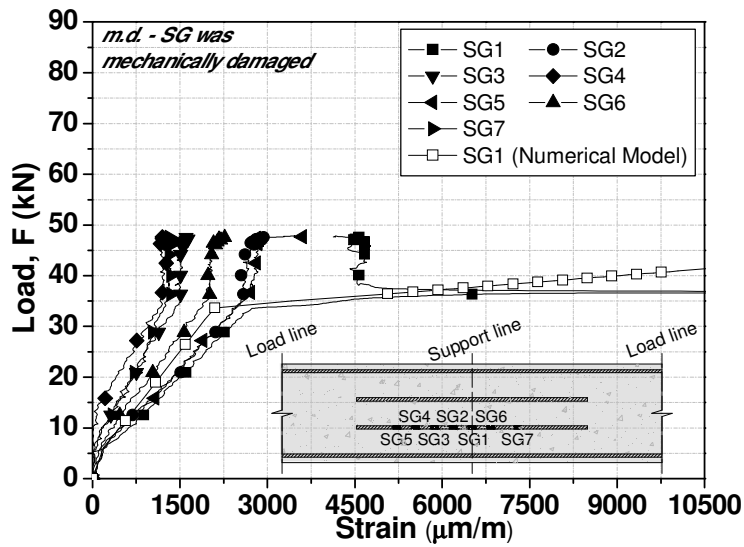
(a)
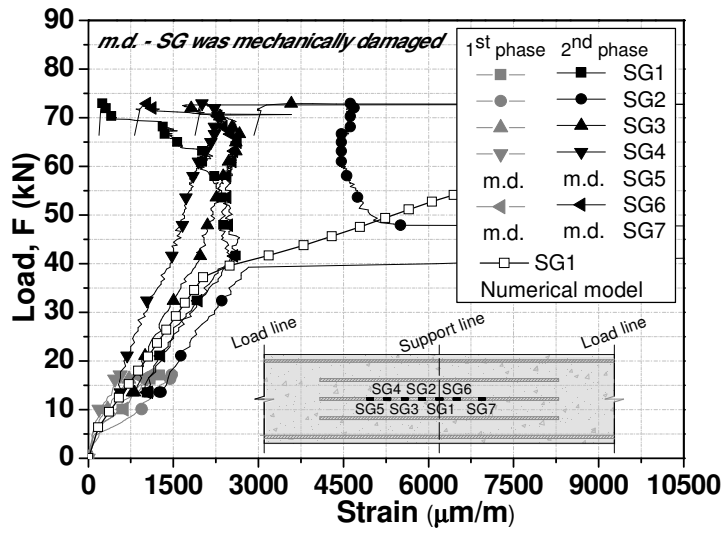
(b)
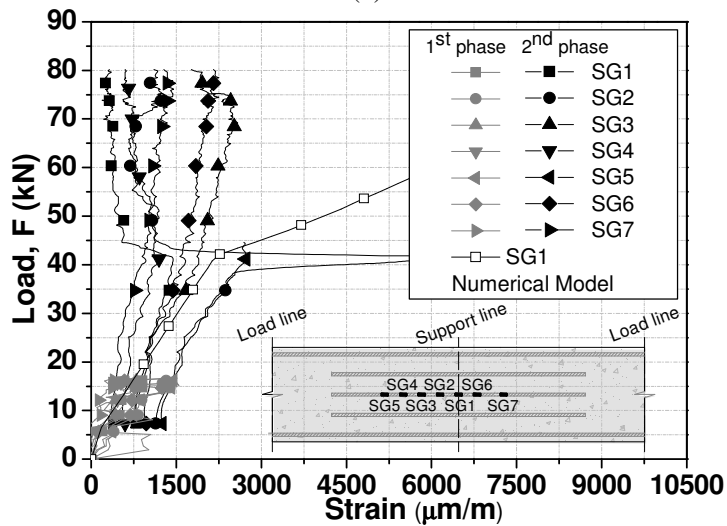
(c)

Figure A4.2: Relationship between applied load and tensile strain of the negative longitudinal steel reinforcement for the (a) SL30-HS, (b) SL30s25-HS and (c) SL30s50-HS slab strips.

Figure A4.3: Relationship between applied load and tensile strain of the positive longitudinal steel reinforcement for the (a) SL30-HS, (b) SL30s25-HS and (c) SL30s50-HS slab strips.
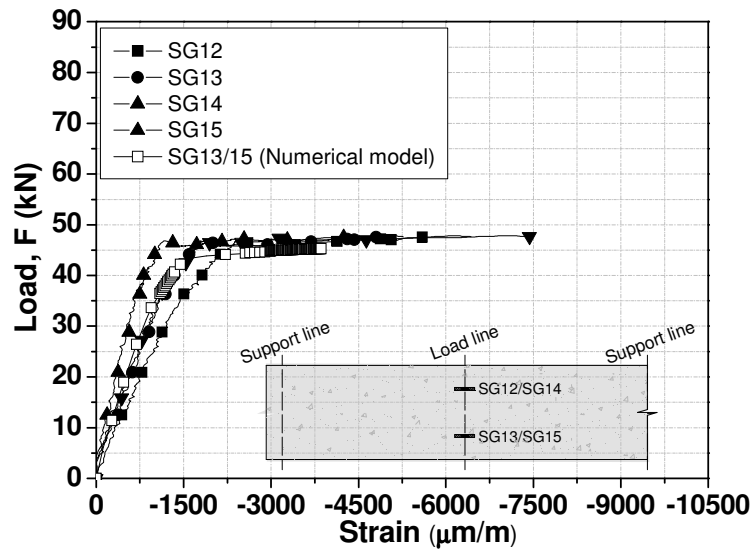
(a)
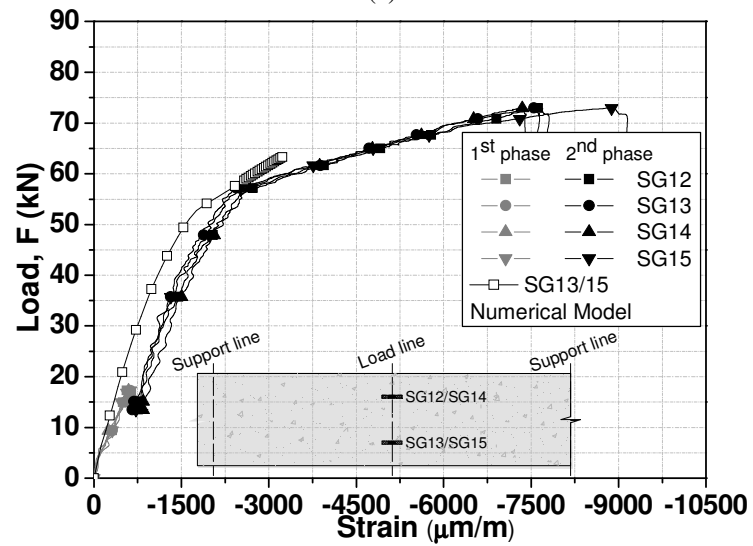
(b)
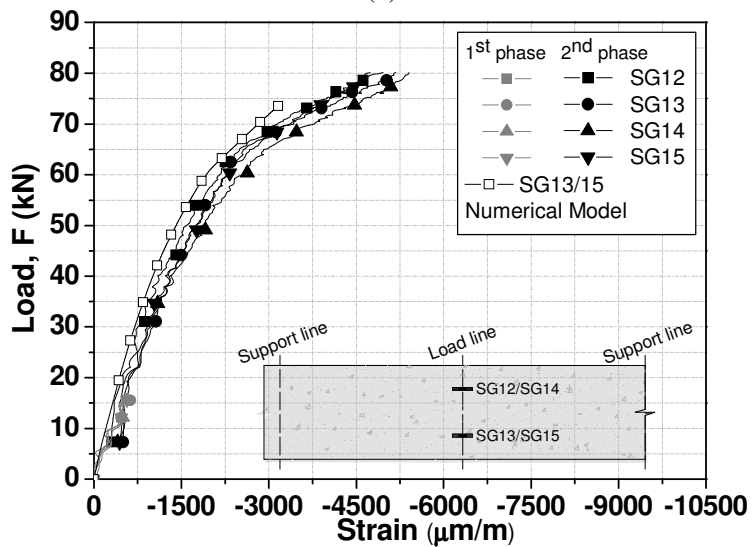
(c)

Figure A4.4: Relationship between applied load and compressive strain of the concrete at sagging region for the (a) SL30-HS, (b) SL30s25-HS and (c) SL30s50-HS slab strips.
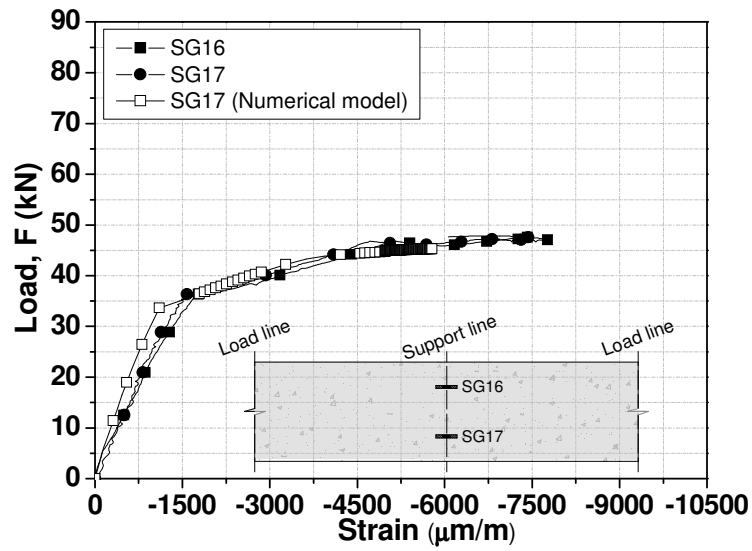
(a)
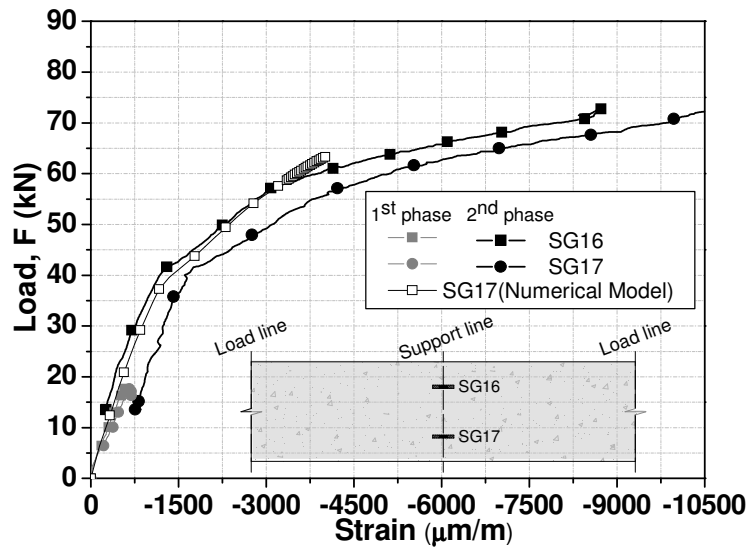
(b)
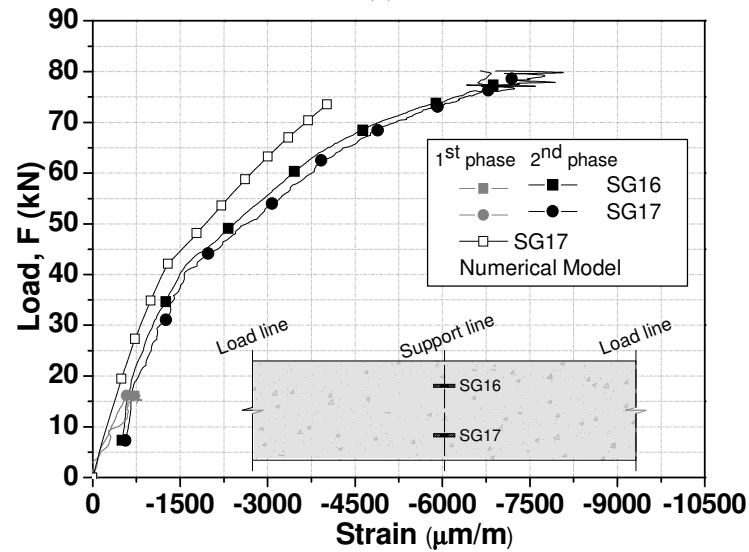
(c)

Figure A4.5: Relationship between applied load and compressive strain of the concrete at hogging region for the (a) SL30-HS, (b) SL30s25-HS and (c) SL30s50-HS slab strips.
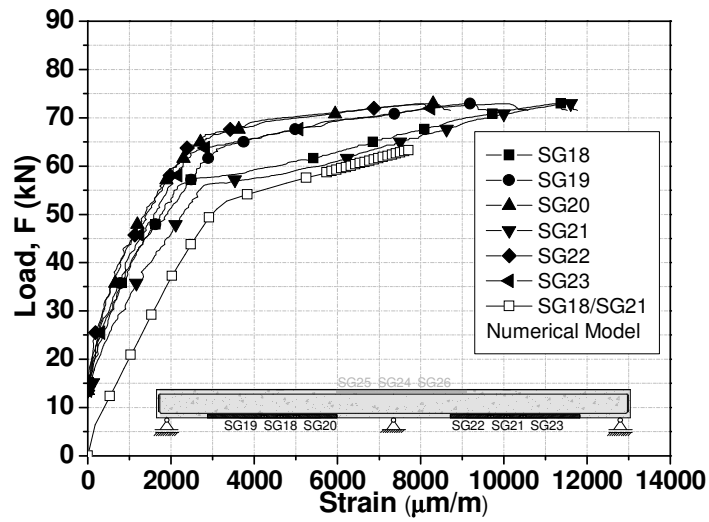
(a)
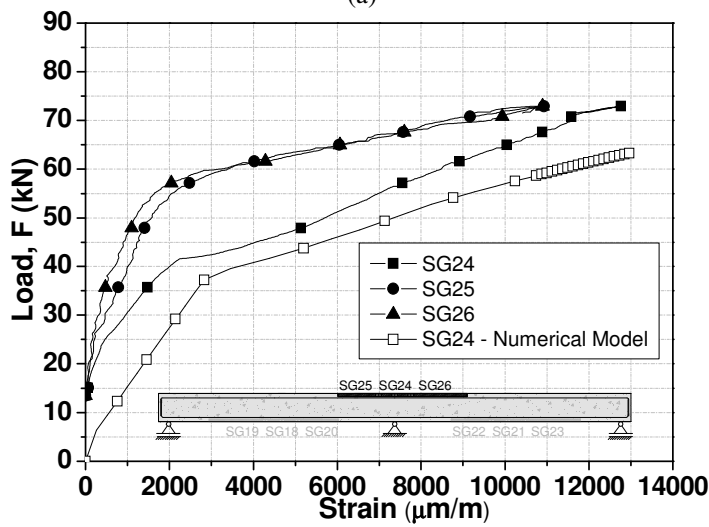
(b)

Figure A4.6: Relationship between applied load and tensile strain of the CFRP laminate at (a) sagging and (b) hogging regions for the SL30s25-HS slab strip.

(a)

(b)

Figure A4.7: Relationship between applied load and tensile strain of the CFRP laminate at (a) sagging and (b) hogging regions for the SL30s50-HS slab strip.

**Data of the numerical simulations of the SL45-HS series**
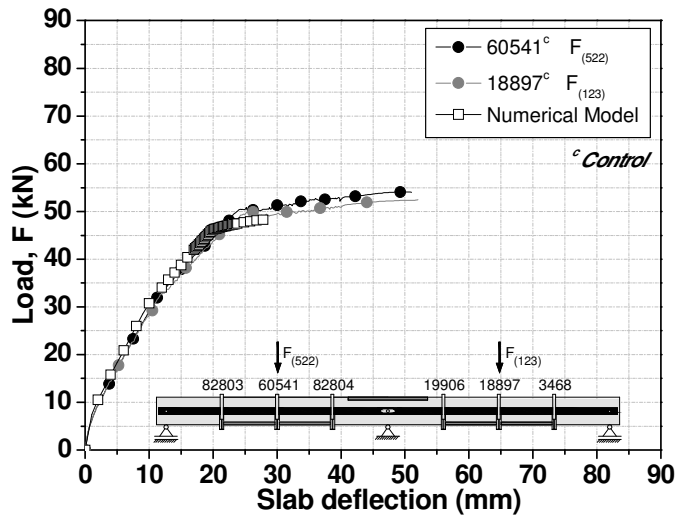
(a)
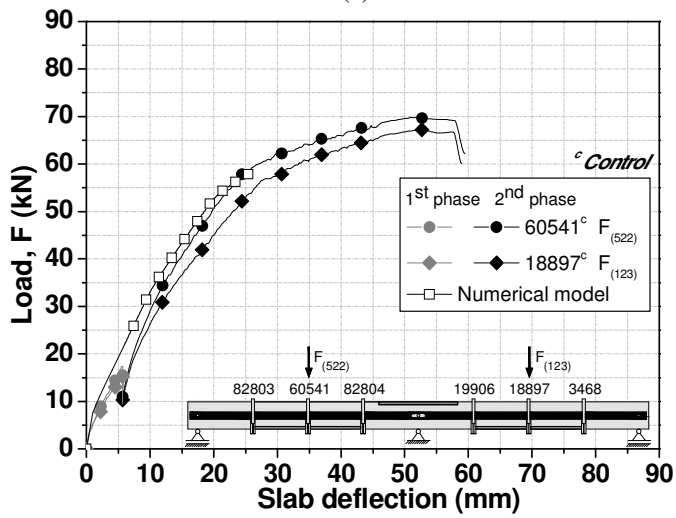
(b)
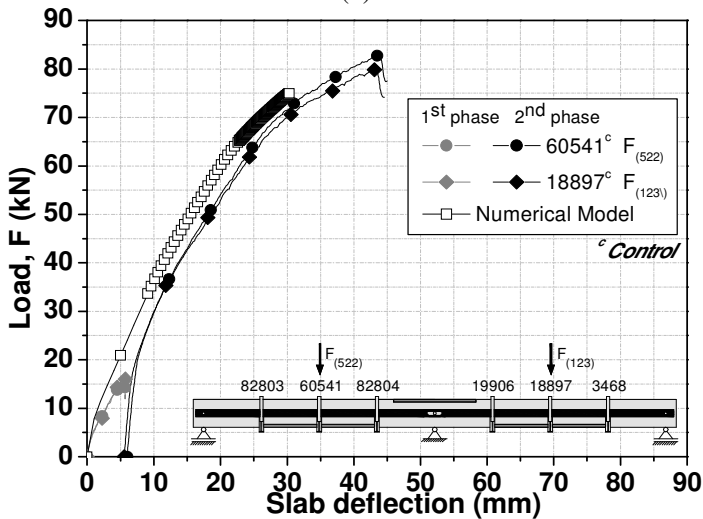

(c)

Figure A4.8: Relationship between applied load and deflections at spans of the (a) SL45-HS, (b) SL45s25-HS and (c) SL45s50-HS slab strips.
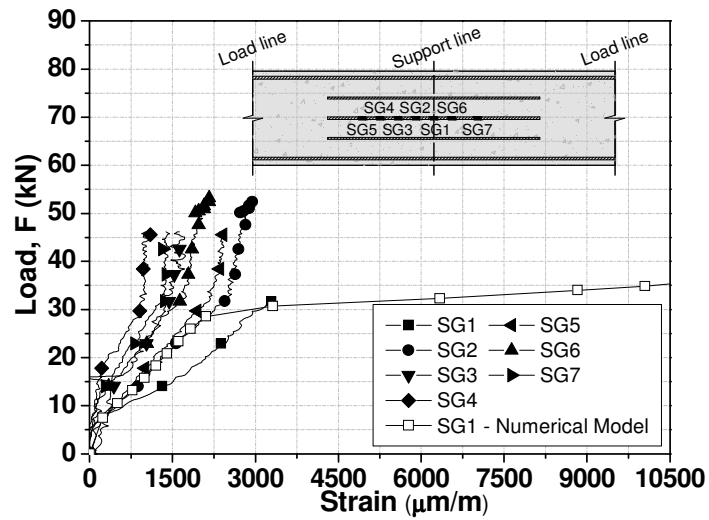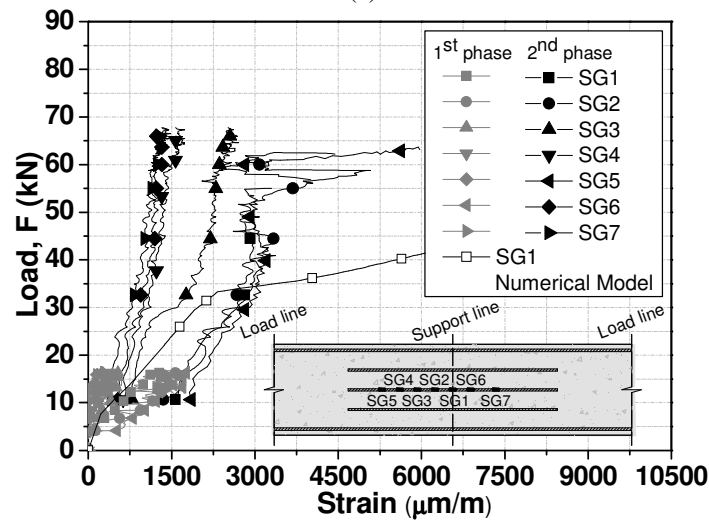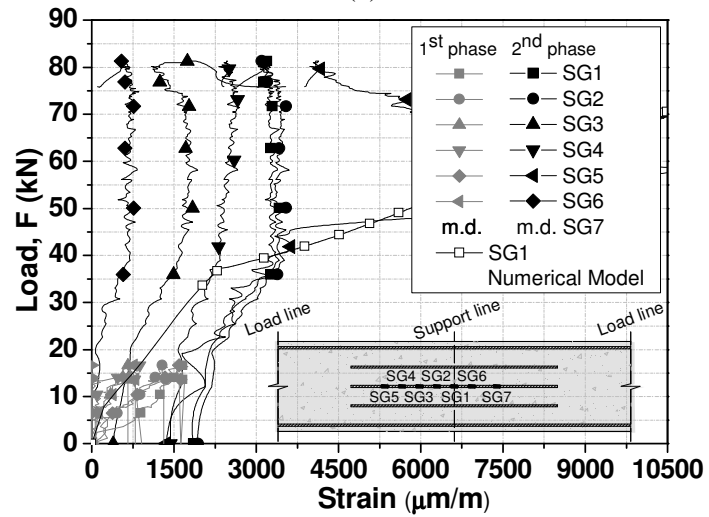
Figure A4.9: Relationship between applied load and tensile strain of the negative longitudinal steel reinforcement for the (a) SL45-HS, (b) SL45s25-HS and (c) SL45s50-HS slab strips.
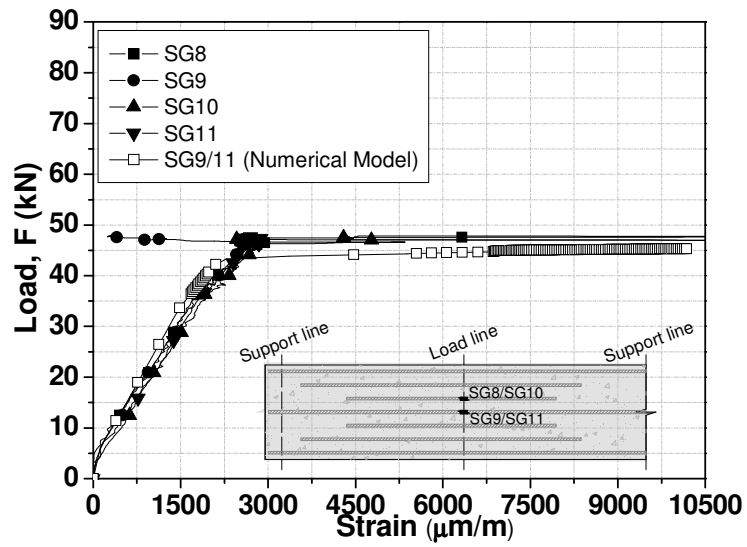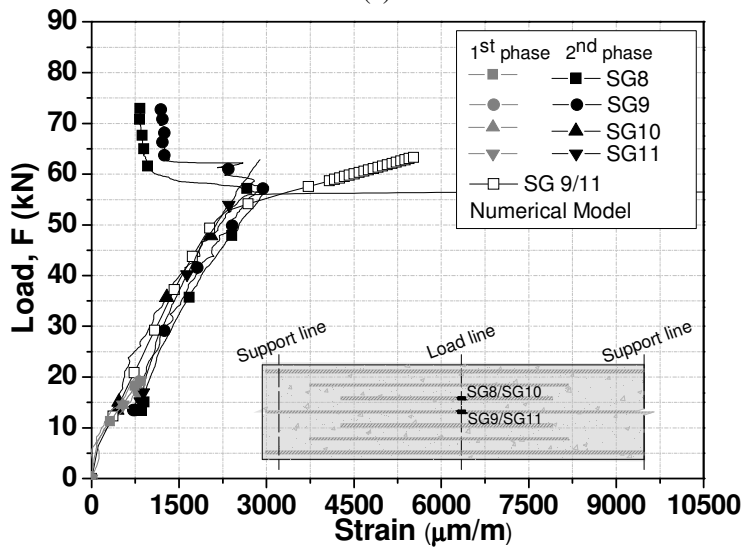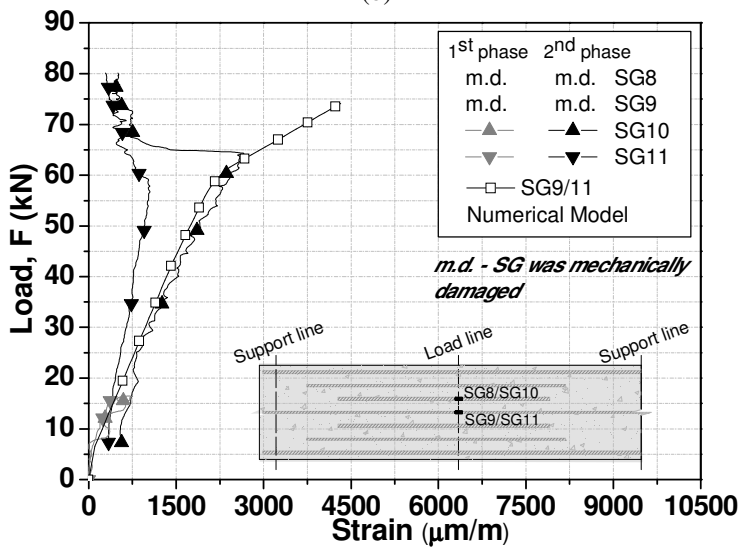
(a)

(b)

(c)
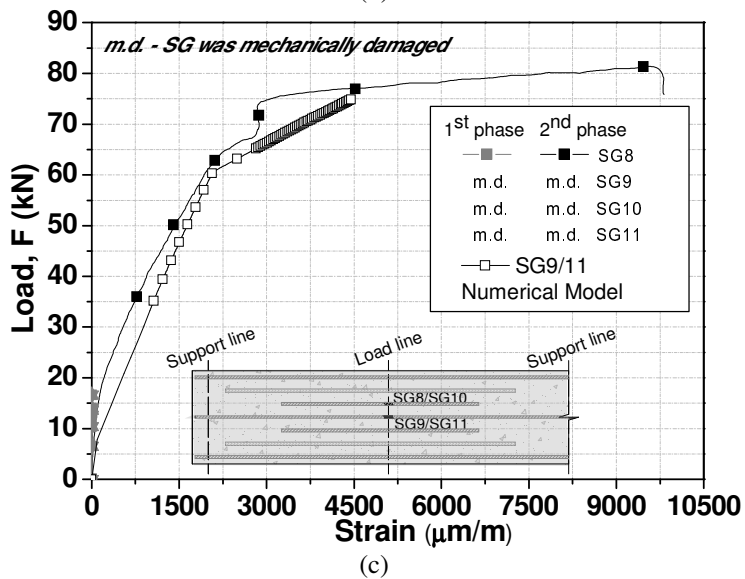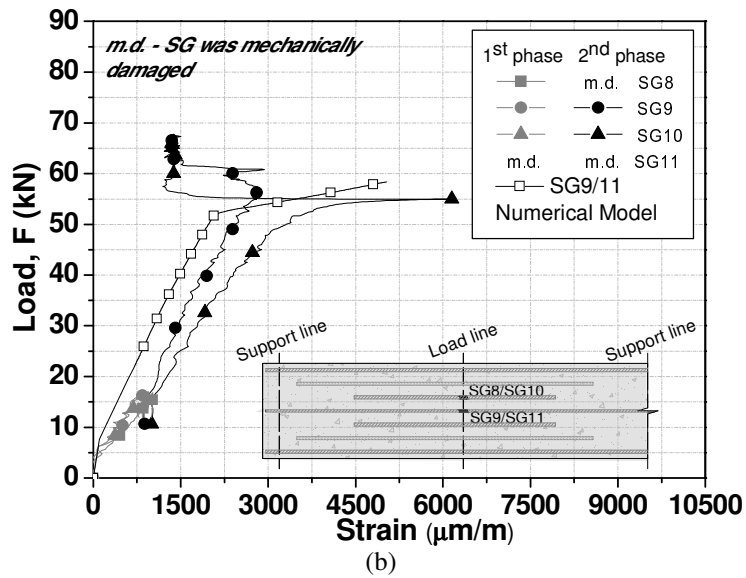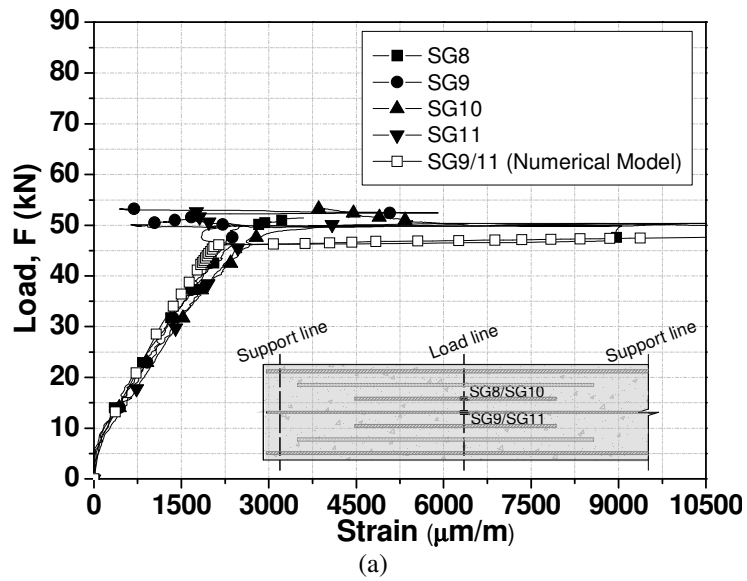
Figure A4.10: Relationship between applied load and tensile strain of the positive longitudinal steel reinforcement for the (a) SL45-HS, (b) SL45s25-HS and (c) SL45s50-HS slab strips.
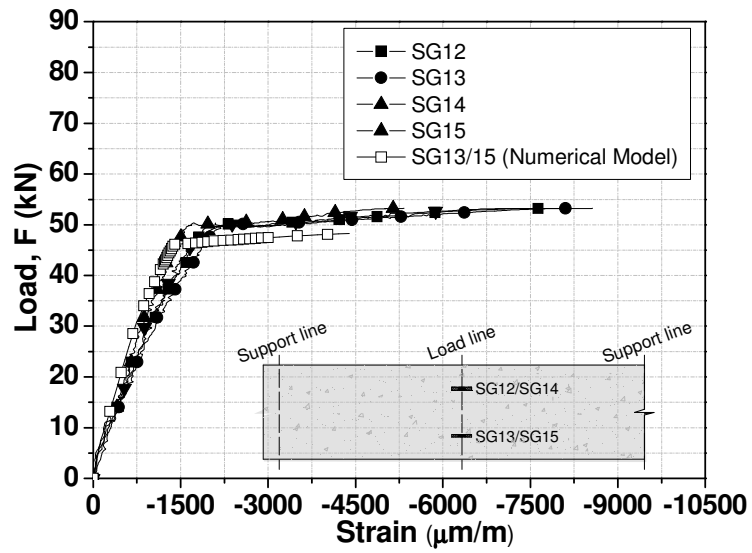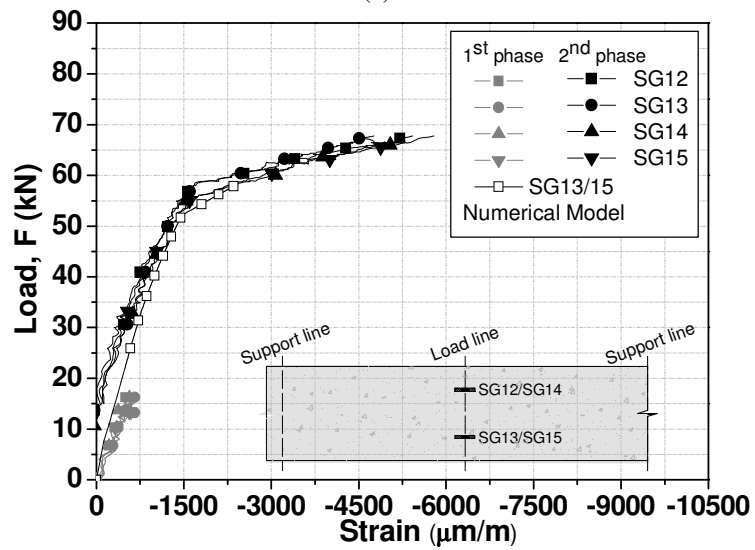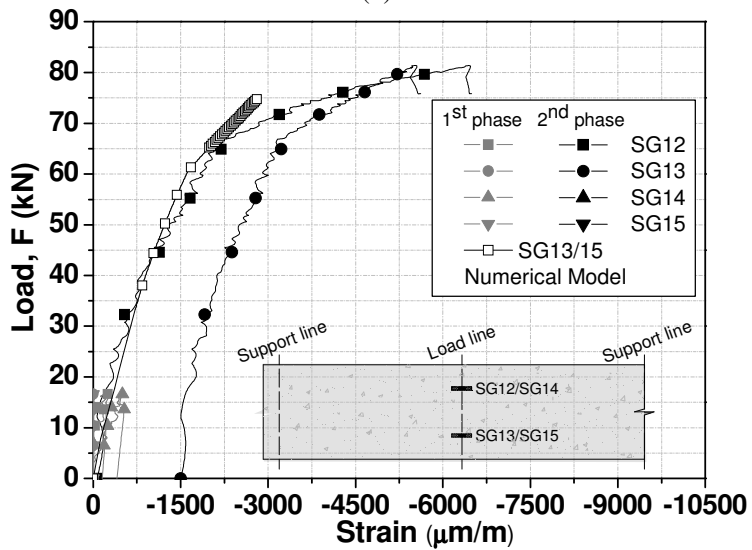
Figure A4.11: Relationship between applied load and compressive strain of the concrete at sagging region for the (a) SL45-HS, (b) SL45s25-HS and (c) SL45s50-HS slab strips.

(a)

(b)

(c)
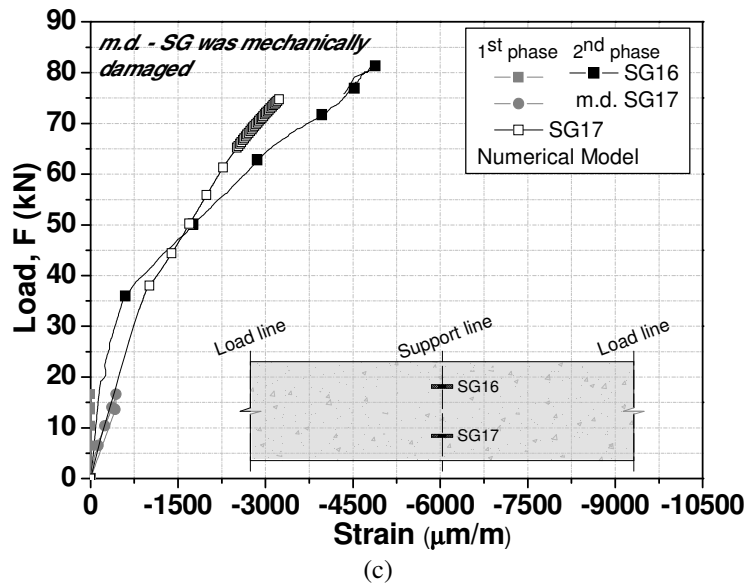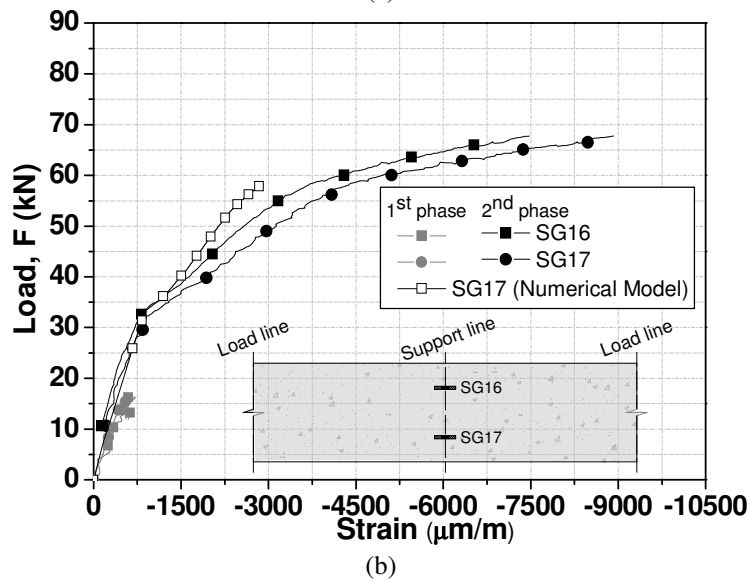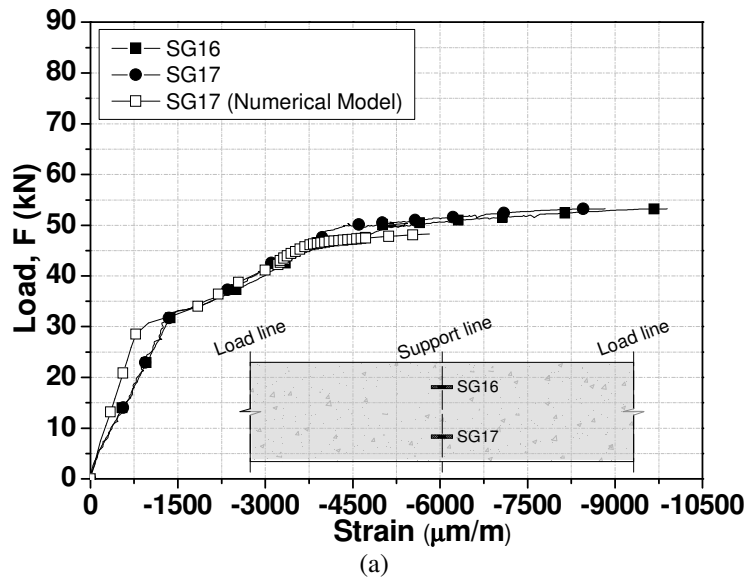
Figure A4.12: Relationship between applied load and compressive strain of the concrete at hogging region for the (a) SL45-HS, (b) SL45s25-HS and (c) SL45s50-HS slab strips.
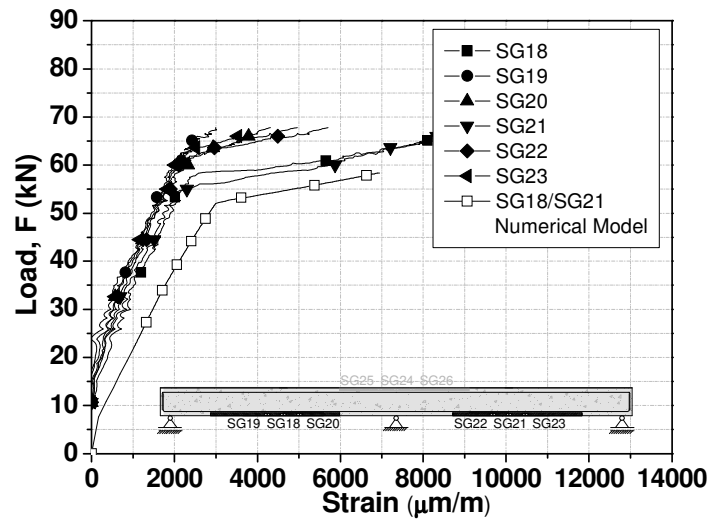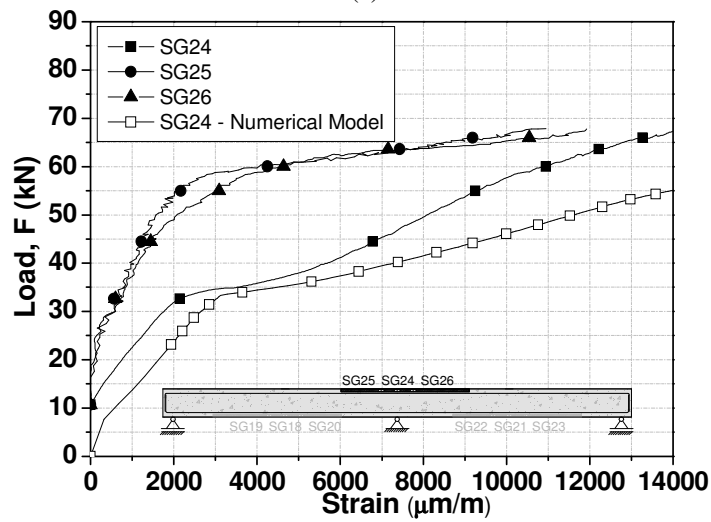
Figure A4.13: Relationship between applied load and tensile strain of the CFRP laminate at (a) sagging and (b) hogging regions for the SL45s25-HS slab strip.
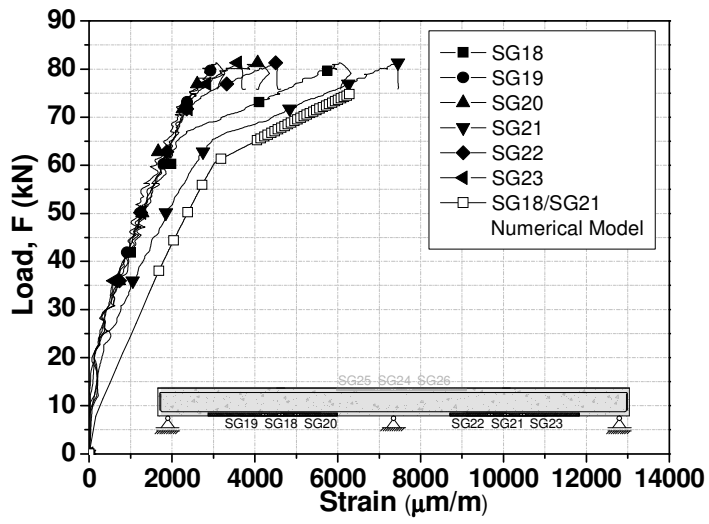
(a)
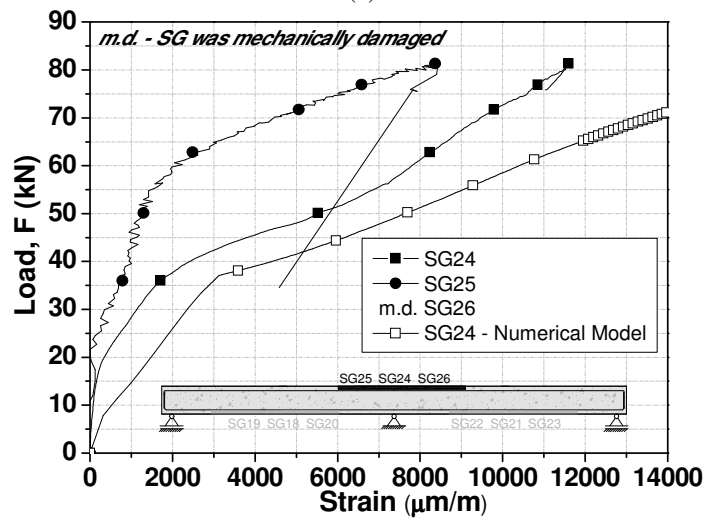
(b)

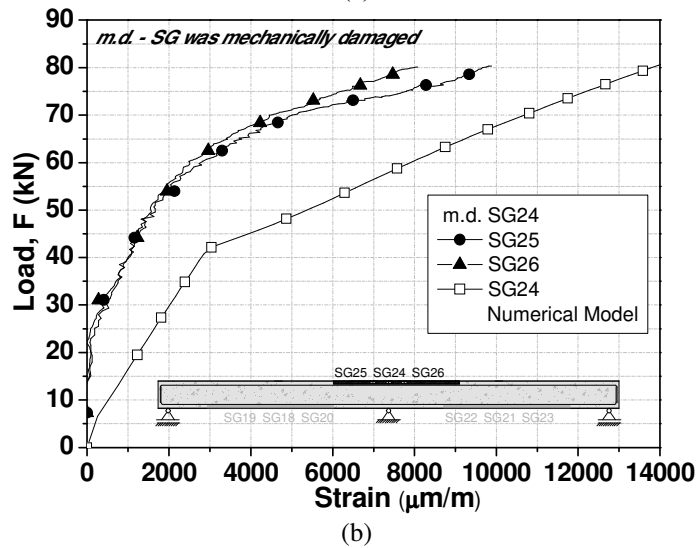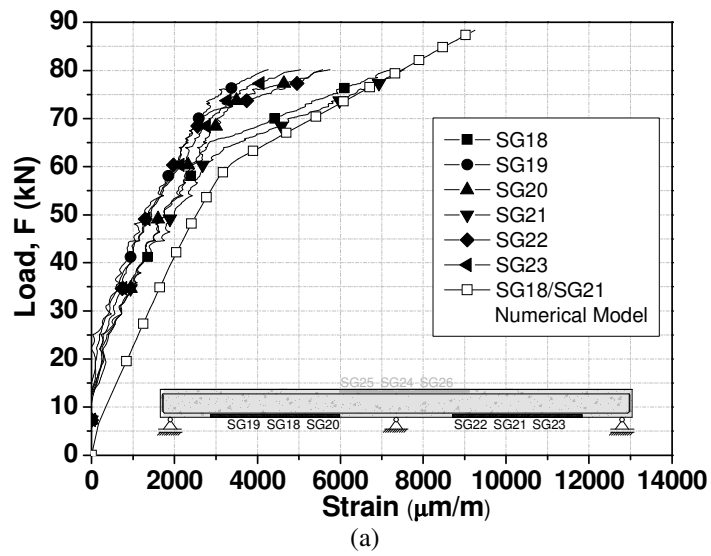Figure A4.14: Relationship between applied load and tensile strain of the CFRP laminate at (a) sagging and (b) hogging regions for the SL45s50-HS slab strip.

Table A.4.1: Main results obtained in the experimental program at the average maximum load.

Slab strip ID	F_{max} (kN)	$u_{F_{max}}$ (mm)	$\varepsilon^S_{c,max,F_{max}}$ (‰)	$\varepsilon^H_{c,max,F_{max}}$ (‰)	$\varepsilon^S_{s,max,F_{max}}$ (‰)	$\varepsilon^H_{s,max,F_{max}}$ (‰)	$\varepsilon^H_{f,max,F_{max}}$ (‰)	$\varepsilon^S_{f,max,F_{max}}$ (‰)	η (%)	IR (%)
SL15-H	51.36	55.04	-6.44	m.d.	1.39	2.41	-----	-----	7.85	-----
SL15s25-H	57.60	81.01	-3.55	-10.86	0.93	2.41	16.61	-----	-20.40	12.15
SL15s50-H	62.36	46.25	-5.27	-5.12	0.88	2.21	10.27	-----	-27.64	21.42
SL30-H	49.84	38.63	-5.59	-7.05	0.46	2.95	-----	-----	27.71	-----
SL30s25-H	54.87	70.27	-9.04	-12.53	1.30	3.62	15.19	-----	6.36	10.09
SL30s50-H	58.09	57.62	-8.35	-7.70	2.39	2.35	13.30	-----	-2.42	16.55
SL45-H	52.55	41.29	-5.44	-6.69	0.96	m.d.	-----	-----	43.62	-----
SL45s25-H	54.49	71.12	m.d.	-4.34	0.27	m.d.	13.31	-----	32.58	3.69
SL45s50-H	57.79	51.55	-6.43	-5.60	1.25	m.d.	12.59	-----	16.73	9.97
SL15-HS	47.61	54.45	-11.26	-14.43	11.54	9.64	-----	-----	(na)	-----
SL15s25-HS	69.24	47.73	-5.34	-7.07	m.d.	m.d.	7.64	8.24	8.85	45.43
SL30-HS	47.85	53.00	-7.06	-7.46	4.53	4.19	-----	-----	19.69	-----
SL30s25-HS	72.96	65.18	-8.85	-10.83	4.26	4.62	12.75	11.48	26.58	52.48
SL30s50-HS	80.42	49.19	-5.47	-6.91	0.57	2.22	9.85	7.60	31.67	68.07
SL45-HS	53.27	51.52	-8.05	-9.89	1.79	2.69	-----	-----	38.93	-----
SL45s25-HS	68.48	52.33	-5.26	-10.08	1.51	11.07	14.73	10.44	37.66	28.55
SL45s50-HS	81.57	43.64	-6.58	-5.33	m.d.	9.68	11.62	7.49	47.04	53.13

(na) – is not presented since the reactions are not available due to a deficient functioning of the data acquisition system during the test of this slab; m.d. – SG mechanically damaged

$$\begin{bmatrix} \Delta \overline{F}_1 \\ \Delta \overline{F}_2 \\ \Delta R \end{bmatrix} = \begin{bmatrix} f_{\Delta F_1 \Delta R} & f_{\Delta F_1 \Delta R} & f_{\Delta F_1 \Delta R} \\ f_{\Delta F_2 \Delta F_1} & f_{\Delta F_2 \Delta R} & f_{\Delta F_2 \Delta R} \\ f_{\Delta R \Delta F_1} & f_{\Delta R \Delta F_1} & f_{\Delta R \Delta R} \end{bmatrix}^{-1} \begin{bmatrix} \Delta u_1 \\ \Delta u_2 \\ 0 \end{bmatrix}$$

Chapter 5
ANNEXES

SL15s25-H slab strip

(a)

955   955

Support line   Load line   Support line   Load line   Support line

375

125   1400   1400

5850   VIEW OF TOP REINFORCEMENT

(b)

238 240   121   583   583   121

Support line   Load line   Support line   Load line   Support line

375

125   1400   1400

5850   VIEW OF BOTTOM REINFORCEMENT

(c)

A_s' S_1 S_2 CFRP Laminates (3x) S_1

A_s 120

S_1' S_2' S_1'

125   500   900   445   955

5600   SIDE VIEW

Figure A5.1: Arrangement of the (a-b) longitudinal steel reinforcement and
(c) CFRP laminates of the SL15s25-H slab strip.

Support line   Load line   Support line   Load line   Support line

1   2   3   4   5-6 7   8   8   7 5-6   4   3   2 1

CFRP Laminates (3x)

ΔF ΔF

1 2   3   4   5-6 7   8   8   7 5-6   4   3   2 1

a b   c   d   e   f g   h   i j   k   l   m n o

$(EI)_1$ $(EI)_2$ $(EI)_3$ $(EI)_4$ $(EI)_{5-6}$ $(EI)_7$ $(EI)_8$

238 240   923   445   252 121   583

1400   1400   1400   1400
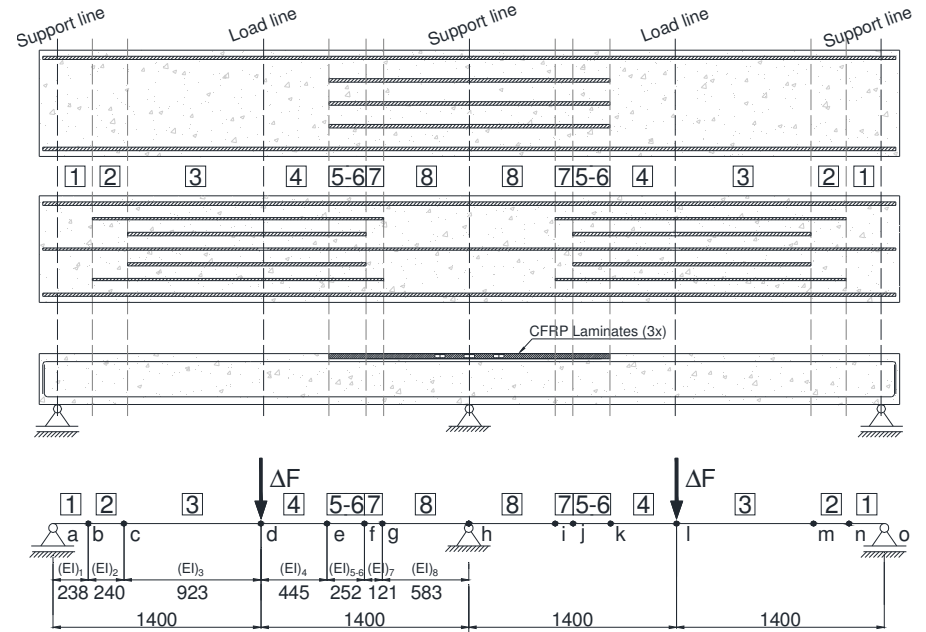
Figure A5.2: Discretization of the slab strip.

CS1 $A_s' = 2\phi12$ 26   120   26
$A_s = 2\phi12$ / 375   + 1\phi8

CS2 $A_s' = 2\phi12$ 26   120   26
$A_s = 2\phi12$ / 375   + 3\phi8

CS3/4 $A_s' = 2\phi12$ 375   26   120   26
$A_s = 4\phi12$ / 375   + 3\phi8

CS5/6 $A_s = 5\phi12$ 26   120   26
$A_s = 4\phi12$ / 375   + 3\phi8

CS7 $A_s = 5\phi12$ 26   120   26
$A_s = 2\phi12$ / 375   + 3\phi8

CS8 $A_s = 5\phi12$ 26   120   26
$A_s = 2\phi12$ / 375   + 1\phi8

Figure A5.3: Resume of the cross-section according to the longitudinal steel reinforcement.

Table A5.1: Relation M$-\chi$ of the cross sections of the SL15s25-H slab strip.

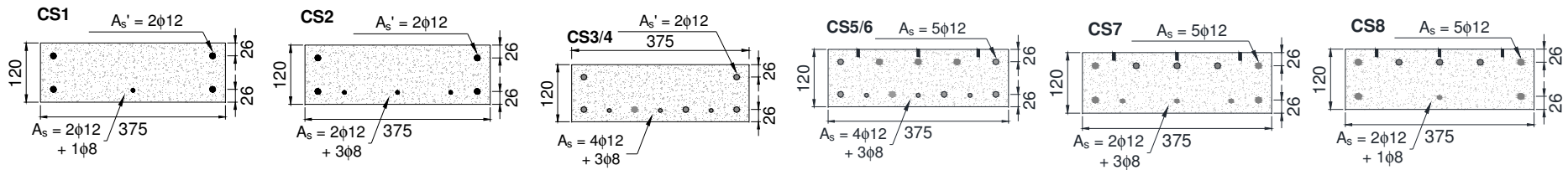| Element 1		Element 2		Element 3		Element 4		Element 5/6		Element 5/6		Element 7		Element 7		Element 8	
M^+	χ	M^+	χ	M^+	χ	M^+	χ	M^+	χ	M^-	χ	M^+	χ	M^-	χ	M^+	χ
0.00	1.89E+12	0.00	1.91E+12	0.00	1.95E+12	0.00	1.95E+12	0.00	2.01E+12	0.00	2.05E+12	0.00	1.97E+12	0.00	2.01E+12	0.00	1.99E+12
3.05	1.68E+12	3.07	1.71E+12	3.12	1.76E+12	3.12	1.76E+12	3.23	1.81E+12	3.33	1.84E+12	3.18	1.75E+12	3.23	1.81E+12	3.18	1.80E+12
5.00	1.15E+12	5.19	1.23E+12	5.49	1.37E+12	5.49	1.37E+12	5.59	1.37E+12	5.82	1.41E+12	5.24	1.22E+12	5.71	1.42E+12	5.65	1.42E+12
4.57	4.70E+11	5.30	6.14E+11	6.35	8.56E+11	6.35	8.56E+11	6.39	8.43E+11	6.84	8.97E+11	5.28	6.02E+11	6.75	9.13E+11	6.71	9.21E+11
5.55	3.60E+11	6.32	4.66E+11	7.59	6.72E+11	7.59	6.72E+11	7.65	6.70E+11	8.33	7.30E+11	6.28	4.64E+11	8.17	7.34E+11	8.09	7.36E+11
6.92	3.39E+11	7.82	4.36E+11	9.26	6.22E+11	9.26	6.22E+11	9.34	6.22E+11	10.22	6.83E+11	7.74	4.35E+11	9.99	6.82E+11	9.88	6.82E+11
8.31	3.30E+11	9.37	4.24E+11	11.04	6.03E+11	11.04	6.03E+11	11.14	6.04E+11	12.19	6.64E+11	9.27	4.23E+11	11.92	6.62E+11	11.78	6.61E+11
9.63	3.23E+11	10.91	4.17E+11	12.81	5.92E+11	12.81	5.92E+11	12.93	5.94E+11	14.16	6.54E+11	10.78	4.16E+11	13.84	6.51E+11	13.67	6.50E+11
10.74	3.07E+11	12.38	4.10E+11	14.55	5.85E+11	14.55	5.85E+11	14.70	5.88E+11	16.10	6.47E+11	12.22	4.09E+11	15.72	6.44E+11	15.53	6.43E+11
11.37	2.70E+11	13.68	3.97E+11	16.25	5.80E+11	16.25	5.80E+11	16.43	5.82E+11	17.99	6.42E+11	13.50	3.98E+11	17.56	6.39E+11	17.35	6.37E+11
11.54	2.24E+11	14.63	3.71E+11	17.88	5.74E+11	17.88	5.74E+11	18.10	5.76E+11	19.83	6.36E+11	14.45	3.74E+11	19.35	6.33E+11	19.11	6.32E+11
11.66	1.94E+11	15.12	3.33E+11	19.43	5.66E+11	19.43	5.66E+11	19.67	5.67E+11	21.59	6.29E+11	14.98	3.39E+11	21.07	6.27E+11	20.81	6.25E+11
11.78	1.71E+11	15.30	2.85E+11	20.84	5.54E+11	20.84	5.54E+11	21.08	5.52E+11	23.23	6.18E+11	15.18	2.97E+11	22.68	6.18E+11	22.41	6.17E+11
11.88	1.52E+11	15.37	2.45E+11	22.04	5.33E+11	22.04	5.33E+11	22.18	5.26E+11	24.69	6.01E+11	15.29	2.62E+11	24.16	6.05E+11	23.88	6.05E+11
11.97	1.37E+11	15.47	2.18E+11	22.88	4.98E+11	22.88	4.98E+11	22.83	4.86E+11	25.89	5.74E+11	15.40	2.36E+11	25.44	5.84E+11	25.18	5.88E+11
12.07	1.25E+11	15.56	1.97E+11	23.27	4.52E+11	23.27	4.52E+11	23.15	4.45E+11	26.80	5.41E+11	15.51	2.16E+11	26.47	5.56E+11	26.25	5.63E+11
12.15	1.15E+11	15.65	1.81E+11	23.47	4.11E+11	23.47	4.11E+11	23.34	4.08E+11	27.53	5.09E+11	15.61	2.00E+11	27.27	5.22E+11	27.10	5.31E+11
12.23	1.07E+11	15.73	1.67E+11	23.61	3.77E+11	23.61	3.77E+11	23.48	3.76E+11	28.17	4.80E+11	15.70	1.86E+11	27.93	4.91E+11	27.79	4.98E+11
12.31	1.01E+11	15.80	1.55E+11	23.72	3.48E+11	23.72	3.48E+11	23.59	3.48E+11	28.76	4.56E+11	15.79	1.74E+11	28.54	4.65E+11	28.40	4.70E+11
12.37	9.50E+10	15.86	1.45E+11	23.81	3.23E+11	23.81	3.23E+11	23.67	3.22E+11	29.32	4.35E+11	15.86	1.64E+11	29.10	4.42E+11	28.96	4.47E+11
12.43	9.01E+10	15.91	1.36E+11	23.89	3.01E+11	23.89	3.01E+11	23.72	2.98E+11	29.84	4.16E+11	15.94	1.56E+11	29.62	4.22E+11	29.49	4.26E+11
12.48	8.58E+10	15.96	1.28E+11	23.94	2.80E+11	23.94	2.80E+11	23.74	2.77E+11	30.35	4.00E+11	16.00	1.48E+11	30.12	4.05E+11	29.99	4.09E+11
12.52	8.19E+10	15.99	1.21E+11					23.77	2.59E+11	30.83	3.85E+11	16.05	1.41E+11	30.59	3.90E+11	30.45	3.93E+11
12.55	7.84E+10	16.02	1.15E+11					23.80	2.45E+11	31.28	3.72E+11	16.09	1.35E+11	31.03	3.76E+11	30.89	3.79E+11
12.58	7.54E+10	16.04	1.10E+11					23.81	2.32E+11	31.70	3.60E+11	16.13	1.29E+11	31.44	3.64E+11	31.30	3.67E+11
12.60	7.27E+10	16.06	1.05E+11					23.83	2.20E+11	32.10	3.49E+11	16.15	1.24E+11	31.83	3.53E+11	31.68	3.56E+11
12.62	7.01E+10	16.07	1.01E+11					23.83	2.10E+11	32.47	3.39E+11	16.17	1.19E+11	32.20	3.43E+11	32.03	3.45E+11
										37.71	2.17E+11	16.18	1.11E+11	37.28	1.98E+11	35.85	2.11E+11

M (N.mm); χ (1/mm); M^+ (Positive bending moment); M^- (Negative bending moment)

(a)

955   955

Support line   Load line   Support line   Load line   Support line

375

125   1400   1400

5850   VIEW OF TOP REINFORCEMENT

(b)

238 240   121   583   583   121

Support line   Load line   Support line   Load line   Support line

375

125   1400   1400

5850   VIEW OF BOTTOM REINFORCEMENT

(c)

A_s' S_1 S_2 CFRP Laminates (7x) S_1

120

A_s S_1' S_2' S_1'

125   500   900   445   955

5600   SIDE VIEW

Figure A5.4: Arrangement of the (a-b) longitudinal steel reinforcement and
(c) CFRP laminates of the SL15s25-H slab strip.

Support line   Load line   Support line   Load line   Support line

CFRP Laminates (7x)

ΔF ΔF

1 2   3   4 5-6 7   8   8   7 5-6   4   3   2 1

a b   c   d   e f g   h   i j   k   l   m   n o

$(EI)_1$ $(EI)_2$ $(EI)_3$ $(EI)_4$ $(EI)_{5-6}$ $(EI)_7$ $(EI)_8$

238 240   923   445 252 121   583

1400   1400   1400   1400

Figure A5.5: Discretization of the slab strip.

CS1 $A_s' = 2\phi12$

120   26   26

$A_s = 2\phi12$ 375
$+ 1\phi8$

CS2 $A_s' = 2\phi12$

120   26   26

$A_s = 2\phi12$ 375
$+ 3\phi8$

CS3/4 $A_s' = 2\phi12$
375

120   26   26

$A_s = 4\phi12$ 375
$+ 3\phi8$

CS5/6 $A_s = 5\phi12$

120   26   26

$A_s = 4\phi12$ 375
$+ 3\phi8$

CS7 $A_s = 5\phi12$

120   26   26

$A_s = 2\phi12$ 375
$+ 3\phi8$

CS8 $A_s = 5\phi12$

120   26   26

$A_s = 2\phi12$ 375
$+ 1\phi8$

Figure A5.6: Resume of the cross-section according to the longitudinal steel reinforcement.

Table A5.2: Relation M−χ of the cross sections of the SL15s50-H slab strip.

Element 1		Element 2		Element 3		Element 4		Element 5/6		Element 5		Element 6		Element 6		Element 7	
M^+	χ	M^+	χ	M^+	χ	M^+	χ	M^+	χ	M^-	χ	M^+	χ	M^-	χ	M^+	χ
0.00	1.89E+12	0.00	1.91E+12	0.00	1.95E+12	0.00	1.95E+12	0.00	2.00E+12	0.00	2.09E+12	0.00	1.96E+12	0.00	2.05E+12	0.34	2.01E+12
3.46	1.64E+12	3.48	1.66E+12	3.54	1.73E+12	3.54	1.73E+12	3.63	1.76E+12	3.23	1.91E+12	4.32	1.58E+12	6.53	1.31E+12	0.84	1.98E+12
4.93	8.94E+11	5.29	1.01E+12	5.82	1.20E+12	5.82	1.20E+12	5.86	1.19E+12	7.25	1.08E+12	5.21	6.52E+11	10.44	8.07E+11	1.34	1.95E+12
4.86	3.95E+11	5.60	5.16E+11	6.82	7.51E+11	6.82	7.51E+11	6.82	7.44E+11	12.73	7.81E+11	6.62	4.51E+11	15.39	7.58E+11	1.82	1.93E+12
6.33	3.45E+11	7.16	4.44E+11	8.52	6.37E+11	8.52	6.37E+11	8.52	6.35E+11	18.81	7.52E+11	8.74	4.24E+11	20.21	7.42E+11	2.30	1.90E+12
7.92	3.32E+11	8.92	4.26E+11	10.53	6.07E+11	10.53	6.07E+11	10.52	6.06E+11	24.50	7.36E+11	10.88	4.14E+11	24.71	7.28E+11	2.77	1.88E+12
9.45	3.24E+11	10.70	4.18E+11	12.56	5.94E+11	12.56	5.94E+11	12.55	5.93E+11	29.48	7.07E+11	12.86	4.03E+11	28.73	7.06E+11	3.23	1.85E+12
10.74	3.07E+11	12.38	4.10E+11	14.55	5.85E+11	14.55	5.85E+11	14.56	5.86E+11	33.23	6.49E+11	14.36	3.75E+11	31.96	6.67E+11	3.67	1.81E+12
11.41	2.63E+11	13.84	3.94E+11	16.48	5.79E+11	16.48	5.79E+11	16.51	5.80E+11	36.09	5.84E+11	15.04	3.25E+11	34.42	6.16E+11	7.14	1.08E+12
11.57	2.14E+11	14.81	3.61E+11	18.33	5.72E+11	18.33	5.72E+11	18.39	5.72E+11	38.49	5.35E+11	15.23	2.70E+11	36.46	5.70E+11	12.35	7.76E+11
11.71	1.83E+11	15.23	3.14E+11	20.05	5.62E+11	20.05	5.62E+11	20.13	5.61E+11	40.53	4.99E+11	15.39	2.32E+11	38.22	5.33E+11	18.16	7.45E+11
11.83	1.60E+11	15.34	2.60E+11	21.56	5.44E+11	21.56	5.44E+11	21.60	5.39E+11	42.25	4.70E+11	15.53	2.06E+11	39.73	5.03E+11	23.60	7.28E+11
11.95	1.41E+11	15.44	2.25E+11	22.69	5.10E+11	22.69	5.10E+11	22.58	5.01E+11	43.70	4.46E+11	15.66	1.86E+11	40.98	4.78E+11	28.42	7.04E+11
12.05	1.26E+11	15.55	2.00E+11	23.23	4.58E+11	23.23	4.58E+11	23.04	4.54E+11	44.93	4.26E+11	15.78	1.70E+11	42.04	4.57E+11	32.19	6.59E+11
12.15	1.15E+11	15.65	1.81E+11	23.47	4.11E+11	23.47	4.11E+11	23.27	4.11E+11	45.99	4.08E+11	15.88	1.57E+11	42.92	4.39E+11	34.91	6.01E+11
12.24	1.06E+11	15.74	1.65E+11	23.63	3.72E+11	23.63	3.72E+11	23.43	3.75E+11	46.92	3.93E+11	15.96	1.46E+11	43.66	4.22E+11	37.08	5.52E+11
12.33	9.90E+10	15.82	1.52E+11	23.75	3.40E+11	23.75	3.40E+11	23.55	3.43E+11	47.74	3.79E+11	16.02	1.36E+11	44.26	4.08E+11	38.86	5.13E+11
12.40	9.28E+10	15.88	1.41E+11	23.85	3.13E+11	23.85	3.13E+11	23.64	3.15E+11	48.45	3.67E+11	16.07	1.28E+11	44.68	3.95E+11	40.28	4.83E+11
12.46	8.76E+10	15.94	1.31E+11	23.92	2.89E+11	23.92	2.89E+11	23.68	2.89E+11	49.07	3.56E+11	16.10	1.21E+11	45.05	3.83E+11	41.43	4.57E+11
12.51	8.29E+10	15.98	1.23E+11					23.71	2.67E+11	49.56	3.46E+11	16.11	1.15E+11	45.48	3.71E+11	42.32	4.35E+11
12.55	7.89E+10	16.02	1.16E+11					23.73	2.49E+11	49.88	3.37E+11			45.83	3.60E+11	42.92	4.16E+11
12.58	7.54E+10	16.04	1.10E+11					23.75	2.34E+11	50.33	3.28E+11			46.10	3.50E+11	43.50	3.98E+11
12.60	7.23E+10	16.06	1.04E+11					23.76	2.21E+11	50.61	3.19E+11			46.25	3.41E+11	43.94	3.82E+11
12.62	6.95E+10	16.07	9.98E+10							50.72	3.11E+11					44.26	3.68E+11
12.63	6.69E+10															44.44	3.55E+11

M (N.mm); χ (1/mm); M^+ (Positive bending moment); M^- (Negative bending moment)

ANNEX 5.3 – SL15-HS
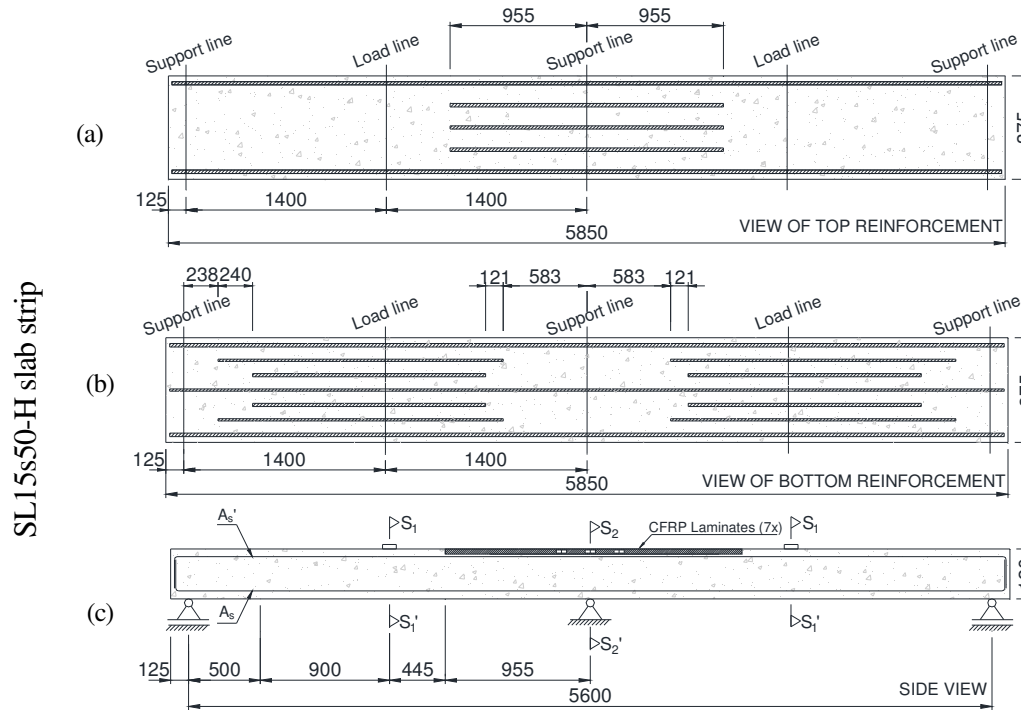
Figure A5.7: Arrangement of the (a-b) longitudinal steel reinforcement of the SL15-HS slab strip.
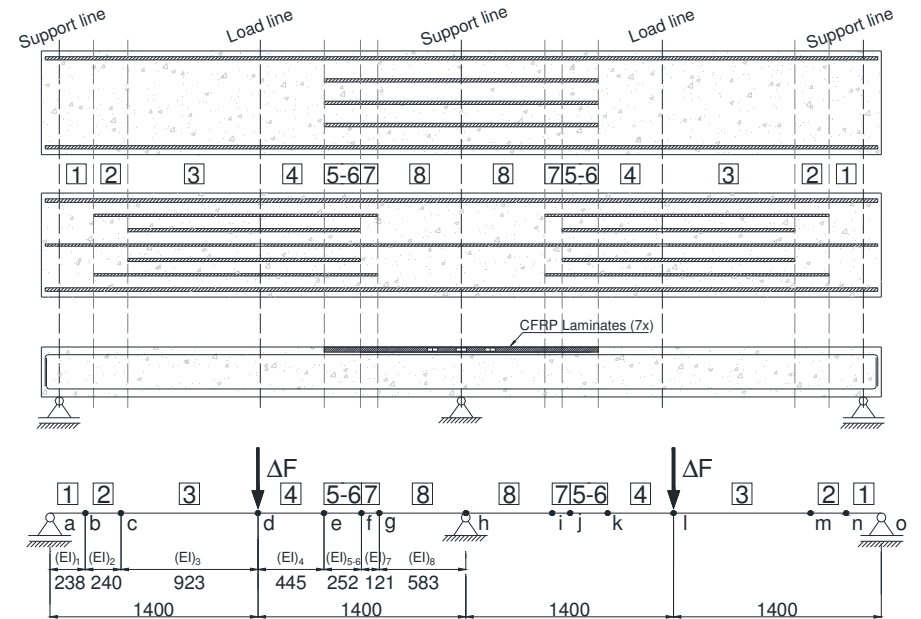
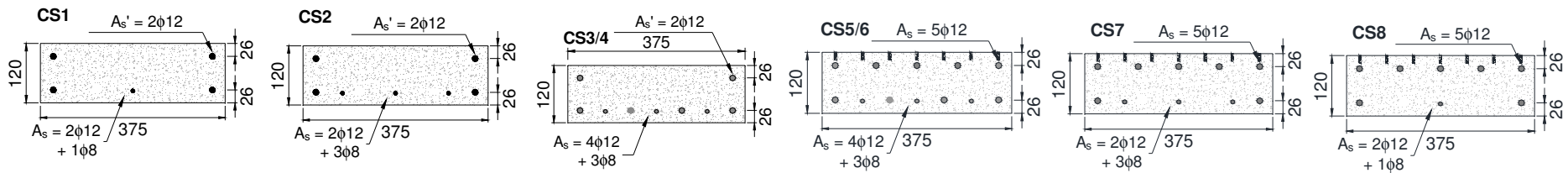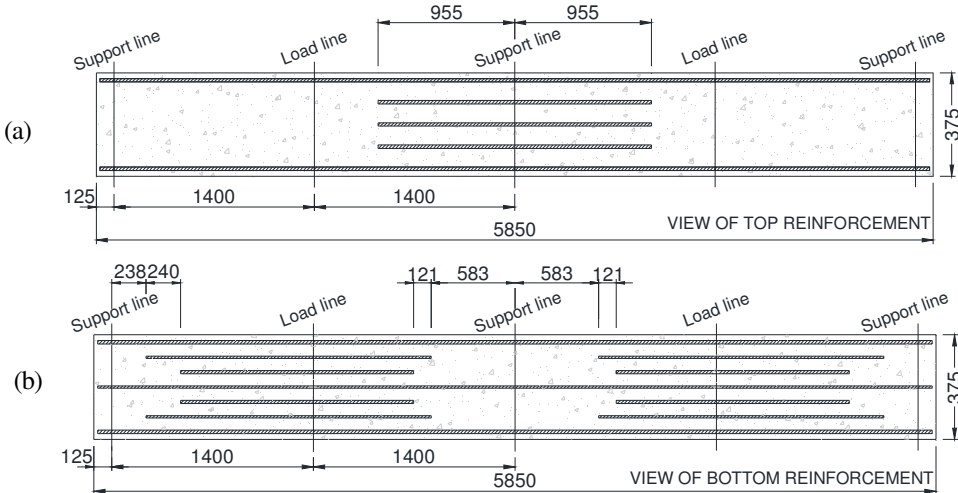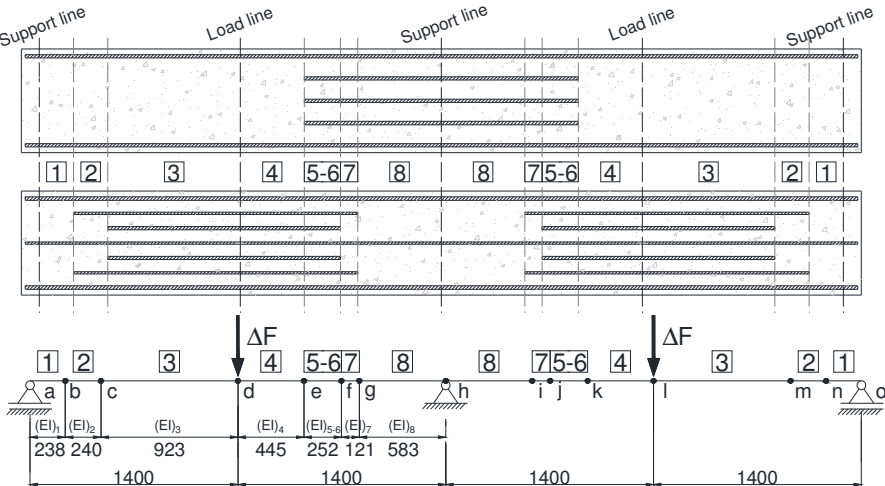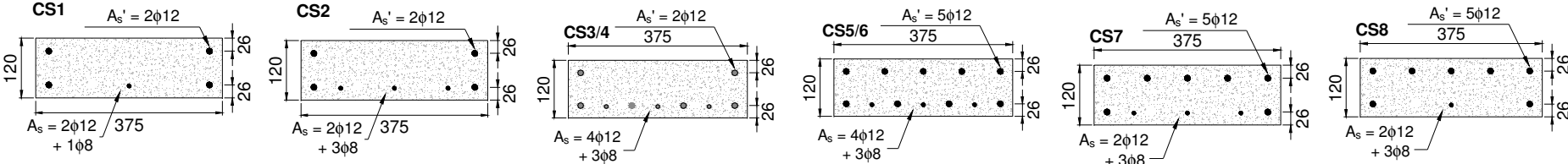Figure A5.8: Discretization of the slab strip.

Figure A5.9: Resume of the cross-section according to the longitudinal steel reinforcement.

Table A5.3: Relation M− χ of the cross sections of the SL15-HS slab strip.

Element 1		Element 2		Element 3		Element 4		Element 5/6		Element 5/6		Element 7		Element 7		Element 8	
M^+	χ	M^+	χ	M^+	χ	M^+	χ	M^+	χ	M^-	χ	M^+	χ	M^-	χ	M^+	χ
0.00	1.68E+12	0.00	1.70E+12	0.00	1.74E+12	0.00	1.74E+12	0.00	1.81E+12	0.00	1.81E+12	0.00	1.76E+12	0.00	1.76E+12	0.00	1.74E+12
1.24	1.54E+12	1.25	1.56E+12	1.27	1.62E+12	1.27	1.62E+12	1.35	1.67E+12	1.35	1.67E+12	1.33	1.62E+12	1.30	1.63E+12	1.28	1.62E+12
3.38	1.17E+12	3.46	1.22E+12	3.59	1.31E+12	3.59	1.31E+12	3.77	1.33E+12	3.76	1.31E+12	3.61	1.22E+12	3.65	1.31E+12	3.59	1.30E+12
3.84	4.19E+11	4.42	5.44E+11	5.26	7.54E+11	5.26	7.54E+11	5.43	7.38E+11	5.31	7.02E+11	4.50	5.22E+11	5.22	7.13E+11	5.17	7.19E+11
5.28	3.30E+11	5.96	4.22E+11	7.05	5.99E+11	7.05	5.99E+11	7.38	6.00E+11	7.23	5.71E+11	6.15	4.21E+11	7.04	5.71E+11	6.94	5.71E+11
6.93	3.15E+11	7.79	4.01E+11	9.12	5.64E+11	9.12	5.64E+11	9.59	5.69E+11	9.41	5.42E+11	8.05	4.02E+11	9.14	5.40E+11	9.00	5.39E+11
8.50	3.07E+11	9.56	3.92E+11	11.14	5.48E+11	11.14	5.48E+11	11.75	5.55E+11	11.54	5.29E+11	9.89	3.93E+11	11.19	5.26E+11	11.00	5.24E+11
9.89	2.96E+11	11.23	3.84E+11	13.07	5.37E+11	13.07	5.37E+11	13.82	5.45E+11	13.58	5.20E+11	11.62	3.84E+11	13.14	5.16E+11	12.91	5.14E+11
10.84	2.70E+11	12.74	3.73E+11	14.89	5.28E+11	14.89	5.28E+11	15.78	5.37E+11	15.51	5.12E+11	13.13	3.70E+11	14.98	5.08E+11	14.72	5.06E+11
11.20	2.28E+11	13.92	3.50E+11	16.60	5.19E+11	16.60	5.19E+11	17.62	5.27E+11	17.31	5.03E+11	14.14	3.40E+11	16.71	4.99E+11	16.41	4.97E+11
11.29	1.87E+11	14.52	3.12E+11	18.18	5.09E+11	18.18	5.09E+11	19.29	5.15E+11	18.91	4.88E+11	14.58	3.00E+11	18.28	4.88E+11	17.96	4.86E+11
11.37	1.61E+11	14.76	2.73E+11	19.61	4.96E+11	19.61	4.96E+11	20.71	4.96E+11	20.19	4.64E+11	14.76	2.61E+11	19.63	4.71E+11	19.31	4.71E+11
11.45	1.42E+11	14.89	2.39E+11	20.80	4.78E+11	20.80	4.78E+11	21.72	4.65E+11	20.93	4.23E+11	14.85	2.28E+11	20.62	4.43E+11	20.37	4.49E+11
11.52	1.27E+11	14.96	2.10E+11	21.68	4.52E+11	21.68	4.52E+11	22.22	4.19E+11	21.21	3.77E+11	14.91	2.02E+11	21.15	4.03E+11	21.03	4.16E+11
11.58	1.16E+11	14.99	1.84E+11	22.20	4.19E+11	22.20	4.19E+11	22.38	3.74E+11	21.33	3.39E+11	14.97	1.82E+11	21.33	3.58E+11	21.32	3.74E+11
11.63	1.06E+11	15.02	1.66E+11	22.45	3.82E+11	22.45	3.82E+11	22.47	3.38E+11	21.42	3.08E+11	15.02	1.66E+11	21.41	3.22E+11	21.41	3.34E+11
11.67	9.86E+10	15.05	1.52E+11	22.54	3.46E+11	22.54	3.46E+11	22.53	3.08E+11	21.48	2.82E+11	15.07	1.54E+11	21.46	2.94E+11	21.46	3.02E+11
11.70	9.19E+10	15.07	1.40E+11	22.56	3.13E+11	22.56	3.13E+11	22.57	2.84E+11	21.51	2.59E+11	15.09	1.43E+11	21.50	2.70E+11	21.49	2.77E+11
11.73	8.62E+10	15.08	1.30E+11	22.56	2.87E+11	22.56	2.87E+11	22.59	2.63E+11	21.54	2.42E+11	15.11	1.34E+11	21.52	2.51E+11	21.51	2.57E+11
11.74	8.13E+10	15.09	1.22E+11					22.60	2.46E+11	21.56	2.26E+11	15.12	1.26E+11	21.53	2.34E+11		
11.74	7.70E+10																

M (N.mm); χ (1/mm); M^+ (Positive bending moment); M^- (Negative bending moment)
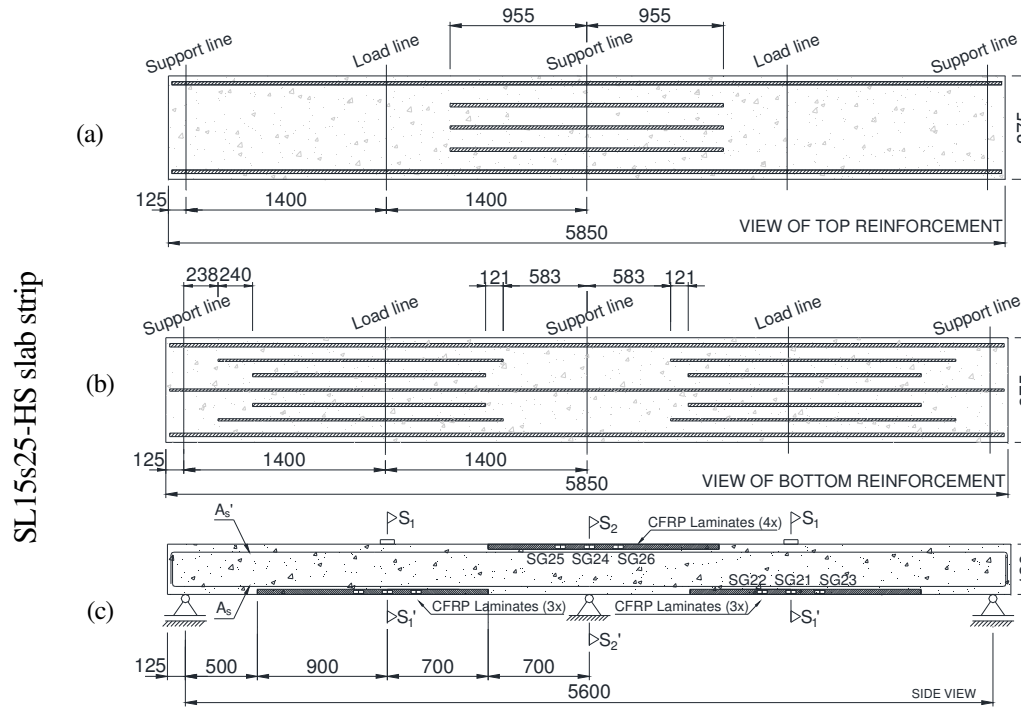
ANNEX 5.4– SL15s25-HS

Figure A5.10: Arrangement of the (a-b) longitudinal steel reinforcement and (c) CFRP laminates of the SL15s25-H slab strip.
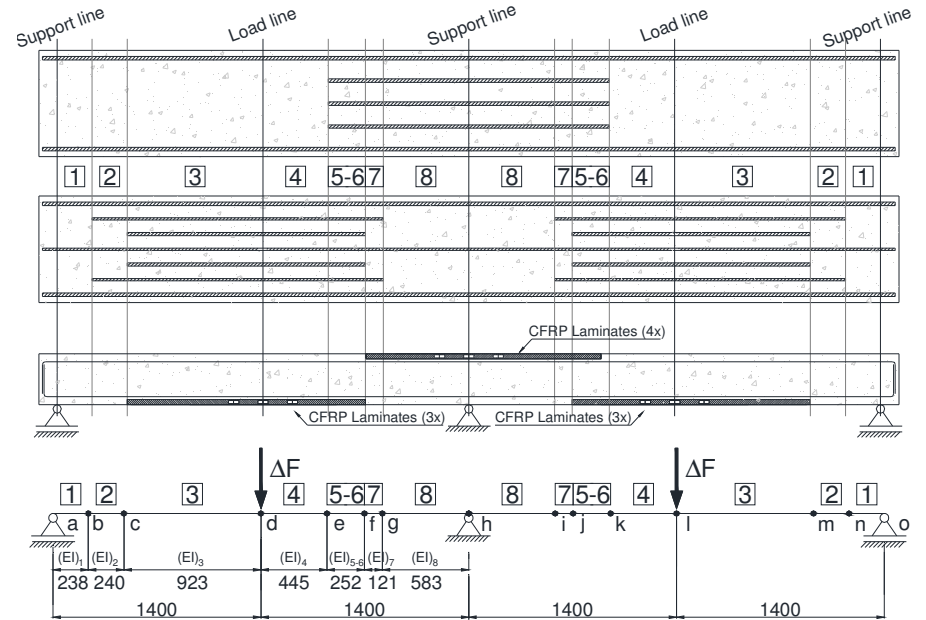

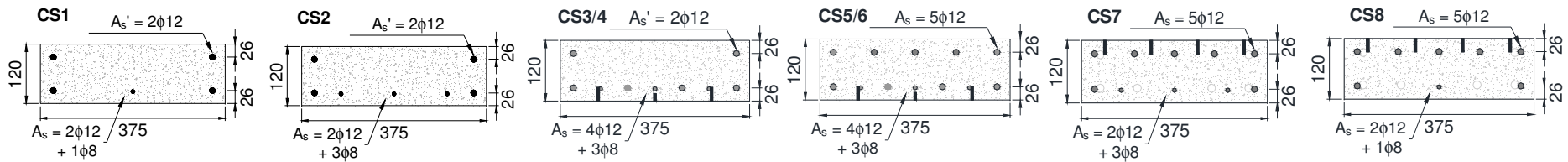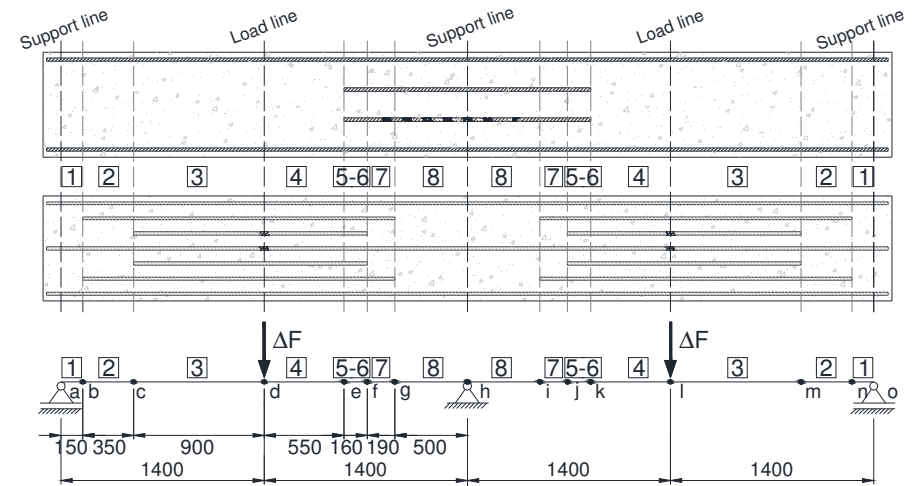Figure A5.11: Discretization of the slab strip.

Figure A5.12: Resume of the cross-section according to the longitudinal steel reinforcement.

Table A5.4: Relation M$-\chi$ of the cross sections of the SL15s25-HS slab strip.

Element 1		Element 2		Element 3		Element 4		Element 5/6		Element 5/6		Element 7		Element 7		Element 8	
M^+	χ	M^+	χ	M^+	χ	M^+	χ	M^+	χ	M^-	χ	M^+	χ	M^-	χ	M^+	χ
0.00	1.68E+12	0.00	1.70E+12	0.00	1.76E+12	0.00	1.76E+12	0.00	1.83E+12	0.00	1.80E+12	0.00	1.75E+12	0.00	1.80E+12	0.00	1.78E+12
2.45	1.38E+12	2.48	1.41E+12	2.56	1.51E+12	2.56	1.51E+12	2.71	1.55E+12	2.70	1.50E+12	2.63	1.44E+12	2.63	1.53E+12	2.59	1.52E+12
2.96	1.29E+12	3.01	1.32E+12	4.59	1.12E+12	4.59	1.12E+12	5.45	8.65E+11	3.28	1.41E+12	3.17	1.34E+12	5.40	8.86E+11	5.35	8.91E+11
3.73	5.67E+11	4.17	6.91E+11	7.04	6.77E+11	7.04	6.77E+11	9.37	6.36E+11	4.87	8.22E+11	4.21	6.40E+11	9.24	6.43E+11	9.09	6.41E+11
4.46	3.50E+11	5.08	4.52E+11	10.06	6.17E+11	10.06	6.17E+11	13.54	6.07E+11	6.25	6.02E+11	5.28	4.42E+11	13.31	6.11E+11	13.07	6.08E+11
5.83	3.23E+11	6.57	4.13E+11	12.99	5.96E+11	12.99	5.96E+11	17.37	5.89E+11	8.05	5.55E+11	6.87	4.10E+11	17.05	5.93E+11	16.72	5.89E+11
7.20	3.14E+11	8.09	3.99E+11	15.71	5.81E+11	15.71	5.81E+11	20.82	5.71E+11	9.89	5.37E+11	8.46	3.98E+11	20.42	5.76E+11	20.00	5.72E+11
8.50	3.07E+11	9.56	3.92E+11	18.23	5.68E+11	18.23	5.68E+11	23.65	5.41E+11	11.68	5.27E+11	10.01	3.91E+11	23.33	5.53E+11	22.84	5.51E+11
9.67	2.99E+11	10.96	3.85E+11	20.50	5.54E+11	20.50	5.54E+11	25.49	4.89E+11	13.40	5.20E+11	11.47	3.84E+11	25.54	5.17E+11	25.08	5.19E+11
10.59	2.81E+11	12.26	3.77E+11	22.50	5.36E+11	22.50	5.36E+11	26.56	4.28E+11	15.04	5.13E+11	12.78	3.73E+11	27.01	4.70E+11	26.61	4.76E+11
11.08	2.50E+11	13.39	3.63E+11	24.10	5.10E+11	24.10	5.10E+11	27.37	3.78E+11	16.60	5.06E+11	13.80	3.53E+11	28.08	4.28E+11	27.67	4.33E+11
11.23	2.12E+11	14.18	3.38E+11	25.24	4.75E+11	25.24	4.75E+11	28.07	3.42E+11	18.04	4.96E+11	14.37	3.21E+11	28.97	3.93E+11	28.51	3.98E+11
11.30	1.82E+11	14.58	3.05E+11	25.99	4.37E+11	25.99	4.37E+11	28.69	3.13E+11	19.32	4.82E+11	14.63	2.86E+11	29.74	3.65E+11	29.22	3.70E+11
11.37	1.61E+11	14.76	2.73E+11	26.54	4.03E+11	26.54	4.03E+11	29.24	2.90E+11	20.32	4.58E+11	14.76	2.54E+11	30.40	3.42E+11	29.81	3.46E+11
11.44	1.45E+11	14.87	2.45E+11	26.98	3.75E+11	26.98	3.75E+11	29.74	2.72E+11	20.91	4.23E+11	14.83	2.27E+11	30.97	3.23E+11	30.32	3.26E+11
11.50	1.31E+11	14.94	2.20E+11	27.36	3.51E+11	27.36	3.51E+11	30.18	2.56E+11	21.16	3.83E+11	14.88	2.04E+11	31.48	3.06E+11	30.75	3.09E+11
11.55	1.21E+11	14.98	1.96E+11	27.68	3.30E+11	27.68	3.30E+11	30.59	2.42E+11	21.28	3.49E+11	14.93	1.86E+11	31.93	2.92E+11	31.11	2.94E+11
11.60	1.12E+11	15.00	1.78E+11	27.95	3.13E+11	27.95	3.13E+11	30.97	2.31E+11	21.36	3.20E+11	14.98	1.72E+11	32.31	2.79E+11	31.42	2.81E+11
11.64	1.05E+11	15.03	1.63E+11	28.18	2.97E+11	28.18	2.97E+11	31.33	2.21E+11	21.42	2.96E+11	15.02	1.60E+11	32.68	2.68E+11	31.68	2.70E+11
11.67	9.86E+10	15.05	1.52E+11	28.37	2.84E+11	28.37	2.84E+11	31.69	2.11E+11	21.46	2.75E+11	15.05	1.50E+11	33.02	2.57E+11	31.88	2.59E+11
11.70	9.30E+10	15.07	1.42E+11	28.53	2.72E+11	28.53	2.72E+11	32.03	2.03E+11	21.49	2.57E+11	15.07	1.41E+11	33.30	2.48E+11	32.02	2.50E+11
11.72	8.80E+10	15.08	1.33E+11	28.67	2.61E+11	28.67	2.61E+11	32.37	1.96E+11	21.52	2.41E+11	15.08	1.33E+11	33.53	2.40E+11		
11.73	8.37E+10	15.09	1.26E+11	28.78	2.51E+11	28.78	2.51E+11	32.72	1.90E+11	21.53	2.28E+11	15.09	1.26E+11	33.68	2.32E+11		
11.74	7.98E+10			28.88	2.41E+11	28.88	2.41E+11	33.06	1.84E+11					33.74	2.26E+11		
				28.96	2.33E+11	28.96	2.33E+11	33.39	1.78E+11								
				29.02	2.26E+11	29.02	2.26E+11	33.71	1.73E+11								
				29.05	2.19E+11	29.05	2.19E+11	34.02	1.69E+11								
								34.27	1.65E+11								

M (N.mm); χ (1/mm); M^+ (Positive bending moment); M^- (Negative bending moment)

SL30-H slab strip

(a)

850 | 850

Support line   Load line   Support line   Load line   Support line

SG4 SG2 SG6
SG5 SG3 SG1 SG7

(5x100) 200

375

125 | 1400 | 1400

5850

VIEW OF TOP REINFORCEMENT

(b)

150 350   190 500 500 190

Support line   Load line   Support line   Load line   Support line

SG8   SG10
SG9   SG11

375

125 | 1400 | 1400

5850

VIEW OF BOTTOM REINFORCEMENT
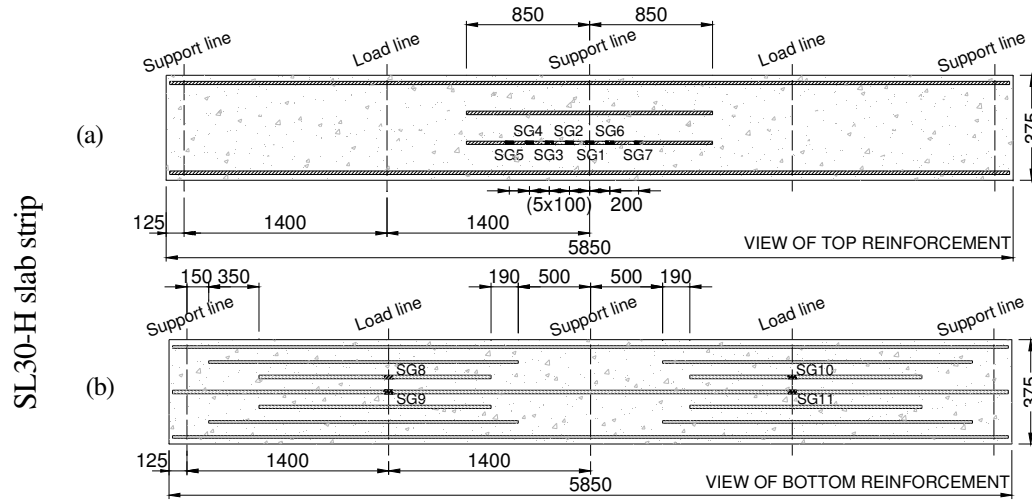
Figure A5.13: Arrangement of the (a-b) longitudinal steel
of the SL30-H slab strip.

Support line   Load line   Support line   Load line   Support line

1 2   3   4 5-6 7 8   8 7 5-6 4   3   2 1

ΔF   ΔF

1 2   3   4 5-6 7 8   8 7 5-6 4   3   2 1
a b   c   d   e f g   h   i j k   l   m   n o

150 350   900   550 160 190 500   1400   1400

1400   1400

Figure A5.14: Discretization of the slab strip.

CS1 $A_s' = 2\phi12$

120 | 26 / 26

$A_s = 1\phi12$ / 375
+ $2\phi10$

CS2 $A_s' = 2\phi12$

120 | 26 / 26

$A_s = 3\phi12$ / 375
+ $2\phi10$

CS3/4 $A_s' = 2\phi12$

120 | 26 / 26

$A_s = 3\phi12$ / 375
+ $4\phi10$

CS5/6 $A_s = 4\phi12$

120 | 26 / 26

$A_s = 3\phi12$ / 375
+ $4\phi10$

CS7 $A_s = 4\phi12$

120 | 26 / 26

$A_s = 3\phi12$ / 375
+ $2\phi10$

CS8 $A_s = 4\phi12$

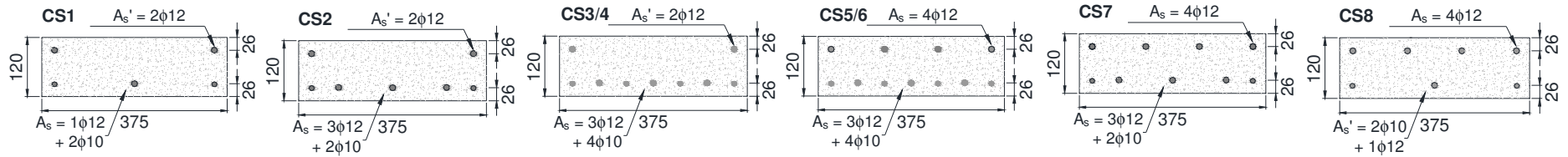120 | 26 / 26

$A_s' = 2\phi10$ / 375
+ $1\phi12$

Figure A5.15: Resume of the cross-section according to the longitudinal steel reinforcement.

Table A5.5: Relation M$-\chi$ of the cross sections of the SL30-H slab strip.

Element 1		Element 2		Element 3		Element 4		Element 5/6		Element 5/6		Element 7		Element 7		Element 8	
M^+	χ	M^+	χ	M^+	χ	M^+	χ	M^+	χ	M^-	χ	M^+	χ	M^-	χ	M^+	χ
0.00	1.83E+12	0.00	1.87E+12	0.00	1.90E+12	0.00	1.90E+12	0.00	1.94E+12	0.00	1.94E+12	0.00	1.92E+12	0.00	1.92E+12	0.00	1.87E+12
1.38	1.73E+12	1.40	1.78E+12	1.41	1.81E+12	1.41	1.81E+12	1.46	1.85E+12	1.49	1.84E+12	1.45	1.82E+12	1.45	1.82E+12	1.40	1.78E+12
3.42	1.52E+12	3.49	1.59E+12	3.53	1.63E+12	3.53	1.63E+12	3.65	1.66E+12	3.68	1.63E+12	3.61	1.62E+12	3.61	1.61E+12	3.49	1.59E+12
4.40	7.01E+11	5.29	9.67E+11	5.64	1.08E+12	5.64	1.08E+12	5.71	1.06E+12	5.25	8.87E+11	5.33	9.37E+11	5.24	9.06E+11	5.22	9.38E+11
4.70	3.47E+11	6.18	5.89E+11	6.84	7.19E+11	6.84	7.19E+11	6.98	7.11E+11	6.19	5.50E+11	6.28	5.81E+11	6.13	5.53E+11	6.04	5.61E+11
6.20	3.15E+11	7.92	5.21E+11	8.67	6.31E+11	8.67	6.31E+11	8.90	6.31E+11	8.00	4.96E+11	8.09	5.20E+11	7.92	4.97E+11	7.77	4.98E+11
7.75	3.05E+11	9.83	5.02E+11	10.71	6.05E+11	10.71	6.05E+11	11.00	6.07E+11	9.94	4.80E+11	10.04	5.02E+11	9.84	4.80E+11	9.64	4.80E+11
9.21	2.98E+11	11.71	4.93E+11	12.74	5.93E+11	12.74	5.93E+11	13.10	5.96E+11	11.86	4.72E+11	11.97	4.94E+11	11.74	4.72E+11	11.50	4.71E+11
10.46	2.83E+11	13.54	4.86E+11	14.72	5.85E+11	14.72	5.85E+11	15.14	5.89E+11	13.71	4.65E+11	13.85	4.87E+11	13.57	4.65E+11	13.31	4.64E+11
11.20	2.47E+11	15.30	4.79E+11	16.63	5.79E+11	16.63	5.79E+11	17.11	5.82E+11	15.41	4.55E+11	15.64	4.79E+11	15.28	4.55E+11	15.00	4.56E+11
11.40	2.05E+11	16.92	4.69E+11	18.45	5.72E+11	18.45	5.72E+11	19.00	5.75E+11	16.79	4.33E+11	17.26	4.67E+11	16.70	4.35E+11	16.48	4.39E+11
11.53	1.76E+11	18.28	4.48E+11	20.17	5.64E+11	20.17	5.64E+11	20.77	5.66E+11	17.61	3.96E+11	18.53	4.42E+11	17.58	3.99E+11	17.49	4.06E+11
11.65	1.54E+11	19.17	4.14E+11	21.74	5.53E+11	21.74	5.53E+11	22.36	5.52E+11	17.98	3.52E+11	19.28	4.05E+11	17.97	3.56E+11	17.95	3.63E+11
11.75	1.37E+11	19.61	3.72E+11	23.10	5.36E+11	23.10	5.36E+11	23.67	5.29E+11	18.15	3.09E+11	19.64	3.64E+11	18.16	3.14E+11	18.18	3.22E+11
11.85	1.23E+11	19.83	3.34E+11	24.18	5.11E+11	24.18	5.11E+11	24.57	4.93E+11	18.24	2.73E+11	19.83	3.27E+11	18.26	2.75E+11	18.29	2.83E+11
11.93	1.12E+11	19.96	3.01E+11	24.89	4.74E+11	24.89	4.74E+11	25.01	4.49E+11	18.33	2.46E+11	19.94	2.92E+11	18.33	2.46E+11	18.34	2.48E+11
12.01	1.04E+11	20.04	2.70E+11	25.19	4.29E+11	25.19	4.29E+11	25.22	4.09E+11	18.42	2.25E+11	20.00	2.62E+11	18.41	2.24E+11	18.40	2.22E+11
12.07	9.65E+10	20.07	2.42E+11	25.33	3.90E+11	25.33	3.90E+11	25.34	3.75E+11	18.49	2.08E+11	20.05	2.38E+11	18.48	2.06E+11	18.45	2.03E+11
12.13	9.05E+10	20.10	2.20E+11	25.42	3.59E+11	25.42	3.59E+11	25.43	3.46E+11	18.55	1.94E+11	20.09	2.20E+11	18.53	1.92E+11	18.50	1.88E+11
12.17	8.54E+10	20.12	2.03E+11	25.48	3.32E+11	25.48	3.32E+11	25.49	3.21E+11	18.60	1.82E+11	20.13	2.05E+11	18.58	1.79E+11	18.54	1.75E+11
12.21	8.10E+10	20.14	1.89E+11	25.52	3.10E+11	25.52	3.10E+11	25.53	3.01E+11	18.63	1.71E+11	20.16	1.92E+11	18.61	1.69E+11	18.56	1.64E+11
12.23	7.71E+10	20.15	1.78E+11	25.54	2.91E+11	25.54	2.91E+11	25.56	2.83E+11	18.65	1.62E+11	20.17	1.81E+11	18.63	1.60E+11	18.58	1.55E+11
12.25	7.37E+10			25.55	2.75E+11	25.55	2.75E+11			18.66	1.54E+11			18.64	1.51E+11	18.58	1.47E+11
12.26	7.06E+10																

M (N.mm); χ (1/mm); M^+ (Positive bending moment); M^- (Negative bending moment)
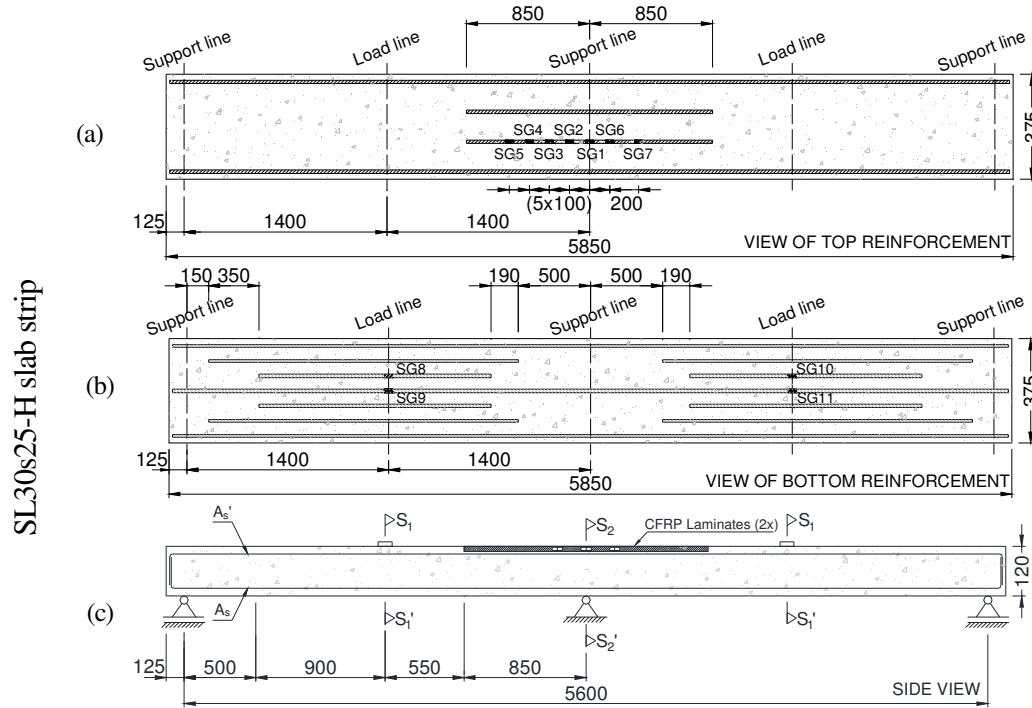
Figure A5.16: Arrangement of the (a-b) longitudinal steel reinforcement and (c) CFRP laminates of the SL30s25-H slab strip.
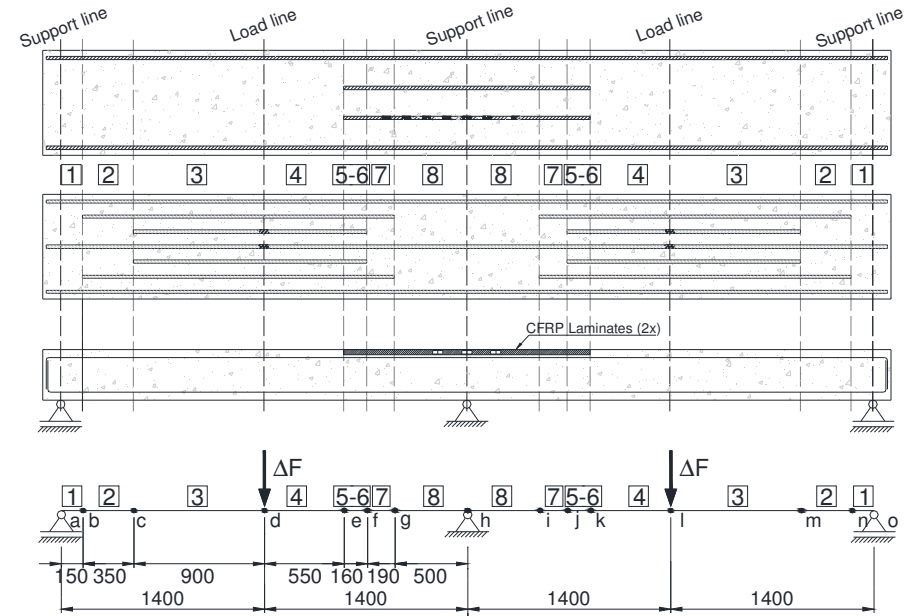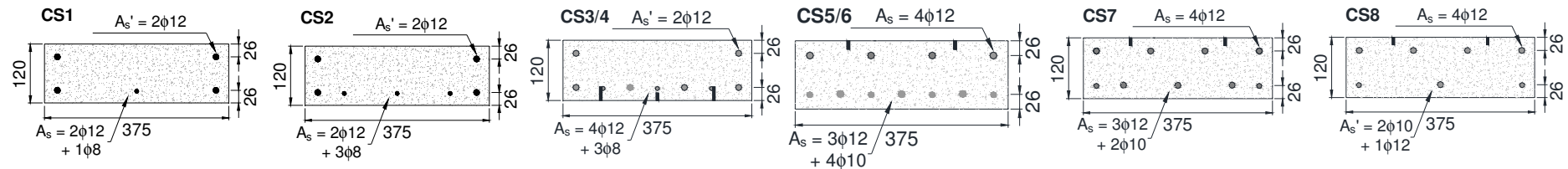
Figure A5.17: Discretization of the slab strip.

CS1 $A_s' = 2\phi12$

$A_s = 2\phi12$
$+ 1\phi8$ / 375

CS2 $A_s' = 2\phi12$

$A_s = 2\phi12$
$+ 3\phi8$ / 375

CS3/4 $A_s' = 2\phi12$

$A_s = 4\phi12$
$+ 3\phi8$ / 375

CS5/6 $A_s = 4\phi12$

$A_s = 3\phi12$
$+ 4\phi10$ / 375

CS7 $A_s = 4\phi12$

$A_s = 3\phi12$
$+ 2\phi10$ / 375

CS8 $A_s = 4\phi12$

$A_s' = 2\phi10$
$+ 1\phi12$ / 375

Figure A5.18: Resume of the cross-section according to the longitudinal steel reinforcement.

343

Table A5.6: Relation M−χ of the cross sections of the SL30s25-H slab strip.

Element 1		Element 2		Element 3		Element 4		Element 5		Element 5		Element 6		Element 6		Element 7	
M^+	χ	M^+	χ	M^+	χ	M^+	χ	M^+	χ	M^-	χ	M^+	χ	M^-	χ	M^+	χ
0.00	1.83E+12	0.00	1.87E+12	0.00	1.90E+12	0.00	1.90E+12	0.00	1.94E+12	0.00	1.95E+12	0.00	1.91E+12	0.00	1.93E+12	0.00	1.88E+12
1.38	1.73E+12	1.40	1.78E+12	1.41	1.81E+12	1.41	1.81E+12	1.43	1.84E+12	1.49	1.85E+12	1.42	1.82E+12	1.46	1.83E+12	1.41	1.79E+12
3.42	1.52E+12	3.49	1.59E+12	3.53	1.63E+12	3.53	1.63E+12	3.57	1.67E+12	5.13	1.26E+12	4.97	1.28E+12	5.09	1.27E+12	4.99	1.28E+12
4.40	7.01E+11	5.29	9.67E+11	5.64	1.08E+12	5.64	1.08E+12	5.65	1.09E+12	6.80	5.68E+11	6.39	5.69E+11	6.73	5.71E+11	6.61	5.76E+11
4.70	3.47E+11	6.18	5.89E+11	6.84	7.19E+11	6.84	7.19E+11	6.80	7.25E+11	9.96	5.16E+11	9.25	5.05E+11	9.85	5.16E+11	9.64	5.15E+11
6.20	3.15E+11	7.92	5.21E+11	8.67	6.31E+11	8.67	6.31E+11	8.58	6.35E+11	13.15	5.02E+11	12.20	4.91E+11	13.00	5.02E+11	12.72	5.01E+11
7.75	3.05E+11	9.83	5.02E+11	10.71	6.05E+11	10.71	6.05E+11	10.59	6.08E+11	16.14	4.90E+11	15.03	4.81E+11	15.97	4.90E+11	15.63	4.89E+11
9.21	2.98E+11	11.71	4.93E+11	12.74	5.93E+11	12.74	5.93E+11	12.61	5.96E+11	18.51	4.57E+11	17.51	4.62E+11	18.40	4.60E+11	18.13	4.66E+11
10.46	2.83E+11	13.54	4.86E+11	14.72	5.85E+11	14.72	5.85E+11	14.58	5.88E+11	19.74	3.98E+11	19.08	4.15E+11	19.69	4.01E+11	19.60	4.09E+11
11.20	2.47E+11	15.30	4.79E+11	16.63	5.79E+11	16.63	5.79E+11	16.50	5.83E+11	20.45	3.42E+11	19.64	3.54E+11	20.42	3.46E+11	20.36	3.52E+11
11.40	2.05E+11	16.92	4.69E+11	18.45	5.72E+11	18.45	5.72E+11	18.35	5.76E+11	21.04	2.97E+11	19.85	2.99E+11	21.02	3.01E+11	20.96	3.08E+11
11.53	1.76E+11	18.28	4.48E+11	20.17	5.64E+11	20.17	5.64E+11	20.09	5.68E+11	21.58	2.64E+11	19.93	2.54E+11	21.56	2.66E+11	21.52	2.72E+11
11.65	1.54E+11	19.17	4.14E+11	21.74	5.53E+11	21.74	5.53E+11	21.70	5.57E+11	22.05	2.40E+11	20.00	2.23E+11	22.05	2.41E+11	22.02	2.43E+11
11.75	1.37E+11	19.61	3.72E+11	23.10	5.36E+11	23.10	5.36E+11	23.08	5.39E+11	22.47	2.22E+11	20.06	2.00E+11	22.47	2.22E+11	22.46	2.23E+11
11.85	1.23E+11	19.83	3.34E+11	24.18	5.11E+11	24.18	5.11E+11	24.15	5.11E+11	22.83	2.07E+11	20.09	1.82E+11	22.83	2.07E+11	22.83	2.07E+11
11.93	1.12E+11	19.96	3.01E+11	24.89	4.74E+11	24.89	4.74E+11	24.77	4.72E+11	23.14	1.94E+11			23.15	1.94E+11	23.15	1.94E+11
12.01	1.04E+11	20.04	2.70E+11	25.19	4.29E+11	25.19	4.29E+11	25.06	4.31E+11	23.41	1.84E+11			23.42	1.84E+11	23.41	1.84E+11
12.07	9.65E+10	20.07	2.42E+11	25.33	3.90E+11	25.33	3.90E+11	25.21	3.95E+11	23.63	1.75E+11			23.64	1.75E+11	23.63	1.75E+11
12.13	9.05E+10	20.10	2.20E+11	25.42	3.59E+11	25.42	3.59E+11	25.32	3.64E+11	23.82	1.67E+11			23.83	1.67E+11	23.80	1.67E+11
12.17	8.54E+10	20.12	2.03E+11	25.48	3.32E+11	25.48	3.32E+11	25.40	3.39E+11	23.99	1.60E+11			23.99	1.60E+11	23.94	1.61E+11
12.21	8.10E+10	20.14	1.89E+11	25.52	3.10E+11	25.52	3.10E+11	25.45	3.16E+11	24.13	1.53E+11			24.12	1.54E+11	24.05	1.55E+11
12.23	7.71E+10	20.15	1.78E+11	25.54	2.91E+11	25.54	2.91E+11	25.49	2.97E+11	24.26	1.48E+11			24.23	1.48E+11	24.13	1.50E+11
12.25	7.37E+10			25.55	2.75E+11	25.55	2.75E+11	25.52	2.80E+11	24.37	1.43E+11			24.33	1.43E+11	24.18	1.45E+11
12.26	7.06E+10																

M (N.mm); χ (1/mm); M^+ (Positive bending moment); M^- (Negative bending moment)
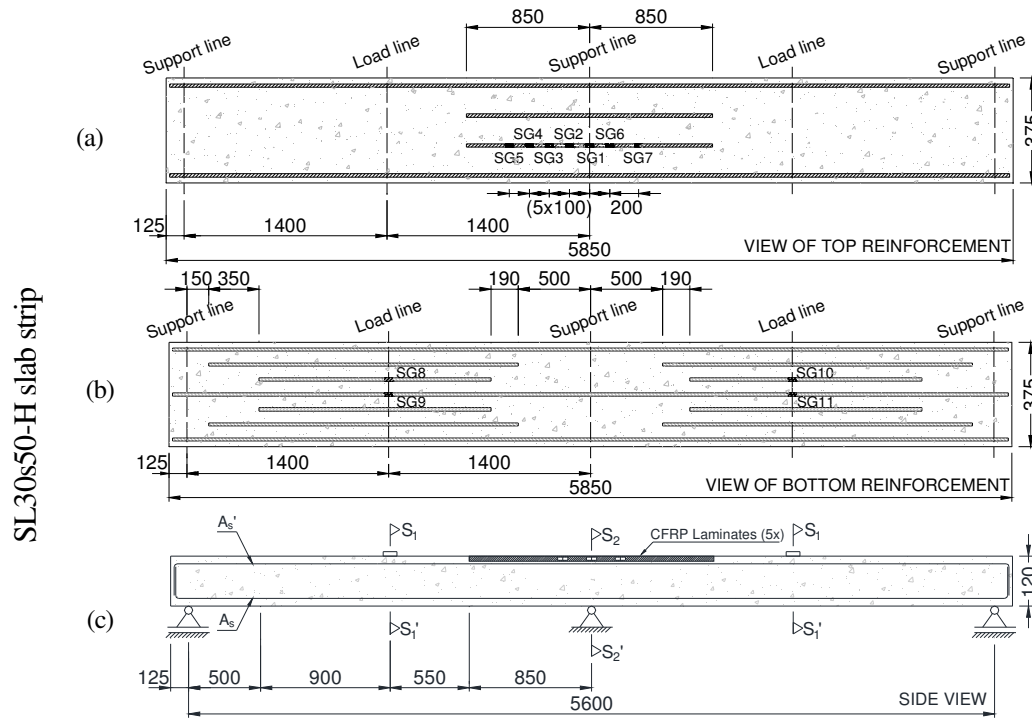
Figure A5.19: Arrangement of the (a-b) longitudinal steel reinforcement and (c) CFRP laminates of the SL30s50-H slab strip.
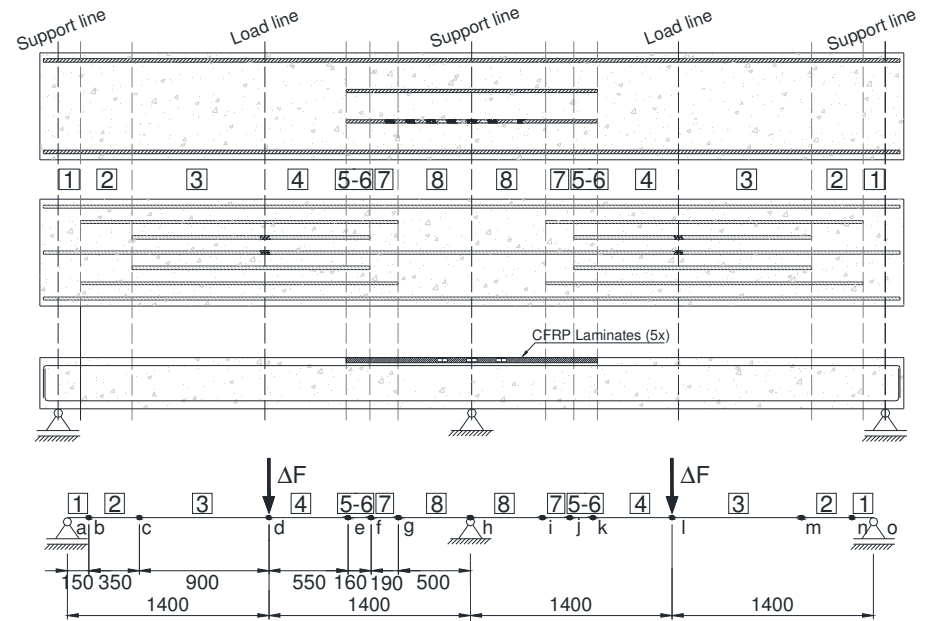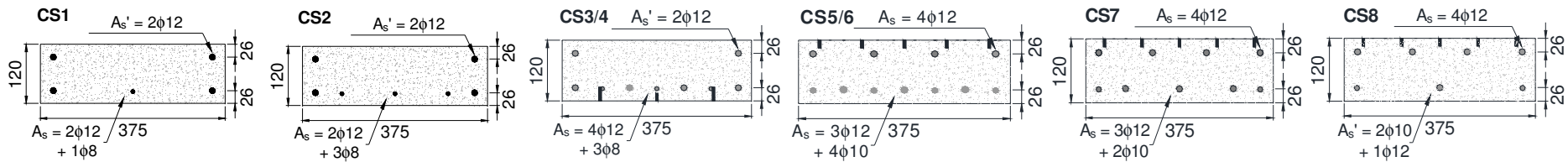
Figure A5.20: Discretization of the slab strip.

Figure A5.21: Resume of the cross-section according to the longitudinal steel reinforcement.

345

Table A5.7: Relation M–χ of the cross sections of the SL30s50-H slab strip.

Element 1		Element 2		Element 3		Element 4		Element 5		Element 5		Element 6		Element 6		Element 7	
M^+	χ	M^+	χ	M^+	χ	M^+	χ	M^+	χ	M^-	χ	M^+	χ	M^-	χ	M^+	χ
0.00	1.83E+12	0.00	1.87E+12	0.00	1.90E+12	0.00	1.90E+12	0.00	1.94E+12	0.00	1.97E+12	0.00	1.91E+12	0.00	1.94E+12	0.00	1.90E+12
2.79	1.60E+12	2.83	1.66E+12	2.86	1.70E+12	2.86	1.70E+12	2.92	1.73E+12	3.04	1.74E+12	2.89	1.69E+12	2.98	1.72E+12	2.87	1.69E+12
3.42	1.52E+12	3.49	1.59E+12	3.53	1.63E+12	3.53	1.63E+12	3.60	1.66E+12	5.46	1.14E+12	2.89	1.69E+12	5.18	1.31E+12	5.53	1.03E+12
4.40	7.01E+11	5.29	9.67E+11	5.64	1.08E+12	5.64	1.08E+12	5.67	1.08E+12	7.94	5.92E+11	4.99	1.27E+12	7.07	6.20E+11	8.47	5.77E+11
4.70	3.47E+11	6.18	5.89E+11	6.84	7.19E+11	6.84	7.19E+11	6.86	7.18E+11	11.73	5.53E+11	5.51	7.37E+11	10.33	5.60E+11	12.52	5.46E+11
6.20	3.15E+11	7.92	5.21E+11	8.67	6.31E+11	8.67	6.31E+11	8.70	6.32E+11	15.43	5.40E+11	6.47	5.64E+11	13.63	5.45E+11	16.36	5.33E+11
7.75	3.05E+11	9.83	5.02E+11	10.71	6.05E+11	10.71	6.05E+11	10.74	6.07E+11	18.81	5.23E+11	7.89	5.20E+11	16.78	5.34E+11	19.74	5.10E+11
9.21	2.98E+11	11.71	4.93E+11	12.74	5.93E+11	12.74	5.93E+11	12.79	5.95E+11	21.28	4.77E+11	9.40	5.04E+11	19.57	5.14E+11	22.01	4.50E+11
10.46	2.83E+11	13.54	4.86E+11	14.72	5.85E+11	14.72	5.85E+11	14.79	5.87E+11	22.73	4.18E+11	10.91	4.95E+11	21.55	4.68E+11	23.39	3.90E+11
11.20	2.47E+11	15.30	4.79E+11	16.63	5.79E+11	16.63	5.79E+11	16.72	5.81E+11	23.88	3.71E+11	12.40	4.90E+11	22.78	4.15E+11	24.54	3.47E+11
11.40	2.05E+11	16.92	4.69E+11	18.45	5.72E+11	18.45	5.72E+11	18.58	5.75E+11	24.92	3.36E+11	13.86	4.85E+11	23.80	3.74E+11	25.54	3.16E+11
11.53	1.76E+11	18.28	4.48E+11	20.17	5.64E+11	20.17	5.64E+11	20.34	5.66E+11	25.86	3.09E+11	15.26	4.79E+11	24.71	3.42E+11	26.40	2.92E+11
11.65	1.54E+11	19.17	4.14E+11	21.74	5.53E+11	21.74	5.53E+11	21.93	5.54E+11	26.71	2.87E+11	16.57	4.71E+11	25.55	3.17E+11	27.12	2.74E+11
11.75	1.37E+11	19.61	3.72E+11	23.10	5.36E+11	23.10	5.36E+11	23.29	5.35E+11	27.46	2.70E+11	17.73	4.58E+11	26.30	2.97E+11	27.73	2.58E+11
11.85	1.23E+11	19.83	3.34E+11	24.18	5.11E+11	24.18	5.11E+11	24.30	5.04E+11	28.10	2.55E+11	18.62	4.36E+11	26.97	2.80E+11	28.23	2.45E+11
11.93	1.12E+11	19.96	3.01E+11	24.89	4.74E+11	24.89	4.74E+11	24.85	4.62E+11	28.65	2.43E+11	19.19	4.07E+11	27.56	2.66E+11	28.65	2.33E+11
12.01	1.04E+11	20.04	2.70E+11	25.19	4.29E+11	25.19	4.29E+11	25.10	4.21E+11	29.14	2.33E+11	19.50	3.75E+11	28.07	2.54E+11	29.01	2.23E+11
12.07	9.65E+10	20.07	2.42E+11	25.33	3.90E+11	25.33	3.90E+11	25.24	3.86E+11	29.57	2.24E+11	19.68	3.45E+11	28.52	2.44E+11	29.31	2.14E+11
12.13	9.05E+10	20.10	2.20E+11	25.42	3.59E+11	25.42	3.59E+11	25.33	3.56E+11	29.96	2.15E+11	19.80	3.17E+11	28.93	2.34E+11	29.57	2.06E+11
12.17	8.54E+10	20.12	2.03E+11	25.48	3.32E+11	25.48	3.32E+11	25.40	3.31E+11	30.30	2.08E+11	19.88	2.91E+11	29.28	2.26E+11	29.79	1.99E+11
12.21	8.10E+10	20.14	1.89E+11	25.52	3.10E+11	25.52	3.10E+11	25.45	3.09E+11	30.62	2.01E+11	19.92	2.67E+11	29.60	2.18E+11	29.98	1.93E+11
12.23	7.71E+10	20.15	1.78E+11	25.54	2.91E+11	25.54	2.91E+11	25.48	2.91E+11	30.89	1.95E+11	19.95	2.47E+11	29.88	2.12E+11	30.15	1.87E+11
12.25	7.37E+10			25.55	2.75E+11	25.55	2.75E+11	25.50	2.74E+11	31.12	1.90E+11	19.99	2.31E+11	30.08	2.06E+11	30.29	1.81E+11
12.26	7.06E+10									31.38	1.85E+11	20.02	2.17E+11	30.35	2.00E+11	30.43	1.76E+11
										31.68	1.80E+11	20.05	2.06E+11	30.60	1.94E+11	30.55	1.72E+11
												20.07	1.95E+11	30.84	1.89E+11	30.67	1.68E+11
												20.08	1.86E+11	31.08	1.84E+11	30.77	1.64E+11
												20.09	1.78E+11	31.31	1.80E+11		

M (N.mm); χ (1/mm); M^+ (Positive bending moment); M^- (Negative bending moment)
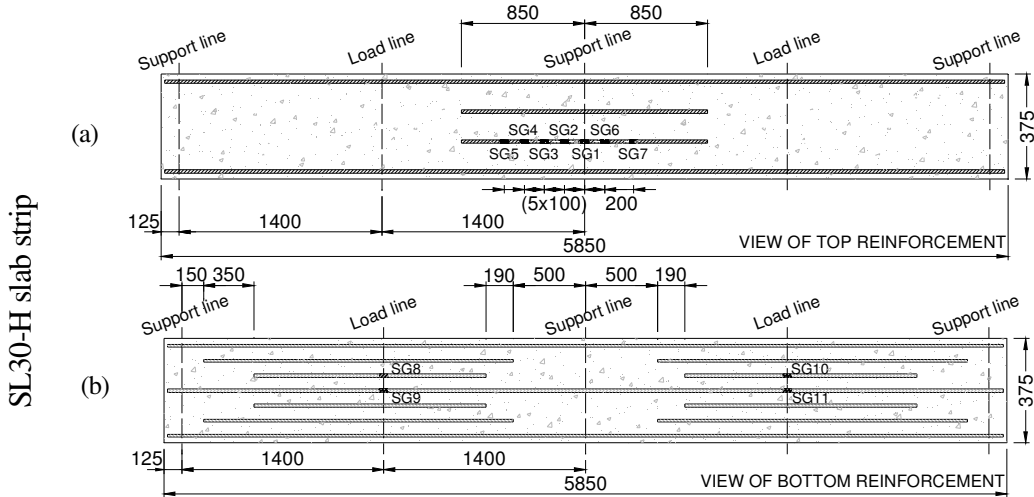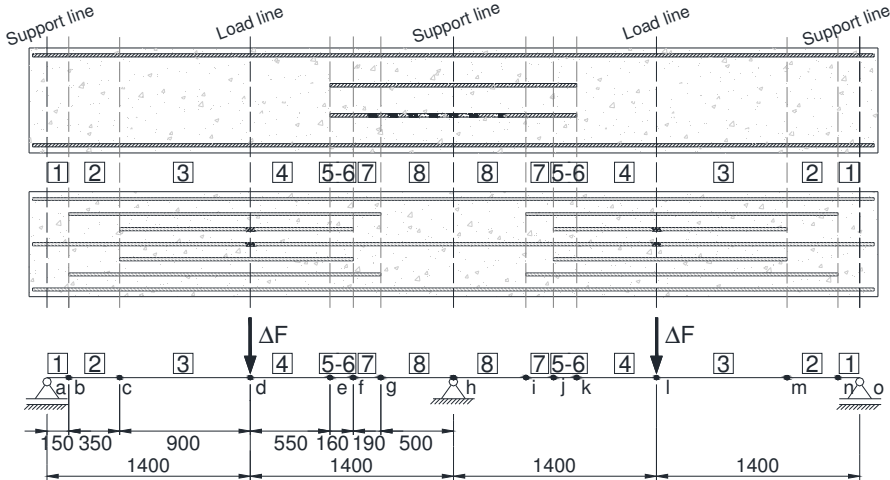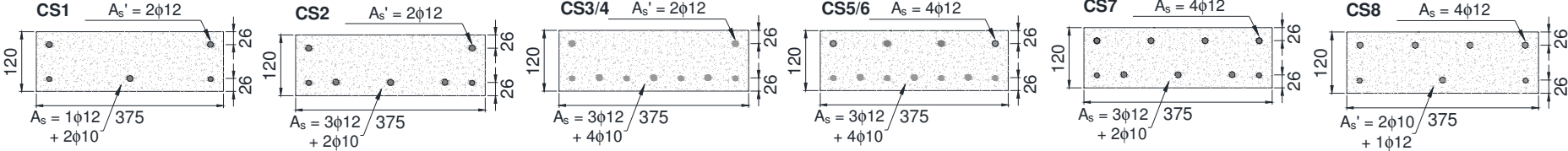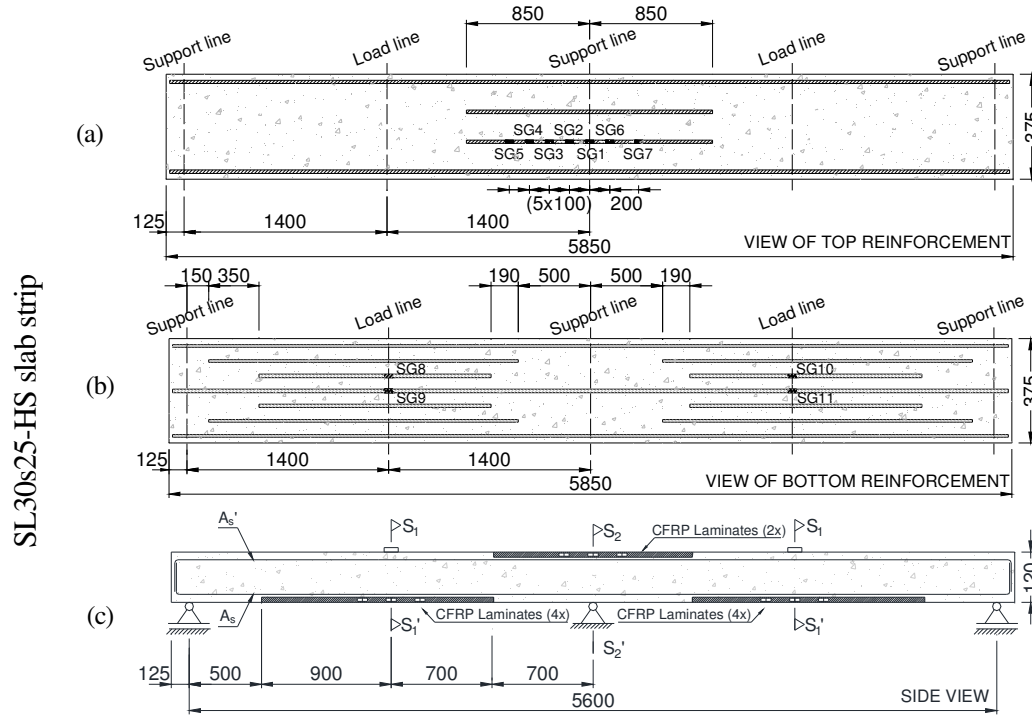
Figure A5.22: Arrangement of the (a-b) longitudinal steel
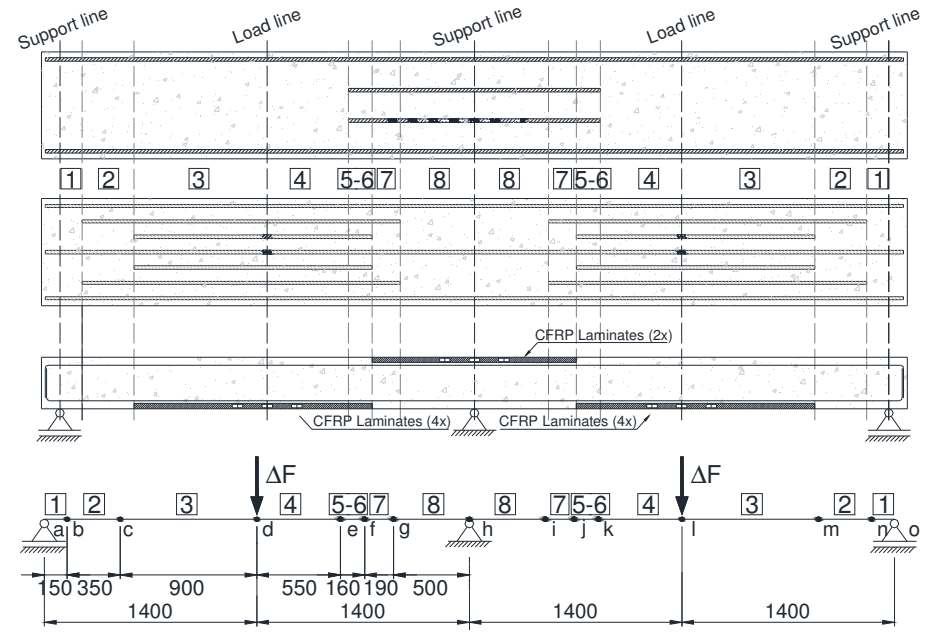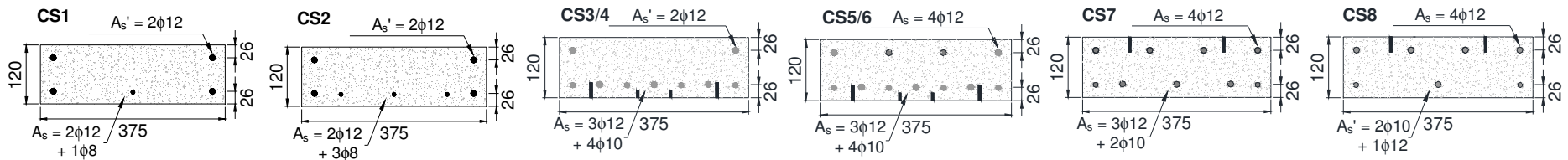of the SL30-H slab strip.

Figure A5.23: Discretization of the slab strip.

Figure A5.24: Resume of the cross-section according to the longitudinal steel reinforcement.

Table A5.8: Relation M−χ of the cross sections of the SL30-HS slab strip.

Element 1		Element 2		Element 3		Element 4		Element 5/6		Element 5/6		Element 7		Element 7		Element 8	
M^+	χ	M^+	χ	M^+	χ	M^+	χ	M^+	χ	M^-	χ	M^+	χ	M^-	χ	M^+	χ
0.00	1.71E+12	0.00	1.75E+12	0.00	1.78E+12	0.00	1.78E+12	0.00	1.82E+12	0.00	1.82E+12	0.00	1.80E+12	0.00	1.80E+12	0.00	1.75E+12
2.52	1.43E+12	2.58	1.49E+12	2.61	1.53E+12	2.61	1.53E+12	2.71	1.56E+12	2.74	1.53E+12	2.68	1.52E+12	2.68	1.52E+12	2.58	1.49E+12
2.85	1.37E+12	2.93	1.45E+12	2.96	1.49E+12	2.96	1.49E+12	3.08	1.51E+12	3.10	1.48E+12	3.04	1.47E+12	3.04	1.46E+12	2.93	1.44E+12
3.86	6.86E+11	4.57	9.25E+11	4.84	1.03E+12	4.84	1.03E+12	4.94	1.01E+12	4.58	8.56E+11	4.63	9.00E+11	4.56	8.72E+11	4.51	8.99E+11
4.11	3.48E+11	5.40	5.89E+11	5.95	7.10E+11	5.95	7.10E+11	6.10	7.02E+11	5.43	5.46E+11	5.50	5.78E+11	5.37	5.51E+11	5.28	5.60E+11
5.32	3.10E+11	6.79	5.11E+11	7.43	6.16E+11	7.43	6.16E+11	7.66	6.16E+11	6.91	4.86E+11	6.97	5.09E+11	6.83	4.86E+11	6.66	4.88E+11
6.59	2.99E+11	8.34	4.88E+11	9.08	5.86E+11	9.08	5.86E+11	9.38	5.89E+11	8.52	4.68E+11	8.57	4.88E+11	8.41	4.67E+11	8.20	4.66E+11
7.83	2.93E+11	9.88	4.77E+11	10.72	5.72E+11	10.72	5.72E+11	11.10	5.76E+11	10.10	4.58E+11	10.16	4.78E+11	9.97	4.58E+11	9.71	4.56E+11
8.98	2.87E+11	11.36	4.69E+11	12.32	5.62E+11	12.32	5.62E+11	12.77	5.67E+11	11.65	4.52E+11	11.70	4.71E+11	11.49	4.51E+11	11.17	4.49E+11
9.99	2.77E+11	12.78	4.63E+11	13.86	5.54E+11	13.86	5.54E+11	14.38	5.60E+11	13.13	4.46E+11	13.18	4.65E+11	12.94	4.45E+11	12.58	4.43E+11
10.73	2.58E+11	14.14	4.57E+11	15.33	5.47E+11	15.33	5.47E+11	15.92	5.53E+11	14.52	4.38E+11	14.60	4.59E+11	14.32	4.38E+11	13.91	4.37E+11
11.10	2.26E+11	15.41	4.50E+11	16.75	5.41E+11	16.75	5.41E+11	17.41	5.47E+11	15.75	4.26E+11	15.92	4.51E+11	15.56	4.27E+11	15.14	4.28E+11
11.21	1.94E+11	16.58	4.41E+11	18.09	5.34E+11	18.09	5.34E+11	18.82	5.40E+11	16.69	4.03E+11	17.11	4.39E+11	16.56	4.08E+11	16.21	4.14E+11
11.29	1.71E+11	17.61	4.27E+11	19.36	5.27E+11	19.36	5.27E+11	20.14	5.32E+11	17.23	3.72E+11	18.07	4.20E+11	17.18	3.77E+11	17.01	3.90E+11
11.37	1.54E+11	18.42	4.06E+11	20.54	5.18E+11	20.54	5.18E+11	21.34	5.21E+11	17.50	3.38E+11	18.71	3.92E+11	17.48	3.43E+11	17.43	3.56E+11
11.44	1.39E+11	18.92	3.76E+11	21.59	5.07E+11	21.59	5.07E+11	22.40	5.07E+11	17.65	3.08E+11	19.03	3.59E+11	17.64	3.12E+11	17.62	3.23E+11
11.50	1.28E+11	19.16	3.43E+11	22.52	4.93E+11	22.52	4.93E+11			17.75	2.81E+11	19.20	3.29E+11	17.75	2.86E+11	17.74	2.94E+11
11.56	1.19E+11	19.29	3.14E+11	23.29	4.76E+11	23.29	4.76E+11			17.82	2.57E+11	19.31	3.03E+11	17.83	2.62E+11	17.83	2.70E+11
11.61	1.10E+11	19.38	2.90E+11	23.86	4.55E+11	23.86	4.55E+11			17.86	2.36E+11	19.39	2.80E+11	17.89	2.41E+11	17.90	2.49E+11
11.65	1.03E+11	19.44	2.69E+11	24.25	4.31E+11	24.25	4.31E+11			17.90	2.18E+11	19.45	2.60E+11	17.92	2.22E+11	17.96	2.31E+11
11.69	9.70E+10	19.49	2.51E+11	24.49	4.05E+11	24.49	4.05E+11			17.93	2.03E+11	19.50	2.43E+11	17.94	2.05E+11	17.99	2.14E+11
11.72	9.16E+10	19.53	2.35E+11	24.62	3.79E+11	24.62	3.79E+11			17.95	1.91E+11	19.53	2.27E+11	17.96	1.92E+11	18.00	1.98E+11
11.74	8.69E+10	19.56	2.22E+11	24.67	3.53E+11	24.67	3.53E+11			17.97	1.80E+11	19.55	2.12E+11	17.97	1.80E+11	18.00	1.84E+11
11.76	8.27E+10	19.58	2.10E+11							17.98	1.70E+11			17.98	1.71E+11		
11.77	7.90E+10	19.59	1.99E+11							17.99	1.62E+11			17.99	1.62E+11		
11.78	7.57E+10																
11.78	7.28E+10																

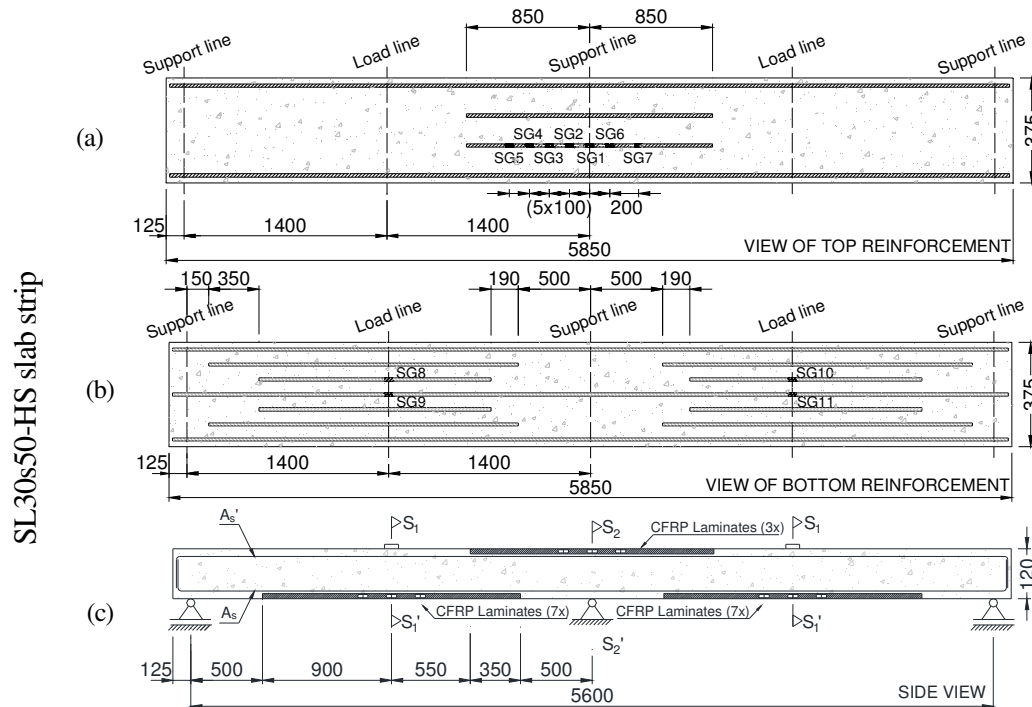M (N.mm); χ (1/mm); M^+ (Positive bending moment); M^- (Negative bending moment)

Figure A5.25: Arrangement of the (a-b) longitudinal steel reinforcement and (c) CFRP laminates of the SL30s25-HS slab strip.
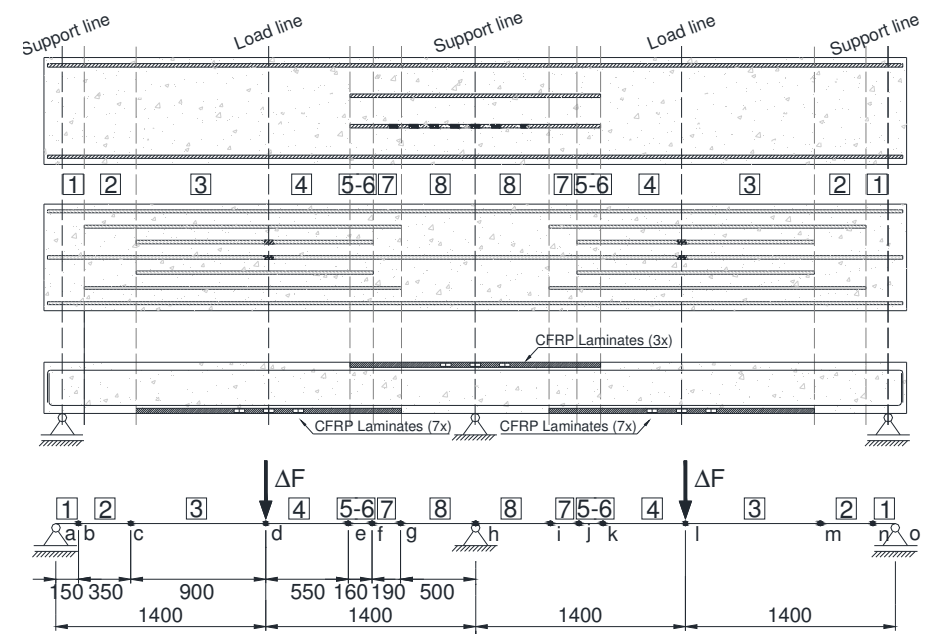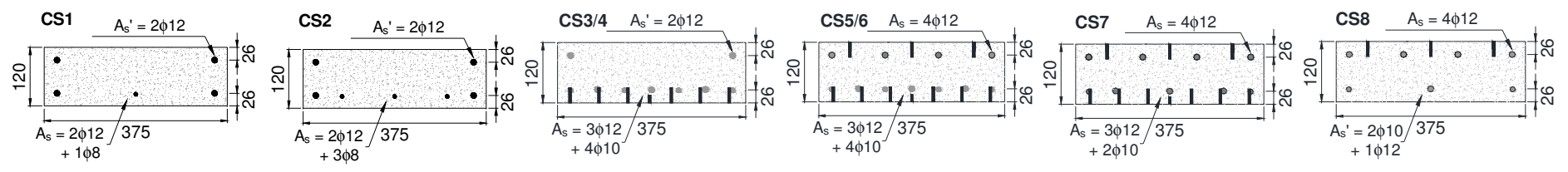
Figure A5.26: Discretization of the slab strip.

Figure A5.27: Resume of the cross-section according to the longitudinal steel reinforcement.

Table A5.9: Relation $M-\chi$ of the cross sections of the SL30s25-HS slab strip.

Element 1		Element 2		Element 3		Element 4		Element 5		Element 5		Element 6		Element 6		Element 7	
M^+	χ	M^+	χ	M^+	χ	M^+	χ	M^+	χ	M^-	χ	M^+	χ	M^-	χ	M^+	χ
0.00	1.71E+12	0.00	1.75E+12	0.00	1.80E+12	0.00	1.80E+12	0.00	1.85E+12	0.00	1.82E+12	0.00	1.79E+12	0.00	1.81E+12	0.00	1.77E+12
2.52	1.43E+12	2.58	1.49E+12	2.64	1.56E+12	2.64	1.56E+12	2.74	1.60E+12	2.75	1.52E+12	2.69	1.51E+12	2.71	1.54E+12	2.61	1.51E+12
2.85	1.37E+12	2.93	1.45E+12	4.51	1.27E+12	4.51	1.27E+12	5.21	1.07E+12	3.34	1.43E+12	3.28	1.43E+12	4.98	7.86E+11	4.92	8.07E+11
3.86	6.86E+11	4.57	9.25E+11	6.80	7.49E+11	6.80	7.49E+11	8.34	6.87E+11	4.67	7.48E+11	4.74	7.92E+11	8.29	5.27E+11	8.06	5.26E+11
4.11	3.48E+11	5.40	5.89E+11	9.59	6.57E+11	9.59	6.57E+11	12.07	6.43E+11	5.84	5.16E+11	5.90	5.43E+11	12.07	5.03E+11	11.71	5.00E+11
5.32	3.10E+11	6.79	5.11E+11	12.44	6.32E+11	12.44	6.32E+11	15.62	6.25E+11	7.57	4.75E+11	7.63	4.97E+11	15.55	4.88E+11	15.04	4.85E+11
6.59	2.99E+11	8.34	4.88E+11	15.15	6.17E+11	15.15	6.17E+11	18.91	6.11E+11	9.33	4.61E+11	9.40	4.81E+11	18.50	4.63E+11	17.93	4.66E+11
7.83	2.93E+11	9.88	4.77E+11	17.69	6.05E+11	17.69	6.05E+11	21.93	5.97E+11	11.05	4.53E+11	11.12	4.73E+11	20.31	4.05E+11	19.99	4.21E+11
8.98	2.87E+11	11.36	4.69E+11	20.05	5.94E+11	20.05	5.94E+11	24.58	5.77E+11	12.71	4.46E+11	12.78	4.66E+11	21.30	3.47E+11	21.09	3.59E+11
9.99	2.77E+11	12.78	4.63E+11	22.21	5.81E+11	22.21	5.81E+11	26.73	5.49E+11	14.27	4.39E+11	14.36	4.59E+11	22.11	3.07E+11	21.90	3.15E+11
10.73	2.58E+11	14.14	4.57E+11	24.14	5.66E+11	24.14	5.66E+11	28.26	5.10E+11	15.65	4.26E+11	15.83	4.51E+11	22.82	2.77E+11	22.59	2.83E+11
11.10	2.26E+11	15.41	4.50E+11	25.80	5.46E+11	25.80	5.46E+11	29.28	4.67E+11	16.70	4.01E+11	17.14	4.38E+11	23.46	2.54E+11	23.19	2.59E+11
11.21	1.94E+11	16.58	4.41E+11	27.14	5.22E+11	27.14	5.22E+11	30.04	4.28E+11	17.27	3.66E+11	18.18	4.16E+11	24.00	2.35E+11	23.70	2.40E+11
11.29	1.71E+11	17.61	4.27E+11	28.15	4.93E+11	28.15	4.93E+11	30.67	3.95E+11	17.53	3.29E+11	18.80	3.82E+11	24.48	2.20E+11	24.14	2.24E+11
11.37	1.54E+11	18.42	4.06E+11	28.87	4.62E+11	28.87	4.62E+11	31.22	3.68E+11	17.67	2.97E+11	19.09	3.46E+11	24.89	2.07E+11	24.51	2.11E+11
11.44	1.39E+11	18.92	3.76E+11	29.41	4.33E+11	29.41	4.33E+11	31.71	3.44E+11	17.76	2.68E+11	19.24	3.15E+11	25.25	1.97E+11	24.83	2.00E+11
11.50	1.28E+11	19.16	3.43E+11	29.85	4.08E+11	29.85	4.08E+11	32.14	3.25E+11	17.83	2.43E+11	19.34	2.87E+11	25.58	1.87E+11	25.10	1.90E+11
11.56	1.19E+11	19.29	3.14E+11	30.21	3.85E+11	30.21	3.85E+11	32.51	3.08E+11	17.87	2.22E+11	19.42	2.65E+11	25.89	1.78E+11	25.33	1.82E+11
11.61	1.10E+11	19.38	2.90E+11	30.51	3.66E+11	30.51	3.66E+11	32.84	2.94E+11	17.90	2.05E+11	19.48	2.45E+11	26.17	1.71E+11	25.53	1.74E+11
11.65	1.03E+11	19.44	2.69E+11	30.77	3.49E+11	30.77	3.49E+11	33.14	2.82E+11	17.93	1.90E+11	19.52	2.27E+11	26.45	1.64E+11	25.71	1.68E+11
11.69	9.70E+10	19.49	2.51E+11	30.99	3.33E+11	30.99	3.33E+11	33.41	2.70E+11	17.95	1.78E+11	19.53	2.11E+11	26.71	1.58E+11	25.86	1.62E+11
11.72	9.16E+10	19.53	2.35E+11	31.17	3.20E+11	31.17	3.20E+11	33.67	2.60E+11	17.96	1.68E+11			26.97	1.53E+11	26.00	1.56E+11
11.74	8.69E+10	19.56	2.22E+11	31.33	3.07E+11	31.33	3.07E+11	33.91	2.51E+11	17.96	1.59E+11			27.23	1.48E+11	26.13	1.51E+11
11.76	8.27E+10	19.58	2.10E+11	31.45	2.96E+11	31.45	2.96E+11	34.13	2.43E+11					27.49	1.43E+11	26.25	1.47E+11
11.77	7.90E+10	19.59	1.99E+11	31.55	2.86E+11	31.55	2.86E+11	34.34	2.35E+11					27.75	1.39E+11	26.36	1.43E+11
11.78	7.57E+10	0.00	0.00E+00	31.63	2.77E+11	31.63	2.77E+11	34.50	2.29E+11					28.02	1.35E+11	26.46	1.39E+11
11.78	7.28E+10	0.00	0.00E+00	31.69	2.68E+11	31.69	2.68E+11	34.59	2.23E+11							26.54	1.36E+11
				31.72	2.60E+11	31.72	2.60E+11	34.67	2.17E+11							26.59	1.33E+11

M (N.mm); χ (1/mm); M^+ (Positive bending moment); M^- (Negative bending moment)

Figure A5.28: Arrangement of the (a-b) longitudinal steel reinforcement and
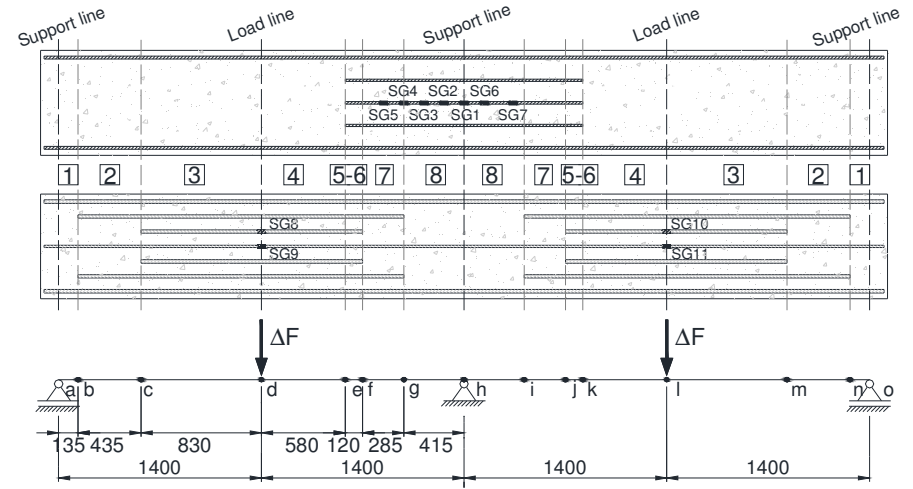(c) CFRP laminates of the SL30s50-HS slab strip.

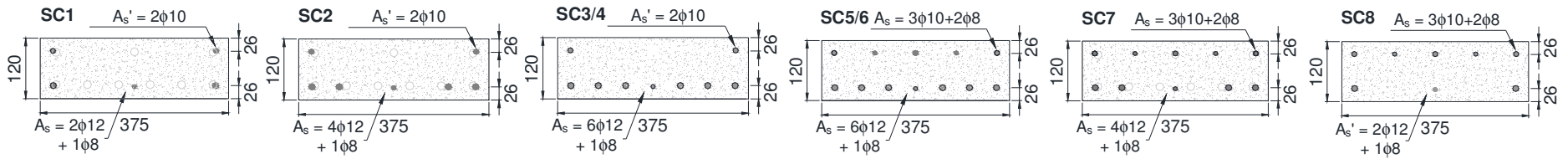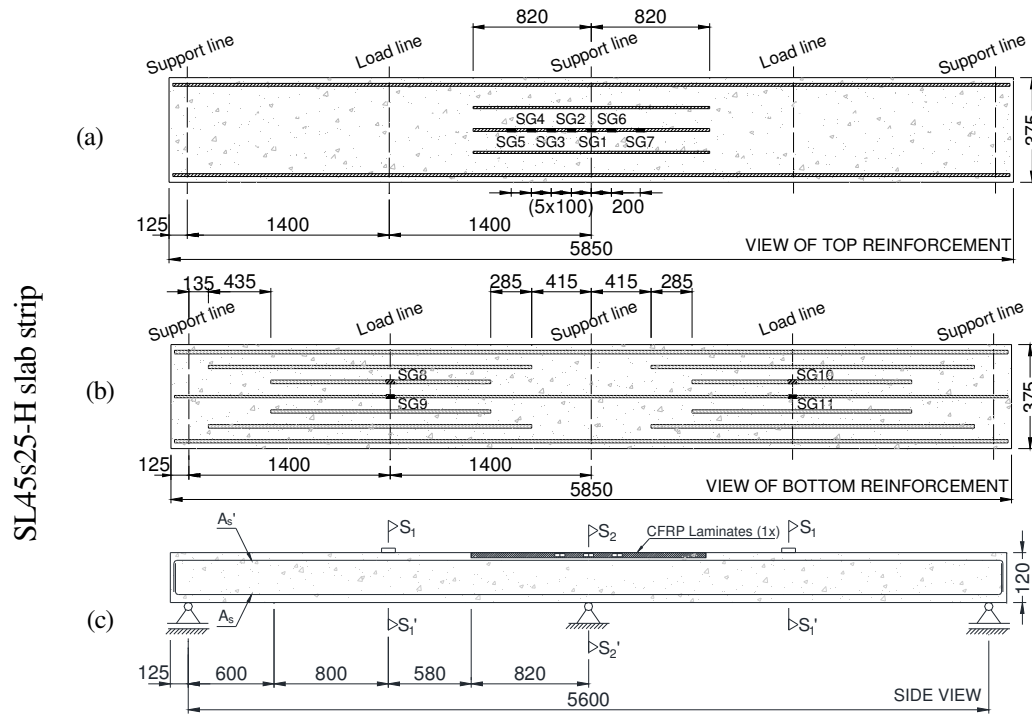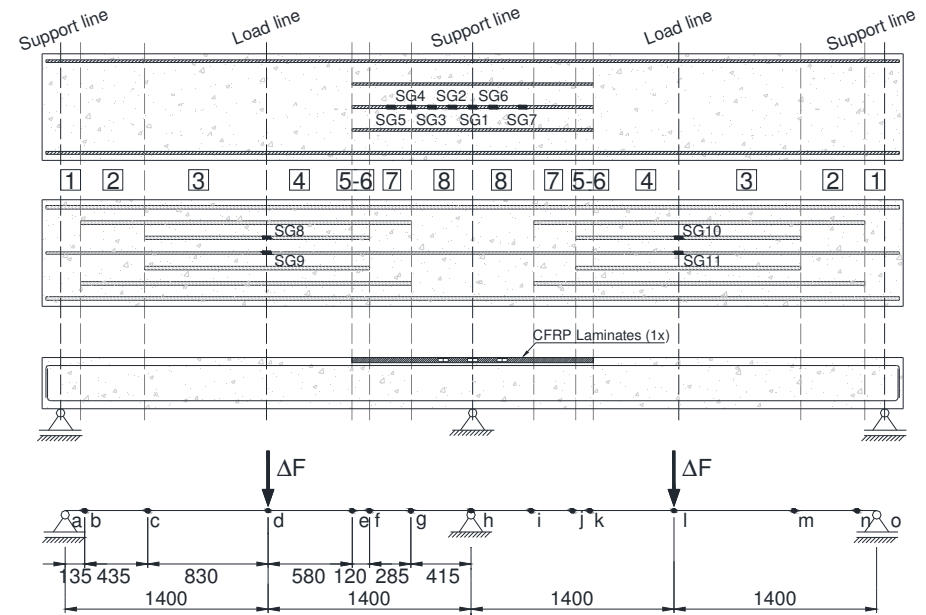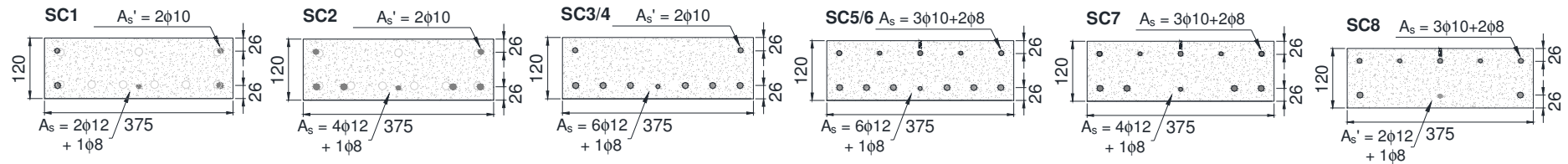Figure A5.29: Discretization of the slab strip.

Figure A5.30: Resume of the cross-section according to the longitudinal steel reinforcement.

351

Table A5.10: Relation M−χ of the cross sections of the SL30s50-HS slab strip.

Element 1		Element 2		Element 3		Element 4		Element 5		Element 5		Element 6		Element 6		Element 7	
M^+	χ	M^+	χ	M^+	χ	M^+	χ	M^+	χ	M^-	χ	M^+	χ	M^-	χ	M^+	χ
0.00	1.71E+12	0.00	1.75E+12	0.00	1.83E+12	0.00	1.83E+12	0.00	1.88E+12	0.00	1.81E+12	0.00	1.79E+12	0.00	1.82E+12	0.00	1.78E+12
1.27	1.58E+12	1.29	1.63E+12	1.33	1.72E+12	1.33	1.72E+12	1.38	1.76E+12	1.38	1.68E+12	1.35	1.66E+12	1.36	1.70E+12	1.31	1.66E+12
3.06	1.33E+12	3.15	1.41E+12	4.36	1.38E+12	4.36	1.38E+12	5.10	1.25E+12	3.33	1.42E+12	3.28	1.43E+12	5.18	7.85E+11	5.10	8.04E+11
3.78	5.70E+11	4.68	8.31E+11	6.80	8.72E+11	6.80	8.72E+11	8.08	7.99E+11	4.66	7.51E+11	4.73	7.92E+11	8.82	5.49E+11	8.56	5.48E+11
4.40	3.31E+11	5.72	5.55E+11	9.47	7.46E+11	9.47	7.46E+11	11.59	7.30E+11	5.81	5.16E+11	5.89	5.43E+11	12.82	5.25E+11	12.42	5.22E+11
5.76	3.05E+11	7.33	5.00E+11	12.27	7.12E+11	12.27	7.12E+11	15.04	7.06E+11	7.52	4.75E+11	7.61	4.97E+11	16.49	5.10E+11	15.92	5.07E+11
7.14	2.96E+11	9.01	4.82E+11	14.96	6.94E+11	14.96	6.94E+11	18.29	6.91E+11	9.27	4.60E+11	9.38	4.81E+11	19.61	4.86E+11	18.96	4.87E+11
8.44	2.90E+11	10.66	4.72E+11	17.50	6.81E+11	17.50	6.81E+11	21.33	6.78E+11	10.98	4.52E+11	11.10	4.72E+11	21.69	4.31E+11	21.20	4.47E+11
9.62	2.82E+11	12.23	4.65E+11	19.89	6.69E+11	19.89	6.69E+11	24.14	6.65E+11	12.63	4.46E+11	12.75	4.66E+11	22.99	3.75E+11	22.61	3.90E+11
10.54	2.65E+11	13.73	4.59E+11	22.11	6.58E+11	22.11	6.58E+11	26.70	6.49E+11	14.18	4.38E+11	14.33	4.59E+11	24.06	3.35E+11	23.68	3.45E+11
11.05	2.34E+11	15.14	4.52E+11	24.16	6.46E+11	24.16	6.46E+11	28.97	6.31E+11	15.57	4.25E+11	15.80	4.51E+11	25.01	3.06E+11	24.59	3.13E+11
11.20	1.97E+11	16.44	4.42E+11	26.04	6.33E+11	26.04	6.33E+11	30.89	6.07E+11	16.63	4.02E+11	17.11	4.38E+11	25.84	2.83E+11	25.38	2.89E+11
11.29	1.72E+11	17.57	4.28E+11	27.73	6.19E+11	27.73	6.19E+11	32.46	5.78E+11	17.22	3.67E+11	18.15	4.16E+11	26.58	2.64E+11	26.06	2.70E+11
11.37	1.53E+11	18.45	4.05E+11	29.23	6.03E+11	29.23	6.03E+11	33.72	5.48E+11	17.49	3.31E+11	18.79	3.83E+11	27.24	2.49E+11	26.63	2.54E+11
11.44	1.38E+11	18.96	3.72E+11	30.52	5.85E+11	30.52	5.85E+11	34.74	5.18E+11	17.64	2.98E+11	19.08	3.47E+11	27.82	2.36E+11	27.11	2.41E+11
11.51	1.26E+11	19.20	3.37E+11	31.60	5.65E+11	31.60	5.65E+11	35.62	4.92E+11	17.74	2.70E+11	19.23	3.15E+11	28.35	2.25E+11	27.51	2.30E+11
11.57	1.16E+11	19.32	3.07E+11	32.51	5.44E+11	32.51	5.44E+11	36.38	4.68E+11	17.80	2.45E+11	19.33	2.88E+11	28.83	2.15E+11	27.84	2.20E+11
11.62	1.08E+11	19.40	2.82E+11	33.26	5.23E+11	33.26	5.23E+11	37.07	4.48E+11	17.84	2.24E+11	19.41	2.65E+11	29.27	2.06E+11	28.12	2.11E+11
11.67	1.00E+11	19.47	2.61E+11	33.87	5.03E+11	33.87	5.03E+11	37.68	4.29E+11	17.87	2.06E+11	19.47	2.45E+11	29.68	1.99E+11	28.35	2.04E+11
11.70	9.39E+10	19.51	2.42E+11	34.38	4.83E+11	34.38	4.83E+11	38.24	4.13E+11	17.90	1.92E+11	19.51	2.28E+11	30.08	1.92E+11	28.54	1.97E+11
11.73	8.84E+10	19.55	2.27E+11	34.81	4.66E+11	34.81	4.66E+11	38.75	3.99E+11	17.92	1.79E+11	19.52	2.12E+11	30.46	1.85E+11	28.69	1.91E+11
11.75	8.37E+10	19.58	2.13E+11	35.16	4.49E+11	35.16	4.49E+11	39.20	3.85E+11	17.93	1.69E+11			30.83	1.80E+11	28.81	1.85E+11
11.77	7.96E+10	19.59	2.01E+11	35.46	4.34E+11	35.46	4.34E+11	39.61	3.73E+11					31.21	1.75E+11	28.88	1.80E+11
11.78	7.60E+10			35.71	4.20E+11	35.71	4.20E+11	39.97	3.62E+11					31.58	1.70E+11		
11.78	7.28E+10			35.90	4.07E+11	35.90	4.07E+11	40.27	3.52E+11					31.94	1.66E+11		
				36.03	3.95E+11	36.03	3.95E+11	40.50	3.43E+11					32.30	1.62E+11		
								40.63	3.35E+11					32.65	1.58E+11		
														32.98	1.55E+11		

M (N.mm); χ (1/mm); M^+ (Positive bending moment); M^- (Negative bending moment)
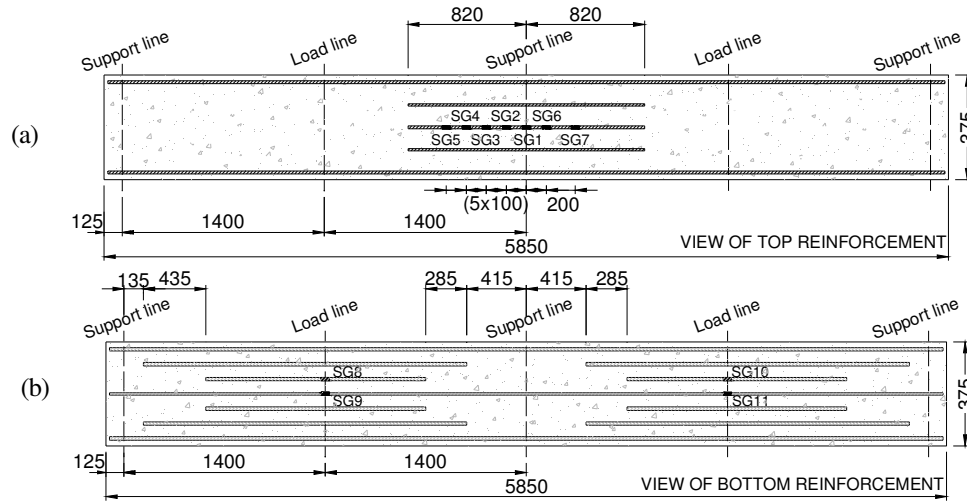
Figure A5.31: Arrangement of the (a-b) longitudinal steel
of the SL45-H slab strip.

Figure A5.32: Discretization of the slab strip.

Figure A5.33: Resume of the cross-section according to the longitudinal steel reinforcement.

Table A5.11: Relation M−χ of the cross sections of the SL45-H slab strip.

Element 1		Element 2		Element 3		Element 4		Element 5		Element 5		Element 6		Element 6		Element 7	
M^+	χ	M^+	χ	M^+	χ	M^+	χ	M^+	χ	M^-	χ	M^+	χ	M^-	χ	M^+	χ
0.00	1.89E+12	0.00	1.94E+12	0.00	1.97E+12	0.00	1.97E+12	0.00	2.01E+12	0.00	2.01E+12	0.00	1.97E+12	0.00	1.97E+12	0.00	1.92E+12
1.43	1.81E+12	1.44	1.86E+12	1.46	1.90E+12	1.46	1.90E+12	1.50	1.93E+12	1.56	1.91E+12	1.48	1.88E+12	1.51	1.88E+12	1.46	1.84E+12
3.59	1.64E+12	3.65	1.70E+12	3.70	1.76E+12	3.70	1.76E+12	3.80	1.78E+12	3.89	1.70E+12	3.74	1.72E+12	3.78	1.68E+12	3.67	1.66E+12
4.98	8.54E+11	5.73	1.09E+12	6.18	1.26E+12	6.18	1.26E+12	6.26	1.24E+12	5.01	7.86E+11	5.76	1.07E+12	5.06	8.26E+11	5.10	8.71E+11
5.04	3.88E+11	6.51	6.39E+11	7.50	8.41E+11	7.50	8.41E+11	7.61	8.34E+11	5.44	4.19E+11	6.58	6.30E+11	5.40	4.22E+11	5.35	4.27E+11
6.62	3.44E+11	8.28	5.51E+11	9.41	7.24E+11	9.41	7.24E+11	9.59	7.24E+11	7.09	3.78E+11	8.40	5.50E+11	7.05	3.78E+11	6.98	3.79E+11
8.30	3.32E+11	10.29	5.29E+11	11.61	6.91E+11	11.61	6.91E+11	11.85	6.92E+11	8.84	3.66E+11	10.45	5.29E+11	8.80	3.66E+11	8.73	3.66E+11
9.87	3.22E+11	12.29	5.19E+11	13.83	6.76E+11	13.83	6.76E+11	14.12	6.78E+11	10.54	3.59E+11	12.51	5.20E+11	10.49	3.59E+11	10.42	3.60E+11
11.09	2.97E+11	14.26	5.12E+11	16.02	6.67E+11	16.02	6.67E+11	16.35	6.70E+11	12.09	3.49E+11	14.51	5.12E+11	12.04	3.49E+11	11.97	3.50E+11
11.49	2.37E+11	16.14	5.04E+11	18.14	6.59E+11	18.14	6.59E+11	18.52	6.63E+11	13.27	3.24E+11	16.41	5.04E+11	13.25	3.25E+11	13.21	3.28E+11
11.63	1.94E+11	17.84	4.90E+11	20.19	6.52E+11	20.19	6.52E+11	20.61	6.56E+11	13.81	2.82E+11	18.08	4.87E+11	13.81	2.79E+11	13.81	2.78E+11
11.75	1.64E+11	19.16	4.60E+11	22.13	6.44E+11	22.13	6.44E+11	22.59	6.48E+11	14.05	2.45E+11	19.26	4.54E+11	14.02	2.40E+11	13.98	2.34E+11
11.85	1.40E+11	19.82	4.11E+11	23.93	6.33E+11	23.93	6.33E+11	24.42	6.35E+11	14.23	2.18E+11	19.86	4.09E+11	14.18	2.12E+11	14.13	2.03E+11
11.96	1.23E+11	20.11	3.64E+11	25.52	6.16E+11	25.52	6.16E+11	26.01	6.14E+11	14.39	1.97E+11	20.14	3.62E+11	14.33	1.90E+11	14.25	1.81E+11
12.06	1.11E+11	20.29	3.22E+11	26.77	5.89E+11	26.77	5.89E+11	27.15	5.74E+11	14.54	1.80E+11	20.26	3.14E+11	14.47	1.73E+11	14.38	1.63E+11
12.15	1.01E+11	20.35	2.80E+11	27.60	5.50E+11	27.60	5.50E+11	27.71	5.21E+11	14.68	1.67E+11	20.32	2.74E+11	14.60	1.59E+11	14.49	1.48E+11
12.23	9.31E+10	20.40	2.46E+11	27.99	4.98E+11	27.99	4.98E+11	27.95	4.71E+11	14.81	1.55E+11	20.40	2.46E+11	14.72	1.48E+11	14.58	1.35E+11
12.30	8.63E+10	20.46	2.23E+11	28.12	4.46E+11	28.12	4.46E+11	28.11	4.31E+11	14.92	1.46E+11	20.47	2.25E+11	14.82	1.38E+11	14.66	1.25E+11
12.36	8.05E+10	20.51	2.04E+11	28.21	4.06E+11	28.21	4.06E+11	28.22	3.97E+11	15.02	1.37E+11	20.54	2.08E+11	14.91	1.29E+11	14.73	1.17E+11
12.42	7.55E+10	20.55	1.89E+11	28.29	3.74E+11	28.29	3.74E+11	28.31	3.68E+11	15.09	1.30E+11	20.59	1.93E+11	14.98	1.22E+11	14.79	1.10E+11
12.46	7.11E+10	20.59	1.77E+11	28.34	3.48E+11	28.34	3.48E+11	28.38	3.44E+11	15.15	1.23E+11	20.64	1.81E+11	15.03	1.15E+11	14.84	1.04E+11
12.49	6.75E+10	20.61	1.66E+11	28.38	3.26E+11	28.38	3.26E+11	28.44	3.23E+11	15.20	1.17E+11	20.67	1.71E+11	15.08	1.10E+11	14.88	9.84E+10
12.52	6.44E+10	20.62	1.56E+11	28.40	3.07E+11	28.40	3.07E+11	28.47	3.05E+11	15.23	1.12E+11	20.69	1.62E+11	15.11	1.05E+11	14.90	9.38E+10
12.54	6.18E+10									15.25	1.07E+11	20.69	1.54E+11	15.13	1.00E+11	14.92	8.97E+10
12.54	5.94E+10									15.26	1.03E+11			15.13	9.62E+10	14.93	8.60E+10

M (N.mm); χ (1/mm); M^+ (Positive bending moment); M^- (Negative bending moment)
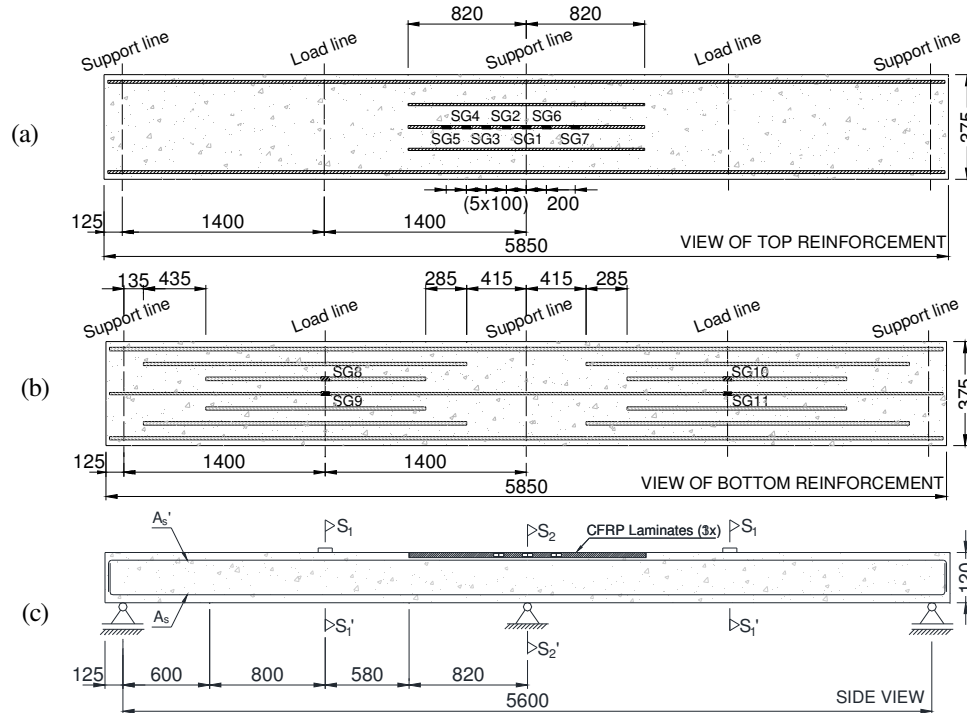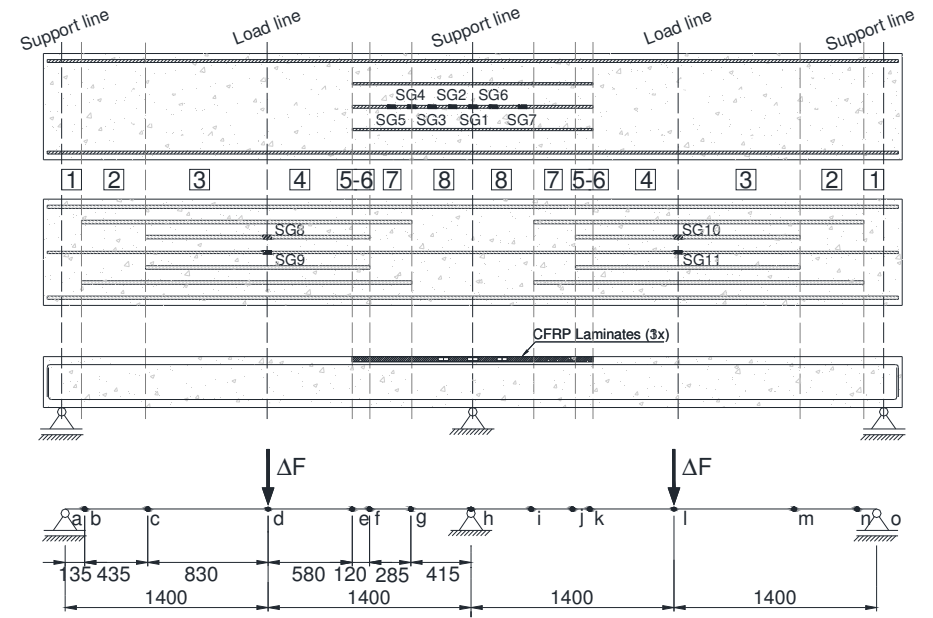
ANNEX 5.12– SL45s25-H

Figure A5.34: Arrangement of the (a-b) longitudinal steel reinforcement and (c) CFRP laminates of the SL45s25-H slab strip.

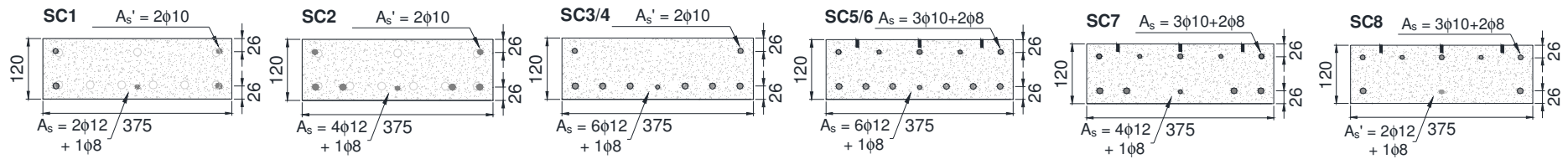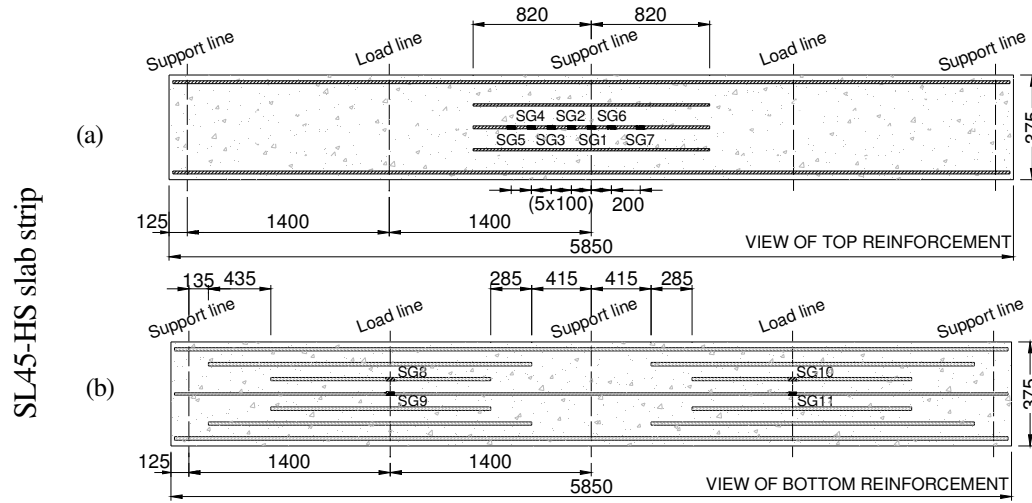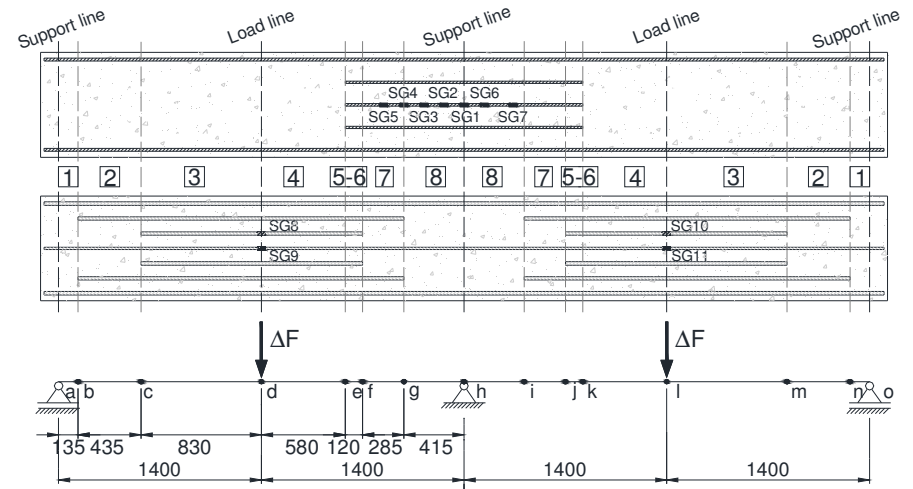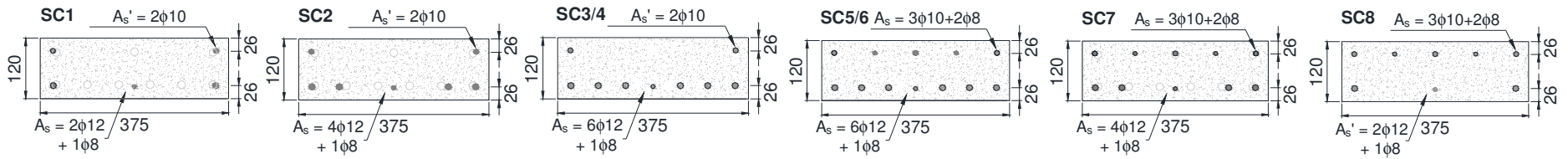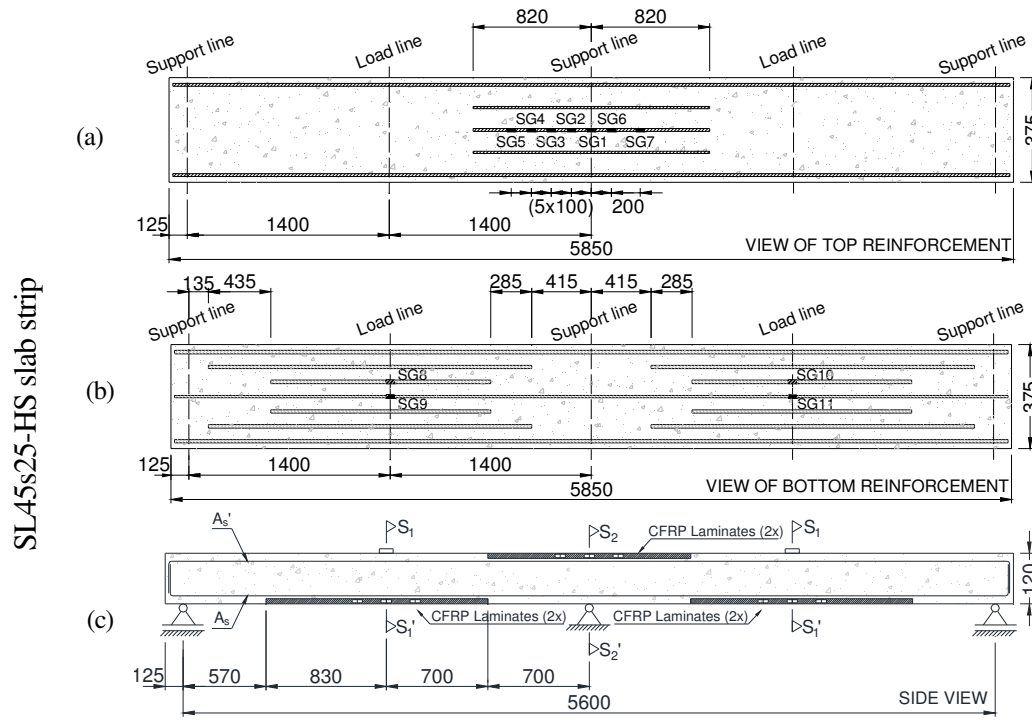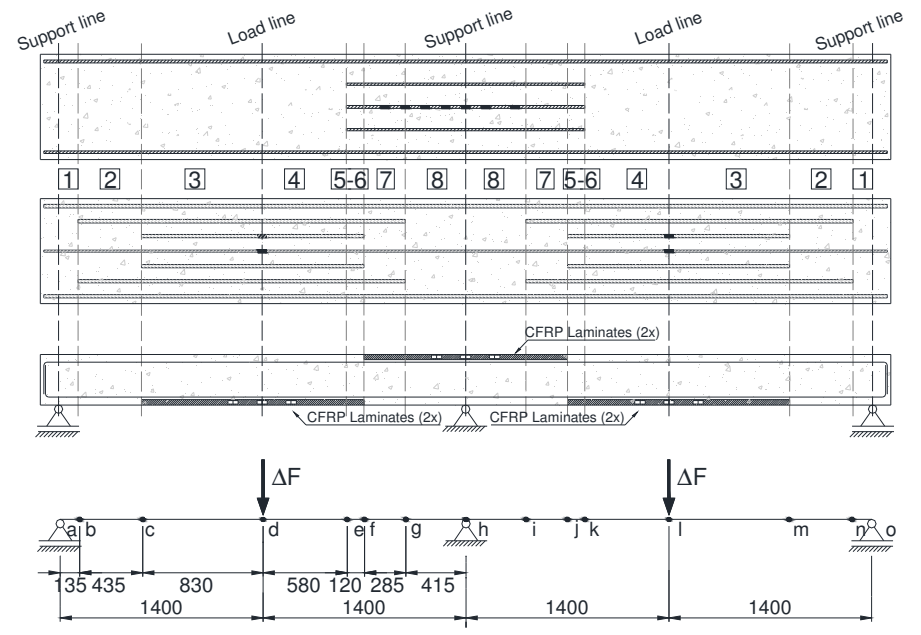Figure A5.35: Discretization of the slab strip.
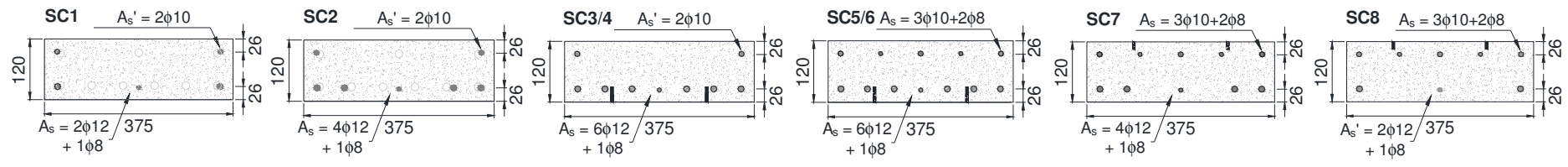

Figure A5.36: Resume of the cross-section according to the longitudinal steel reinforcement.

Table A5.12: Relation $M-\chi$ of the cross sections of the SL45s25-H slab strip.

Element 1		Element 2		Element 3		Element 4		Element 5		Element 5		Element 6		Element 6		Element 7	
M^+	χ	M^+	χ	M^+	χ	M^+	χ	M^+	χ	M^-	χ	M^+	χ	M^-	χ	M^+	χ
0.00	1.89E+12	0.00	1.94E+12	0.00	1.97E+12	0.00	1.97E+12	0.00	2.00E+12	0.00	2.01E+12	0.00	1.96E+12	0.00	1.97E+12	0.00	1.93E+12
1.43	1.81E+12	1.44	1.86E+12	1.46	1.90E+12	1.46	1.90E+12	1.46	1.93E+12	1.56	1.92E+12	1.45	1.88E+12	1.52	1.88E+12	1.46	1.84E+12
3.59	1.64E+12	3.65	1.70E+12	3.70	1.76E+12	3.70	1.76E+12	3.71	1.78E+12	4.53	1.60E+12	4.30	1.65E+12	4.42	1.59E+12	4.30	1.58E+12
4.98	8.54E+11	5.73	1.09E+12	6.18	1.26E+12	6.18	1.26E+12	6.18	1.27E+12	5.03	5.62E+11	5.88	8.45E+11	5.04	5.82E+11	5.05	6.06E+11
5.04	3.88E+11	6.51	6.39E+11	7.50	8.41E+11	7.50	8.41E+11	7.45	8.51E+11	6.61	4.06E+11	7.35	5.75E+11	6.56	4.08E+11	6.48	4.10E+11
6.62	3.44E+11	8.28	5.51E+11	9.41	7.24E+11	9.41	7.24E+11	9.29	7.30E+11	8.77	3.86E+11	9.63	5.34E+11	8.71	3.86E+11	8.64	3.86E+11
8.30	3.32E+11	10.29	5.29E+11	11.61	6.91E+11	11.61	6.91E+11	11.44	6.94E+11	10.89	3.78E+11	12.00	5.20E+11	10.83	3.78E+11	10.75	3.78E+11
9.87	3.22E+11	12.29	5.19E+11	13.83	6.76E+11	13.83	6.76E+11	13.63	6.79E+11	12.82	3.66E+11	14.31	5.12E+11	12.76	3.66E+11	12.67	3.67E+11
11.09	2.97E+11	14.26	5.12E+11	16.02	6.67E+11	16.02	6.67E+11	15.79	6.70E+11	14.27	3.35E+11	16.49	5.02E+11	14.24	3.37E+11	14.18	3.41E+11
11.49	2.37E+11	16.14	5.04E+11	18.14	6.59E+11	18.14	6.59E+11	17.89	6.64E+11	14.96	2.87E+11	18.33	4.80E+11	14.96	2.86E+11	14.96	2.85E+11
11.63	1.94E+11	17.84	4.90E+11	20.19	6.52E+11	20.19	6.52E+11	19.93	6.57E+11	15.39	2.51E+11	19.47	4.38E+11	15.39	2.46E+11	15.39	2.41E+11
11.75	1.64E+11	19.16	4.60E+11	22.13	6.44E+11	22.13	6.44E+11	21.89	6.50E+11	15.77	2.24E+11	19.96	3.85E+11	15.77	2.18E+11	15.77	2.12E+11
11.85	1.40E+11	19.82	4.11E+11	23.93	6.33E+11	23.93	6.33E+11	23.72	6.40E+11	16.13	2.03E+11	20.16	3.32E+11	16.13	1.98E+11	16.13	1.90E+11
11.96	1.23E+11	20.11	3.64E+11	25.52	6.16E+11	25.52	6.16E+11	25.36	6.23E+11	16.46	1.87E+11	20.22	2.83E+11	16.46	1.81E+11	16.47	1.74E+11
12.06	1.11E+11	20.29	3.22E+11	26.77	5.89E+11	26.77	5.89E+11	26.67	5.94E+11	16.77	1.74E+11	20.29	2.50E+11	16.77	1.69E+11	16.79	1.61E+11
12.15	1.01E+11	20.35	2.80E+11	27.60	5.50E+11	27.60	5.50E+11	27.45	5.47E+11	17.04	1.64E+11	20.37	2.25E+11	17.05	1.58E+11	17.09	1.50E+11
12.23	9.31E+10	20.40	2.46E+11	27.99	4.98E+11	27.99	4.98E+11	27.78	4.97E+11	17.29	1.54E+11	20.44	2.06E+11	17.31	1.49E+11	17.36	1.40E+11
12.30	8.63E+10	20.46	2.23E+11	28.12	4.46E+11	28.12	4.46E+11	27.96	4.53E+11	17.51	1.46E+11	20.50	1.90E+11	17.53	1.41E+11	17.61	1.33E+11
12.36	8.05E+10	20.51	2.04E+11	28.21	4.06E+11	28.21	4.06E+11	28.10	4.17E+11	17.71	1.39E+11	20.55	1.77E+11	17.73	1.34E+11	17.82	1.26E+11
12.42	7.55E+10	20.55	1.89E+11	28.29	3.74E+11	28.29	3.74E+11	28.20	3.87E+11	17.87	1.33E+11	20.58	1.66E+11	17.90	1.28E+11	18.01	1.20E+11
12.46	7.11E+10	20.59	1.77E+11	28.34	3.48E+11	28.34	3.48E+11	28.28	3.60E+11	18.01	1.28E+11	20.60	1.56E+11	18.05	1.23E+11	18.17	1.15E+11
12.49	6.75E+10	20.61	1.66E+11	28.38	3.26E+11	28.38	3.26E+11	28.35	3.38E+11	18.14	1.23E+11	20.60	1.48E+11	18.18	1.18E+11	18.31	1.11E+11
12.52	6.44E+10	20.62	1.56E+11	28.40	3.07E+11	28.40	3.07E+11	28.40	3.19E+11	18.24	1.18E+11			18.29	1.14E+11	18.43	1.07E+11
12.54	6.18E+10							28.43	3.02E+11	18.32	1.14E+11			18.38	1.10E+11		
12.54	5.94E+10									18.39	1.10E+11			18.45	1.06E+11		
										18.45	1.06E+11						
										18.49	1.03E+11						

M (N.mm); χ (1/mm); M^+ (Positive bending moment); M^- (Negative bending moment)

SL45s50-H slab strip

(a)

820 | 820

Support line   Load line   Support line   Load line   Support line

SG4 SG2 SG6
SG5 SG3 SG1 SG7

375

125   1400   1400
(5x100)   200
5850

VIEW OF TOP REINFORCEMENT

(b)

135 435   285 415 415 285

Support line   Load line   Support line   Load line   Support line

SG8   SG10
SG9   SG11

375

125   1400   1400
5850

VIEW OF BOTTOM REINFORCEMENT

(c)

A$_s$' $\triangleright$S$_1$ $\triangleright$S$_2$ CFRP Laminates (3x) $\triangleright$S$_1$

120

A$_s$ $\triangleright$S$_1$' $\triangleright$S$_2$' $\triangleright$S$_1$'

125   600   800   580   820
5600

SIDE VIEW

Figure A5.37: Arrangement of the (a-b) longitudinal steel reinforcement and
(c) CFRP laminates of the SL45s50-H slab strip.

Support line   Load line   Support line   Load line   Support line

SG4 SG2 SG6
SG5 SG3 SG1 SG7

1 | 2 | 3 | 4 | 5-6 | 7 | 8 | 8 | 7 | 5-6 | 4 | 3 | 2 | 1

SG8   SG10
SG9   SG11

CFRP Laminates (3x)

ΔF   ΔF

a b   c   d   e f   g   h   i   j k   l   m   n   o

135 435   830   580 120 285   415
1400   1400   1400   1400

Figure A5.38: Discretization of the slab strip.

SC1 A$_s$' = 2φ10   26   120   26
A$_s$ = 2φ12   375
+ 1φ8

SC2 A$_s$' = 2φ10   26   120   26
A$_s$ = 4φ12   375
+ 1φ8

SC3/4 A$_s$' = 2φ10   26   120   26
A$_s$ = 6φ12   375
+ 1φ8

SC5/6 A$_s$ = 3φ10+2φ8   26   120   26
A$_s$ = 6φ12   375
+ 1φ8

SC7 A$_s$ = 3φ10+2φ8   26   120   26
A$_s$ = 4φ12   375
+ 1φ8

SC8 A$_s$ = 3φ10+2φ8   26   120   26
A$_s$' = 2φ12   375
+ 1φ8

Figure A5.39: Resume of the cross-section according to the longitudinal steel reinforcement.

357

Table A5.13: Relation M−χ of the cross sections of the SL45s50-H slab strip.

Element 1		Element 2		Element 3		Element 4		Element 5		Element 5		Element 6		Element 6		Element 7	
M^+	χ	M^+	χ	M^+	χ	M^+	χ	M^+	χ	M^-	χ	M^+	χ	M^-	χ	M^+	χ
0.00	1.89E+12	0.00	1.94E+12	0.00	1.97E+12	0.00	1.97E+12	0.00	2.00E+12	0.00	2.02E+12	0.00	1.96E+12	0.00	1.98E+12	0.00	1.94E+12
1.43	1.81E+12	1.44	1.86E+12	1.46	1.90E+12	1.46	1.90E+12	1.46	1.92E+12	1.57	1.93E+12	1.45	1.88E+12	1.52	1.89E+12	1.47	1.86E+12
3.59	1.64E+12	3.65	1.70E+12	3.70	1.76E+12	3.70	1.76E+12	3.71	1.78E+12	4.88	1.54E+12	4.63	1.59E+12	4.78	1.54E+12	4.66	1.53E+12
4.98	8.54E+11	5.73	1.09E+12	6.18	1.26E+12	6.18	1.26E+12	6.17	1.27E+12	5.47	5.36E+11	6.04	7.45E+11	5.45	5.48E+11	5.42	5.65E+11
5.04	3.88E+11	6.51	6.39E+11	7.50	8.41E+11	7.50	8.41E+11	7.43	8.51E+11	7.68	4.34E+11	7.99	5.56E+11	7.61	4.35E+11	7.51	4.37E+11
6.62	3.44E+11	8.28	5.51E+11	9.41	7.24E+11	9.41	7.24E+11	9.27	7.29E+11	10.21	4.19E+11	10.55	5.26E+11	10.13	4.18E+11	10.02	4.18E+11
8.30	3.32E+11	10.29	5.29E+11	11.61	6.91E+11	11.61	6.91E+11	11.41	6.94E+11	12.64	4.10E+11	13.13	5.15E+11	12.56	4.10E+11	12.44	4.10E+11
9.87	3.22E+11	12.29	5.19E+11	13.83	6.76E+11	13.83	6.76E+11	13.60	6.78E+11	14.79	3.94E+11	15.60	5.06E+11	14.70	3.95E+11	14.58	3.95E+11
11.09	2.97E+11	14.26	5.12E+11	16.02	6.67E+11	16.02	6.67E+11	15.75	6.69E+11	16.35	3.58E+11	17.80	4.88E+11	16.30	3.61E+11	16.22	3.65E+11
11.49	2.37E+11	16.14	5.04E+11	18.14	6.59E+11	18.14	6.59E+11	17.85	6.63E+11	17.33	3.12E+11	19.28	4.48E+11	17.33	3.12E+11	17.31	3.15E+11
11.63	1.94E+11	17.84	4.90E+11	20.19	6.52E+11	20.19	6.52E+11	19.88	6.56E+11	18.13	2.79E+11	19.90	3.91E+11	18.16	2.77E+11	18.19	2.75E+11
11.75	1.64E+11	19.16	4.60E+11	22.13	6.44E+11	22.13	6.44E+11	21.83	6.49E+11	18.87	2.55E+11	20.15	3.34E+11	18.93	2.52E+11	18.98	2.48E+11
11.85	1.40E+11	19.82	4.11E+11	23.93	6.33E+11	23.93	6.33E+11	23.66	6.39E+11	19.57	2.36E+11	20.21	2.80E+11	19.64	2.33E+11	19.72	2.29E+11
11.96	1.23E+11	20.11	3.64E+11	25.52	6.16E+11	25.52	6.16E+11	25.30	6.23E+11	20.22	2.21E+11	20.29	2.45E+11	20.30	2.18E+11	20.41	2.14E+11
12.06	1.11E+11	20.29	3.22E+11	26.77	5.89E+11	26.77	5.89E+11	26.62	5.94E+11	20.82	2.09E+11	20.38	2.20E+11	20.92	2.05E+11	21.05	2.02E+11
12.15	1.01E+11	20.35	2.80E+11	27.60	5.50E+11	27.60	5.50E+11	27.41	5.48E+11	21.37	1.99E+11	20.45	1.99E+11	21.48	1.95E+11	21.63	1.92E+11
12.23	9.31E+10	20.40	2.46E+11	27.99	4.98E+11	27.99	4.98E+11	27.76	4.98E+11	21.87	1.90E+11	20.51	1.84E+11	22.00	1.87E+11	22.16	1.83E+11
12.30	8.63E+10	20.46	2.23E+11	28.12	4.46E+11	28.12	4.46E+11	27.94	4.54E+11	22.33	1.82E+11	20.55	1.70E+11	22.47	1.79E+11	22.64	1.76E+11
12.36	8.05E+10	20.51	2.04E+11	28.21	4.06E+11	28.21	4.06E+11	28.07	4.18E+11	22.74	1.75E+11	20.57	1.59E+11	22.89	1.73E+11	23.07	1.70E+11
12.42	7.55E+10	20.55	1.89E+11	28.29	3.74E+11	28.29	3.74E+11	28.17	3.88E+11	23.12	1.69E+11	20.58	1.50E+11	23.27	1.67E+11	23.46	1.64E+11
12.46	7.11E+10	20.59	1.77E+11	28.34	3.48E+11	28.34	3.48E+11	28.25	3.61E+11	23.46	1.64E+11			23.62	1.61E+11	23.81	1.59E+11
12.49	6.75E+10	20.61	1.66E+11	28.38	3.26E+11	28.38	3.26E+11	28.32	3.39E+11	23.77	1.59E+11			23.93	1.57E+11	24.12	1.54E+11
12.52	6.44E+10	20.62	1.56E+11	28.40	3.07E+11	28.40	3.07E+11	28.38	3.20E+11	24.05	1.54E+11			24.21	1.52E+11	24.40	1.50E+11
12.54	6.18E+10							28.41	3.02E+11	24.31	1.50E+11			24.47	1.48E+11	24.65	1.47E+11
12.54	5.94E+10									24.54	1.46E+11						
										24.76	1.42E+11						

M (N.mm); χ (1/mm); M^+ (Positive bending moment); M^- (Negative bending moment)

(a)

820   820

Support line   Load line   Support line   Load line   Support line

SG4 SG2 SG6
SG5 SG3 SG1 SG7

375

125   1400   1400   (5x100)   200   VIEW OF TOP REINFORCEMENT
5850

(b)

135 435   285 415 415 285

Support line   Load line   Support line   Load line   Support line

SG8   SG10
SG9   SG11

375

125   1400   1400   VIEW OF BOTTOM REINFORCEMENT
5850

Figure A5.40: Arrangement of the (a-b) longitudinal steel
of the SL45-HS slab strip.

SL45-HS slab strip

Support line   Load line   Support line   Load line   Support line

SG4 SG2 SG6
SG5 SG3 SG1 SG7

1 2   3   4 5-6 7 8   8 7 5-6 4   3   2 1

SG8   SG10
SG9   SG11

ΔF   ΔF

a b   c   d   e f   g   h   i   j k   l   m   n o

135 435   830   580 120 285 415   1400   1400   1400
1400

Figure A5.41: Discretization of the slab strip.

SC1 $A_s' = 2\phi10$ **SC2** $A_s' = 2\phi10$ **SC3/4** $A_s' = 2\phi10$ **SC5/6** $A_s = 3\phi10+2\phi8$ **SC7** $A_s = 3\phi10+2\phi8$ **SC8** $A_s = 3\phi10+2\phi8$

120   26   26   120   26   26   120   26   26   120   26   26   120   26   26   120   26   26

$A_s = 2\phi12$ / 375 $A_s = 4\phi12$ / 375 $A_s = 6\phi12$ / 375 $A_s = 6\phi12$ / 375 $A_s = 4\phi12$ / 375 $A_s' = 2\phi12$ / 375
$+ 1\phi8$ $+ 1\phi8$ $+ 1\phi8$ $+ 1\phi8$ $+ 1\phi8$ $+ 1\phi8$

Figure A5.42: Resume of the cross-section according to the longitudinal steel reinforcement.

Table A5.14: Relation M$-\chi$ of the cross sections of the SL45-HS slab strip.

Element 1		Element 2		Element 3		Element 4		Element 5		Element 5		Element 6		Element 6		Element 7	
M^+	χ	M^+	χ	M^+	χ	M^+	χ	M^+	χ	M^-	χ	M^+	χ	M^-	χ	M^+	χ
0.00	1.91E+12	0.00	1.95E+12	0.00	1.99E+12	0.00	1.99E+12	0.00	2.02E+12	0.00	2.02E+12	0.00	1.98E+12	0.00	1.98E+12	0.00	1.94E+12
1.44	1.82E+12	1.45	1.87E+12	1.47	1.91E+12	1.47	1.91E+12	1.51	1.94E+12	1.57	1.93E+12	1.49	1.90E+12	1.52	1.89E+12	1.47	1.85E+12
4.23	1.57E+12	4.33	1.64E+12	4.41	1.71E+12	4.41	1.71E+12	4.51	1.72E+12	4.56	1.61E+12	4.43	1.66E+12	4.45	1.60E+12	4.32	1.59E+12
4.71	5.49E+11	5.96	8.39E+11	6.71	1.04E+12	6.71	1.04E+12	6.78	1.03E+12	4.92	5.43E+11	5.99	8.20E+11	4.93	5.62E+11	4.95	5.87E+11
5.98	3.54E+11	7.55	5.73E+11	8.64	7.56E+11	8.64	7.56E+11	8.79	7.54E+11	6.43	3.88E+11	7.66	5.71E+11	6.39	3.89E+11	6.33	3.91E+11
8.02	3.34E+11	9.95	5.33E+11	11.24	6.98E+11	11.24	6.98E+11	11.47	6.99E+11	8.53	3.69E+11	10.10	5.34E+11	8.49	3.69E+11	8.43	3.69E+11
9.93	3.23E+11	12.38	5.21E+11	13.93	6.78E+11	13.93	6.78E+11	14.22	6.81E+11	10.60	3.60E+11	12.59	5.21E+11	10.55	3.60E+11	10.49	3.60E+11
11.29	2.86E+11	14.75	5.12E+11	16.58	6.67E+11	16.58	6.67E+11	16.91	6.71E+11	12.43	3.45E+11	15.01	5.12E+11	12.39	3.46E+11	12.32	3.47E+11
11.57	2.15E+11	16.98	5.01E+11	19.13	6.59E+11	19.13	6.59E+11	19.52	6.63E+11	13.61	3.06E+11	17.24	4.99E+11	13.61	3.06E+11	13.60	3.09E+11
11.73	1.74E+11	18.83	4.74E+11	21.56	6.50E+11	21.56	6.50E+11	22.00	6.54E+11	14.00	2.57E+11	18.96	4.69E+11	13.98	2.52E+11	13.95	2.47E+11
11.86	1.42E+11	19.80	4.18E+11	23.80	6.38E+11	23.80	6.38E+11	24.28	6.40E+11	14.23	2.22E+11	19.84	4.16E+11	14.19	2.15E+11	14.13	2.07E+11
11.99	1.22E+11	20.17	3.61E+11	25.73	6.17E+11	25.73	6.17E+11	26.22	6.13E+11	14.44	1.96E+11	20.19	3.59E+11	14.37	1.89E+11	14.29	1.79E+11
12.11	1.08E+11	20.35	3.09E+11	27.16	5.81E+11	27.16	5.81E+11	27.45	5.60E+11	14.62	1.77E+11	20.30	2.99E+11	14.54	1.69E+11	14.44	1.58E+11
12.22	9.68E+10	20.40	2.59E+11	27.93	5.25E+11	27.93	5.25E+11	27.91	4.95E+11	14.79	1.61E+11	20.40	2.59E+11	14.70	1.54E+11	14.57	1.41E+11
12.31	8.79E+10	20.48	2.28E+11	28.16	4.58E+11	28.16	4.58E+11	28.14	4.42E+11	14.94	1.49E+11	20.50	2.31E+11	14.84	1.41E+11	14.68	1.28E+11
12.39	8.04E+10	20.55	2.05E+11	28.28	4.08E+11	28.28	4.08E+11	28.29	4.00E+11	15.06	1.38E+11	20.58	2.09E+11	14.95	1.30E+11	14.77	1.17E+11
12.46	7.42E+10	20.61	1.87E+11	28.38	3.70E+11	28.38	3.70E+11	28.41	3.65E+11	15.16	1.30E+11	20.66	1.92E+11	15.04	1.21E+11	14.85	1.09E+11
12.51	6.92E+10	20.65	1.72E+11	28.45	3.40E+11	28.45	3.40E+11	28.50	3.37E+11	15.24	1.22E+11	20.71	1.78E+11	15.11	1.14E+11	14.91	1.02E+11
12.55	6.52E+10	20.68	1.60E+11	28.50	3.15E+11	28.50	3.15E+11	28.56	3.13E+11	15.29	1.15E+11	20.75	1.66E+11	15.16	1.07E+11	14.95	9.58E+10
12.58	6.18E+10	20.69	1.50E+11	28.51	2.93E+11	28.51	2.93E+11			15.33	1.09E+11	20.77	1.56E+11	15.19	1.01E+11	14.98	9.07E+10
12.60	5.89E+10									15.34	1.04E+11			15.21	9.65E+10	14.99	8.62E+10

M (N.mm); χ (1/mm); M^+ (Positive bending moment); M^- (Negative bending moment)

Figure A5.43: Arrangement of the (a-b) longitudinal steel reinforcement and
(c) CFRP laminates of the SL45s25-HS slab strip.

Figure A5.44: Discretization of the slab strip.

Figure A5.45: Resume of the cross-section according to the longitudinal steel reinforcement.

Table A5.15: Relation M−χ of the cross sections of the SL45s25-HS slab strip.

Element 1		Element 2		Element 3		Element 4		Element 5		Element 5		Element 6		Element 6		Element 7	
M^+	χ	M^+	χ	M^+	χ	M^+	χ	M^+	χ	M^-	χ	M^+	χ	M^-	χ	M^+	χ
0.00	1.91E+12	0.00	1.95E+12	0.00	2.00E+12	0.00	2.00E+12	0.00	2.02E+12	0.00	2.03E+12	0.00	1.98E+12	0.00	1.99E+12	0.00	1.95E+12
1.44	1.82E+12	1.45	1.87E+12	1.47	1.93E+12	1.47	1.93E+12	1.47	1.94E+12	1.58	1.94E+12	1.46	1.90E+12	1.53	1.90E+12	1.48	1.86E+12
3.62	1.66E+12	3.68	1.72E+12	5.06	1.65E+12	5.06	1.65E+12	3.74	1.80E+12	5.09	1.48E+12	3.69	1.74E+12	4.99	1.49E+12	4.88	1.49E+12
5.05	8.72E+11	5.80	1.11E+12	7.50	9.50E+11	7.50	9.50E+11	6.24	1.29E+12	5.53	4.86E+11	5.79	1.13E+12	5.49	4.93E+11	5.44	5.02E+11
5.07	3.89E+11	6.55	6.43E+11	10.28	7.67E+11	10.28	7.67E+11	7.49	8.57E+11	7.96	4.13E+11	6.47	6.53E+11	7.90	4.13E+11	7.81	4.14E+11
6.66	3.44E+11	8.33	5.53E+11	13.52	7.30E+11	13.52	7.30E+11	9.33	7.32E+11	10.57	4.00E+11	8.12	5.56E+11	10.50	4.00E+11	10.41	4.00E+11
8.35	3.33E+11	10.36	5.31E+11	16.73	7.14E+11	16.73	7.14E+11	11.50	6.96E+11	13.01	3.88E+11	10.07	5.32E+11	12.94	3.89E+11	12.84	3.89E+11
9.93	3.23E+11	12.38	5.21E+11	19.84	7.04E+11	19.84	7.04E+11	13.70	6.81E+11	14.96	3.60E+11	12.06	5.21E+11	14.91	3.62E+11	14.82	3.65E+11
11.14	2.96E+11	14.36	5.14E+11	22.79	6.94E+11	22.79	6.94E+11	15.88	6.72E+11	16.03	3.08E+11	14.01	5.14E+11	16.04	3.07E+11	16.03	3.09E+11
11.51	2.34E+11	16.26	5.06E+11	25.51	6.81E+11	25.51	6.81E+11	18.00	6.66E+11	16.74	2.67E+11	15.88	5.07E+11	16.76	2.63E+11	16.78	2.60E+11
11.66	1.93E+11	17.98	4.91E+11	27.88	6.59E+11	27.88	6.59E+11	20.07	6.59E+11	17.38	2.38E+11	17.57	4.93E+11	17.41	2.34E+11	17.45	2.29E+11
11.77	1.62E+11	19.27	4.58E+11	29.68	6.22E+11	29.68	6.22E+11	22.04	6.52E+11	17.97	2.17E+11	18.89	4.68E+11	18.02	2.12E+11	18.08	2.07E+11
11.88	1.38E+11	19.89	4.08E+11	30.85	5.72E+11	30.85	5.72E+11	23.89	6.41E+11	18.52	2.01E+11	19.65	4.28E+11	18.58	1.96E+11	18.67	1.90E+11
11.99	1.22E+11	20.17	3.61E+11	31.61	5.18E+11	31.61	5.18E+11	25.53	6.24E+11	19.02	1.88E+11	20.00	3.83E+11	19.10	1.83E+11	19.21	1.77E+11
12.09	1.10E+11	20.33	3.18E+11	32.19	4.67E+11	32.19	4.67E+11	26.82	5.92E+11	19.48	1.77E+11	20.18	3.38E+11	19.57	1.72E+11	19.70	1.67E+11
12.18	1.00E+11	20.38	2.73E+11	32.68	4.29E+11	32.68	4.29E+11	27.54	5.43E+11	19.89	1.68E+11	20.22	2.93E+11	19.99	1.63E+11	20.14	1.58E+11
12.26	9.21E+10	20.44	2.42E+11	33.11	3.99E+11	33.11	3.99E+11	27.86	4.93E+11	20.26	1.60E+11	20.29	2.62E+11	20.36	1.56E+11	20.53	1.51E+11
12.34	8.53E+10	20.50	2.20E+11	33.47	3.74E+11	33.47	3.74E+11	28.04	4.50E+11	20.58	1.53E+11	20.36	2.39E+11	20.70	1.49E+11	20.88	1.44E+11
12.40	7.93E+10	20.56	2.02E+11	33.77	3.54E+11	33.77	3.54E+11	28.17	4.14E+11	20.87	1.46E+11	20.43	2.20E+11	20.99	1.43E+11	21.18	1.39E+11
12.46	7.42E+10	20.61	1.87E+11	34.01	3.36E+11	34.01	3.36E+11	28.28	3.84E+11	21.12	1.41E+11	20.48	2.04E+11	21.25	1.38E+11	21.46	1.34E+11
12.51	7.00E+10	20.64	1.74E+11	34.20	3.21E+11	34.20	3.21E+11	28.37	3.58E+11	21.34	1.36E+11	20.54	1.91E+11	21.48	1.33E+11		
12.54	6.64E+10	20.67	1.64E+11	34.35	3.07E+11	34.35	3.07E+11	28.44	3.36E+11	21.54	1.31E+11	20.58	1.80E+11	21.68	1.28E+11		
12.57	6.34E+10	20.69	1.55E+11	34.46	2.95E+11	34.46	2.95E+11	28.49	3.17E+11	21.71	1.27E+11	20.62	1.70E+11	21.86	1.24E+11		
12.59	6.08E+10	20.70	1.47E+11	34.54	2.85E+11	34.54	2.85E+11	28.52	2.98E+11	21.87	1.23E+11	20.64	1.62E+11				
12.60	5.85E+10	0.00	0.00E+00	34.58	2.75E+11	34.58	2.75E+11					20.66	1.54E+11				
				34.59	2.66E+11	34.59	2.66E+11					20.67	1.47E+11				

M (N.mm); χ (1/mm); M^+ (Positive bending moment); M^- (Negative bending moment)

Figure A5.46: Arrangement of the (a-b) longitudinal steel reinforcement and
(c) CFRP laminates of the SL45s50-HS slab strip.
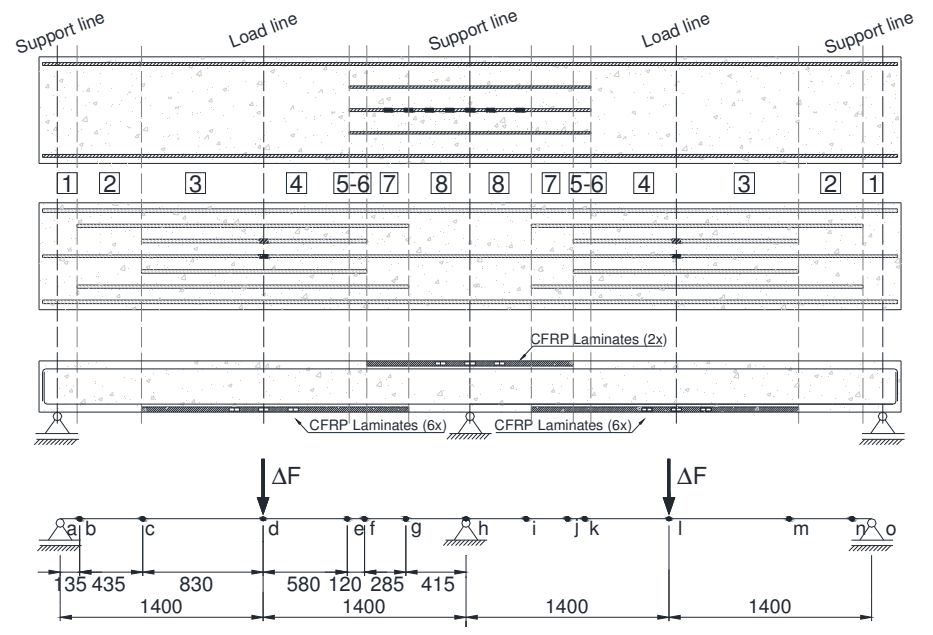
Figure A5.47: Discretization of the slab strip.
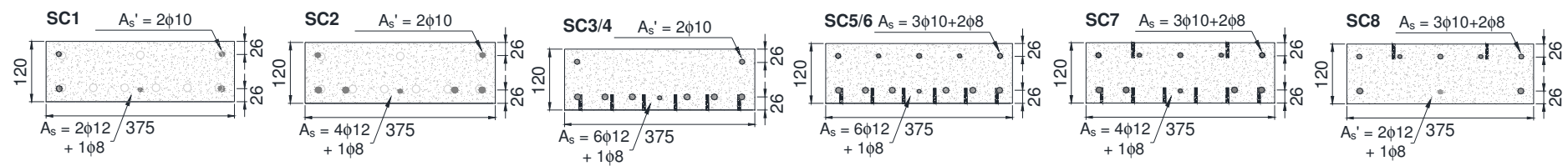
Figure A5.48: Resume of the cross-section according to the longitudinal steel reinforcement.

Table A5.16: Relation M−χ of the cross sections of the SL45s50-HS slab strip.

Element 1		Element 2		Element 3		Element 4		Element 5		Element 5		Element 6		Element 6		Element 7	
M^+	χ	M^+	χ	M^+	χ	M^+	χ	M^+	χ	M^-	χ	M^+	χ	M^-	χ	M^+	χ
0.00	1.91E+12	0.00	1.95E+12	0.00	2.04E+12	0.00	2.04E+12	0.00	2.01E+12	0.00	2.04E+12	0.00	1.97E+12	0.00	2.00E+12	0.00	1.96E+12
1.44	1.82E+12	1.45	1.87E+12	1.49	1.97E+12	1.49	1.97E+12	1.50	1.94E+12	1.58	1.95E+12	1.49	1.89E+12	1.53	1.91E+12	1.48	1.87E+12
3.62	1.66E+12	3.68	1.72E+12	5.17	1.71E+12	5.17	1.71E+12	3.81	1.79E+12	5.13	1.50E+12	3.76	1.73E+12	5.02	1.50E+12	4.91	1.50E+12
5.05	8.72E+11	5.80	1.11E+12	8.02	1.07E+12	8.02	1.07E+12	6.30	1.26E+12	5.77	5.21E+11	5.82	1.09E+12	5.72	5.29E+11	5.67	5.40E+11
5.07	3.89E+11	6.55	6.43E+11	11.06	8.72E+11	11.06	8.72E+11	7.64	8.39E+11	8.28	4.42E+11	6.60	6.34E+11	8.20	4.42E+11	8.10	4.43E+11
6.66	3.44E+11	8.33	5.53E+11	14.51	8.28E+11	14.51	8.28E+11	9.61	7.26E+11	11.01	4.27E+11	8.41	5.51E+11	10.92	4.27E+11	10.80	4.27E+11
8.35	3.33E+11	10.36	5.31E+11	17.95	8.10E+11	17.95	8.10E+11	11.87	6.93E+11	13.59	4.17E+11	10.46	5.30E+11	13.50	4.17E+11	13.37	4.17E+11
9.93	3.23E+11	12.38	5.21E+11	21.28	7.99E+11	21.28	7.99E+11	14.15	6.79E+11	15.78	3.96E+11	12.53	5.20E+11	15.70	3.98E+11	15.58	3.99E+11
11.14	2.96E+11	14.36	5.14E+11	24.47	7.89E+11	24.47	7.89E+11	16.39	6.71E+11	17.30	3.53E+11	14.54	5.13E+11	17.25	3.57E+11	17.17	3.62E+11
11.51	2.34E+11	16.26	5.06E+11	27.47	7.78E+11	27.47	7.78E+11	18.57	6.64E+11	18.34	3.10E+11	16.45	5.04E+11	18.35	3.10E+11	18.33	3.12E+11
11.66	1.93E+11	17.98	4.91E+11	30.24	7.64E+11	30.24	7.64E+11	20.68	6.57E+11	19.26	2.80E+11	18.12	4.87E+11	19.30	2.78E+11	19.33	2.77E+11
11.77	1.62E+11	19.27	4.58E+11	32.70	7.43E+11	32.70	7.43E+11	22.68	6.49E+11	20.12	2.58E+11	19.29	4.54E+11	20.18	2.55E+11	20.25	2.53E+11
11.88	1.38E+11	19.89	4.08E+11	34.74	7.14E+11	34.74	7.14E+11	24.53	6.36E+11	20.92	2.40E+11	19.87	4.07E+11	21.01	2.38E+11	21.10	2.35E+11
11.99	1.22E+11	20.17	3.61E+11	36.34	6.77E+11	36.34	6.77E+11	26.12	6.13E+11	21.66	2.26E+11	20.15	3.60E+11	21.77	2.23E+11	21.89	2.21E+11
12.09	1.10E+11	20.33	3.18E+11	37.59	6.39E+11	37.59	6.39E+11	27.23	5.72E+11	22.34	2.15E+11	20.26	3.11E+11	22.46	2.12E+11	22.60	2.09E+11
12.18	1.00E+11	20.38	2.73E+11	38.61	6.04E+11	38.61	6.04E+11	27.75	5.18E+11	22.97	2.05E+11	20.32	2.71E+11	23.10	2.02E+11	23.25	2.00E+11
12.26	9.21E+10	20.44	2.42E+11	39.49	5.73E+11	39.49	5.73E+11	27.99	4.69E+11	23.53	1.96E+11	20.40	2.44E+11	23.67	1.94E+11	23.84	1.92E+11
12.34	8.53E+10	20.50	2.20E+11	40.23	5.47E+11	40.23	5.47E+11	28.14	4.28E+11	24.04	1.89E+11	20.48	2.23E+11	24.19	1.87E+11	24.36	1.85E+11
12.40	7.93E+10	20.56	2.02E+11	40.86	5.23E+11	40.86	5.23E+11	28.26	3.94E+11	24.50	1.82E+11	20.54	2.06E+11	24.66	1.80E+11	24.83	1.79E+11
12.46	7.42E+10	20.61	1.87E+11	41.40	5.03E+11	41.40	5.03E+11	28.35	3.65E+11	24.92	1.76E+11	20.60	1.92E+11	25.08	1.75E+11	25.25	1.73E+11
12.51	7.00E+10	20.64	1.74E+11	41.84	4.84E+11	41.84	4.84E+11	28.44	3.42E+11	25.30	1.71E+11	20.64	1.80E+11	25.45	1.70E+11	25.62	1.68E+11
12.54	6.64E+10	20.67	1.64E+11	42.20	4.67E+11	42.20	4.67E+11	28.49	3.21E+11	25.64	1.66E+11	20.67	1.70E+11	25.79	1.65E+11	25.94	1.64E+11
12.57	6.34E+10	20.69	1.55E+11	42.48	4.52E+11	42.48	4.52E+11	28.52	3.02E+11	25.95	1.61E+11	20.69	1.61E+11	26.09	1.60E+11	26.23	1.59E+11
12.59	6.08E+10	20.70	1.47E+11	42.70	4.38E+11	42.70	4.38E+11			26.23	1.57E+11	20.70	1.53E+11	26.36	1.56E+11	26.48	1.56E+11
12.60	5.85E+10			42.86	4.24E+11	42.86	4.24E+11			26.50	1.53E+11						
				42.97	4.12E+11	42.97	4.12E+11			26.74	1.50E+11						
				43.02	4.01E+11	43.02	4.01E+11										

M (N.mm); χ (1/mm); M^+ (Positive bending moment); M^- (Negative bending moment)

ANNEX 5.17 - RESUME OF THE APPLIED DISPLACEMENT X OBTAINED LOAD

Table A5.17: Resume of the applied displacement x obtained load for the SL15 series.

SL15-H		SL15s25-H		SL15s50-H		SL15-HS		SL15s25-HS	
Applied displacement (mm)	Obtained load (kN)	Applied displacement (mm)	Obtained load (kN)	Applied displacement (mm)	Obtained load (kN)	Applied displacement (mm)	Obtained load (kN)	Applied displacement (mm)	Obtained load (kN)
0.00	0.00	0.00	0.00	0.00	0.00	0.00	0.00	0.00	0.00
1.00	8.81	1.00	8.90	1.00	8.95	1.00	7.19	5.00	17.50
2.00	12.43	3.00	14.06	2.00	13.09	2.00	10.02	10.00	31.44
3.00	13.60	5.00	18.06	3.00	14.69	3.00	11.57	12.50	38.11
5.00	17.31	7.50	25.12	5.00	19.01	5.00	15.73	15.00	44.22
7.50	23.99	10.00	32.59	7.50	26.50	7.50	22.07	17.50	49.27
10.00	31.11	12.50	39.49	10.00	34.39	10.00	28.29	20.00	52.93
12.50	37.58	15.00	45.82	12.50	41.69	12.50	34.19	22.50	55.49
15.00	42.96	17.50	50.27	15.00	48.60	15.00	39.38	25.00	57.22
20.00	47.86	20.00	52.66	17.50	53.85	20.00	45.89	27.50	58.52
22.50	49.03	22.50	53.84	20.00	56.72	25.00	47.34	30.00	59.61
25.00	49.62	25.00	54.69	22.50	58.35	27.50	47.51	32.50	60.55
27.50	49.91	27.50	55.43	25.00	59.64	32.80	47.60	35.00	61.37
30.00	50.10	30.00	56.09	30.00	61.80			37.50	62.10
37.50	50.44	35.00	57.20	35.00	63.37			40.00	62.72
		44.70	59.81	41.70	66.23			42.50	63.24
								45.00	63.61
								47.50	63.98
								53.50	64.42

Table A5.18: Resume of the Applied Displacement x Obtained Load for the SL30 series.

SL30-H		SL30s25-H		SL30s50-H		SL30-HS		SL30s25-HS		SL30s50-HS	
Applied displacement (mm)	Obtained load (kN)	Applied displacement (mm)	Obtained load (kN)	Applied displacement (mm)	Obtained load (kN)	Applied displacement (mm)	Obtained load (kN)	Applied displacement (mm)	Obtained load (kN)	Applied displacement (mm)	Obtained load (kN)
0.00	0.00	0.00	0.00	0.00	0.00	0.00	0.00	0.00	0.00	0.00	0.00
3.00	10.00	5.00	16.70	5.00	17.12	7.40	1.00	5.00	17.08	5.00	18.52
5.00	16.38	10.00	30.06	10.00	30.88	10.15	2.00	10.00	30.70	10.00	33.24
10.00	29.41	15.50	41.82	12.50	37.24	11.54	3.00	12.50	37.02	15.50	47.18
13.20	35.00	20.00	47.94	15.00	42.82	15.48	5.00	15.00	42.47	20.00	55.22
17.50	42.59	22.50	50.17	17.50	47.14	21.65	7.50	17.50	45.58	25.00	62.15
20.00	47.40	25.00	51.27	20.00	50.50	27.86	10.00	20.00	50.17	27.50	64.68
22.50	47.09	27.50	51.85	22.50	52.72	33.40	12.50	22.50	53.33	30.00	66.66
25.00	48.56	30.00	52.25	25.00	53.92	37.80	15.00	25.00	55.71	32.50	68.24
27.50	49.21	32.50	52.59	27.50	54.67	45.25	20.00	27.50	57.42	35.00	69.53
30.00	49.41	35.00	52.88	30.00	55.27	45.50	22.50	30.00	58.69	37.50	70.56
32.50	49.55	37.50	53.12	32.50	55.78	46.72	25.00	32.50	59.70	40.00	71.38
41.00	49.77	40.00	53.31	35.00	56.23	47.72	27.50	35.00	60.55	42.50	71.97
		44.50	53.78	37.50	56.60	48.11	32.50	37.50	61.29	44.20	72.20
				42.50	57.49			40.00	61.93		
				45.00	58.11			42.50	62.49		
				47.00	58.52			45.00	62.96		
								47.50	63.37		
								50.00	63.71		
								52.50	63.99		
								55.00	64.20		
								57.30	64.33		

Table A5.19: Resume of the Applied Displacement x Obtained Load for the SL45 series.

SL45-H		SL45s25-H		SL45s50-H		SL45-HS		SL45s25-HS		SL45s50-HS	
Applied displacement (mm)	Obtained load (kN)	Applied displacement (mm)	Obtained load (kN)	Applied displacement (mm)	Obtained load (kN)	Applied displacement (mm)	Obtained load (kN)	Applied displacement (mm)	Obtained load (kN)	Applied displacement (mm)	Obtained load (kN)
0.00	0.00	0.00	0.00	0.00	0.00	0.00	0.00	0.00	0.00	0.00	0.00
5.00	16.78	2.50	12.49	5.00	17.40	3.00	13.22	5.00	17.98	5.00	19.77
10.00	29.40	5.00	16.99	7.50	24.04	5.00	16.86	7.50	24.85	12.50	41.59
15.00	38.57	7.50	23.42	10.00	30.68	7.50	23.19	10.00	31.53	15.00	47.47
20.00	44.38	10.00	29.84	12.50	36.57	8.50	25.86	12.50	37.52	17.50	52.88
22.50	47.57	12.50	35.27	15.00	41.57	10.00	29.53	15.00	42.07	20.00	57.98
25.00	49.76	16.50	42.15	17.50	46.03	15.00	38.75	17.50	46.71	22.50	62.48
30.00	50.68	20.00	47.26	20.00	49.84	20.00	44.48	20.00	51.06	25.00	66.06
46.00	51.25	22.50	49.94	22.50	52.59	22.50	47.69	22.50	54.47	27.50	68.83
		25.00	51.47	25.00	54.16	25.00	49.85	25.00	56.75	30.00	71.06
		27.50	52.18	27.50	54.95	30.00	50.78	27.50	58.28	32.50	73.01
		30.00	52.53	30.00	55.50	35.00	51.11	30.00	59.38	35.00	74.74
		32.50	52.83	32.50	55.99	47.20	51.45	32.50	60.28	37.50	76.29
		46.00	53.81	35.00	56.46			35.00	61.10	40.00	77.63
				37.50	56.89			37.50	61.87	50.30	80.43
				40.00	57.27			56.00	64.86		
				42.50	57.60						
				46.00	58.25						

Figure A5.49 (continued).

Figure A5.49: Moment diagram to the calculation of the flexibility influence coefficients.

Chapter 6
ANNEXES

Technical Data Sheet

S&P
Clever Reinforcement Company AG
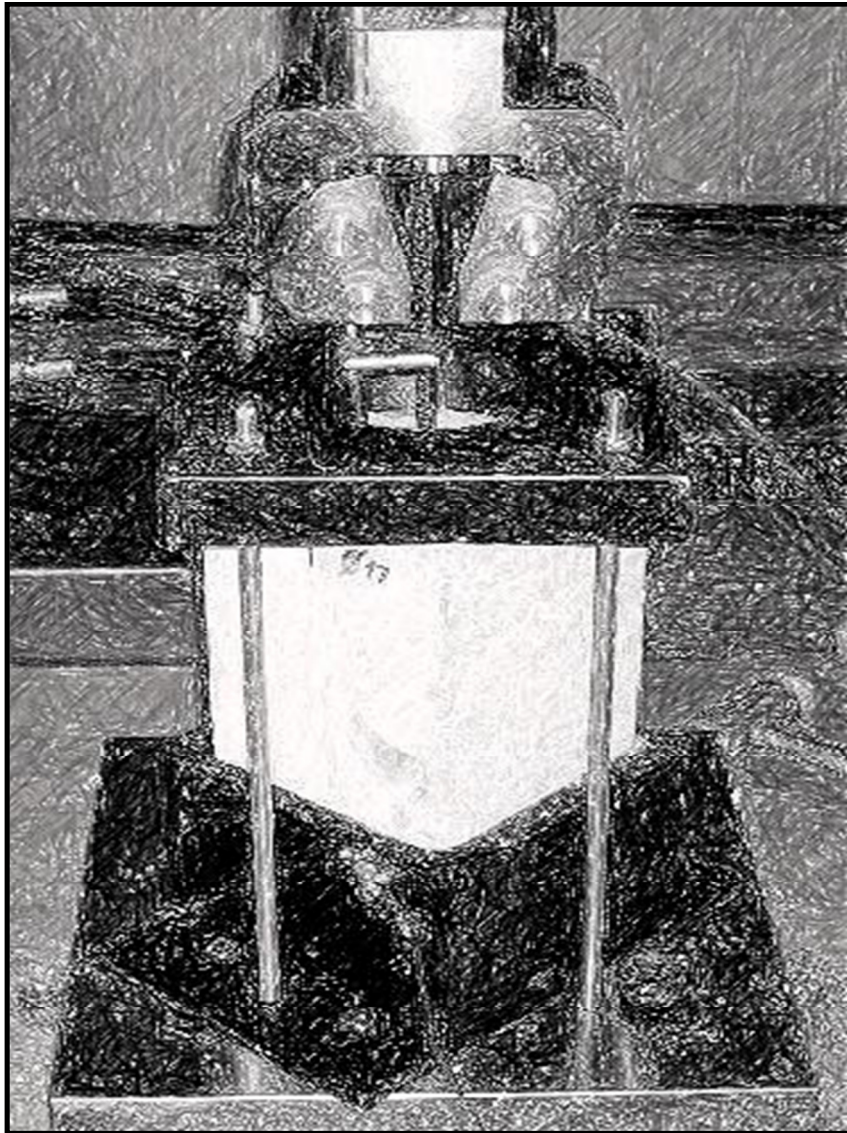
S&P Resin Epoxy 55
S&P Resin Epoxy 50
Laminating resin

10/12

Application
The S&P Resin Epoxy 55/50 is used as a laminating resin for the following S&P Sheet systems:

S&P C-Sheet
S&P G-Sheet
S&P A-Sheet

Its high wet ability and thixotropy allow bonding of FRP systems of up to 400 g/ m². Sheets of 400 - 800 g/ m² are preimpregnated with S&P Resin Epoxy 55/50 and wet applied.

Description of product
Solvent-free, transparent 2-component epoxy resin with a formulated amine hardener.

Performance
When fully cured the S&P Resin Epoxy 55/50 is resistant against bases, diluted acids, saline solutions, mineral oils and aliphatics. The S&P Resin Epoxy 55/50 is weather resistant and is almost non-yellowing. The S&P Resin Epoxy 55/50 is resistant to constant as well as changing temperatures within the range of -30°C up to +45°C with dry exposure and up to +40°C with wet exposure.

Processing
The S&P Resin Epoxy 55/50 is delivered in the prescribed mixing ratios. The hardener (Comp. II) is poured into the resin (Comp. I). It is important that the hardener is used up completely. Mixing of both components is preferably done by means of a low speed drill equipped with a mixing paddle. Mix thoroughly and carefully scrape the sides and bottom of the container while mixing to ensure that the hardener is evenly distributed also vertically. After blending the mix must be homogeneous, i.e. without streaks. The temperature of both components at the moment of mixing shall be 15°-20°C. Higher temperatures considerably reduce the open time.

The S&P Resin Epoxy 55/50 must be protected from moisture during 6-8 hours after the application. Should any contact with moisture occur during this period, the surface will turn white and tacky; the resin below, however, cures perfectly. In discoloured or tacky areas the bond to any subsequent coating is either reduced or completely prevented. If the product is used as a primer, special attention has to be paid to this circumstance.

Safety precautions
When fully cured the S&P Resin Epoxy 55/50 is physiologically harmless. The hardener (Comp. II) is caustic. Care must be taken that no skin contact with the resin (Comp. I) or the hardener (Comp. II) takes place. It is recommended to wear rubber gloves during handling and application. If skin contact occurs, rinse with soap and plenty of water. If eye contact occurs, rinse at once with plenty of water and additionally use an eye rinsing kit (available in drugstores). Seek medical advice immediately.

Cleaning of tools
In case of any work interruption exceeding 15 minutes all tools must be thoroughly and carefully cleaned with the S&P Cleaner and rinsed.

Safety directions
For directions regarding dangers, safety and waste disposal please refer to the EN material safety data sheet and the label on the containers.

1/2   www.sp-reinforcement.eu   ISO 9001 BUREAU VERITAS

Technical Data Sheet

S&P
Clever Reinforcement Company AG

Approvals
Certified in accordance with EN 1504-4

Technical data
(The standard values below indicated are based on +20°C and 50% relative humidity of air.)

Density			1.11 kg/l
Mixing ratio by weight			2:1 (resin to hardener)
Application temperature	+8°C to +35°C		
Application time at	+ 10°C		3 h
	+ 20°C		45 min
	+ 30°C		30 min
Dust-dry after			4 h
Hardening time			7 days
Glass transition temperature EMPA 461.427/2			44°C
Tensile strength after ISO 527-2:1993(E) EMPA 461'427	14 days		35.8 MPa
Elongation at break ISO 527-2:1993(E) EMPA 461'427	14 days		2.3 %
Modulus of elasticity static ISO 7500-1:2004-11 (EMPA 461'427)	14 days		2'581.8 MPa
Modulus of elasticity dynamic EMPA 461.427/2	14 days 14 days	+20 °C -20 °C	2'515 MPa 2'989 MPa
Modulus of elasticity dynamic EMPA 461.427/2	14 days 14 days	+20 °C -20 °C	2'515 MPa 2'989 MPa
Pull off strength on concrete job-site tests			failure in concrete
Pull off strength on steel In-house tests			> 15 N/mm²
Toxicity class	**Comp. I**	**9**	
Toxicity class	**Comp. II**	**8**	
Transport class / UN No.	Comp. I	III / 3082	
	Comp. II	III / 2735	

Packaging
Units of 6 kg or container of 1'000 l

Storage
In original containers, at +5°C to +25°C, 24 months

374

ANNEX 6.2 – TECHNICAL DATA SHEET OF THE K BOND AGENT

Sikadur®-32 N

Wet to dry epoxy resin bonding agent

Product Description	Sikadur®-32 N is a two component solvent free, moisture insensitive, medium viscosity, structural epoxy bonding agent. Complies with ASTM C 881-78 type II, Grade 2 Class B & C.
Uses	Sikadur®-32 N is used for bonding fresh concrete to an existing concrete or mortar substrate. It is also suitable for vertical anchor bolt grouting.
Characteristics / Advantages	■ Easy to mix and apply ■ Solvent-free ■ Components of different colours to ensure thorough mixing ■ Excellent adhesion to concrete and a wide variety of other substrates ■ Tensile strength far greater than concrete ■ Can be applied to damp substrates

Product Data

Form

Appearance / Colours	Part A: White Part B: Grey Mixed: Light Grey
Packaging	Pre batched Part A+B 1litre and 5 litre kits

Storage

Storage Conditions / Shelf-Life	12 months from date of production if stored properly in unopened, undamaged and sealed original packaging, in dry conditions at temperatures between +5°C and +30°C.

Technical Data

Chemical Base	Solvent free two-part epoxy resin.
Density	Part A+B mixed: 1,40 kg/litre

Construction

Sika®

1

Mechanical / Physical Properties

Compressive Strength	$60 - 70 \text{ N/mm}^2$
Bond Strength	$2.5 - 3.0 \text{ N/mm}^2$
Tensile Strength	$18 - 20 \text{ N/mm}^2$

System Information

Application Details

Consumption / Dosage	$2 - 4 \text{ m}^2$ per litre depending on the porosity of the substrate.
Substrate Preparation	Requirements: Sound, clean, free from oil and grease, old coatings and surface treatments, etc. Pre-treatment for good bond: Concrete, mortar and stone should be thoroughly prepared by high pressure water jetting or mechanical means such as grinding, chiselling, etc. Cracks must be cleaned with compressed air to remove dust.

Application Conditions / Limitations

Substrate Temperature	Min.5 °C - Max.30 °C
Ambient Temperature	Min.5 °C - Max.35 °C
Substrate Humidity	Dry or damp (SSD - Saturated Surface Dry: no standing water)
Relative Air Humidity	80 %
Dew Point	Substrate temperature must always be at least 3 °C above the dew point.

Application Instructions

Mixing (Ratio/Dosage)	Mix both components thoroughly before use. Pour both components into a suitable, clean mixing container. Mix thoroughly using a slow speed drill (set at 400 - 600 rpm) with a clean, rust free, mixing paddle until the two components are evenly blended to a uniform colour (minimum 3 minutes). **Use immediately.**
Application Method / Tools	For bonding fresh concrete to an existing concrete or mortar substrate. Apply Sikadur®-32 N to the prepared substrate by brush or roller. On damp surfaces ensure that it is worked well into the substrate. Place the fresh concrete while the Sikadur®-32 N is still tacky. If the Sikadur®-32 N loses tackiness and becomes glossy, recoat with additional material and continue. Calculation of Grout Quantities Volume of Bolt Hole **Less:** Volume of Embedded Bolt **=** Volume of Sikadur®-32 N Volume of Sikadur®-32 N = $(\pi r^2 H - \pi r^2 L) \times 1000$ Where H = Depth of Hole (in metres) L = Length of Embedded Bolt (in metres)

2

	Vertical anchor bolt grouting:
	The correct quantity of Sikadur®-32 N required to completely fill the annular gap between the bolt and the sides of the hole should be determined before installation is attempted. (In most cases, the bolthole will be no greater than 5 mm larger in diameter than the bolt). Place the pre-determined quantity of Sikadur®-32 N directly into the bolthole. Lower the anchor bolt into the hole and press it gently to the bottom, displacing the Sikadur®-32 N and filling the annulus around the bolt. A slight agitation of the bolt will assist the Sikadur®-32 N to fill the annulus evenly. Centre or locate the bolt in the desired position, using shims if necessary, and then leave undisturbed until the Sikadur®-32 N is tack free.
	If the Sikadur®-32 N does not fill the annular gap evenly during bolt insertion, withdraw the bolt, insert additional Sikadur®-32 N, and re-insert the bolt. Do not attempt to add additional Sikadur®-32 N with the bolt in place.
Cleaning of Tools	Remove uncured Sikadur®-32 N from tools and equipment with Kwiklean water-soluble solvent immediately after use. Cured material can only be removed mechanically.
Pot Life	Pot Life at 20°C - 25 minutes.
Open Time	Open Time at 20°C and 1mm thickness – 1.5 hours. Open Time at 30°C and 1mm thickness – 1 hour.
Waiting Time / Overcoatability	
Notes on Application / Limits	Cured Sikadur®-32 N is a vapour barrier.
	Concrete should be a minimum of 28 days old.
	The normal precautions pertaining to dew point should be observed.
Local Restrictions	Please note that as a result of specific local regulations the performances of this product may vary from country to country. Please consult the local Product Data Sheet for the exact description of the application fields.

Health and Safety Information

Protective Measures	Use personal protective clothing and avoid contact with eyes and skin. Change soiled work clothes and wash hands before breaks and after finishing work. Allow for sufficient ventilation when applying.
	Local regulations as well as health and safety advice on packaging labels must be observed.
Ecology	
Transportation Class	
Important Notes	Residues of material must be removed according to local regulations. Fully cured material can be disposed of as household waste under agreement with the responsible local authorities.
	Detailed health and safety information as well as detailed precautionary measures e.g. physical, toxicological and ecological data can be obtained from the Material Safety Data Sheet.
Toxicity	

Construction
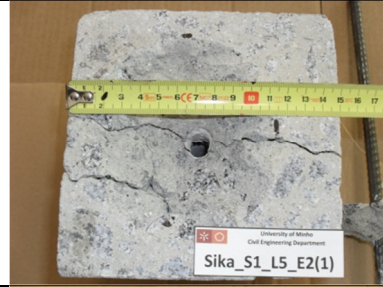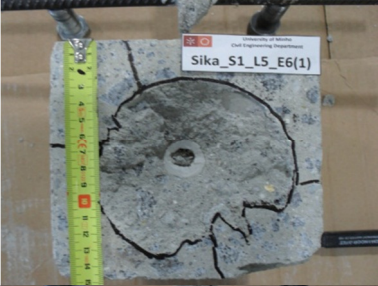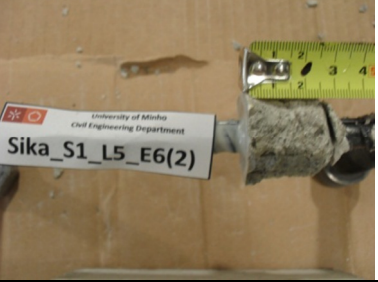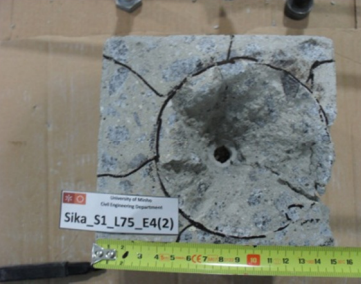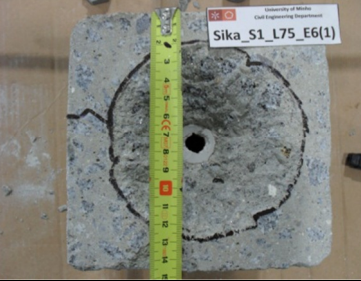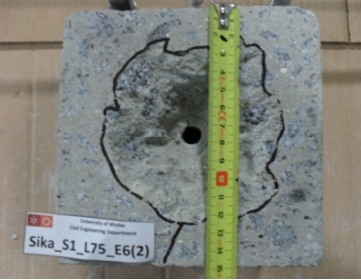
ANNEX 6.3 – DETAILS OF THE SPECIMENS AFTER TEST

Specimen	Details after test			
S2 (12 mm) AK_D12_L50_T2-1				
AK_D12_L50_T2-2				
AK_D12_L50_T4-1				
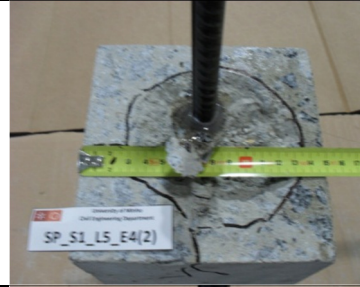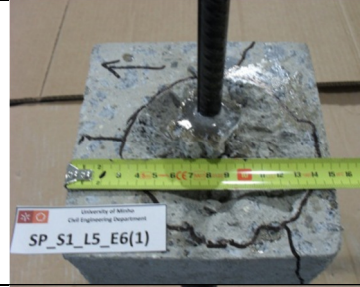
Specimen	Details after test			
S2 **(12 mm)** AK_D12_L50_T4-2				
AK_D12_L50_T6-1				
AK_D12_L50_T6-2				

	Specimen	Details after test			
S2 (12 mm)	AK_D12_L75_T2-1				
	AK_D12_L75_T2-2				
	AK_D12_L75_T4-1				

Specimen	Details after test			
S2 **(12 mm)** AK_D12_L75_T4-2				
AK_D12_L75_T6-1				
AK_D12_L75_T6-2				

	Specimen	Details after test			
S2 (12 mm)	AS_D12_L75_T2-1				
	AS_D12_L75_T2-2				
	AS_D12_L75_T4-1				

	Specimen	Details after test			
S2 (12 mm)	AS_D12_L75_T4-2				
	AS_D12_L75_T6-1				
	AS_D12_L75_T6-2				

Specimen	Details after test			
S2 (12 mm) AS_D12_L75_T2-1				
AS_D12_L75_T2-2				
AS_D12_L75_T4-1				

Specimen		Details after test			
S2 (12 mm)	AS_D12_L75_T4-2				
	AS_D12_L75_T6-1				
	AS_D12_L75_T6-2				

Chapter 7

ANNEXES

ANNEX 7.1 - DATA OF THE NUMERICAL SIMULATIONS OF THE BEAMS OF A SERIES
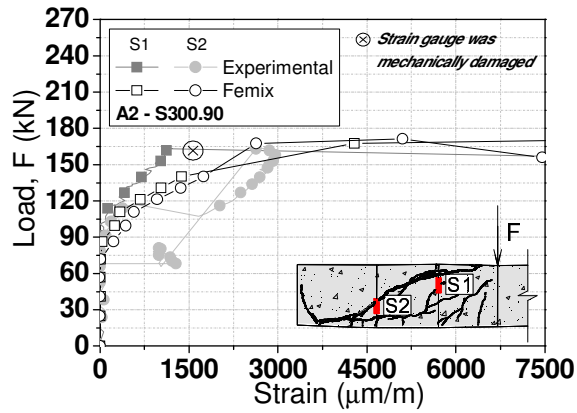
Figure A7.1: Relationship between Load *versus* Strain in the steel stirrups for the beamA.2.
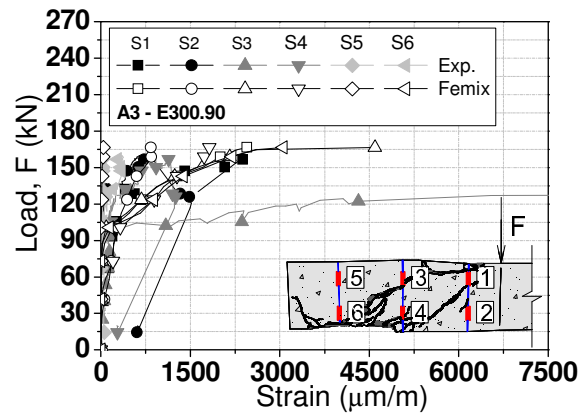
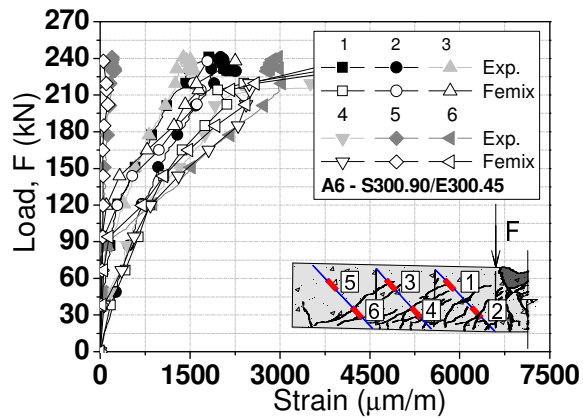Figure A7.2: Relationship between Load *versus* Strain in the ETS bars for the beam A.3.
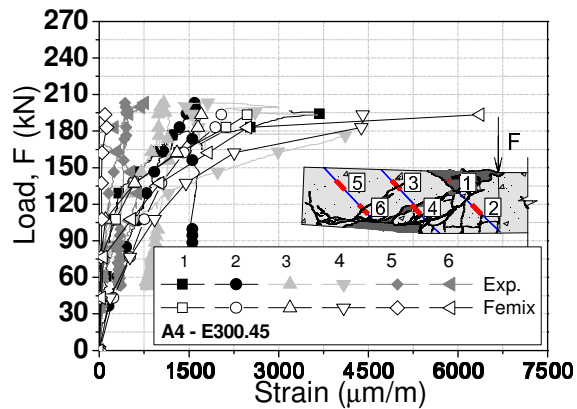
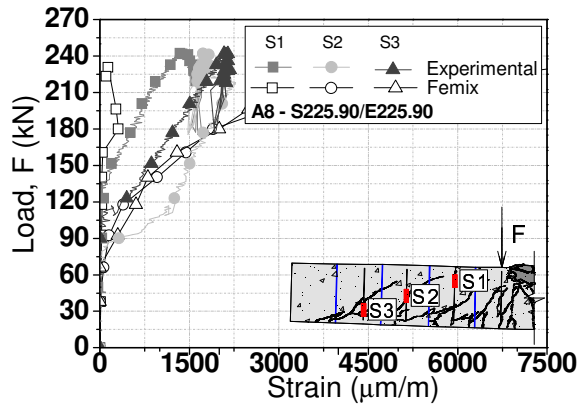Figure A7.3: Relationship between Load *versus* Strain in the ETS bars for the beam A.4.
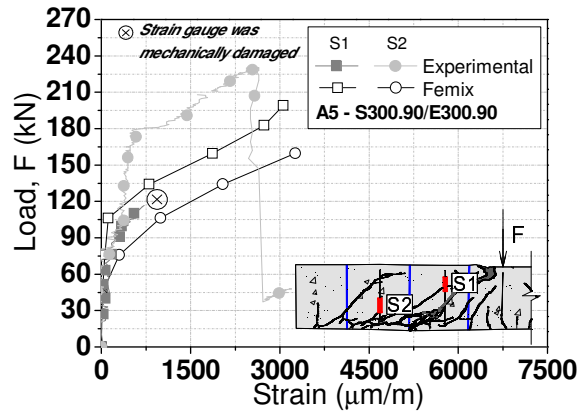
Figure A7.4: Relationship between Load *versus* Strain in the steel stirrups for the beam A.5.
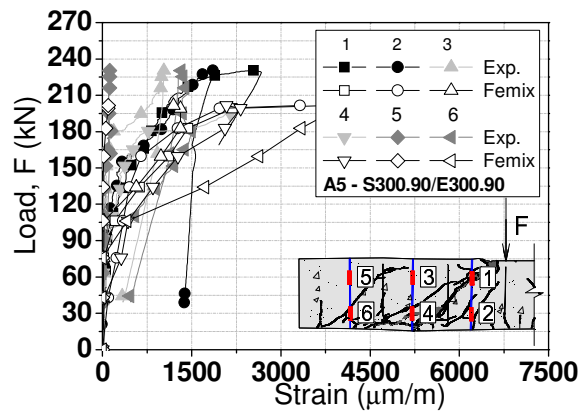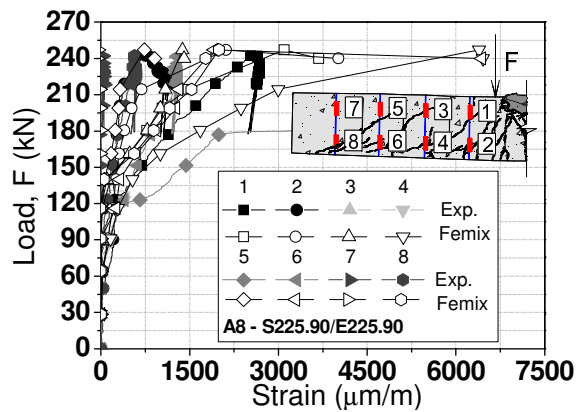

Figure A7.5: Relationship between Load *versus* Strain in the ETS bars for the beam A.5.

Figure A7.6: Relationship between Load *versus* Strain in the ETS bars for the beam A.6.

Figure A7.7: Relationship between Load *versus* Strain in the Steel stirrups for the beam A.8.

Figure A7.8: Relationship between Load *versus* Strain in the ETS bars for the beam A.8.

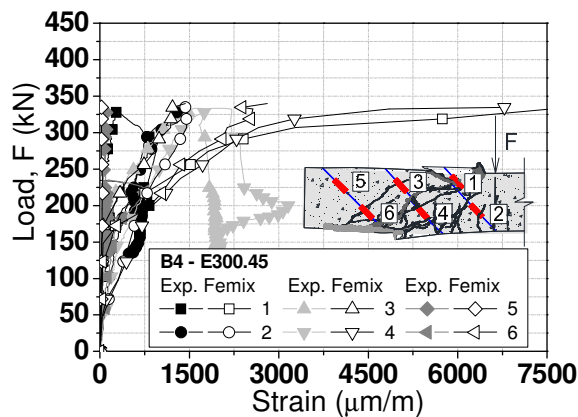## ANNEX 7.2 - DATA OF THE NUMERICAL SIMULATIONS OF THE BEAMS OF B SERIES

Figure A7.9: Relationship between Load *versus* Strain in ETS bars for the beam B.4.
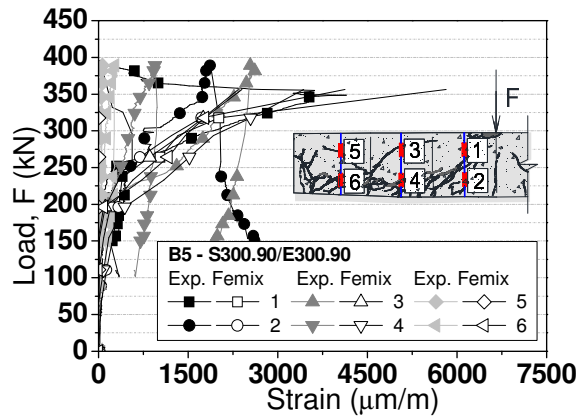
Figure A7.10: Relationship between Load *versus* Strain in ETS bars for the beam B.5.
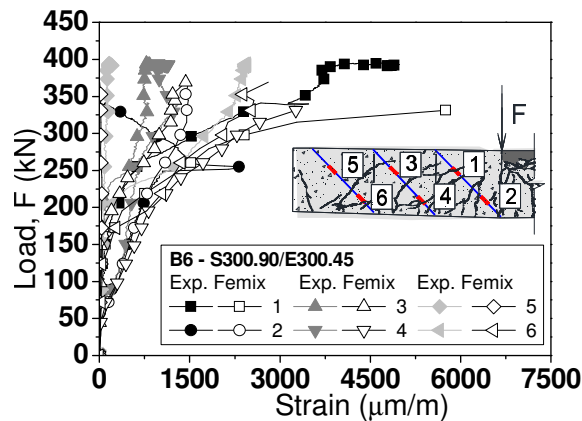

Figure A7.11: Relationship between Load *versus* Strain in ETS bars for the beam B.6.

ANNEX 7.3 - PREDICTION OF THE RC BEAMS CAPACITY

7.2.1 Shear resistance of RC beams according to ACI 440 and ACI318

To evaluate the nominal shear resistance of the tested beams (V_n), the recommendations of the ACI 440 (2008) were adopted by assuming that ETS bars can be regarded, from the strengthening point-of-view, like a fiber reinforced polymer (FRP) system. Therefore,

$$\phi V_n = \phi(V_c + V_s + \psi_f V_f) \tag{A7.1}$$

where V_c, V_s and V_f are the contributions from the concrete, steel stirrups and ETS bars, respectively, ψ_f is a reduction applied to the contribution of the shear strengthening system and has a value of 0.85, and ϕ is the strength-reduction factor required by ACI 318 (2008) that, for shear strengthening of concrete elements and has value of 0.95 (full wrapped conditions for the section). In equation (A7.1), V_c has been computed using the upper limit indicated in Section 11.2.2.1 of the ACI 318 (2008), given by $V_c = 3.5\sqrt{f_c'} \cdot b_w \cdot d$,

where f_c' is the concrete compressive strength (in psi), b_w is the web width (in inches), and d is the distance from the extreme compression fiber of the cross section to the centroid of the longitudinal reinforcement (in inches). Thus, the average concrete compressive strengths are 30.78 MPa (4464.26 psi) and 27.81MPa (4033.50 psi) for the batches 1 and 2, respectively; the web widths (b_w) are equal to 150 mm (5.91 inches) and 300 mm (11.81 inches) for the A and B series, respectively; and the distance from the extreme compression fiber of the cross section to the centroid of the longitudinal reinforcement (d) is 261.50 mm (10.30 inches).

For the calculations according to the ACI 440 and ACI318 recommendations the contributions from the concrete for the A series, for the batches 1 and 2, are:

$$V_c = \phi(3.5\sqrt{f_c'} \cdot b_w \cdot d) \tag{A7.2}$$
$$V_c = 0.85(3.5\sqrt{4464.26psi} \cdot 5.91in \cdot 10.30in)$$
$$V_c = 12100.03lb$$
$$V_c = 53.77kN$$

and

$$V_c = \phi(3.5\sqrt{f_c'} \cdot b_w \cdot d) \tag{A7.3}$$
$$V_c = 0.85(3.5\sqrt{4033.50\,psi} \cdot 5.91in \cdot 10.30in)$$
$$V_c = 11501.45lb$$
$$V_c = 52.02kN$$

For the calculations according to the ACI 440 and ACI318 recommendations the contributions from the concrete for the B series, for the batches 1 and 2, are:

$$V_c = \phi(3.5\sqrt{f_c'} \cdot b_w \cdot d) \tag{A7.4}$$
$$V_c = 0.85(3.5\sqrt{4464.26psi} \cdot 11.81in \cdot 10.30in)$$
$$V_c = 24179.58lb$$
$$V_c = 107.45kN$$

and

$$V_c = \phi(3.5\sqrt{f_c'} \cdot b_w \cdot d) \tag{A7.5}$$
$$V_c = 0.85(3.5\sqrt{4033.50\,psi} \cdot 11.81in \cdot 10.30in)$$
$$V_c = 22983.44lb$$
$$V_c = 103.96kN$$

The contribution of the vertical steel stirrups has been computed according to Section 11.4.7.2 of the ACI 318 Code, by applying the equation

$$V_s = \phi\left(\frac{A_v \cdot f_{yt} \cdot d}{s}\right) \tag{A7.6}$$

where A_v is the cross sectional area of steel stirrups of spacing s, and f_{yt} is the yield stress of the steel stirrup. When inclined bars are used as shear reinforcement,

$$V_s = \phi \left(\frac{A_v \cdot f_{yt} \cdot (\sin \alpha + \cos \alpha) \cdot d}{s} \right) \tag{A7.7}$$

where α is the angle between inclined stirrups and longitudinal axis of the member, and s is measured in direction parallel to longitudinal reinforcement. Using the equation (A7.7) and the materials properties presented in Table 7.2, the contribution of the vertical steel stirrups placed at a spacing of 300 mm and 225 mm are:

$$V_{stirrups} = 0.85 \frac{[(6mm/2)^2 \cdot \Pi \cdot 2] \cdot 559.14 MPa \cdot (\sin 90 + \cos 90) \cdot 261.50 mm}{300 mm} \tag{A7.8}$$

$$V_{stirrups} = 23.42 kN$$

and

$$V_{stirrups} = 0.85 \frac{[(6mm/2)^2 \cdot \Pi \cdot 2] \cdot 559.14 MPa \cdot (\sin 90 + \cos 90) \cdot 261.50 mm}{225 mm} \tag{A7.9}$$

$$V_{stirrups} = 31.21 kN$$

The contribution of ETS bars is evaluated by introducing convenient adjustments in equations (A7.10) and (A7.11):

$$V_f = \phi \psi_f \left(\frac{A_f \cdot f_{yt} \cdot d}{s_f} \right) \tag{A7.10}$$

and

$$V_f = \phi \psi_f \left(\frac{A_f \cdot f_{yt} \cdot (\sin \alpha + \cos \alpha) \cdot d}{s_f} \right) \tag{A7.11}$$

where A_f is the cross sectional area of the ETS bars of spacing s_f and f_{yt} is the yield stress of the ETS bar. Using the equation (A7.11) and the materials properties presented in Table 7.2, the contribution of the vertical and inclined ETS bars in the beams of the A series is, respectively:

$$V_f = 0.85 \cdot 0.95 \left\{ \frac{[(10mm/2)^2 \cdot \Pi] \cdot 541.60 MPa \cdot (\sin 90 + \cos 90) \cdot 261.50 mm}{300 mm} \right\} \tag{A7.12}$$

$$V_f = 29.93 kN$$

and

$$V_f = 0.85 \cdot 0.95 \left\{ \frac{[(10mm/2)^2 \cdot \Pi] \cdot 541.60 MPa \cdot (\sin 45 + \cos 45) \cdot 261.50 mm}{300 mm} \right\} \tag{A7.13}$$

$V_f = 42.32 kN$

The contribution of the vertical ETS bars in the beams of the A series, at a spacing of 225 mm, is:

$$V_f = 0.85 \cdot 0.95 \left\{ \frac{[(10mm/2)^2 \cdot \Pi] \cdot 541.60 MPa \cdot (\sin 90 + \cos 90) \cdot 261.50mm}{225mm} \right\}$$ (A7.14)

$V_f = 39.89 kN$

Concerning to the beams of the B series, the contribution of the vertical and inclined ETS bars in is, respectively:

$$V_f = 0.85 \cdot 0.95 \left\{ \frac{[(8mm/2)^2 \cdot \Pi \cdot 2] \cdot 566.50 MPa \cdot (\sin 90 + \cos 90) \cdot 261.50mm}{300mm} \right\}$$ (A7.15)

$V_f = 40.07 kN$

and

$$V_f = 0.85 \cdot 0.95 \left\{ \frac{[(8mm/2)^2 \cdot \Pi \cdot 2] \cdot 566.50 MPa \cdot (\sin 45 + \cos 45) \cdot 261.50mm}{300mm} \right\}$$ (A7.16)

$V_f = 56.66 kN$

7.2.2 Shear resistance of RC beams according to the Eurocode 2 (2004)

In the case of the reference beams, the design value for the shear resistance, $V_{Rd,c}$, for members not requiring shear reinforcement is determined from:

$$V_{Rd,c} = [C_{Rd,c} k (100 \rho_l f_{ck} + k_1 \sigma_{cp})^{1/3}] b_w d \geq (V_{min} + k_1 \sigma_{cp}) b_w d$$ (A7.17)

where f_{ck} is the characteristic value of concrete compressive strength, $k = 1 + \sqrt{200/d} \leq 2.0$ (width d in mm), $\rho_l = A_{sl}/b_w d \leq 0.02$ being A_{sl} the cross sectional area of the tensile reinforcement. The recommended value for $C_{Rd,c}$ is $0.18/\gamma_c$, where γ_c is the partial safety factor for concrete. Additionally, σ_{cp} is the stress due to the axial load, $k_1 = 0.15$ (recommended value) and $V_{min} = 0.035 k^{3/2} f_{ck}^{1/2}$.

Thus, for the design value calculation, the following parameters were adopted:

- f_{cm} of 30.78 MPa and 27.81MPa for the batches 1 and 2, which correspond to an f_{ck} of 22.78 MPa and 19.81MPa respectively;

- $C_{Rd,c} = 0.18/\gamma_c$, being γ_c equal to 1.50, obtaining a value of 0.12;

- web widths (b_w) equal to 150 mm and 300 mm for the A and B series, respectively;

- distance from the extreme compression fiber of the cross section to the centroid of the longitudinal reinforcement (d) equal to 261.50 mm;

- $k = 1 + \sqrt{200/d} \leq 2.0$, obtaining a value of 1.87; and

- $\rho_l = A_{sl}/b_w d \leq 0.02$, obtaining the values of 0.02 and 0.018 for the A and B series, respectively.

The design value for the shear resistance for members not requiring shear reinforcement is:

$$V_{Rd,c} = [0.12 \cdot 1.87(100 \cdot 0.02 \cdot 22.78MPa)^{1/3}]150mm \cdot 261.50mm \tag{A7.18}$$

$$V_{Rd,c} = 31.51kN$$

and

$$V_{Rd,c} = [0.12 \cdot 1.87(100 \cdot 0.018 \cdot 22.78MPa)^{1/3}]300mm \cdot 261.50mm \tag{A7.19}$$

$$V_{Rd,c} = 61.70kN$$

For reinforced concrete members with vertical steel stirrups, the $V_{Rd,s}$ is the smaller value between

$$V_{Rd,s} = \frac{A_{sw}}{s} \cdot z \cdot f_{ywd} \cdot \cot\theta \tag{A7.20}$$

and

$$V_{Rd,max} = \alpha_{cw} b_w z \nu_1 f_{cd} / (\cot\theta + \tan\theta) \tag{A7.21}$$

For members with inclined shear reinforcement, the $V_{Rd,s}$ is the smaller value between

$$V_{Rd,s} = \frac{A_{sw}}{s} \cdot z \cdot f_{ywd} \cdot (\cot\theta + \cot\alpha)\sin\alpha \tag{A7.22}$$

and

$$V_{Rd,max} = \alpha_{cw} b_w z \nu_1 f_{cd} (\cot\theta + \tan\alpha) / (1 + \cot^2\theta) \tag{A7.23}$$

where $V_{Rd,max}$ is the design value of the maximum shear force that can be sustained by the member, limited by crushing of the compression struts; A_{sw} is the cross-sectional area of the shear reinforcement; s is the spacing of the stirrups; z is the lever arm (that may be considered as $z = 0.9 \cdot d$), f_{ywd} is the design value of the yield stress of the shear reinforcement; θ is the angle of the inclined struts ($1 \leq \cot\theta \leq 2.5$), α is the angle between the inclined bars and the axis of the beam, ν_1 is a strength reduction factor to take into account that concrete is cracked in the shear region (considered as 0.6 for $f_{ck} < 60\,MPa$); α_{cw} is a coefficient to take into account

the stress state in the compression chord (recommended values of 1 for non-prestressed structures) and f_{cd} is the design value of concrete compressive strength.

Using the equations (A7.22) and (A7.23), the materials properties presented in Table 7.2 and $\cot\theta = 2.5 => \theta = 21.8°$, the $V_{Rd,s}$ of the vertical steel stirrups, at a spacing of 300 mm, is the smaller value between:

$$V_{Rd,s} = \frac{[2 \cdot (6mm/2)^2 \cdot \Pi]}{300mm} \cdot (0.9 \cdot 261.50mm) \cdot \frac{(559.14MPa)}{1.15}(\cot 21.8° + \cot 90°)\sin 90° \tag{A7.24}$$
$$V_{Rd,s} = 53.93kN$$

and

$$V_{Rd,max} = 1.00 \cdot 150mm \cdot (0.9 \cdot 261.50mm) \cdot 0.60 \cdot \frac{(22.78MPa)}{1.50}(\cot 21.8° + \tan 90°)/(1 + \cot^2 21.8°)$$
$$V_{Rd,max} = 110.92kN \tag{A7.25}$$

or

$$V_{Rd,max} = 1.00 \cdot 150mm \cdot (0.9 \cdot 261.50mm) \cdot 0.60 \cdot \frac{(19.81MPa)}{1.50}(\cot 21.8° + \tan 90°)/(1 + \cot^2 21.8°)$$
$$V_{Rd,max} = 96.45kN$$

or

$$V_{Rd,max} = 1.00 \cdot 300mm \cdot (0.9 \cdot 261.50mm) \cdot 0.60 \cdot \frac{(22.78MPa)}{1.50}(\cot 21.8° + \tan 90°)/(1 + \cot^2 21.8°)$$
$$V_{Rd,max} = 221.83kN$$

or

$$V_{Rd,max} = 1.00 \cdot 300mm \cdot (0.9 \cdot 261.50mm) \cdot 0.60 \cdot \frac{(19.81MPa)}{1.50}(\cot 21.8° + \tan 90°)/(1 + \cot^2 21.8°)$$
$$V_{Rd,max} = 192.91kN$$

So, $V_{Rd,s} = 53.93kN$.

Similarly, considering $\cot\theta = 1.0 => \theta = 45°$, the $V_{Rd,s}$ of the vertical steel stirrups, at a spacing of 300 mm, is the smaller value between:

$$V_{Rd,s} = \frac{[2 \cdot (6mm/2)^2 \cdot \Pi]}{300mm} \cdot (0.9 \cdot 261.50mm) \cdot \frac{(559.14MPa)}{1.15}(\cot 45° + \cot 90°)\sin 90° \tag{A7.26}$$
$$V_{Rd,s} = 21.58kN$$

and

$$V_{Rd,max} = 1.00 \cdot 150mm \cdot (0.9 \cdot 261.50mm) \cdot 0.60 \cdot \frac{(22.78MPa)}{1.50}(\cot 45° + \tan 90°)/(1 + \cot^2 45°)$$
$$V_{Rd,max} = 160.84kN \tag{A7.27}$$

or

$$V_{Rd,\max} = 1.00 \cdot 150mm \cdot (0.9 \cdot 261.50mm) \cdot 0.60 \cdot \frac{(19.81MPa)}{1.50}(\cot 45\text{º} + \tan 90\text{º})/(1 + \cot^2 45\text{º})$$

$$V_{Rd,\max} = 139.87kN$$

or

$$V_{Rd,\max} = 1.00 \cdot 300mm \cdot (0.9 \cdot 261.50mm) \cdot 0.60 \cdot \frac{(22.78MPa)}{1.50}(\cot 45\text{º} + \tan 90\text{º})/(1 + \cot^2 45\text{º})$$

$$V_{Rd,\max} = 321.68kN$$

or

$$V_{Rd,\max} = 1.00 \cdot 300mm \cdot (0.9 \cdot 261.50mm) \cdot 0.60 \cdot \frac{(19.81MPa)}{1.50}(\cot 45\text{º} + \tan 90\text{º})/(1 + \cot^2 45\text{º})$$

$$V_{Rd,\max} = 279.74kN$$

So, $V_{Rd,s} = 21.58kN$.

Taking into account the materials properties presented in Table 7.2 and $\cot\theta = 2.5 \Rightarrow \theta = 21.8°$, the $V_{Rd,s}$ of the vertical steel stirrups, at a spacing of 225 mm, is the smaller value between:

$$V_{Rd,s} = \frac{[2 \cdot (6mm/2)^2 \cdot \Pi]}{225mm} \cdot (0.9 \cdot 261.50mm) \cdot \frac{(559.14MPa)}{1.15}(\cot 21.8\text{º} + \cot 90\text{º})\sin 90\text{º} \qquad \text{(A7.28)}$$

$$V_{Rd,s} = 71.90kN$$

and

$$V_{Rd,\max} = 1.00 \cdot 150mm \cdot (0.9 \cdot 261.50mm) \cdot 0.60 \cdot \frac{(22.78MPa)}{1.50}(\cot 21.8\text{º} + \tan 90\text{º})/(1 + \cot^2 21.8\text{º})$$

$$V_{Rd,\max} = 110.92kN \qquad \text{(A7.29)}$$

or

$$V_{Rd,\max} = 1.00 \cdot 150mm \cdot (0.9 \cdot 261.50mm) \cdot 0.60 \cdot \frac{(19.81MPa)}{1.50}(\cot 21.8\text{º} + \tan 90\text{º})/(1 + \cot^2 21.8\text{º})$$

$$V_{Rd,\max} = 96.45kN$$

or

$$V_{Rd,\max} = 1.00 \cdot 300mm \cdot (0.9 \cdot 261.50mm) \cdot 0.60 \cdot \frac{(22.78MPa)}{1.50}(\cot 21.8\text{º} + \tan 90\text{º})/(1 + \cot^2 21.8\text{º})$$

$$V_{Rd,\max} = 221.83kN$$

or

$$V_{Rd,\max} = 1.00 \cdot 300mm \cdot (0.9 \cdot 261.50mm) \cdot 0.60 \cdot \frac{(19.81MPa)}{1.50}(\cot 21.8\text{º} + \tan 90\text{º})/(1 + \cot^2 21.8\text{º})$$

$$V_{Rd,\max} = 192.92kN$$

So, $V_{Rd,s} = 71.90kN$.

Similarly, considering $\cot\theta = 1.0 \Rightarrow \theta = 45°$, the $V_{Rd,s}$ of the vertical steel stirrups, at a spacing of 225 mm, is the smaller value between:

$$V_{Rd,s} = \frac{[2 \cdot (6mm/2)^2 \cdot \Pi]}{225mm} \cdot (0.9 \cdot 261.50mm) \cdot \frac{(559.14MPa)}{1.15}(\cot 45° + \cot 90°)\sin 90° \qquad \text{(A7.30)}$$
$$V_{Rd,s} = 27.78kN$$

and

$$V_{Rd,max} = 1.00 \cdot 150mm \cdot (0.9 \cdot 261.50mm) \cdot 0.60 \cdot \frac{(22.78MPa)}{1.50}(\cot 45° + \tan 90°)/(1+\cot^2 45°)$$
$$V_{Rd,max} = 160.84kN \qquad \text{(A7.31)}$$

or

$$V_{Rd,max} = 1.00 \cdot 150mm \cdot (0.9 \cdot 261.50mm) \cdot 0.60 \cdot \frac{(19.81MPa)}{1.50}(\cot 45° + \tan 90°)/(1+\cot^2 45°)$$
$$V_{Rd,max} = 139.87kN$$

or

$$V_{Rd,max} = 1.00 \cdot 300mm \cdot (0.9 \cdot 261.50mm) \cdot 0.60 \cdot \frac{(22.78MPa)}{1.50}(\cot 45° + \tan 90°)/(1+\cot^2 45°)$$
$$V_{Rd,max} = 321.68kN \qquad \text{(A7.29)}$$

or

$$V_{Rd,max} = 1.00 \cdot 300mm \cdot (0.9 \cdot 261.50mm) \cdot 0.60 \cdot \frac{(19.81MPa)}{1.50}(\cot 45° + \tan 90°)/(1+\cot^2 45°)$$
$$V_{Rd,max} = 279.74kN$$

So, $V_{Rd,s} = 27.78kN$.

To take into account the contribution of the ETS bars ($V_{Rd,f}$) for the shear strengthening of a shear reinforced element, in equation (7.7), the term $V_{Rd,f}$ was also added:

$$V_{Rd} = V_{Rd,s} + V_{Rd,f} \qquad \text{(A7.30)}$$

where $V_{Rd,f}$ is the design value of the maximum shear force that can be sustained by the ETS bars:

$$V_{Rd,f} = \frac{A_{sf}}{s_f} \cdot z \cdot f_{ywd} \cdot (\cot\theta + \cot\alpha)\sin\alpha \qquad \text{(A7.31)}$$

being A_{sf} and f_{ywd} the cross-sectional area and the design value of the yield stress of a ETS bar ($f_{ywd} = f_{ym}/\gamma_s$), and s_f is the spacing of ETS bars.

Taking into account the materials properties presented in Table 7.2 and $\cot\theta=2.5 \Rightarrow \theta=21.8°$ and $\cot\theta=1.0 \Rightarrow \theta=45°$, the $V_{Rd,f}$ of the vertical ETS bars of the A series, at a spacing of 300 mm, are:

$$V_{Rd,f}=\frac{\left[(10mm/2)^2\cdot\Pi\right]}{300mm}\cdot(0.9\cdot261.50mm)\cdot\frac{(541.60MPa)}{1.15}\cdot(\cot21.8°+\cot90°)\sin90° \tag{A7.32}$$
$$V_{Rd,f}=72.55kN$$

and

$$V_{Rd,f}=\frac{\left[(10mm/2)^2\cdot\Pi\right]}{300mm}\cdot(0.9\cdot261.50mm)\cdot\frac{(541.60MPa)}{1.15}\cdot(\cot45°+\cot90°)\sin90°$$
$$V_{Rd,f}=29.04kN$$

The $V_{Rd,f}$ of the vertical ETS bars of the B series, at a spacing of 300mm, are:

$$V_{Rd,f}=\frac{\left[(8mm/2)^2\cdot\Pi\cdot2\right]}{300mm}\cdot(0.9\cdot261.50mm)\cdot\frac{(566.50MPa)}{1.15}\cdot(\cot21.8°+\cot90°)\sin90° \tag{A7.33}$$
$$V_{Rd,f}=97.13kN$$

and

$$V_{Rd,f}=\frac{\left[(8mm/2)^2\cdot\Pi\cdot2\right]}{300mm}\cdot(0.9\cdot261.50mm)\cdot\frac{(566.50MPa)}{1.15}\cdot(\cot45°+\cot90°)\sin90°$$
$$V_{Rd,f}=37.88kN$$

The $V_{Rd,f}$ of the inclined ETS bars of the A series, at a spacing of 300 mm and taking into account the materials properties presented in Table 7.2 and $\cot\theta=2.5 \Rightarrow \theta=21.8°$ and $\cot\theta=1.0 \Rightarrow \theta=45°$, are:

$$V_{Rd,f}=\frac{\left[(8mm/2)^2\cdot\Pi\cdot2\right]}{300mm}\cdot(0.9\cdot261.50mm)\cdot\frac{(566.50MPa)}{1.15}\cdot(\cot21.8°+\cot45°)\sin45° \tag{A7.34}$$
$$V_{Rd,f}=96.15kN$$

and

$$V_{Rd,f}=\frac{\left[(8mm/2)^2\cdot\Pi\cdot2\right]}{300mm}\cdot(0.9\cdot261.50mm)\cdot\frac{(566.50MPa)}{1.15}\cdot(\cot45°+\cot45°)\sin45°$$
$$V_{Rd,f}=54.98kN$$